CR-12866

Space Shuttle Program

MSC-03321

IBM

GD

AA

H
HONEYWELL

Phase B Final Report
Expendable Second Stage
Reusable Space Shuttle Booster
Volume XII. Design Data Book

Contract NAS9-10960, Exhibit B
DRL MSFC-DRL-221, DRL Line Item 6
DRD MA-078-U2
SD 71-140-12
25 June 1971

Space Division • North American Rockwell 12214 Lakewood Boulevard, Downey, California 90241

SD 71-140-12
(MSC-03321)

25 June 1971

PHASE B FINAL REPORT
EXPENDABLE SECOND STAGE
REUSABLE SPACE SHUTTLE BOOSTER

Volume XII
Design Data Book

Contract NAS9-10960, Exhibit B
DRL MSFC-DRL-221, DRL Line Item 6
DRD MA-078-U2

Approved by

B. Hello
Vice President and General Manager
Space Shuttle Program

Space Division • North American Rockwell 12214 LAKEWOOD BOULEVARD • DOWNEY, CALIFORNIA 90241

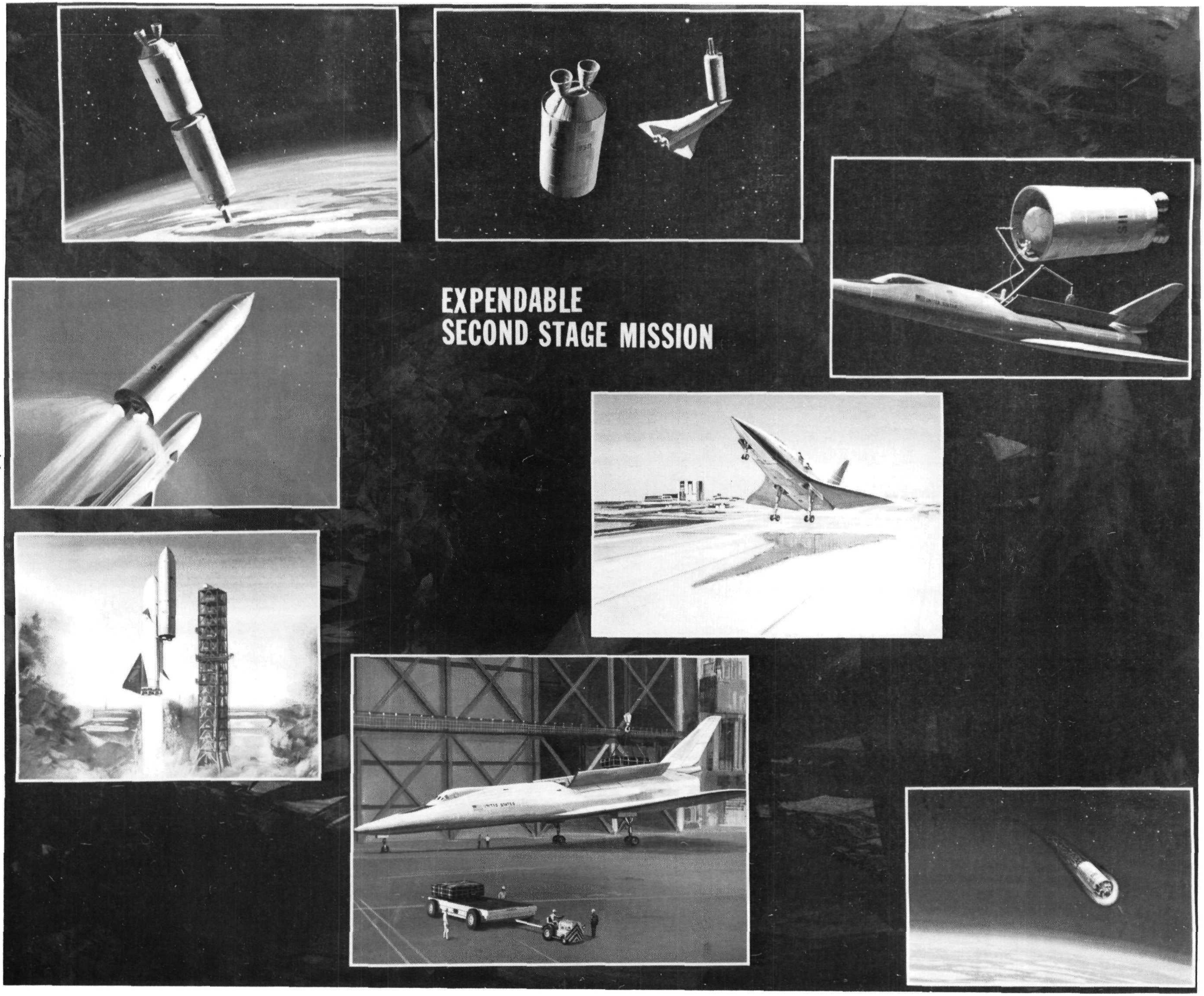
EXPENDABLE
SECOND STAGE MISSION

FOREWORD

The Space Shuttle Phase B studies are directed toward the definition of an economical space transportation system. In addition to the missions which can be satisfied with the shuttle payload capability, the National Aeronautics and Space Administration has missions planned that require space vehicles to place payloads in excess of 100,000 pounds in earth orbit. To satisfy this requirement, a cost-effective multimission space shuttle system with large lift capability is needed. Such a system would utilize a reusable shuttle booster and an expendable second stage. The expendable second stage would be complementary to the space shuttle system and impose minimum impact on the reusable booster.

To assist the expendable second stage concept, a two-phase study was authorized by NASA. Phase A efforts, which ended in December 1970, concentrated on performance, configuration, and basic aerodynamic considerations. Basic trade studies were carried out on a relatively large number of configurations. At the conclusion of Phase A, the contractor proposed a single configuration. Phase B commenced on February 1, 1971 (per Technical Directive Number 503) based on the recommended system. Whereas a large number of payload configurations were considered in the initial phase, Phase B was begun with specific emphasis placed on three representative payload configurations. The entire Phase B activity has been directed toward handling the three representative payload configurations in the most acceptable manner. Results of this activity are reported in this 12-volume Phase B final report.

Volume I	Executive Summary	SD 71-140-1
Volume II	Technical Summary	SD 71-140-2
Volume III	Wind Tunnel Test Data	SD 71-140-3
Volume IV	Detail Mass Properties Data	SD 71-140-4
Volume V	Operations and Resources	SD 71-140-5
Volume VI	Interface Control Drawings	SD 71-140-6
Volume VII	Preliminary Design Drawings	SD 71-140-7
Volume VIII	Preliminary CEI Specification - Part 1	SD 71-140-8
Volume IX	Preliminary System Specification	SD 71-140-9
Volume X	Technology Requirements	SD 71-140-10
Volume XI	Cost and Schedule Estimates	SD 71-140-11
Volume XII	Design Data Book	SD 71-140-12

This document is Volume XII, Design Data Book.

PRECEDING PAGE BLANK NOT FILMED

CONTENTS

Section | Page

Section		Page

INTRODUCTION

This volume of the final report is intended to provide NASA with preliminary engineering definition information generated during program phases which displays current system requirements and configuration. The data contained herein are of preliminary engineering nature and have been used to develop description of the selected system. Insofar as feasible, the data have been arranged in four sections as follows:

Section 1.0 General and Design Criteria

Section 2.0 Requirements

Section 3.0 Configuration Definition

Section 4.0 Program Concepts

Where not otherwise covered in the text of the previous volumes of this report, analytical methods including mathematical equations in key design areas are given.

It may be noted that in general the design criteria and requirements associated with the selected system are given in Volume II, Technical Summary, at the beginning of the sections to which they apply. Similarly, the evolution of the configuration of the selected system is described in the other volumes of this report.

In those areas where additional engineering information has been developed, such data are included in this volume.

Page Intentionally Left Blank

PRECEDING PAGE BLANK NOT FILMED

1.0 GENERAL AND DESIGN CRITERIA

1.1 AERODYNAMIC DATA

1.1.1 TRAJECTORY DEVELOPMENT

The following trajectory data were developed and used in the course of the study. Each trajectory is identified by payload type (where appropriate) and by date. A brief discussion of its significance to the study is included. The trajectory dated 2/15/71 was the first developed during Phase B. Much of the initial aerodynamic heating analysis was based on it.

The 3/1/71 trajectory was an updating of certain performance parameters and represented steering based on nominal (no wind) angle of attack equal to zero. Loads analyses conducted on this trajectory revealed that attachment loads were high and that load reduction schemes by trajectory shaping should be investigated.

NOMINAL ESS REFERENCE TRAJECTORY (2/15/71)

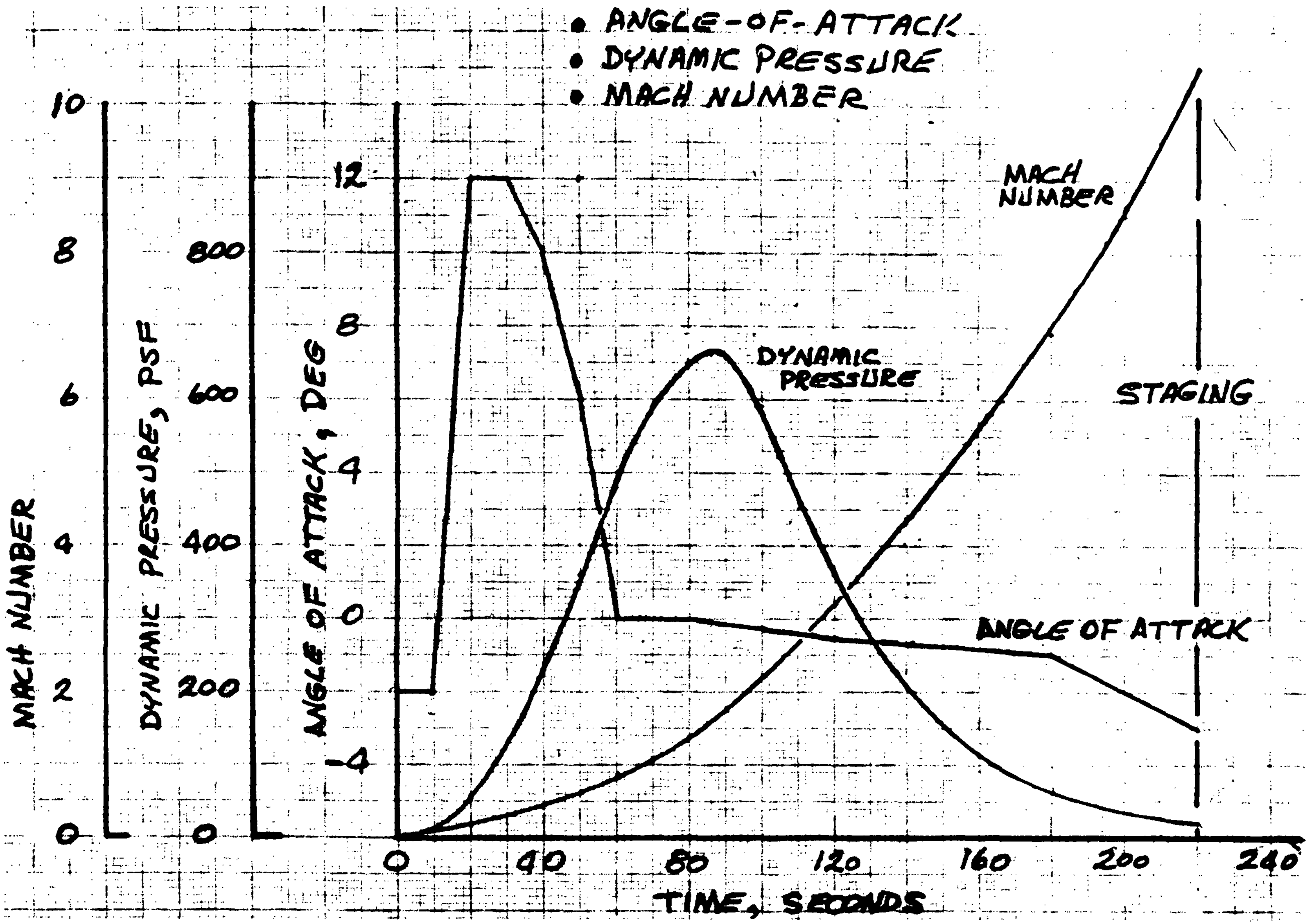

NOMINAL ESS REFERENCE TRAJECTORY (2/15/71)

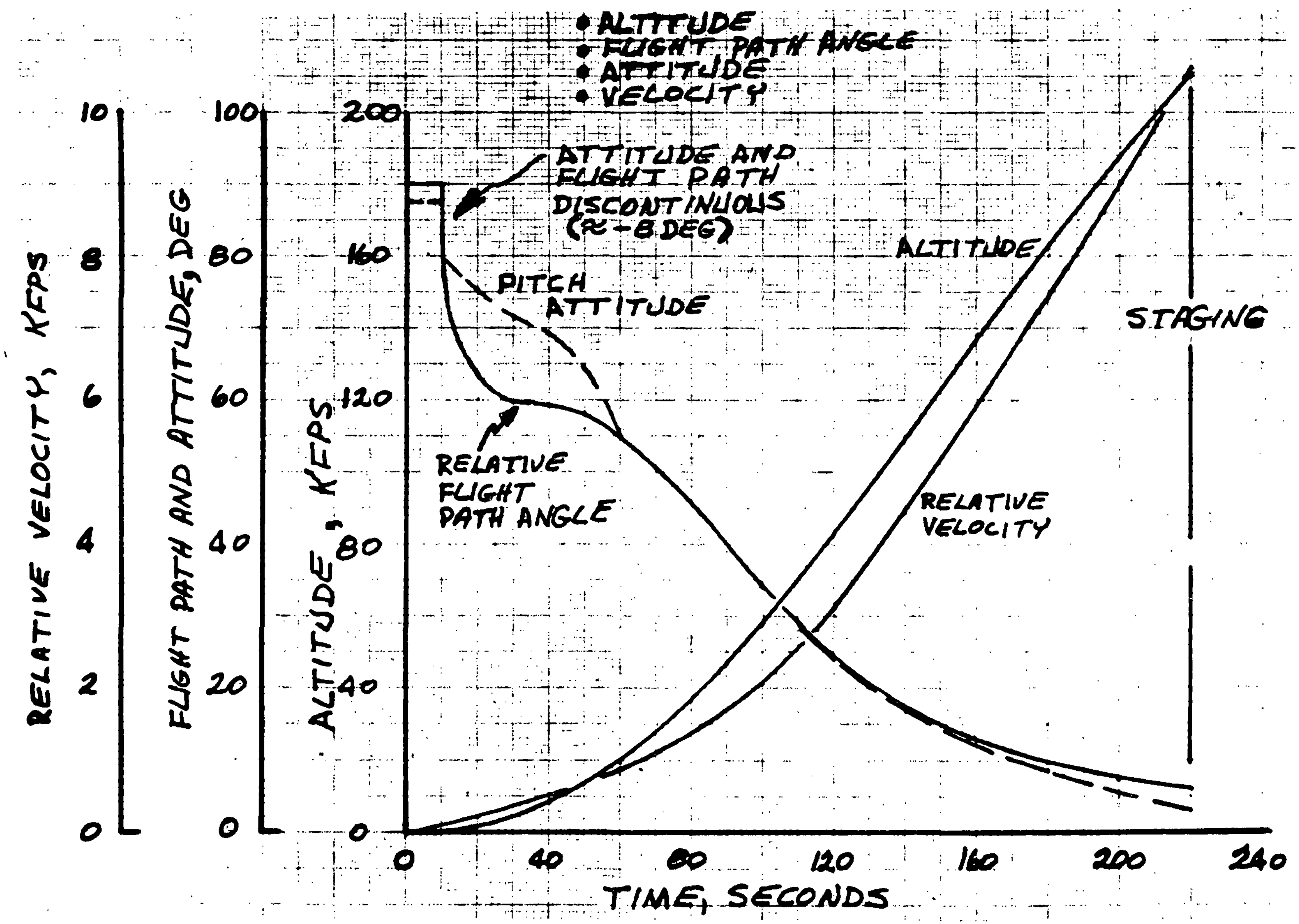

NOMINAL ESS REFERENCE TRAJECTORY (2/15/71)

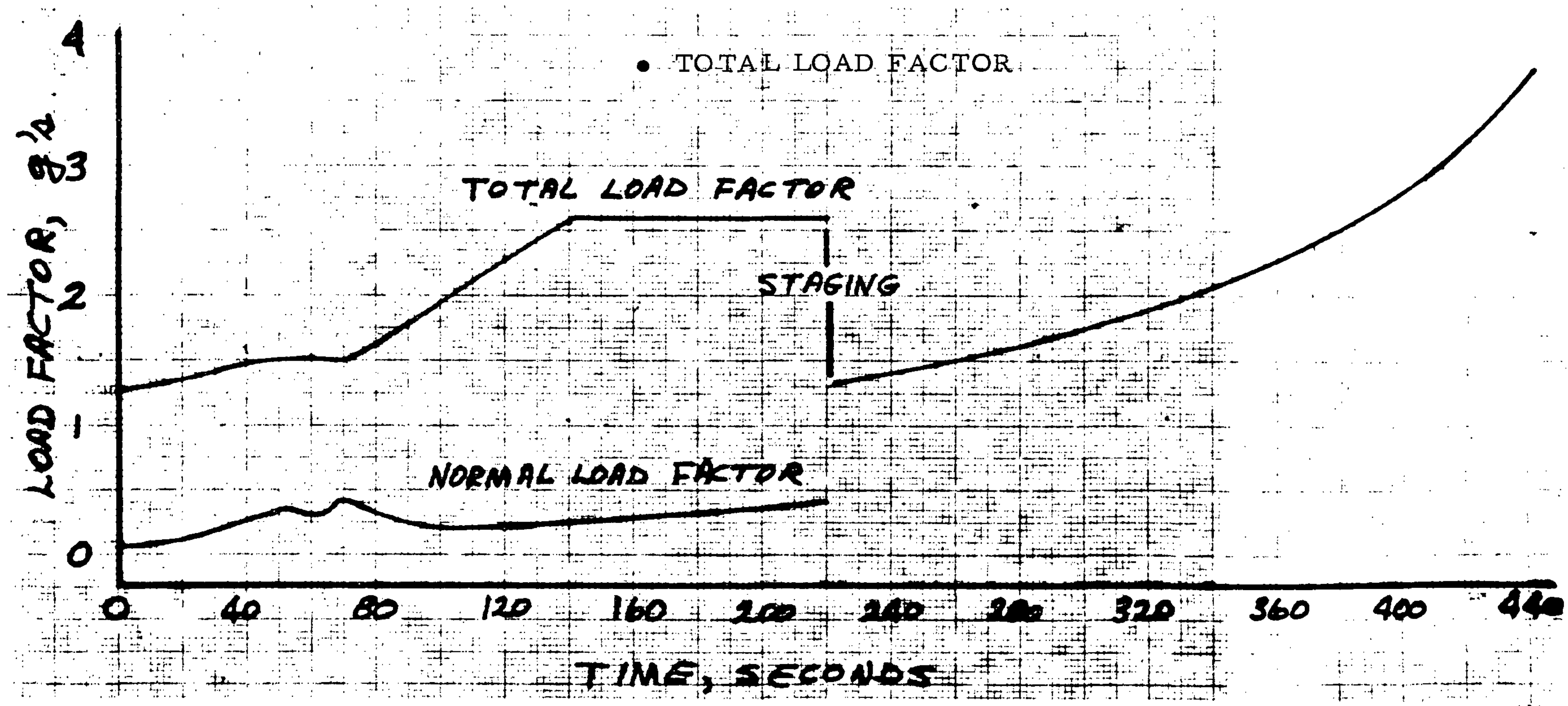

NOMINAL BASELINE ESS ASCENT TRAJECTORY (3/1/71)

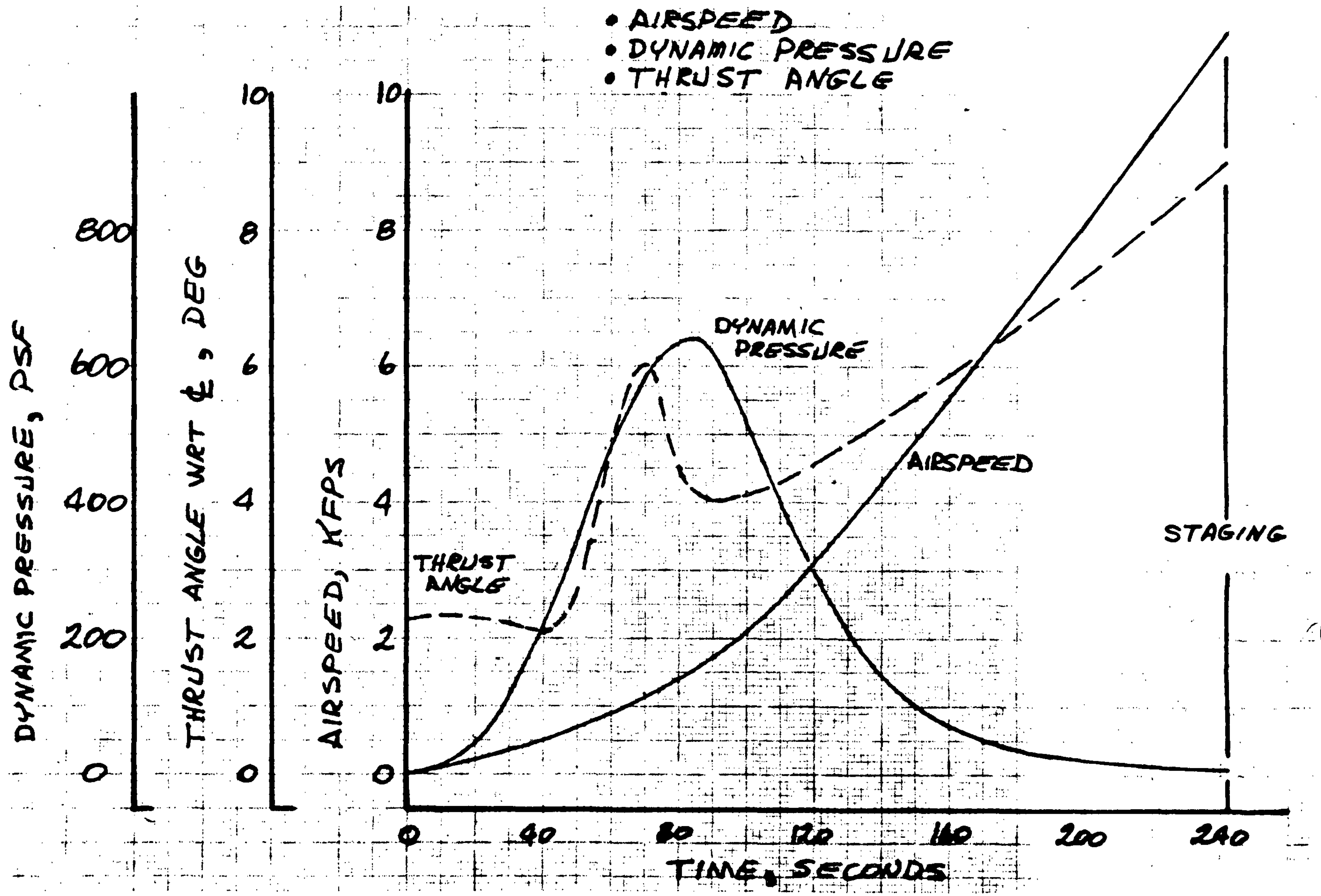

NOMINAL BASELINE ESS ASCENT TRAJECTORY (3/1/71)

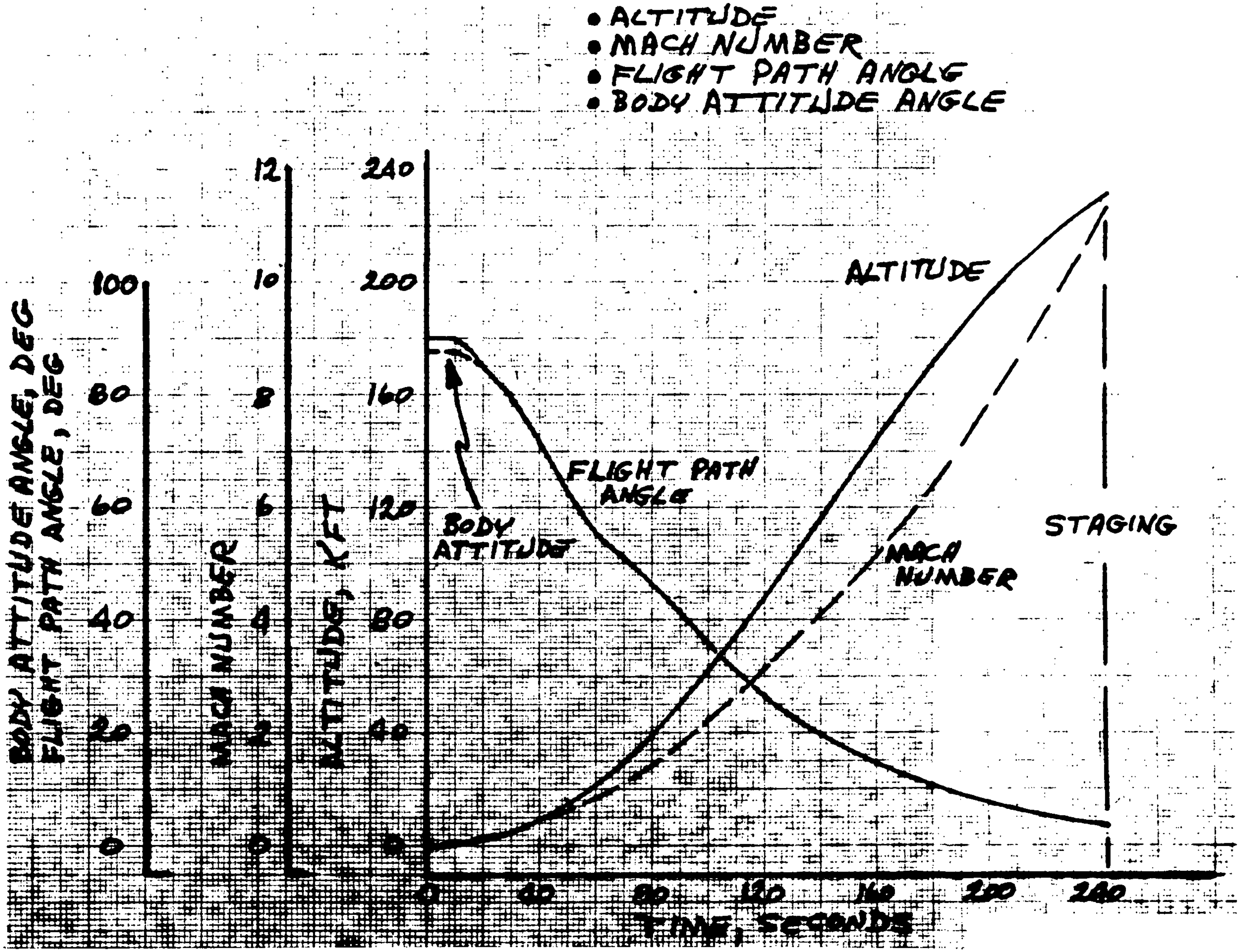

NOMINAL BASELINE ESS ASCENT TRAJECTORY (3/1/71)

- TOTAL LOAD FACTOR
- NORMAL LOAD FACTOR (MATED FLIGHT ONLY)

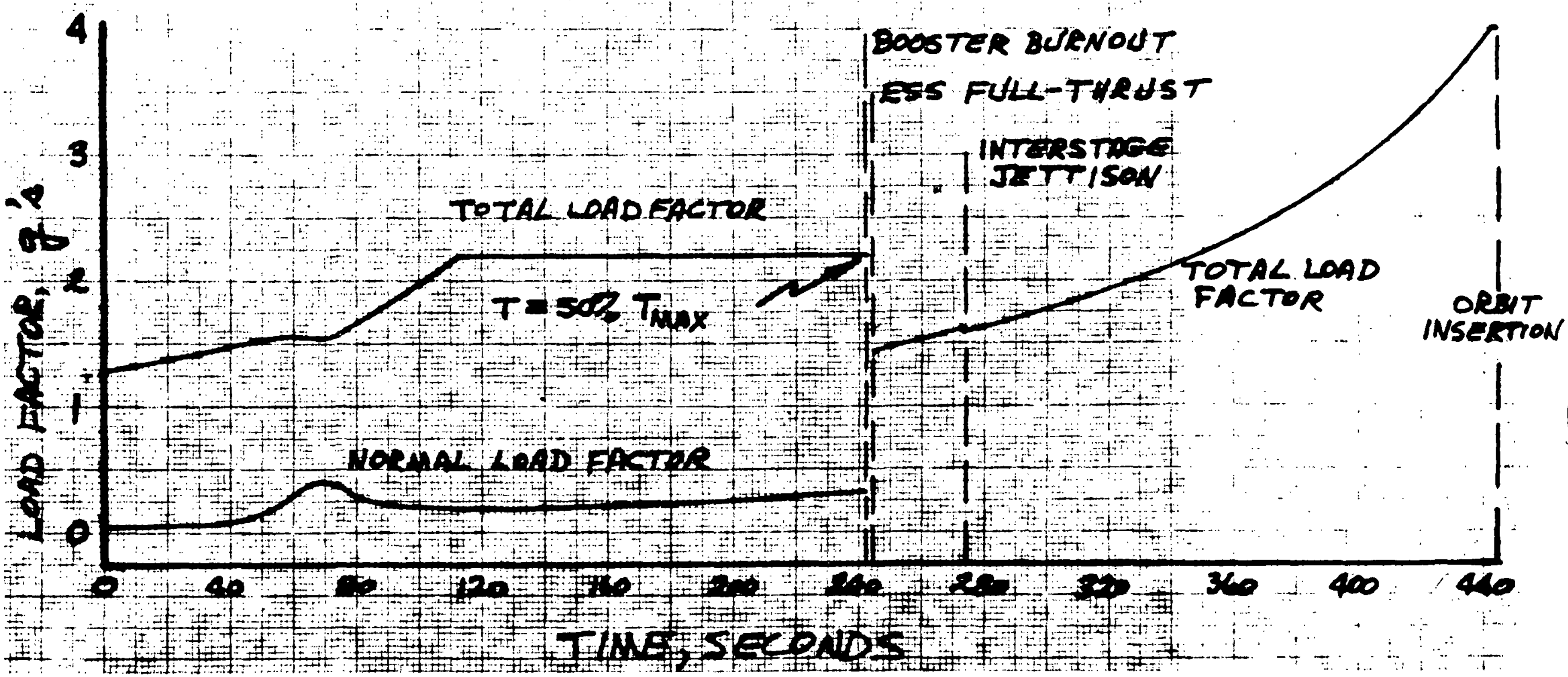

NOMINAL BASELINE ESS ASCENT TRAJECTORY (3/1/71)

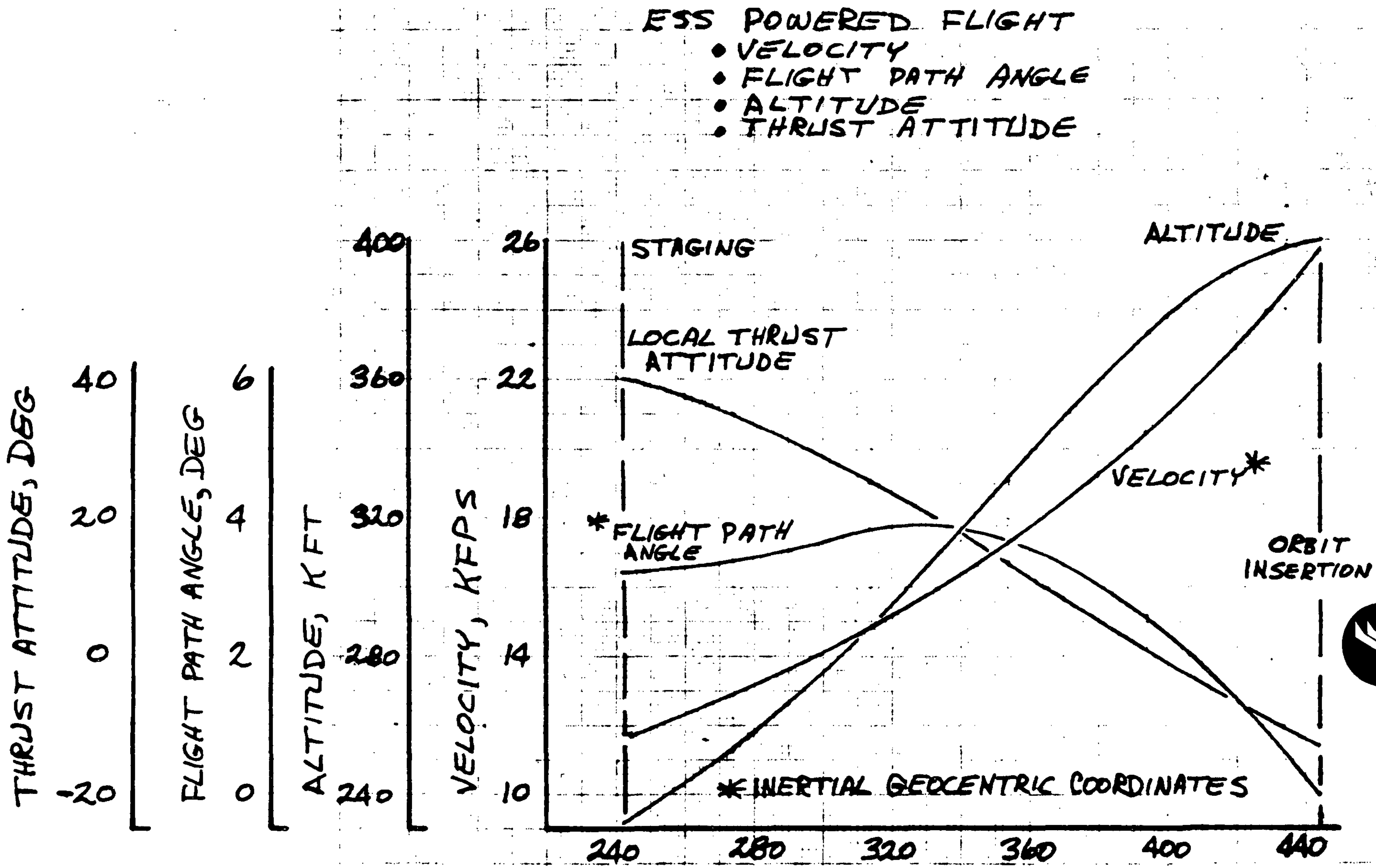

NOMINAL BASELINE ESS ASCENT TRAJECTORY (3/1/71)

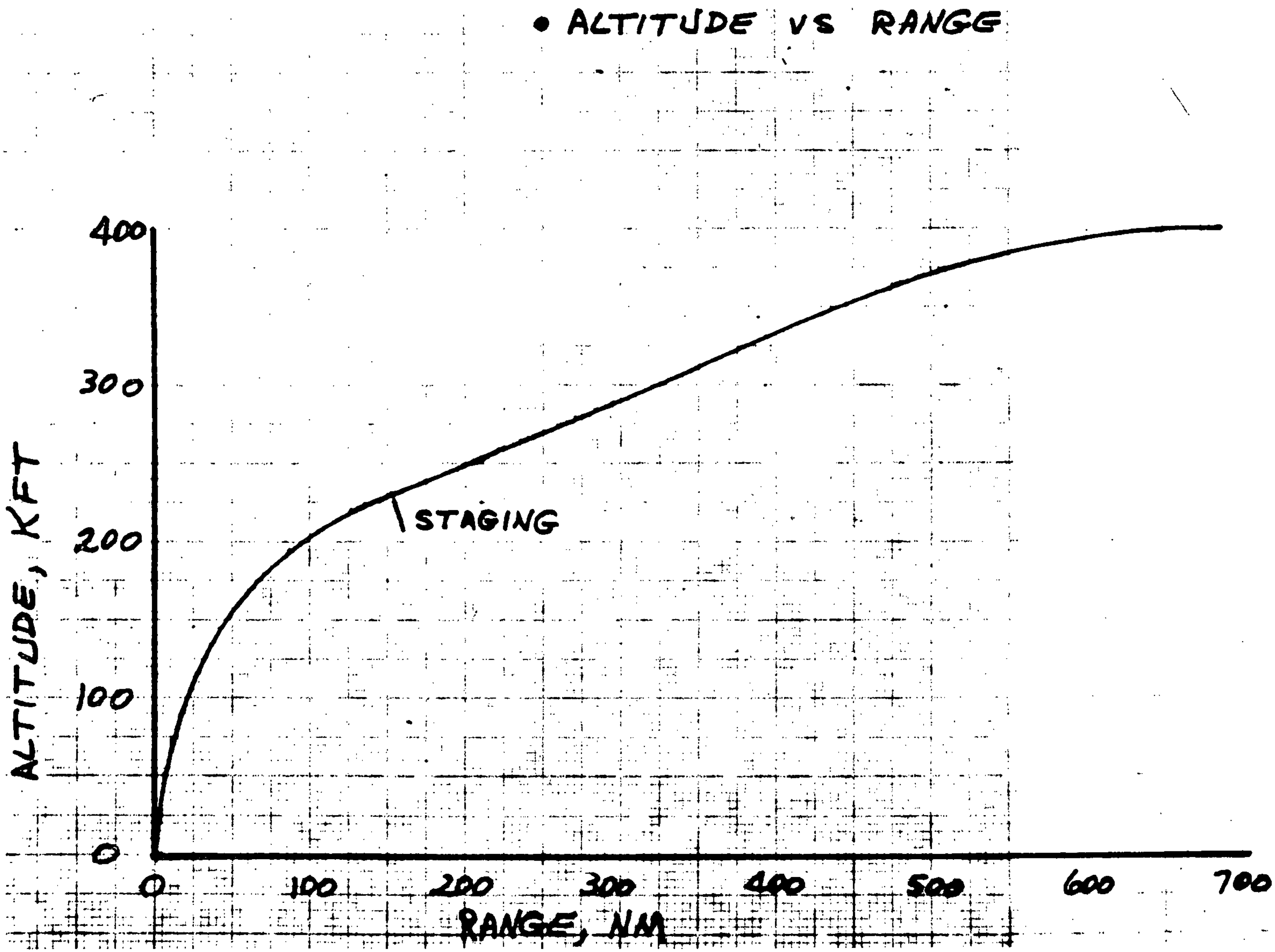

1.1.2 NOMINAL ESS ASCENT TRAJECTORY FOR RNS PAYLOAD (4/7/71)

This trajectory was the first to reflect trajectory shaping rationale designed to minimize attachment loads at maximum $q\alpha$. It is based on off-loading the booster and the ESS to provide minimum residual propellant in the ESS and employs throttling and trajectory shaping to reduce the maximum dynamic pressure to 372 psf and to permit the nominal (no wind) angle of attack to be negative in the max q region.

Booster propellant of 900, 000 pounds was off-loaded. Throttling of 27 percent was employed to give a liftoff T/W of 1.2. The trajectory climbs nearly vertically for 60 seconds after which negative angle of attack is introduced to provide negative angle of attack at max q and permit acceptable staging conditions.

The computer printout is included as are plots of selected parameters.

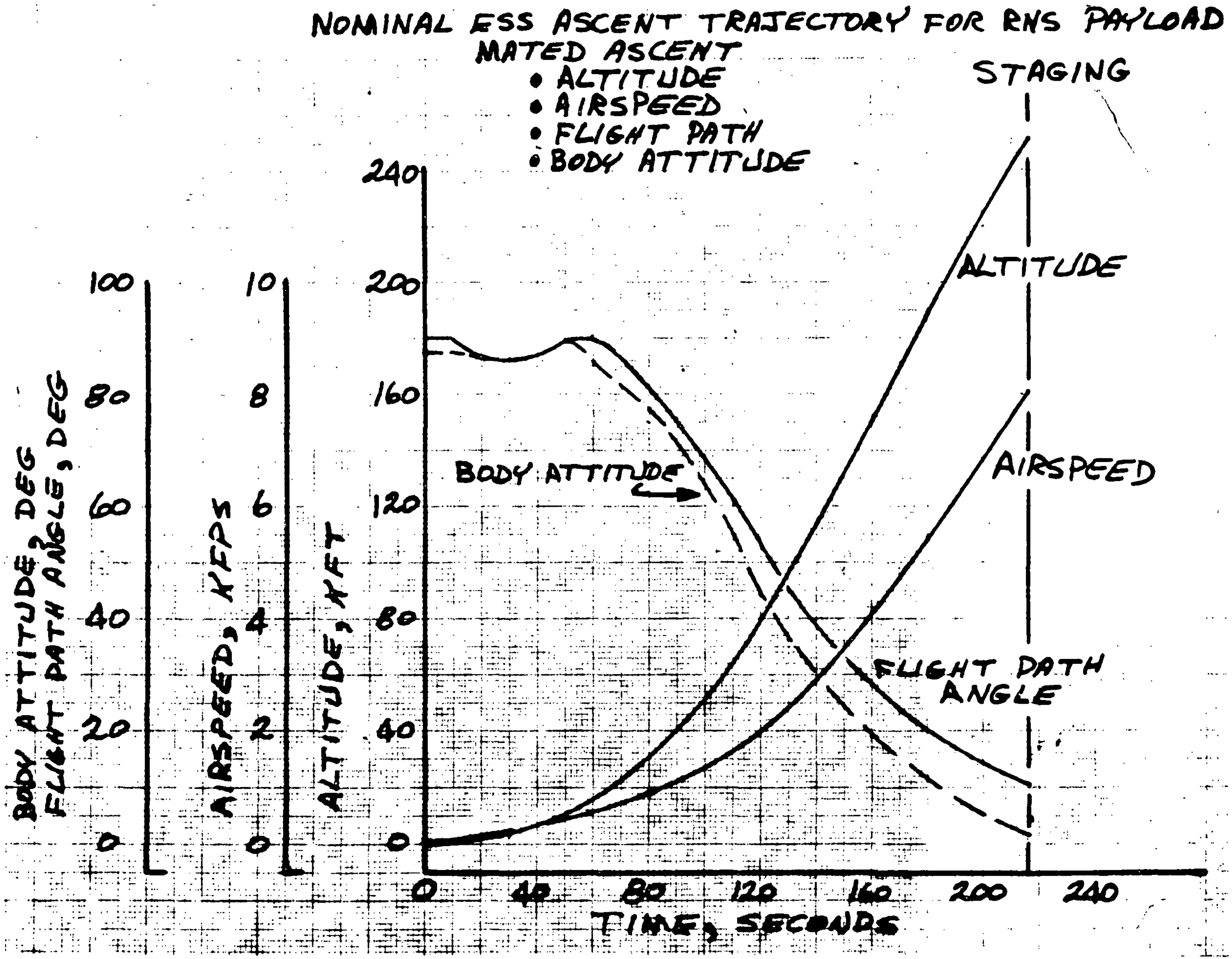
NOMINAL ESS ASCENT TRAJECTORY FOR RNS PAYLOAD
MATED ASCENT
• ALTITUDE
• AIRSPEED
• FLIGHT PATH
• BODY ATTITUDE
STAGING
ALTITUDE
AIRSPEED
BODY ATTITUDE
FLIGHT PATH ANGLE
BODY ATTITUDE, DEG
FLIGHT PATH ANGLE, DEG
AIRSPEED, KFPS
ALTITUDE, KFT
TIME, SECONDS
0
40
80
120
160
200
240
0
20
40
60
80
100
0
2
4
6
8
10

NOMINAL ESS ASCENT TRAJECTORY FOR RNS PAYLOAD (CON'

MATED ASCENT

- DYNAMIC PRESSURE
- MACH NUMBER

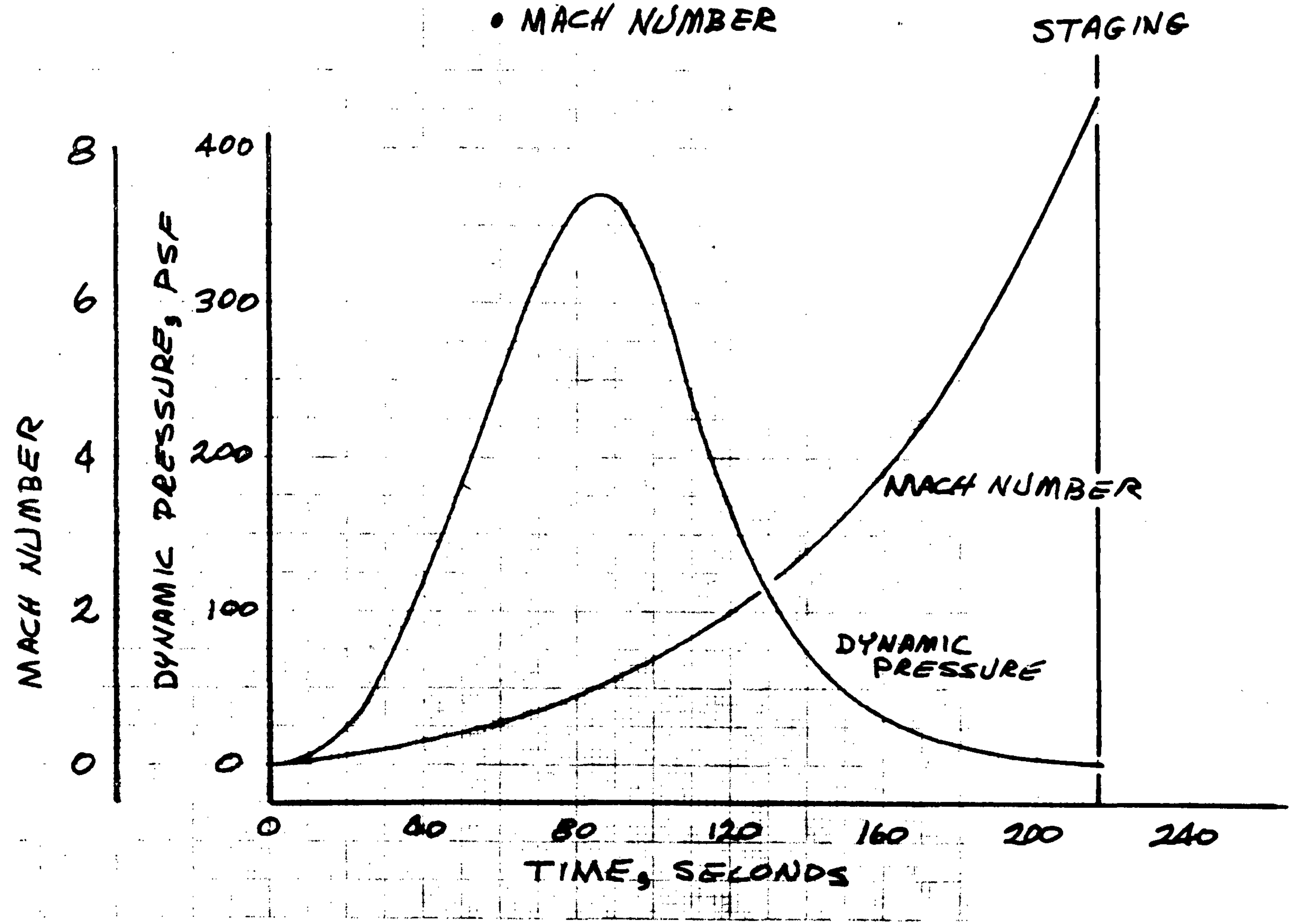

NOMINAL ESS ASCENT TRAJECTORY FOR RNS PAYLOAD (CONT)

MATED ASCENT

- THRUST DEFLECTION ANGLE FOR TRIM
- ANGLE OF ATTACK
- $q\alpha$ PRODUCT

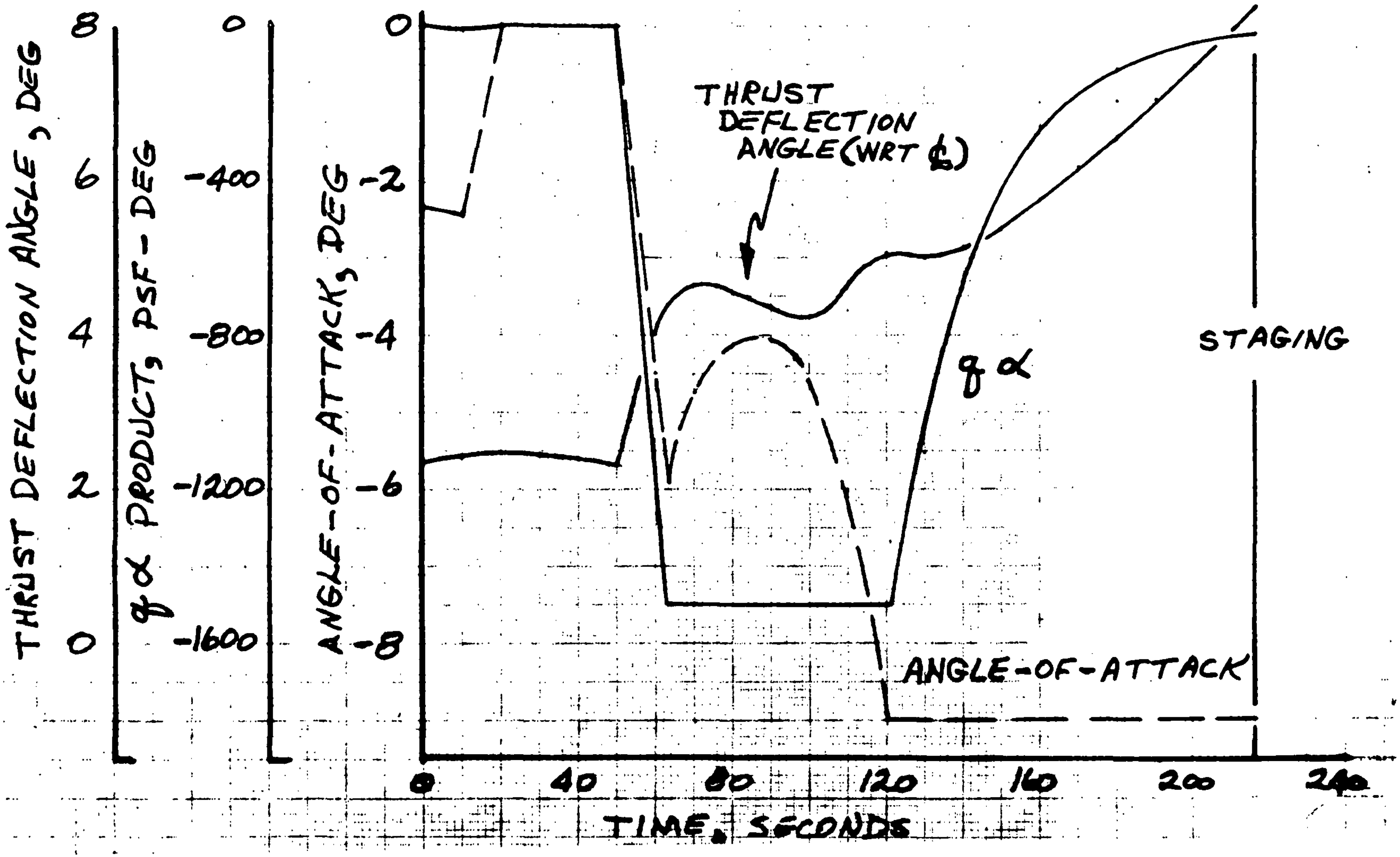

NOMINAL ESS ASCENT TRAJECTORY FOR RNS PAYLOAD (CONT

• LOAD FACTORS

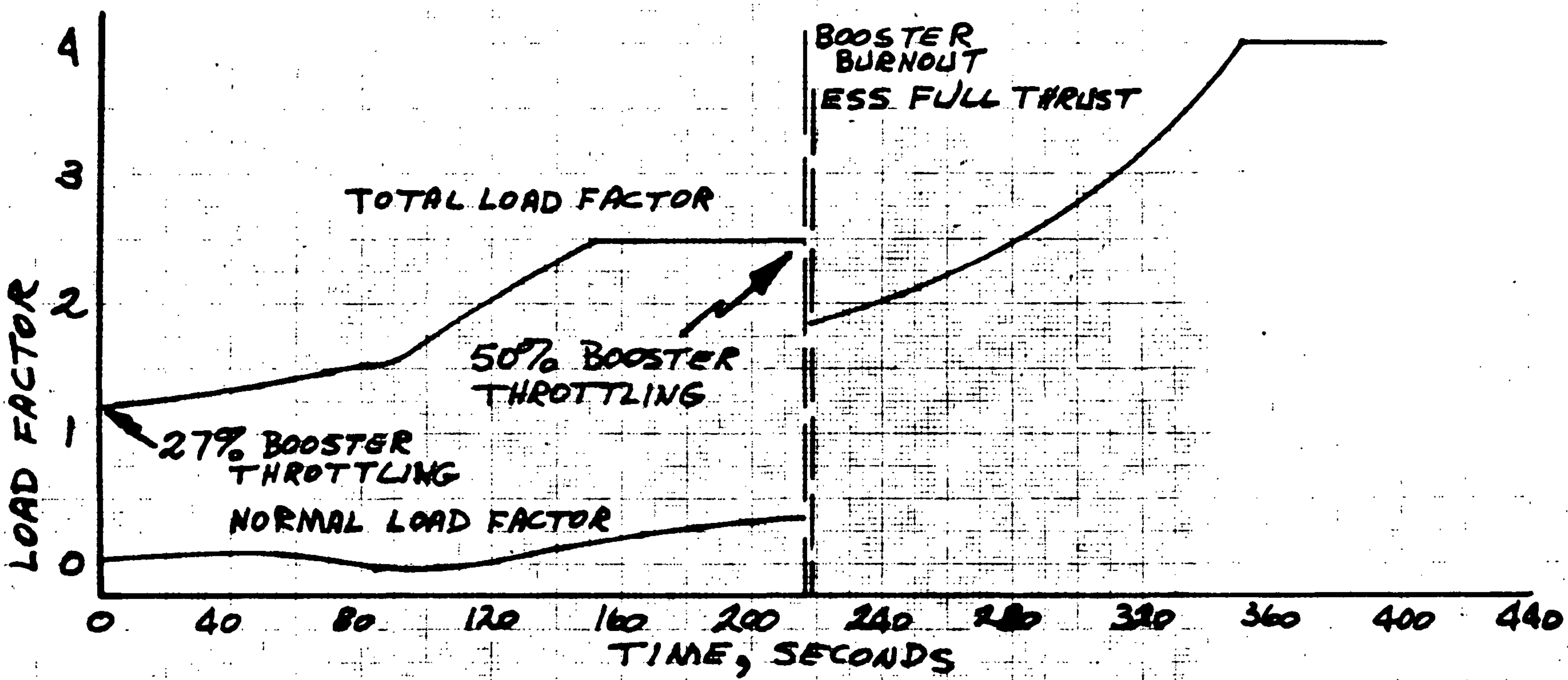

NOMINAL ESS ASCENT TRAJECTORY FOR RNS PAYLOAD (CONT)

• ALTITUDE VS RANGE

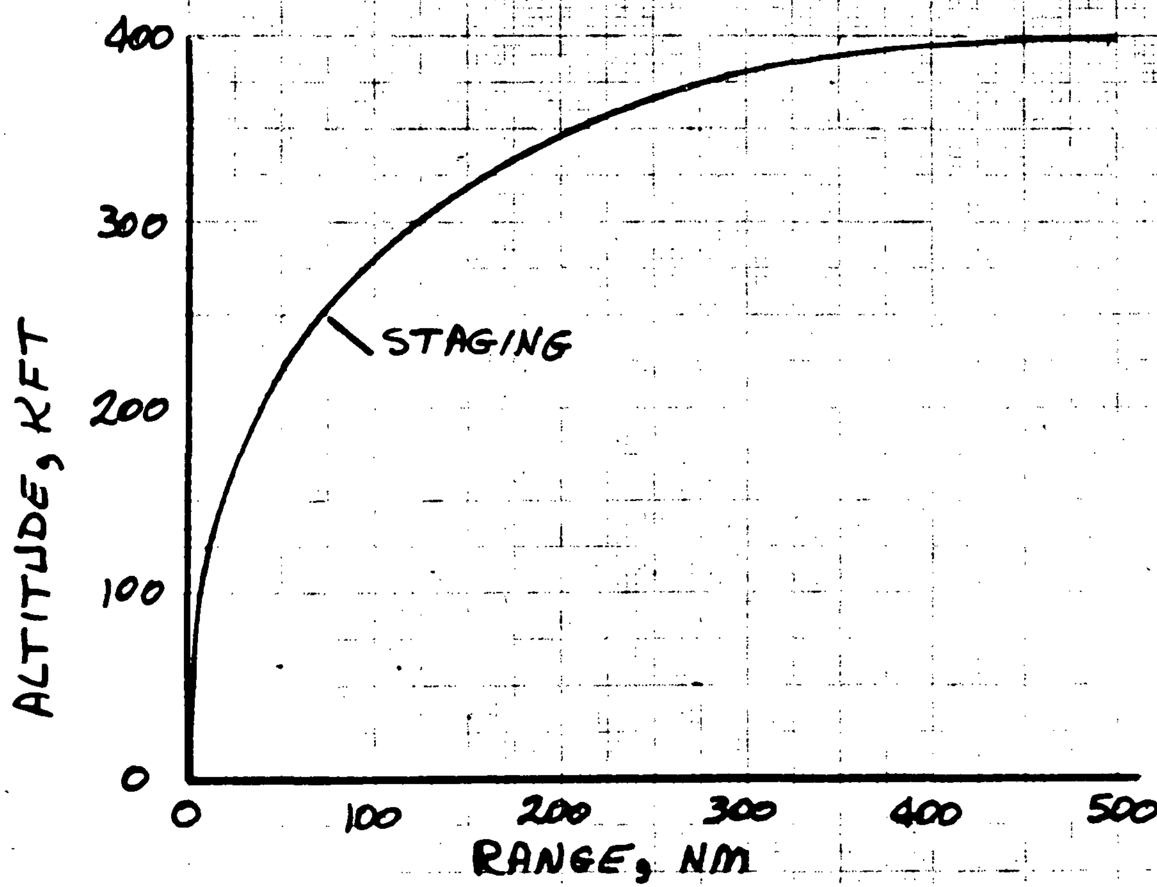

NOMINAL ESS ASCENT TRAJECTORY FOR RNS PAYLOAD (CONT)

ESS POWERED ASCENT

- ALTITUDE
- VELOCITY
- FLIGHT PATH ANGLE
- THRUST ATTITUDE

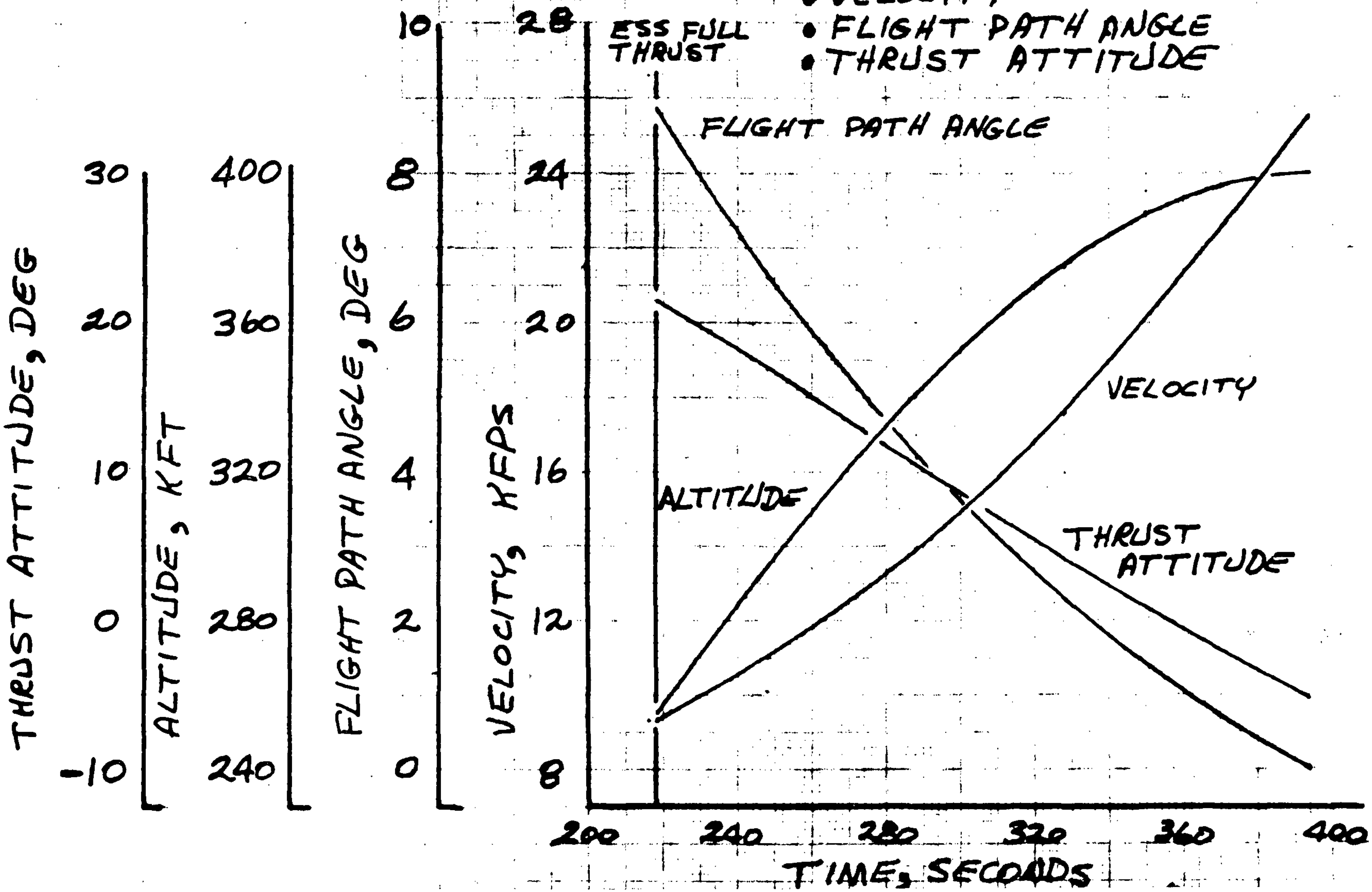

NOMINAL ESS ASCENT TRAJECTORY FOR RNS PAYLOAD

VEHICLE CHARACTERISTICS — CASE 3

STAGE	1	2	3	4
GROSS STAGE WEIGHT,(LB)	3974835.0	686600.0	680000.0	599000.0
GROSS STAGE THRUST/WEIGHT	1.660	0.0	1.859	2.110
THRUST,(LB)	7243500.0	0.0	1263810.0	1263810.0
ISP,(SEC)	439.000	2.500	459.000	459.000
STRUCTURE,(LB)	660335.0	6600.0	0.0	106820.0
PROPELLANT,(LB)	2479900.0	0.0	81000.0	386339.6
PERF. FRAC.,(NU)	0.6239	0.0	0.1191	0.6450
PROPELLANT FRAC.,(NUB)	0.7897	0.0	1.0000	0.7834
BURNOUT TIME,(SEC)	216.250	218.750	248.168	394.050
BURNOUT VELOCITY,(FT/SEC)	9343.488	9331.055	11042.387	25762.266
BURNOUT GAMMA,(DEGREES)	9.302	8.888	6.620	-0.001
BURNOUT ALTITUDE,(FT)	251695.1	255328.0	295280.0	400000.0
BURNOUT RANGE,(NM)	72.7	75.9	117.8	497.4
IDEAL VELOCITY,(FT/SEC)	13468.3	0.0	1873.0	14991.1

(Handwritten, beside the boxed stage 3 and 4 propellant values: → 467,340 LBS)

INJECTION VELOCITY,(FT/SEC) 302.0 — FLYBACK RANGE(NM) 346.7
INJECTION PROPELLANT,(LB) 4393.7 — FLYBACK PROP(LBS) 148000.0

ON ORBIT DELTA-V,(FT/SEC) 740.0
ON ORBIT PROPELLANT,(LB) 10782.4
ON ORBIT ISP,(SEC) 451.4

(Handwritten: + DEORBIT 2300 + BOILOFF AND CHILLDOWN (10%) 1308 = TOTAL OMS 14390 LBS)

THETA= 21.44 PITCH RATE= 0.00354 ATTEMPTS TO CONVERGE= 3

PAYLOAD,(LB) 95057.9

(Handwritten: − ΔOMS 3608 − MARGIN 8,458 = RNS PAYLOAD 83,000 LBS)

TIME W ALPHA ATTITUDE	VREL VDOT MACH TVC DEFL 2*Q*V	ALT GDT LIFT XCG(IN) AERO HEAT	GAMMA VGRAV RANGE ZCG(IN) Q*ALPHA	QBAR VDRG DRAG PITCH AC(IN) AERO MOM(IN-LB)	LOAD FACTOR THRUST THROTTLE RATIO NORMAL LF AXIAL LF
0.0	0.0	0.0	0.900000E 02	0.0	0.119955E 01
0.397484E 07	0.645824E 01	0.0	0.0	0.0	0.481800E 07
-0.236409E 01	0.0	0.0	0.0	0.500000E 05	0.730000E 00
0.876359E 02	0.236409E 01	0.230379E 04	0.466849E 03	0.294800E 04	0.499996E-01
0.0	0.0	0.0	0.0	0.0	0.119850E 01
0.100000E 02	0.704524E 02	0.342875E 03	0.900001E 02	0.564656E 01	0.123597E 01
0.385413E 07	0.763120E 01	0.117719E-04	0.322165E 03	0.438247E 01	0.482358E 07
-0.245828E 01	0.619922E-01	0.388260E 03	-0.636523E-07	0.599864E 05	0.730000E 00
0.875418E 02	0.244115E 01	0.232002E 04	0.468958E 03	0.294800E 04	0.527400E-01
0.0	0.795627E 03	0.198383E 04	-0.138808E 02	-0.298782E 07	0.123484E 01
0.100000E 02	0.704524E 02	0.342875E 03	0.891228E 02	0.564656E 01	0.123597E 01
0.385413E 07	0.763498E 01	-0.400135E 00	0.322165E 03	0.438247E 01	0.482358E 07
-0.245828E 01	0.619922E-01	0.388260E 03	-0.636523E-07	0.599864E 05	0.730000E 00
0.866645E 02	0.244115E 01	0.232002E 04	0.468958E 03	0.294800E 04	0.527400E-01
0.0	0.795627E 03	0.198383E 04	-0.138808E 02	-0.298782E 07	0.123484E 01
0.200000E 02	0.152763E 03	0.144822E 04	0.864523E 02	0.257493E 02	0.127179E 01
0.373343E 07	0.880490E 01	-0.287675E-01	0.643965E 03	0.107258E 02	0.484122E 07
0.0	0.134972E 00	0.119684E 05	0.990779E-02	0.937030E 05	0.730000E 00
0.864523E 02	0.245794E 01	0.233601E 04	0.471230E 03	0.294800E 04	0.588170E-01
0.0	0.786710E 04	0.367821E 05	0.0	-0.150301E 08	0.127043E 01
0.300000E 02	0.246340E 03	0.343107E 04	0.864401E 02	0.632671E 02	0.130575E 01
0.361272E 07	0.989429E 01	0.364004E-01	0.965423E 03	0.214561E 02	0.487149E 07
0.0	0.219128E 00	-0.294068E 05	0.314375E-01	0.155718E 06	0.730000E 00
0.864401E 02	0.245523E 01	0.235643E 04	0.473653E 03	0.295098E 04	0.659048E-01
0.0	0.311705E 05	0.214310E 06	0.0	-0.315452E 08	0.130409E 01

TIME W ALPHA ATTITUDE	VREL VDOT MACH TVC DEFL 2*Q*V	ALT GDT LIFT XCG(IN) AERO HEAT	GAMMA VGRAV RANGE ZCG(IN) Q*ALPHA	QBAR VDRG DRAG PITCH AC(IN) AERO MOM(IN-LB)	LOAD FACTOR THRUST THROTTLE RATIO NORMAL LF AXIAL LF
0.400000E 02	0.350467E 03	0.640199E 04	0.873780E 02	0.117228E 03	0.134028E 01
0.349202E 07	0.109725E 02	0.160206E 00	0.128694E 04	0.393219E 02	0.491367E 07
0.0	0.314646E 00	0.544883E 05	0.585523E-01	0.236328E 06	0.730000E 00
0.873780E 02	0.240947E 01	0.237866E 04	0.476261E 03	0.296558E 04	0.747599E-01
0.0	0.821692E 05	0.754504E 06	0.0	-0.553677E 08	0.133819E 01
0.500000E 02	0.466260E 03	0.104739E 05	0.898041E 02	0.183087E 03	0.138111E 01
0.337131E 07	0.122473E 02	0.331171E 00	0.160871E 04	0.652973E 02	0.496562E 07
0.0	0.423736E 00	0.850999E 05	0.735297E-01	0.314233E 06	0.730000E 00
0.898041E 02	0.233967E 01	0.240043E 04	0.479088E 03	0.298231E 04	0.853715E-01
0.0	0.170733E 06	0.198603E 07	0.0	-0.837461E 08	0.137847E 01
0.600000E 02	0.596211E 03	0.157746E 05	0.903920E 02	0.253570E 03	0.142494E 01
0.325061E 07	0.136638E 02	-0.256061E 00	0.193045E 04	0.997146E 02	0.502409E 07
-0.450000E 01	0.551201E 00	-0.260645E 06	0.637491E-01	0.401686E 06	0.730000E 00
0.858920E 02	0.406417E 01	0.242169E 04	0.482158E 03	0.299605E 04	0.199096E-01
0.0	0.302363E 06	0.431821E 07	-0.114107E 04	0.122848E 09	0.142480E 01
0.700000E 02	0.740964E 03	0.224409E 05	0.862099E 02	0.317066E 03	0.148040E 01
0.312990E 07	0.154747E 02	-0.457291E 00	0.225183E 04	0.144207E 03	0.508502E 07
-0.473088E 01	0.702909E 00	-0.371562E 06	0.104502E 00	0.466968E 06	0.730000E 00
0.814790E 02	0.465580E 01	0.244238E 04	0.485500E 03	0.300212E 04	0.125849E-02
0.0	0.469869E 06	0.815243E 07	-0.150000E 04	0.177788E 09	0.148040E 01
0.800000E 02	0.905862E 03	0.306088E 05	0.813630E 02	0.362716E 03	0.152653E 01
0.300920E 07	0.173018E 02	-0.526657E 00	0.257123E 04	0.196918E 03	0.514385E 07
-0.413546E 01	0.892362E 00	-0.374799E 06	0.265760E 00	0.562679E 06	0.730000E 00
0.772275E 02	0.452514E 01	0.246243E 04	0.489147E 03	0.300323E 04	-0.284781E-02
0.0	0.657142E 06	0.137910E 08	-0.150000E 04	0.135618E 09	0.152653E 01

TIME W ALPHA ATTITUDE	VREL VDOT MACH TVC DEFL 2*Q*V	ALT GDT LIFT XCG(IN) AERO HEAT	GAMMA VGRAV RANGE ZCG(IN) Q*ALPHA	QBAR VDRG DRAG PITCH AC(IN) AERO MOM(IN-LB)	LOAD FACTOR THRUST THROTTLE RATIO NORMAL LF AXIAL LF
0.900000E 02	0.108602E 04	0.403498E 05	0.754577E 02	0.366835E 03	0.155818E 01
0.288849E 07	0.189341E 02	-0.659370E 00	0.288574E 04	0.267279E 03	0.519557E 07
-0.408903E 01	0.112108E 01	-0.438509E 06	0.616000E 00	0.713803E 06	0.730000E 00
0.713687E 02	0.436141E 01	0.248223E 04	0.493089E 03	0.299268E 04	-0.322598E-01
0.0	0.796780E 06	0.211348E 08	-0.150000E 04	0.870157E 08	0.155784E 01
0.100000E 03	0.130521E 04	0.516636E 05	0.686192E 02	0.322239E 03	0.171361E 01
0.276779E 07	0.251642E 02	-0.705780E 00	0.319073E 04	0.337421E 03	0.523517E 07
-0.465494E 01	0.139167E 01	-0.358595E 06	0.125435E 01	0.508741E 06	0.730000E 00
0.639643E 02	0.423736E 01	0.250943E 04	0.496596E 03	0.297577E 04	-0.429231E-02
0.0	0.841178E 06	0.294062E 08	-0.150000E 04	0.424806E 08	0.171361E 01
0.110000E 03	0.159260E 04	0.647201E 05	0.612718E 02	0.240473E 03	0.188250E 01
0.264708E 07	0.322276E 02	-0.771631E 00	0.348089E 04	0.384395E 03	0.526056E 07
-0.623772E 01	0.167236E 01	-0.377904E 06	0.230699E 01	0.302921E 06	0.730000E 00
0.550341E 02	0.465991E 01	0.253545E 04	0.500570E 03	0.294039E 04	0.709980E-02
0.0	0.765955E 06	0.375173E 08	-0.150000E 04	0.656974E 08	0.188249E 01
0.120000E 03	0.194955E 04	0.795391E 05	0.532244E 02	0.168241E 03	0.203421E 01
0.252638E 07	0.391828E 02	-0.835553E 00	0.374990E 04	0.413797E 03	0.527444E 07
-0.891576E 01	0.199709E 01	-0.405937E 06	0.394195E 01	0.179933E 06	0.730000E 00
0.443086E 02	0.535862E 01	0.256011E 04	0.505076E 03	0.288648E 04	0.143105E-01
0.0	0.655989E 06	0.446358E 08	-0.150000E 04	0.817782E 08	0.203416E 01
0.130000E 03	0.238056E 04	0.958373E 05	0.453913E 02	0.114047E 03	0.218087E 01
0.240567E 07	0.470008E 02	-0.727283E 00	0.399162E 04	0.428822E 03	0.528145E 07
-0.900000E 01	0.239152E 01	-0.254616E 06	0.633999E 01	0.592829E 05	0.730000E 00
0.363913E 02	0.499270E 01	0.258320E 04	0.510199E 03	0.282101E 04	0.826728E-01
0.0	0.542990E 06	0.506352E 08	-0.102642E 04	0.360201E 08	0.217931E 01

TIME W ALPHA ATTITUDE	VREL VDOT MACH TVC DEFL 2*Q*V	ALT GDT LIFT XCG(IN) AERO HEAT	GAMMA VGRAV RANGE ZCG(IN) Q*ALPHA	QBAR VDRG DRAG PITCH AC(IN) AERO MOM(IN-LB)	LOAD FACTOR THRUST THROTTLE RATIO NORMAL LF AXIAL LF
0.140000E 03	0.288820E 04	0.113353E 06	0.386500E 02	0.739855E 02	0.232098E 01
0.228497E 07	0.544662E 02	-0.623511E 00	0.420466E 04	0.431927E 03	0.528483E 07
-0.900000E 01	0.282629E 01	-0.160015E 06	0.964099E 01	-0.536427E 04	0.730000E 00
0.296500E 02	0.513203E 01	0.260512E 04	0.515916E 03	0.273513E 04	0.138088E 00
0.0	0.427370E 06	0.554805E 08	-0.665870E 03	0.128659E 08	0.231687E 01
0.150000E 03	0.346959E 04	0.131814E 06	0.328823E 02	0.469476E 02	0.246470E 01
0.216426E 07	0.618072E 02	-0.531786E 00	0.439036E 04	0.428334E 03	0.528639E 07
-0.900000E 01	0.329861E 01	-0.101866E 06	0.139678E 02	-0.406142E 05	0.730000E 00
0.238823E 02	0.538772E 01	0.263183E 04	0.521208E 03	0.263689E 04	0.185794E 00
0.0	0.325778E 06	0.592304E 08	-0.422528E 03	0.297107E 07	0.245769E 01
0.160000E 03	0.410647E 04	0.150904E 06	0.279837E 02	0.297133E 02	0.248674E 01
0.204615E 07	0.649551E 02	-0.450288E 00	0.455099E 04	0.420415E 03	0.502222E 07
-0.900000E 01	0.380977E 01	-0.664021E 05	0.194257E 02	-0.619632E 05	0.693427E 00
0.189837E 02	0.575162E 01	0.265516E 04	0.527404E 03	0.253057E 04	0.218663E 00
0.0	0.244034E 06	0.620649E 08	-0.267420E 03	0.148558E 07	0.247711E 01
0.170000E 03	0.476697E 04	0.170198E 06	0.238197E 02	0.193573E 02	0.248669E 01
0.193472E 07	0.671009E 02	-0.384924E 00	0.468928E 04	0.409311E 03	0.473514E 07
-0.900000E 01	0.443116E 01	-0.476080E 05	0.260651E 02	-0.734363E 05	0.653748E 00
0.148197E 02	0.616915E 01	0.267416E 04	0.534340E 03	0.245780E 04	0.244647E 00
0.0	0.184551E 06	0.641870E 08	-0.174216E 03	0.304900E 07	0.247462E 01
0.180000E 03	0.544760E 04	0.189277E 06	0.202442E 02	0.126216E 02	0.248664E 01
0.182954E 07	0.689876E 02	-0.331890E 00	0.480783E 04	0.396144E 03	0.446738E 07
-0.900000E 01	0.519986E 01	-0.362402E 05	0.339129E 02	-0.804413E 05	0.616761E 00
0.112442E 02	0.658853E 01	0.269403E 04	0.540810E 03	0.239861E 04	0.267483E 00
0.0	0.137515E 06	0.657918E 08	-0.113594E 03	0.504900E 07	0.247221E 01

TIME W ALPHA ATTITUDE	VREL VDOT MACH TVC DEFL 2*Q*V	ALT GDT LIFT XCG(IN) AERO HEAT	GAMMA VGRAV RANGE ZCG(IN) Q*ALPHA	QBAR VDRG DRAG PITCH AC(IN) AERO MOM(IN-LB)	LOAD FACTOR THRUST THROTTLE RATIO NORMAL LF AXIAL LF
0.190000E 03	0.614593E 04	0.207787E 06	0.171525E 02	0.796304E 01	0.248659E 01
0.173023E 07	0.706476E 02	-0.287624E 00	0.490897E 04	0.381065E 03	0.421548E 07
-0.900000E 01	0.606937E 01	-0.284407E 05	0.429683E 02	-0.858844E 05	0.581974E 00
0.815254E 01	0.703006E 01	0.271194E 04	0.547531E 03	0.233535E 04	0.289718E 00
0.0	0.978806E 05	0.669624E 08	-0.716673E 02	0.758428E 07	0.246966E 01
0.200000E 03	0.685984E 04	0.225438E 06	0.144680E 02	0.485836E 01	0.248655E 01
0.163643E 07	0.721043E 02	-0.250390E 00	0.499479E 04	0.364274E 03	0.397899E 07
-0.900000E 01	0.702063E 01	-0.230895E 05	0.533045E 02	-0.894356E 05	0.549322E 00
0.546799E 01	0.747640E 01	0.272986E 04	0.553935E 03	0.231276E 04	0.310995E 00
0.0	0.666551E 05	0.677781E 08	-0.437252E 02	0.104328E 08	0.246702E 01
0.210000E 03	0.758740E 04	0.241992E 06	0.121265E 02	0.289055E 01	0.248651E 01
0.154782E 07	0.733827E 02	-0.218656E 00	0.506711E 04	0.345946E 03	0.375662E 07
-0.900000E 01	0.803403E 01	-0.197455E 05	0.648713E 02	-0.916588E 05	0.518621E 00
0.312649E 01	0.793661E 01	0.274485E 04	0.560843E 03	0.228869E 04	0.331782E 00
0.0	0.438636E 05	0.683242E 08	-0.260150E 02	0.126755E 08	0.246427E 01
0.216250E 03	0.804832E 04	0.251695E 06	0.108157E 02	0.207808E 01	0.248692E 01
0.149494E 07	0.741144E 02	-0.201016E 00	0.510618E 04	0.333763E 03	0.362495E 07
-0.900000E 01	0.869482E 01	-0.183817E 05	0.727364E 02	-0.925670E 05	0.500443E 00
0.181569E 01	0.824083E 01	0.275113E 04	0.565857E 03	0.227300E 04	0.345101E 00
0.0	0.334502E 05	0.685645E 08	-0.187027E 02	0.138646E 08	0.246286E 01

EXO-ATMOSPHERIC TRAJECTORY

TIME W	V(R) V(I)	GAM(R) GAM(I)	ALT THETA(R)	RANGE	T/W
0.216250E 03 0.686601E 06	0.804832E 04 0.934349E 04	0.108157E 02 0.930203E 01	0.251695E 06 0.214437E 02	0.727364E 02	0.0
0.218750E 03 0.686601E 06	0.803391E 04 0.933105E 04	0.103376E 02 0.888793E 01	0.255328E 06 0.215061E 02	0.759496E 02	0.0
0.218750E 03 0.680001E 06	0.803391E 04 0.933105E 04	0.103376E 02 0.888793E 01	0.255328E 06 0.215061E 02	0.759496E 02	0.185854E 01
0.248168E 03 0.599001E 06	0.973437E 04 0.110424E 05	0.751424E 01 0.661990E 01	0.295280E 06 0.169593E 02	0.117783E 03	0.210986E 01
0.248168E 03 0.599001E 06	0.973437E 04 0.110424E 05	0.751424E 01 0.661990E 01	0.295280E 06 0.169593E 02	0.117783E 03	0.210986E 01
0.288168E 03 0.488865E 06	0.125777E 05 0.138946E 05	0.463374E 01 0.419373E 01	0.341232E 06 0.105513E 02	0.189353E 03	0.258519E 01
0.328168E 03 0.378729E 06	0.162638E 05 0.175857E 05	0.247435E 01 0.228826E 01	0.375340E 06 0.417573E 01	0.281954E 03	0.333697E 01
0.350968E 03 0.315953E 06	0.189160E 05 0.202395E 05	0.147148E 01 0.137525E 01	0.389408E 06 0.713195E 00	0.346579E 03	0.399999E 01
0.390968E 03 0.222964E 06	0.240426E 05 0.253671E 05	0.833535E-01 0.790014E-01	0.399984E 06 -0.477079E 01	0.485333E 03	0.399999E 01
0.394050E 03 0.217054E 06	0.244378E 05 0.257623E 05	-0.785188E-03 -0.744820E-03	0.400000E 06 -0.515492E 01	0.497401E 03	0.399999E 01

1.1.3 LOW Q TRAJECTORY FOR MDAC SS ANALYSIS (4/12/71)

The trajectory represents the lowest aero loading environment (q_{max}) practical for launch of the reusable booster/ESS system with the MDAC space station payload. Preliminary analyses conducted previously indicated that attachment loads at max q would be excessive. Those trajectory analyses reflected "zero alpha" steering and made no attempt at reducing the max q.

A performance analysis was conducted to find a trajectory with low maximum dynamic pressure, negative angle of attack at max q, and would provide performance adequate to launch the MDAC space station. The enclosed trajectory represents the results.

The trajectory was derived assuming liftoff T/W of 1.2 and employed steering designed to force the trajectory nearly vertically until shortly before max q when negative α is introduced as a load-relieving technique, and also to force the trajectory to acceptable staging conditions. Maximum booster throttling of 50 percent is employed at end boost to limit the attachment loads.

Related mass properties for the ESS are:

ESS gross weight: 991,687 lb
X cg: S-II station = 475
Booster station = 2222
Z cg: 450 inches above booster ℄

Radii of gyration:
K_x = 87 inches
K_y = 465 inches
K_z = 465 inches

NOMINAL ASCENT TRAJECTORY FOR LAUNCH OF SPACE STATION

VEHICLE CHARACTERISTICS — CASE 1

STAGE	1	2	3	4	
GROSS STAGE WEIGHT,(LB)	5186522.0	998287.0	991687.0	903187.0	ESS GROSS WEIGHT
GROSS STAGE THRUST/WEIGHT	1.273	0.0	1.274	1.399	
THRUST,(LB)	7243500.0	0.0	1263810.0	1263810.0	
ISP,(SEC)	439.000	2.500	459.000	459.000	
STRUCTURE,(LB)	660335.0	6600.0	7500.0	99320.0	
PROPELLANT,(LB)	3379900.0	0.0	81000.0 +	593685.8	= 674686 LBS
PERF. FRAC.,(NU)	0.6517	0.0	0.0817	0.6573	
PROPELLANT FRAC.,(NUP)	0.8366	0.0	0.9153	0.8567	
BURNOUT TIME,(SEC)	249.664	252.164	281.582	494.898	
BURNOUT VELOCITY,(FT/SEC)	9927.375	9921.828	10932.844	25762.848	
BURNOUT GAMMA,(DEGREES)	4.245	3.860	3.276	-0.000	
BURNOUT ALTITUDE,(FT)	278500.0	280208.0	299168.0	400000.0	
BURNOUT RANGE,(NM)	110.7	114.4	159.8	710.6	
IDEAL VELOCITY,(FT/SEC)	14585.3	0.0	1258.3	15514.8	

INJECTION VELOCITY,(FT/SEC) 302.0 — FLYBACK RANGE(NM) 376.4
INJECTION PROPELLANT,(LB) 6394.4 — FLYBACK PROP(LBS) 148000.0

ON ORBIT DELTA-V,(FT/SEC) 740.0
ON ORBIT PROPELLANT,(LB) 15692.5 + 2375 (DEORBIT) + 1807 (LOSSES) = 19,875 (TOTAL)
ON ORBIT ISP,(SEC) 451.4

THETA= 37.38 PITCH RATE= 0.00427 ATTEMPTS TO CONVERGE= 3

PAYLOAD,(LB) 194488.8 − 4183 (AOMS) − 13346 (MARGIN) = 176960 (MDAC SS)

- 27 -

SD 71-140-12

TIME W ALPHA ATTITUDE	VREL VDOT MACH TVC DEFL 2*Q*V	ALT GDT LIFT XCG(IN) AERO HEAT	GAMMA VGRAV RANGE ZCG(IN) Q*ALPHA	QBAR VDRG DRAG PITCH AC(IN) AERO MOM(IN-LB)	LOAD FACTOR THRUST THROTTLE RATIO NORMAL LF AXIAL LF
0.0	0.0	0.0	0.900000E 02	0.0	0.120130E 01
0.518652E 07	0.647034E 01	0.0	0.0	0.0	0.628056E 07
-0.256019E 01	0.0	0.0	0.0	0.500000E 05	0.951600E 00
0.874398E 02	0.256019E 01	0.217464E 04	0.478176E 03	0.300900E 04	0.540914E-01
0.0	0.0	0.0	0.0	0.0	0.120008E 01
0.100000E 02	0.705925E 02	0.343523E 03	0.900001E 02	0.566894E 01	0.123793E 01
0.502949E 07	0.764991E 01	-0.205487E-04	0.322165E 03	0.339401E 01	0.628785E 07
-0.266614E 01	0.621157E-01	0.300616E 03	-0.541660E-07	0.617066E 05	0.951600E 00
0.873239E 02	0.265488E 01	0.219597E 04	0.480449E 03	0.300900E 04	0.573980E-01
0.0	0.800369E 03	0.100528E 04	-0.151142E 02	-0.230458E 07	0.123660E 01
0.200000E 02	0.152579E 03	0.145199E 04	0.900001E 02	0.258192E 02	0.127430E 01
0.487245E 07	0.882353E 01	0.132620E-05	0.644307E 03	0.855360E 01	0.631090E 07
-0.275239E 01	0.135164E 00	-0.757183E 04	-0.315128E-06	0.101937E 06	0.951600E 00
0.872477E 02	0.280348E 01	0.221699E 04	0.492902E 03	0.300900E 04	0.607930E-01
0.0	0.793557E 04	0.369534E 05	-0.710644E 02	0.403319E 07	0.127235E 01
0.200000E 02	0.152579E 03	0.145199E 04	0.880525E 02	0.258192E 02	0.127430E 01
0.487245E 07	0.884212E 01	-0.409539E 00	0.644307E 03	0.855360E 01	0.631090E 07
-0.275239E 01	0.135164E 00	-0.757183E 04	-0.315128E-06	0.101937E 06	0.951600E 00
0.853001E 02	0.280348E 01	0.221699E 04	0.432902E 03	0.300900E 04	0.607930E-01
0.0	0.793557E 04	0.369534E 05	-0.710644E 02	0.403319E 07	0.127285E 01
0.300000E 02	0.247458E 03	0.344039E 04	0.853631E 02	0.638252E 02	0.130994E 01
0.471542E 07	0.100206E 02	-0.721679E-01	0.965746E 03	0.176641E 02	0.635047E 07
0.0	0.220128E 00	0.295875E 05	0.234663E-01	0.175237E 06	0.951600E 00
0.853631E 02	0.274205E 01	0.223766E 04	0.485554E 03	0.301309E 04	0.704903E-01
0.0	0.315881E 05	0.216166E 06	0.0	-0.306720E 08	0.130804E 01

TIME W ALPHA ATTITUDE	VREL VDOT MACH TVC DEFL 2*Q*V	ALT GDT LIFT XCG(IN) AERO HEAT	GAMMA VGRAV RANGE ZCG(IN) Q*ALPHA	QBAR VDRG DRAG PITCH AC(IN) AERO MOM(IN-LB)	LOAD FACTOR THRUST THROTTLE RATIO NORMAL LF AXIAL LF
0.400000E 02	0.353425E 03	0.642384E 04	0.846516E 02	0.119137E 03	0.134597E 01
0.455838E 07	0.112095E 02	-0.672217E-01	0.128654E 04	0.332890E 02	0.640566E 07
0.0	0.317322E 00	0.533617E 05	0.687087E-01	0.273467E 06	0.951600E 00
0.846516E 02	0.275900E 01	0.225796E 04	0.488424E 03	0.303286E 04	0.793478E-01
0.0	0.842117E 05	0.767120E 06	0.0	-0.523664E 08	0.134363E 01
0.500000E 02	0.472267E 03	0.105195E 05	0.835000E 02	0.187569E 03	0.138652E 01
0.440135E 07	0.126139E 02	-0.167920E 00	0.160677E 04	0.566301E 02	0.647370E 07
-0.666667E 00	0.429254E 00	0.444756E 05	0.141394E 00	0.373484E 06	0.951600E 00
0.828333E 02	0.295473E 01	0.227783E 04	0.491537E 03	0.305561E 04	0.849345E-01
0.0	0.177165E 06	0.203806E 07	-0.125046E 03	-0.428044E 08	0.138392E 01
0.600000E 02	0.606589E 03	0.158529E 05	0.812171E 02	0.261828E 03	0.143186E 01
0.424431E 07	0.142791E 02	-0.289023E 00	0.192573E 04	0.880954E 02	0.655025E 07
-0.133333E 01	0.560549E 00	0.106808E 05	0.264805E 00	0.473696E 06	0.951600E 00
0.798837E 02	0.330911E 01	0.229724E 04	0.494919E 03	0.307325E 04	0.890024E-01
0.0	0.317644E 06	0.447345E 07	-0.349104E 03	-0.600822E 07	0.142909E 01
0.700000E 02	0.758702E 03	0.225488E 05	0.777123E 02	0.331283E 03	0.147861E 01
0.408728E 07	0.161797E 02	-0.411848E 00	0.224193E 04	0.128915E 03	0.662978E 07
-0.200000E 01	0.720067E 00	-0.458585E 05	0.480321E 00	0.585170E 06	0.951600E 00
0.757123E 02	0.383582E 01	0.231614E 04	0.498601E 03	0.308174E 04	0.923021E-01
0.0	0.502691E 06	0.854435E 07	-0.662567E 03	0.604371E 08	0.147573E 01
0.800000E 02	0.928032E 03	0.307031E 05	0.732953E 02	0.379475E 03	0.149193E 01
0.393024E 07	0.172506E 02	-0.480398E 00	0.255305E 04	0.183818E 03	0.670610E 07
-0.200000E 01	0.914622E 00	-0.656110E 05	0.844753E 00	0.840802E 06	0.951600E 00
0.712953E 02	0.397214E 01	0.233848E 04	0.502595E 03	0.308543E 04	0.940466E-01
0.0	0.704330E 06	0.145970E 08	-0.758950E 03	0.497179E 08	0.148896E 01

TIME W ALPHA ATTITUDE	VREL VDOT MACH TVC DEFL 2*Q*V	ALT GDT LIFT XCG(IN) AERO HEAT	GAMMA VGRAV RANGE ZCG(IN) Q*ALPHA	QBAR VDRG DRAG PITCH AC(IN) AERO MOM(IN-LB)	LOAD FACTOR THRUST THROTTLE RATIO NORMAL LF AXIAL LF
0.900000E 02	0.119706E 04	0.402863E 05	0.681463E 02	0.382133E 03	0.153116E 01
0.377321E 07	0.194891E 02	-0.535546E 00	0.285610E 04	0.264899E 03	0.677239E 07
-0.200000E 01	0.114248E 01	-0.527709E 05	0.142050E 01	0.993810E 06	0.951600E 00
0.661463E 02	0.391580E 01	0.236426E 04	0.506943E 03	0.305341E 04	0.990900E-01
0.0	0.846085E 06	0.224099E 08	-0.764265E 03	-0.351215E 07	0.152795E 01
0.100000E 03	0.133141E 04	0.513145E 05	0.626236E 02	0.341054E 03	0.168142E 01
0.361617E 07	0.255388E 02	-0.559002E 00	0.314763E 04	0.341240E 03	0.682314E 07
-0.234567E 01	0.141906E 01	-0.289642E 05	0.228598E 01	0.742289E 06	0.951600E 00
0.602779E 02	0.498507E 01	0.238904E 04	0.511720E 03	0.304304E 04	0.118010E 00
0.0	0.908167E 06	0.312640E 08	-0.800000E 03	-0.147370E 08	0.167728E 01
0.110000E 03	0.162239E 04	0.640157E 05	0.569509E 02	0.259386E 03	0.185139E 01
0.345914E 07	0.327516E 02	-0.577739E 00	0.342443E 04	0.394812E 03	0.685621E 07
-0.308421E 01	0.170694E 01	-0.883708E 05	0.354871E 01	0.450257E 06	0.951600E 00
0.538667E 02	0.460349E 01	0.241268E 04	0.516984E 03	0.300275E 04	0.126566E 00
0.0	0.842170E 06	0.401040E 08	-0.800000E 03	0.316193E 08	0.184706E 01
0.120000E 03	0.198607E 04	0.785519E 05	0.511186E 02	0.183406E 03	0.200944E 01
0.330210E 07	0.397861E 02	-0.586919E 00	0.369333E 04	0.427016E 03	0.687474E 07
-0.436192E 01	0.203728E 01	-0.147893E 06	0.534416E 01	0.239066E 06	0.951600E 00
0.467567E 02	0.509832E 01	0.243502E 04	0.522804E 03	0.294329E 04	0.134846E 00
0.0	0.728511E 06	0.479772E 08	-0.800000E 03	0.681366E 08	0.200491E 01
0.130000E 03	0.240809E 04	0.948691E 05	0.452144E 02	0.122244E 03	0.206037E 01
0.314759E 07	0.435982E 02	-0.596784E 00	0.392131E 04	0.443129E 03	0.657529E 07
-0.654426E 01	0.242257E 01	-0.173040E 06	0.781965E 01	0.958490E 05	0.908881E 00
0.386701E 02	0.548327E 01	0.245942E 04	0.528773E 03	0.287394E 04	0.141530E 00
0.0	0.588750E 06	0.545958E 08	-0.800000E 03	0.767238E 08	0.205550E 01

TIME W ALPHA ATTITUDE	VREL VDOT MACH TVC DEFL 2*Q*V	ALT GDT LIFT XCG(IN) AERO HEAT	GAMMA VGRAV RANGE ZCG(IN) Q*ALPHA	QBAR VDRG DRAG PITCH AC(IN) AERO MOM(IN-LB)	LOAD FACTOR THRUST THROTTLE RATIO NORMAL LF AXIAL LF
0.140000E 03	0.285566E 04	0.112501E 06	0.392706E 02	0.752045E 02	0.206020E 01
0.300199E 07	0.460019E 02	-0.567393E 00	0.413555E 04	0.448751E 03	0.619449E 07
-0.800000E 01	0.279815E 01	-0.136535E 06	0.110964E 02	0.168814E 05	0.855670E 00
0.312706E 02	0.566157E 01	0.248645E 04	0.534485E 03	0.280236E 04	0.157744E 00
0.0	0.429516E 06	0.596741E 08	-0.601636E 03	0.488704E 08	0.205415E 01
0.150000E 03	0.332803E 04	0.130863E 06	0.339389E 02	0.450090E 02	0.206002E 01
0.286453E 07	0.484479E 02	-0.500438E 00	0.432513E 04	0.447566E 03	0.586595E 07
-0.800000E 01	0.316861E 01	-0.848784E 05	0.152498E 02	-0.313094E 05	0.810039E 00
0.259389E 02	0.585694E 01	0.253998E 04	0.540595E 03	0.273074E 04	0.181145E 00
0.0	0.299582E 06	0.632890E 08	-0.360072E 03	0.253986E 08	0.205204E 01
0.160000E 03	0.382404E 04	0.149522E 06	0.292313E 02	0.272353E 02	0.205990E 01
0.273410E 07	0.507254E 02	-0.442410E 00	0.449135E 04	0.442437E 03	0.557219E 07
-0.800000E 01	0.355245E 01	-0.551520E 05	0.203251E 02	-0.577717E 05	0.769367E 00
0.212313E 02	0.614608E 01	0.253024E 04	0.547132E 03	0.265653E 04	0.201197E 00
0.0	0.208298E 06	0.657388E 08	-0.217383E 03	0.158836E 08	0.205005E 01
0.170000E 03	0.434191E 04	0.169084E 06	0.250644E 02	0.173319E 02	0.205984E 01
0.261004E 07	0.529212E 02	-0.392113E 00	0.463590E 04	0.434464E 03	0.530243E 07
-0.800000E 01	0.402739E 01	-0.389262E 05	0.263570E 02	-0.727281E 05	0.732073E 00
0.170644E 02	0.648096E 01	0.254735E 04	0.554116E 03	0.256890E 04	0.218733E 00
0.0	0.150507E 06	0.675671E 08	-0.138656E 03	0.125184E 08	0.204820E 01
0.180000E 03	0.487581E 04	0.186195E 06	0.213665E 02	0.113449E 02	0.205979E 01
0.249185E 07	0.547325E 02	-0.348366E 00	0.476056E 04	0.424818E 03	0.505209E 07
-0.800000E 01	0.463459E 01	-0.301712E 05	0.333717E 02	-0.799398E 05	0.697488E 00
0.133665E 02	0.685864E 01	0.256771E 04	0.560424E 03	0.254462E 04	0.234593E 00
0.0	0.110722E 06	0.688653E 08	-0.907596E 02	0.130024E 08	0.204639E 01

TIME W ALPHA ATTITUDE 	VREL VDOT MACH TVC DEFL 2*Q*V	ALT GDT LIFT XCG(IN) AERO HEAT	GAMMA VGRAV RANGE ZCG(IN) Q*ALPHA	QBAR VDRG DRAG PITCH AC(IN) AERO MOM(IN-LB)	LOAD FACTOR THRUST THROTTLE RATIO NORMAL LF AXIAL LF
0.190000E 03	0.543593E 04	0.203541E 06	0.180791E 02	0.734397E 01	0.205975E 01
0.237917E 07	0.564655E 02	-0.309891E 00	0.486710E 04	0.413860E 03	0.481466E 07
-0.800000E 01	0.532408E 01	-0.243784E 05	0.413893E 02	-0.854711E 05	0.664697E 00
0.100791E 02	0.724890E 01	0.258456E 04	0.567312E 03	0.251704E 04	0.250200E 00
0.0	0.798426E 05	0.698116E 08	-0.587518E 02	0.140076E 08	0.204450E 01
0.200000E 03	0.600852E 04	0.219848E 06	0.151530E 02	0.469943E 01	0.205972E 01
0.227170E 07	0.580287E 02	-0.276007E 00	0.495722E 04	0.401762E 03	0.458985E 07
-0.800000E 01	0.607933E 01	-0.205010E 05	0.504248E 02	-0.890569E 05	0.633656E 00
0.715302E 01	0.765675E 01	0.259776E 04	0.574830E 03	0.248564E 04	0.265720E 00
0.0	0.564733E 05	0.704876E 08	-0.375955E 02	0.151495E 08	0.204251E 01
0.210000E 03	0.659595E 04	0.234880E 06	0.125452E 02	0.299712E 01	0.205970E 01
0.216918E 07	0.594334E 02	-0.246221E 00	0.503254E 04	0.388678E 03	0.437656E 07
-0.800000E 01	0.688285E 01	-0.179468E 05	0.604894E 02	-0.912804E 05	0.604207E 00
0.454518E 01	0.806774E 01	0.260989E 04	0.582389E 03	0.244144E 04	0.280823E 00
0.0	0.395377E 05	0.709629E 08	-0.239770E 02	0.162092E 08	0.204046E 01
0.220000E 03	0.719668E 04	0.248439E 06	0.102166E 02	0.193516E 01	0.205968E 01
0.207136E 07	0.606932E 02	-0.219983E 00	0.509455E 04	0.374708E 03	0.417378E 07
-0.800000E 01	0.772232E 01	-0.163436E 05	0.715920E 02	-0.926533E 05	0.576212E 00
0.221662E 01	0.847730E 01	0.262214E 04	0.589721E 03	0.239527E 04	0.295458E 00
0.0	0.278535E 05	0.712961E 08	-0.154813E 02	0.172022E 08	0.203837E 01
0.230000E 03	0.780934E 04	0.260358E 06	0.813560E 01	0.129105E 01	0.205966E 01
0.197801E 07	0.618207E 02	-0.196706E 00	0.514458E 04	0.359907E 03	0.398076E 07
-0.800000E 01	0.859342E 01	-0.153658E 05	0.837393E 02	-0.934781E 05	0.549563E 00
0.135605E 00	0.889309E 01	0.263213E 04	0.597368E 03	0.234736E 04	0.310001E 00
0.0	0.201645E 05	0.715335E 08	-0.103284E 02	0.181602E 08	0.203620E 01

TIME W ALPHA ATTITUDE	VREL VDOT MACH TVC DEFL 2*Q*V	ALT GDT LIFT XCG(IN) AERO HEAT	GAMMA VGRAV RANGE ZCG(IN) Q*ALPHA	QBAR VDRG DRAG PITCH AC(IN) AERO MOM(IN-LB)	LOAD FACTOR THRUST THROTTLE RATIO NORMAL LF AXIAL LF
0.240000E 03	0.843268E 04	0.270500E 06	0.627363E 01	0.909224E 00	0.205964E 01
0.188891E 07	0.628287E 02	-0.176043E 00	0.518388E 04	0.344301E 03	0.379685E 07
-0.800000E 01	0.949665E 01	-0.147837E 05	0.969369E 02	-0.939636E 05	0.524174E 00
-0.172637E 01	0.930462E 01	0.264182E 04	0.604828E 03	0.229768E 04	0.324168E 00
0.0	0.153344E 05	0.717091E 08	-0.727379E 01	0.190285E 08	0.203397E 01
0.249664E 03	0.904412E 04	0.278509E 06	0.466075E 01	0.674087E 00	0.205969E 01
0.180668E 07	0.637007E 02	-0.158037E 00	0.521270E 04	0.328458E 03	0.362737E 07
-0.800000E 01	0.102310E 02	-0.144202E 05	0.110691E 03	-0.942551E 05	0.500776E 00
-0.333925E 01	0.972072E 01	0.264616E 04	0.613147E 03	0.227700E 04	0.338359E 00
0.0	0.121930E 05	0.718410E 08	-0.539269E 01	0.199565E 08	0.203171E 01

EXO-ATMOSPHERIC TRAJECTORY

TIME / W	V(R) / V(I)	GAM(R) / GAM(I)	ALT / THETA(R)	RANGE	T/W
0.249664E 03	0.904412E 04	0.466075E 01	0.278509E 06	0.110691E 03	0.0
0.998340E 06	0.992739E 04	0.424527E 01	0.373761E 02		
0.252164E 03	0.903803E 04	0.423864E 01	0.280208E 06	0.114350E 03	0.0
0.998340E 06	0.992183E 04	0.386049E 01	0.374430E 02		
0.252164E 03	0.903803E 04	0.423864E 01	0.280208E 06	0.114350E 03	0.127434E 01
0.991740E 06	0.992183E 04	0.386049E 01	0.374430E 02		
0.281582E 03	0.100476E 05	0.356499E 01	0.299168E 06	0.159762E 03	0.138767E 01
0.910740E 06	0.109328E 05	0.327601E 01	0.334415E 02		
0.281582E 03	0.100476E 05	0.356499E 01	0.299168E 06	0.159762E 03	0.139920E 01
0.903240E 06	0.109328E 05	0.327601E 01	0.334415E 02		
0.321582E 03	0.116864E 05	0.294403E 01	0.323584E 06	0.229967E 03	0.159350E 01
0.793104E 06	0.125731E 05	0.273624E 01	0.272098E 02		
0.361582E 03	0.136892E 05	0.243048E 01	0.347248E 06	0.311863E 03	0.185046E 01
0.682968E 06	0.145773E 05	0.228234E 01	0.201358E 02		
0.401582E 03	0.161607E 05	0.186743E 01	0.369568E 06	0.408104E 03	0.220624E 01
0.572833E 06	0.170500E 05	0.177000E 01	0.124812E 02		
0.441582E 03	0.192570E 05	0.116598E 01	0.388272E 06	0.522172E 03	0.273139E 01
0.462697E 06	0.201473E 05	0.111445E 01	0.472712E 01		
0.481582E 03	0.232549E 05	0.312102E 00	0.399152E 06	0.658903E 03	0.358464E 01

0.352561E 06	0.241458E 05	0.300587E 00	-0.250333E 01		
0.494898E 03	0.248718E 05	-0.207446E-04	0.400000E 06	0.710618E 03	0.400069E 01
0.315897E 06	0.257628E 05	-0.200272E-04	-0.468456E 01		

1.1.4 NOMINAL ASCENT TRAJECTORY FOR LAUNCH OF SPACE TUG (4/15/71)

This launch trajectory is to be used for analysis of the space tug payload. As with the RNS and space station trajectories, it is intended to be a low loads trajectory having low q, negative angle of attack at max q, and maximum throttling at end boost. The angle of attack is -2 degrees at max q and max q is 407 psf 84 seconds after lift-off.

Due to the weight and orbit of the payload, the launch system must be either ballasted or off-loaded for this launch. The latter approach is reflected in this trajectory.

The booster propellant tanks were off-loaded by 350,000 pounds and the ESS was loaded with 450,000 pounds of propellant. Throttling was employed at lift-off (16.8 percent) to give a lift T/W = 1.2. A nearly vertical trajectory is followed until shortly before max q when negative angle of attack is introduced as a load-relieving technique in that region and to force the trajectory to acceptable staging conditions. The booster engines are throttled to 50 percent at burnout.

Mass properties of the ESS are:

ESS gross weight (w/o attachment link): 691,523 lb

X cg:	S-II station	443
	Booster station	2254

Z cg: 450 inches above booster ℄

Radii of gyration:

K_x = 71 inches

K_y = 452 inches

K_z = 452 inches

NOMINAL ASCENT TRAJECTORY FOR LAUNCH OF SPACE TUG

VEHICLE CHARACTERISTICS — CASE 3 PAGE 1 OF

STAGE	1	2	3	4	
GROSS STAGE WEIGHT,(LB)	4536358.0	698123.0	691523.0	610523.0	ESS GROSS WEIGHT
GROSS STAGE THRUST/WEIGHT	1.455	0.0	1.828	2.070	
THRUST,(LB)	7243500.0	0.0	1263810.0	1263810.0	
ISP,(SEC)	439.000	2.500	459.000	459.000	
STRUCTURE,(LB)	660335.0	6600.0	0.0	106820.0	
PROPELLANT,(LB)	3029900.0	0.0	81000.0 +	368689.9	= 449,690 LBS
PERF. FRAC.,(NU)	0.6679	0.0	0.1171	0.6039	
PROPELLANT FRAC.,(NUB)	0.8211	0.0	1.0000	0.7754	
BURNOUT TIME,(SEC)	239.484	241.984	271.402	406.736	
BURNOUT VELOCITY,(FT/SEC)	11412.742	11409.020	12927.684	25762.902	
BURNOUT GAMMA,(DEGREES)	2.872	2.555	3.681	0.000	
BURNOUT ALTITUDE,(FT)	251529.0	252848.0	272560.0	400016.0	
BURNOUT RANGE,(NM)	113.7	117.8	169.3	542.7	
IDEAL VELOCITY,(FT/SEC)	15255.5	0.0	1839.6	13375.3	

INJECTION VELOCITY,(FT/SEC)	302.0	FLYBACK RANGE(NM)	349.9
INJECTION PROPELLANT,(LB)	4996.4	FLYBACK PROP(LBS)	148000.0

ORBIT MANEUVERING REQUIREMENTS	RENDEZVOUS	DEORBIT	*LOSSES	TOTALS
DELTA V,(FT/SEC)	130.0	600.0	0.0	730.0
SPECIFIC IMPULSE,(SEC)	451.4	451.4	0.0	0.0
PROPELLANT,(LBS)	2155.0	3796.0	595.1	6546.1

PAYLOAD,(LB) 128466.9 − 10,000 (ADAPTER) − 11,287 (MARGIN) = 107,180 LBS (SPACE TUG)

*LOSSES = 0.0 LBS + 10.0 PERCENT OF USABLE PROPELLANT

TIME W ALPHA ATTITUDE FLOW RATE	VREL VDOT MACH TVC DEFL 2*Q*V	ALT GDT LIFT XCG(IN) AERO HEAT	GAMMA VGRAV RANGE ZCG(IN) Q*ALPHA	QBAR VDRG DRAG PITCH AC(IN) AERO MOM(IN-LB)	LOAD FACTOR THRUST THROTTLE RATIO NORMAL LF AXIAL LF
0.0	0.0	0.0	0.900000E 02	0.0	0.120000E 01
0.453636E 07	0.647785E 01	0.0	0.0	0.0	0.549363E 07
-0.207428E 01	0.0	0.0	0.0	0.500000E 05	0.832368E 00
0.879257E 02	0.207428E 01	0.222666E 04	0.461440E 03	0.309200E 04	0.438331E-01
0.137461E 05	0.0	0.0	0.0	0.0	0.119920E 01
0.100000E 02	0.706935E 02	0.343962E 03	0.900000E 02	0.568510E 01	0.123689E 01
0.439889E 07	0.766580E 01	0.466406E-05	0.322165E 03	0.381826E 01	0.550001E 07
-0.216980E 01	0.622046E-01	0.397373E 03	0.231933E-07	0.590641E 05	0.832368E 00
0.878312E 02	0.215177E 01	0.224609E 04	0.463263E 03	0.309200E 04	0.465274E-01
0.137461E 05	0.803800E 03	0.200327E 04	-0.123298E 02	-0.140687E 07	0.123601E 01
0.200000E 02	0.153381E 03	0.145468E 04	0.900000E 02	0.259534E 02	0.127430E 01
0.426143E 07	0.887279E 01	0.124797E-05	0.644307E 03	0.921503E 01	0.552022E 07
-0.225475E 01	0.135521E 00	-0.567006E 04	0.156014E-06	0.898832E 05	0.832368E 00
0.877452E 02	0.228662E 01	0.226529E 04	0.465233E 03	0.309200E 04	0.495247E-01
0.137461E 05	0.796154E 04	0.371881E 05	-0.585185E 02	0.529231E 07	0.127334E 01
0.200000E 02	0.153381E 03	0.145468E 04	0.883384E 02	0.259534E 02	0.127430E 01
0.426143E 07	0.888630E 01	-0.347960E 00	0.644307E 03	0.921503E 01	0.552022E 07
-0.225475E 01	0.135521E 00	-0.567006E 04	0.156014E-06	0.898832E 05	0.832368E 00
0.860836E 02	0.228662E 01	0.226529E 04	0.465233E 03	0.309200E 04	0.495247E-01
0.137461E 05	0.796154E 04	0.371881E 05	-0.585185E 02	0.529231E 07	0.127334E 01
0.300000E 02	0.248534E 03	0.345112E 04	0.859868E 02	0.643612E 02	0.131187E 01
0.412396E 07	0.101243E 02	-0.749599E-01	0.965918E 03	0.181012E 02	0.555496E 07
0.0	0.221093E 00	0.297242E 05	0.202517E-01	0.146197E 06	0.832368E 00
0.859868E 02	0.219357E 01	0.228425E 04	0.467365E 03	0.309305E 04	0.587649E-01
0.137461E 05	0.319919E 05	0.218311E 06	0.0	-0.255061E 08	0.131056E 01

ATMOSPHERIC TRAJECTORY

TIME W ALPHA ATTITUDE FLOW RATE	VREL VDOT MACH TVC DEFL 2*Q*V	ALT GDT LIFT XCG(IN) AERO HEAT	GAMMA VGRAV RANGE ZCG(IN) Q*ALPHA	QBAR VDRG DRAG PITCH AC(IN) AERO MOM(IN-LB)	LOAD FACTOR THRUST THROTTLE RATIO NORMAL LF AXIAL LF
0.400000E 02	0.355992E 03	0.645449E 04	0.852154E 02	0.120762E 03	0.135100E 01
0.398650E 07	0.114147E 02	-0.773462E-01	0.128699E 04	0.327387E 02	0.560352E 07
0.0	0.319657E 00	0.540953E 05	0.604883E-01	0.220323E 06	0.832368E 00
0.852154E 02	0.217342E 01	0.230294E 04	0.469676E 03	0.309798E 04	0.668768E-01
0.137461E 05	0.859803E 05	0.778835E 06	0.0	-0.458719E 08	0.134935E 01
0.500000E 02	0.477568E 03	0.105915E 05	0.838797E 02	0.191374E 03	0.139597E 01
0.384903E 07	0.129657E 02	-0.196374E 00	0.160748E 04	0.539088E 02	0.566355E 07
-0.666667E 00	0.434168E 00	0.388341E 05	0.128219E 00	0.291875E 06	0.832368E 00
0.832130E 02	0.235938E 01	0.232132E 04	0.472185E 03	0.310371E 04	0.697808E-01
0.137461E 05	0.182789E 06	0.208399E 07	-0.127583E 03	-0.350374E 08	0.139423E 01
0.600000E 02	0.616483E 03	0.160003E 05	0.811766E 02	0.269187E 03	0.144891E 01
0.371157E 07	0.149020E 02	-0.346357E 00	0.192656E 04	0.815339E 02	0.573122E 07
-0.133333E 01	0.570393E 00	-0.508675E 04	0.251146E 00	0.353471E 06	0.832368E 00
0.798433E 02	0.266729E 01	0.233937E 04	0.474913E 03	0.310911E 04	0.682727E-01
0.137461E 05	0.331898E 06	0.461346E 07	-0.358915E 03	-0.650800E 07	0.144730E 01
0.700000E 02	0.777281E 03	0.228224E 05	0.769188E 02	0.344677E 03	0.150907E 01
0.357410E 07	0.173233E 02	-0.505940E 00	0.224234E 04	0.115078E 03	0.580164E 07
-0.200000E 01	0.738564E 00	-0.779975E 05	0.480792E 00	0.407115E 06	0.832368E 00
0.749138E 02	0.308474E 01	0.236459E 04	0.477842E 03	0.311416E 04	0.615665E-01
0.137461E 05	0.535821E 06	0.891059E 07	-0.689354E 03	0.355839E 08	0.150781E 01
0.800000E 02	0.959430E 03	0.311645E 05	0.715914E 02	0.399283E 03	0.152536E 01
0.343664E 07	0.186739E 02	-0.544599E 00	0.255155E 04	0.160160E 03	0.586911E 07
-0.200000E 01	0.947698E 00	-0.644814E 05	0.890110E 00	0.625701E 06	0.832368E 00
0.695914E 02	0.352653E 01	0.238953E 04	0.481045E 03	0.312265E 04	0.799426E-01
0.137461E 05	0.766168E 06	0.154366E 08	-0.798566E 03	0.788422E 08	0.152327E 01

TIME	VREL	ALT	GAMMA	QBAR	LOAD FACTOR
W	VDOT	GDT	VGRAV	VDRG	THRUST
ALPHA	MACH	LIFT	RANGE	DRAG	THROTTLE RATIO
ATTITUDE	TVC DEFL	XCG(IN)	ZCG(IN)	PITCH AC(IN)	NORMAL LF
FLOW RATE	2*Q*V	AERO HEAT	Q*ALPHA	AERO MOM(IN-LB)	AXIAL LF
0.900000E 02	0.114766E 04	0.409716E 05	0.659785E 02	0.399732E 03	0.153849E 01
0.329917E 07	0.202526E 02	-0.583306E 00	0.285080E 04	0.236897E 03	0.592723E 07
-0.200000E 01	0.118785E 01	-0.476165E 05	0.154414E 01	0.850524E 06	0.832368E 00
0.639785E 02	0.362215E 01	0.241383E 04	0.484557E 03	0.312849E 04	0.900802E-01
0.137461E 05	0.917515E 06	0.239521E 08	-0.799465E 03	0.649346E 08	0.153585E 01
0.100000E 03	0.138262E 04	0.521833E 05	0.600486E 02	0.352493E 03	0.170001E 01
0.316171E 07	0.269803E 02	-0.599176E 00	0.313651E 04	0.309546E 03	0.597087E 07
-0.226955E 01	0.147493E 01	-0.800296E 04	0.252178E 01	0.595908E 06	0.832368E 00
0.577791E 02	0.355363E 01	0.243741E 04	0.488420E 03	0.311700E 04	0.107061E 00
0.137461E 05	0.974725E 06	0.335010E 08	-0.800000E 03	0.228754E 08	0.169663E 01
0.110000E 03	0.168896E 04	0.649935E 05	0.539357E 02	0.266560E 03	0.186718E 01
0.302424E 07	0.342625E 02	-0.621631E 00	0.340510E 04	0.358000E 03	0.599867E 07
-0.300120E 01	0.177263E 01	-0.941086E 05	0.394203E 01	0.350874E 06	0.832368E 00
0.509345E 02	0.405884E 01	0.246015E 04	0.492681E 03	0.308601E 04	0.103246E 00
0.137461E 05	0.900419E 06	0.429582E 08	-0.800000E 03	0.665432E 08	0.186432E 01
0.120000E 03	0.206755E 04	0.794764E 05	0.476967E 02	0.189815E 03	0.202195E 01
0.288678E 07	0.414548E 02	-0.623548E 00	0.365298E 04	0.386215E 03	0.601404E 07
-0.421464E 01	0.211815E 01	-0.155818E 06	0.595101E 01	0.178493E 06	0.832368E 00
0.434820E 02	0.446697E 01	0.248339E 04	0.497254E 03	0.304800E 04	0.103882E 00
0.137461E 05	0.784903E 06	0.514017E 08	-0.800000E 03	0.912011E 08	0.201928E 01
0.130000E 03	0.251793E 04	0.954917E 05	0.414900E 02	0.129718E 03	0.216910E 01
0.274931E 07	0.485884E 02	-0.618490E 00	0.387715E 04	0.399496E 03	0.602196E 07
-0.616723E 01	0.253079E 01	-0.180645E 06	0.870484E 01	0.657459E 05	0.832368E 00
0.353227E 02	0.473128E 01	0.251392E 04	0.501512E 03	0.300083E 04	0.112771E 00
0.137461E 05	0.653242E 06	0.586079E 08	-0.800000E 03	0.906820E 08	0.216617E 01

TIME W ALPHA ATTITUDE FLOW RATE	VREL VDOT MACH TVC DEFL 2*Q*V	ALT GDT LIFT XCG(IN) AERO HEAT	GAMMA VGRAV RANGE ZCG(IN) Q*ALPHA	QBAR VDRG DRAG PITCH AC(IN) AERO MOM(IN-LB)	LOAD FACTOR THRUST THROTTLE RATIO NORMAL LF AXIAL LF
0.140000E 03	0.303790E 04	0.112659E 06	0.352755E 02	0.844953E 02	0.230626E 01
0.261185E 07	0.554617E 02	-0.617368E 00	0.407513E 04	0.404345E 03	0.602582E 07
-0.900000E 01	0.297599E 01	-0.181344E 06	0.123638E 02	0.179657E 05	0.832368E 00
0.262755E 02	0.490706E 01	0.254284E 04	0.506412E 03	0.292603E 04	0.127697E 00
0.137461E 05	0.513377E 06	0.644308E 08	-0.760457E 03	0.725330E 08	0.230272E 01
0.150000E 03	0.362961E 04	0.130408E 06	0.295446E 02	0.546038E 02	0.245006E 01
0.247438E 07	0.628701E 02	-0.530247E 00	0.424541E 04	0.403575E 03	0.602761E 07
-0.900000E 01	0.345815E 01	-0.115884E 06	0.170774E 02	-0.256488E 05	0.832368E 00
0.205446E 02	0.498513E 01	0.256988E 04	0.512059E 03	0.284503E 04	0.167047E 00
0.137461E 05	0.396381E 06	0.689559E 08	-0.491434E 03	0.358491E 08	0.244435E 01
0.160000E 03	0.427617E 04	0.148313E 06	0.246488E 02	0.357568E 02	0.246767E 01
0.234008E 07	0.659398E 02	-0.451101E 00	0.438985E 04	0.398320E 03	0.571772E 07
-0.900000E 01	0.397739E 01	-0.762936E 05	0.229510E 02	-0.514689E 05	0.789465E 00
0.156488E 02	0.523349E 01	0.259416E 04	0.518426E 03	0.275780E 04	0.194112E 00
0.130435E 05	0.305804E 06	0.724490E 08	-0.321812E 03	0.187419E 08	0.246002E 01
0.170000E 03	0.494679E 04	0.165914E 06	0.204680E 02	0.243303E 02	0.246761E 01
0.221337E 07	0.681415E 02	-0.387279E 00	0.451130E 04	0.389917E 03	0.539249E 07
-0.900000E 01	0.457927E 01	-0.569246E 05	0.300300E 02	-0.657106E 05	0.744510E 00
0.114680E 02	0.556021E 01	0.262064E 04	0.524278E 03	0.269491E 04	0.215301E 00
0.123078E 05	0.240714E 06	0.751563E 08	-0.218973E 03	0.134558E 08	0.245820E 01
0.180000E 03	0.563808E 04	0.182772E 06	0.168654E 02	0.171671E 02	0.246756E 01
0.209375E 07	0.700806E 02	-0.334722E 00	0.461248E 04	0.379426E 03	0.508978E 07
-0.900000E 01	0.532655E 01	-0.448515E 05	0.383374E 02	-0.742199E 05	0.702694E 00
0.786543E 01	0.592342E 01	0.264488E 04	0.530460E 03	0.261869E 04	0.235258E 00
0.116238E 05	0.193580E 06	0.773218E 08	-0.154504E 03	0.108823E 08	0.245632E 01

TIME W ALPHA ATTITUDE FLOW RATE	VREL VDOT MACH TVC DEFL 2*Q*V	ALT GDT LIFT XCG(IN) AERO HEAT	GAMMA VGRAV RANGE ZCG(IN) Q*ALPHA	QBAR VDRG DRAG PITCH AC(IN) AERO MOM(IN-LB)	LOAD FACTOR THRUST THROTTLE RATIO NORMAL LF AXIAL LF
0.190000E 03	0.634758E 04	0.198515E 06	0.137451E 02	0.121312E 02	0.246753E 01
0.198076E 07	0.717867E 02	-0.290515E 00	0.469578E 04	0.367126E 03	0.480498E 07
-0.900000E 01	0.615835E 01	-0.363920E 05	0.478890E 02	-0.808740E 05	0.663363E 00
0.474511E 01	0.632823E 01	0.266482E 04	0.537383E 03	0.254505E 04	0.255626E 00
0.109805E 05	0.154008E 06	0.790535E 08	-0.109181E 03	0.102655E 08	0.245425E 01
0.200000E 03	0.707308E 04	0.212843E 06	0.110325E 02	0.864064E 01	0.246749E 01
0.187399E 07	0.732838E 02	-0.253082E 00	0.476338E 04	0.353250E 03	0.453787E 07
-0.900000E 01	0.705556E 01	-0.303407E 05	0.586955E 02	-0.849865E 05	0.626482E 00
0.203246E 01	0.675519E 01	0.268310E 04	0.544456E 03	0.251701E 04	0.275938E 00
0.103773E 05	0.122232E 06	0.804284E 08	-0.777658E 02	0.108631E 08	0.245201E 01
0.210000E 03	0.781261E 04	0.225511E 06	0.866437E 01	0.628233E 01	0.246746E 01
0.177309E 07	0.745963E 02	-0.221279E 00	0.481720E 04	0.337984E 03	0.428642E 07
-0.900000E 01	0.799693E 01	-0.262340E 05	0.707645E 02	-0.877465E 05	0.591765E 00
-0.335630E 00	0.718265E 01	0.270225E 04	0.551109E 03	0.248760E 04	0.295394E 00
0.980931E 04	0.981627E 05	0.815244E 08	-0.565409E 02	0.116214E 08	0.244971E 01
0.220000E 03	0.856444E 04	0.236324E 06	0.659233E 01	0.474262E 01	0.246743E 01
0.167769E 07	0.757471E 02	-0.193834E 00	0.485890E 04	0.321432E 03	0.404946E 07
-0.900000E 01	0.896354E 01	-0.235434E 05	0.841017E 02	-0.895389E 05	0.559050E 00
-0.240767E 01	0.762687E 01	0.271885E 04	0.558132E 03	0.245739E 04	0.314839E 00
0.927385E 04	0.812358E 05	0.824159E 08	-0.426836E 02	0.124864E 08	0.244726E 01
0.230000E 03	0.932704E 04	0.245131E 06	0.477519E 01	0.378661E 01	0.246740E 01
0.158750E 07	0.767552E 02	-0.170068E 00	0.488996E 04	0.303657E 03	0.382597E 07
-0.900000E 01	0.994013E 01	-0.218720E 05	0.987114E 02	-0.906511E 05	0.528194E 00
-0.422481E 01	0.807055E 01	0.273540E 04	0.564897E 03	0.242687E 04	0.333678E 00
0.876853E 04	0.706358E 05	0.831705E 08	-0.340795E 02	0.132645E 08	0.244474E 01

ATMOSPHERIC TRAJECTORY CASE 3 PAGE 7 OF 8

TIME	VREL	ALT	GAMMA	QBAR	LOAD FACTOR
W	VDOT	GDT	VGRAV	VDRG	THRUST
ALPHA	MACH	LIFT	RANGE	DRAG	THROTTLE RATIO
ATTITUDE	TVC DEFL	XCG(IN)	ZCG(IN)	PITCH AC(IN)	NORMAL LF
FLOW RATE	2*Q*V	AERO HEAT	Q*ALPHA	AERO MOM(IN-LB)	AXIAL LF
0.239484E 03	0.100590E 05	0.251529E 06	0.325905E 01	0.327161E 01	0.246751E 01
0.150651E 07	0.775989E 02	-0.150025E 00	0.491078E 04	0.285705E 03	0.362588E 07
-0.900000E 01	0.108633E 02	-0.209423E 05	0.113741E 03	-0.912203E 05	0.500571E 00
-0.574095E 01	0.852754E 01	0.274550E 04	0.572583E 03	0.242500E 04	0.352635E 00
0.831584E 04	0.658185E 05	0.838138E 08	-0.294445E 02	0.142519E 08	0.244218E 01

EXO-ATMOSPHERIC TRAJECTORY

TIME W	V(R) V(I)	GAM(R) GAM(I)	ALT THETA(R)	RANGE	T/W
0.239484E 03	0.100590E 05	0.325905E 01	0.251529E 06	0.113741E 03	0.0
0.698174E 06	0.114127E 05	0.287214E 01	0.381393E 02		
0.241984E 03	0.100548E 05	0.289926E 01	0.252848E 06	0.117824E 03	0.0
0.698174E 06	0.114090E 05	0.255488E 01	0.382165E 02		
0.241984E 03	0.100548E 05	0.289926E 01	0.252848E 06	0.117824E 03	0.182744E 01
0.691574E 06	0.114090E 05	0.255488E 01	0.382165E 02		
0.271402E 03	0.115738E 05	0.411190E 01	0.272560E 06	0.169307E 03	0.206987E 01
0.610574E 06	0.129277E 05	0.368066E 01	0.307509E 02		
0.271402E 03	0.115738E 05	0.411190E 01	0.272560E 06	0.169307E 03	0.206987E 01
0.610574E 06	0.129277E 05	0.368066E 01	0.307509E 02		
0.311402E 03	0.142316E 05	0.470261E 01	0.313168E 06	0.252402E 03	0.252541E 01
0.500438E 06	0.155871E 05	0.429288E 01	0.181494E 02		
0.351402E 03	0.177781E 05	0.372445E 01	0.361296E 06	0.355240E 03	0.323803E 01
0.390302E 06	0.191381E 05	0.345945E 01	0.368394E 01		
0.378405E 03	0.208443E 05	0.214244E 01	0.388224E 06	0.439195E 03	0.399999E 01
0.315953E 06	0.222078E 05	0.201084E 01	-0.593374E 01		
0.406736E 03	0.243977E 05	0.325273E-03	0.400016E 06	0.542706E 03	0.399999E 01
0.246830E 06	0.257629E 05	0.308037E-03	-0.148668E 02		

1.2 COMBINED SYSTEM HEATING RATES

This section presents the local heating rates on the ESS during ascent when used as an expendable second stage with the following three payload configurations:

Reusable nuclear stage (ESS/RNS)

McDonnell Douglas space station (ESS/MDAC)

North American Rockwell space tug (ESS/space tug)

It is assumed that the heating rates on the B9U booster are identical to those computed on the ESS at the same station.

The effect of a fairing shroud around the separation mechanism, and of the trajectory on the local heating rates has been analyzed; the results are presented herein.

When the ESS is used in connection with a GDC/ B9U booster, larger and heavier payloads can be put into orbit than with the present shuttle/B9U system. However, the mated configuration of the ESS in the presence of the booster presents thermal problems that did not exist when the S-II was used as the second stage of the Saturn V. For instance, the flow field between the two mated vehicles will generate a complex pattern of shock waves that could create serious damage to the vehicle if the thermal protection system (TPS) is not locally reinforced when compared with the original S-II design. The present analysis provides the local heating rates on the S-II and on the B9U in mated configuration for three different payloads. The results will permit beef-up of the local regions affected by the presence of the main booster.

1.2.1 VEHICLE CONFIGURATIONS, TRAJECTORY, AND FLOW REGIMES

The three payloads to be considered in the study (RNS, Space Station, Space Tug) are presented in Figure 1. (The existing protuberances and fitting attachment are not shown here.)

The launch trajectory used for the thermal environment (2/15/71 trajectory) is shown in Figure 2. The flight angle of attack varies slowly between $0 \leq \mathring{\alpha} \leq -2$. By analogy with the analysis performed on the shuttle/booster configuration, it is assumed that the flow is turbulent at t = 0 (takeoff) and becomes laminar at higher altitude. Transition is reached when, at a given location, the Reynolds number based on the momentum thickness is 150 times the local Mach number or

$$\frac{R_{e}\theta}{M_{e}} = 150$$

This relationship points out that, as the flight time increases, the transition location moves forward on the ESS. However, in the present analysis, it was assumed that the flow on the ESS remains fully turbulent as long as the transition point is still located on the vehicle. However, this traveling time of transition along the second stage is rather short and occurs at an altitude when local film coefficients have already dropped by more than two orders of magnitude when compared with the peak heating value. As a consequence, the effect of this traveling on the wall temperature will be negligible.

The present calculations have been performed using the 2/15/71 trajectory. Shortly after the effort had started, a second trajectory (3/1/71 trajectory) was computed. Both trajectories are presented on Figure 2. The influence of the trajectory on the local heating rates has been analyzed for a typical case; the results will be presented later in this section.

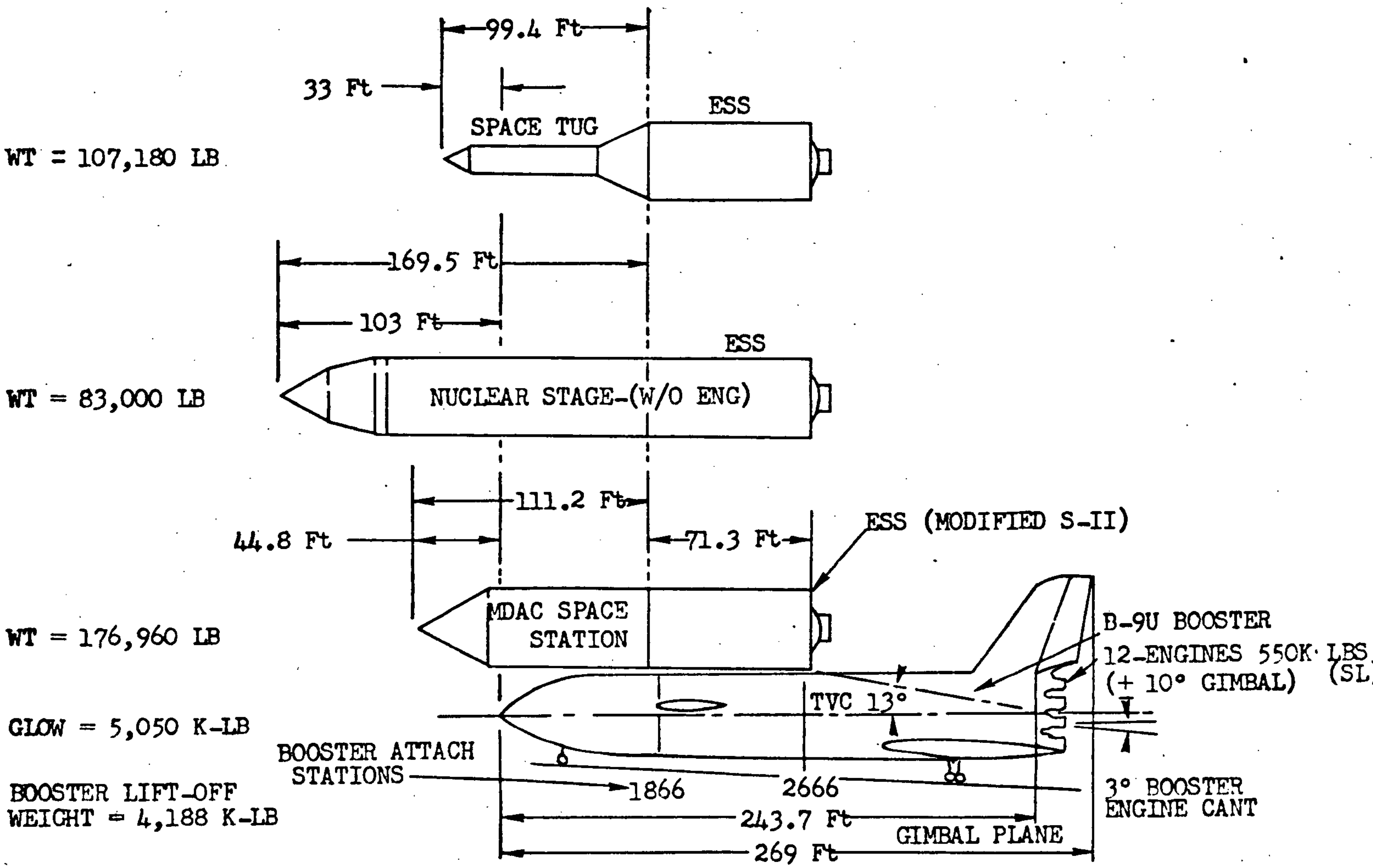

Figure 1. Booster/ESS Configuration with Specified Payloads

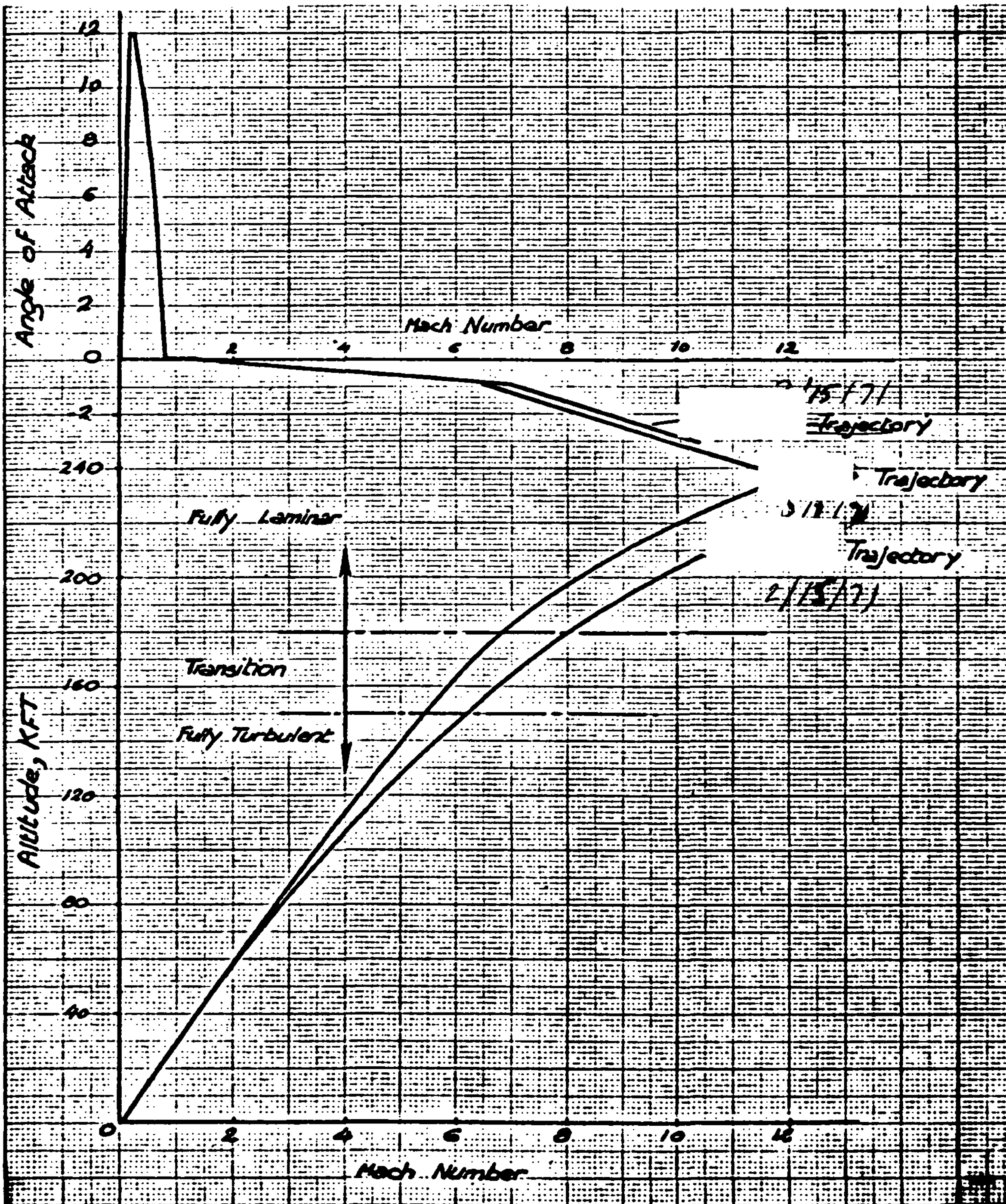

Figure 2. Trajectory Comparison

1.2.2 DETERMINATION OF THE LOCAL HEATING RATES

The determination of the local aerodynamic heating rates on the three payloads is not part of the present analysis. However, the influence of each payload on the ESS (protuberances) or on the booster (shock interaction, shock impingement) is of significant interest and has been investigated. In all analyses, it was assumed that the flight angle of attack was equal to zero. The results must not be extrapolated to cases where significant flight angle of attack ($|\alpha|>5$ deg) exists. The present experimental results showing no influence between $\alpha^o = 0$ and $\alpha^o = -5$.

a. Payload/ESS Stage Alone

The present analysis deals with the complete second-stage independent of the booster effect. The local heating rates have been computed on the ESS (no protuberance) at three longitudinal locations and a linear interpolation is used for other intermediate stations. The reference conditions corresponding to the 2/15/71 trajectory have been obtained using the PATRICK 63 atmosphere. The present heating rates do not account for any separated flow region exhaust gas heating. The film coefficient and the recovery temperature have been selected to represent the local aerodynamic heating. These heat transfer coefficients have been determined for calorically and thermally perfect gas ($\gamma = 1.4$). These assumptions are compatible with the flight Mach numbers encountered during the launch phase. No correction due to vorticity interactions have been applied. The heat transfer rates calculations have been performed assuming $T_W = 540$ degrees and using the following relationship:

$$\dot{q} = h_c\left(T_r - T_w\right)$$

For other wall temperatures, following NASA/MSFC practice, it is assumed that the film coefficient, h_c, remains unchanged with T_{wall}.

The protuberances on the ESS and the associated protuberance-influenced regions are shown on Figure 3. It should be noted that the attachment struts are included as integral part of the ESS. The heating rates on these protuberances and on the protuberance-influenced regions are computed following the relationship:

$$\dot{q} = (PF)\, h_c\left(T_r - T_w\right)$$

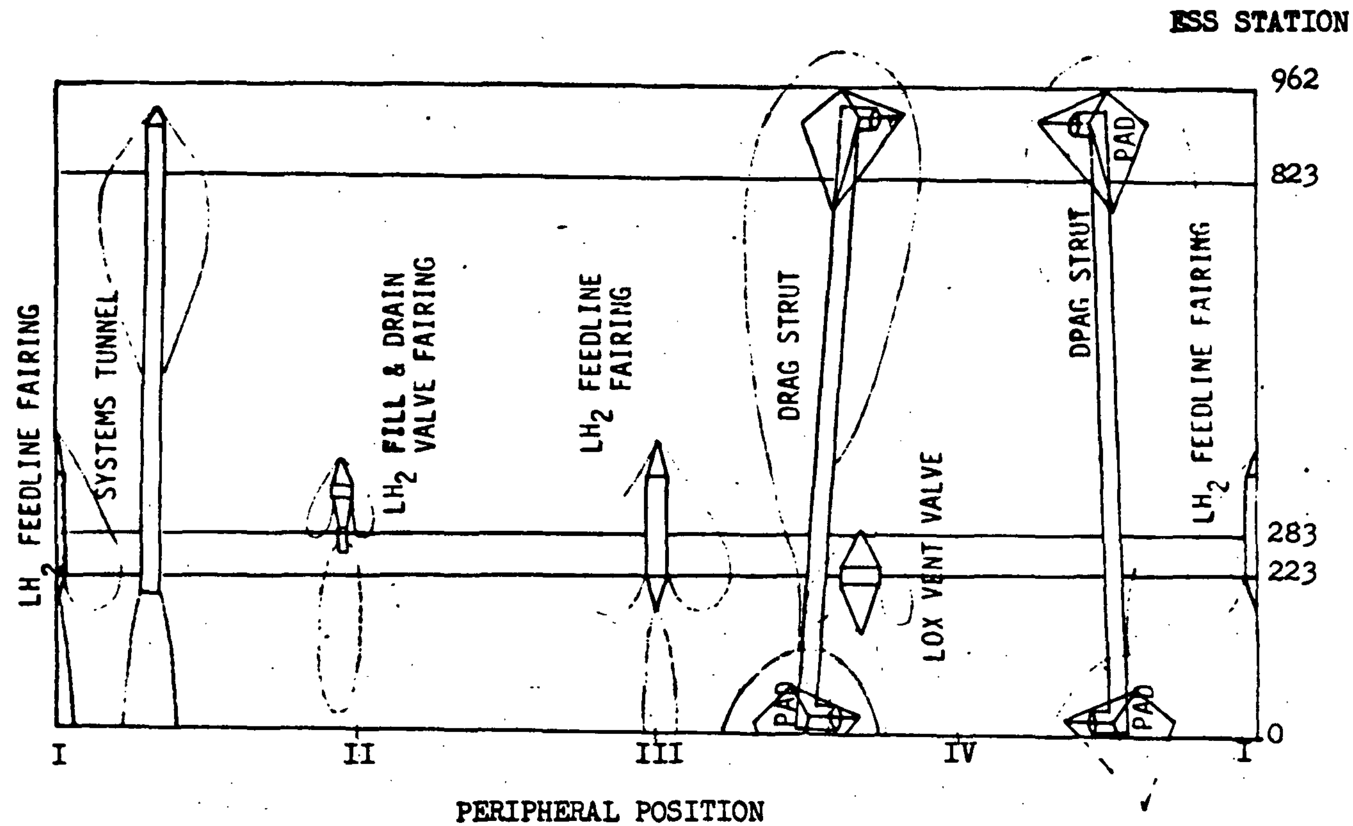

Figure 3. ESS Protuberance and Protuberance Influenced Regions

where PF is a protuberance factor. Where protuberance regions overlap, the product of the individual protuberance factors is used.

Large protuberances exist for the MDAC space station, and their influence on the ESS has already been included in the basic sidewall heating rates calculations.

b. <u>ESS/B9U Interference Heating, Including Mated Effects</u>

The influence of mated configuration has been incorporated to the ESS-alone results. This assumes that the effect of the booster can simply be included as a new protuberance factor that will be added to the base sidewall configuration.

The analysis of the booster interference has been derived from NR wind tunnel test (References 1 and 2) and other sources theoretical and experimental data (References 5 through 9).

E

1.2.3 DESCRIPTION OF SPACE SHUTTLE LAUNCH HEATING TESTS

Interference heating factors for the mated ESS/booster combination were based on the following two launch heating tests run as part of the NR Phase B Space Shuttle Program.

1. NASA/ARC 3.5-Foot HWT Test 107 (Reference 1), Conducted During the Period September 28, 1970 through October 9, 1970

   The 0.006-scale, thin-skin models of the NR 9992-134B delta wing orbiter, the NR 9992-130C straight wing orbiter (modified to the 9992-130G wing position) and the GD/Convair 7620-010 straight wing booster were used for these tests. The models were instrumented with iron-constantan thermocouples.

   Heat transfer data were obtained at a nominal Mach number of 7.4, a nominal total temperature of 1400 degrees R and nominal Reynolds numbers of 0.7×10^6 and 3.5×10^6 per foot. Angles of attack of zero degrees and -5 degrees were investigated.

   Mating of the two vehicles was accomplished by sting-mounting the orbiter to the booster sting, which was in turn mounted to the wind tunnel model support system. The actual mounting attachments between the two vehicles were not simulated. The gap between the orbiter and booster was completely open as shown in Figure 4. Longitudinal positions of the orbiter with respect to the booster were obtained by sliding the orbiter sting fore and aft, while lateral positions were obtained by shimming the orbiter sting support. Longitudinal positions tested ranged from orbiter nose 550 inches, full-scale, ahead of the booster nose, to orbiter nose 167 inches, full-scale, behind the booster nose. Minimum gaps between the orbiter and booster ranged from 3.3 inches to 24 inches full-scale.

   A typical shadowgraph taken during this test showing the interference shock pattern between the mated vehicles is presented in Figure 5.

2. NASA/LRC UPWT Test 945 (Reference 2), Conducted During the Period from January 13 through January 22, 1971

   The models used for these investigations were 0.006-scale, thin skin thermocouple models of the NR 9992-134B delta wing orbiter and the GD/Convair WT-70-105610 delta wing booster.

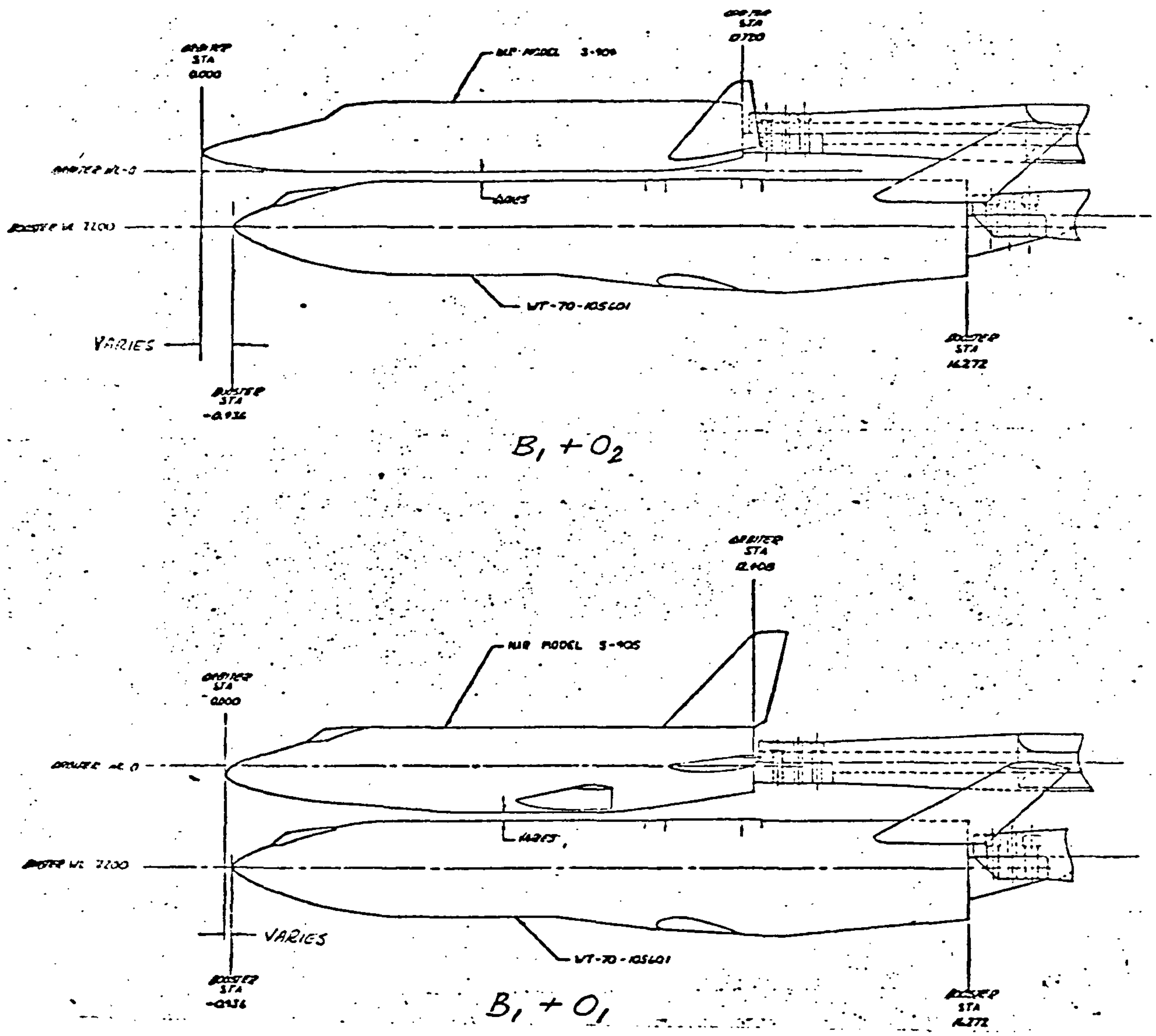

Figure 4. Wind Tunnel Mated Configuration Sting Mounting System

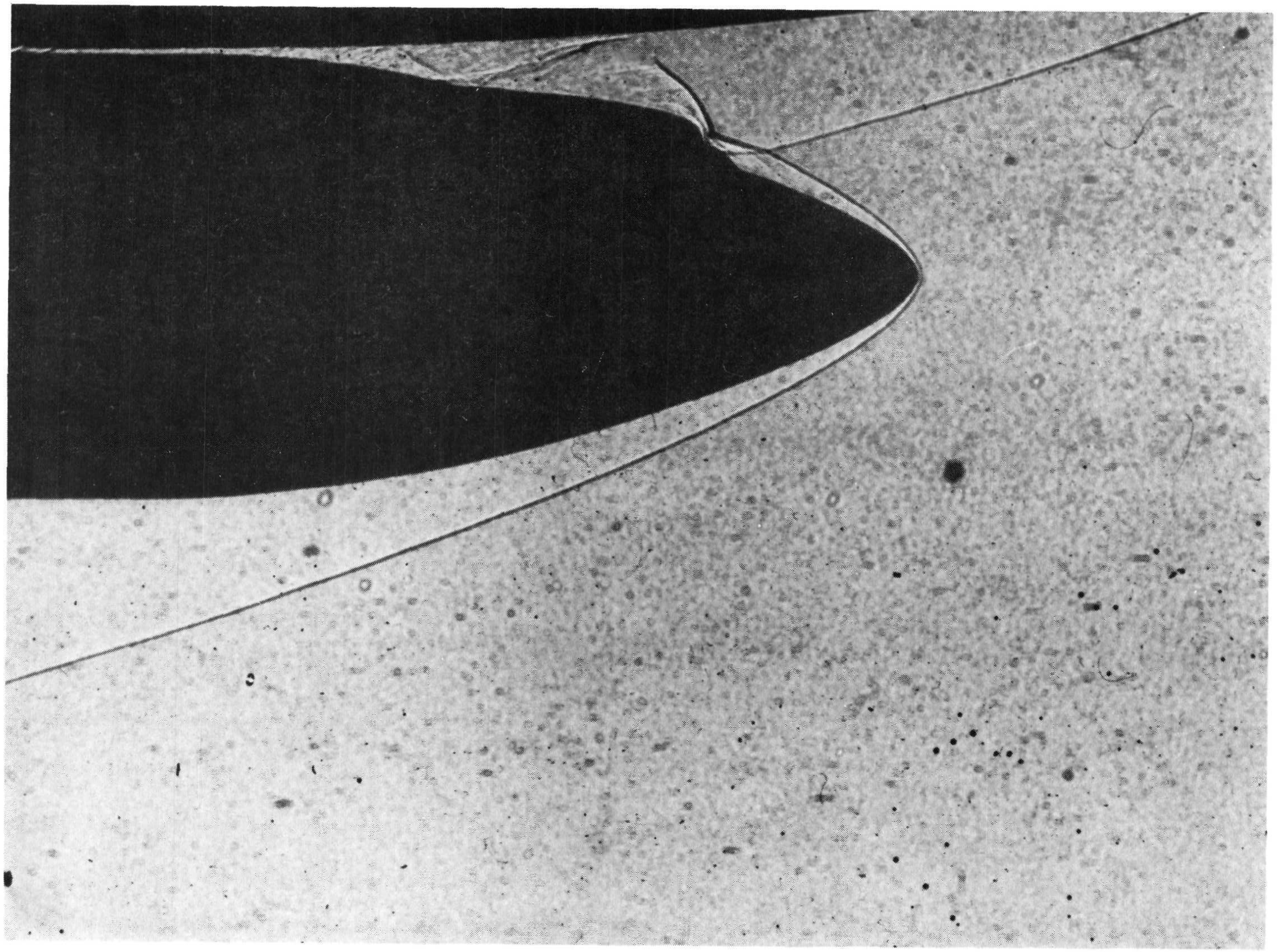

Figure 5. Flow Visualization of Mated Orbiter/Booster Shock Wave Interactions
at M = 7.4, = 0°, Re/Ft = 3.5 X 10^6
NASA/ARC 3.5-Ft. HWT Test 107
Orbiter Nose 467 in. (Full Scale) Ahead of Booster Nose
Minimum Gap = 3.3 in. (Full Scale)

Heat transfer data were obtained at supersonic Mach numbers of 2.5 and 3.7, and at Reynolds numbers of 2.5×10^6 and 5×10^6 per foot. Angles of attack of zero degrees and -5 degrees were investigated.

Mounting of the mated models in the wind tunnel was identical with that of the NASA/ARC test. Data were obtained at orbiter nose longitudinal positions of zero, 223, and 417 inches, full-scale, ahead of the booster nose. Minimum vertical gaps between the orbiter and booster were 3.3 and 23 inches, full-scale.

A typical shadowgraph obtained during this test is presented in Figure 6, illustrating the complex shock interference patterns between the mated vehicles.

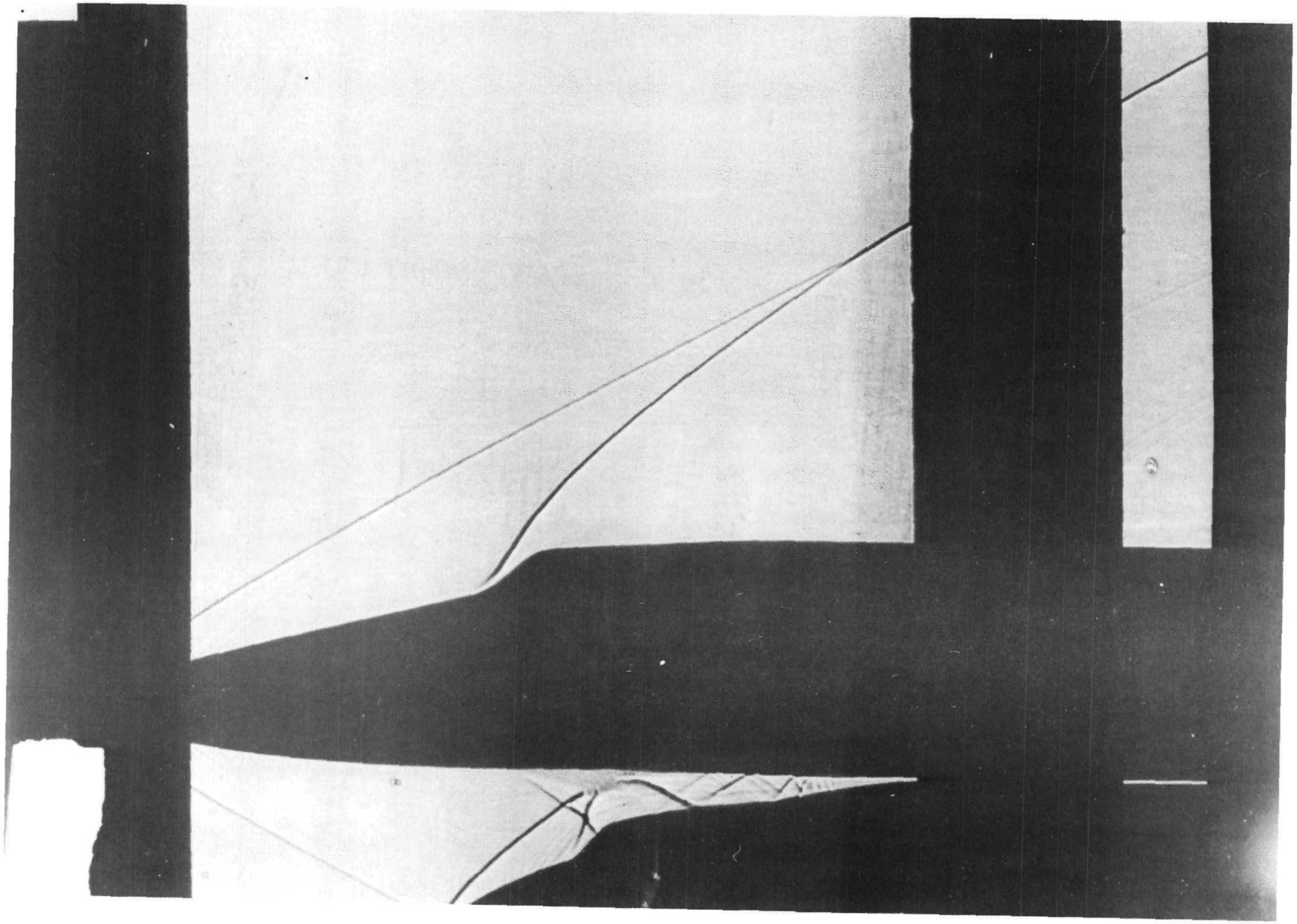

Figure 6. Flow Visualization of Mated Orbiter/Booster Shock Wave Interactions at $M = 3.7$, $\alpha = 0°$, $Re/Ft = 3 \times 10^6$
NASA/LRC UPTW Test 945
Orbiter Nose 417 in. (Full Scale) Ahead of Booster Nose
Minimum Gap = 3.3 in. (Full Scale)

1.2.4 TEST DATA ANALYSIS

A search of existing literature dealing with shock interference heating was made (References 3 through 9). Based on these, it was concluded that the interference heating problem is formidable where geometric characteristics are strongly coupled with the aerodynamic parameters and requires experimental programs on specific configurations in order to make accurate predictions. Many empirical relations have been developed, based on experimental investigations, relating the heating rise to the pressure rise across the shock interaction. The simplest equations are usually of the form:

$$\frac{\dot{q}_2}{\dot{q}_1} = \left(\frac{p_2}{p_1}\right)^{1-n}$$

where n is about 0.5 for laminar flow and about 0.2 for turbulent flow (e.g., Reference 3). Even though the relationship appears simple, it gives reasonable results when the two geometric configurations to be investigated are similar to those where existing experimental data at different aerodynamic conditions already exist.

Model Configuration

For the present study, predictions of interference heating on a body (ESS) in close proximity to another body (GDC B9U booster) is required. In lieu of a wind tunnel program using these specific configurations, the Phase B Space Shuttle wind tunnel tests previously described would provide the best available means of estimating the interference heating to the ESS. It must be pointed out that at the start of this study, no experimental pressure data similar to those made for the heat transfer study existed. For instance, the influence of the geometric (gap and stagger distance) and aerodynamic conditions on the pressure rise was not investigated, so that a direct heat rate-pressure relationship as that presented above is not available from this preliminary set of data. Instead of it, the flight Reynolds numbers (valid for both interaction and clean configurations) are used to correlate the data and extend them to the actual flight conditions. The cross-sectional shapes at the ESS location of the space shuttle vehicles used in the launch heating tests are compared with the ESS/B9U configuration in Figure 7. On this figure, only one gap distance is shown, but this parameter was variable during the test. The NR straight wing orbiter was chosen as being most representative, considering that the present booster (7620-010)/shuttle configuration is almost identical to the ESS/booster B9U geometry. Analysis was, therefore, concentrated on the data obtained with the NR straight wing orbiter as well as on the GDC booster. Test data analysis was also restricted to the vehicle's lower centerline due to shape

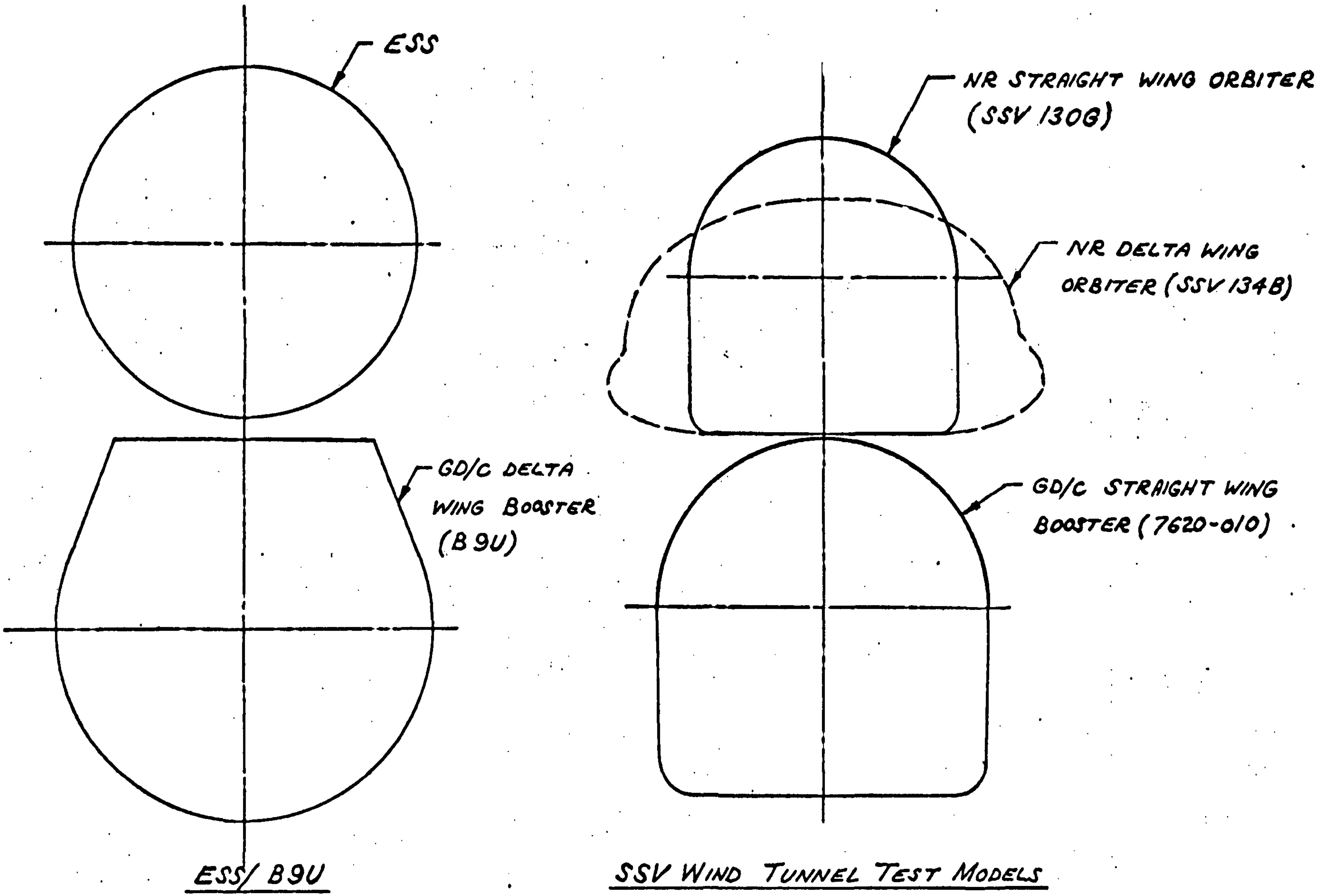

Figure 7. Comparison of Cross-Sectional Shapes

differences and limited instrumentation of the models in that area making any rigorous survey outside the pitch plane rather difficult. A cosine law decay in interference heating was assumed on the cylindrical portion from the lower centerline (θ = 0 degrees) to the side centerline (θ = 90 degrees) of the ESS.

Influence of the Reynolds Number

Typical mated orbiter/booster and orbiter-alone experimental heating distributions are presented in Figure 8. Ratioing the local heat transfer rate to the theoretical stagnation heating rate of a scaled one-foot-radius sphere emphasizes the influence of Reynolds number on interference heating. The relative locations of the ESS and the payload are also indicated in Figure 8. It is immediately apparent that the shock pattern due to mated configuration rapidly decays along the axis as previously shown in the literature (see References 4, 5, 6, and 9). As a result, the payload experiences much higher interference heating than the ESS.

The shadowgraphs of Figures 5 and 6 clearly show the axial damping of the shock wave interaction effects which results in a rapid decrease in interference heating to the level of the orbiter-alone as the gap between the two vehicles decreases to a minimum. The shadowgraphs also indicate the complexity of the flow phenomena occurring in the shock interaction region. However, in the present series of tests, no solid connections (struts, attachments) exist between the two vehicles. When such fittings exist, the local supersonic regions (where they exist) could regenerate a new shock network system that would significantly increase the heat transfer rates shown here.

Influence of Gap and Stagger Distances

Figure 9 shows the effect of vertical separation of the interference heating along the lower centerline of the orbiter. A decrease in interference heating with increasing gap is indicated on the payload. In the area corresponding to the ESS location, no significant change in heating is shown as the minimum gap is varied between 3.3 and 24 inches, full-scale. This "pattern"-type result is very important and should be investigated in order to understand the influence of the scaling effect for the next phase of the investigation. The influence of the stagger was also investigated but the results show no variation at the ESS location.

Influence of Angle of Attack

The effect of angle of attack on lower surface centerline interference heating is presented in Figure 10. A small decrease is shown in the payload area over an angle of attack range of zero degrees to -5 degrees.

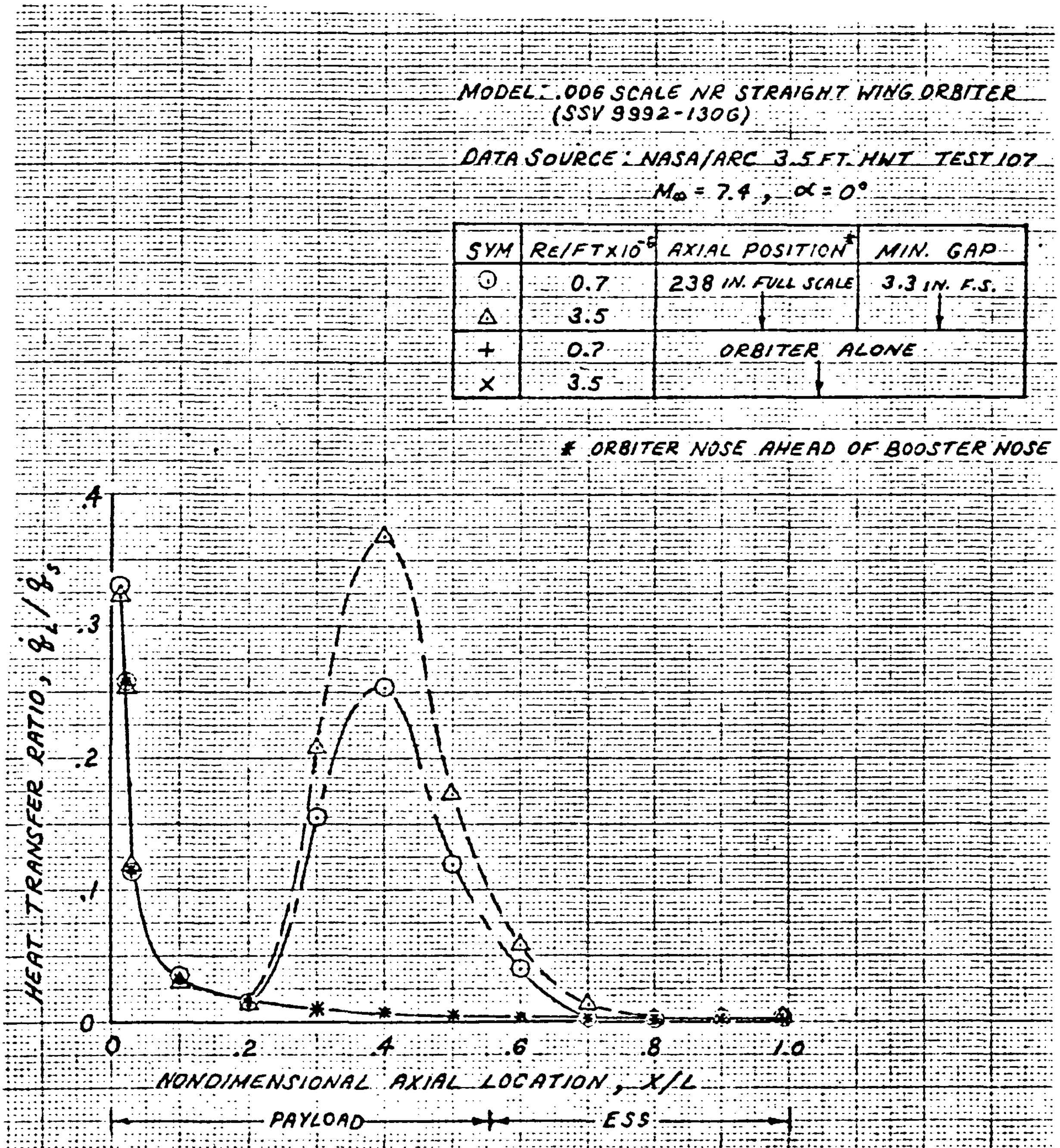

Figure 8. Typical Heating Distributions on the NR Straight Wing Orbiter Fuselage Lower Centerline, Effect of Reynolds Number on Mated Interference Heating

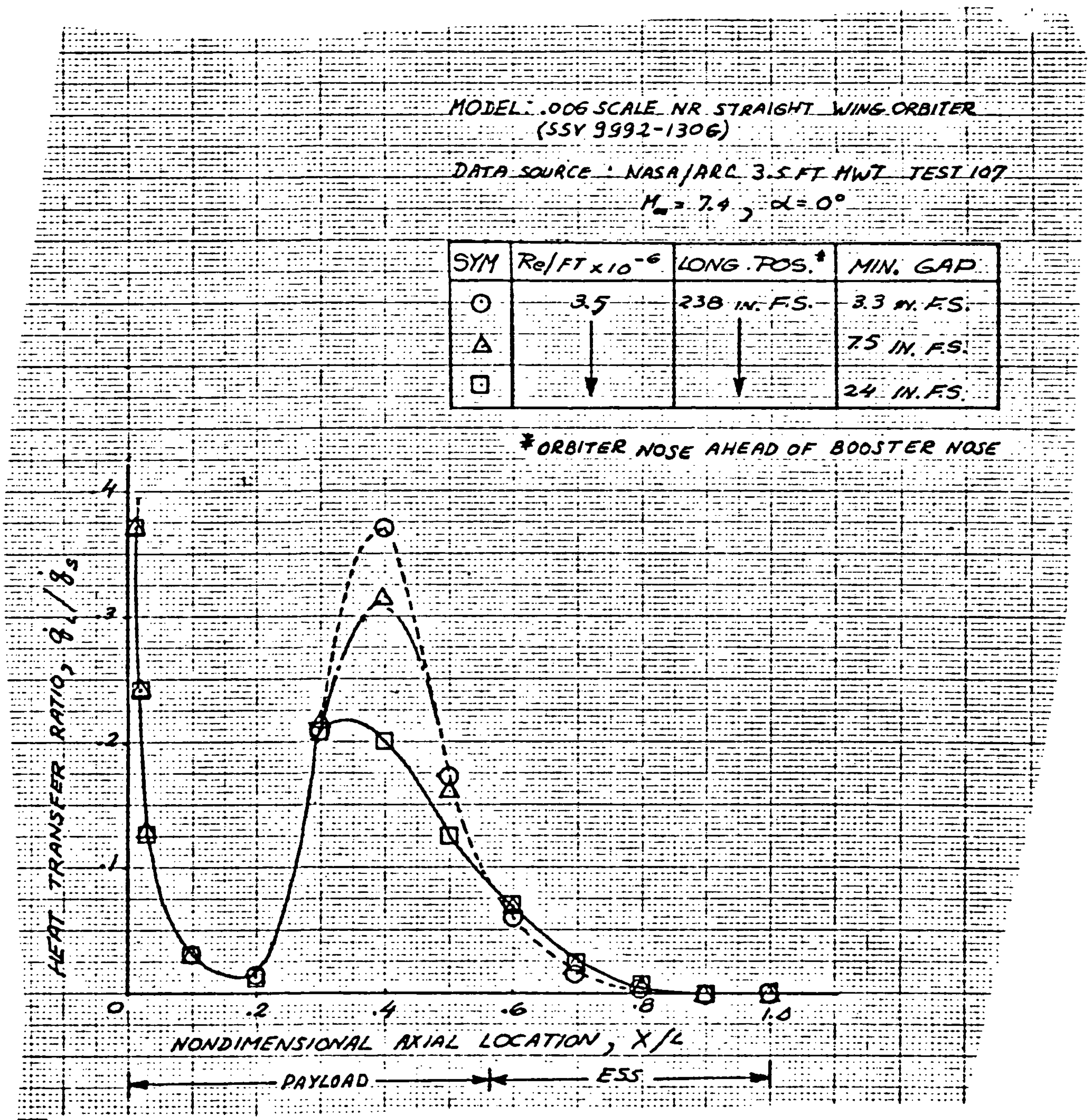

Figure 9. Effect of Gap Distance on Mated Interference Heating, NR Straight Wing Orbiter Fuselage Lower Centerline

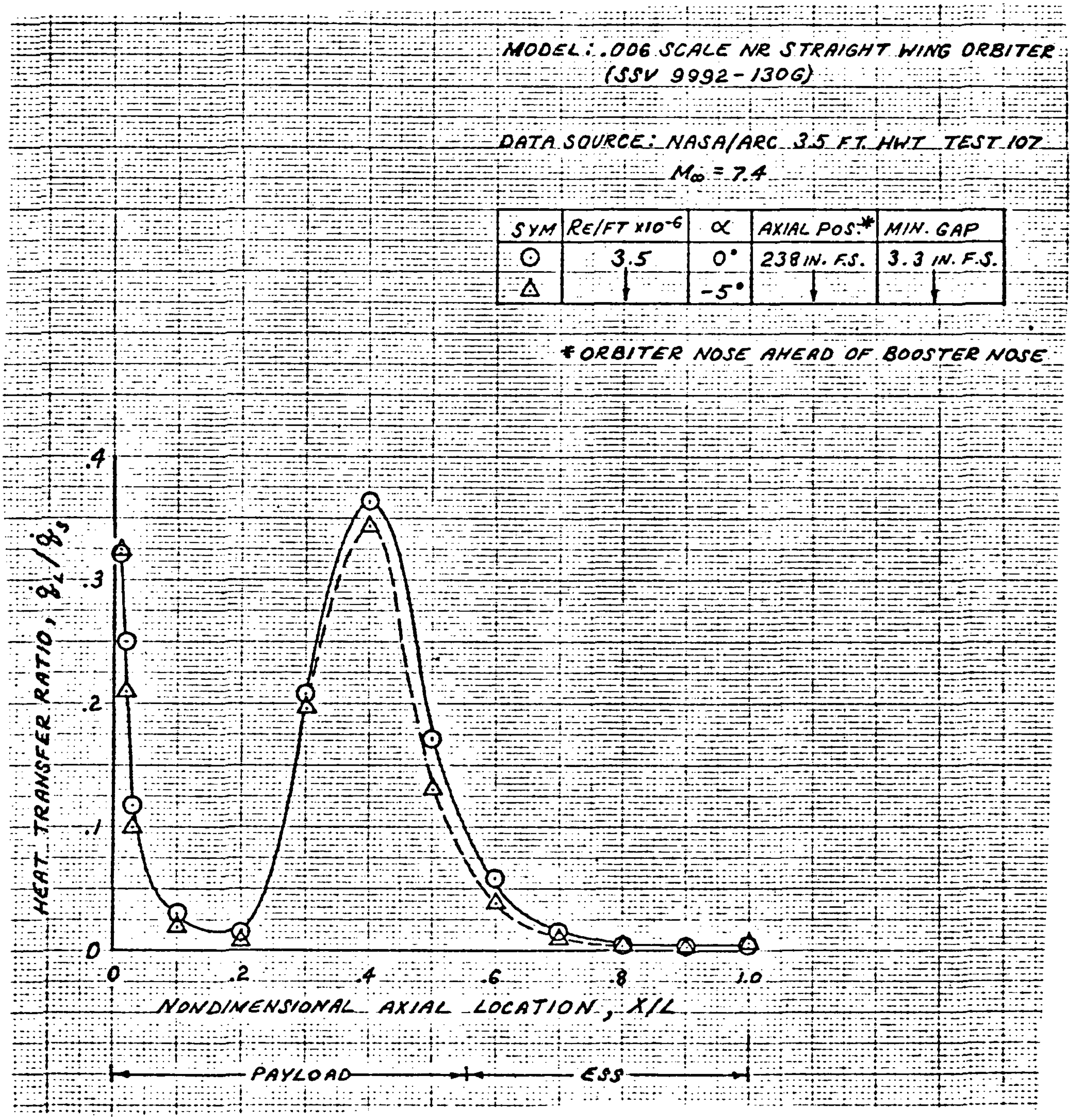

Figure 10. Effect of Angle of Attack on Mated Interference Heating, NR Straight Wing Orbiter Fuselage Lower Centerline

Again, in the area where the ESS would be located, no significant effect of angle of attack is indicated for the present (no solid contact) configuration.

Influence of the Mach Number

The variation of interference heating factor on the low surface centerline for the test Mach numbers of 3.7 and 7.4 is shown in Figure 11. Interference heating factors were determined as a function of ESS axial location using the appropriate test data with the aft end of the orbiter location in approximately the same position on the booster as the ESS. It appears that the interference heating factor decays more rapidly with distance for $M_\infty = 7.4$ (laminar flow) than for $M = 3.7$ (turbulent flow). This behavior is still not well understood because of the lack of data at the same viscous flow regime. A literature survey did not provide any more quantitative information but, qualitatively, it was shown that downstream of the region of strong shock interference, the Mach number influence could be considered as a perturbation effect when compared with the Reynolds number effect. This secondary effect is illustrated on Figure 12 when the ratio $\log (\dot{q}_{int}/\dot{q}_{clean})$ for turbulent flow is plotted versus $\log (p_{int}/p_{clean}) \approx \log (Re_{int}/Re_{clean})$. Even though the Mach number varies significantly, the results can still be represented on the same straight line.

Application of Test Data to Ascent Flight Trajectory

The local Reynolds number along the ESS determined from the nominal ESS 2/15/71 reference trajectory is presented in Figure 13.

As a result of the experimental data analysis, the effect of flight Mach number on interference heating in the hypersonic range ($M_\infty \geq 7.4$) was assumed to be small and was neglected in the present study. The interference heating factors predicted for $M_\infty = 7.4$ (Figure 11), therefore, were used for $M_\infty \geq 6$. These interference heating factors at the two test Reynolds numbers were then used for extrapolation to flight Reynolds numbers as shown in Figure 14 following the results from Figure 12. A similar plot was derived for the $M_\infty = 3.7$ heating factors. Between $M_\infty = 3.7$ and $M_\infty = 6$, the interference heating factors were smoothly faired.

From $M_\infty = 1$ to $M_\infty = 3.7$, the following relation was used to determine the interference heating factor:

$$\frac{Q_{M_\infty = 1}}{Q_{N_\infty = 3.7}} = \frac{\left(Re_{\infty_X}\right)_{M_\infty = 1}}{\left(Re_{\infty_X}\right)_{M_\infty = 3.7}}$$

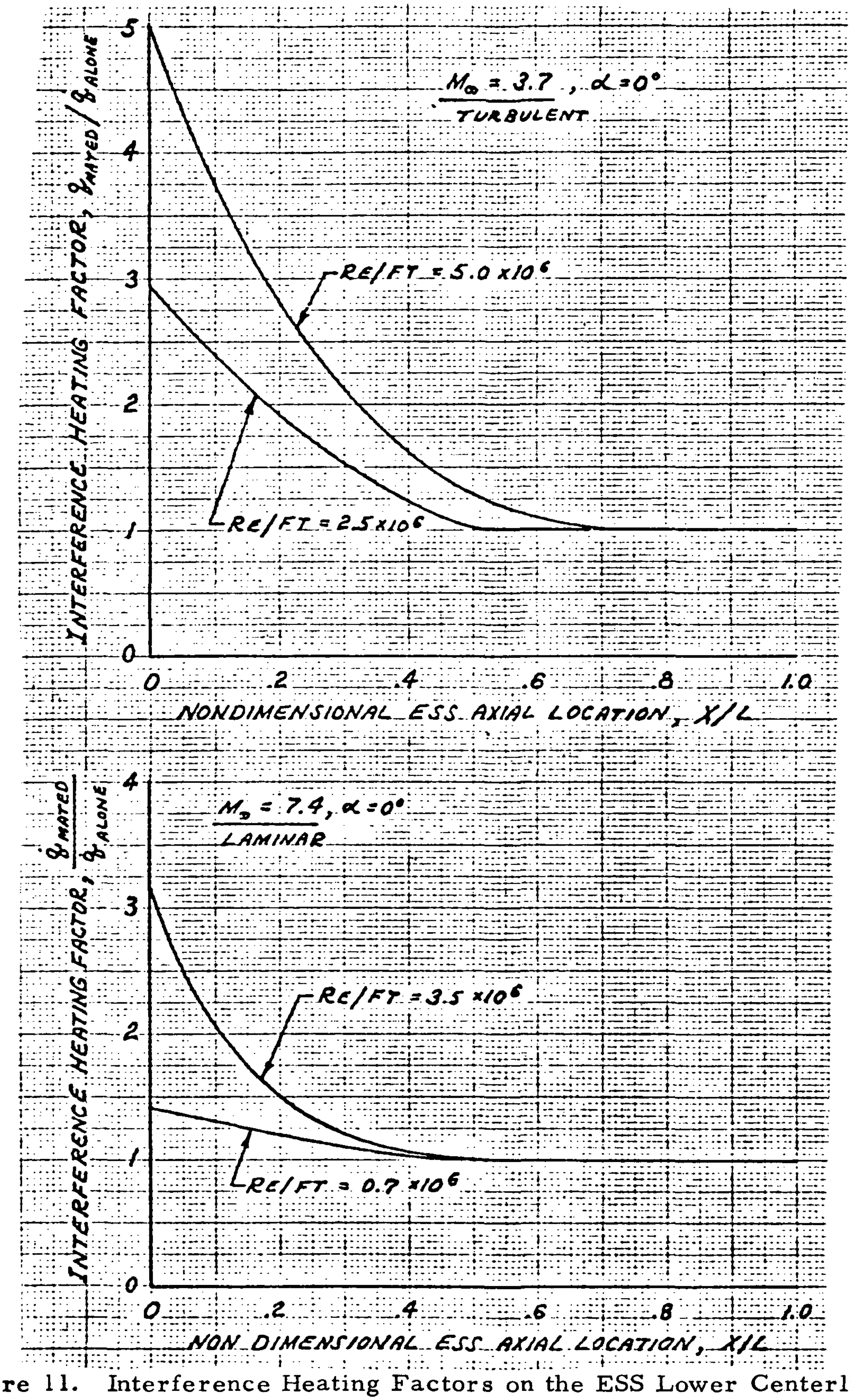

Figure 11. Interference Heating Factors on the ESS Lower Centerline from SSV Phase B Wind Tunnel Test Data Predicted

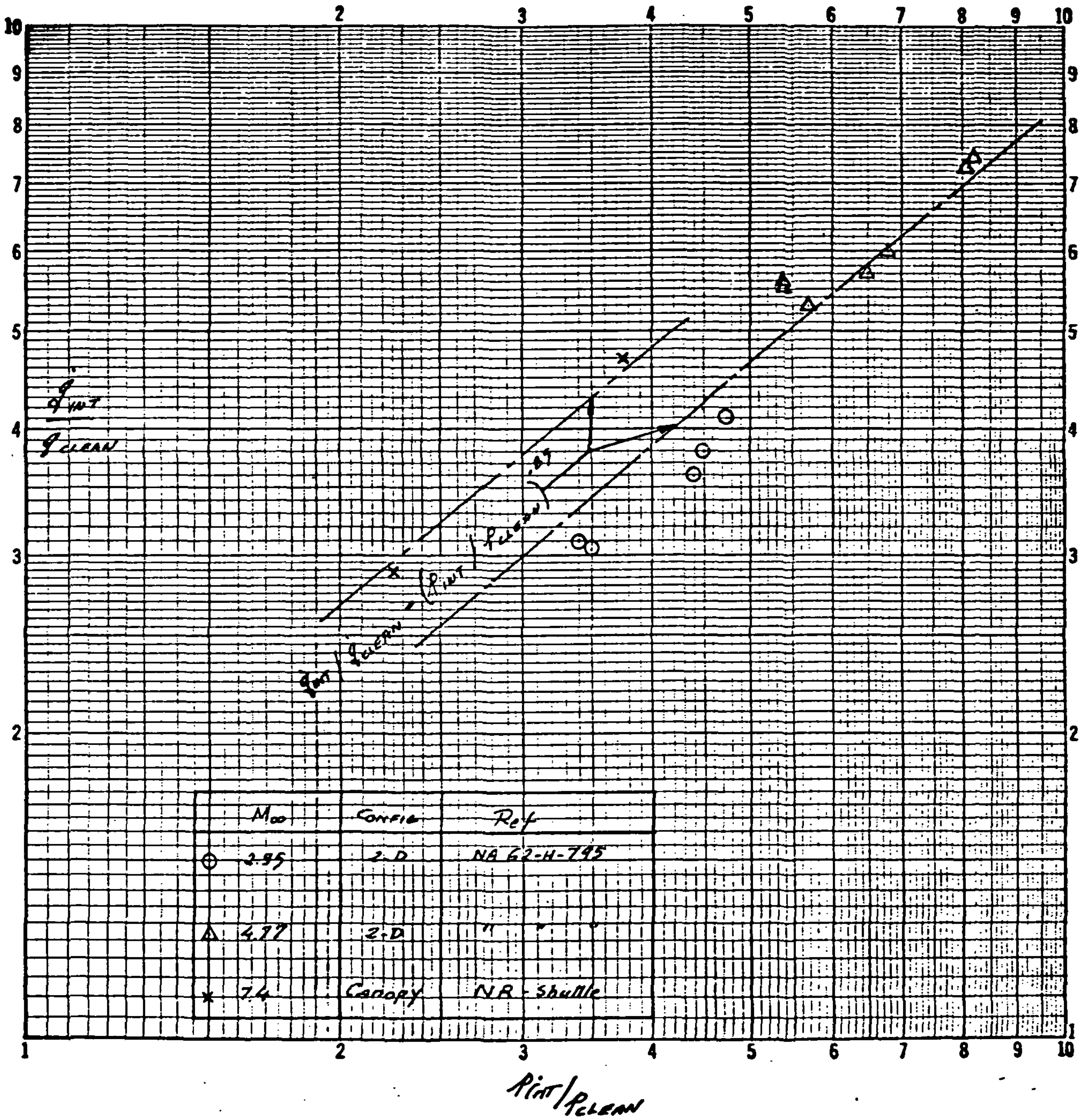

Figure 12. Variation of the Interference Heating Rate with the Interference Pressure

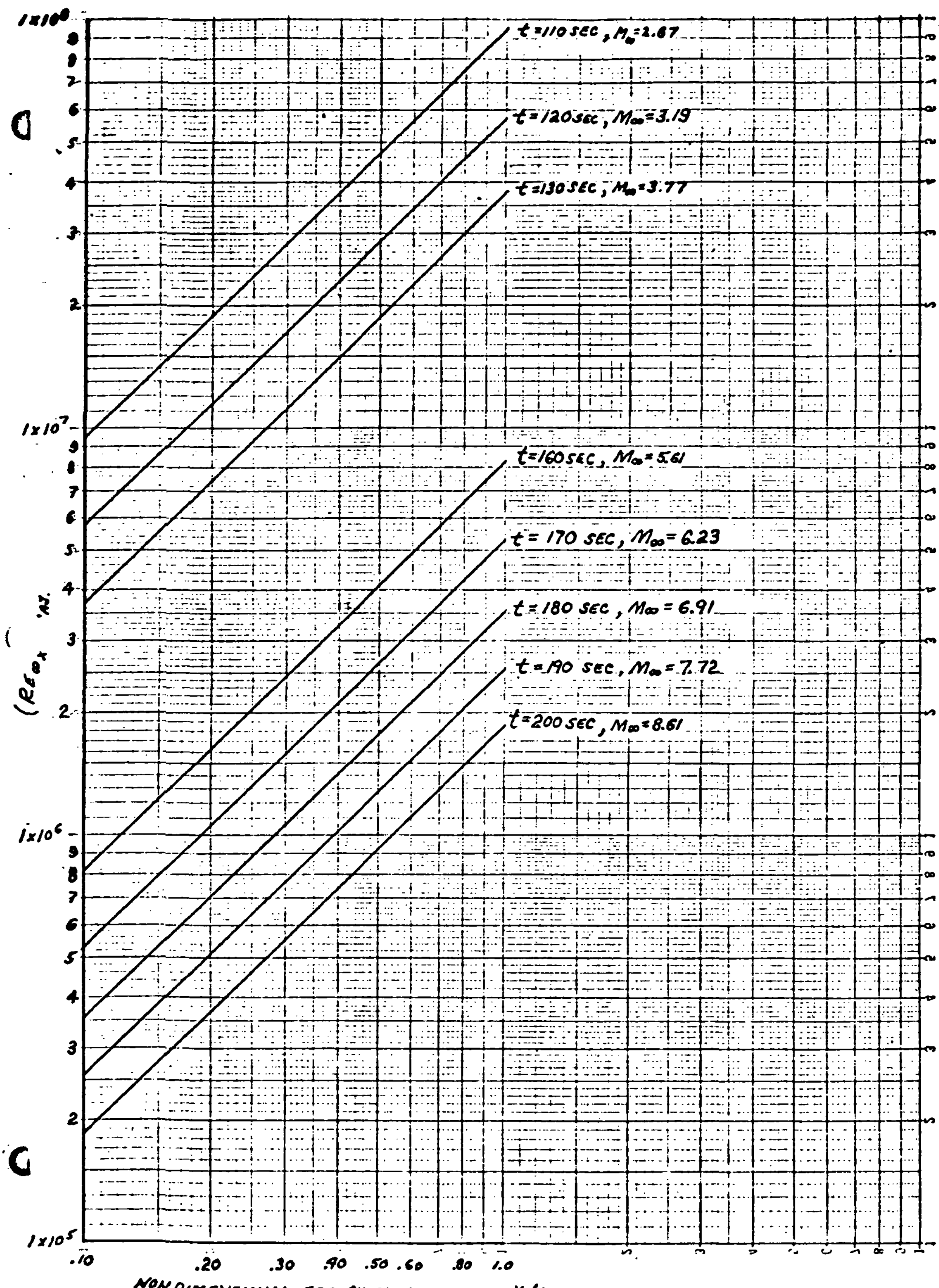

Figure 13. Local ESS Reynolds Number Based on Nominal 2-15-71 Reference Trajectory

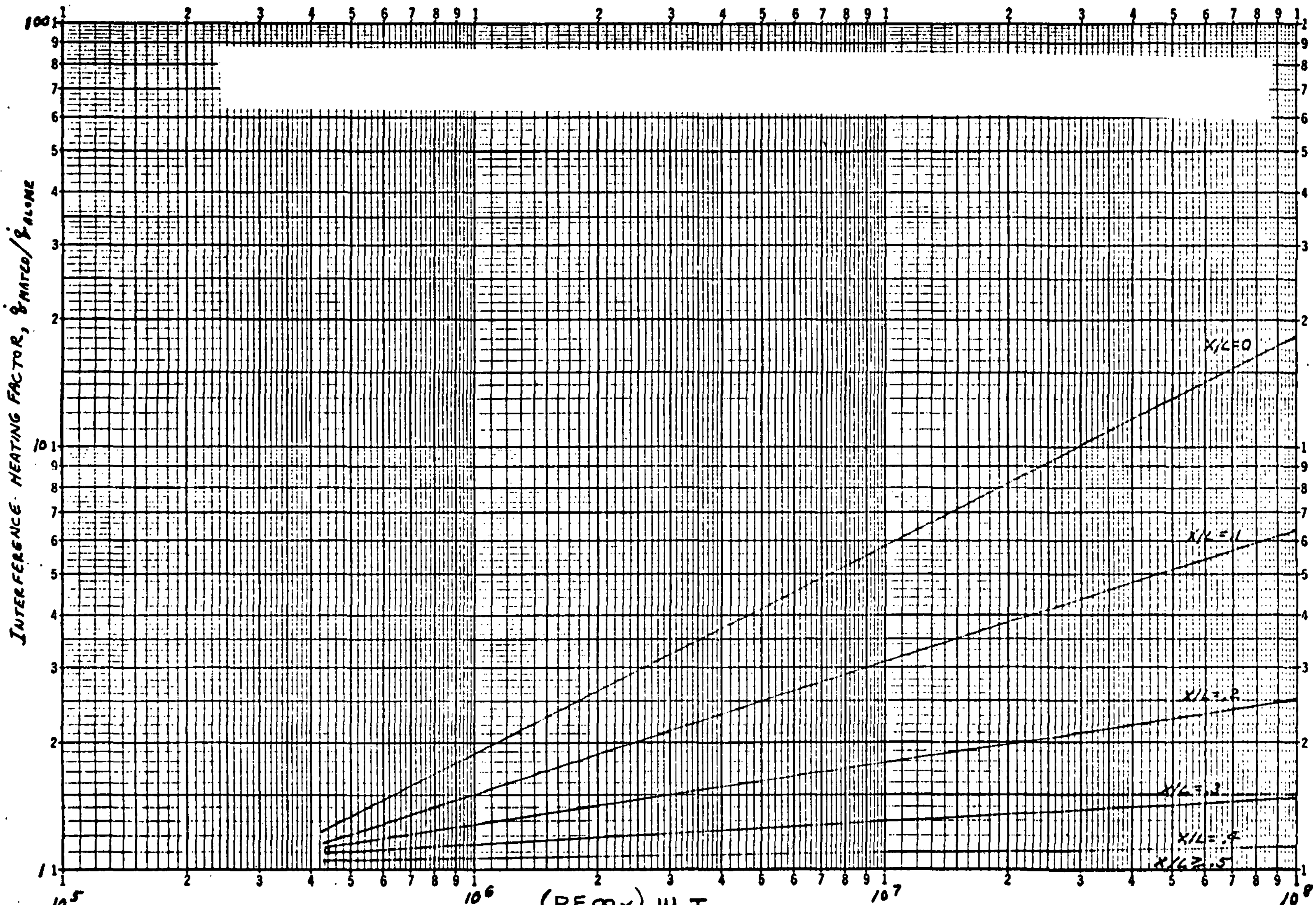

Figure 14. ESS Lower Centerline Interference Heating Factors As a Function of Reynolds Number, $M_\infty \geq 6$

where

Q = interference heating factor

Re_{∞_X} = local Reynolds number based on freestream properties

The end result presented in Figure 15 shows the predicted variation of interference heating factor along the ESS lower centerline with trajectory time. The factors of Figure 15 were then applied to the local heating rates on the non-mated ESS configuration. The predicted heating rates to the ESS including mated interference heating are presented in the appendixes of this volume for the MDAC Space Station payloads.

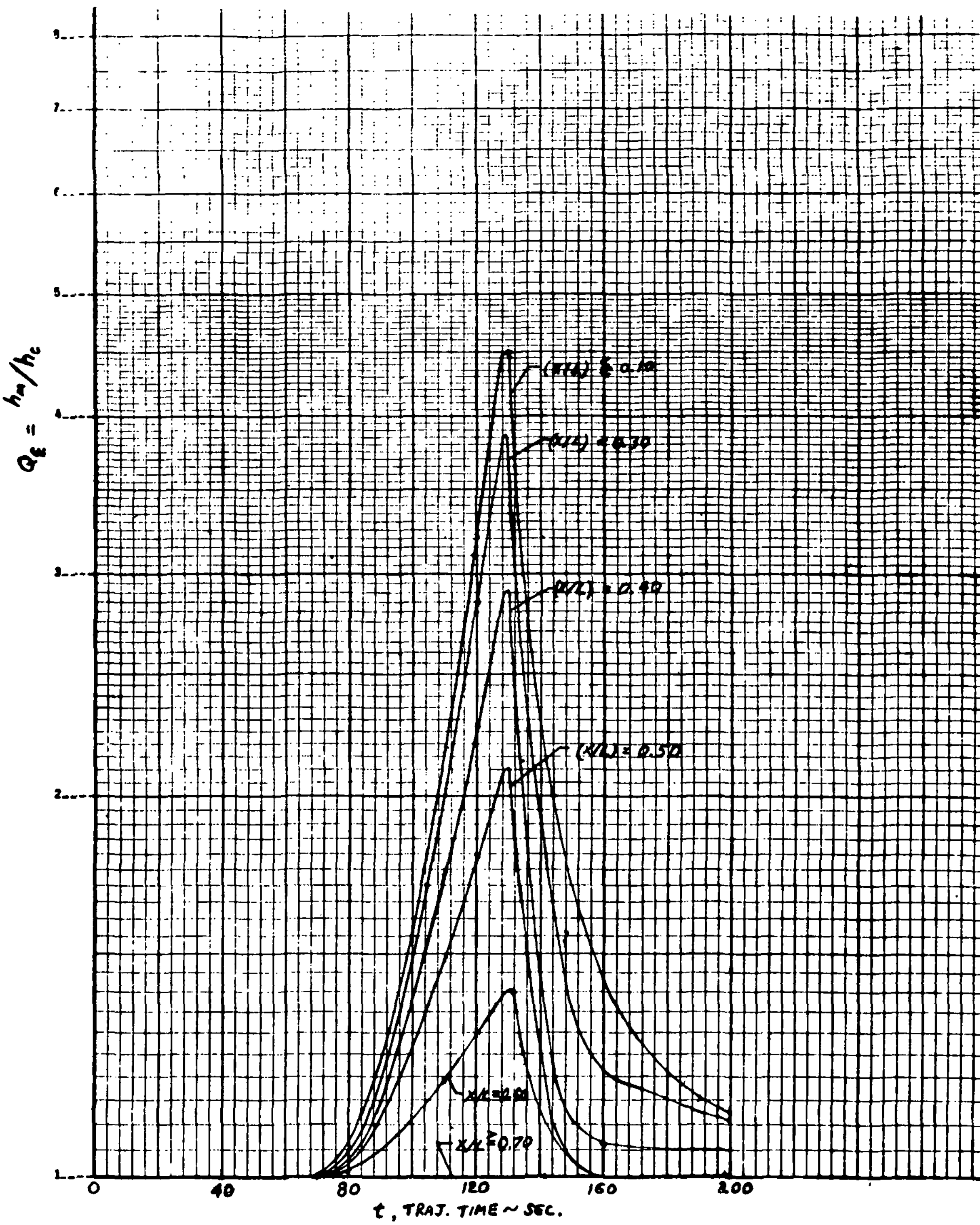

Figure 15. ESS Lower ℄ Interference Heating Factors

1.2.5 AERODYNAMIC HEATING ON THE BASIC PAYLOADS

The methods previously discussed for the analysis of the aerodynamic heating have been applied to the three basic payloads. The results on the mated configurations are given as a function of time and include:

the film coefficient

the recovery temperature

the protuberance factor and interaction regions

The following comments should be made:

Even though the trajectory is identical for the three payloads, the local base heating rates are slightly different for each configuration due to the shape and size of the payloads that modify the local edge properties on the ESS.

The MDAC Space Station payload has large protuberances (see Figure 16) while the other payloads do not have any. The influence of these protuberance on the flow downstream will create a region of interaction heating that will be even amplified by the presence of the booster. The exact increase of heating due to the "12 feet" docking ports has not yet been experimentally investigated and very few published data exist on such large protuberance. A conservative approach was then taken where the protuberance factor due to the docking ports is increased by the protuberance factor due to the mated configuration. The approach leads to local heating rates that are 50 times greater than those obtained on the present clean and nonmated ESS. The influence of these large heating rates on the wall temperature is significant and local additional protection will have to be considered.

The influence of the present attachment struts will, at a lesser extent, create a similar problem on the end section of the ESS. This is due to the interaction of the separation mechanism merging into the inviscid flow, generating shock waves that impinge on the surfaces producing locally insensitive heating rates. The same protuberance-style approach as above has been taken during the investigation. However, the region of influence is smaller and decays rapidly.

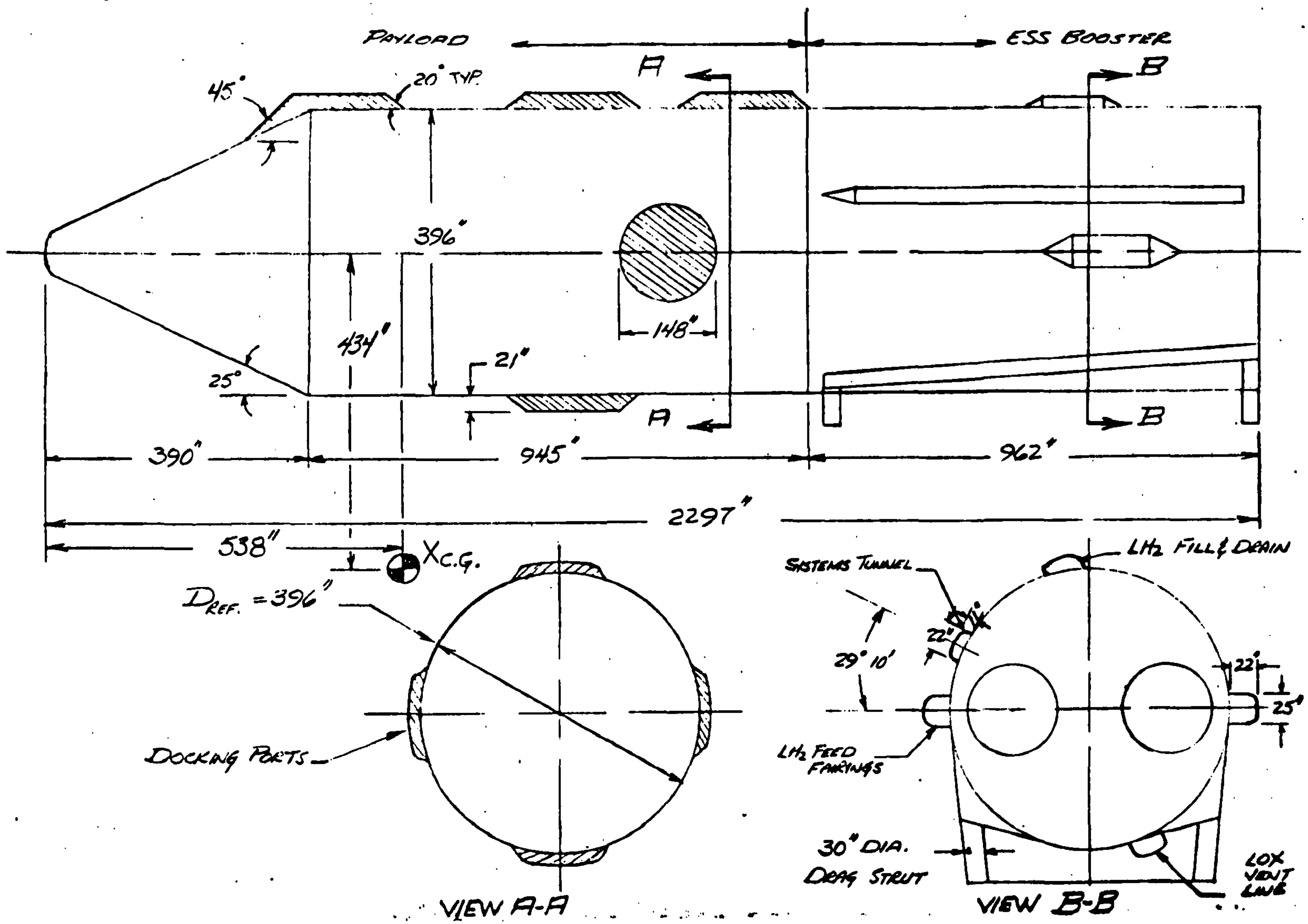

Figure 16. MDAC Space Station and ESS Booster

The convective heating increase due to protuberance can be significantly reduced by the use of a fairing shroud that will prevent the interaction from the MDAC Space Station protuberances to impinge on the ESS, but, instead be diverted on the forebody of the fairing shroud; and cover the struts attachment so that no shock will be introduced by the attachment sticking out in the undisturbed flow.

The preliminary design of such a device and its influence on the local aerodynamic heating is presented in a later section.

1.2.6 AERODYNAMIC HEATING ON THE GDC/B9U BOOSTER

The influence of the ESS payloads on the local heating rates on the booster are of two types:

a. The influence of the close proximity of the ESS that will increase the local heat transfer rates when compared with the booster-alone configuration. This problem exists also with the present shuttle/booster configuration. In this analysis, it has been assumed that by reason of symmetry, the local heating rates on the booster at a given station were identical to those on the ESS at the same location. This was later substantiated by the aerodynamic test tunnel data on the booster provided by GDC on the shuttle/booster configuration (no protuberance)

   For the ESS study, the effect of the protuberances (in the case of the MDAC Space Station) and, for all payloads, the effects of the struts fitting have been included. As a result, the data presented earlier in this volume have also been used for the aerodynamic heating calculations on the booster in the presences of the ESS.

b. The space tug payload presents a conical interstage inducing a shock wave at its junction with the cylindrical section that impinges on the booster upper surface. This shock impingement will create local overpressure and heating rates that are more severe than those existing for the other payloads, shuttle included. Also, the impingement point on the booster being a function of the flight Mach number will vary during the ascent phase. An analysis of the phenomena has been made based upon the following methods and assumptions:

   The pressure rise ratio p_{int}/p_{clean} across the impinging shock is obtained assuming the shock is conical and that upstream conditions correspond to perfect gas. This assumption is compatible with the Mach numbers encountered during the boost phase.

   The increase in the film coefficient h_{int}/h_{clean} due to the shock impingement is obtained, as a function of the pressure rise ratio, following the analysis of Reference 5. The results are obtained from empirical compilation of turbulent flow data on 2-D bodies and can be expressed as follows (see Figure 12):

$$\frac{h_{int}}{h_{clean}} = \left(\frac{p_{int}}{p_{clean}}\right)^{0.85}$$

No reliable data are available for laminar flow. However, during NR laminar flow tests (References 1 and 2), it was noticed that the canopy region experiences also the influence of an impinging shock. For this region, the pressure ratio and the heat transfer coefficient rise has also been plotted on Figure 12 together with the turbulent flow data of Reference 5. It can be seen that the same exponent of 0. 85 applies also for the canopy and as a result, a 0. 85 exponent will be used for both laminar and turbulent flow. As mentioned previously, all results seem to be independent of the Mach number.

No low density corrections have been made relative to the influence of the shock wave (pressure or/and heat transfer rates) for the high altitude/high Mach numbers flight case.

Application of the above methods for the ascent phase has been performed where the flight Mach number was used to compute the pressure jump across the impinging shock neglecting the weak influence of the shock from the booster's nose. The result of the analysis is presented on Figure 17, (a and b) as a function of the flight time. Figure 17-a presents the shock impingement location of the GDC/B9U booster as a function of time. Figure 17-b presents the pressure and heat transfer increase. It must be pointed out that the most significant increases occur at high altitude where vorticity interaction and low density effects exist and would tend to attenuate the shock strength and to reduce the present values. However, as mentioned in the assumptions, these effects are not taken into account in the present analysis and the results of the figure could be used as an upper limit for the effects to be encountered.

The influence on the booster of the impinging shock wave could be avoided by a better fairing design of the interstage and it is recommended to improve the present configuration.

Influence of the Fairing Shroud

The present design of the separation mechanism creates on the ESS local heating rates that are 20 times greater than those obtained on the clean vehicle. Also, it has been shown that the booster interaction was more sensitive near the pitch plane where shock-impingement effects are more likely to have a greater intensity and, as a consequence, where higher convective local heating rates could be expected. Addition of a fairing shroud around the separation mechanism could alleviate these phenomena.

A typical design is presented in Figure 18. With such a configuration, the influence of the booster on the ESS only exists for $\theta \geq 30$ degrees. Also, all additional interference heating rates due to the struts are eliminated. The present design of the forebody creates several zones of interactions for

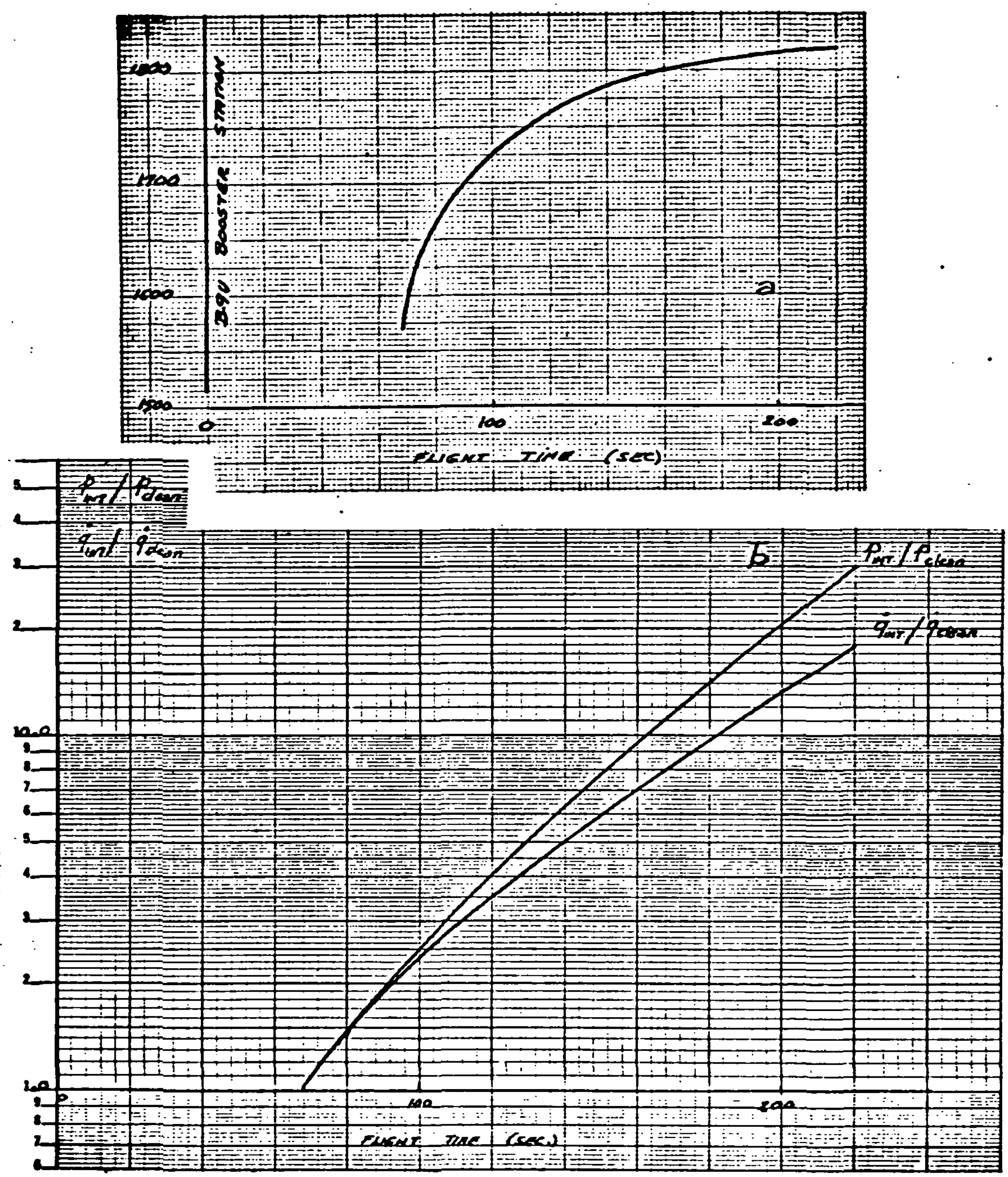

Figure 17. Space Tug - Influence of Impingement Shock on GD/C B—9U Booster

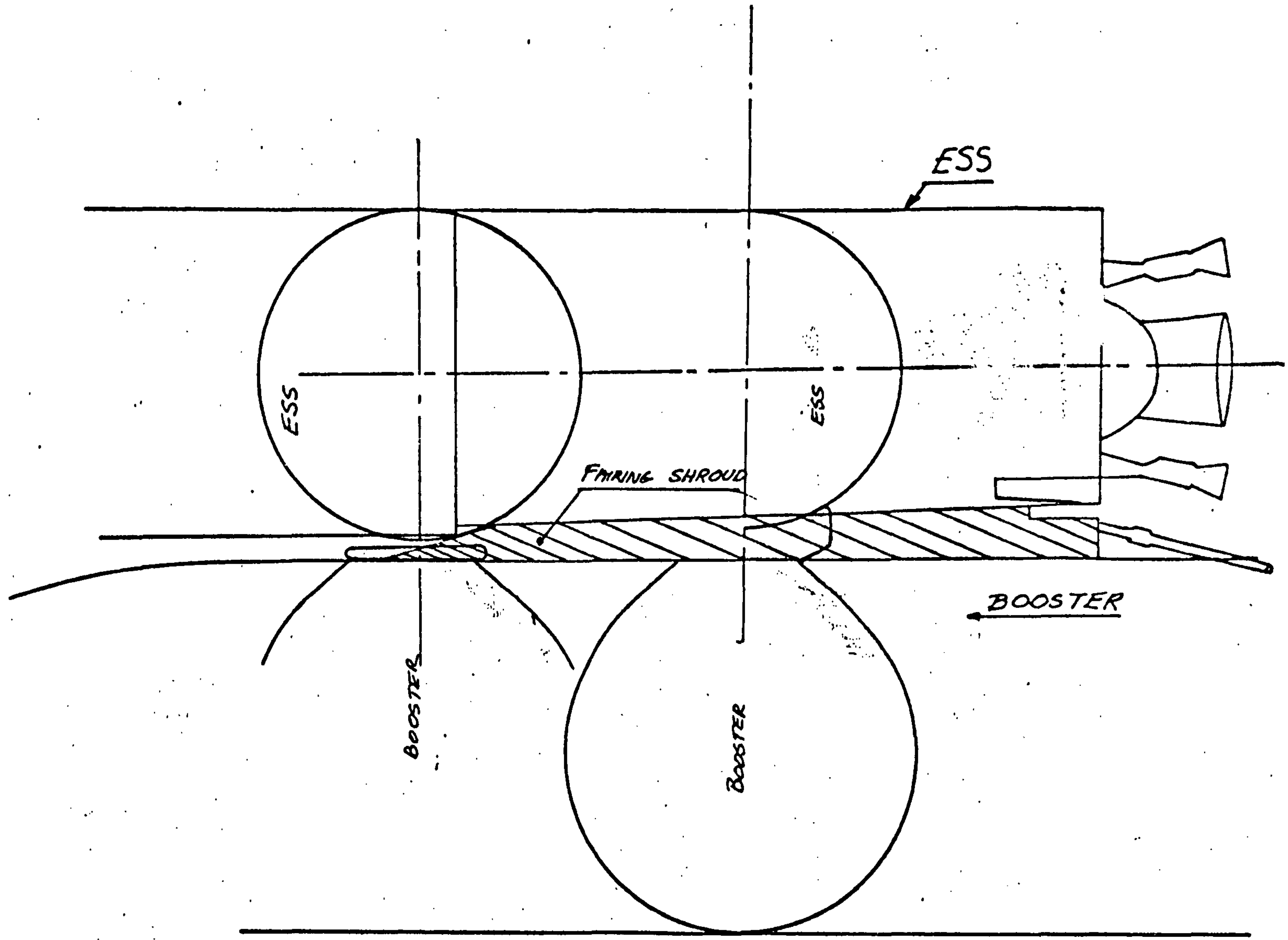

Figure 18. Fairing Shroud - ESS to SS Booster Drag Link Structure

which heating rates will be locally slightly increased when compared with the present (non-fairing) configuration. However, additional study of the forebody shape (Figure 19) (OSWATITCH-like fairing) would be desirable as a result of the preliminary analysis and would possibly eliminate to a significant extent the region of local interactions. No experimental data are presently available on the system configuration with fairing and the aerodynamic heating method adopted here was the same as that developed previously, but for $30 \leq \theta \leq 90$.

The analysis was applied to the MDAC/ESS configuration and the results presented in the appendixes. It can be seen that the value of the film coefficients have been significantly reduced and that the severe penalty due to the struts are now eliminated.

<u>Influence of the Trajectory</u>

Shortly after the 2/15/71 trajectory was computed, a more refined trajectory (dated 3/1/71) was issued. These two trajectories are represented on Figure 2. The first calculations were performed with the 2/15/71 trajectory. The effect of the trajectory on the local heating rates was analyzed. Here again, the MDAC/ESS configuration was used.

The results obtained from the 2/15/71 trajectory have been used and modified to account for the slight variation in flow properties following the analysis of Reference 10 for the laminar flow and that of Reference 11 for turbulent flow. Obviously, this analysis is based upon small perturbations and is only valid when the two flight conditions do not differ significantly.

Laminar Boundary Layer Analysis

In Reference 10, the laminar film coefficient for a cylinder is given by the following relationship:

$$h = \frac{\dot{q}}{Cp \, \Delta T} = \left(\sim \frac{\overline{S'_w}}{S_w} \right) \sqrt{Re_w \frac{\mu_w}{P_r}}$$

where $\overline{S'_w}/S_w$ is a constant for the zero pressure gradient case and already includes a 2-D to axisymmetric transformation,

and

$$Re_w = \frac{w \, u_e}{\mu_w}$$

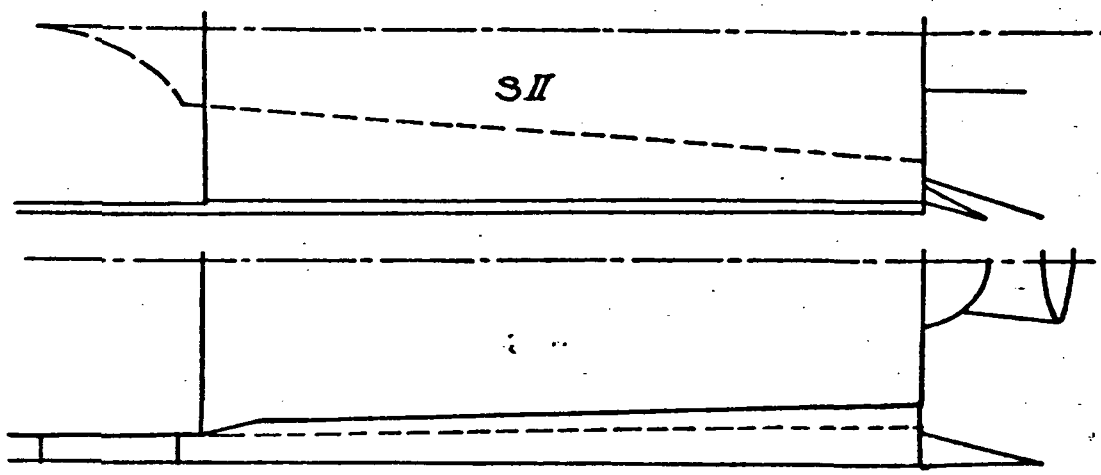

19A - "Oswatitch" Type

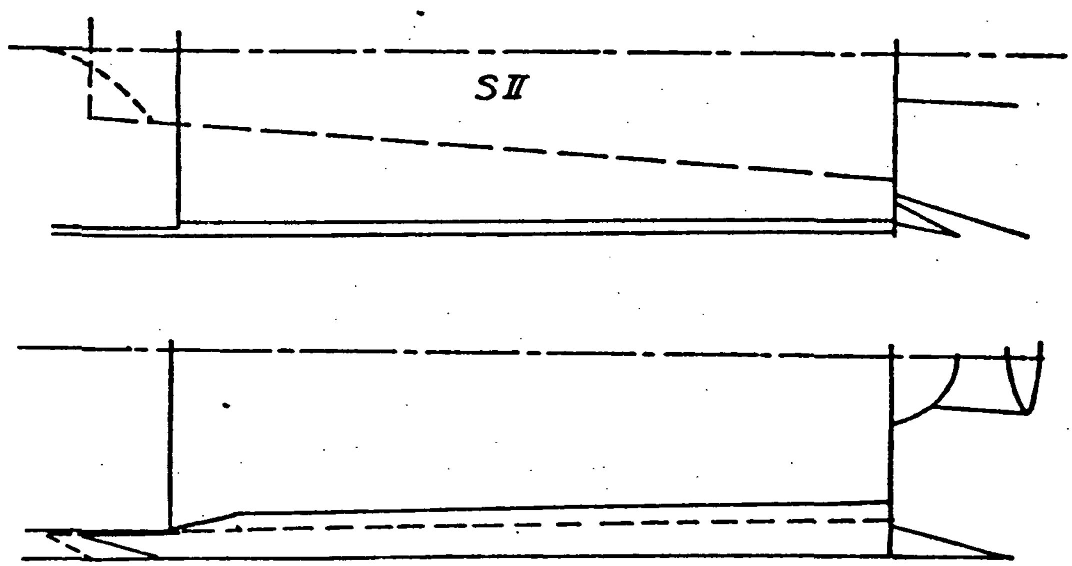

19B - Inverted Wedge Type
(May also be combined with the
Oswatitch type)

Figure 19. Fairing Shroud - Proposed Design Improvements

with

$$\rho_w = \frac{p_e}{Z_w \; R \; T_w}$$

In the following development, the edge and wall conditions for the 2/15/71 trajectory will be affected by the subscript (1) and the same parameters for the current trajectory will be affected by the subscript (2).

At a given time and location the film coefficient ratio between the two trajectories is given by

$$\frac{h_1}{h_2} = \sqrt{\frac{u_{e_1} \; (\rho_w \; \mu_w)_1}{u_{e_2} \; (\rho_w \; \mu_w)_2}} \qquad (1)$$

assuming that,

$$T_{w_1} (x) \approx T_{w_2} (x)$$

and

$$P_e = \phi(p_{stag}) = \tau \, p_\infty M_\infty^2 \qquad \text{(see Reference 13)}$$

gives

$$\frac{\rho_{w_1}}{\rho_{w_2}} = \frac{p_{\infty_1} \; M_{\infty_1}^2}{p_{\infty_2} \; M_{\infty_2}^2}$$

Introducing these results into Eq. 1,

$$\frac{h_1}{h_2} = \frac{M_{\infty_1}}{M_{\infty_2}} \sqrt{\frac{p_{\infty_1} \; u_{e_1}}{p_{\infty_2} \; u_{e_2}}} \qquad (2)$$

and the film coefficient for the current trajectory is then

$$h_{2_{(x)}} = h_{1_{(x)}} \frac{M_{\infty_2}}{M_{\infty_1}} \sqrt{\frac{p_{\infty_2} u_{e_2}}{p_{\infty_1} u_{e_1}}} \qquad (3)$$

The recovery temperature is given by the following relationship:

$$T_{ad} = T_{\infty}\left(1 + \frac{\gamma - 1}{2} r_{laminar} M_{\infty_2}^2\right) \qquad (4)$$

Turbulent Boundary Layer Analysis

In Reference 11, it is shown that Colburn's relationship for incompressible turbulent boundary layer could be used for moderate supersonic Mach numbers. Applying the same small perturbation analysis for the turbulent flow as previously described for the laminar flow, the film coefficient for the current trajectory is given by the following relationship:

$$h_{2_{(x)}} = h_1(x) \left[\frac{M_{\infty_2}^2 \, p_{\infty_2} \, u_{e_2}}{M_{\infty_1}^2 \, p_{\infty_1} \, u_{e_1}}\right]^{0.2} \qquad (5)$$

The recovery temperature is given by

$$T_{ad} = T_{\infty}\left(1 + \frac{\gamma - 1}{2} r_{turbulent} M_{\infty_2}^2\right)$$

The film coefficient versus time for both the current and the 2/15/71 trajectory is given in the Appendixes. However, on the semilog plot, it is difficult to accurately read and discriminate among the values for the two trajectories. During the analysis of the 2/15/71 trajectory, the film coefficient was carefully computed and included in the thermal model. To take advantage of this previous setup, the ration $h_2/h_1 = f(t)$ was also given. All results are presented with the recovery temperature in the appendixes.

A parametric thermal analysis has been made for the two trajectories in order to analyze the variation of the peak wall temperature.

The following parameters were investigated:

Wall thickness:	$0.2 \leq \Delta \text{inch} \leq 0.16$
Radiation to space factor:	$0.085 \leq \mathcal{F} \leq 0.8$
Solar absorption factor:	yes/no

The difference between the two peak wall temperatures has been computed and is represented on Figure 20. It can be seen that the maximum difference is of the order of 13 degrees and that, furthermore, this result is obtained for a very low radiation to space factor, unlikely to occur on the present system.

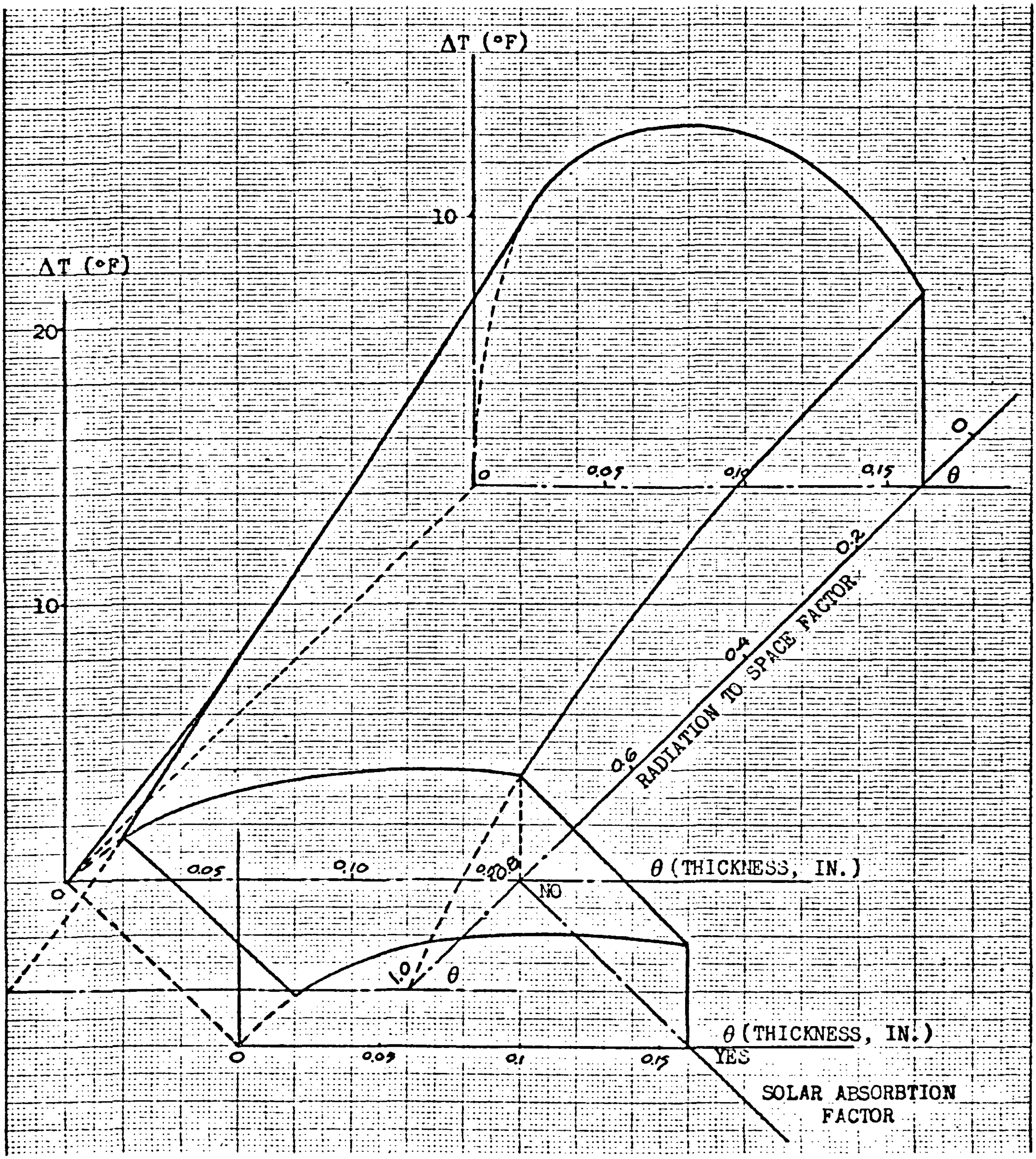

Figure 20. Peak Wall Temperature Difference Due to Change in Trajectory

1.2.7 CONCLUSION

The aerodynamic heating on the expendable second stage has been computed for three basic payloads, the details on one of which have been included. The results include the interaction effects due to protuberances and mated configuration.

The methods used have been derived from heat transfer (no pressure data) shuttle/booster wind tunnel tests when the two bodies are in close proximity, without any solid junction connecting the vehicles. These tests were conducted for two Mach numbers, two Reynolds numbers, two angle of attack α, and several values of the gap and stagger distances.

The vehicle geometry tested differ significantly from the payload-ESS/B9U configuration but, at the ESS location, the booster/straight wing model offers an excellent simulation of the ESS/B9U. The limited amount of heat transfer gauges did not always permit detection of the exact value and location of the peak heating. However, the phenomena always occurred on the payload and the heating rates decay very rapidly on the ESS.

The results of the present test program on the interference heating can be summarized as follows:

The Reynolds number is the most significant parameter influencing the local heating rates.

The Mach number and angle of attack have almost no influence.

The effect of the gap distance can reasonably be predicted.

The results of the literature survey show that the aerodynamic simulation of the protuberances as a function of the boundary layer thickness could create a serious problem when applying the general wind tunnel results to actual flight cases.

The method was applied within these assumptions to predict the local heating rates during the ascent trajectory. For this preliminary phase of the ESS program, the ascent trajectory used (identical for each payload) may not represent the envelope of the most critical flight conditions, so that the results obtained should only be used for the identification of the most crucial problems associated with each payload configuration.

However, the methods discussed here are believed to be for a generalized parametric study. More precision may be needed for a specific configuration where protuberances and attachment struts create significant modifications in the inviscid flow field, increasing local heating rates by over one order of magnitude. When the booster definition is selected and the trajectories known, a wind tunnel test program is needed. Protuberances and the gap distance should be aerodynamically simulated, and the flight conditions (M_∞, α) should be analyzed as a function of the Reynolds number. With such test data, a more adequate analysis could be performed including vorticity effects for high altitude cases.

Wind tunnel heating data on aerodynamic heat transfer distribution on the Phase B space shuttle booster vehicles at angles of attack from -5 degrees to +60 degrees is given in Reference 14.

REFERENCES

1. SSV Launch Phase Testing in the NASA/Ames Research Center 3.5-Foot Hypersonic Wind Tunnel, Test 107. (To be published)

2. SSV Launch Phase Testing in the NASA/Langley Research Center Unitary Plan Wind Tunnel, Test 945. (To be published)

3. Back, L. H., and R. F. Cuffel. "Changes in Heat Transfer from Turbulent Boundary Layers Interacting with Shock Waves and Expansion Waves," AIAA J. Vol. 8, No. 10 (October 1970).

4. Edney, B. E., "Effects of Shock Impingement on the Heat Transfer Around Blunt Bodies," AIAA J., Vol. 6, No. 1, (January 1968) pp. 15-21.

5. Levin, V., and T. J. Fabish. "Thermal Effects of Shockwave Turbulent Boundary Layer Interaction at Mach Numbers 3 and 5," Columbus Division, North American Rockwell Corporation, NA62H (12 Nov. 1962).

6. Sayano, S., C. R. Erickson, and J. S. Murphy. "Aerodynamic Interference Associated with Two Parallel Bodies in Close Proximity in Hypersonic Flow." AFFDL-TR-64-158 (prepared under Contract No. AF 33(657)-10660 by MSSD, Douglas Aircraft Company) (December 1964).

7. Schadt, G. H., "Aerodynamic Heating Problems and Their Influence on Earth Orbit Lifting Entry Spacecraft." AIAA Paper No. 68-1126, AIAA 5th Annual Meeting and Technical Display, Philadelphia, Pennsylvania (October 1968).

8. Truitt, R. W., "Hypersonic Turbulent Boundary-Layer Interference Heat Transfer in the Vicinity of Protuberances." AIAA J., Vol. 3, No. 9 (Sept. 1965) pp. 1754-1755.

9. Edney, B., Anomalous Heat Transfer and Pressure Distributions on Blunt Bodies at Hypersonic Speeds in the Presence of an Impinging Shock. FFA Report 115 (February 1968).

10. Cohen, N., and E. Reshotho. Similar Solutions for Compressible Boundary Layer with Heat Transfer and Pressure Gradient. NACA TN-3325 (Feb. 1955).

11. Michel, R. Aerodynamique - Couches Limites, Frottement et Transport de Chaleur. Ecole Nationale Supérieure de l'Aeronautique (1927).

12. Casey, W. Expendable Second Stage Thermal Analysis - Influence of the Trajectory. Internal Letter No. TA-190-201-71-31 (1971).

13. Waiter, S.A., and P.R. Choudhury. "Correlation Equations for Determining the Equilibrium Conditions Behind a Strong Shock." JAS J. (May 1962).

14. Aerodynamic Heat Transfer Distribution on Phase B Space Shuttle Booster Vehicles at Angles of Attack from -5° to 60°. Convair Aerospace Division, General Dynamics Corporation, Report No. 76-549-4-083 (3 Mar. 1971).

2.0 REQUIREMENTS

2.1 ESS TVC ACTUATOR ORIENTATION, GIMBAL CAPABILITY, AND CANT REQUIREMENTS

A summary of the actuator orientation, gimbal capability, and cant requirements for the selected ESS main engines and OMS engines is presented in Figure 2-1.

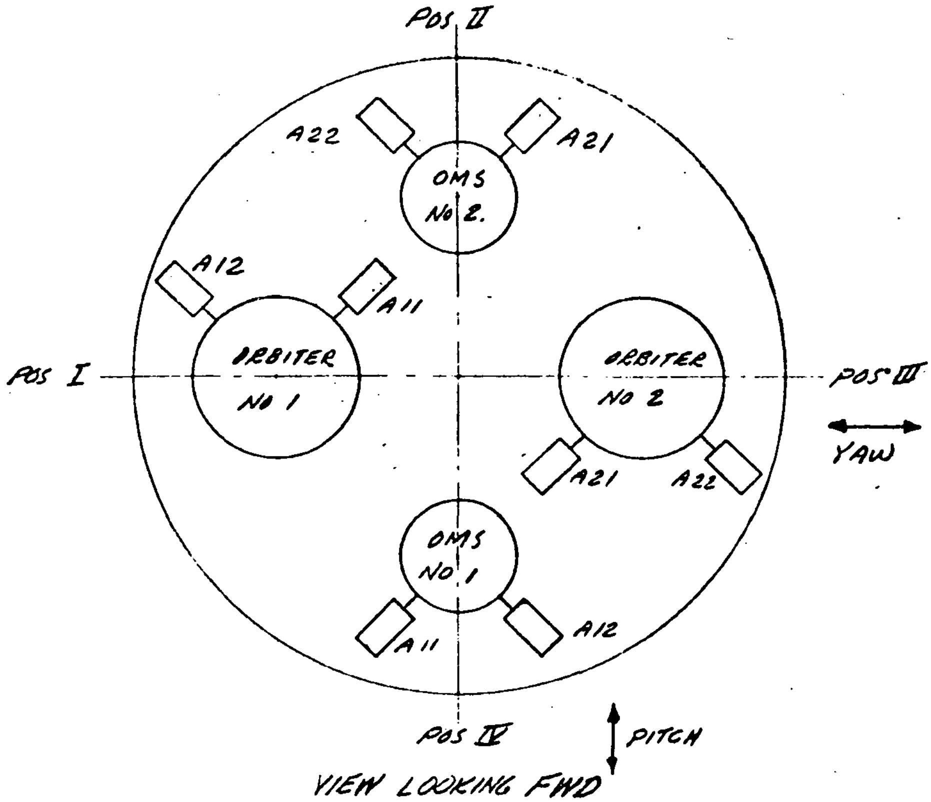

ENGINE	ACT.	* ACTUATOR POLARITY + PITCH	+ YAW	+ ROLL
ORBITER 1	A11	−	−	+
	A12	−	+	+
ORBITER 2	A21	+	+	+
	A22	+	−	+
OMS 1	A11	+	+	+
	A12	+	−	−
OMS 2	A21	−	−	+
	A22	−	+	−

* ACTUATOR EYTEND (+)

ORBITER ENG
± 7° SQ PATTERN
13° STATIC PRECANT
12° DYNAMIC PRECANT

OMS ENG
± 4.3° SQ. PATTERN
9° STATIC PRECANT
8° DYNAMIC [redacted]CANT

Figure 2-1. ESS TVC Actuator Orientation, Gimbal Capability and Cant Requirements

2.2 ESS OMS ENGINE CANT-ANGLE AND DEFLECTION REQUIREMENTS

The engine cant-angle and deflection requirements are outlined for the orbital maneuvering system (OMS) during the expendable second stage flight. The effect of engine cant angle on vehicle payload penalty is given. The data are generated as flight-control requirements for the ESS.

The study indicated that the use of a single OMS engine for flight control during orbital ΔV maneuvers is feasible. The recommended engine cant-angle and deflection requirements for all ESS vehicle configurations examined are 8 degrees and ±6 degrees, respectively. With this required cant angle, the vehicle payload penalty is 400 pounds.

If a single OMS engine is used for both orbital ΔV maneuvers and ESS deorbit, the cant-angle and deflection requirements are 16 degrees and ±12 degrees. The corresponding vehicle payload penalty is 950 pounds. In view of the known deflection capabilities (±7 degrees) of the ESS and the orbiter engines, the design for single OMS engine deorbit without additional attitude control is not practical and is therefore not recommended. The attitude control and propulsion system (ACPS) should be used to provide this additional attitude control.

The ESS plus payload vehicle configuration, coordinate system, and the OMS engine deflection angles are defined in Figure 2-2. Three types of payload are considered in this study: MDAC space station, NR reusable nuclear shuttle (RNS), and NR space tug. The OMS engines are used for orbital ΔV maneuvers such as orbit circularization, orbit phasing, and rendezvous. They also may be used for ESS deorbit. The total propellant for the OMS control operations is 23,000 pounds of which 3000 is reserved for ESS deorbit. The nominal thrust per OMS engine is 10, 000 pounds.

The OMS engines are gimbaled (with equal deflection capability) about the pitch and yaw vehicle-body axes for thrust-vector control. These engines are also canted (before launch) to provide adequate pitch-axis control in the event of one engine failure. The cant angles are measured on the X-Z plane and are β_{CT} degrees outboard.

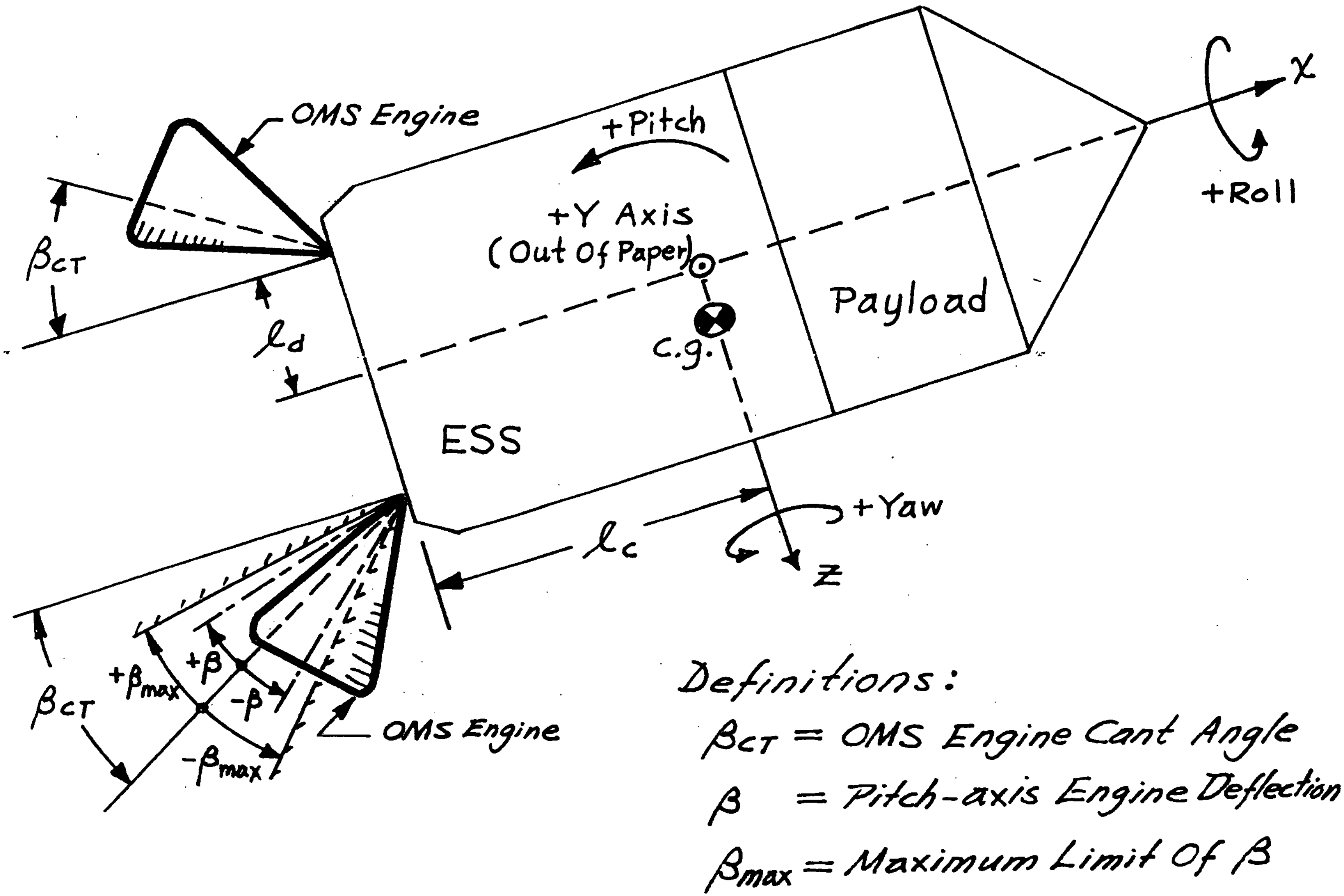

Figure 2-2. ESS Vehicle Configuration, Coordinate System and OMS Engine Deflection Angles

ANALYSIS

The problem of this study is to determine the OMS engine cant-angle and deflection requirements for the following conditions:

Study Case	Assumptions	Vehicle Configurations
1	One OMS engine has failed. The remaining OMS engine is required to provide thrust-vector control for orbital ΔV maneuvers.	ESS + NR tug ESS + MDAC space station ESS + NR RNS
2	Same as study case 1 except that single-engine thrust vector control is also required for ESS deorbit.	ESS + NR tug ESS + MDAC space station ESS + NR RNS

In particular, the study questions are as follows:

1. What is the recommended engine cant angle (β_{CT}) for all ESS plus payload vehicle configurations?

2. With this recommended cant angle, what maximum pitch-axis engine deflection (β_{max}) is required?

3. What is the vehicle payload penalty due to the required engine cant angle?

The yaw-axis deflection requirement need not be determined because it is expected to be much less than that of the pitch axis. An engine deflection requirement adequate for the pitch axis is also adequate for the yaw-axis control.

The determination of β_{CT} and β_{max} requirements involves calculations of engine deflections for pitch-axis static and dynamic trims under one engine-failure condition. The effect of cant angle on payload penalty is determined by calculating the propellant wasted to produce the sine components of the engine thrust vectors. The techniques and input data used for these calculations are summarized in the paragraphs that follow.

Results of these analyses are given in Volume II, Book 2.

The calculations of engine deflections and vehicle payload penalties for study case 1 (single OMS engine orbital ΔV maneuvers) are summarized below. The calculations for study case 2 (orbital ΔV maneuvers and ESS deorbit) are not presented but are similar to those of case 1. For specific results of calculations, refer to Volume II, Book 2.

Engine Deflection Requirement

The engine deflection requirement ($|\beta_{max}|$) for each ESS plus payload vehicle is determined by the following steps:

1. Calculate engine deflection β_s for pitch-axis static trim:

$$\beta_s = 57.3 \left(\frac{l_d}{l_c} \right) \text{degrees}$$

$$l_c = X_{cg} + 48 \text{ inches}$$

$$l_d = 128 \text{ inches}$$

2. Calculate engine deflection β_D for pitch-axis dynamic trim:

$$\beta_D = \left(\frac{I_{YY}}{n\ F\ l_c} \right) \dot{q} \text{ degrees}$$

n = 1 engine

F = 10,000 pounds thrust per engine

$\dot{q}$ = pitch-axis angular acceleration

3. Calculate the maximum engine deflection (β_{max}) as a function of cant angle (β_{CT}).

$$\beta_{max} \text{ (OMS propellant full)} = 1.25\ (\beta_{D1} + \beta_{S1} - \beta_{CT})$$

$$\beta_{max} \text{ (OMS propellant at 3,000 pounds)} = 1.25\ (-\beta_{D2} + \beta_{S2} - \beta_{CT})$$

Vehicle Payload Penalty

The vehicle payload penalty (ΔW) as a function of engine cant angle (β_{CT}) is calculated by the following equation:

$$\Delta W = W_f \left[1 - \left(\frac{W_o}{W_f} \right) \left(\frac{W_f}{W_o} \right) \frac{1}{\cos \beta_{CT}} \right]$$

where W_o and W_f are vehicle weights when the OMS propellant is 23,000 and 3000 pounds, respectively.

C2

2.3 ESS MAIN ENGINE CANT-ANGLE AND DEFLECTION REQUIREMENTS

The engine cant-angle and deflection requirements are examined for the expendable second stage during boost flight. It also shows vehicle payload penalties as a result of cant-angle requirements.

The ESS + payload vehicle configuration, coordinate system, and the engine deflection angles are defined in Figure 2-3. Three types of payload are considered in this study: MDAC space station, NR reusable nuclear shuttle, and NR space tug. Following first-stage separation, this ESS + payload vehicle is boosted into earth orbit by two orbiter engines. The thrusting time is approximately 200 seconds.

The orbiter engines are gimbaled to deflect about the pitch and yaw vehicle-body axes for thrust-vector control. The proposed nominal deflection capability in each of these axes is ±7 degrees. Because of the engine gimbaling geometry, this deflection capability may be extended to an angle as defined by the following equations:

$$\left|\begin{array}{l}\text{Maximum}\\ \text{yaw-axis}\\ \text{deflection}\\ \text{capability}\end{array}\right| = 10^\circ - \left|\begin{array}{l}\text{pitch-axis}\\ \text{deflection}\\ \text{requirement}\end{array}\right| \qquad (1)$$

$$\left|\begin{array}{l}\text{Maximum}\\ \text{pitch-axis}\\ \text{deflection}\\ \text{capability}\end{array}\right| = 10^\circ - \left|\begin{array}{l}\text{yaw-axis}\\ \text{deflection}\\ \text{requirement}\end{array}\right| \qquad (2)$$

The engines are also canted (before launch) to provide adequate yaw-axis control in event of one engine failure.

ANALYSIS

The problem of this study is to determine the cant-angle and maximum yaw-axis deflection requirements for the orbiter engines. In particular, the study questions are as follows:

1. What is the recommended engine cant angle (δ_{CT}) for each ESS + payload vehicle configuration?

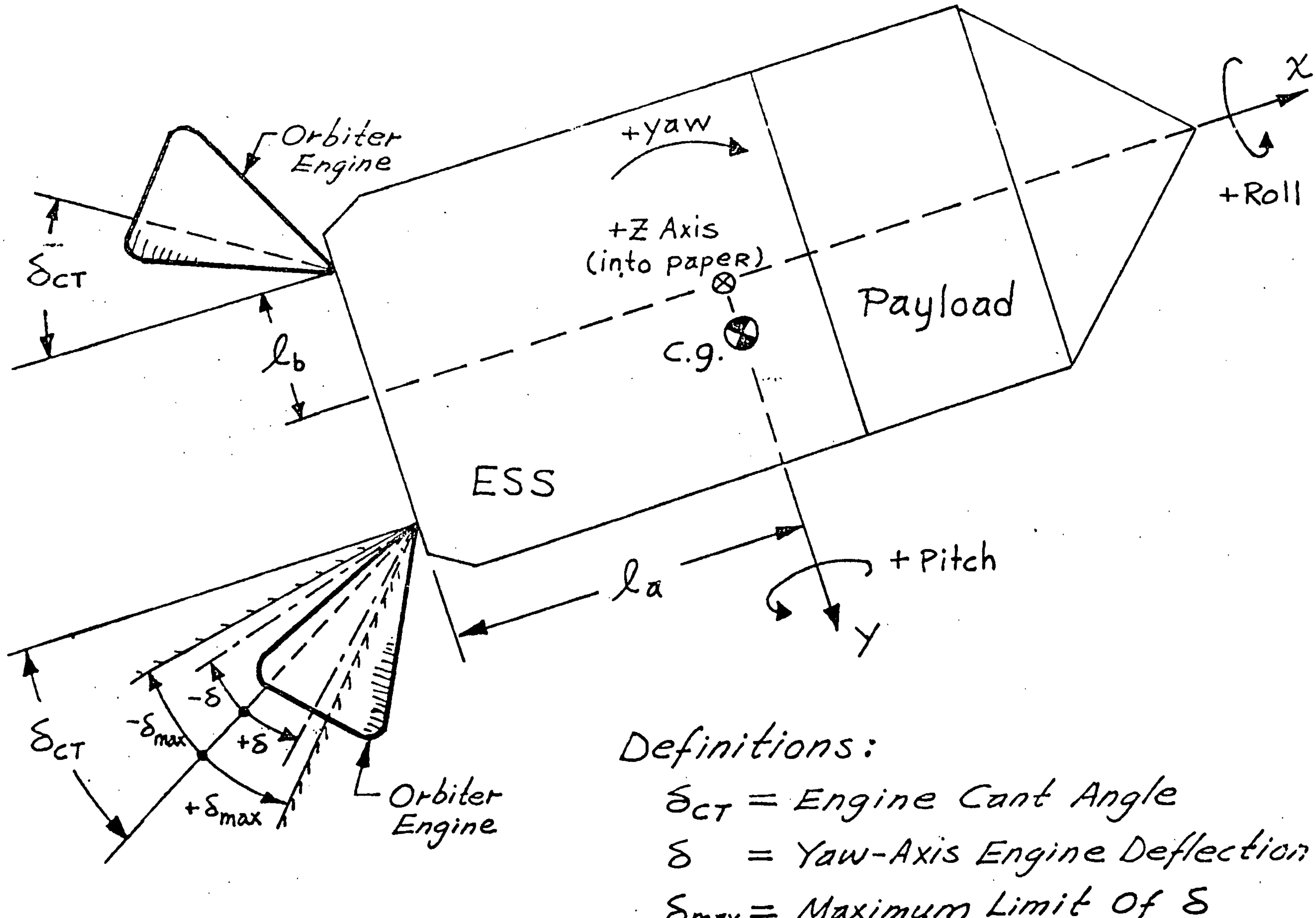

Figure 2-3. ESS Vehicle Configuration, Coordinate System and Orbiter Engine Deflection

2. With the recommended cant angle, is the proposed nominal deflection capability of ±7 degrees adequate for yaw-axis control?

3. If this ±7 degrees capability is not adequate, what maximum yaw-axis deflection (δ_{max}) is required?

4. What is the vehicle payload penalty as a result of the required cant angle?

The pitch-axis deflection requirement (for orbit-insertion maneuver, ESS/shuttle separation transient damping, and engine-failure-mode dynamic trim) is estimated to be 2 degrees. This pitch-axis deflection requirement is well within the proposed nominal capability of the orbiter engine and needs no further calculation.

The determination of δ_{CT} and δ_{max} requirements involves calculations of engine deflections for yaw-axis static and dynamic trims under one engine failure condition. The effect of cant angle on payload penalty is determined by calculating the propellant wasted to produce the sine components of the engine thrust vectors. The techniques and input data used for these calculations are summarized in the paragraphs that follow.

RESULTS

The engine deflection requirements (plus or minus δ_{max}) and the vehicle payload penalty as functions of cant angle are plotted in Figure 2-4 where two important indications should be noted. First, there is no acceptable cant angle for design if the engine deflection capability falls below 5.5 degrees. Secondly, the engine cant angle need not be greater than 13 degrees. With these indications and the limiting capability of the orbiter engine, the possible combinations of cant-angle and maximum-deflection requirements are tabulated in Table 2-1 for comparison.

CONCLUSIONS

The main conclusion is that the proposed nominal deflection capability of ±7 degrees is adequate for yaw-axis control, provided the required engine cant angles are as follows:

Vehicle Configuration	Minimum Engine Cant Angle
ESS + MDAC space station	10 degrees
ESS + NR RNS	12 degrees
ESS + NR tug	12 degrees

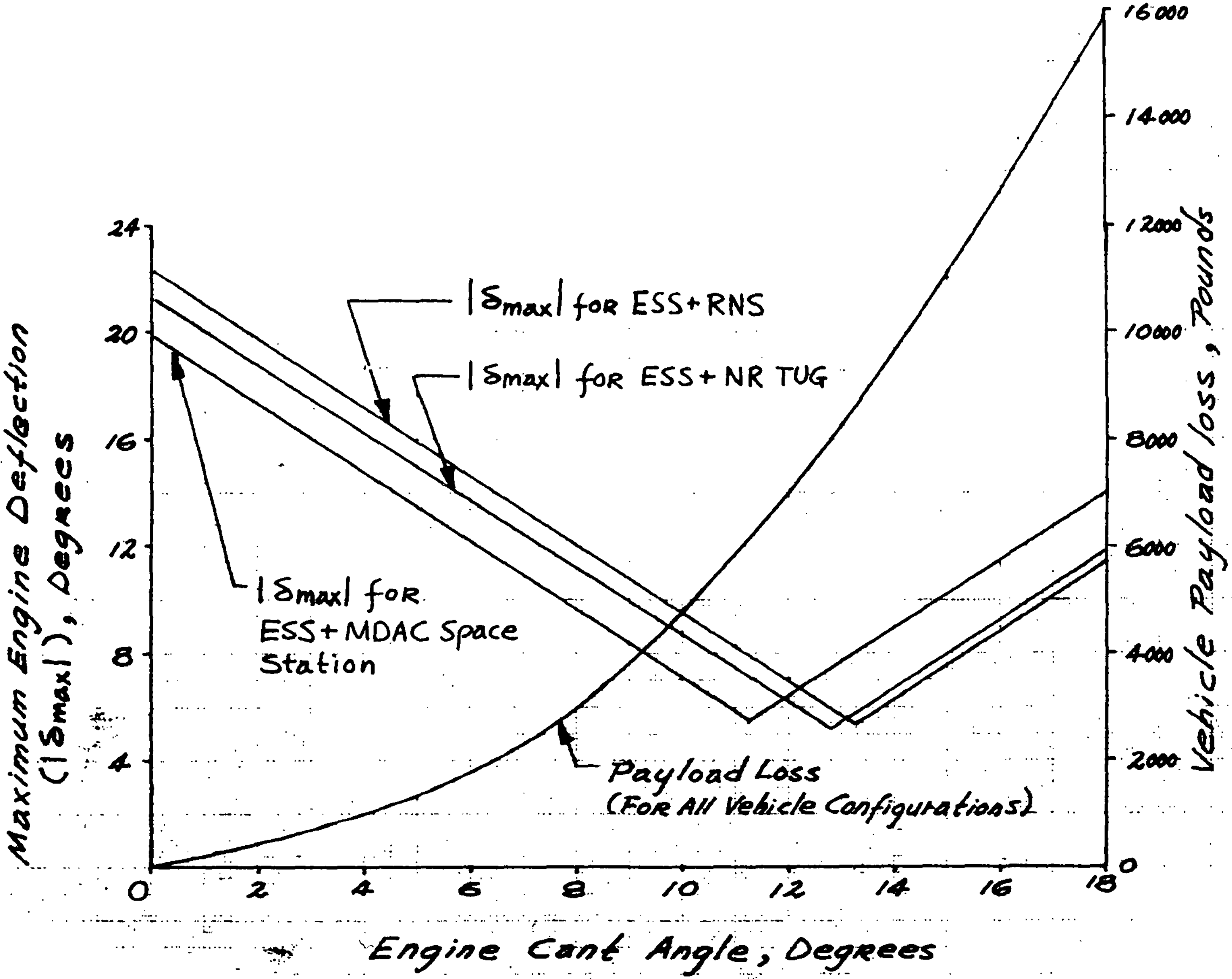

Figure 2-4. Engine Deflection Requirement and Vehicle Payload Loss versus Cant Angle

Table 2-1. ESS Flight Control Requirements*

Maximum Engine Deflection Requirement (Degrees)	Engine Cant Angle Requirement (Degrees)		
	MDAC Space Station	NR RNS	NR Tug
±6	11	13	13
±7	10	12	12
±8	9	11	11
±9	9	11	10
±10	8	10	9

* DESIGN RECOMMENDATION FOR ALL ABOVE ESS VEHICLE CONFIGURATIONS:

MAXIMUM ENGINE DEFLECTION REQUIREMENT = ± 7 DEGREES
(PROPOSED NOMINAL CAPABILITY OF ORBITER ENGINE)
ENGINE CANT ANGLE REQUIREMENT = 12 DEGREES

The vehicle payload penalties corresponding to these required cant angles range from 4800 to 7000 pounds (or 1.6 to 2.3 percent of the in-orbit ESS + payload vehicle weight) if no engine-deflection bias is provided. This payload penalty can be reduced to 2000 pounds if the engine deflection angle is biased by using a control signal to deflect the engine 6 degrees in the opposite direction to the cant angle during normal thrusting.

With the estimated 2 degrees pitch-axis deflection requirement, the maximum yaw-axis deflection capability of the proposed orbiter engine may be extended to ±8 degrees (see Equation 1). If the yaw-axis deflection requirement (δ_{max}) is set to match this extendable capability, the required cant angles for the three vehicle configurations examined can be reduced to 9 degrees, 11 degrees, 11 degrees, respectively. In this case, the payload penalties range from 3800 to 5800 pounds.

For the sake of design commonality, the recommended cant angle for all ESS vehicle configurations examined is 12 degrees. This recommendation is based on two reasons: (1) match the yaw-axis deflection requirement to the proposed nominal capability (±7 degrees) of the orbiter engine, and (2) compromise between conservation of control capability and minimization of payload penalty. Until further information on design tolerances and control-dynamic uncertainties are available, specifying the cant-angle requirement to fit the extended deflection capability is not recommended.

METHOD

The techniques for calculations of engine-deflection requirements and vehicle payload penalties as functions of cant angle are summarized below. The vehicle mass properties used for these calculations are tabulated in Table 2-2. In the calculations of δ_{max}, one of the orbiter engines is assumed to be inoperative.

Engine Deflection Requirement

The engine deflection requirement (δ_{max}) for each ESS + payload vehicle is determined by the following steps:

1. Calculate engine deflection δ_s for yaw-axis static trim:

$$\delta_s = 57.3 \left(\frac{\ell_b}{\ell_a}\right) \text{degrees}$$

$$\ell_a = X_{cg} - 44 \text{ inches}$$

$$\ell_b = 108 \text{ inches}$$

Table 2-2. ESS Vehicle Mass Properties

2 April, 1971

Engine Thrust Time	ESS Payload	ESS+ Payload Weight (lbs)	Vehicle Center Of Gravity (Inches)			Vehicle Moment Of Inertia (Slug-ft^2)		
			X_{cg}	Y_{cg}	Z_{cg}	I_{xx}	I_{yy}	I_{zz}
Beginning Burn ($t=0$)	NR Tug	861,000	444	0	0	0.7×10^6	32×10^6	32×10^6
	MDAC Space Station	861,000	493	0	0	1.6×10^6	45×10^6	45×10^6
	NR RNS	861,000	440	0	0	1.3×10^6	47×10^6	47×10^6
End Of Burn ($t=200$ Seconds)	NR Tug	304,000	713	0	0	0.7×10^6	22×10^6	22×10^6
	MDAC Space Station	304,000	898	0	0	1.5×10^6	27×10^6	27×10^6
	NR RNS	304,000	689	0	0	1.2×10^6	37×10^6	37×10^6

The results are plotted in Figure 2-5. The noted data points are used for δ_{max} calculation.

2. Calculate engine deflection δ_D for yaw-axis dynamic trim:

$$\delta_D = \left(\frac{I_{ZZ}}{NF \ell_a}\right) \dot{r} \text{ degrees}$$

N = 1 engine

F = 632,000 pounds thrust per engine

$\dot{r}$ = yaw-axis angular acceleration

The results are plotted in Figure 2-6. The noted data points are used for δ_{max} calculation.

3. Calculate the maximum engine deflection (δ_{max}) as function of cant angle (δ_{CT}) at the beginning and the end of engine thrusting:

$$\delta_{max} \text{ (beginning burn)} = (1 + 0.25)\ (\delta_{D1} + \delta_{S1} - \delta_{CT})$$

$$\delta_{max} \text{ (end of burn)} = (1 + 0.25)\ (-\delta_{D2} + \delta_{S2} - \delta_{CT})$$

where δ_s and δ_D are obtained from Figures 2-5 and 2-6. (See the noted data points in these figures.) The 25-percent safety factor is added to cover uncertainties such as structure compliance, thrust misalignments, and other design tolerances. The results of this calculation are plotted in Figures 2-7 through 2-9.

Finally the $|\delta_{max}|$ characteristics of Figure 2-4 are constructed by taking the maximum absolute values of the upper and lower curves (begin and end of burn) as shown in Figures 2-7 through 2-9.

Vehicle Payload Penalty

The vehicle payload penalty (ΔW) as function of engine cant angle (δ_{CT}) is calculated by the following equation:

$$\Delta W = W_f \left[1 - \left(\frac{W_o}{W_f}\right) \left(\frac{W_f}{W_o}\right) \frac{1}{\cos \delta_{CT}} \right]$$

where W_o and W_f are vehicle weights at the beginning and at the end of engine thrusting.

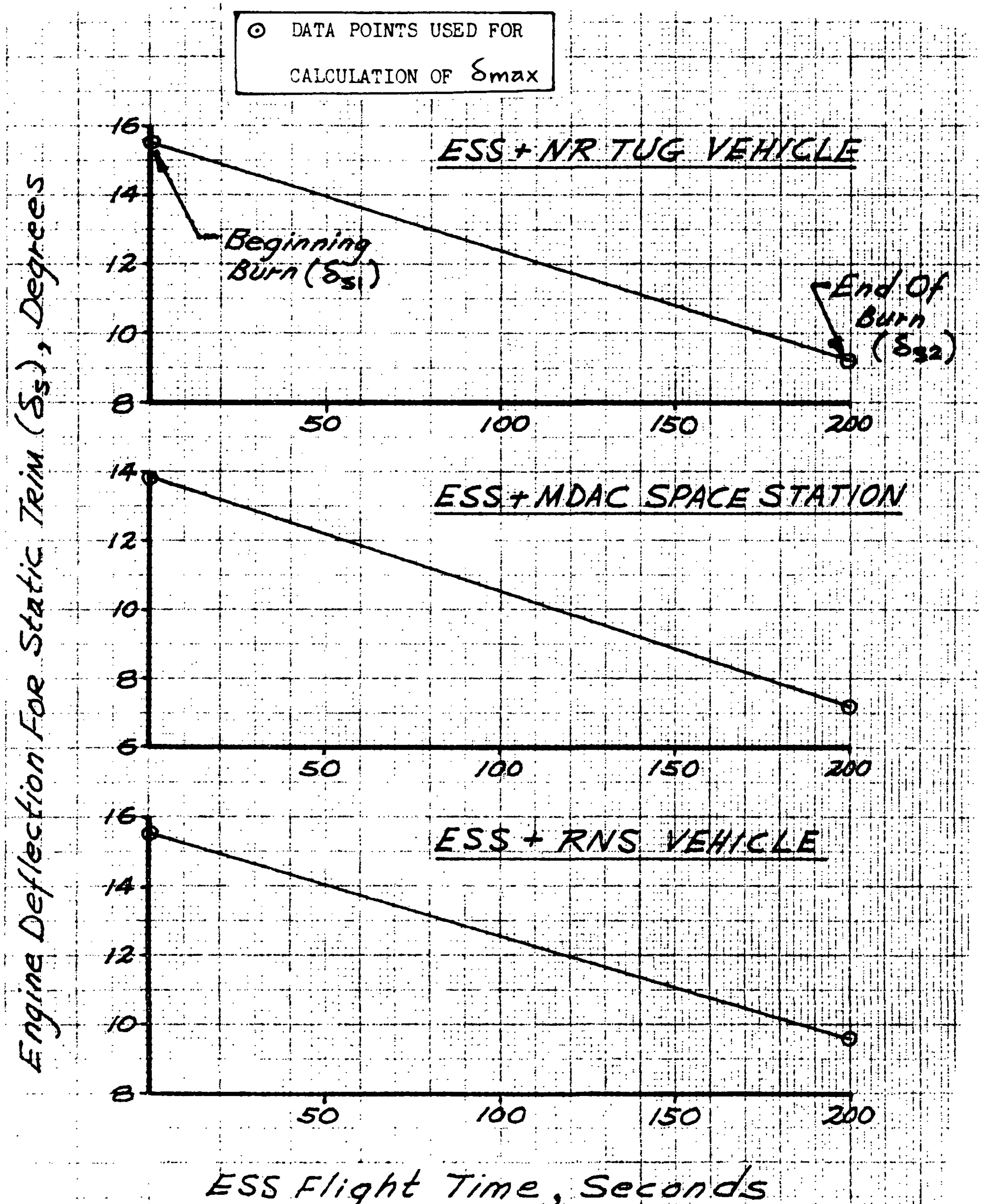

Figure 2-5. Engine Deflection for Static Trim (S_s)

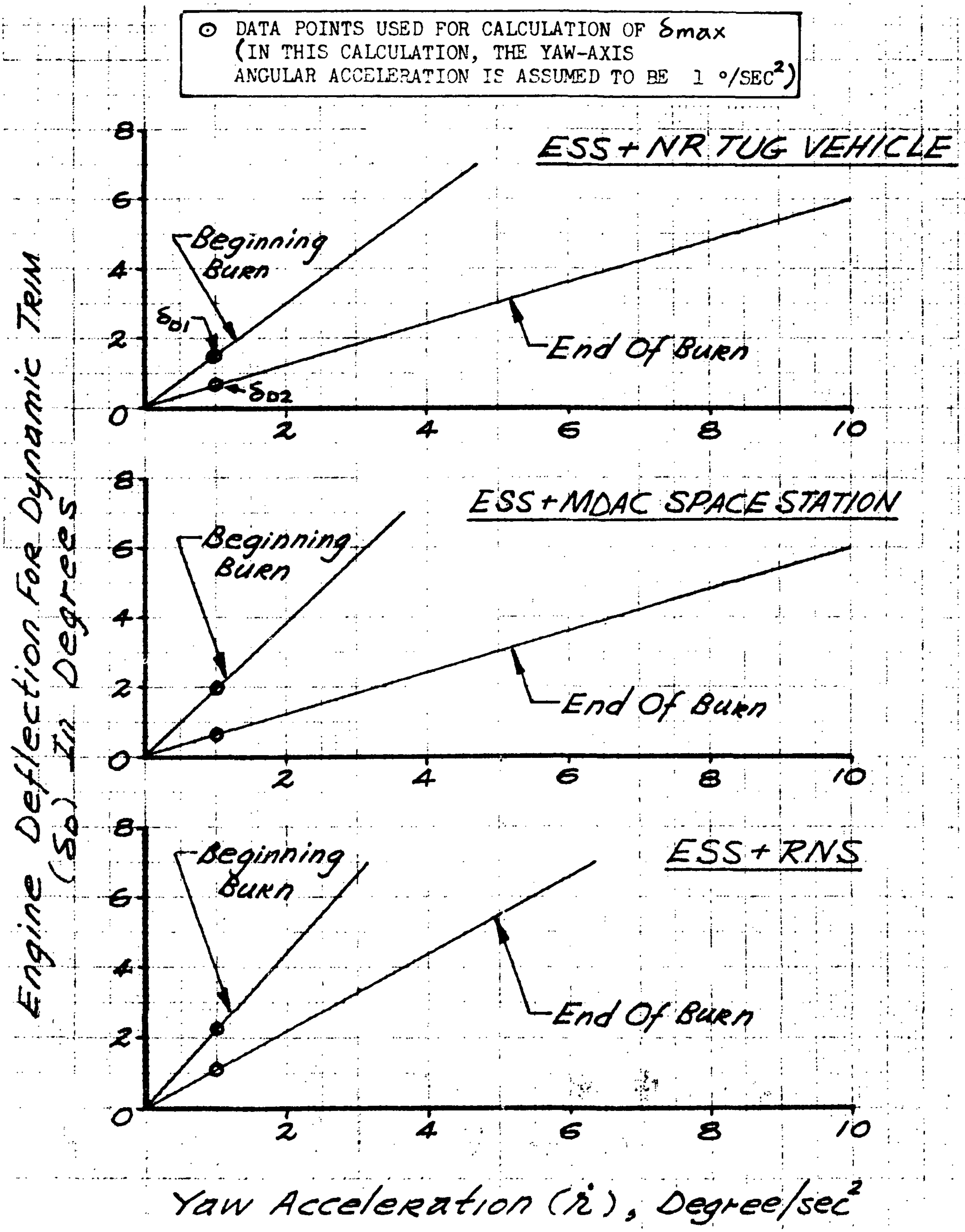

Figure 2-6. Engine Deflection for Dynamic Trim

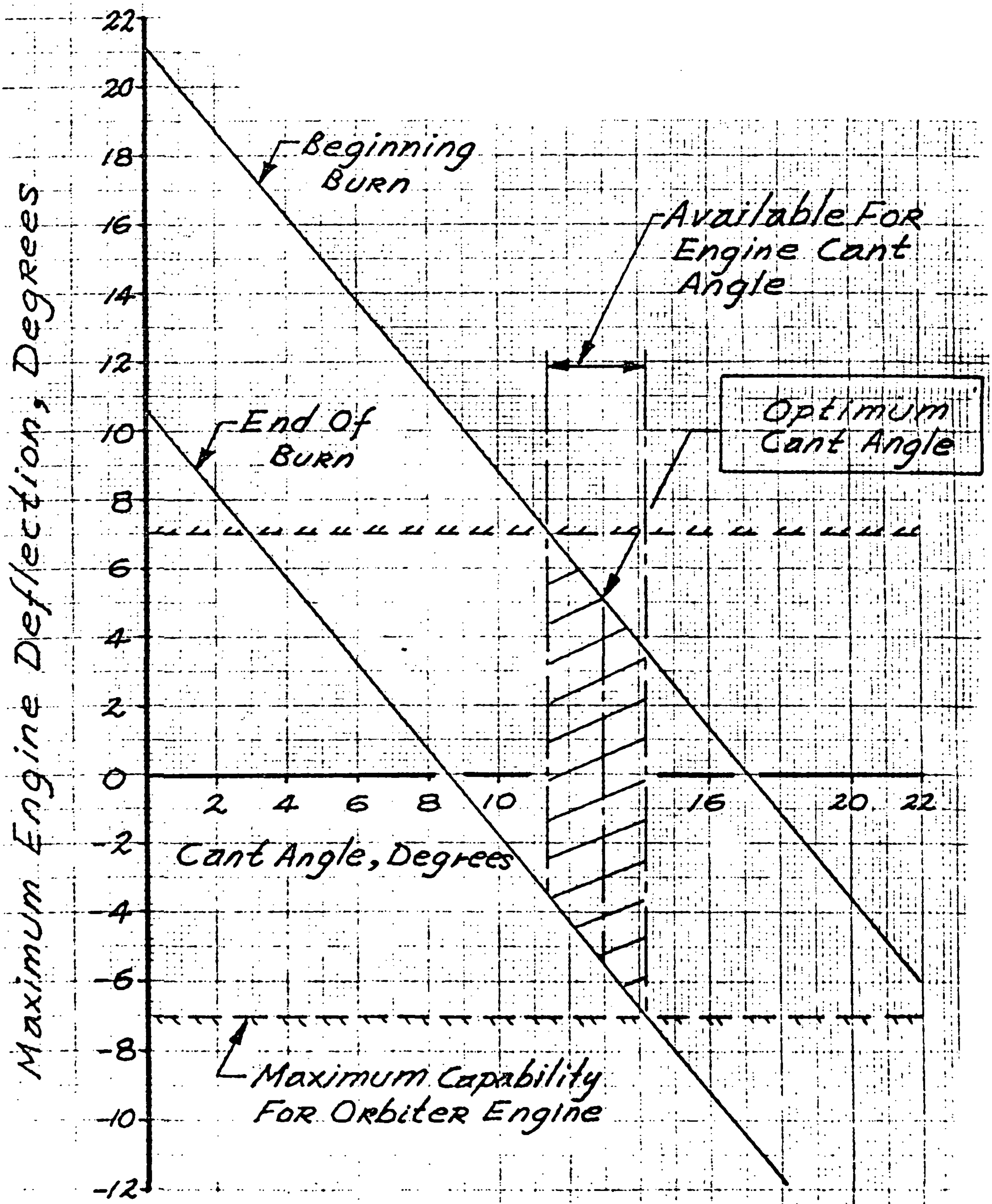

Figure 2-7. Engine Deflection Requirement versus Cant Angle (ESS+NR Tug Vehicle)

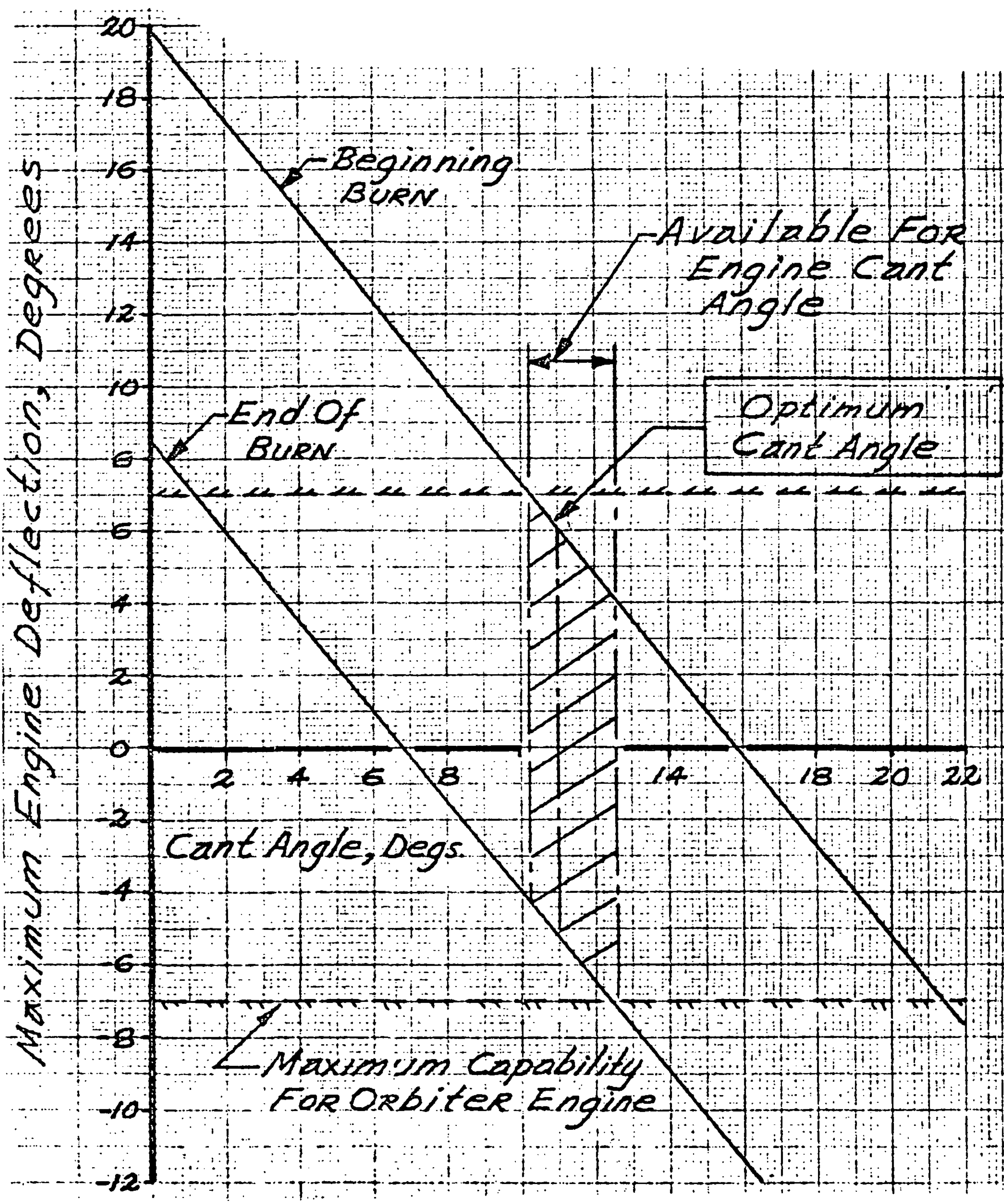

Figure 2-8. Engine Deflection Requirement versus Cant Angle (ESS+MDAC Space Station Vehicle)

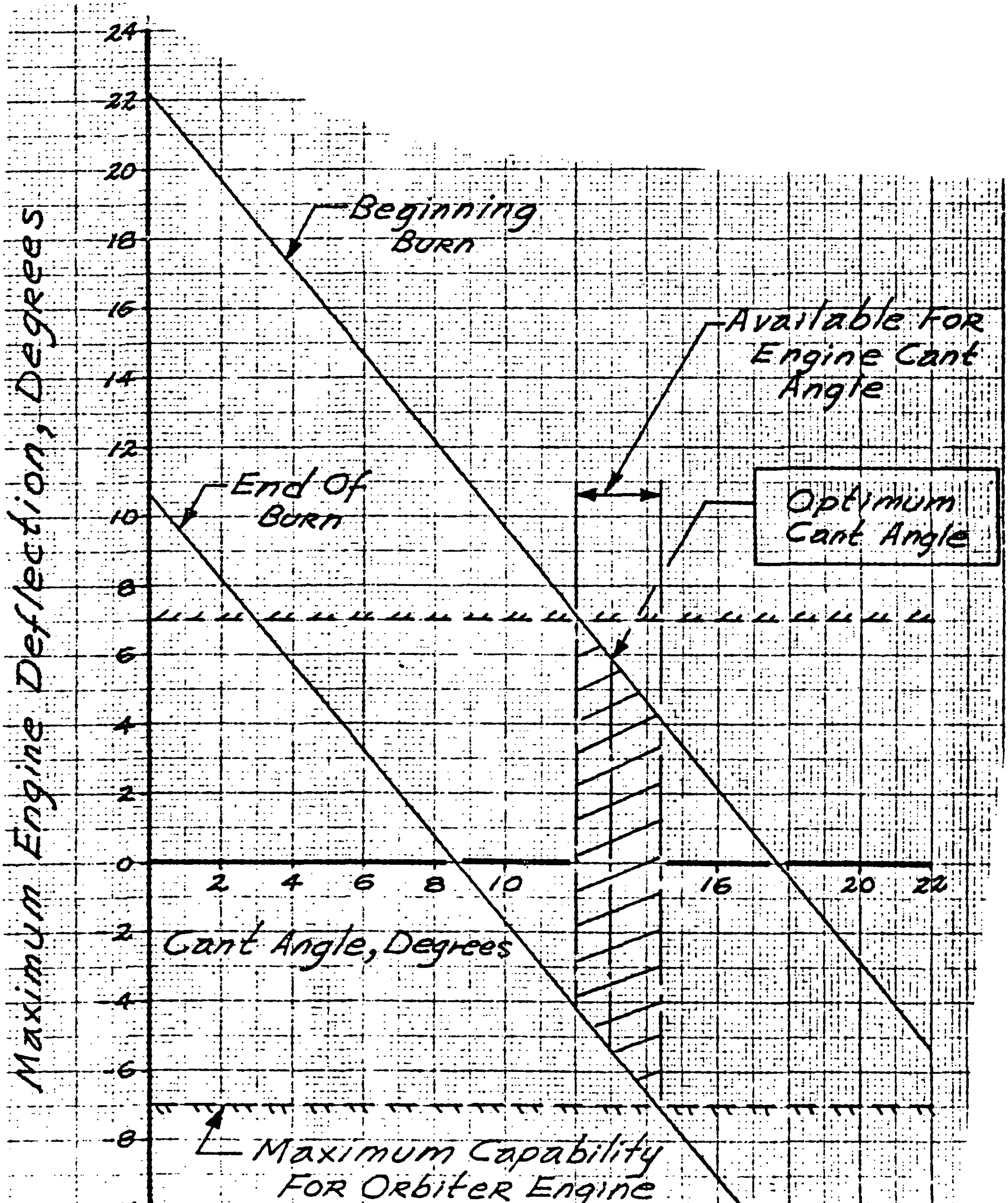

Figure 2-9. Engine Deflection Requirement versus Cant Angle (ESS+NR RNS Vehicle)

2.4 PROPELLANT FEED SYSTEM CHARACTERISTICS FOR DESIGN OF ESS PRESSURIZATION SYSTEM

A pressure drop analysis of the propellant feed system was performed utilizing the loss factors used in design of the shuttle orbiter feed system. The results are shown in Tables 2-3 through 2-5. Table 2-3 shows the pressure drop for nominal engine operation (6.0 mr, 100-percent thrust). Table 2-4 presents the pressure drop at 100-percent thrust for mixture ratio excursions. Table 2-5 shows the drop at emergency power level (109-percent thrust). While the drop for nominal engine operation should be used for baseline design the engine shall be capable of operating at off-nominal conditions, including emergency power level.

Thirteen inches has tentatively been selected as the diameter of both the LO_2 and LH_2 feed systems. While the use of thirteen inch diameter lines should be considered highly desirable to maintain shuttle compatibility the size may be changed if required by pressurization system design.

Table 2-3.

Pressure Drop at Nominal Engine Operation				
Line Size	12-in.	13-in.	14-in.	15-in.
LO_2	6.48 psi	4.69 psi	3.49 psi	2.62 psi
LH_2	3.65 psi	2.65 psi	1.96 psi	1.48 psi

Table 2-4.

Max. Pressure Drop at Off-Nominal Mixture Ratio (Max. LH_2 Drop at 5.5 to 1, LO_2 at 6.5 to 1)				
Line Size	12-in.	13-in.	14-in.	15-in.
LO_2	6.85 psi	4.96 psi	3.68 psi	2.80 psi
LH_2	4.27 psi	3.07 psi	2.29 psi	1.71 psi

Table 2-5.

Pressure Drop at Emergency Power Level				
Line Size	12-in.	13-in.	14-in.	15-in.
LO_2	7.39 psi	5.34 psi	3.97 psi	3.00 psi
LH_2	4.40 psi	3.16 psi	2.45 psi	1.80 psi

The analysis follows:

LH_2 FEED SYSTEM

1. DESIGN FLOW RATES

A. EMERGENCY POWER LEVEL (EPL)

EMR = 6.0

ISP = 456 SEC MIN

THRUST = 109% (632,200) = 689,100 LB

689,100 / 456 = 1511.2 LB/SEC

1/7 (1511.2 LB/SEC) = **215.9 LB/SEC**

B. NORMAL POWER LEVEL (NPL)

a) NOMINAL

EMR = 6.0

ISP = 459 SEC NOM

THRUST = 632,200 LB

632,200 / 459 = 1377.3 LB/SEC

1/7 (1377.3 LB/SEC) = **196.7 LB/SEC**

b) MAXIMUM

EMR = 5.5

ISP = 458 SEC MIN

THRUST = 632,200 LB

632,200 / 458 = 1380.4 LB/SEC

1/6.5 (1380.4) = **212.5 LB/SEC**

ρ_{LH_2} = 4.4 LB/FT³

Q IN FT³/SEC @ EPL = 215.9/4.4 = 49.07 FT³/SEC

@ NPL, NOM = 196.7/4.4 = 44.70 FT³/SEC

@ NPL, MAX = 212.5/4.4 = 48.30 FT³/SEC

2. LINE SIZES, VELOCITIES, DYNAMIC PRESS

A. SIZES

CONSIDER

Size	Area
9.58"	0.501 FT^2
12"	0.785 FT^2
13"	0.922 FT^2
14"	1.069 FT^2
15"	1.228 FT^2

B. VELOCITY

$V = Q/A$ FT/SEC

LINE SIZE →	9.58	12	13	14	15
@ EPL	96.03	62.51	53.22	45.90	39.96
@ NPL, NOM	87.48	56.94	48.48	41.81	36.40
@ NPL, MAX	94.52	61.53	52.39	45.18	39.33

C. DYNAMIC PRESSURE

$$q = \frac{1}{2g} \rho V^2 \left(\frac{1}{144}\right) \quad \text{PSI}$$

LINE SIZE →	9.58	12	13	14	15
@ EPL	4.38	1.85	1.34	1.00	.76
@ NPL, NOM	3.63	1.54	1.12	.83	.63
@ NPL, MAX	4.24	1.80	1.30	.97	.73

3. PRESSURE DROP PER FOOT

A. REYNOLDS NUMBER

$$N_{RE} = \frac{DV\rho}{\mu}$$

$\mu = 9.0 \times 10^{-6}$ LB/SEC-FT

$\rho = 4.4$ LB/FT^3

LINE SIZE	CASE	D, FT	V FT/SEC	DV	NRE
9.58	EPL	.798	96.03	76.63	3.746 × 10^7
9.58	NPL, NOM	.798	87.48	69.81	3.413
9.58	NPL, MAX	.798	94.52	75.43	3.688
12	EPL	1	62.51	62.51	3.056
12	NPL, NOM	1	56.94	56.94	2.784
12	NPL, MAX	1	61.53	61.53	3.008
13	EPL	1.083	53.22	57.64	2.818
13	NPL, NOM	1.083	48.48	52.50	2.567
13	NPL, MAX	1.083	52.39	56.74	2.774
14	EPL	1.167	45.90	53.57	2.619
14	NPL, NOM	1.167	41.81	48.79	2.385
14	NPL, MAX	1.167	45.18	52.73	2.578
15	EPL	1.25	39.96	49.95	2.442
15	NPL, NOM	1.25	36.40	45.50	2.224
15	NPL, MAX	1.25	39.33	49.16	2.403 × 10^7

B. TAKING f FROM CURVE

LINE SIZE	CASE	f	4f	4f/D	$\frac{1}{2}\rho V^2$	ΔP, PSI/FT
9.58	EPL	.00164	.00656	.00822	4.38	.0360
9.58	NPL, NOM	.00168	.00672	.00842	3.63	.0306
9.58	NPL, MAX	.00164	.00656	.00822	4.24	.0349
12	EPL	.00170	.00680	.00680	1.85	.0126
12	NPL, NOM	.00172	.00688	.00688	1.54	.0106
12	NPL, MAX	.00170	.00680	.00680	1.80	.0122
13	EPL	.00172	.00688	.00635	1.34	.00851
13	NPL, NOM	.00175	.00700	.00646	1.12	.00724
13	NPL, MAX	.00172	.00688	.00635	1.30	.00826
14	EPL	.00175	.00700	.00600	1.00	.00600
14	NPL, NOM	.00178	.00712	.00610	.83	.00506
14	NPL, MAX	.00175	.00700	.00600	.97	.00582
15	EPL	.00178	.00712	.00570	.76	.00433
15	NPL, NOM	.00180	.00720	.00576	.63	.00363
15	NPL, MAX	.00178	.00712	.00570	.73	.00416

4. SYSTEM DROP

A. CONFIGURATION

TANK OUTLET, $k = 0.5$
30° BEND $k = 0.1$
LENGTH, TANK-PVLV = 42" = 3.5 FT
PREVALVE $k = 0.6$
3 FLEX $k = 0.2$ EA
2 45° BENDS $k = 0.2$ EA
LENGTH, PVLV-ENG = 268" = 22.3 FT

UPSTREAM OF PREVALVE
3.5 FT + k OF 0.6
PREVALVE TO ENGINE
22.3 FT + k OF 1.6

B. PRESSURE DROP

a. EMERGENCY POWER LEVEL

	9.58"	12"	13"	14"	15"
TANK OUTLET	2.19	.93	.67	.50	.38
30° BEND	.44	.19	.13	.10	.08
LINE - TANK/PREVALVE	.13	.04	.03	.02	.02
SUBTOTAL	2.76	1.16	.83	.62	.48
PREVALVE	2.63	1.11	.80	.60	.46
3 FLEX JOINTS	2.63	1.11	.80	.60	.46
2 45° BENDS	1.75	.74	.54	.40	.30
LINE - PREVALVE/ENG	.80	.28	.19	.13	.10
SUBTOTAL	7.81	3.24	2.33	1.73	1.32
TOTAL	10.57	4.40	3.16	2.45	1.80

b. NORMAL POWER - NOMINAL

	9.58"	12"	13"	14"	15"
TANK OUTLET	1.82	.77	.56	.42	.32
30° BEND	.36	.15	.11	.08	.06
LINE - TANK/PREVALVE	.11	.04	.03	.02	.01
SUBTOTAL	2.29	.96	.70	.52	.39
PREVALVE	2.18	.92	.67	.50	.38
3 FLEX JOINTS	2.18	.92	.67	.50	.38
2 45° BENDS	1.45	.62	.45	.33	.25
LINE-PREVALVE/ENG	.68	.23	.16	.11	.08
SUBTOTAL	6.49	2.69	1.95	1.44	1.09
TOTAL	8.78	3.65	2.65	1.96	1.48

c. NORMAL POWER - MAX

	9.58	12	13	14	15
TANK OUTLET	2.12	.90	.65	.49	.37
30° BEND	.42	.18	.13	.10	.07
LINE - TANK/PREVALVE	.12	.04	.03	.02	.01
SUBTOTAL	2.66	1.12	.81	.61	.45
PREVALVE	2.54	1.08	.78	.58	.44
3 FLEX JOINTS	2.54	1.08	.78	.58	.44
2 45° BENDS	1.70	.72	.52	.39	.29
LINE - PREVALVE/ENG	.78	.27	.18	.13	.09
SUBTOTAL	7.56	3.15	2.26	1.68	1.26
TOTAL	10.22	4.27	3.07	2.29	1.71

LO_2 FEED SYSTEM

1. DESIGN FLOW RATES

   A. EMERGENCY POWER LEVEL

   $6/7\,(1511.2) = \underline{\underline{1295.3\ LB/SEC}}$

   B. NORMAL POWER LEVEL

   a) NOMINAL

   $6/7\,(1377.3) = \underline{\underline{1180.6\ LB/SEC}}$

   b) MAXIMUM

   EMR = 6.5

   ISP = 451 SEC MIN

   THRUST = 632,200 LB

   $632{,}200/451 = 1401.8\ LB/SEC$

   $1401.8\left(\frac{6.5}{7.5}\right) = \underline{\underline{1214.8\ LB/SEC}}$

$\rho_{LOX} = 71\ LB/FT^3$

Q IN FT^3/SEC

@EPL $1295.3/71 = 18.24\ FT^3/SEC$

@NPL, NOM $1180.6/71 = 16.63\ FT^3/SEC$

@NPL, MAX $1214.8/71 = 17.11\ FT^3/SEC$

2. LINE SIZES, VELOCITIES, DYNAMIC PRESS

   A. SIZES

CONSIDER	9.58"	AREA = 0.511 FT^2
	12"	0.785 FT^2
	13"	0.922 FT^2
	14"	1.069 FT^2
	15"	1.228 FT^2

B. VELOCITY

$V = Q/A$

LINE SIZE →	9.58	12	13	14	15
@ EPL	35.69	23.24	19.78	17.06	14.85
@ NPL, NOM.	32.54	21.18	18.04	15.56	13.54
@ NPL, MAX.	33.48	21.80	18.56	16.01	13.93

C. DYNAMIC PRESSURE

$$q = \frac{1}{2g} \rho V^2 \left(\frac{1}{144}\right) \quad \text{PSI}$$

LINE SIZE →	9.58	12	13	14	15
@ EPL	9.75	4.14	3.00	2.23	1.69
@ NPL, NOM	8.12	3.43	2.49	1.86	1.40
@ NPL, MAX	8.58	3.64	2.64	1.96	1.49

3. PRESSURE DROP PER FOOT

A. REYNOLDS NUMBER

$$N_{RE} = \frac{DV\rho}{\mu} \qquad \mu = 130 \times 10^{-6} \text{ LB/SEC-FT}$$

$$\rho = 71 \text{ LB/FT}^3$$

(TO NEXT SHEET)

LINE SIZE	CASE	D, FT	V, FT/SEC	DV	NRe
9.58	EPL	.798	35.69	28.48	1.555×10^7
9.58	NPL, NOM	.798	32.54	25.97	1.428
9.58	NPL, MAX	.798	33.48	26.72	1.459
12	EPL	1	23.24	23.24	1.269
12	NPL, NOM	1	21.18	21.18	1.157
12	NPL, MAX	1	21.80	21.80	1.191
13	EPL	1.083	19.78	21.42	1.170
13	NPL, NOM	1.083	18.04	19.54	1.067
13	NPL, MAX	1.083	18.56	20.10	1.098
14	EPL	1.167	17.06	19.91	1.087
14	NPL, NOM	1.167	15.56	18.16	.992
14	NPL, MAX	1.167	16.01	18.68	1.020
15	EPL	1.25	14.85	18.56	1.014
15	NPL, NOM	1.25	13.54	16.93	.924
15	NPL, MAX	1.25	13.93	17.41	$.951 \times 10^7$

B. TAKING f FROM CURVE

LINE SIZE	CASE	f	4f	4f/D	$\frac{1}{2}\rho V^2$	ΔP, PSI/FT
9.58	EPL	.00190	.00760	.009524	9.75	.09286
9.58	NPL, NOM	.00194	.00776	.009724	8.12	.07896
9.58	NPL, MAX	.00193	.00772	.009674	8.58	.08300
12	EPL	.00198	.00792	.007920	4.14	.03279
12	NPL, NOM	.00201	.00804	.008040	3.43	.02758
12	NPL, MAX	.00200	.00800	.008000	3.64	.02912
13	EPL	.00201	.00804	.007424	3.00	.02227
13	NPL, NOM	.00204	.00816	.007535	2.49	.01876
13	NPL, MAX	.00203	.00812	.007498	2.64	.01979
14	EPL	.00203	.00812	.006958	2.23	.01552
14	NPL, NOM	.00207	.00828	.007095	1.86	.01320
14	NPL, MAX	.00206	.00824	.007061	1.96	.01384
15	EPL	.00206	.00824	.006592	1.69	.01114
15	NPL, NOM	.00209	.00836	.006688	1.40	.009363
15	NPL, MAX	.00208	.00832	.006656	1.49	.009917

4. SYSTEM DROP

A. CONFIGURATION

TANK OUTLET , $k = 0.5$
PREVALVE , $k = 0.6$
90° BEND , $k = 0.3$
2 FLEX , $k = 0.2$ EA $\quad \Sigma k = 1.8$
LENGTH = 128" = 10.7 FT

B. PRESSURE DROP

a. EMERGENCY POWER LEVEL

	9.58"	12"	13"	14"	15"
TANK OUTLET	4.88	2.07	1.50	1.12	.85
PREVALVE	5.85	2.48	1.80	1.34	1.01
90° BEND	1.95	.83	.60	.45	.34
2 FLEX	3.90	1.66	1.20	.89	.68
LINE	.99	.35	.24	.17	.12
TOTAL	17.57	7.39	5.34	3.97	3.00

b. NORMAL POWER LEVEL - NOMINAL

	9.58	12	13	14	15
TANK OUTLET	4.06	1.72	1.25	.93	.70
PREVALVE	4.87	2.06	1.49	1.12	.84
90° BEND	2.44	1.03	.75	.56	.42
2 FLEX	3.25	1.37	1.00	.74	.56
LINE	.84	.30	.20	.14	.10
TOTAL	15.46	6.48	4.69	3.49	2.62

C. NORMAL POWER LEVEL - MAXIMUM

	9.58	12	13	14	15
TANK OUTLET	4.29	1.82	1.32	.98	.75
PREVALVE	5.15	2.18	1.58	1.18	.89
90° BEND	2.57	1.09	.79	.59	.45
2 FLEX	3.43	1.45	1.06	.78	.60
LINE	.89	.31	.21	.15	.11
TOTAL	16.33	6.85	4.96	3.68	2.80

2.5 ESS STABILITY AND CONTROL REQUIREMENTS

Data, information, and definitions used in the ESS stability and control analyses are presented below. Included are a list of Nomenclature, Coordinate System Definitions and Descriptions, Flight Dynamics Equations and Data, Guidance and Control System Information, Engine System Dynamics Information, and a Bibliography.

2.5.1 NOMENCLATURE

2.5.1.1 Parameters

Symbol	Designation	Units
A	Acceleration	ft/sec^2
A	Actuator	-
a	Control System Gain Factor	deg/deg or deg/deg/sec
d	Pitch Axis Body Bending Displacement	ft
e	Yaw Axis Body Bending Displacement	ft
F	Thrust Level	lb
F	Transfer Function	ND
f	Fluid Level	sta-inches
f	Natural Frequency	cycles/sec
g.	Acceleration of Gravity	ft/sec^2
i	Current	Milliamperes
I	Moment of Inertia	$slug\text{-}ft^2$
J	Torsional Moment of Inertia	$Slug\text{-}ft^2$

Symbol	Designation	Units
K	Scale Factor	TBD
l	Distance	ft
L	Torques about X-Axis	ft-lb
M	Torques about Y-Axis	ft-lb
N	Torques abouts Z-Axis	ft-lb
M	Mass	slugs
n	Number of Engines	ND
p	Body Rate about X-Axis	deg/sec
q	Body Rate y-Axis	deg/sec
Q	Generalized Pitch Axis Bending Force	
r	Body Rate Z-Axis	deg/sec
R	Generalized Yaw Bending Force	
S	Laplace Operator	sec
U	Elastic Displacement	ft or deg
U	Linear Velocity - X-Axis	ft sec
U	Linear Velocity - Y-Axis	ft/sec
V	Voltage Variable	volts
W	Linear Velocity Z-Axis	ft/sec
X, Y, Z	Right Hand Coordinate System Displacement	ft
Y	Bending Model Shape	ft/ft
Y	Bending Model slope	deg/ft

Symbol	Designation	Units
δ	Control Engine Deflection	deg
Δ	Slosh Mass Deflection	ft
Γ	Scale factor to Convert Slosh SMS Deflection to Wave Deflection at Tank Wall	ND
θ	Torsional Displacement	deg
ξ	Slosh Wave Height at Wall	ft
ζ	Damping Ratio	ND
χ	Guidance Commands Inertial Angles	deg
ϕ, θ, ψ	Euler Angles	deg
θ	Torsional Modal Displacement	deg
ω	Natural Frequency	rad/sec

2.5.1.2 Subscripts

Symbol	Designation
B	Booster
C	Command
ct	Cant Angle
e	Error; Engine
f	Fluid Level
H	Hydrogen
i	i^{th} mode of a flexiblity model
I	Inertial

Symbol	Designation
O	Oxygen
o	Reference Value; Initial Value

2.5.1.3 Acronyms

Acronym	Meaning
ACPS	Attitude Control Propulsion System
CG	Center of Gravity
ESS	Expendable Second Stage
IU	Instrument Unit
MDAC	McDonnell Douglas Aircraft Company
MPS	Main Propulsion System
NR	North American Rockwell Corporation
ORB	Orbital Engine
RNS	Re-usable Nuclear Shuttle
SMS	Spring Mass System

2.5.2 SYSTEM DESCRIPTION AND AXES SYSTEM

2.5.2.1 Description

The Expendable Section Stage (ESS) is used for orbital missions and is basically a Saturn V S-II stage with new propulsion system, new payloads and with shuttle technology guidance and control subsystem. A sketch of the ESS is shown in Figure 2-1. Instead of the S-IC stage, the Shuttle Booster is used as the first stage booster. Instead of the S-IV-B plus Apollo spacecraft payload, different payloads are placed on top of the stage for earth orbital insertion. The baseline ESS configuration for analysis has a space station payload.

After separation from the Shuttle Booster, the ESS is propelled to earth orbital velocity by two orbiter engines. This phase is second stage main-stage boost. During this phase, guidance and control signals are calculated and used to position the orbiter engines for mainstage control. During the orbital operation phase, guidance and control signals are used to either position the orbital maneuvering system (OMS) engines or to fire RCS jets.

After the orbital mission has ended, the ESS is safely disposed in the ocean with a de-orbit system.

2.5.2.2 Axes Systems

2.5.2.2.1 Launch Point Ground Axes

The launch point ground axes system is fixed to the launch site and is used to align the ESS guidance system. Since the distances are small between the origin of the launch point ground axes, the vehicular gimbal plane and location of the inertial platform, the origin of the ground axes system will be assumed to coincide with the gimbal plane at launch. Because this axes system is fixed to the launch site, it will move through space as the earth moves. However, for the purpose of stability and control analysis, the earth will be assumed fixed in space and the launch pointground axes system will be assumed to be an inertial system.

2.5.2.2.2 Inertial Axes

The inertial axes system is designated by X_e, Y_e, and Z_e, and is defined as a system where Newton's laws of motion are valid. The stabilized guidance platform is an inertial system and is aligned with the launch point ground axes prior to launch.

2.5.2.2.3 Body Axes System

The body axes system is designated by X, Y, and Z. The body axes system translates and rotates with the vehicle during flight. Figure 2-10 depicts the body axes system. The origin of the body axes system is at the engine gimbal plane. The X-axis is along the ESS center line and is positive toward the nose. The orientation of the Y and Z are shown in Figure 2-10. The Y-axis is parallel to position III and the Z-axis is parallel to position IV.

2.5.3 FLIGHT DYNAMICS

2.5.3.1 General Remarks

For purposes of flight dynamics analysis, the ESS flight is divided into two phases: ascent boost to orbital velocity and orbital operational phase. This section of the manual presents data and equations applicable for either

REFERENCES: 1, 6, 8

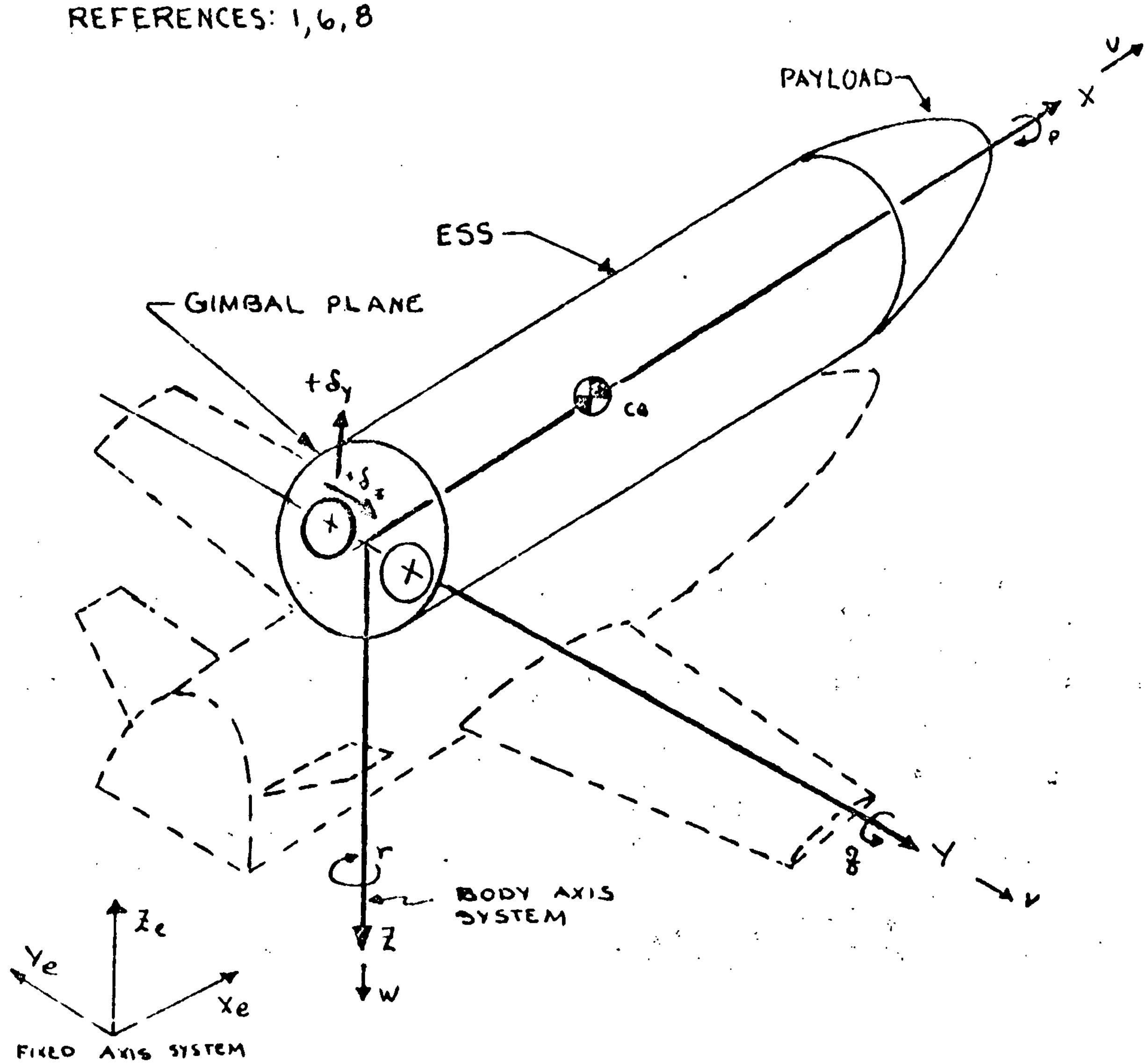

Figure 2-10. Axes System

one of the two phases or for both phases. These data are properly designated with respect to flight phase in those sections of the manual that describe the data.

Linearized perturbation equations are given for flight dynamic stability studies. Data are presented which describes the ESS mass properties, flexibility characteristics and slosh dynamics (g-field model). At the time of this publication a "zero-g" slosh model has not been developed for ESS orbital operational flight dynamic studies.

The dynamics of both liquid propellant sloshing and vehicular flexibility are expressed in terms of generalized spring mass system (SMS). The generalized deflection of the SMS may be corrected to slosh wave displacement or to an elasticity displacement by using the proper scale factors (Γ, θ_i, Y_i) indicated by Equations (3-78) through (3-72).

2.5.3.2 Perturbation Equations

The linear perturbation equations presented in this section are for use in flight dynamic studies at fixed points in the flight. These perturbation equations are applicable during ascent control or orbital operation phase when the orbiter engine and the OMS engines are used.

Because of the axially symmetrical geometry of the ESS stage, adequate control system design may be achieved through separate analysis of each degree of freedom.

Perturbation equations representing vehicular motion are given for the pitch, yaw and roll axis in subsequent paragraphs.

2.5.3.2.1 Pitch Plane Perturbation Equation

The equation matrix presented in Table 2-6 is to be used for pitch plane control system studies. The equations represent the linearized dynamics of pitch plane rigid body motion coupled with linear models for propellant sloshing and body bending. These linear models are made up of two slosh (one LO_2 and one LH_2) and three body bending modes. The coefficients in the matrix are evaluated from auxiliary Equations 3-2 through 3-29. Note that in these equations, i = 1, 2, 3. The matrix equation and auxiliary equations are basically the same equations in Reference

2.5.3.2.2 Yaw Plane Perturbation Equations

The equation Matrix shown in Table 2-7 is for use in yaw plane control system studies. The equations represent linearized rigid body dynamics coupled with linear models for sloshing and body bending. These linear models are made up of two slosh modes: one LO_2 and one LH_2 and three bending modes (i = 1, 2, 3). The coefficients in the matrix are calculated from auxiliary Equations 3-31 through 3-54. Note that in these equations, the subscript i varies from 1 through 3 for the 3 bending modes.

Table 2-6. Pitch Plane Perturbation Dynamics Matrix-Equation 3-1

	θ (DEG)	θ_{IU} (DEG)	d_1 (FT)	d_2 (FT)	d_3 (FT)	Δ_0 (FT)	Δ_H (FT)		δ_Y (DEG)
PITCH MOMENT	S^2	0	$M_{\ddot{d}_1}S^2+M_{d1}$	$M_{\ddot{d}_2}S^2+M_{d2}$	$M_{\ddot{d}_3}S^2+M_{d3}$	$M_{\ddot{\Delta}_0}S^2+M_{\Delta 0}$	$M_{\ddot{\Delta}_H}S^2+M_{\Delta H}$		$M_{\ddot{\delta}}S^2+M_{\delta}$
ATTITUDE AT IU	-1	1	$-Y'_{IU1}$	$-Y'_{IU2}$	$-Y'_{IU3}$	0	0		0
BENDING MODE 1	$Q_{\ddot{\theta}1}S^2$	0	$(1+\frac{m_{g1}}{m})S^2 +2\zeta_1\omega_{m1}S +\omega_{m1}^2-\omega_{1e}^2$	$Q_{12}S^2$	$Q_{13}S^2$	$Q_{1\ddot{\Delta}_0}S^2$	$Q_{1\ddot{\Delta}_H}S^2$	=	$Q_{\ddot{\delta}1}S^2+Q_{\delta 1}$
BENDING MODE 2	$Q_{\ddot{\theta}2}S^2$	0	$Q_{21}S^2$	$(1+\frac{m_{g2}}{m})S^2 +2\zeta_2\omega_{m2}S +\omega_{m2}^2-\omega_{2e}^2$	$Q_{23}S^2$	$Q_{2\ddot{\Delta}_0}S^2$	$Q_{2\ddot{\Delta}_H}S^2$		$Q_{\ddot{\delta}2}S^2+Q_{\delta 2}$
BENDING MODE 3	$Q_{\ddot{\theta}3}S^2$	0	$Q_{31}S^2$	$Q_{32}S^2$	$(1+\frac{m_{g3}}{m})S^2 +2\zeta_3\omega_{m3}S +\omega_{m3}^2-\omega_{3e}^2$	$Q_{3\ddot{\Delta}_0}S^2$	$Q_{3\ddot{\Delta}_H}S^2$		$Q_{\ddot{\delta}3}S^2+Q_{\delta 3}$
LOX SLOSH	$A_{0\ddot{\theta}}S^2$	0	$A_{\ddot{d}1}S^2+A_{d1}$	$A_{\ddot{d}2}S^2+A_{d2}$	$A_{\ddot{d}3}S^2+A_{d3}$	$S^2+2\zeta_0\omega_0 S +\omega_0^2$	$-\frac{m_0 S^2}{m}$		$A_{\ddot{\delta}}S^2+A_{\delta}$
LH2 SLOSH	$A_{H\ddot{\theta}}S^2$	0	$A_{\ddot{d}1}S^2+A_{d1}$	$A_{\ddot{d}2}S^2+A_{d2}$	$A_{\ddot{d}3}S^2+A_{d3}$	$-\frac{m_H S^2}{m}$	$S^2+2\zeta_H\omega_H S +\omega_H^2$		$A_{\ddot{\delta}}S^2+A_{\delta}$

AUXILIARY EQUATIONS

PITCH PLANE

$$M_\delta = +2F\ell_{cg}/I_{YY} \qquad (3\text{-}2)$$

$$M_{\ddot{\delta}} = +2(m_e \ell_e \ell_{cg} + I_e)/I_{YY} \qquad (3\text{-}3)$$

$$M_{d_i} = 2F\ell_{cg} Y'_{ei}/I_{YY} \qquad (3\text{-}4)$$

$$M_{\ddot{d}_i} = 2\left[Y'_{ei}(m_e \ell_e \ell_{cg} + I_e) - Y_{ei} m_e(\ell_e + \ell_{cg})\right]/I_{YY} \qquad (3\text{-}5)$$

$$M_{\Delta_o} = A_x m_o/I_{YY} \qquad (3\text{-}6)$$

$$M_{\ddot{\Delta}_o} = m_o(\ell_{cg} - X_o)/I_{YY} \qquad (3\text{-}7)$$

$$M_{\Delta_H} = A_x m_H/I_{YY} \qquad (3\text{-}8)$$

$$M_{\ddot{\Delta}_H} = m_H(\ell_{cg} - X_H)/I_{YY} \qquad (3\text{-}9)$$

$$Q_{\ddot{\theta}i} = -2m_e \ell_{cg} Y_{ei}/m_i \qquad (3\text{-}10)$$

$$m_{ei} = 2m_e Y_{ei}\left(Y_{ei} - 2m_e Y_{ei}/m + 2m_e \ell_{cg} Y'_{ei}/m - Y'_{ei}\ell_e\right) \qquad (3\text{-}11)$$

$$\omega_i^2 = \omega_{m_i}^2 - \omega_{ei}^2 \qquad (3\text{-}12)$$

$$\omega_{ei}^2 = 2F Y_{ei} Y'_{ei}(1 - 2m_e/m)/m_i \qquad 3\text{-}13$$

CROSS-COUPLING COEFFICIENTS

$$Q_{12} = 2 m_e Y_{e1} Y_{e2} / m_1 \quad (3-14)$$

$$Q_{13} = 2 m_e Y_{e1} Y_{e3} / m_1 \quad (3-15)$$

$$Q_{21} = 2 m_e Y_{e2} Y_{e1} / m_2 \quad (3-16)$$

$$Q_{23} = 2 m_e Y_{e2} Y_{e3} / m_2 \quad (3-17)$$

$$Q_{31} = 2 m_e Y_{e3} Y_{e1} / m_3 \quad (3-18)$$

$$Q_{32} = 2 m_e Y_{e3} Y_{e2} / m_3 \quad (3-19)$$

ENGINE DEFLECTION AND i^{th} BENDING MODE

$$Q_{i\ddot{\delta}} = -2 m_e \ell_e Y_{ei} (1 - 2 m_e / m) / m_i \quad (3-20)$$

$$Q_{i\delta} = -2 F Y_{ei} (1 - 2 m_e / m) / m_i \quad (3-21)$$

BODY BENDING AND SLOSH

$$Q_{i\ddot{\Delta}_0} = 2 Y_{ei} m_e m_0 / m m_i \quad (3-22)$$

$$Q_{i\ddot{\Delta}_H} = 2 Y_{ei} m_e m_H / m m_i \quad (3-23)$$

SLOSH COEFFICIENTS

$$A_{0\ddot{\theta}} = -(\ell_{cg} - X_0) \quad (3-24)$$

$$A_{H\ddot{\theta}} = -(\ell_{cg} - X_H) \quad (3-25)$$

$$A_{\delta} = -2F/\mathcal{M} \qquad (3\text{-}26)$$

$$A_{\ddot{\delta}} = -2\, m_e \ell_e/\mathcal{M} \qquad (3\text{-}27)$$

$$A_{di} = -A_x Y'_{ei} \qquad (3\text{-}28)$$

$$A_{\ddot{d}i} = 2 m_e \left(Y_{ei} - \ell_e Y'_{ei} \right)/\mathcal{M} \qquad (3\text{-}29)$$

Table 2-7. Yaw Plane Perturbation Dynamics Matrix

	ψ (DEG)	ψ_{IU} (DEG)	e_1 (FT)	e_2 (FT)	e_3 (FT)	Δ_o (FT)	Δ_H (FT)		δ_z (DEG)
YAW MOMENT	S^2	0	$N_{\ddot{e}1}S^2+N_{e1}$	$N_{\ddot{e}2}S^2+N_{e2}$	$N_{\ddot{e}3}S^2+N_{e3}$	$N_{\ddot{\Delta}o}S^2+N_{\Delta o}$	$N_{\ddot{\Delta}H}S^2+N_{\Delta H}$		$N_{\ddot{\delta}}S^2+N_{\delta}$
ATTITUDE AT IU	-1	1	$-Y'_{IU1}$	$-Y'_{IU2}$	$-Y'_{IU3}$	0	0		0
BENDING MODE 1	$R_{\ddot{\psi}1}S^2$	0	$(1+\frac{m_{e1}}{m})S^2+2\zeta_1\omega_{m1}S+\omega_{m1}^2$	$R_{12}S^2$	$R_{13}S^2$	$R_{1\ddot{\Delta}o}S^2$	$R_{1\ddot{\Delta}H}S^2$	=	$R_{\ddot{\delta}1}S^2+R_{\delta 1}$
BENDING MODE 2	$R_{\ddot{\psi}2}S^2$	0	$R_{21}S^2$	$(1+\frac{m_{e2}}{m})S^2+2\zeta_2\omega_{m2}S+\omega_{m2}^2$	$R_{23}S^2$	$R_{2\ddot{\Delta}o}S^2$	$R_{2\ddot{\Delta}H}S^2$		$R_{\ddot{\delta}2}S^2+R_{\delta 2}$
BENDING MODE 3	$R_{\ddot{\psi}3}S^2$	0	$R_{31}S^2$	$R_{32}S^2$	$(1+\frac{m_{e3}}{m})S^2+2\zeta_3\omega_{m3}S+\omega_{m3}^2$	$R_{3\ddot{\Delta}o}S^2$	$R_{3\ddot{\Delta}H}S^2$		$R_{\ddot{\delta}3}S^2+R_{\delta 3}$
LOX SLOSH	$A_{o\ddot{\psi}}S^2$	0	$A_{\ddot{e}1}S^2+A_{e1}$	$A_{\ddot{e}2}S^2+A_{e2}$	$A_{\ddot{e}3}S^2+A_{e3}$	$S^2+2\zeta_o\omega_oS+\omega_o^2$	$-\frac{m_o}{m}S^2$		$A_{\ddot{\delta}}S^2+A_{\delta}$
LH2 SLOSH	$A_{H\ddot{\psi}}S^2$	0	$A_{\ddot{e}1}S^2+A_{e1}$	$A_{\ddot{e}2}S^2+A_{e2}$	$A_{\ddot{e}3}S^2+A_{e3}$	$-\frac{m_H}{m}S^2$	$S^2+2\zeta_H\omega_HS+\omega_H^2$		$A_{\ddot{\delta}}S^2+A_{\delta}$

YAW PLANE

$$N_{\delta} = +2\, F \ell_{cg} / I_{zz} \tag{3-31}$$

$$N_{\ddot{\delta}} = +2\left(m_e \ell_e \ell_{cg} + I_e\right) / I_{zz} \tag{3-32}$$

$$N_{e_i} = 2\, F \ell_{cg}\, Y'_{ei} / I_{zz} \tag{3-33}$$

$$N_{\ddot{e}_i} = 2\left[Y'_{ei}\left(m_e \ell_e \ell_{cg} + I_e\right) - Y_{ei} m_e \left(\ell_e + \ell_{cg}\right)\right] / I_{zz} \tag{3-34}$$

$$N_{\Delta o} = A_x m_o / I_{zz} \tag{3-35}$$

$$N_{\ddot{\Delta} o} = m_o \left(\ell_{cg} - X_o\right) / I_{zz} \tag{3-36}$$

$$N_{\Delta H} = A_x m_H / I_{zz} \tag{3-37}$$

$$N_{\ddot{\Delta}_H} = m_H \left(\ell_{cg} - X_H\right) / I_{zz} \tag{3-38}$$

$$R_{\ddot{\psi}_i} = -2\, m_e \ell_{cg} Y_{ei} / m_i \tag{3-39}$$

$$m_{ei} = 2\, m_e Y_{ei}\Big(Y_{ei} - 2\, m_e Y_{ei} / m + 2\, m_e \ell_{cg} Y'_{ei} / m - Y'_{ei} \ell_e\Big) \tag{3-40}$$

$$\omega_i^2 = \omega_{mi}^2 - \omega_{ei}^2 \tag{3-41}$$

$$\omega_{ei}^2 = 2F\, Y_{ei} Y'_{ei} (1 - 2m_e/m)/m_i \tag{3-42}$$

CROSS-COUPLING COEFFICIENTS - BENDING

$$R_{12} = 2m_e Y_{e1} Y_{e2}/m_1 \tag{3-43}$$

$$R_{13} = 2m_e Y_{e1} Y_{e3}/m_1 \tag{3-44}$$

$$R_{21} = 2m_e Y_{e2} Y_{e1}/m_2 \tag{3-45}$$

$$R_{23} = 2m_e Y_{e2} Y_{e3}/m_2 \tag{3-46}$$

$$R_{31} = 2m_e Y_{e3} Y_{e1}/m_3 \tag{3-47}$$

$$R_{32} = 2m_e Y_{e3} Y_{e2}/m_3 \tag{3-48}$$

ENGINE DEFLECTION AND i^{th} BENDING MODE

$$R_{i\ddot{\delta}} = -2m_e \ell_e Y_{ei} (1 - 2m_e/m)/m_i \tag{3-49}$$

$$R_{i\delta} = -2F\, Y_{ei} (1 - 2m_e/m)/m_i \tag{3-50}$$

BODY BENDING AND SLOSH

$$R_{i\ddot{\Delta}_0} = 2Y_{ei}\, m_e m_0/m\, m_i \tag{3-51}$$

$$R_{i\ddot{\Delta}_H} = 2Y_{ei}\, m_e m_H/m\, m_i \tag{3-52}$$

SLOSH COEFFICIENTS

$$A_{0\ddot{\psi}} = -(\ell_{cg} - X_0) \tag{3-53}$$

$$A_{H\ddot{\psi}} = -(\ell_{cg} - X_H) \tag{3-54}$$

2.5.3.2.3 Roll Axis Perturbation Equations

The equation matrix shown in Table 2-8 is for use in roll axis flight dynamic studies. The equations represent linearized rigid body dynamics coupled to the torsional dynamics. The torsional dyanmics are represented by two modes. Auxiliary Equations 3-6 through 3-7 are used to calculate the matrix coefficients.

2.5.3.4 Liquid Propellant Dynamics

2.5.3.4.1 G-Field Slosh Model

The slosh model described in this section is usable when a g-field is created when the Orbital or OMS engines are used. Two Spring Mass Systems (SMS) are used to represent the slosh dynamics. One SMS is for the liquid oxygen (LO_2) propellant and another SMS for the liquid hydrogen (LH_2) slosh dynamics. Data for these models were obtained from Saturn V data, References 1, 9, 10, and 11.

Slosh data in Figure 2-11 through 2-21 consist of slosh masses, frequencies, slosh mass locations, damping ratios, and conversion factors. These data are plotted as functions of propellant fluid measured in station numbers. SMS slosh natural frequencies are given in cycles per second for the first mode only for LO_2 and LH_2. The frequencies are normalized to one standard acceleration ($g_o = 32.2$ ft/sec^2). To obtain slosh frequencies at flight conditions multiply by the square root of flight axial acceleration (A_x) to one standard acceleration, g_o, i.e., $\sqrt{A_x/g_o}$. SMS damping ratios, ζ_o and ζ_H are given in Figures 2-18 and 2-19 as functions of fluid levels for LO_2 and LH_2, respectively. For preliminary design studies, damping ratios of 0.002 and 0.005 are recommended for LO_2 and LH_2, respectively. Scale factors, Γ_o and Γ_H to convert from spring mass deflections to slosh planar wave amplitude at the tank wall are given in Figures 3-20 and 3-21 for LO_2 and LH_2, respectively. This conversion process is indicated by Equations (3-68) and (3-69).

2.5.3.5 Vehicular Flexibility Dynamics

This section describes the flexible body dynamics and data for stability and control analysis of the ESS. These data are applicable during both the ascent boost and orbital operation phases. The manner in which flexible body dynamics are included in the analysis is indicated by perturbation Equations 3-1, 3-30, and 3-55.

Table 2-8. Roll Axis Perturbation Equation

	ϕ_{IU} (DEG)	ϕ (DEG)	P_{IU} (DEG/SEC)	η_1 (DEG)	η_2 (DEG)		δ_x (DEG)
ROLL ACCELERATION	0	S^2	0	$L_{\ddot{\eta}_1} S^2$	$L_{\ddot{\eta}_2} S^2$		$+\left(L_{\ddot{\delta}} S^2 + L_\delta\right)$
ROLL POSITION GYRO	1	-1	0	$-\theta_{IU_1}$	$-\theta_{IU_2}$	=	0
ROLL RATE GYRO	0	$-S$	1	$-\theta_{IU_1} S$	$-\theta_{IU_2} S$		0
FIRST TORSIONAL MODE	0	$P_{1\ddot{\phi}} S^2$	0	$(1+\theta_{1e} P_{1\ddot{\phi}}) S^2 + 2\zeta_1\omega_1 S + \omega_1^2$	$P_{12} S^2$		$+\left(P_{1\ddot{\delta}} S^2 + P_{1\delta}\right)$
SECOND TORSIONAL MODE	0	$P_{2\ddot{\phi}} S^2$	0	$P_{21} S^2$	$(1+\theta_{2e} P_{2\ddot{\phi}}) S^2 + 2\zeta_2\omega_2 S + \omega_2^2$		$+\left(P_{2\ddot{\delta}} + P_{2\delta}\right)$

ROLL PLANE

$$L_{\delta} = 2 F \ell_Y / I_{xx} \qquad (3\text{-}56)$$

$$L_{\ddot{\delta}} = 2 M_e \ell_e \ell_Y / I_{xx} \qquad (3\text{-}57)$$

$$L_{\ddot{\eta}_1} = 2 \theta_{1e} \left(I_{ex} + M_e \ell_Y^2 \right) / I_{xx} \qquad (3\text{-}58)$$

$$L_{\ddot{\eta}_2} = 2 \theta_{2e} \left(I_{ey} + M_e \ell_Y^2 \right) / I_{xx} \qquad (3\text{-}59)$$

$$P_{1\ddot{\delta}} = 2 \theta_{e} M_e \ell_e \ell_Y / J_1 \qquad (3\text{-}60)$$

$$P_{1\delta} = 2 F \ell_Y \theta_{1e} / J_1 \qquad (3\text{-}61)$$

$$P_{2\ddot{\delta}} = 2 \theta_{2e} M_e \ell_e \ell_Y / J_2 \qquad (3\text{-}62)$$

$$P_{2\delta} = 2 F \ell_Y \theta_{2e} / J_2 \qquad (3\text{-}63)$$

$$P_{1\ddot{\phi}} = 2 \theta_{1e} \left(I_{ex} + M_e \ell_Y^2 \right) / J_1 \qquad (3\text{-}64)$$

$$P_{2\ddot{\phi}} = 2 \theta_{2e} \left(I_{ex} + M_e \ell_Y^2 \right) / J_2 \qquad (3\text{-}65)$$

$$P_{12} = 2 \theta_{1e} \theta_{2e} \left(I_{ex} + M_e \ell_Y^2 \right) / J_1 \qquad (3\text{-}66)$$

$$P_{21} = 2 \theta_{2e} \theta_{1e} \left(I_{ex} + M_e \ell_Y^2 \right) / J_2 \qquad (3\text{-}67)$$

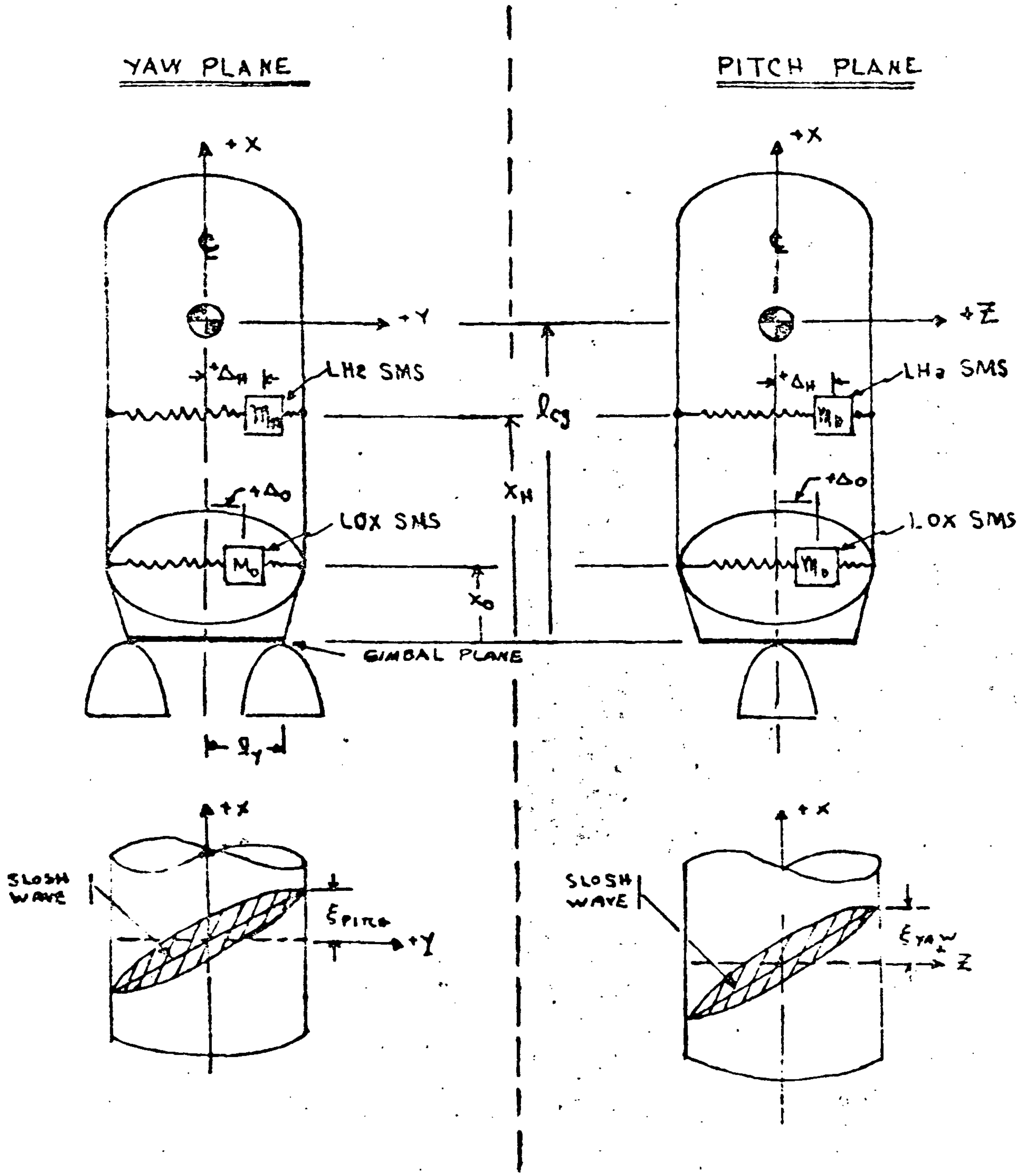

Figure 2-11. Slosh Dynamics Sign Convention

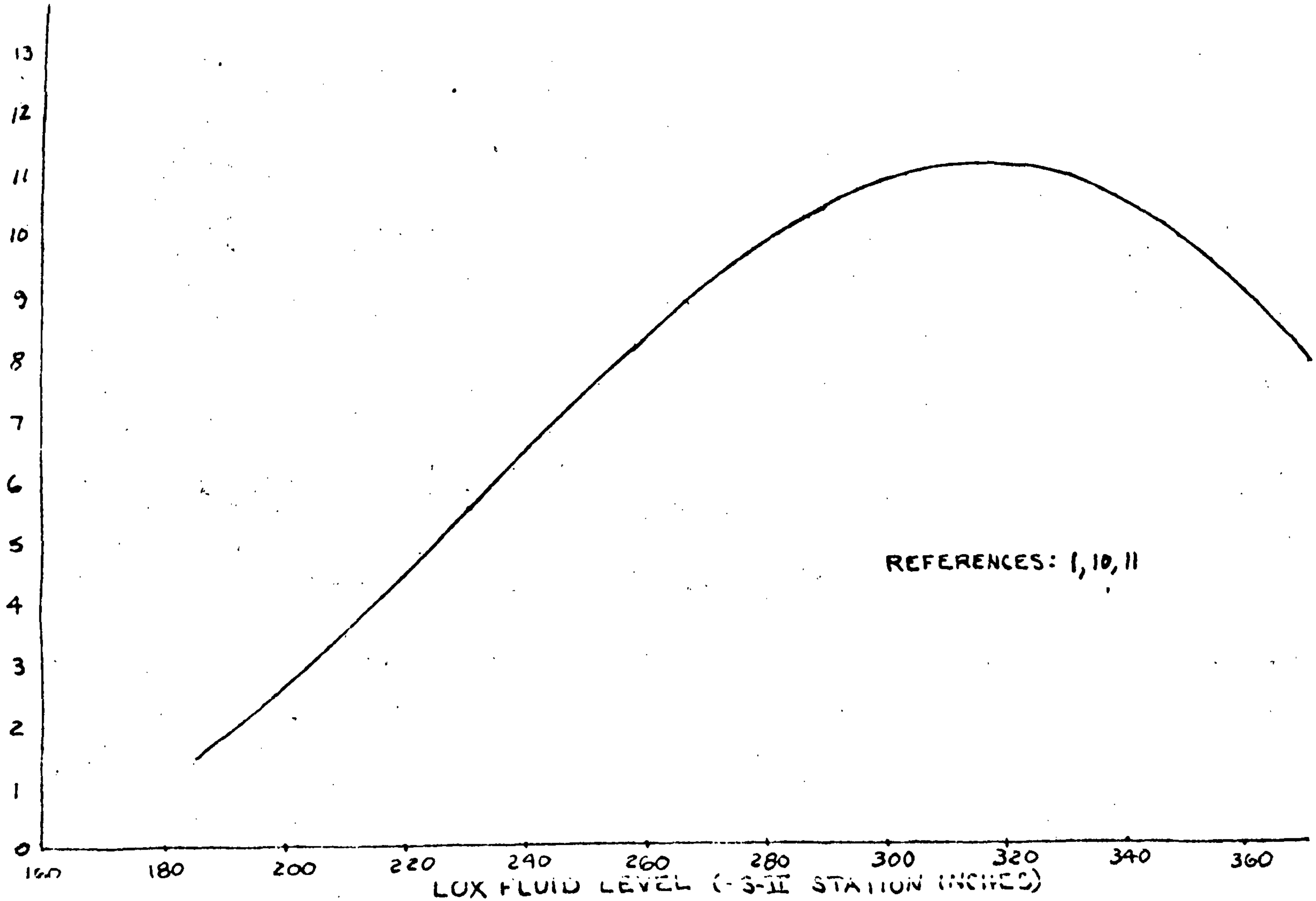

Figure 2-12. LOX Slosh Mass

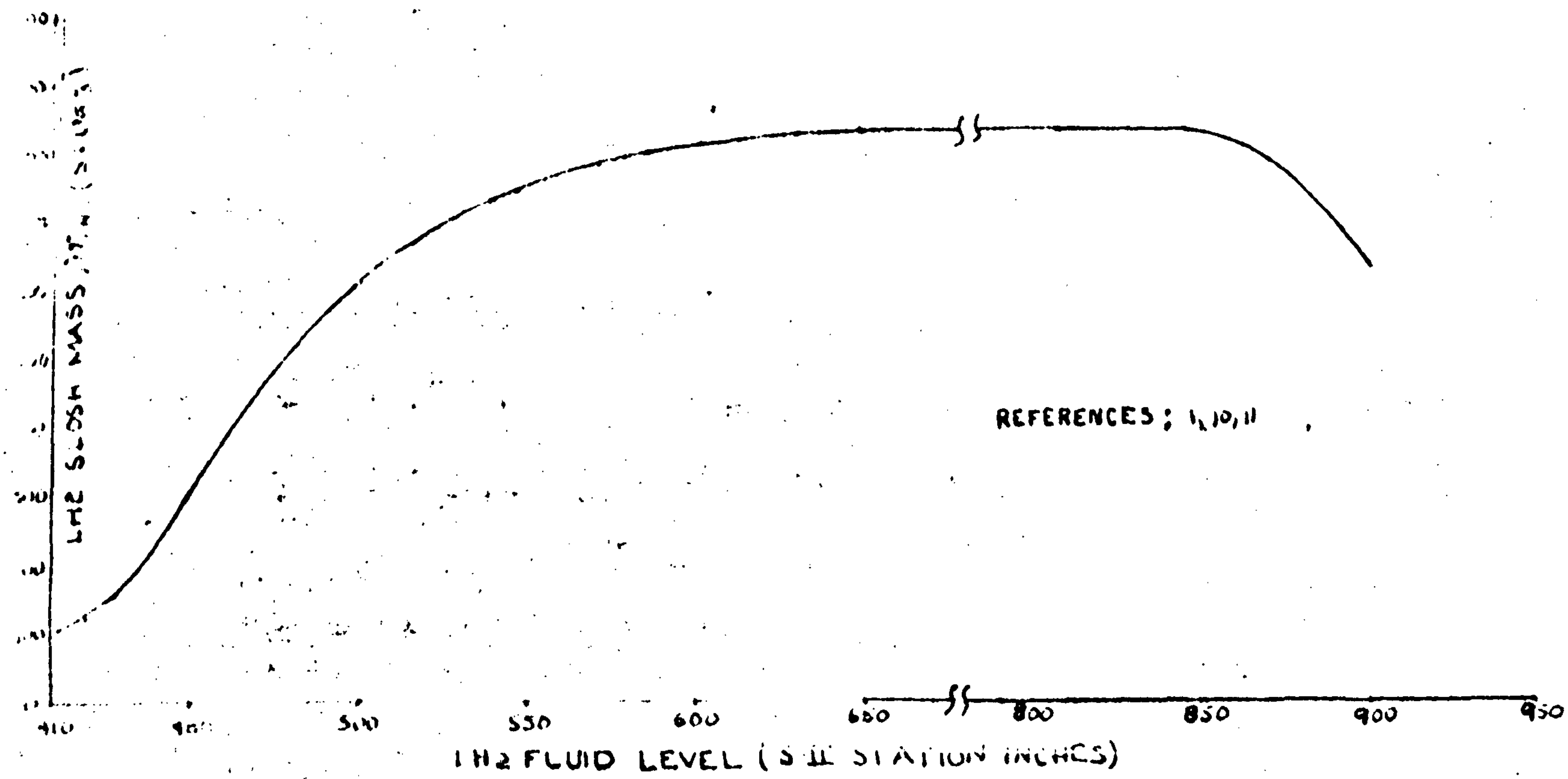

Figure 2-13. LH2 Slosh Mass

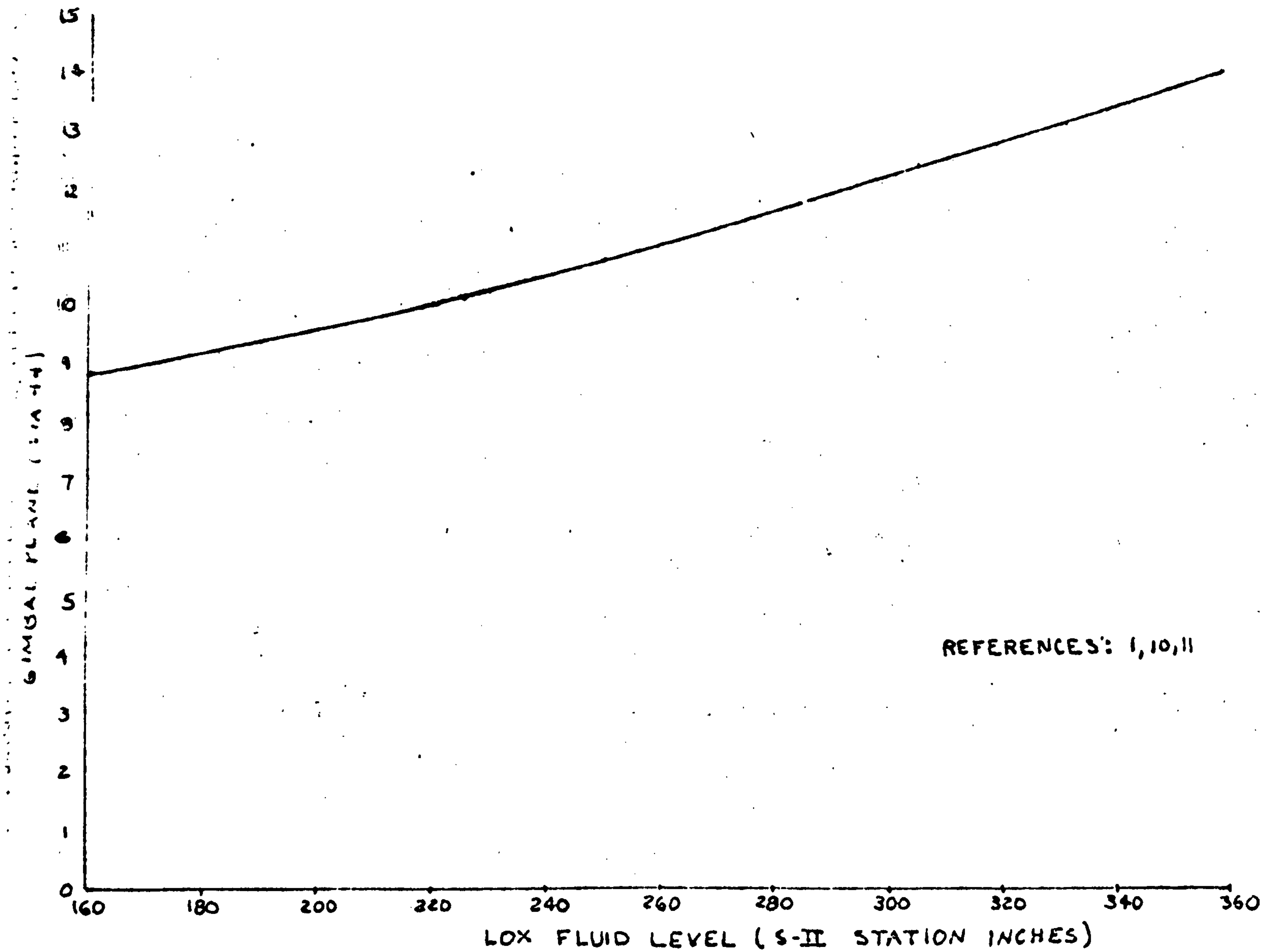

Figure 2-14. LOX Slosh Mass Location

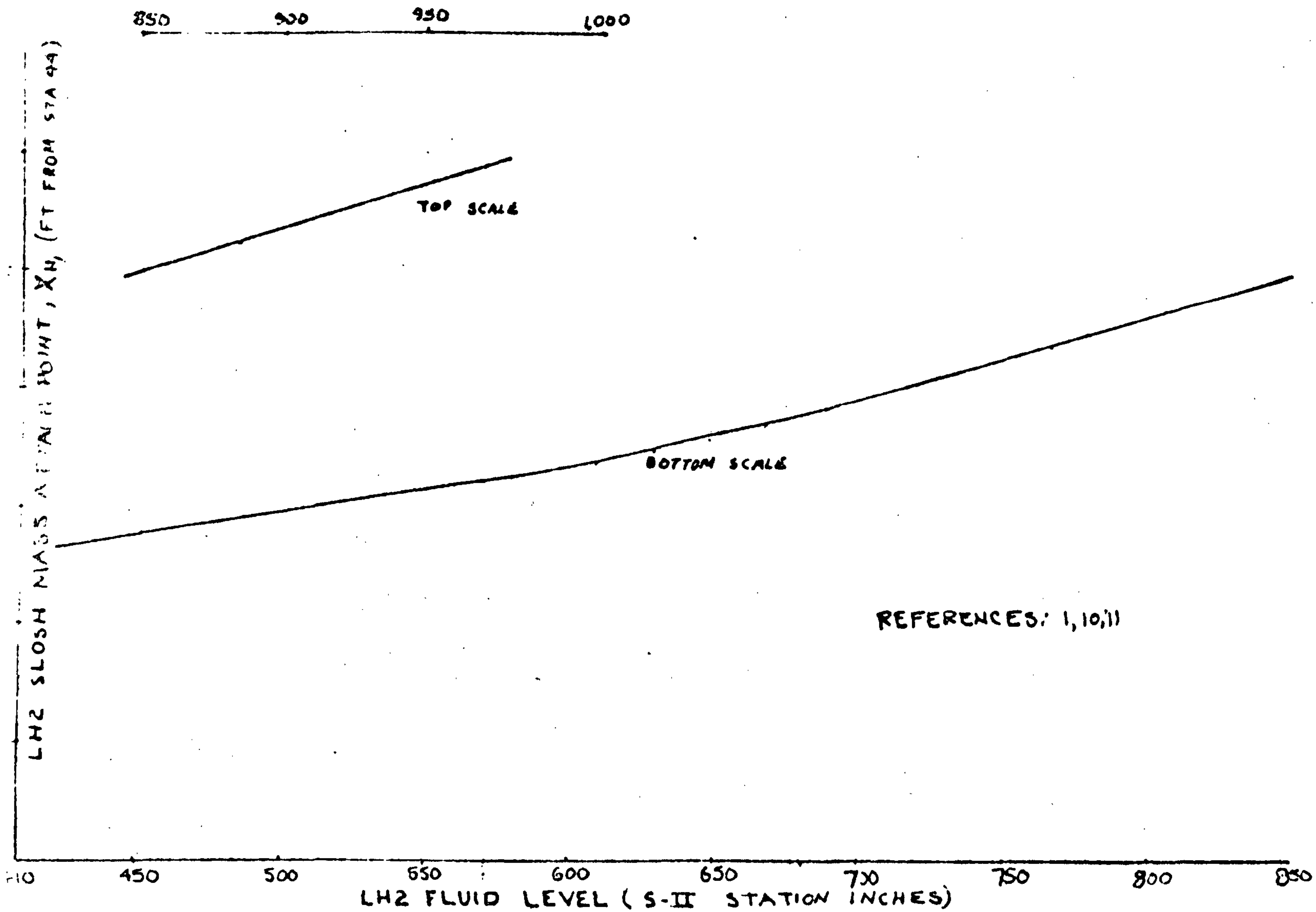

Figure 2-15. LH2 Slosh Mass Location

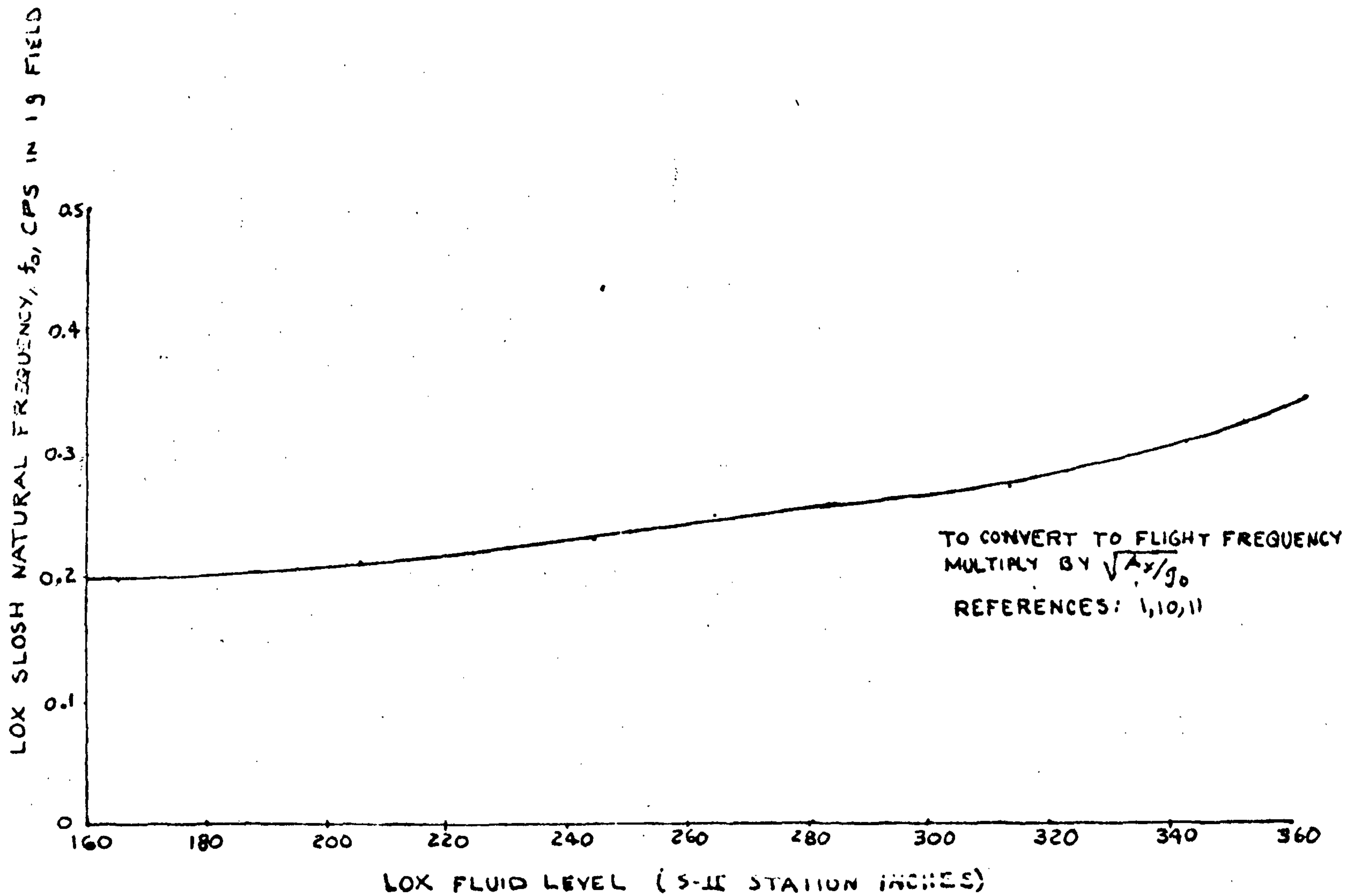

Figure 2-16. LO_2 Slosh Natural Frequency

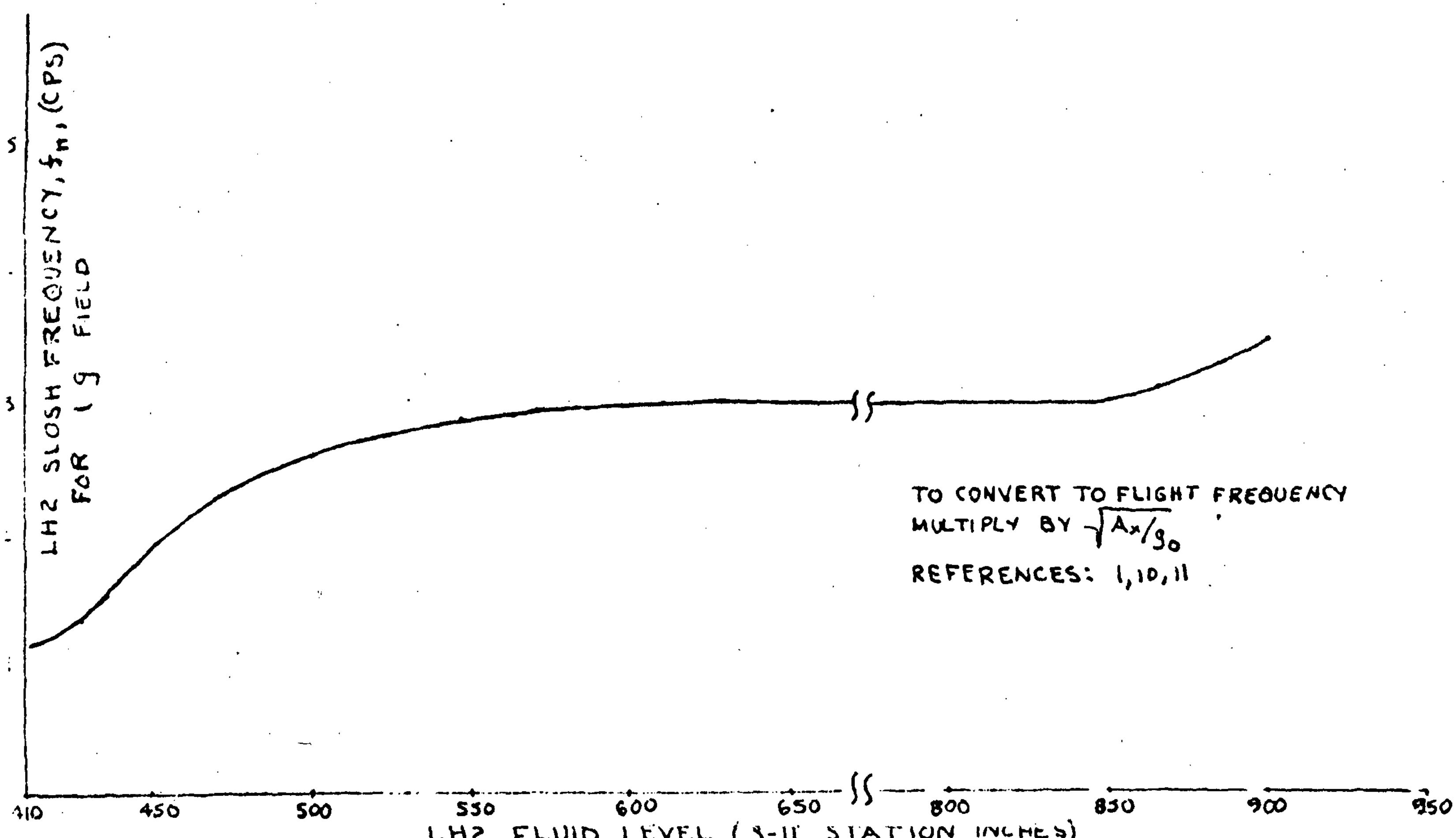

Figure 2-17. LH2 Slosh Frequency

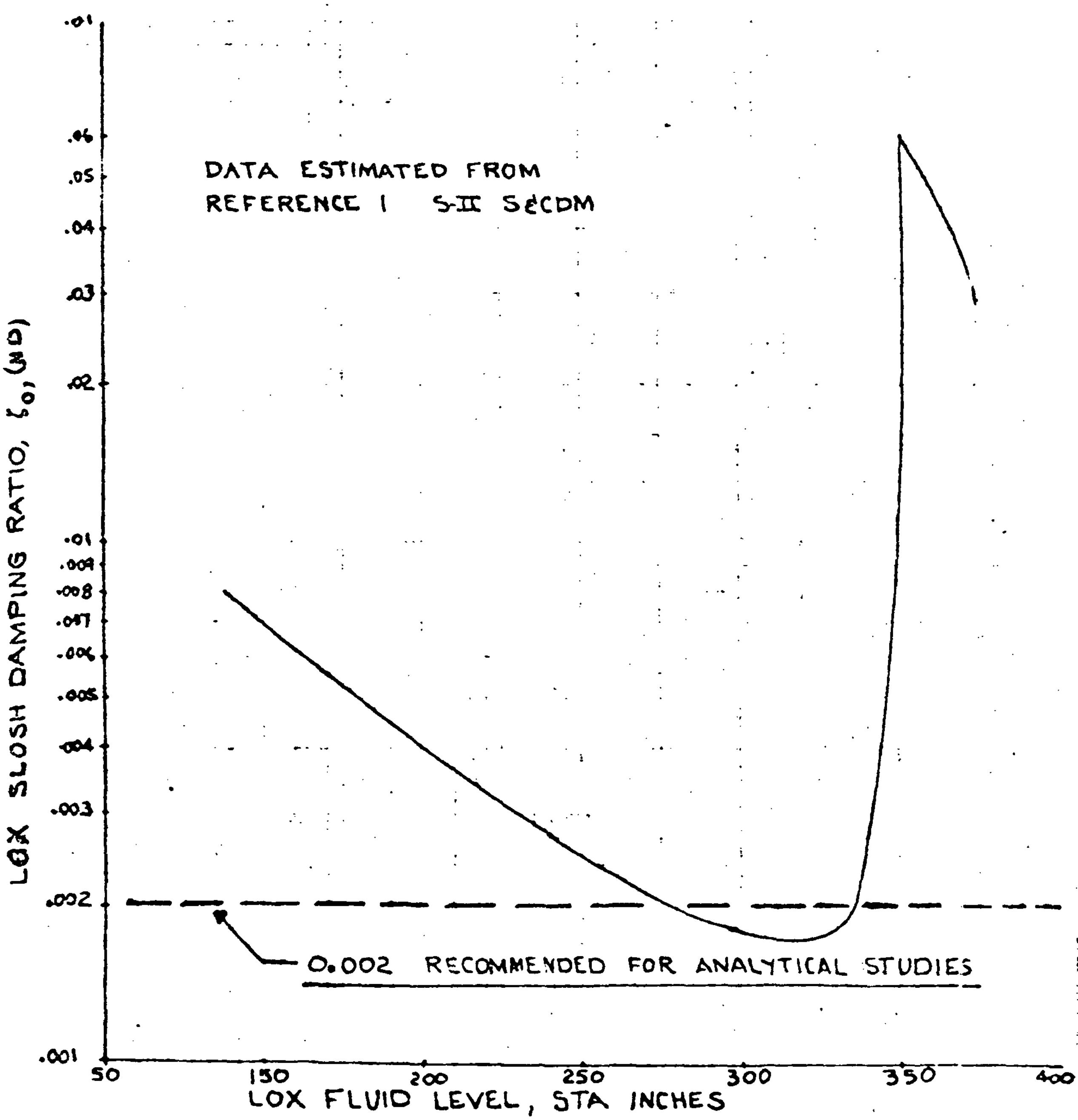

Figure 2-18. Liquid Oxygen Slosh Damping Ratio

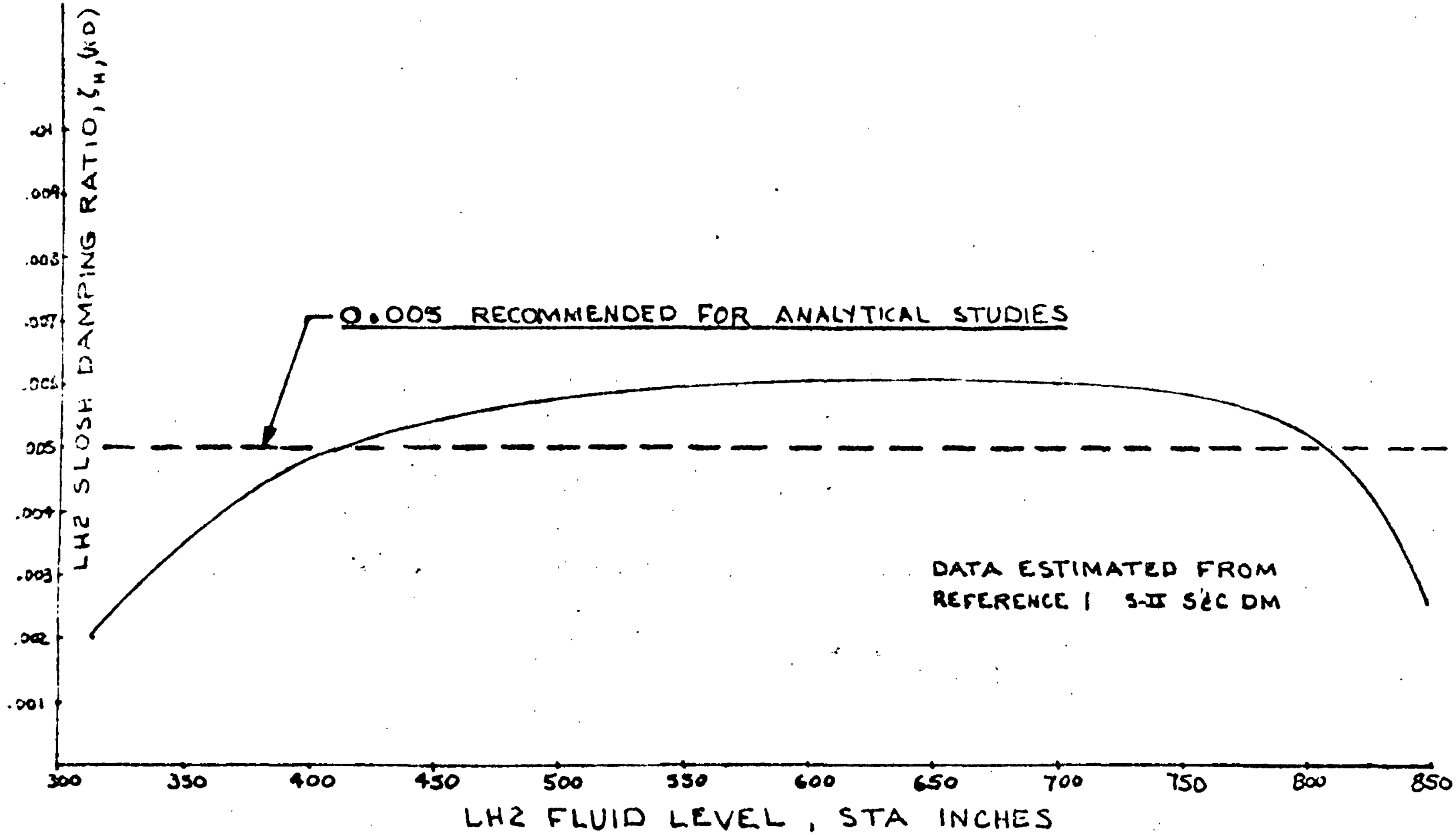

Figure 2-19. Liquid Hydrogen Slosh Damping Ratio

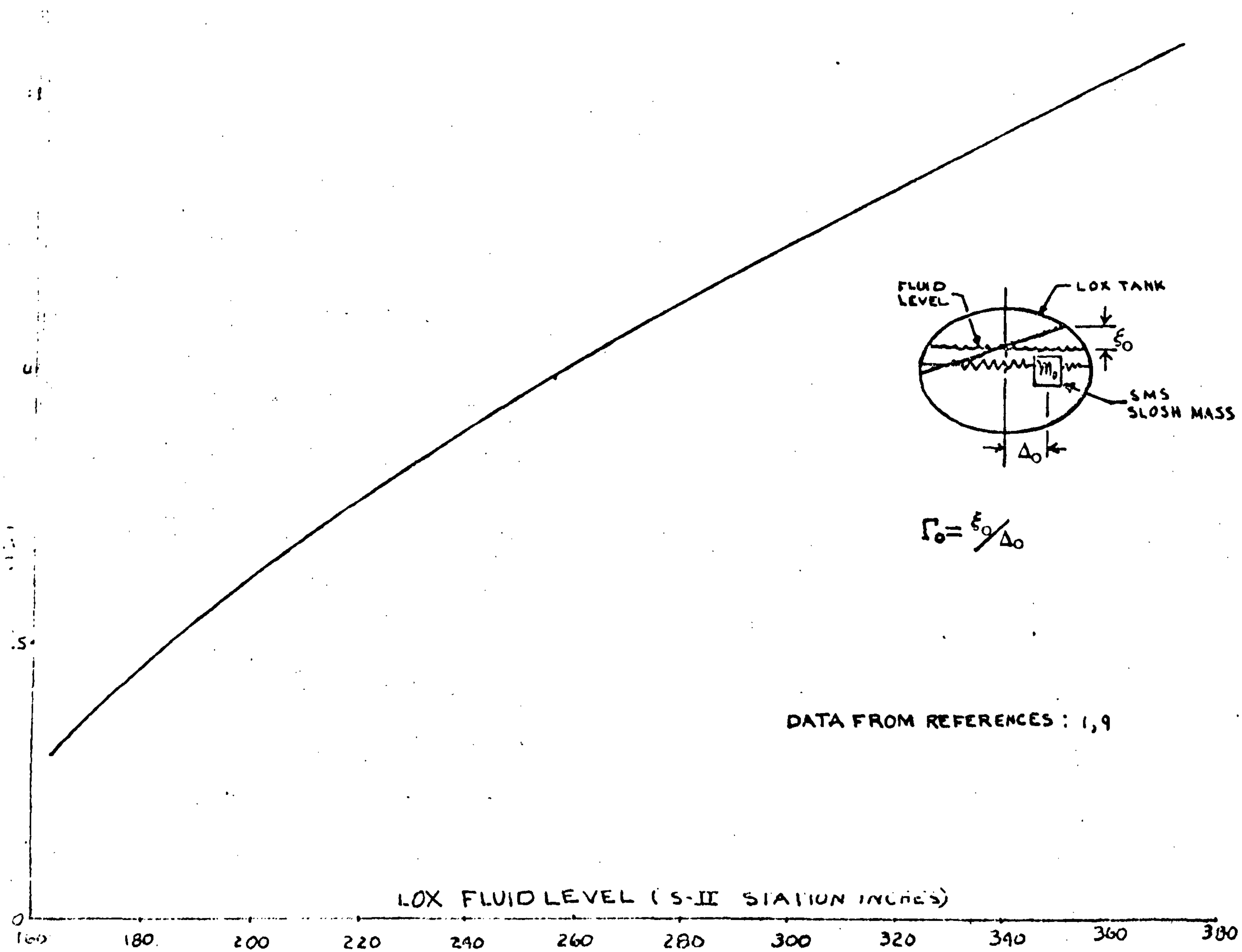

Figure 2-20. LOX Slosh Wave Height Conversion Factor

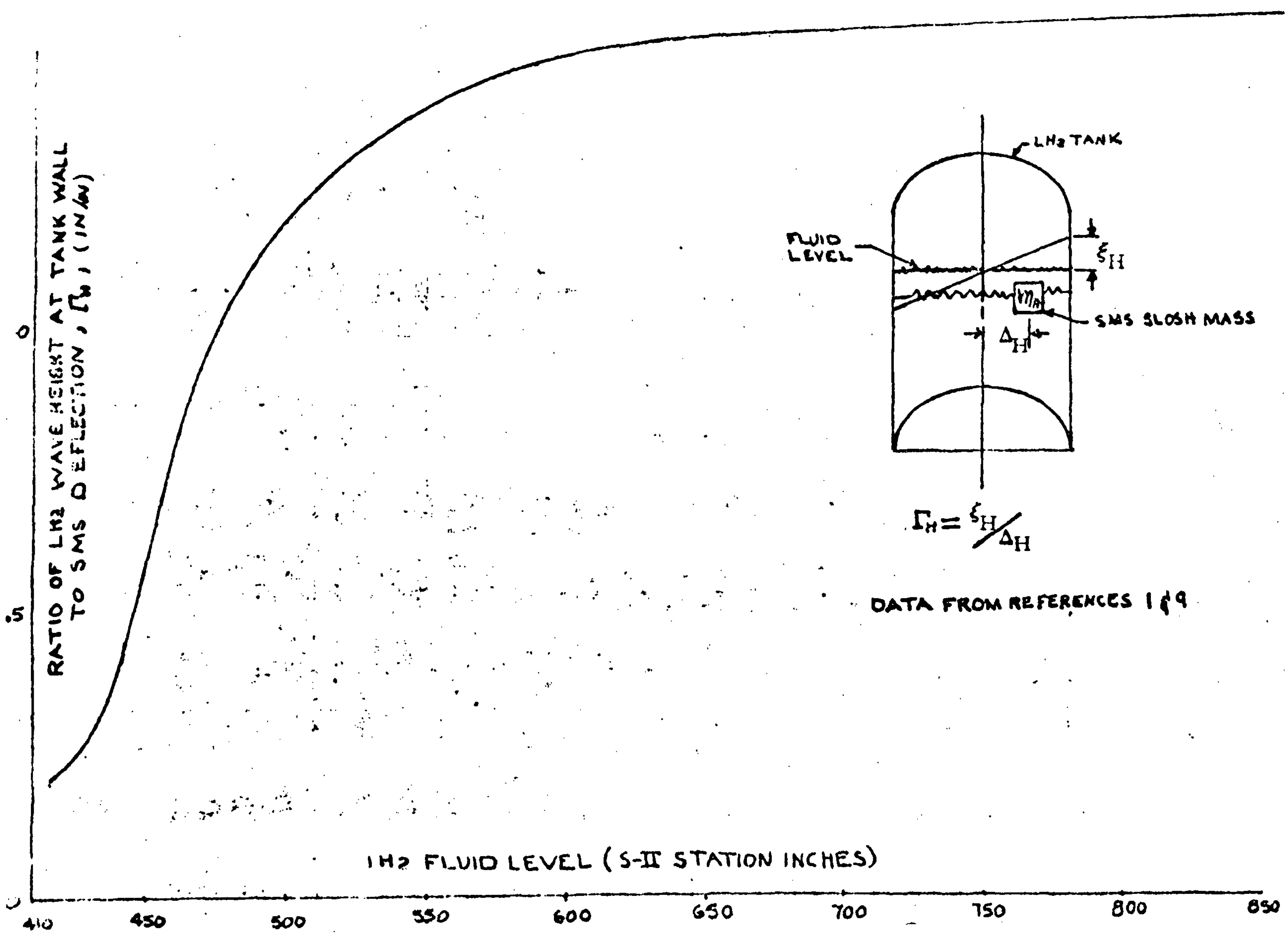

Figure 2-21. LH2 Slosh Wave Height Conversion Factor

In the pitch (yaw) axis, the body bending dynamics are represented by spring mass system (SMS) described by a model mass, M_i; natural frequency, ω_i; damping ratio , ζ_i; and generalized deflection d_i (e_i). These bending modes are coupled to the vehicular angular motion, θ (ψ), and flight control engine angular deflection, through the modal slopes (Y'_{rui} and Y'_{ei}) and model deflection δ_p (δ_y) (Y_{ei}). Data for the bending modes are given in Table 2-9. These data were obtained for INT-21 studies and will require updating when ESS bending data are defined in future studies.

In the roll axis, the vehicular the flexibility dynamics are represented by i number of torsional modes (or degrees-of-freedom). Each mode is described by a moment of inertia, J_i; natural frequency ω_i; damping ratio, ζ_i; and generalized displacement, η_i. The torsional modes are coupled to the vehicular angular motion, ϕ and control engine angular deflections, δ_x through modal deflections at the Instrument Unit (IU) location and control engine gimbal plane location. The sign convention is shown in Figure 2-22. Data for the torsional modes are given in Table 2-10.

The data in Table 2-10were obtained from S-II stage INT-21 studies and at the time of this publication are assumed valid for ESS preliminary stability studies.

To obtain elasticity displacements, use equation (3-70), (3-71) and (3-72).

$$U_y = \Sigma \; Y_i \, e_i \qquad (3\text{-}70)$$

$$U_z = \Sigma \; Y_i \, d_i \qquad (3\text{-}71)$$

$$U_\phi = \Sigma \; \theta_i \, \eta_i \qquad (3\text{-}72)$$

2.5.3.6 Mass Properties

This section of the data manual presents ESS mass moment of inertia, center-of-gravity and propellant fluid levels for various ESS payloads. For the ascent boost phase, these data are given in Figures 2-11 through 2-30. Note that Figures 2-26 through 2-30. the data are plotted versus total vehicular mass and not time. Also in Figure 2-29 more conservative values of Y_{cg} and L_{cg} are recommended for analytical studies than the data shown which were obtained from Reference 7. Roll axis moment of inertia data are given in Table 2-11for the ascent boost phase.

ESS mass properties at the beginning of orbital operations are shown in Table 2-12.

Table 2-9. Bending Mode Parameters

PAYLOAD : REUSABLE NUCLEAR SHUTTLE						
DESIGN CONDITION	MODAL MASS (SLUGS)			NATURAL FREQUENCY (CPS / RAD PER SECOND)		
	m_1	m_2	m_3	ω_1	ω_2	ω_3
FULL TANKS	42,100	42,100	(NOT AVAILABLE)	3.7 (23)	7.3 (46)	(NOT AVAILABLE)
3/4 FULL	34,600	34,600		3.8 (24)	8.1 (51)	
1/2 FULL	26,000	26,000		3.9 (24)	9.3 (58)	
1/4 FULL	19,200	19,200		4.0 (25)	10.8 (68)	
EMPTY	11,700	11,700		4.2 (26)	12.0 (75)	

NOTES: (1) DATA FROM INT-21 S-II ANALYSIS, REFERENCE: 12, 13

(2) USE $\zeta_i = .01$ if $\omega_i \leq 47$ RAD/SEC; $\zeta_i = .02$ if $\omega_i > 47$ RAD/SEC.

Table 2-9. Bending Mode Parameters (Cont)

PAYLOAD : REUSABLE NUCLEAR SHUTTLE — NR						
DESIGN CONDITION	MODAL SLOPE AT GIMBAL PLANE (DEG/FT)			MODAL DEFLECTION AT GIMBAL PLANE (FT/FT)		
	Y'_{e1}	Y'_{e2}	Y'_{e3}	Y_{e1}	Y_{e2}	Y_{e3}
FULL TANKS	-0.2	0.3	(NOT AVAILABLE)	0.9	-1.7	(NOT AVAILABLE)
3/4 FULL	-0.2	0.3		0.8	-1.6	
1/2 FULL	-0.1	0.3		0.7	-1.5	
1/4 FULL	-0.1	0.3		0.6	-1.3	
EMPTY	-0.1	0.2		1.1	-0.9	
NOTE: DATA FROM INT-21 ANALYSIS, REFERENCE: 12, 13						

Table 2-9. Bending Mode Parameters (Cont)

PAYLOAD: REUSABLE NUCLEAR SHUTTLE - NR						
DESIGN CONDITION	MODAL SLOPE AT IU (DEG/FT)			MODAL DEFLECTION AT IU (FT/FT)		
	Y'_{IU1}	Y'_{IU2}	Y'_{IU3}	Y_{IU1}	Y_{IU2}	Y_{IU3}
FULL TANK	3.8	2.8	(NOT AVAILABLE)	3.6	1.8	(NOT AVAILABLE)
3/4 FULL	3.7	2.3	(NOT AVAILABLE)	3.3	1.4	(NOT AVAILABLE)
[illegible] L	3.3	2.0	(NOT AVAILABLE)	3.0	1.2	(NOT AVAILABLE)
1/4 FULL	2.8	2.0	(NOT AVAILABLE)	2.5	1.0	(NOT AVAILABLE)
EMPTY	2.2	1.9	(NOT AVAILABLE)	1.9	0.9	(NOT AVAILABLE)

NOTE: DATA FROM INT-21 S-II ANALYSIS, REFERENCES: 12, 13

Table 2-9. Bending Mode Parameters (Cont)

PAYLOAD: SPACE STATION -NR						
DESIGN CONDITION	MODAL MASS (SLUGS)			NATURAL FREQUENCY (CPS/ RAD PER SECOND)		
	m_1	m_2	m_3	ω_1	ω_2	ω_3
FULL TANK	41,300	41,300	(NOT AVAILABLE)	4.4 (28)	7.6 (48)	(NOT AVAILABLE)
3/4 FULL	33,900	33,900		4.5 (28)	8.3 (52)	
1/2 FULL	26,400	26,400		4.6 (29)	9.3 (58)	
1/4 FULL	18,600	18,600		4.7 (30)	10.2 64	
EMPTY	11,000	11,000		4.9 (31)	10.8 (68)	

NOTES: (1) DATA FROM INT-21 S-II ANALYSIS
(2) USE $\zeta_i = 0.01$ IF $\omega_i \leq 47$ RAD/SEC; $\zeta_i = .02$ IF $\omega_i \geq 47$ RAD/SEC.

Table 2-9. Bending Mode Parameters (Cont)

PAYLOAD: SPACE STATION -NR						
DESIGN CONDITION	MODAL SLOPE AT GIMBAL PLANE (DEG/FT)			MODAL DEFLECTION AT GIMBAL PLANE (FT/FT)		
	Y'_{e1}	Y'_{e2}	Y'_{e3}	Y_{e1}	Y_{e2}	Y_{e3}
TANKS FULL	-0.19	3.0	(NOT AVAILABLE)	0.9	-1.6	(NOT AVAILABLE)
3/4 FULL	-1.7	3.1		0.7	-1.5	
1/2 FULL	-1.5	3.1		0.6	-1.3	
1/4 FULL	-1.2	2.6		0.5	-.9	
EMPTY	-1.2	2.0		0.9	-.9	
NOTE: (1) DATA FROM INT-21 S-II ANALYSIS						

Table 2-9. Bending Mode Parameters (Cont)

PAYLOAD: SPACE STATION —NR						
DESIGN CONDITION	MODAL SLOPE AT IU (DEG/FT)			MODAL DEFLECTION AT IU (FT/FT)		
	Y'_{IU1}	Y'_{IU2}	Y'_{IU2}	Y_{IU1}	Y_{IU2}	Y_{IU3}
TANKS FULL	-0.14	-0.71				
3/4 FULL	-0.18	-0.72				
1/2 FULL	-0.18	-0.72		AVAILABLE	DATA NOT	
1/4 FULL	-0.21	-0.64				
EMPTY	-0.43	-0.35				
NOTE: (1) DATA FROM INT-21 S-II ANALYSIS						

Table 2-10. Torsional Mode Parameters

PAYLOAD: REUSABLE NUCLEAR SHUTTLE — NR						
DESIGN CONDITION	MODAL MOMENT OF INERTIA (SLUG-FT^2)			NATURAL FREQUENCY (CPS/RAD PER SEC)		
	J_1	J_2	J_3	ω_1	ω_2	ω_3
BEGIN BOOST	1.12×10^6	NOT AVAILABLE		11 (69)	NOT AVAILABLE	
END BOOST	1.12×10^6			11 (69)		
	GENERALIZED DISPLACEMENT AT INSTRUMENT UNIT (ND)			GENERALIZED DISPLACEMENT AT GIMBAL PLANE-STA 44 (ND)		
	θ_{IU_1}	θ_{IU_2}	θ_{IU_3}	θ_{e_1}	θ_{e_2}	θ_{e_3}
BEGIN BOOST	1.4	NOT AVAILABLE		-1.2	NOT AVAILABLE	
END BOOST	1.4			-1.2		
NOTE: USE $\zeta_i = .01$ IF $\omega_i \leq 47$ RAD/SEC; $\zeta_i = .02$ IF $\omega > 47$ RAD/SEC.						

Table 2-11. ESS Roll Axis Moment of Inertia Data—Ascent Boost

Flight Condition	Roll Axis Moment of Inertia (million slug-ft^2)		
	MDAC Space Station	NR RNS	NR Tug
Start Boost	1.6	1.3	0.74
End Boost	1.5	1.2	0.67
Reference: 7			

Table 2-12. ESS Mass Properties—Start Orbital Operations

ESS Payload	Total Mass (Slugs)	Center-of-Gravity (station inches)			Moment of Inertia (million slug-ft^2)		
		X_{cg}	Y_{cg}	Z_{cg}	I_{xx}	I_{yy}	I_{zz}
NR Tug	5,440	362	0.2	-1.8	0.57	3.3	3.3
MDAC Space Station	3,180	268	0.3	-3.1	0.53	1.8	1.8
NR RNS	6,190	298	0.1	1.6	0.53	2.4	2.4
Reference: 7							

2.5.4 GUIDANCE AND CONTROL SYSTEM

2.5.4.1 Description

The ESS Guidance and Control System (GN&C) is based on Shuttle developed technology. The main subsystems are the inertial platform (IMU), central computing unit (CPU), gimbal engine servo amplifier, attitude driver unit, rate sensors, and data bus.

2.5.4.2 Guidance System

Inertial Measuring Unit

The inertial unit is a 4 gimbal platform configuration. The Euler angle sequence is pitch-roll-yaw-roll (YXZX) going from inner to outer gimbal transformation.

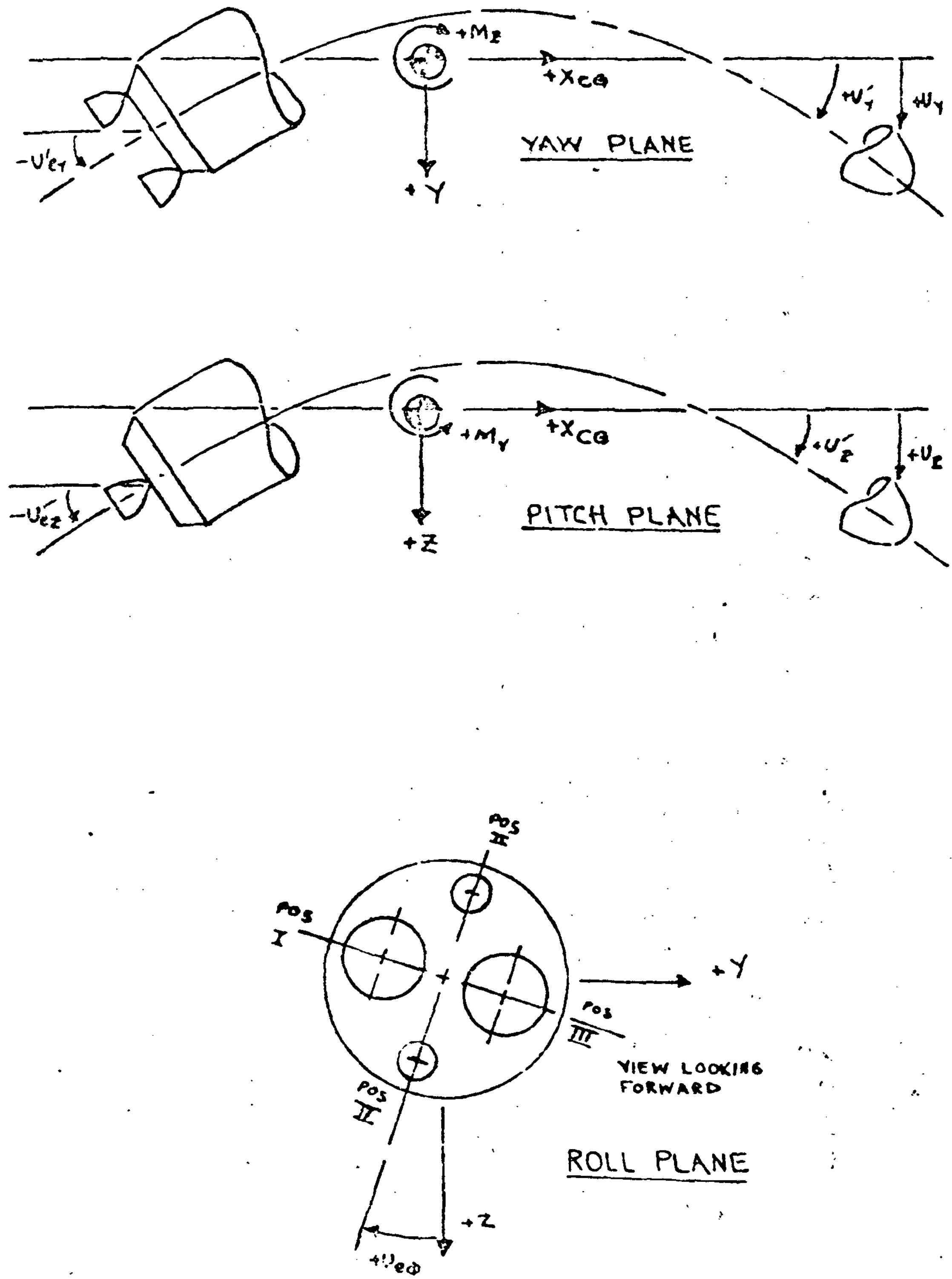

Figure 2-22. Flexibility Dynamics Sign Convention

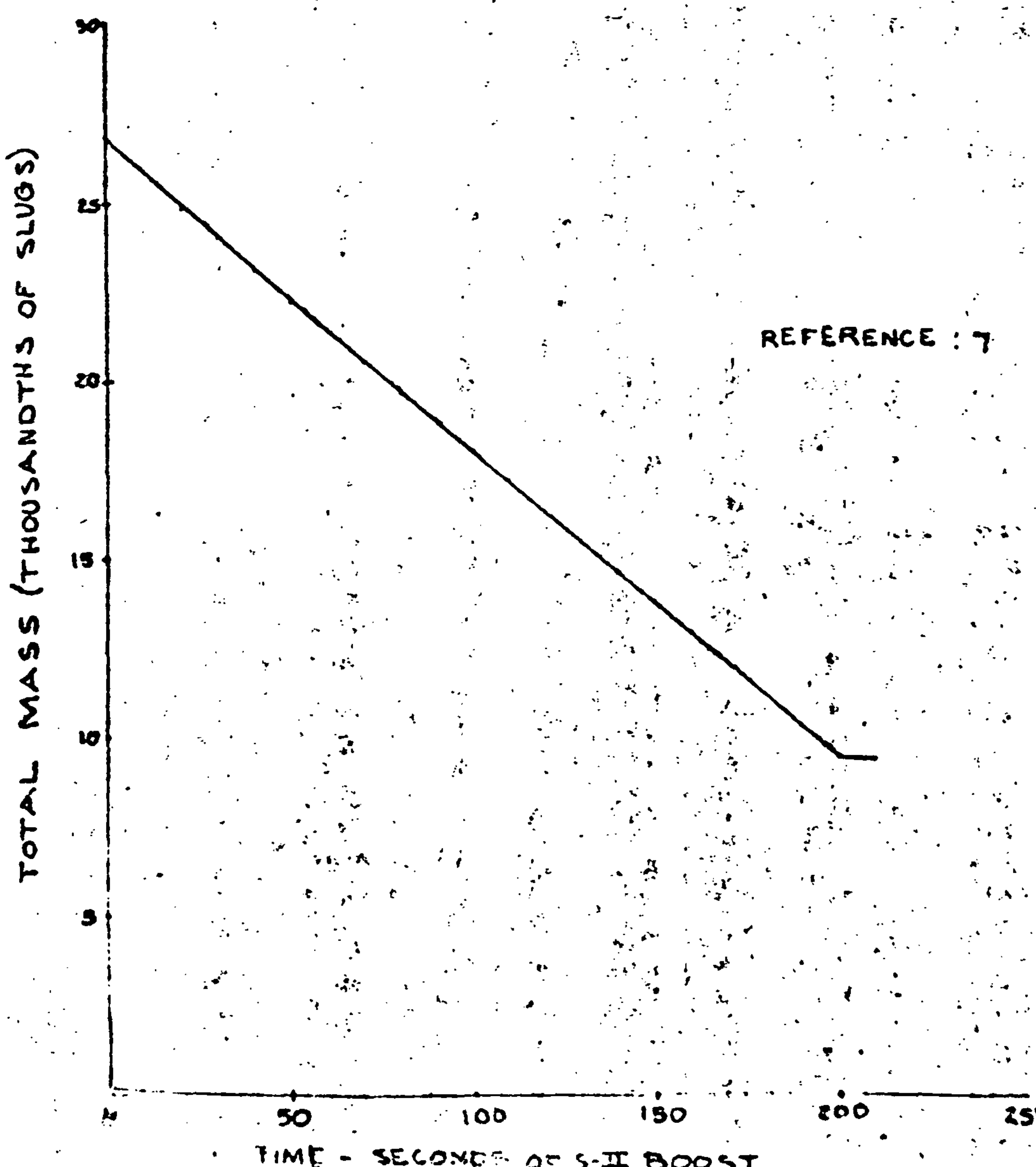

Figure 2-23. ESS Total Mass - NR RNS Payload

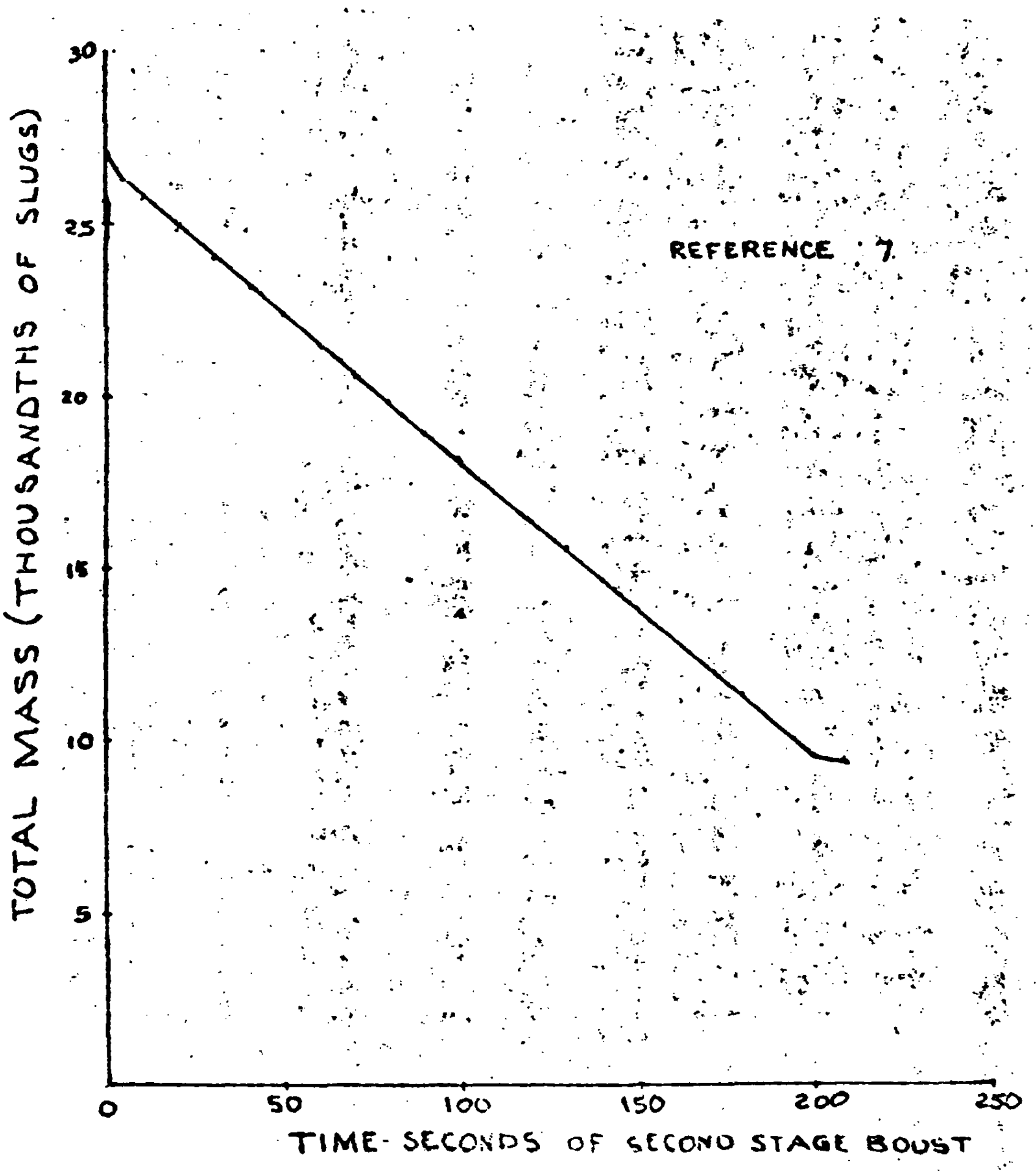

Figure 2-24. ESS Total Mass - NR Tug Payload

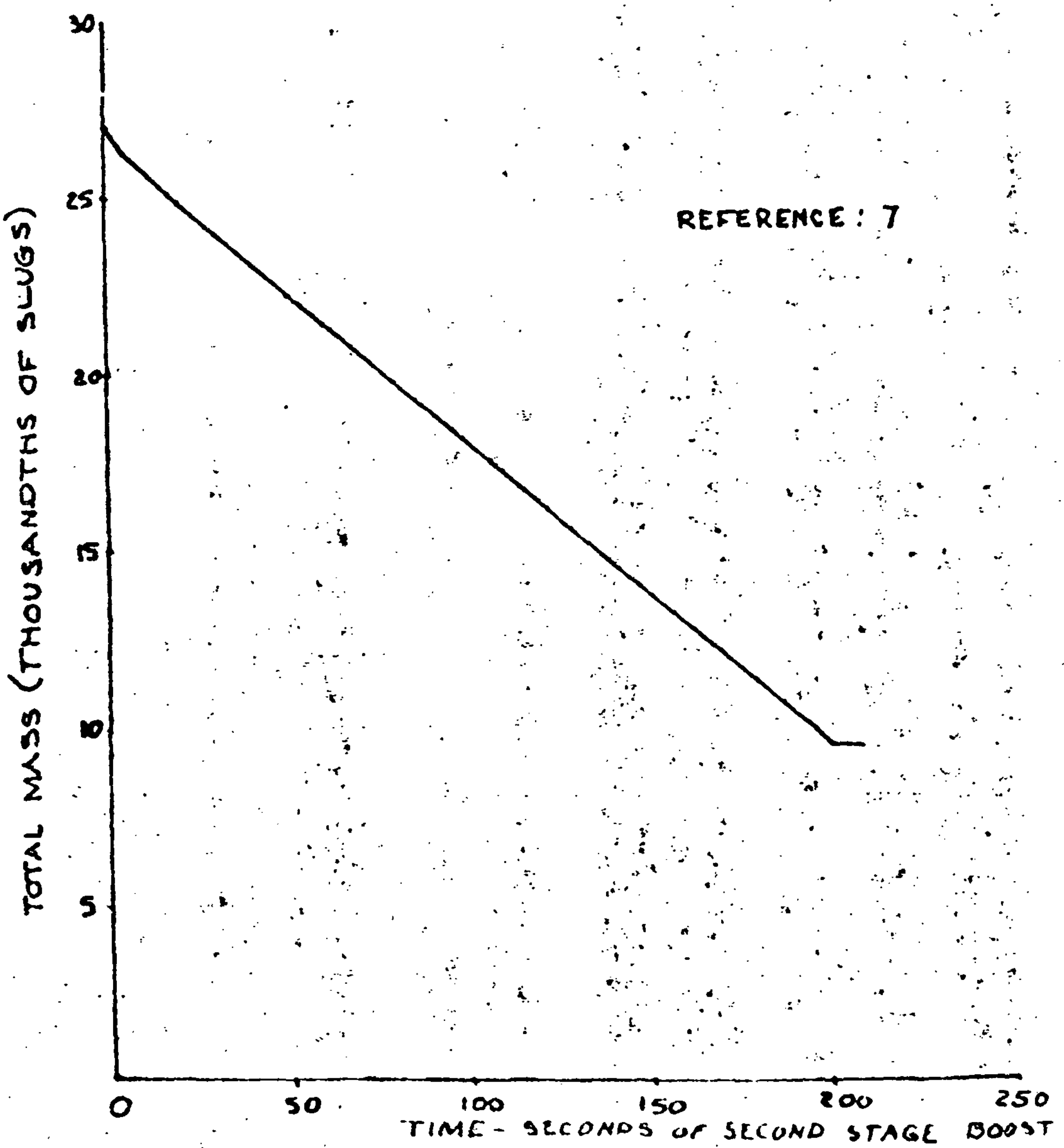

Figure 2-25. ESS Total Mass — MDAC Space Station

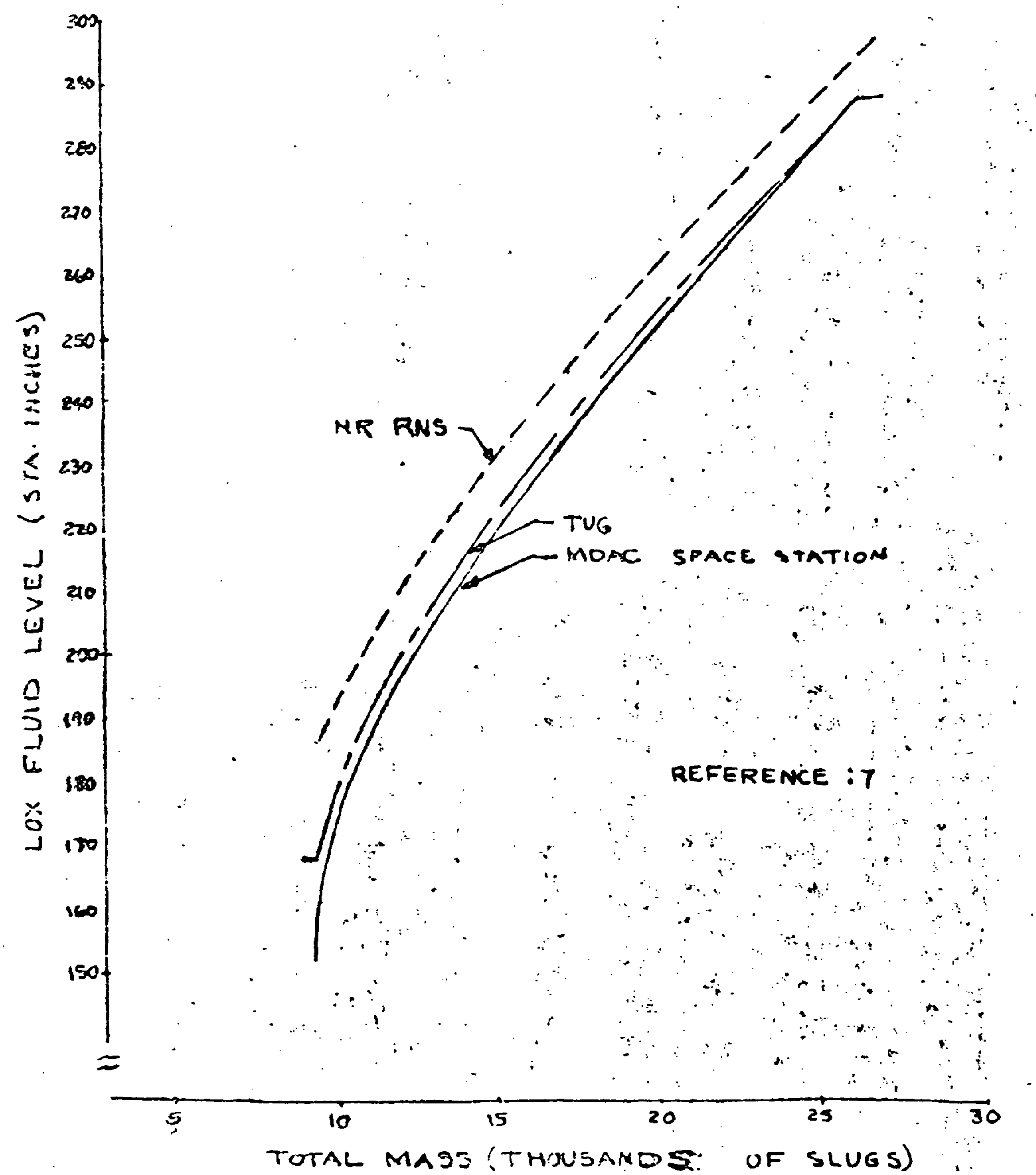

Figure 2-26. LO_2 Fluid Level — NR RNS, NR Tug, and MDAC Space Station Payloads

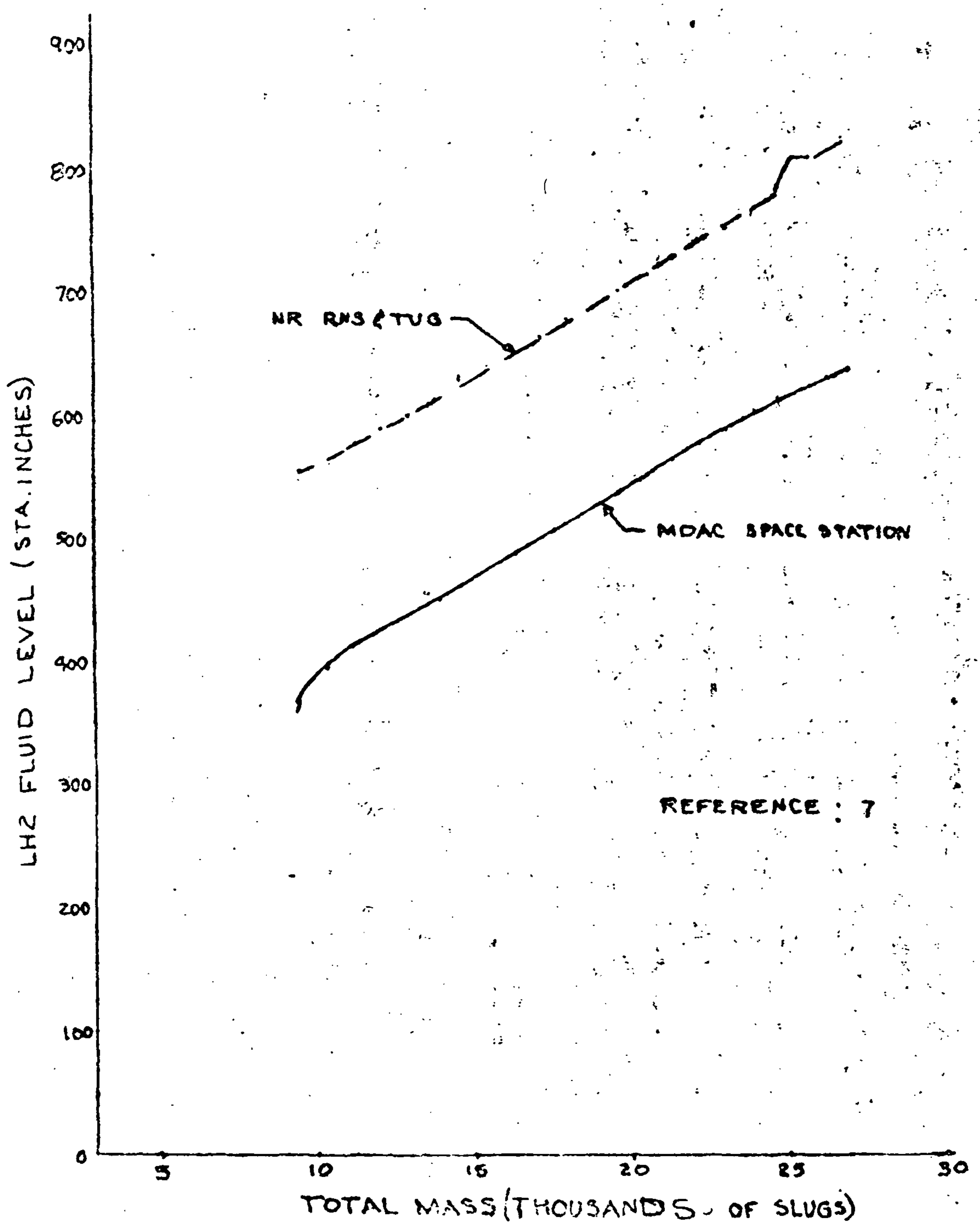

Figure 2-27. LH_2 Fluid Level — NR RNS, NR Tug, and MDAC Space

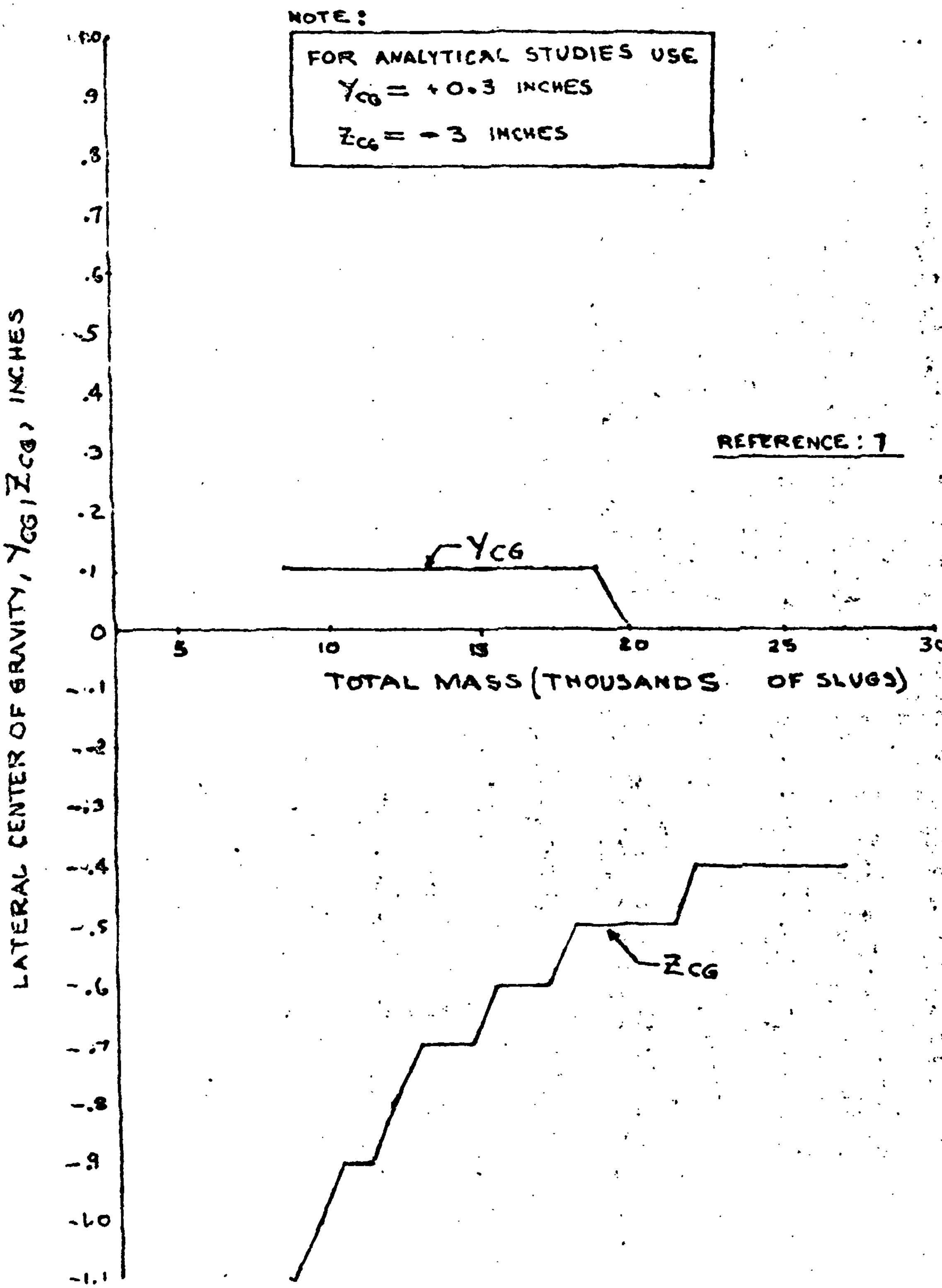

Figure 2-28. ESS Center-of-Gravity, Y_{cg} and Z_{cs} — NR RNS, NR Tug, and MDAC Space Station Payloads

F

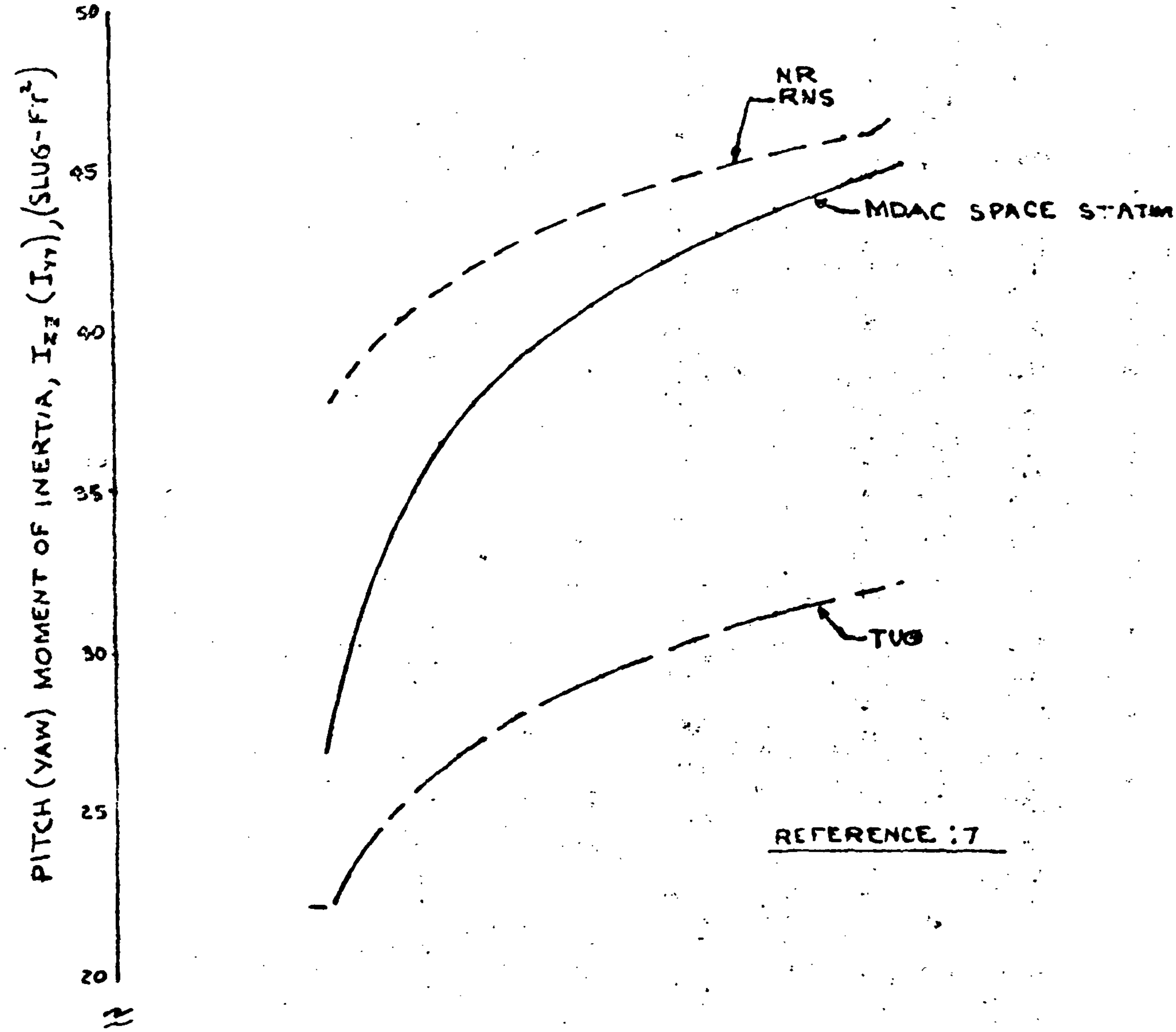

Figure 2-29. ESS Pitch (Yaw) Moment of Inertia – NR RNS, NR Tug, and MDAC Space Station Payloads

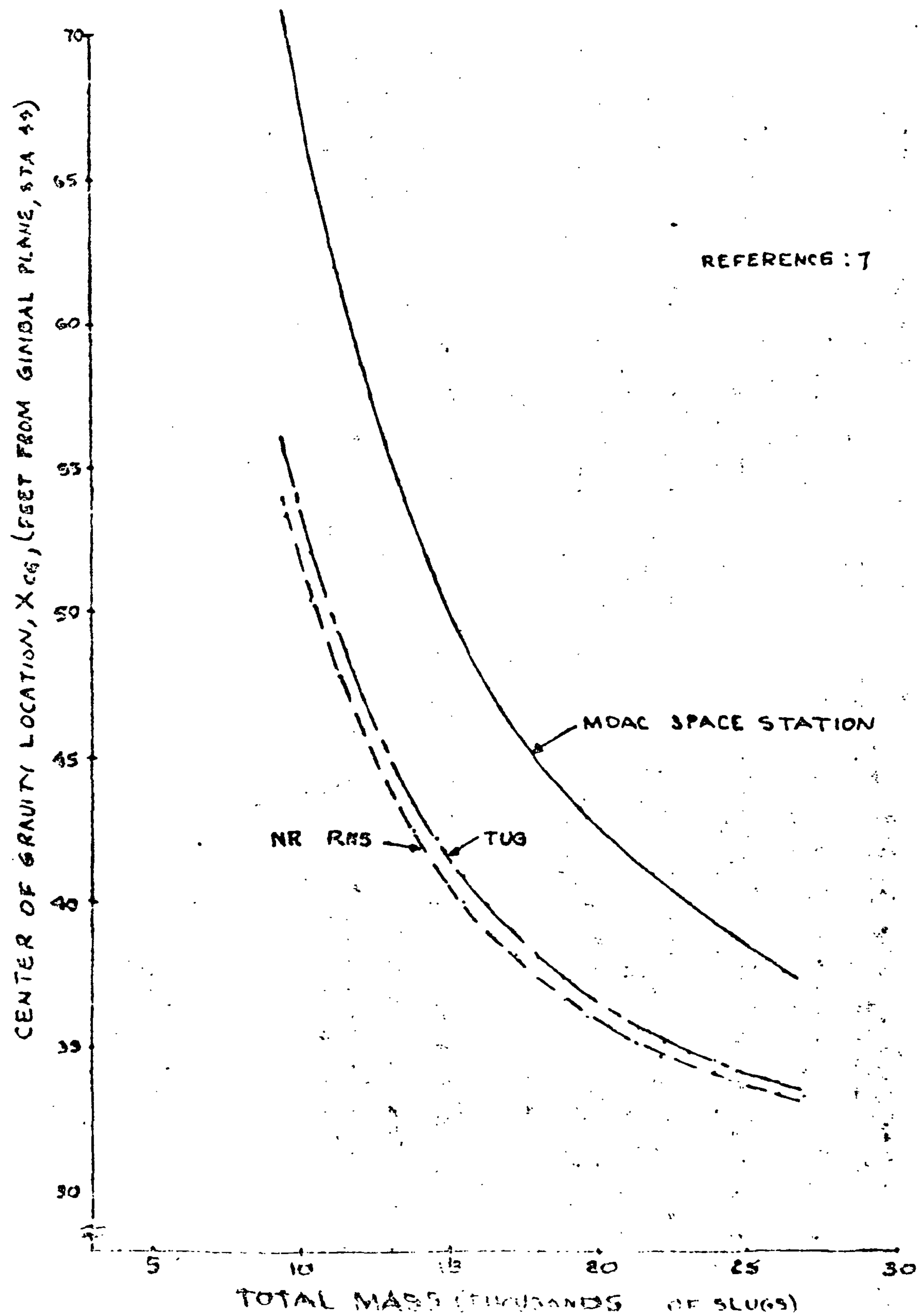

Figure 2-30. ESS Center

2.5.4.3 Flight Control Logic

During mainstage boost, the guidance attitude error commands (θ_e, ψ_e and ϕ_e) are used to point the orbiter and OMS engines with actuators by means of the following control logic equations:

Engine Commands

$$\delta_{cp} = a_\theta F_\theta \theta_e + aq\, Fq\, q_{IU} \qquad (6\text{-}1)$$

Yaw

$$\delta_{cy} = a_\psi F_\psi \psi_e + a_r F_r r_{IU} \qquad (6\text{-}2)$$

Gyro Dynamics

$$q_{IU} = q + \Sigma Y'_{IU_i} \dot{d}_i \qquad (6\text{-}3)$$

$$r_{IU} = r + \Sigma Y'_{IU_i} \dot{e}_i \qquad (6\text{-}4)$$

Actuator Summing Logic

Orbiter Engine Actuator Deflections

$$\delta_{A11} = \sqrt{2}/2 \quad - \delta_{P1} - \delta_{Y1} \qquad (6\text{-}5)$$

$$\delta_{A12} = \sqrt{2}/2 \quad - \delta_{P1} + \delta_{Y1} \qquad (6\text{-}6)$$

$$\delta_{A22} = \sqrt{2}/2 \quad + \delta_{P2} - \delta_{Y2} \qquad (6\text{-}7)$$

$$\delta_{A21} = \sqrt{2}/2 \quad + \delta_{P2} + \delta_{Y2} \qquad (6\text{-}8)$$

OMS Engine Actuator Deflections

$$\delta_{A11} = \sqrt{2}/2 \quad + \delta_{P1} + \delta_{Y1} \qquad (6\text{-}9)$$

$$\delta_{A12} = \sqrt{2}/2 \quad + \delta_{P1} - \delta_{Y1} \qquad (6\text{-}10)$$

$$\delta_{A22} = \sqrt{2}/2 \quad - \delta_{P2} + \delta_{Y2} \tag{6-11}$$

$$\delta_{A12} = \sqrt{2}/2 \quad - \delta_{P2} - \delta_{Y2} \tag{6-12}$$

For point stability and control analysis when single axis perturbation are used to evaluate stability and vehicular response, the attitude errors are approximated by Equations (6-13), (6-14), and (6-15).

$$\theta_e = X_\theta - \theta_{IU} \tag{6-13}$$

$$\psi_e = X_\psi - \psi_{IU} \tag{6-14}$$

$$\phi_e = X_\phi - \phi_{IU} \tag{6-15}$$

A flight control system block diagram is shown in Figure 2-31. The block diagram is conceptual and is for use in determing the stage control requirements such as stability margins and control system response characteristics.

The sign convention used in positioning the flight control engine is shown in Figure 2-32.

2.5.5 ENGINE SYSTEM DYNAMICS

Data are presented on the gimbaled engines used for flight control during the ascent boost and orbital operations flight phases. Actuation system dynamics, engine thrust levels, thrust alignment engine mass data and other data are given for the Orbiter Mainstage Engines and Orbiter Maneuvering System (OMS) engines.

2.5.5.1 Engine Data

Engine data for use in flight dynamics are given in Table 2-13 for the orbiter engine. These data were collected from References 2, 4, and 6. Similar data are given on the OMS engines and were collected from References 5 and 6 and are listed in Table 2-14 and Figure 2-35. Thrust build-up transients are shown in Figures 2-33 and 2-34 for the orbiter and OMS engines, respectively.

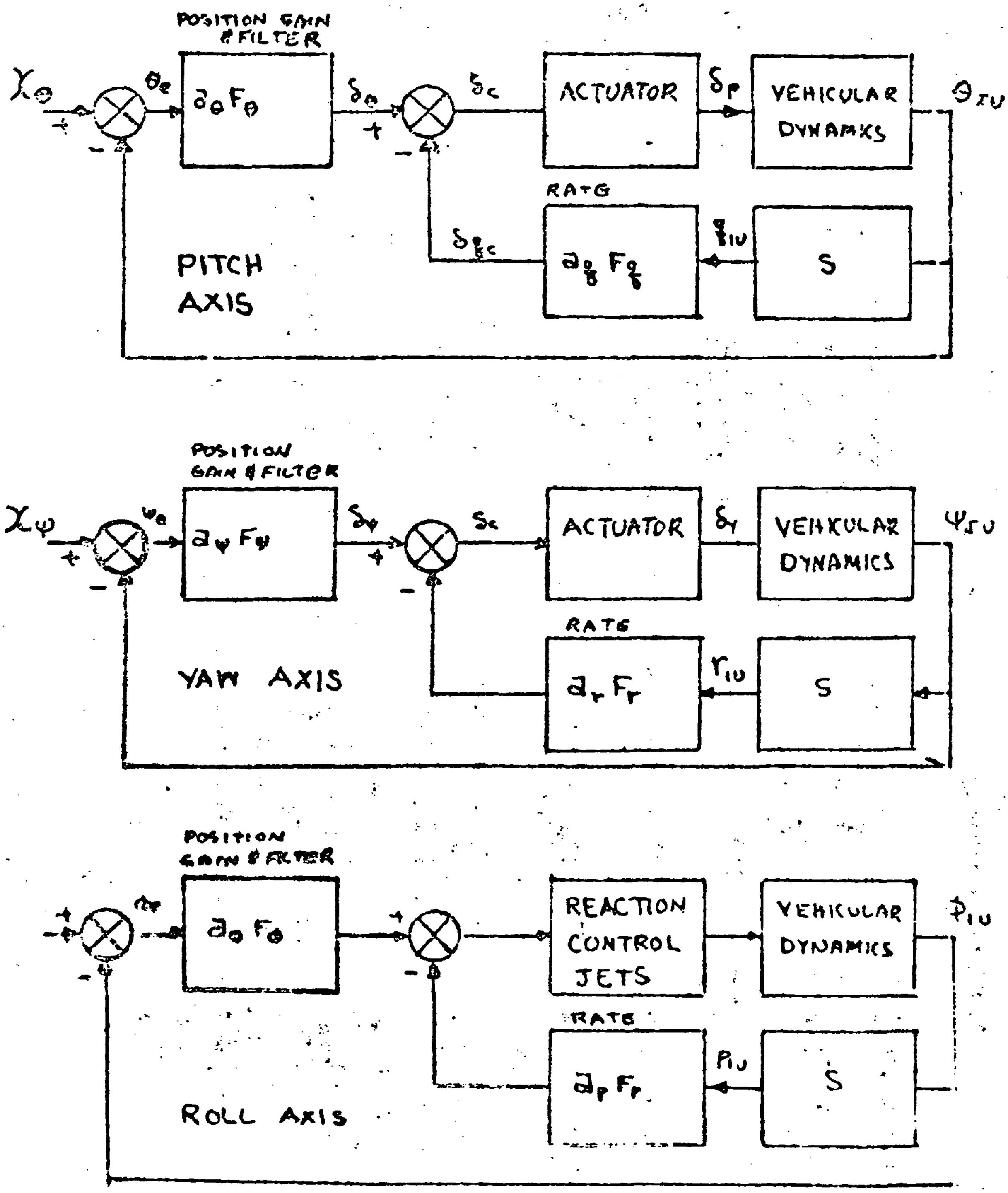

Figure 2-31. 3 Axis Flight Control Diagram

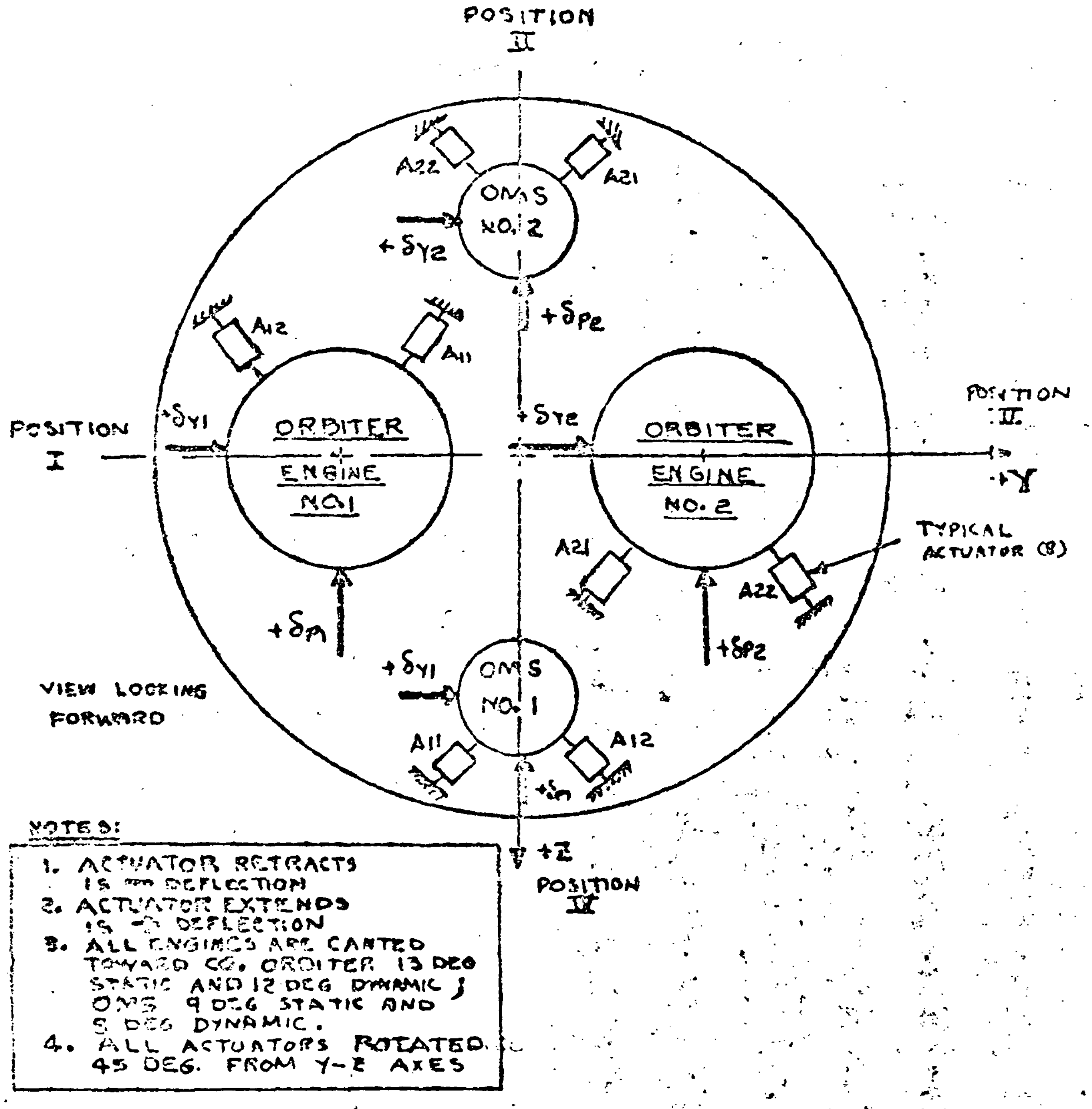

Figure 2-32. Flight Control Engine Sign Convention

Table 2-13. Orbiter Engine Data

PARAMETER	VALUE
THRUST (NOMINAL @VACUUM)	632,000 LB
NOMINAL MIX RATIO	6
THRUST VECTOR ALIGNMENT	30 min FROM ℄
THRUST OFF-SET (FROM GIMBAL CENTER)	0.6 INCH
GIMBAL ANGLE RATE	10 DEG/SEC
GIMBAL ANGLE ACCELERATION	573 DEG/SEC
GIMBAL ANGLE LIMIT	±7 DEG
ACTUATOR LIMIT	±7 DEG
LOADS ALLOWABLE ON ENGINE	
LONGITUDINAL - STEADY STATE	3 g
LONGITUDINAL - DYNAMIC	± 1/4 g
LATERAL - STEADY STATE	± 0.8 g
LATERAL-DYNAMIC	± 0.26 g
THRUST ON-OFF TRANSIENT	FIGURE 4-1
CANT ANGLE - YAW PLANE	13 DEG STATIC 12 DEG DYNAMIC
GIMBAL POINT LOCATION	
X_e	STA 44 IN
Y_e	9.42 FT
Z_e	0
MASS, m_e, WET	205 SLUGS
CENTER-OF-GRAVITY (FROM GIMBAL POINT)	
X	3.68 FT
Y	.15 FT
Z	.08 FT
MOMENT OF INERTIA (GIMBAL POINT)	
I_x	1050 SL-FT^2
I_y	5950 SL-FT^2
I_z	5550 SL-FT^2

REFERENCES: 2, 46

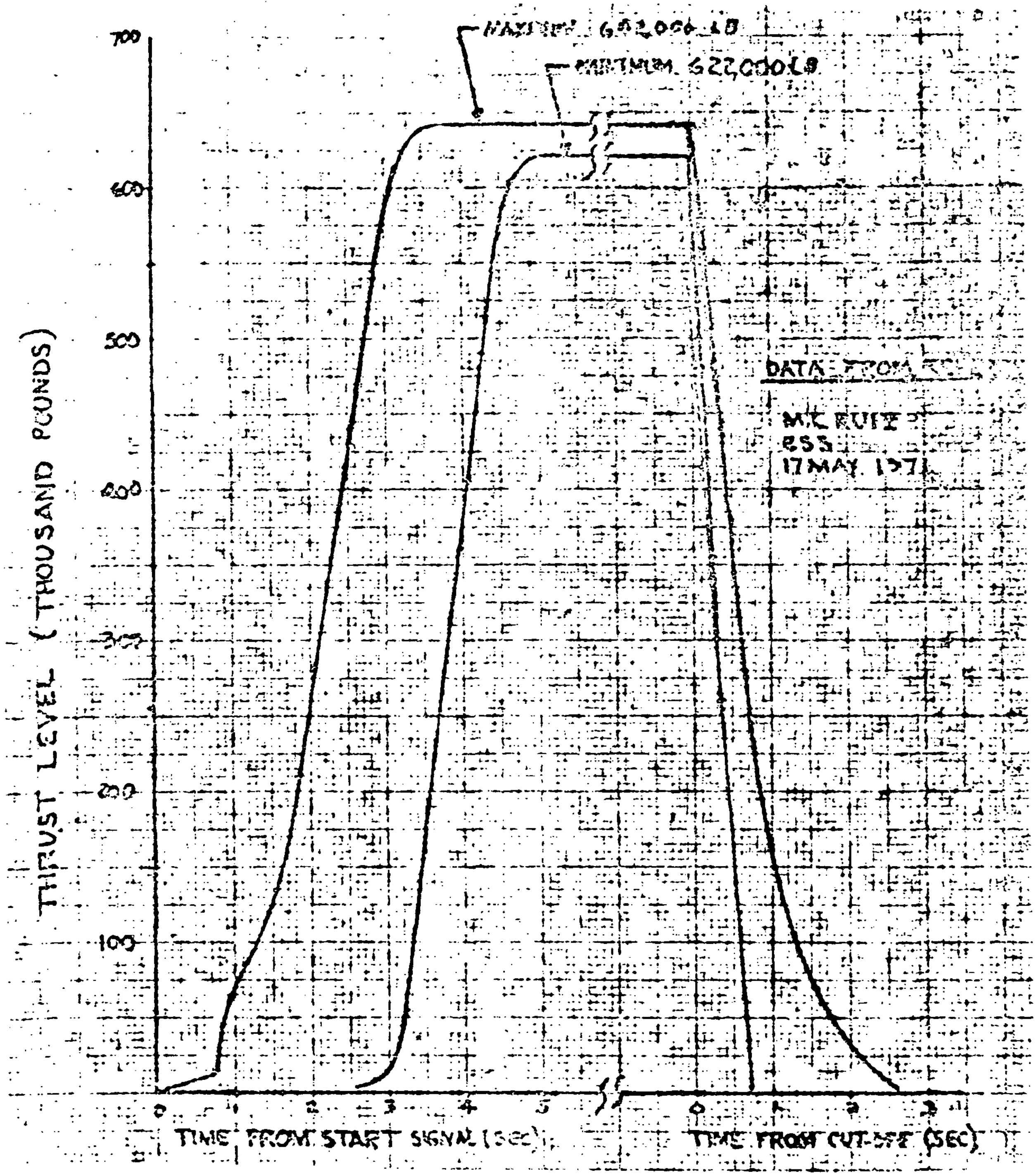

Figure 2-33. Orbiter Engine On-Off Transient

Table 2-14. Orbital Maneuvering Engine

PARAMETER	VALUE
THRUST (NOMINAL @VACUUM)	10,000 LB
NOMINAL MIX RATIO	6
THRUST VECTOR ALIGNMENT	30 MIN FROM ℄
THRUST OFF-SET (FROM GIMBAL CENTER)	1/8 INCH
GIMBAL ANGLE RATE	27 DEG/SEC
GIMBAL ANGLE ACCELERATION	TBD
GIMBAL ANGLE LIMIT	5 DEG
ACTUATOR LIMIT	TBD
LOADS ALLOWABLE ON ENGINE	TBD
THRUST ON-OFF TRANSIENT	FIGURE 4-2
CANT ANGLE - PITCH PLANE	9 DEG STATIC 8 DEG. DYNAMIC
GIMBAL POINT LOCATION	
X_e	STA — 48 IN
Y_e	0
Z_e	10.7 FT
MASS, M_e, WET	4.6[illegible] SLUGS
CENTER-OF-GRAVITY (FROM GIMBAL POINT)	
X	1.8[illegible] FT
Y	.0[illegible] FT
Z	.04 FT
MOMENT OF-INERTIA	
I_x	3.2 SL-FT^2
I_y	29 SL-FT^2
I_z	29 SL-FT^2
REFERENCES: 5,6	

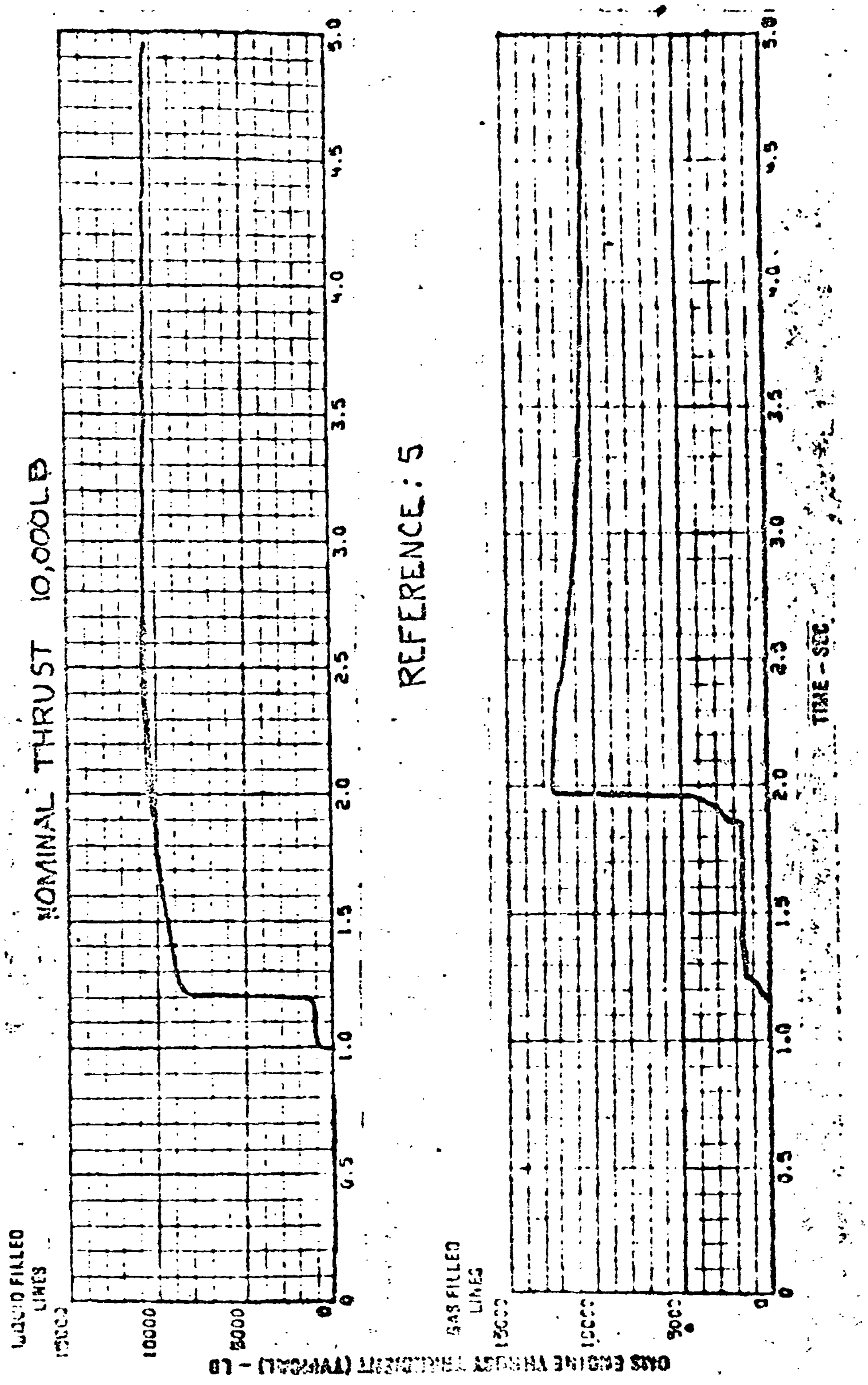

Figure 2-34. Orbital Maneuvering System Engine Start Transient

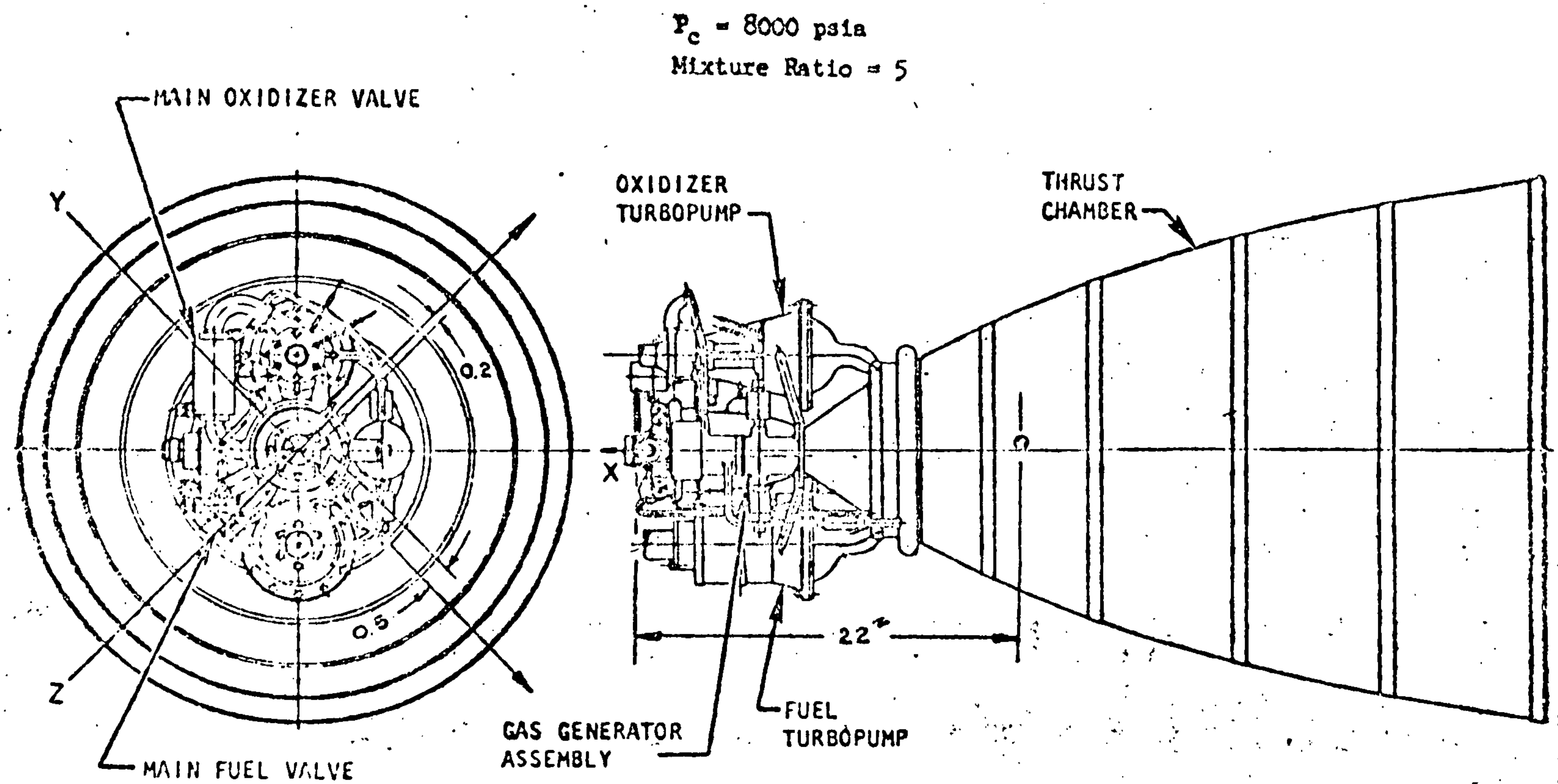

REFERENCE: 5

Weight, pounds	Center of Gravity, inches			Moment of Inertia, slug-ft^2		
	X	Y	Z	I_{xx}	I_{yy}	I_{zz}
152	-22	0.2	0.5	3.2	28.8	23.8

Figure 2-35. OMS Engine Configuration

PRECEDING PAGE BLANK NOT FILMED

BIBLIOGRAPHY

1. SID 62-583, "S-II Stability and Control Data Manual," Revision February 1969.

2. S-II-193-603-71-009, "Shuttle Engine Data for the Expendable Second Stage Study," Revision 18 February 1971.

3. IL S-II-193-603-71-032, "Data Input for Control Analysis of ESS," 25 March 1971.

4. NASA/MSFC ICD 13M1500A, "Space Shuttle/Engine 415 (SL)—Interface Control Document," 12 November 1970.

5. Rocketdyne Report R-8275, "Design Data for the Space Shuttle Orbital Maneuvering System Engine, Rocketdyne Model RS-23," 1 September 1970.

6. SD Dwg. No. V7-923075 (Code ID 03953), "General Arrangement - ESS," Revision 2 April 1971.

7. IL SLV-191-702-71-036, "ESS Mass Properties During Second Flight Stage Burn Time," 9 April 1971.

8. IL S-II-595-201-70/197, "ESS Orientation Relative to the Shuttle Booster," 8 December 1970.

9. MSFC Memo R-Aero-DD-21-77, "Maximum Slosh Height for Saturn IB and Saturn V vehicles by G. Muller," May 1966.

10. MSFC Memo R-Aero-DD-74-67, "Slosh Model Parameters for Saturn V Vehicle as a Function of Propellant Loading," 27 December 1967.

11. MSFC Memo R-Aero-DD-88-68, "Correction to Slosh Parameter for Saturn V Vehicle" 5 March 1968.

12. MSFC Memo R-Aero-DD-92-68, "Saturn V Official Dynamics Data," 26 March 1968.

13. IL S-II-595-401-DA-70-118, "INT-21 With Reusable Nuclear Shuttle (RNS) Body Bending Data," 7 August 1970.

14. IL S-II-193-601-71-065, "Distribution of ESS Flight Timeline Revision," 29 April 1971.

3.0 CONFIGURATION DEFINITION

3.1 USE OF EXISTING LH_2 TANK OUTLET ELBOWS WITH SPACE SHUTTLE ENGINE

The expendable second stage features two space shuttle engines. These engines require much higher fuel flow rates than do J-2 engines and, therefore, need larger feed ducts. To minimize the S-II modifications required for the ESS, an analysis was performed to determine if the existing LH_2 tank outlet elbows can be used with the shuttle engines.

3.1.1 CONCLUSION AND RECOMMENDATIONS

The existing LH_2 tank outlet elbows cannot be used with space shuttle engines. A 13-inch right-angle elbow should be used instead.

3.1.2 DISCUSSION

The analysis performed on the LH_2 tank outlet elbows is presented in the following section. The results may be summarized as follows:

1. At the anticipated flow, a velocity of 98 ft/sec occurs in the existing LH_2 tank elbow. This is considered acceptable as it is slightly below the 100 to 120 ft/sec normally used as an upper design limit.

2. A pressure drop of 3.8 psi occurs. With the existing LH_2 tank structural capability and engine NPSH requirement, this is acceptable.

3. The cavitation constant is less than one. A cavitation constant of two or greater is generally considered acceptable. For this reason, the existing elbow is considered unacceptable.

Research indicates that a 90-degree angle out of the tank represents a more desirable configuration than does the existing LH_2 tank outlet. Since a 90-degree configuration is considered acceptable in terms of pressure drop and cavitation, the selected ESS will utilize a 13-inch 90-degree LH_2 tank outlet elbow. The ESS propellant feed layout shows both a 90-degree and a 30-degree elbow.

ANALYSIS OF THE EXISTING LH_2 TANK OUTLET ELBOWS WITH THE SPACE SHUTTLE ENGINE.

1. ENGINE LH_2 FLOWRATE

   THE MAXIMUM LH_2 FLOWRATE OCCURS WHEN THE ENGINE IS OPERATING @ EMERGENCY POWER LEVEL. USE OF EPL IS PLANNED FOR AN ENGINE OUT CONDITION.

   FROM ICD 13M15000B

   THRUST = 109% (632,000) = 689,000 LB.

   ISP MINIMUM = 456 SECONDS

   $\therefore \dot{W} = 689{,}000/456 = 1511$ LB/SEC

   EMR @ EPL IS FIXED AT 6 TO 1

   $\therefore \dot{W}_{LH_2} = 1/7\,(1511) = \underline{\underline{216\ \text{LB/SEC}}}$

   (FOR J-2 THE MAX LH_2 FLOW = 83.5 LB/SEC)

2. k FACTOR OF LH_2 ELBOW AND LENGTH

   k FACTORS: TANK OUTLET = 0.5
   25° BEND = 0.1
   EXPANSION TO 13" = 0.2
   $\Sigma k = 0.8$

   LENGTH: TANK RING = 2 IN
   ELBOW = 21 IN
   FLANGE = 2 IN
   L = 25 IN = **2.1 FEET**

3. VELOCITY & DYNAMIC PRESSURE IN ELBOW

$\rho_{LH_2} = 4.4 \text{ LB/FT}^3$

$\therefore \quad Q = 216/4.4 = 49.1 \text{ FT}^3/\text{SEC}$

I.D. OF LH_2 TANK ELBOW = 9.600 ± 0.015 IN

$$\therefore \quad A = \frac{\pi (9.58)^2}{4(144)} = 0.50 \text{ FT}^2$$

$$\text{VELOCITY} = 49.1/0.50 = \underline{\underline{98.2 \text{ FT/SEC}}}$$

$$q = \tfrac{1}{2}\rho V^2 = \frac{(4.4)(98.2)^2}{2(32.2)} = 658.9 \text{ PSF}$$

$$658.9/144 = \underline{\underline{4.58 \text{ PSI}}}$$

(FOR J-2 $V = 37.94$ FT/SEC, $q = 0.68$ PSI)

4. PRESSURE LOSS

REYNOLDS NUMBER

$$N_{RE} = \frac{\rho V D}{\mu} \qquad \begin{aligned} \mu &= 9.0 \times 10^{-6} \text{ LB/SEC-FT} \\ \rho &= 4.4 \text{ LB/FT}^3 \\ D &= 9.58/12 \text{ FT} \\ V &= 98.2 \text{ FT/SEC} \end{aligned}$$

$$N_{RE} = \frac{(4.4)(98.2)(9.58)}{(9.0 \times 10^{-6})(12)} = 3.83 \times 10^7$$

FROM CURVE, $f = 0.00165$

$$\Delta P = \tfrac{1}{2}\rho V^2 \left(4f\frac{L}{D} + k\right)$$

$$4f\frac{L}{D} = 4(.00165)(2.1)\left(\frac{12}{\ }\right) = 0.0174$$

$\Delta P = 4.58(.02 + 0.8)$

$= \underline{\underline{3.76 \text{ PSI}}}$

(FOR J-2 THE DROP IS 0.56 PSI)

5. IS THE ΔP ACCEPTABLE?

FOR THE PLANNED 13" FEED SYSTEM THE PRESSURE LOSS IN THE REST OF THE SYSTEM IS 2.49 PSI (BASED ON THE ORIGINAL CALCULATIONS FOR SIZING THE ESS FEED SYSTEM).

$\Sigma \Delta P = 3.76 + 2.49 = 6.25$ PSI

PLANNED LH_2 ULLAGE IS 27.5 - 29.5 PSIA

$\therefore$ INLET PRESS = 27.5 - 6.25 + HEAD
= 21.25 + HEAD

NPSP = INLET PRESS - VAPOR PRESS
= 21.25 + HEAD - P_{VAPOR}

REQUIRED NPSP = 2.5 PSI (FROM ICD 13M15000B)

$2.5 \leq 21.25 + HEAD - P_{VAPOR}$

$\therefore P_{VAPOR} - HEAD \leq 18.75$ PSI

$P_{VAPOR} > 18.75$ PSI ONLY @ END BOOST

AT END BOOST

HEAD = $h \cdot \rho$ (LOAD FACTOR)

@ END BOOST

LIQ STATION = 355 IN
INLET STATION = 55 IN
h = 300 IN = 25 FEET

LOAD FACTOR = 3.3 (ENGINE OUT CASE)

HEAD = (25)(4.4)(3.3) = 363 PSF

363/144 = 2.52 PSI

P_{VAPOR} = 19.6 PSI

P_{VAPOR} - HEAD = 19.6 - 2.5 = 17.1 PSI < 18.75 PSI

∴ PRESSURE DROP IS ACCEPTABLE

6. CAVITATION CONSTANT

THE CAVITATION CONSTANT, σ, IS DEFINED AS

$$\sigma = \frac{P_{STATIC} - P_{VAPOR}}{\frac{1}{2}\rho V^2}$$

$\frac{1}{2}\rho V^2$ = 4.58 PSI P_{VAPOR} MAX = 19.6 PSIA

P_{STATIC} = ULLAGE PRESS + ~~HEAD~~ - $P_{DYNAMIC}$ - P_{FRICT}

ASSUME ZERO HEAD - LIQUID INTERFACE AT END BOOST IS NEAR ELBOW.

ULLAGE PRESS = 27.5 PSIA

P_{STATIC} = 27.5 - 4.58 - 2.75 = 20.17 PSIA

$$\sigma = \frac{20.17 - 19.6}{4.58} = \underline{\underline{0.12}}$$

(FOR J-2 $\sigma = 16$)

THE MINIMUM REQUIRED VALUE OF σ IS SOMEWHAT OPEN TO CONJECTURE AND CAN ONLY BE ESTABLISHED ADEQUATELY BY TESTING. HOWEVER, A VALUE OF 2 IS NORMALLY CONSIDERED NECESSARY. THIS IS TO PREVENT LOCAL CAVITATION AT THE INSIDE OF THE ELBOW WHERE THE VELOCITY IS GREATER.

BY ASSUMING A VELOCITY DISTRIBUTION IN THE BEND LIKE A POTENTIAL VORTEX THE ACTUAL VELOCITY CAN BE CALCULATED AS FOLLOWS FOR TWO DIMENSIONAL FLOW:

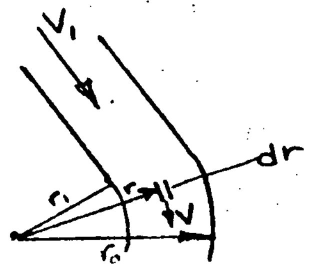

POTENTIAL VORTEX

$Vr = \text{CONSTANT}$

$r_1 = 5.25 \text{ IN} = .438 \text{ FT}$

$r_0 = 14.85 \text{ IN} = 1.238 \text{ FT}$

$V_1 = 98.2 \text{ FT/SEC}$

$$Q = AV = C$$

(2 DIMENSIONAL)

$$dQ = V\,dA = V\,dr = \frac{C}{r}\,dr$$

$$\therefore\ Q = C \operatorname{Ln} r \Big|_{r_0}^{r_1} = C \operatorname{Ln} \frac{1.238}{.438} = C \operatorname{Ln} 2.826$$

$$Q = Vr = 98.2\,(1.238 - .438) = 78.56$$

$$\frac{78.56}{\operatorname{Ln} 2.826} = C \qquad C = \frac{78.56}{1.04} = 75.54$$

$$V_1 = \frac{C}{r_1} = \frac{75.54}{.438} = 172.47 \text{ FT/SEC}$$

@ A VELOCITY OF 172.47 FT/SEC

$$\frac{1}{2}\rho V^2 = \frac{(4.4)(172.47)^2}{2\ (32.2)} = 2032 \text{ psf}$$

$$2032/144 = 14.11 \text{ PSI}$$

$P_{STATIC} = 27.5 - 14.11 - 2.77 = 10.62$ PSIA

THIS IS CONSIDERABLY LESS THAN THE VAPOR PRESSURE - CAVITATION WILL OCCUR.

THE POSSIBILITY OF RAISING THE ULLAGE PRESSURE WAS CONSIDERED. HOWEVER, DUE TO THE RELATIVELY WARM TEMPERATURE OF THE LH_2 REPRESSURIZATION GAS ANTICIPATED WITH THE SHUTTLE ENGINE (+40°F) NO MORE THAN A 1 PSI INCREASE CAN BE ACHIEVED AND STAY WITHIN THE LH_2 TANK STRUCTURAL STRENGTH LIMITATIONS. P_{STATIC} WOULD STILL BE LESS THAN VAPOR PRESSURE IN THE ELBOW.

IT IS THEREFORE CONCLUDED THAT THE EXISTING SII LH_2 TANK OUTLET ELBOWS ARE UNACCEPTABLE FOR THE ESS.

3.2 ENGINE INLET PRESSURE AND TEMPERATURE, ESS PRESSURIZATION SYSTEM BASELINE CONFIGURATION

Estimates have been made for the engine inlet pressure and temperature of an ESS using two space shuttle orbiter engines. The results are based on a pressurization system baseline configuration in which an orifice controls the pressurization flow into the tank and vent valves control propellant tank pressures, which are set at 27.5-29.5 psig for both the LO_2 and LH_2 tanks. The engine inlet temperature, during both the start transient and mainstage operations, should be regarded as typical only, inasmuch as the total heat load to the propellant and the performance of the recirculation (engine inlet prestart conditioning) system have not been established. However, the selected temperature values are based on S-II experience, and are considered conservative.

Figures 3-1 through 3-5 present the data and results relative to the engine inlet pressure and temperature during the ESS burn. More than adequate NPSP is supplied during the start and mainstage periods for the conditions assumed, and it is evident there is room for compromise with other areas of consideration, such as propellant feed line size, tank pressure levels, insulation, and liquid residuals.

LOX ENGINE INLET PRESSURE

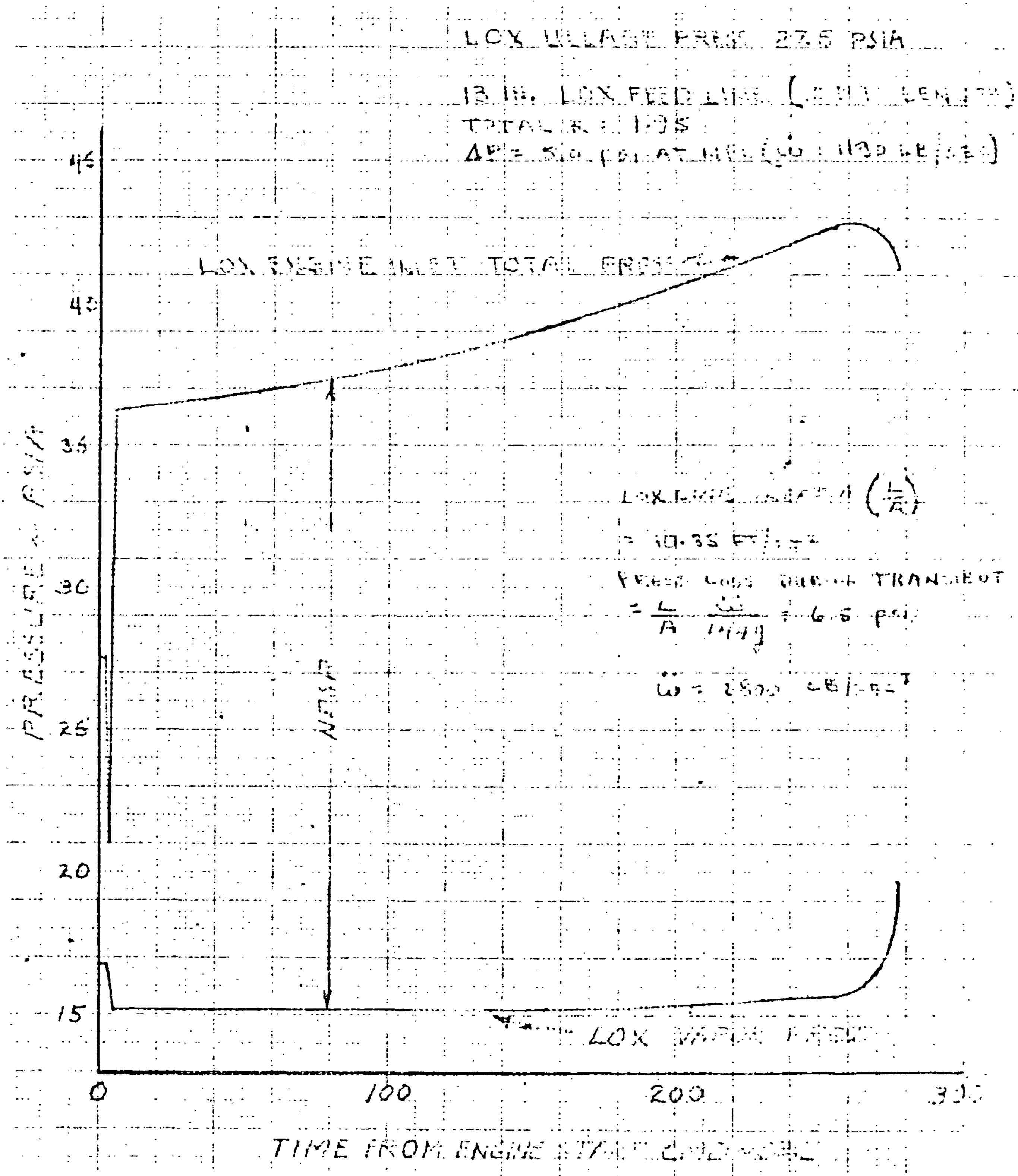

ESS 750 K PROPELLANT-LOAD

LH2 ENGINE INLET PRESSURE

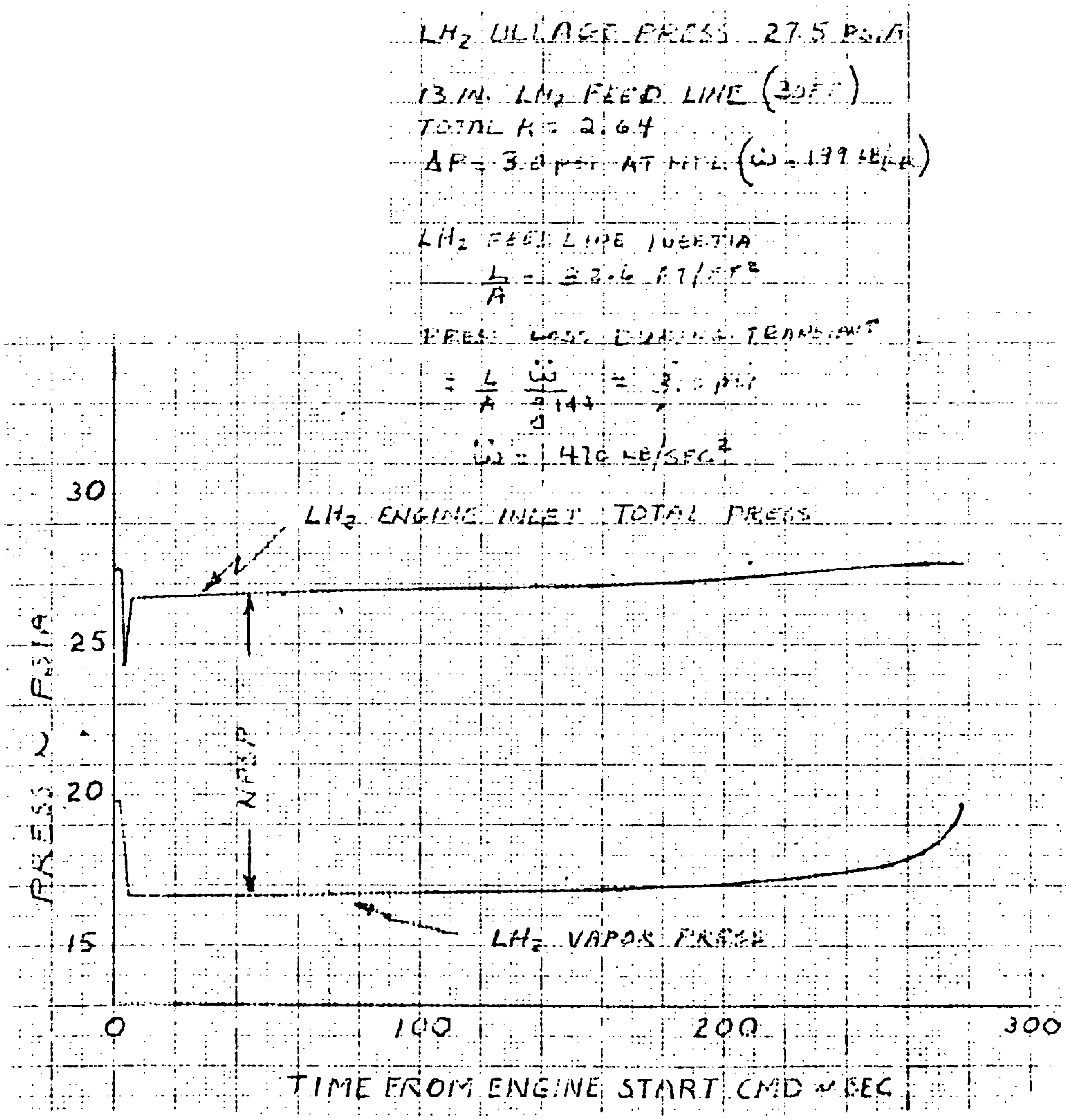

ESS 7504 PROPELLANT LOAD

LOX ENGINE INLET TEMPERATURE

TOTAL HEAT LOAD 107,400 BTU

TOTAL LOX LOADED 653K

1600 LB LOX AT S/O

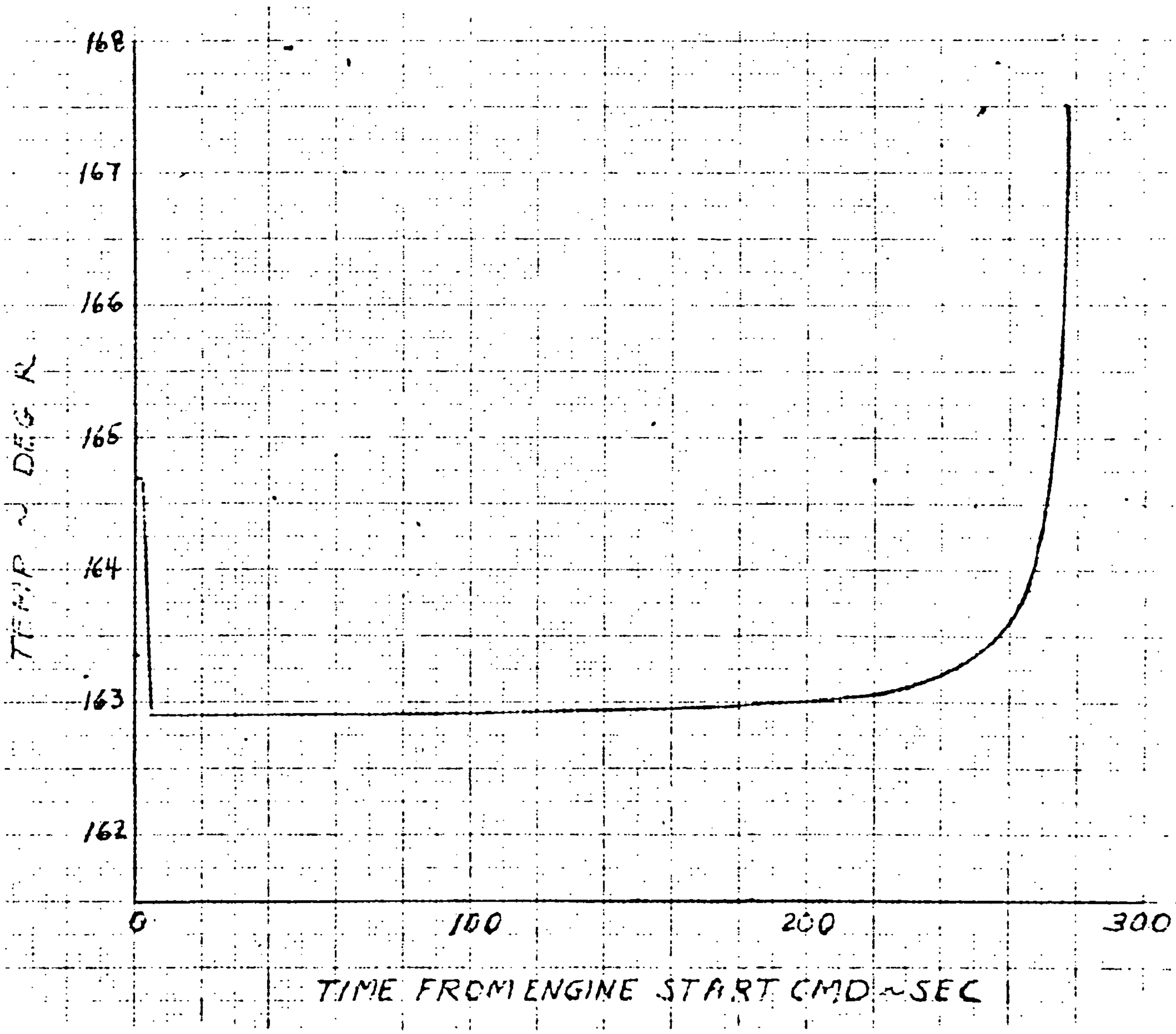

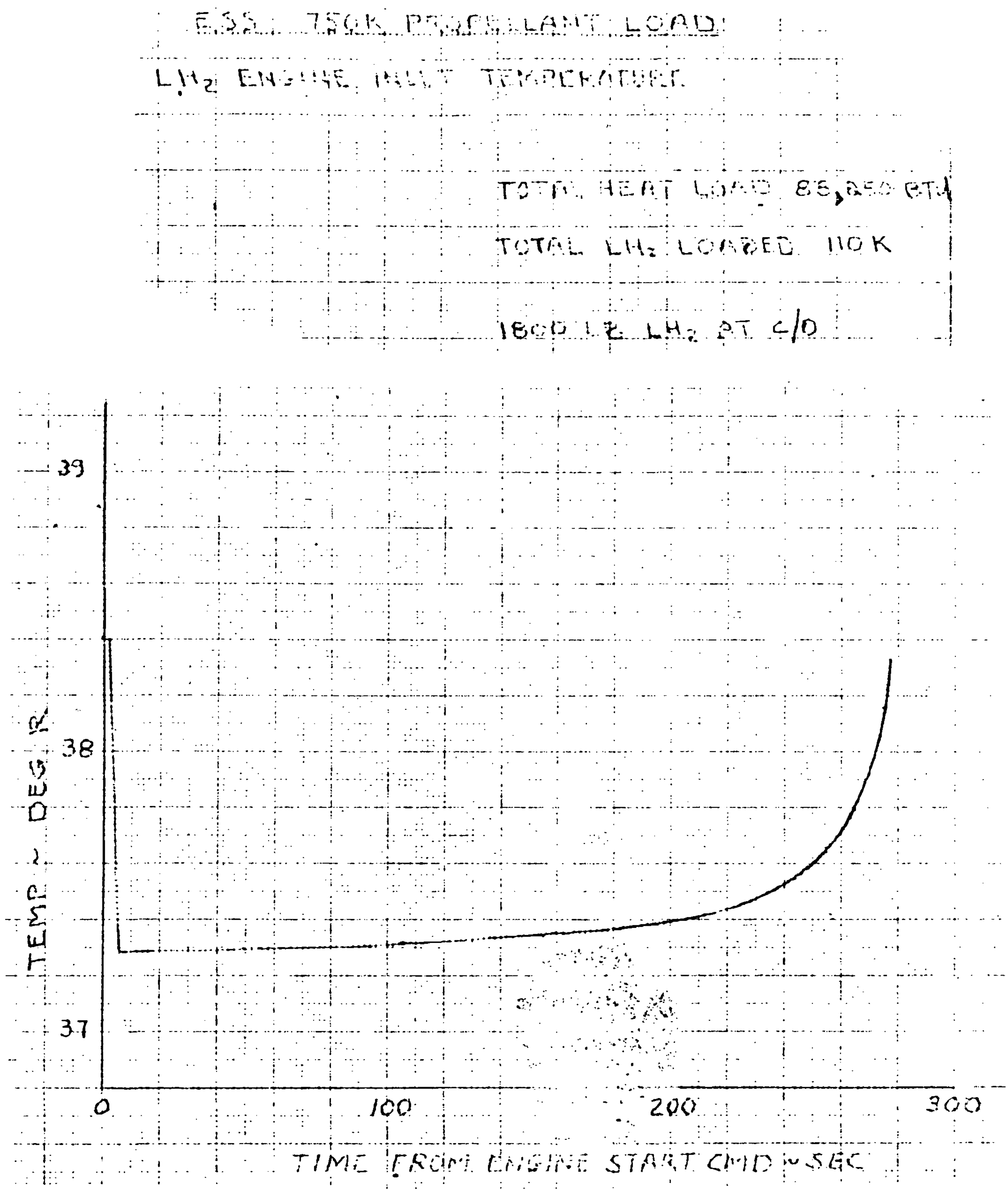
E.S.S. 750K PROPELLANT LOAD
LH2 ENGINE INLET TEMPERATURE
TOTAL HEAT LOAD
TOTAL LH2 LOADED 110K
1800 LB LH2 AT C/O
39
38
37
TEMP ~ DEG R
0
100
200
300
TIME FROM ENGINE START CMD ~ SEC

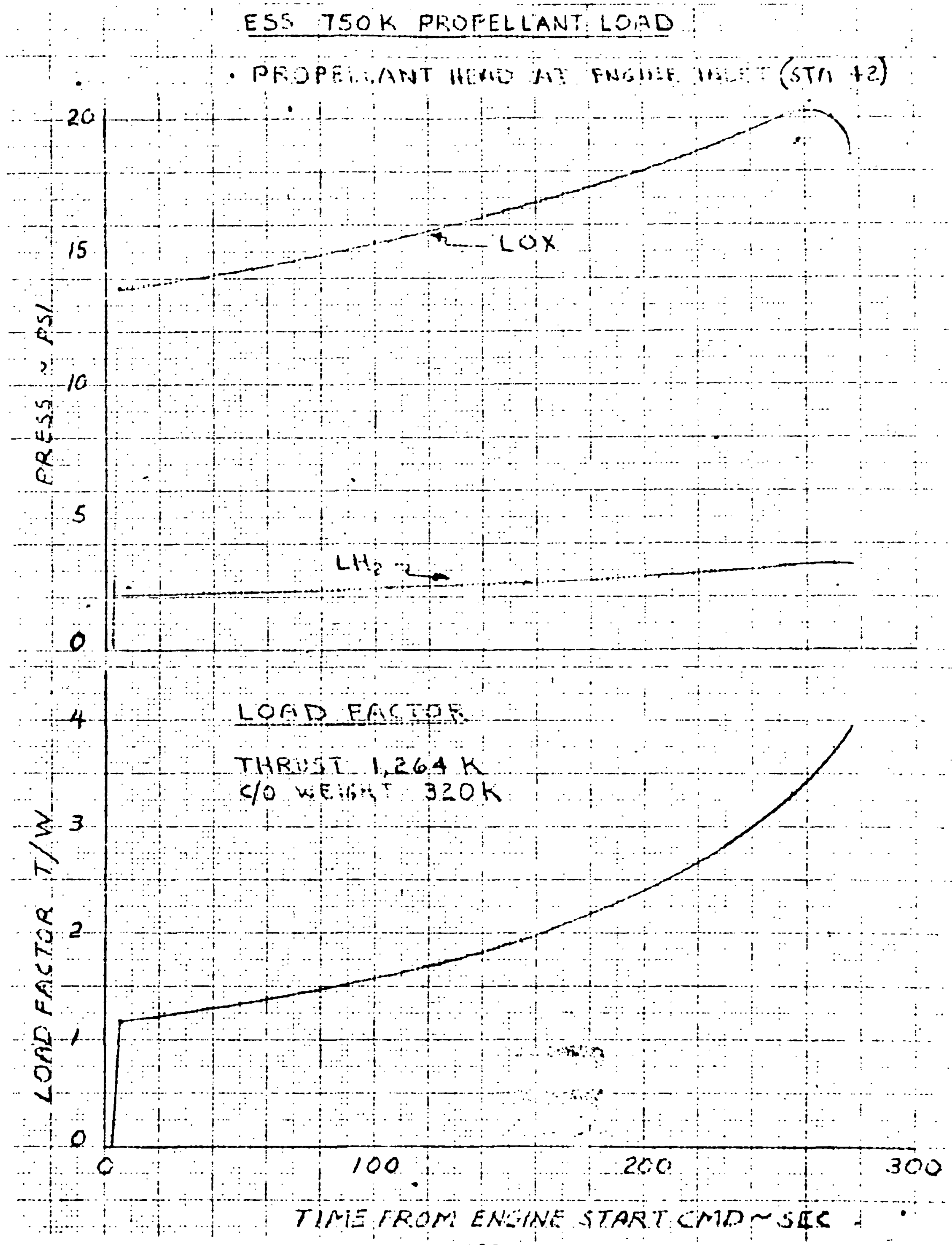

ESS 750 K PROPELLANT LOAD
PROPELLANT HEAD AT ENGINE INLET (STA 42)
PRESS ~ PSI
LOX
LH_2
LOAD FACTOR
THRUST 1,264 K
C/O WEIGHT 320 K
LOAD FACTOR T/W
TIME FROM ENGINE START CMD ~ SEC

3.3 SIZE OF ENGINE HELIUM SUPPLY BOTTLE

3.3.1 IN-FLIGHT AND PRELAUNCH DEMANDS

The in-flight and prelaunch demands are as follows:

1. Prior to liftoff: 130 SCFM
2. First-stage boost: 29 SCFM
3. Nozzle extension: 290 SCFM
4. E/S-1.5 sec to E/S +2.5 sec: 670 SCFM
5. E/S +2.5 sec to E/S +4.0 sec: 11,600 SCFM
6. During ESS burn: 50 SCFM
7. C/O to C/O +1.5 sec: 11,300 SCFM
8. C/O +1.5 sec to C/O +3.0 sec: 1170 SCFM
9. Nozzle retraction: 290 SCFM
10. Propellant dump: two 1-sec bursts at 22 SCFM

3.3.2 TOTAL REQUIREMENTS

The total requirements are as follows:

1.	Allowing for venting the airborne line at T-60 sec 60/60 x 130	= 130 SCF
2.	Boost time ≈ 240 sec 240/60 x 29	= 116 SCF
3.	290 x 8/60	= 39 SCF
4.	670 x 4/60	= 45 SCF
5.	11,600 x 1.5/60	= 290 SCF

6.	ESS burn $\approx$ 200 sec 200/60 x 50	=	167 SCF
7.	11,300 x 1.5/60	=	283 SCF
8.	1170 x 1.5/60	=	30 SCF
9.	290 x 10/60	=	49 SCF
10.	22 x 2/60	=	1 SCF
	Total	=	1150 SCF

ρ_{HE} at STP = 0.01 11.5 lb

For 2 engines
2300 SCF and 23 lb

3.3.3 BOTTLE SIZE

Assuming an initial pressure of 3000 psig and a final pressure of 1400 psig:

$$\Delta P = 1600 \text{ PSIG}$$

$$\text{Vol} = \frac{2300}{1600} \times 14.7 - 21.1 \text{ ft}^3$$

For 4500 psig:

$$\text{Usable} = 1.6 \text{ lb/ft}^3$$

$$\frac{23 \text{ lb}}{1.6 \text{ lb/ft}^3} = 14.4 \text{ ft}^3 \text{ — Use } 15 \text{ ft}^3$$

3.4 ESS ORBIT MANEUVERING SYSTEM (OMS) SIZING

The following design data were developed in sizing the OMS tankage.

Total Impulse = 9.49×10^6 lb-sec (includes contingency and deorbit)

Tank Volumes for Separate Tankage:

RL-10:
- LH_2 = 900 ft^3 + 10% ullage = 990 ft^3
- LO_2 = 279 ft^3 + 10% ullage = 307 ft^3

(10% boil-off and chill-down allowance is included)

LMDE:
- UDMH 50/50 = 216 + 10% ullage = 238 ft^3
- NTO = 216 + 10% ullage = 238 ft^3

Inside Diameters of Tanks:

Single Spherical Tank

RL-10:	LH_2 tank	— 12.4 feet
	LO_2 tank	— 8.4 feet
LMDE:	UDMH 50/50	— 7.7 feet
	NTO tank	— 7.7 feet

Two Spherical Tanks

RL-10:	LH_2 tanks	— 9.8 feet each
	LO_2 tanks	— 6.7 feet each
LMDE	LDMH 50/50	— 6.1 feet each
	NTO tanks	— 6.1 feet each

Note: High-performance insulation will probably add 0.5 foot to cryo tank diameter.

Torus for LH_2 only with 85-inch R - cross section diameter is 5.4 feet (without insulation).

3.4.1 TANK MOUNTING ON ESS

The following are applicable to ESS tank mounting:

LMDE

Two modules (each module containing an engine with a UDMH 50/50 tank and an NTO tank) are mounted on the exterior of the thrust cone.

RL-10

1. The space inside the thrust cone is not adequate for mounting the required LH_2 tankage.
2. There is sufficient space on the exterior of the thrust cone to accommodate the necessary tankage. This means the installation is possible but cannot be considered practicable until the following are completed:
   a. Structures group must analyze to determine if mounting is possible.
   b. An RL-10 thrust structure must be designed.
   c. A thermal protection system must be devised to protect the engine during main engine burn.

3.4.2 TANK SIZE — NEW SHUTTLE OMS ENGINE

I_{sp} = 454 sec

$$\frac{9.49 \times 10^6}{4.54 \times 10^2} = 2.09 \times 10^4 \text{ lb}$$

MR is 5 to 1

$$20,900 \times \frac{1}{6} = 3,483 \text{ lb } LH_2$$

$$20,900 - 3483 = 17,417 \text{ lb } LO_2$$

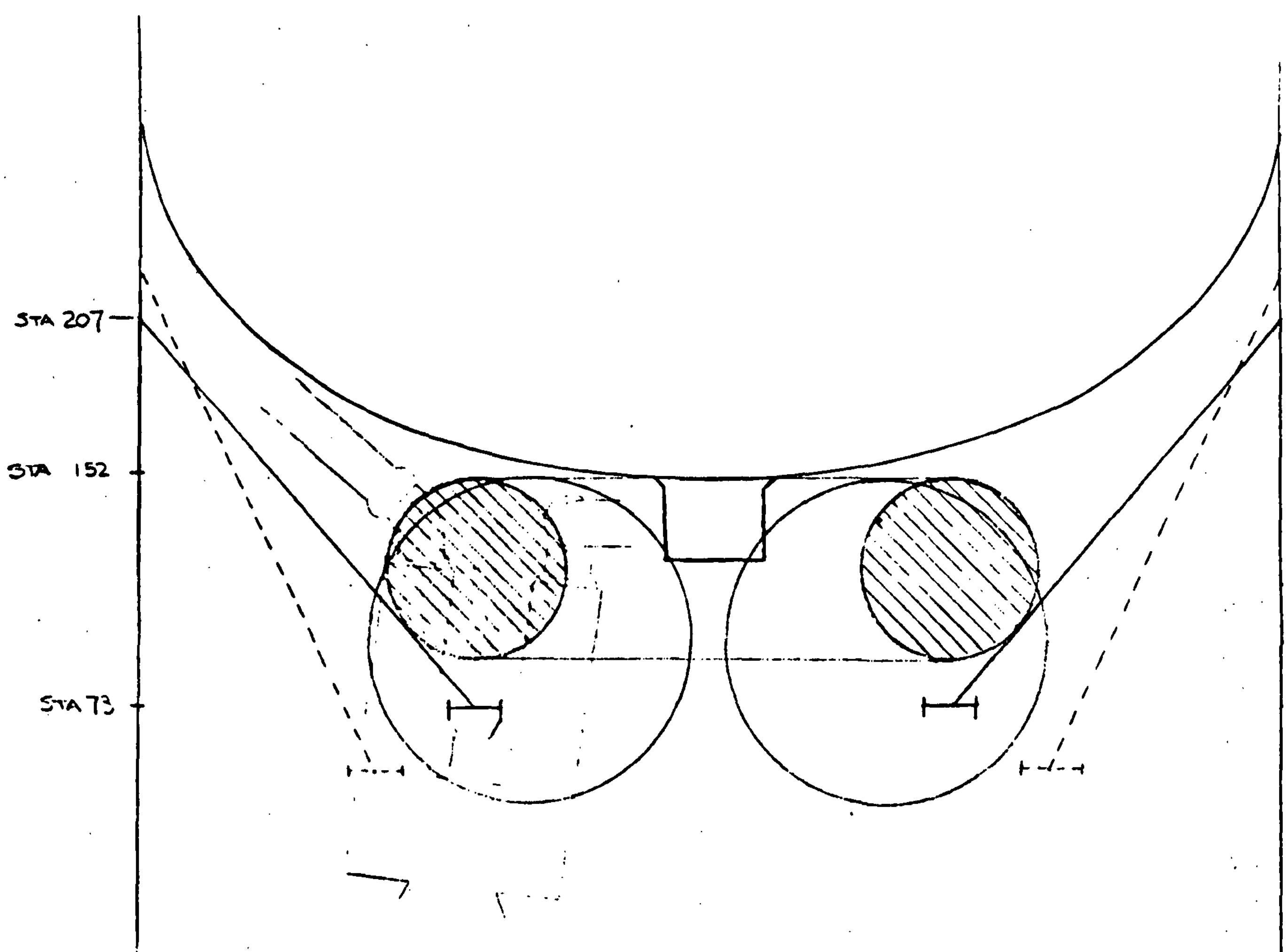

PROPOSED ESS THRUST CONE
2 SPHERICAL RL-10 TANKS
LH_2 ONLY (9.49×10^6 LB-SEC)
(DOTTED LINE IS CIS CONE)

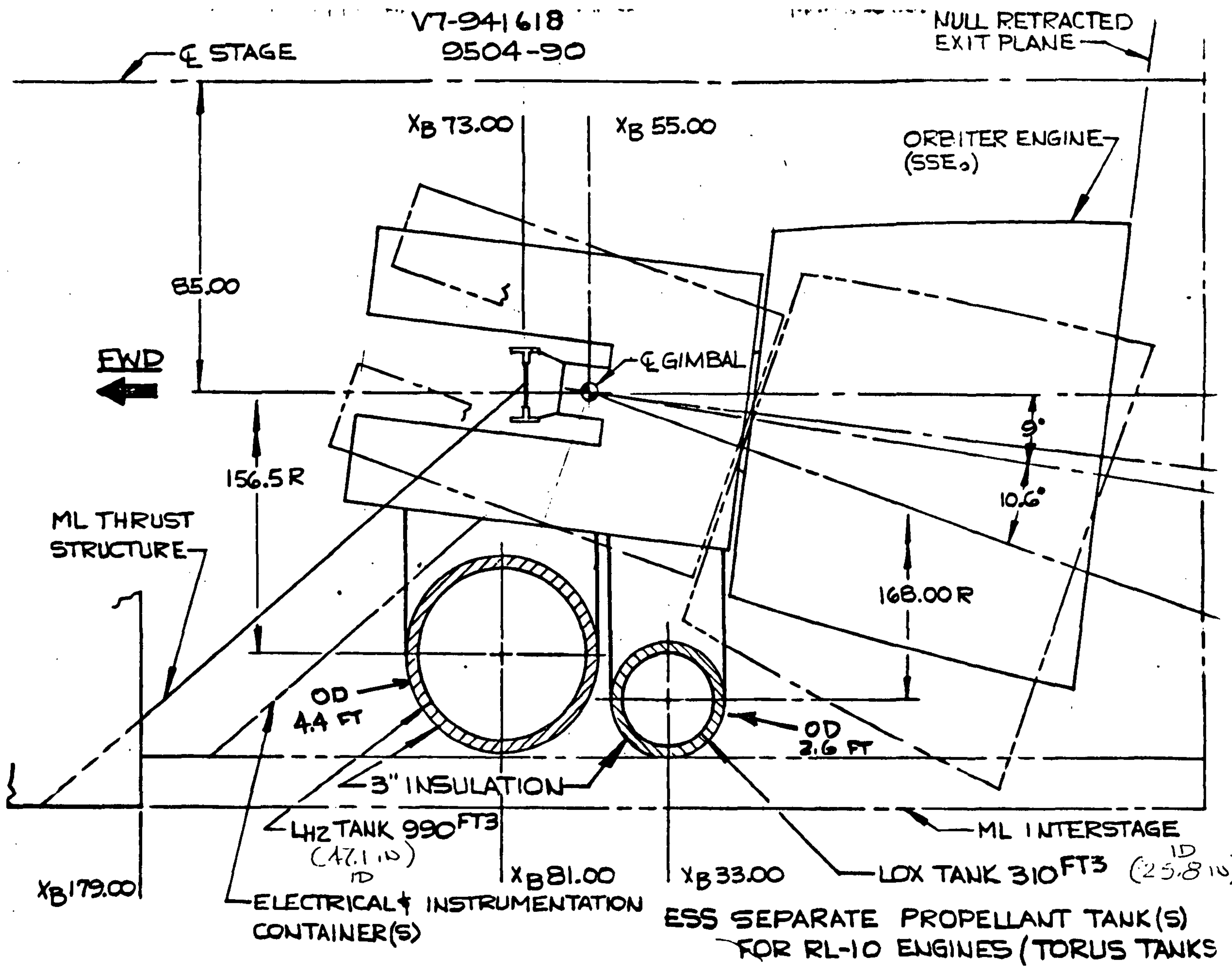

ESS SEPARATE PROPELLANT TANK(S) FOR RL-10 ENGINES (TORUS TANKS

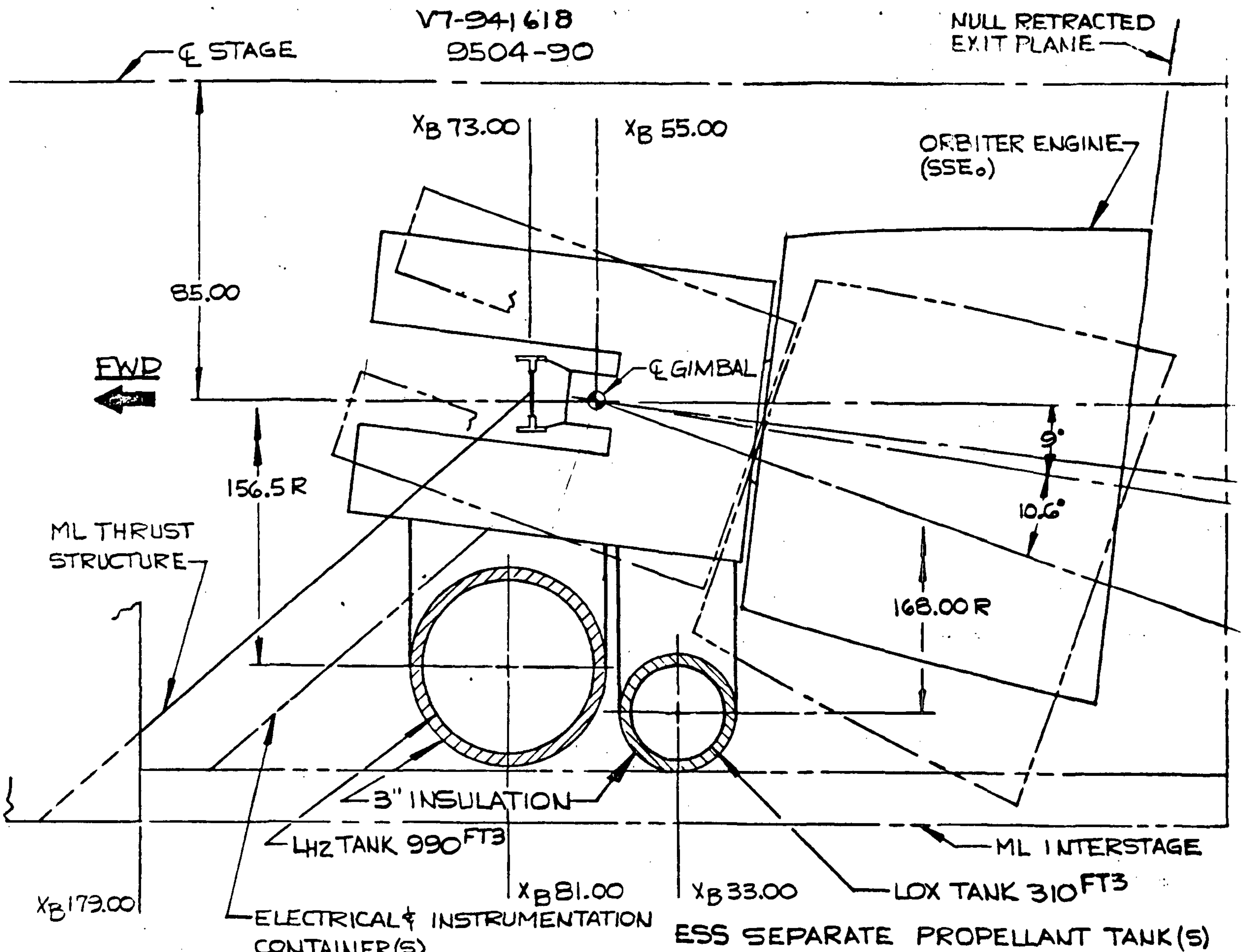

ESS SEPARATE PROPELLANT TANK(S)
FOR RL-10 ENGINES (TORUS TANKS)

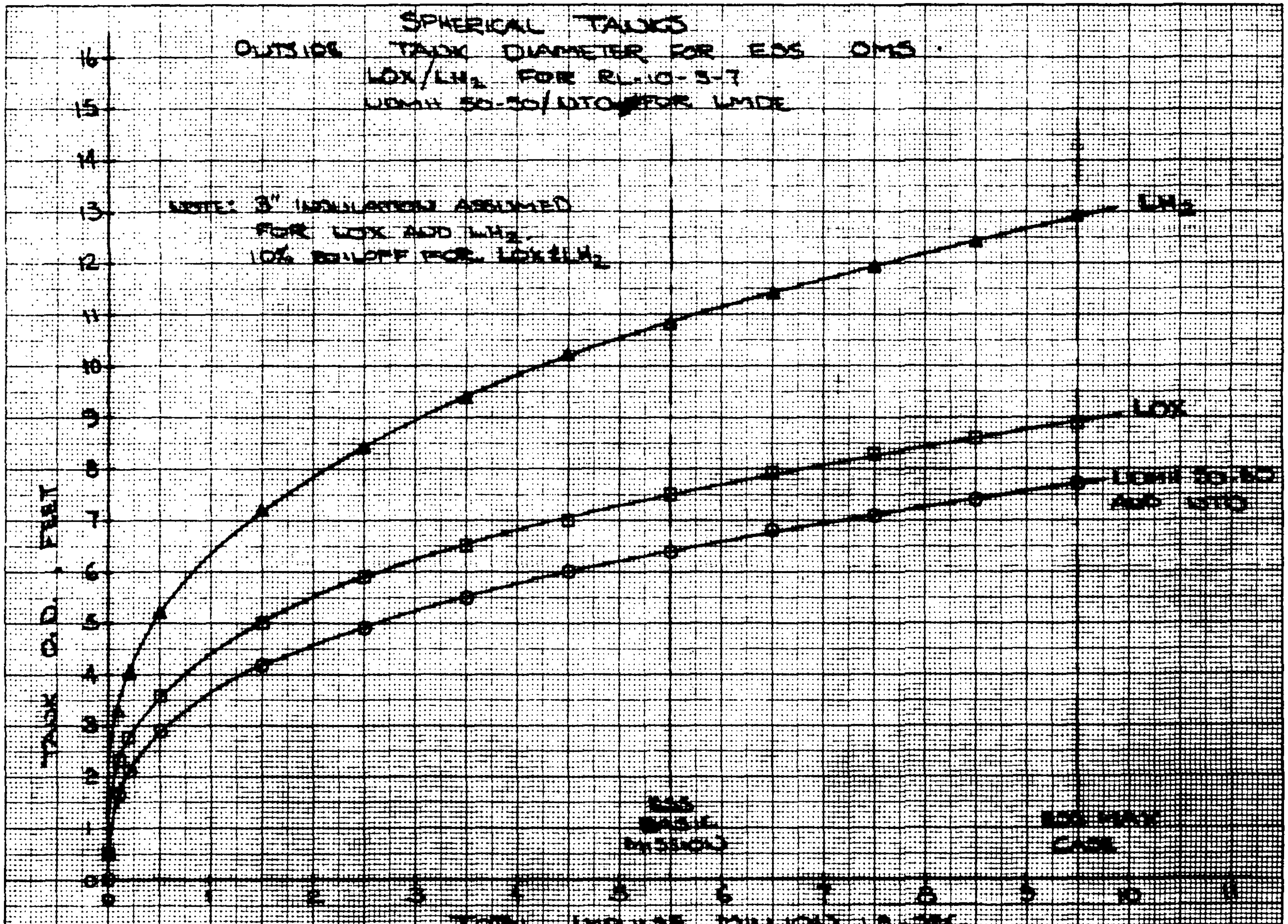
SPHERICAL TANKS
OUTSIDE TANK DIAMETER FOR EOS OMS
LOX/LH2 FOR RL-10-3-7
UDMH 50-50/NTO FOR LMDE
NOTE: 3" INSULATION ASSUMED
FOR LOX AND LH2.
10% BOILOFF FOR LOX & LH2
LH2
LOX
UDMH 50-50
AND NTO
EOS BASIC MISSION
EOS MAX CASE
TANK O.D., FEET
TOTAL IMPULSE, MILLION LB-SEC
0
1
2
3
4
5
6
7
8
9
10
11
12
13
14
15
16

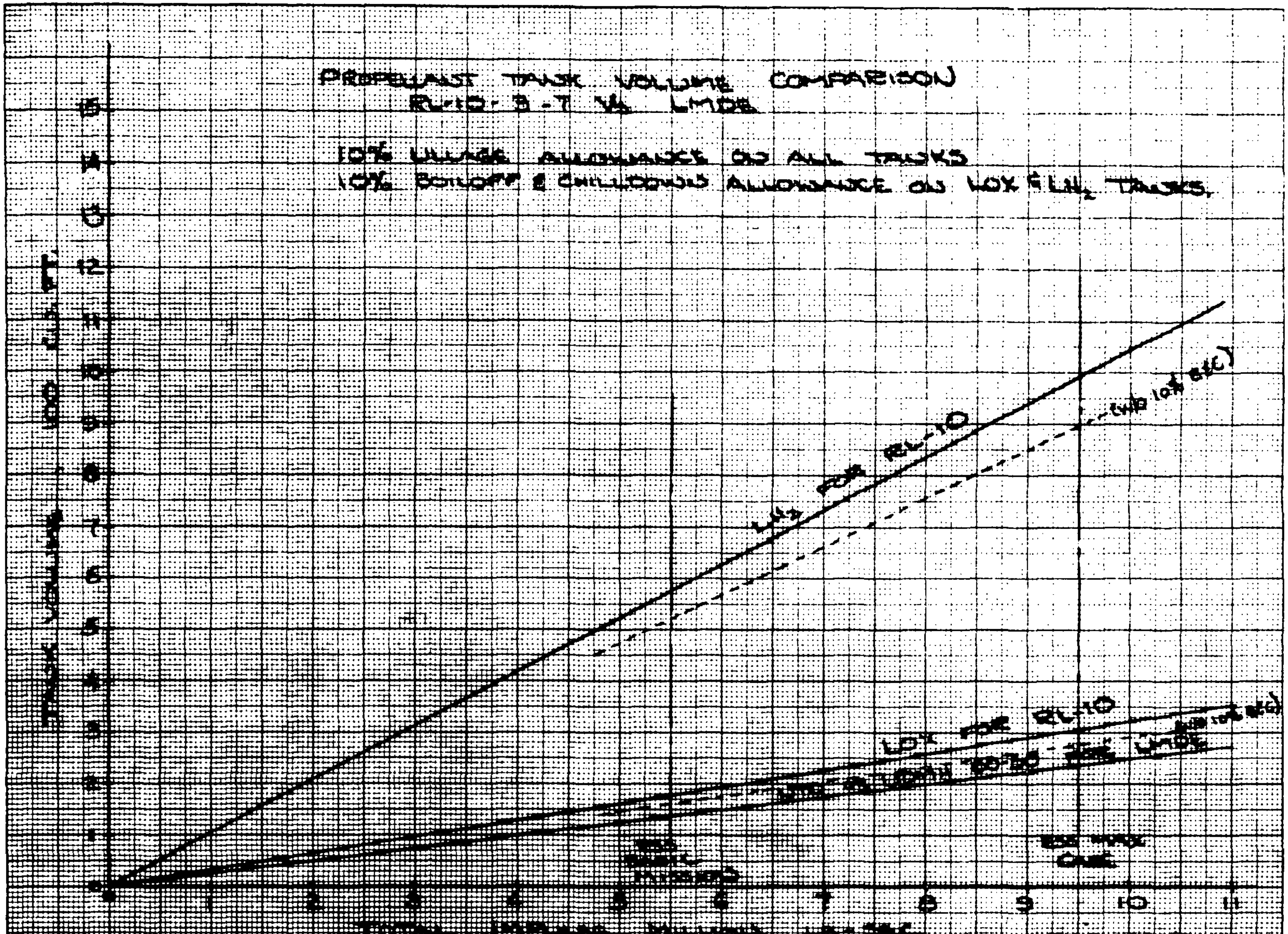
PROPELLANT TANK VOLUME COMPARISON
RL-10-3-7 vs LMDE
10% ULLAGE ALLOWANCE ON ALL TANKS
10% BOILOFF & CHILLDOWN ALLOWANCE ON LOX & LH2 TANKS
LH2 FOR RL-10
LOX FOR RL-10
0
1
2
3
4
5
6
7
8
9
10
11
12
13
14
15

$$\rho_{LH_2} = 4.4 \text{ lb/ft}^3$$

$$\rho_{LO_2} = 71 \text{ lb/ft}^3$$

$$LH_2 \text{ Vol} = \frac{3483}{4.4} = 792 \text{ ft}^3$$

$$LO_2 \text{ Vol} = \frac{17,417}{71} = 245 \text{ ft}^3$$

Add 10 percent ullage:

$$LH_2 = 792 + 79 = 871 \text{ ft}^3$$

$$LO_2 = 245 + 25 = 270 \text{ ft}^3$$

Add 10 percent boil-off and chill-down:

$$LH_2 = 871 + 87 = 958 \text{ ft}^3 \longleftarrow LH_2$$

$$LO_2 = 270 + 27 = 297 \text{ ft}^3 \longleftarrow LO_2$$

Put into 1 LO_2 tank and 4 spherical LH_2 tanks:

LO_2 — 297 ft^3

$$V = \frac{1}{6} \pi D^3$$

$$D^3 = \frac{6(297)}{\pi} = 567.5 \text{ ft}^3$$

D = 8.3 ft +6" insulation (3" each side)

D = 8.8 ft (LO_2)

LH_2 — $958/4 = 240\ ft^3$

$$D^3 = \frac{6(240)}{\pi} = 458.6\ ft^3$$

$D = 7.7$ ft +6" insulation

$D = 8.2$ ft (LH_2)

For CIS tanks, tanks contain 3218 lb LH_2, 13,542 lb LO_2.

13,542 lb = Usable + 10% Usable

$$\text{Usable} = \frac{13,542}{\pi} = 12,311 \text{ lb } LO_2$$

$$\frac{3,218}{11} = 2925 \text{ lb } LH_2$$

$\therefore LO_2$ is limiting

12,311 lb LO_2

Equivalent LH_2 is 1/5 or 2462 lb

$$\sum = 14,773 \text{ lb}$$

14,773 lb x 454 sec

$$I = 6.7 \times 10^6$$

3.4.3 CALCULATE A CURVE

I_{TOT}	Total (lb)	LO_2 (lb)	LH_2 (lb)	LO_2 (ft^3)	LH_2 (ft^3)
1×10^6	2, 203	1, 836	367	25. 86	83. 41
2	4, 405	3, 671	734	51. 70	166. 82
3	6, 608	5, 507	1, 101	77. 56	250. 22
4	8, 811	7, 342	1, 469	103. 41	333. 86
5	11, 101	9, 251	1, 850	130. 30	420. 45
6	13, 216	11, 013	2, 203	155. 11	500. 68
7	15, 419	12, 849	2, 570	180. 97	584. 09
8	17, 621	14, 684	2, 937	206. 82	667. 50
9	19, 824	16, 520	3, 304	232. 68	750. 91
9. 49	20, 903	17, 419	3, 484	245. 34	791. 82
10	22, 030	18, 358	3, 672	258. 56	834. 54

LO_2 + 10% Boiloff (ft^3)	LO_2 + 10% Ullage (ft^3)	LH_2 + 10% Boiloff (ft^3)	LH_2 + 10% Ullage (ft^3)	$I_{TOT} \times 10^6$
28. 45	31. 30	91. 75	100. 93	1
56. 87	62. 56	183. 50	201. 85	2
85. 32	93. 85	275. 24	302. 76	3
113. 75	125. 13	367. 25	403. 98	4
143. 33	157. 66	462. 50	508. 75	5

LO_2 + 10% Boiloff (ft^3)	LO_2 + 10% Ullage (ft^3)	LH_2 + 10% Boiloff (ft^3)	LH_2 + 10% Ullage (ft^3)	$I_{TOT} \times 10^6$
170.62	187.68	550.75	605.83	6
199.07	218.98	642.50	706.75	7
227.50	250.25	734.25	807.68	8
255.95	281.55	826.00	908.60	9
269.87	296.86	871.00	958.10	9.49
284.42	312.86	917.99	1,009.79	10

$6/\pi = 1.9098$

$I \times 10^6$	LO_2 (D^3)	LH_2 (D^3)	$LH_2 \div 4$ (D^3)	LO_2 (D)	LH_2 (D)
1	59.78	192.76	48.19	3.9	3.6
2	119.48	385.49	96.37	4.9	4.6
3	179.23	578.21	144.55	5.6	5.2
4	238.97	771.52	192.88	6.2	5.75
5	301.10	971.61	242.90	6.7	6.2
6	358.43	1,157.01	289.25	7.1	6.6
7	418.21	1,349.75	337.44	7.5	7.0
8	477.93	1,542.51	385.63	7.8	7.3
9	537.70	1,735.24	433.81	8.1	7.6
9.49	566.94	1,829.78	457.45	8.3	7.7
10	597.50	1,928.50	482.13	8.4	7.8

$I \times 10^6$	LO_2 w/Insulation (D)	LH_2 w/Insulation (D)
1	4.4	4.1
2	5.4	5.1
3	6.1	5.7
4	6.7	6.25
5	7.2	6.7
6	7.6	7.1
7	8.0	7.5
8	8.3	7.8
9	8.6	8.1
9.49	8.8	8.2
10	8.9	8.3

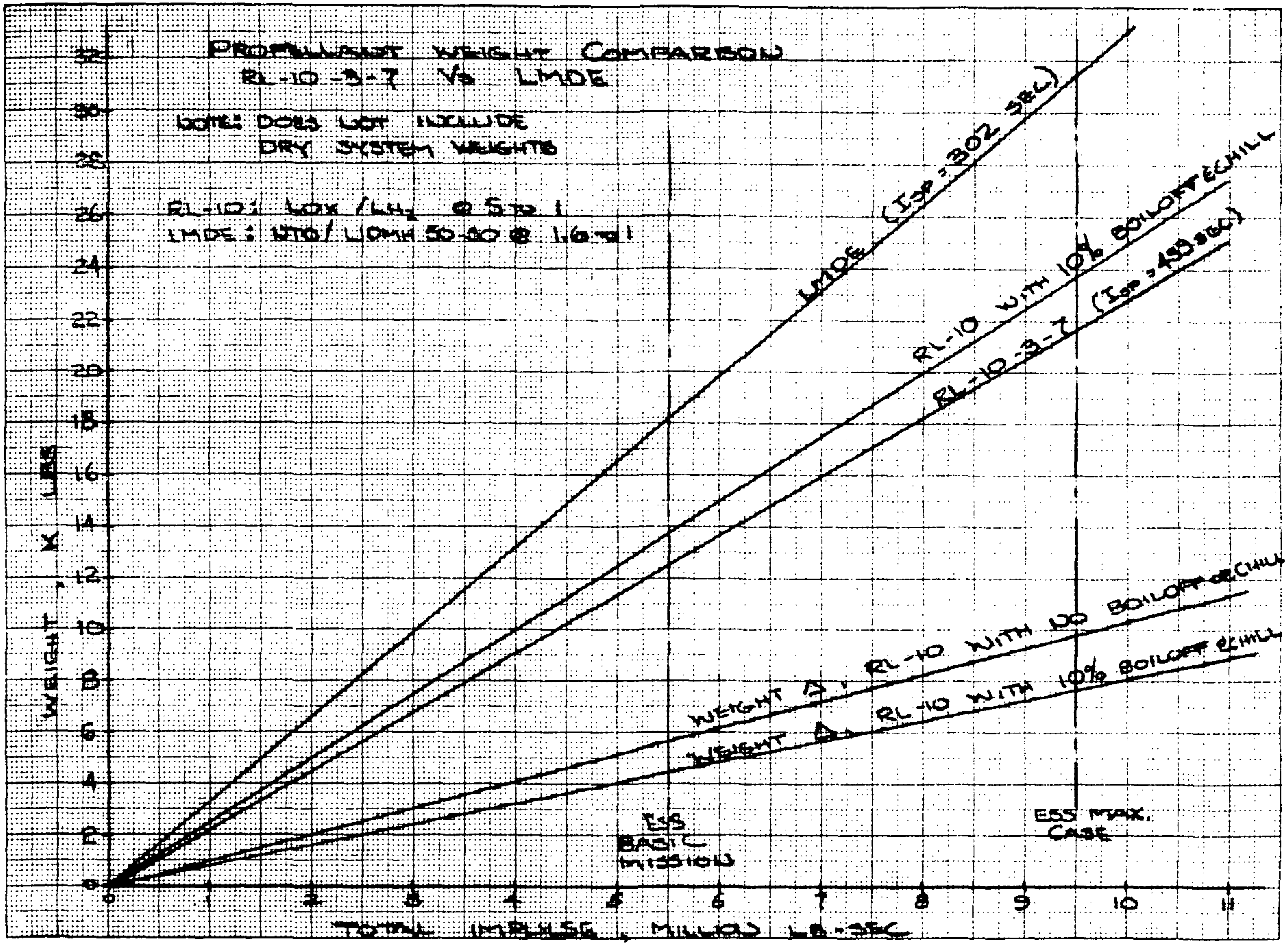
PROPELLANT WEIGHT COMPARISON
RL-10-3-7 VS LMDE
NOTE: DOES NOT INCLUDE
DRY SYSTEM WEIGHTS
RL-10: LOX/LH2 @ 5 TO 1
LMDE: NTO/UDMH 50-50 @ 1.6 TO 1
LMDE (ISP = 302 SEC)
RL-10 WITH 10% BOILOFF & CHILL
RL-10-3-7 (ISP = 455 SEC)
WEIGHT Δ, RL-10 WITH NO BOILOFF & CHILL
WEIGHT Δ, RL-10 WITH 10% BOILOFF & CHILL
ESS BASIC MISSION
ESS MAX. CASE
WEIGHT, K LBS
0
2
4
6
8
10
12
14
16
18
20
22
24
26
28
30
32
TOTAL IMPULSE, MILLION LB-SEC
0
1
2
3
4
5
6
7
8
9
10
11

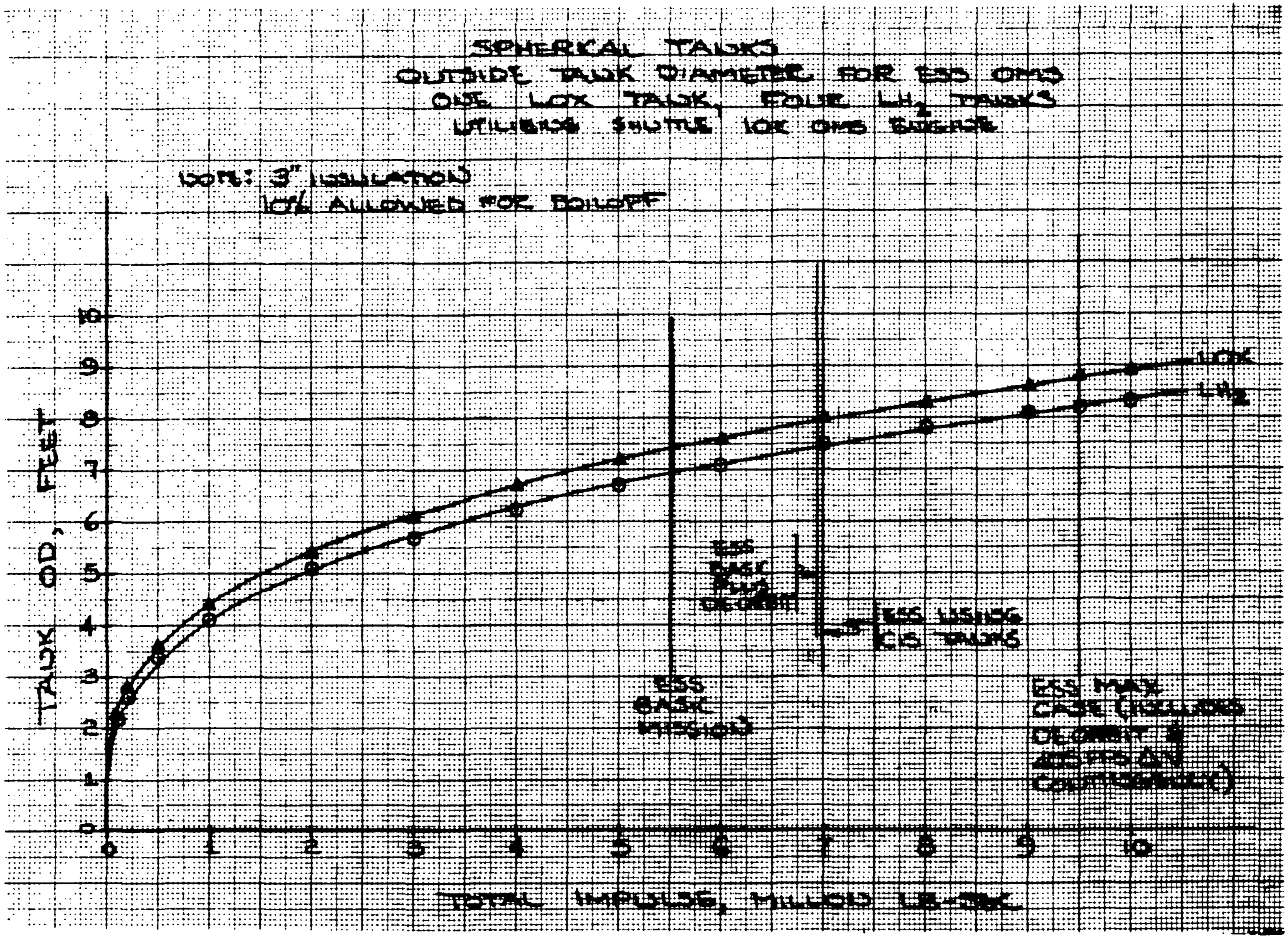
SPHERICAL TANKS
OUTSIDE TANK DIAMETER FOR ESS OMS
ONE LOX TANK, FOUR LH2 TANKS
UTILIZING SHUTTLE 10K OMS ENGINE
NOTE: 3" INSULATION
10% ALLOWED FOR BOILOFF
LOX
LH2
ESS BASIC PLUS DEORBIT
ESS USING CIS TANKS
ESS BASIC MISSION
ESS MAX CASE (INCLUDES DEORBIT &
TANK OD, FEET
TOTAL IMPULSE, MILLION LB-SEC

3.5 NARSAMS COMPUTER SOLUTION

Inputs to the program for structural analysis are:

1. Node point coordinates in an overall coordinate system (X, Y, Z)
2. The elastic properties of the finite elements (modulus of elasticity, moments of inertia, area, thickness, and shear modulus)
3. Applied loads and boundary conditions

The output from NARSAMS consists of:

1. The node point deflections
2. The elastic properties of the finite elements (modulus of elasticity, moments of inertia, area, thickness, and shear modulus)

3.5.1 NARSAMS STRUCTURAL MODEL (Figure 3-6)

To keep the program model to a practical size, the following simplifying assumptions were made:

1. The structure is symmetrical; therefore, only one half of the structure was modeled.
2. The stringers and skin were lumped into ten beam elements for each bay.
3. Each frame was idealized into nine beam elements.
4. The load-carrying capability of some of the frames was proportioned into adjacent frames.
5. The skin panels have shear capability only.
6. The attachment loads were applied at node points. No fitting structure was modeled.

7. To increase the accuracy of the solution for the region of load application, the structural modifications were approximated. This rough sizing made unnecessary the iterating of the program. The frames were estimated for attachment loads through use of the ring frame load coefficients in NR Space Division Structures Manual, Pub. 2546, (October 1969). The skin panels and stringers were estimated through use of the method for solution of shear lag problems in Paul Kuhn's Stress in Aircraft Structures, McGraw-Hill Book Company (1956).

3.5.2 PROBLEMS INVESTIGATED

The following problems were investigated with NARSAMS:

1. Local modification of shell structure required to distribute drag load, thereby minimizing total modification required. The element loads from the computer output were used to determine the local structural modifications.

2. Structural modification to frames required to distribute attachment loads. The element loads from the computer output were used to determine the required frame area, moment of inertia, and web thickness.

The method employed was to use rough-cut structure, sized to the general load intensity curves, as input data to the NARSAMS program, then resize the structure using the program output. This one program provides internal loads for the entire ESS 33-foot-diameter shell structure (forward skirt, LH_2 tank sidewall, and aft skirt). The loads were evaluated, and it was determined that boost of the MDAC space station and RNS payloads at max $q\alpha$ was critical. Figure 3-7 shows the externally applied ultimate loads to the structural model for these two conditions. The loads at intermediate stations listed are applied to the model as load intensities (N_x). Their values are computed to duplicate the applied external bending moment curve and axial load distribution.

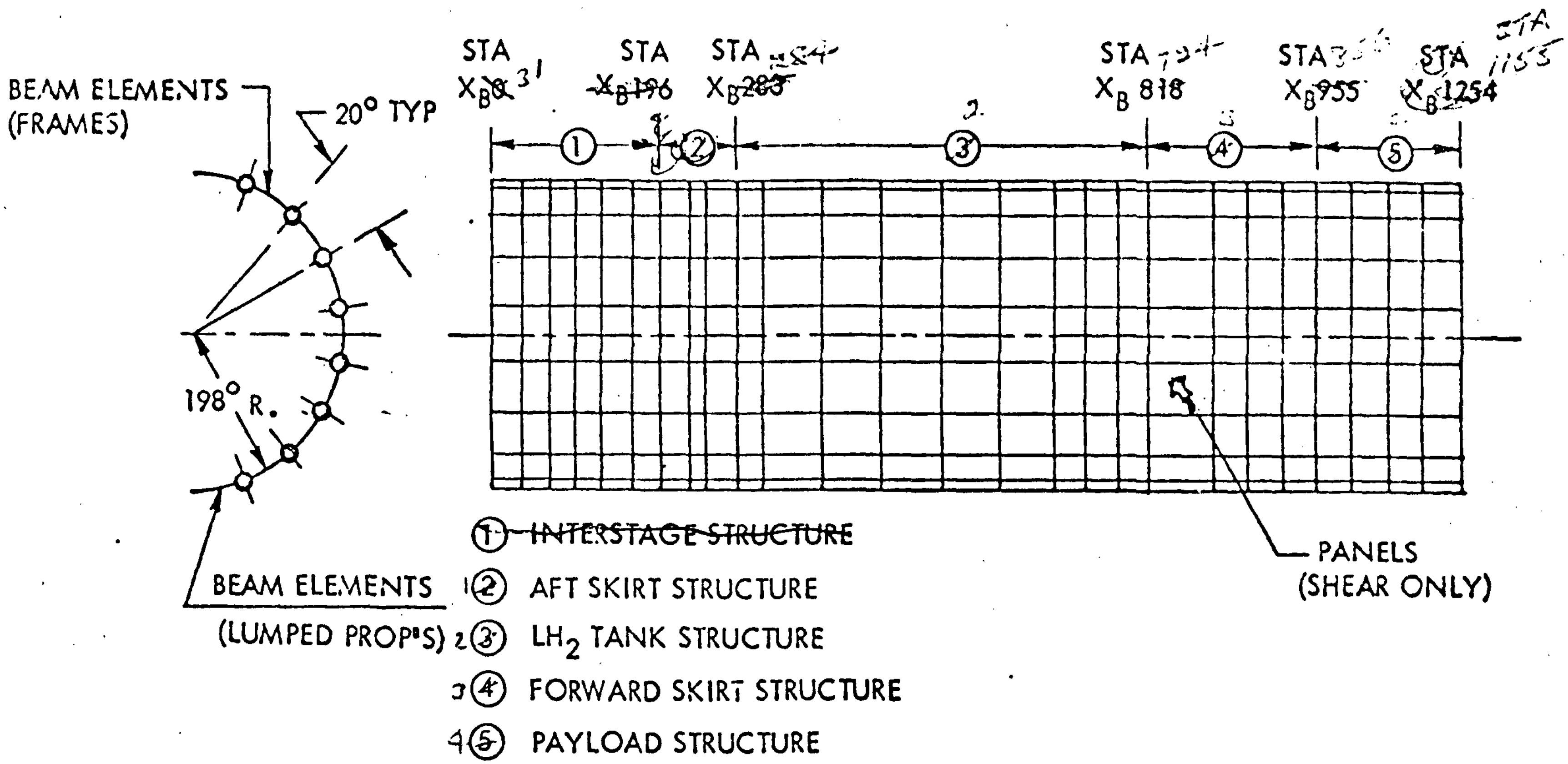

ASSUMPTIONS:
1) ALL BENDING AND AXIAL LOAD IS CARRIED BY BEAM ELEMENTS
2) PANELS CARRY SHEAR ONLY

Figure 3-6. Internal Loads - NARSAMS Model

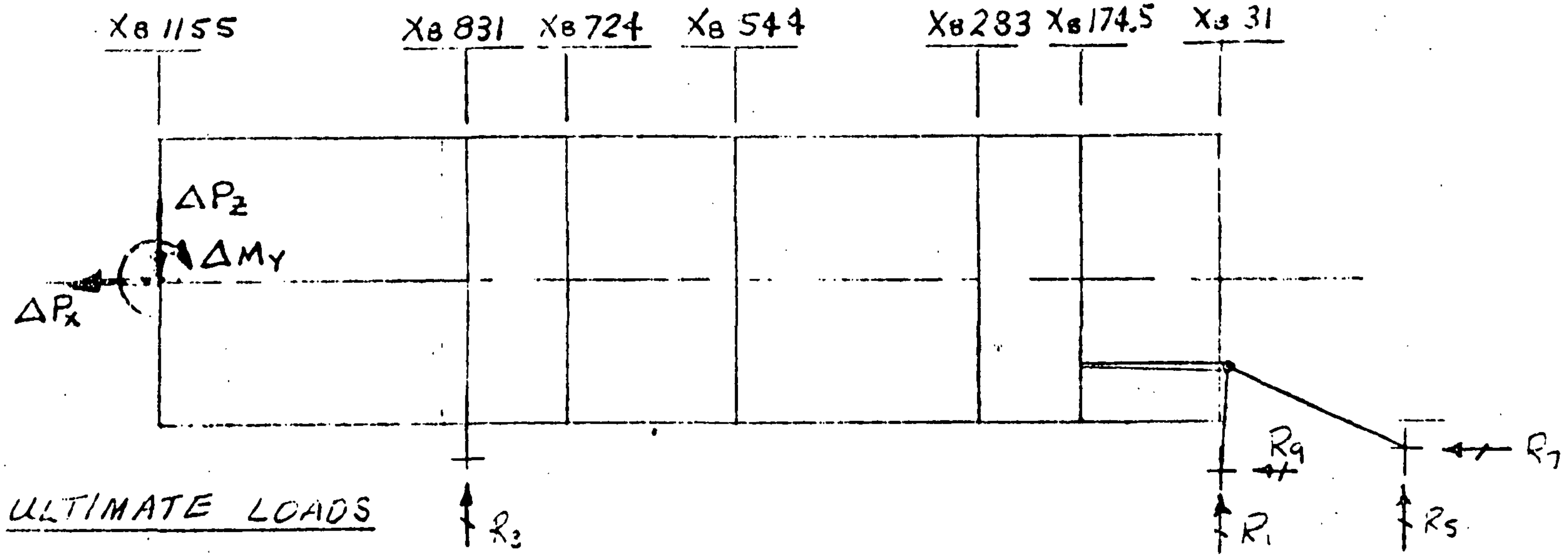

COND	MDAC ~ MAX qα H.W.			R115 ~ MAX qα T.W.		
X_B	ΔP_x	ΔP_z	ΔM_y	ΔP_x	ΔP_z	ΔM_y
1155	-1064	-42	57400.	-420	162.4	-238000.
724	-140	37.8	—	-42	23.8	—
544	-168	33.6	—	-192	9.8	—
283	-1428	273.0	14000.	-1071	-105.0	-6900.
174.5	-378	33.6	1960.	-257	-15.4	—

APPLIED LOADS ~ TOTAL

	MDAC	RNS
R_1	.51	-326.5
R_3	-318.1	65.0
R_5	485.6	279.2
R_7	1589	779.2
R_9	—	7.3

REACTIONS PER SIDE.

Figure 3-7. Loads and Reactions in KIPS, Moments in In-KIPS

THRUST STRUCTURE SKIN

QUARTER PANEL

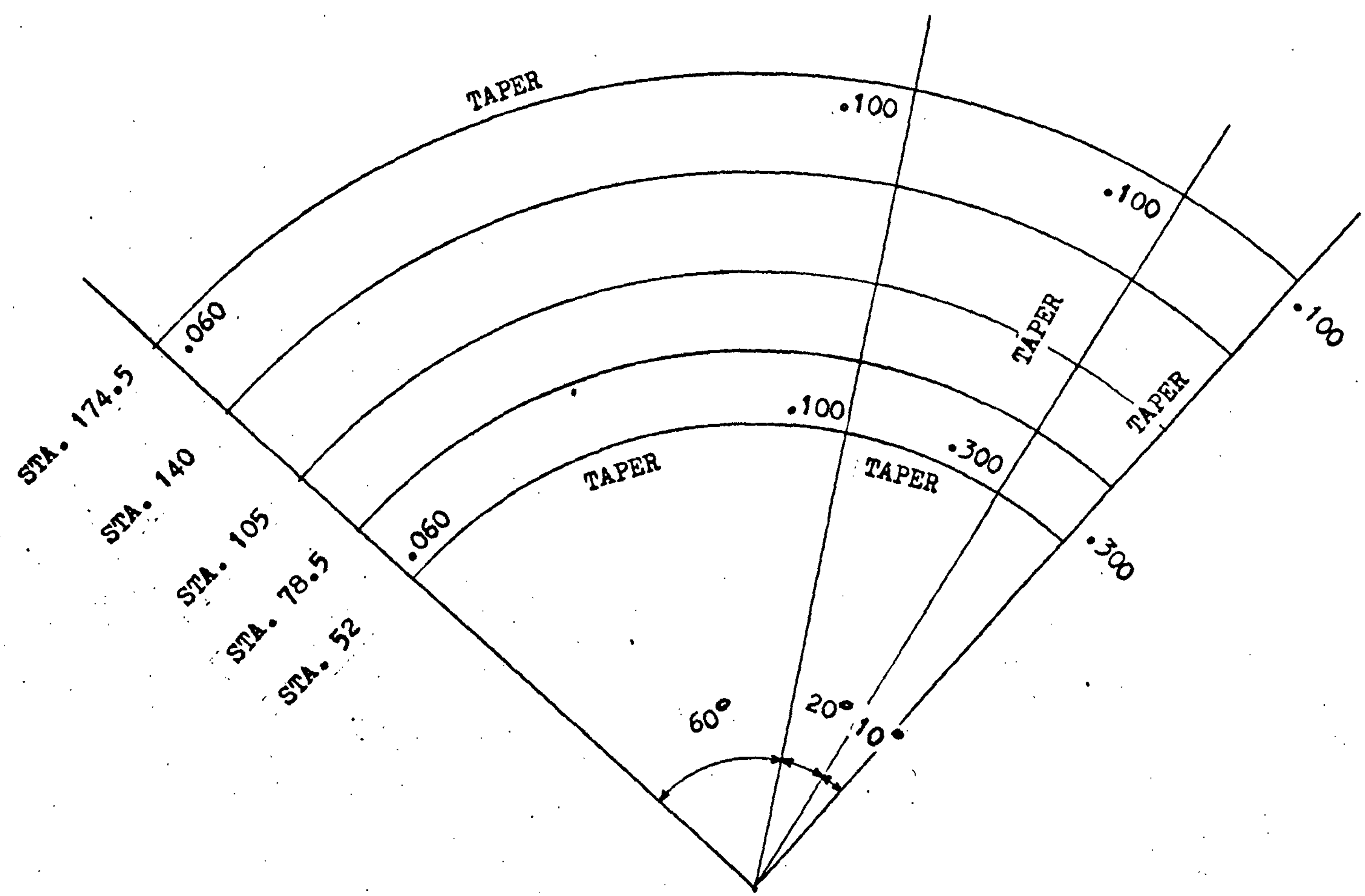

THRUST STRUCTURE STRINGERS

QUARTER PANEL

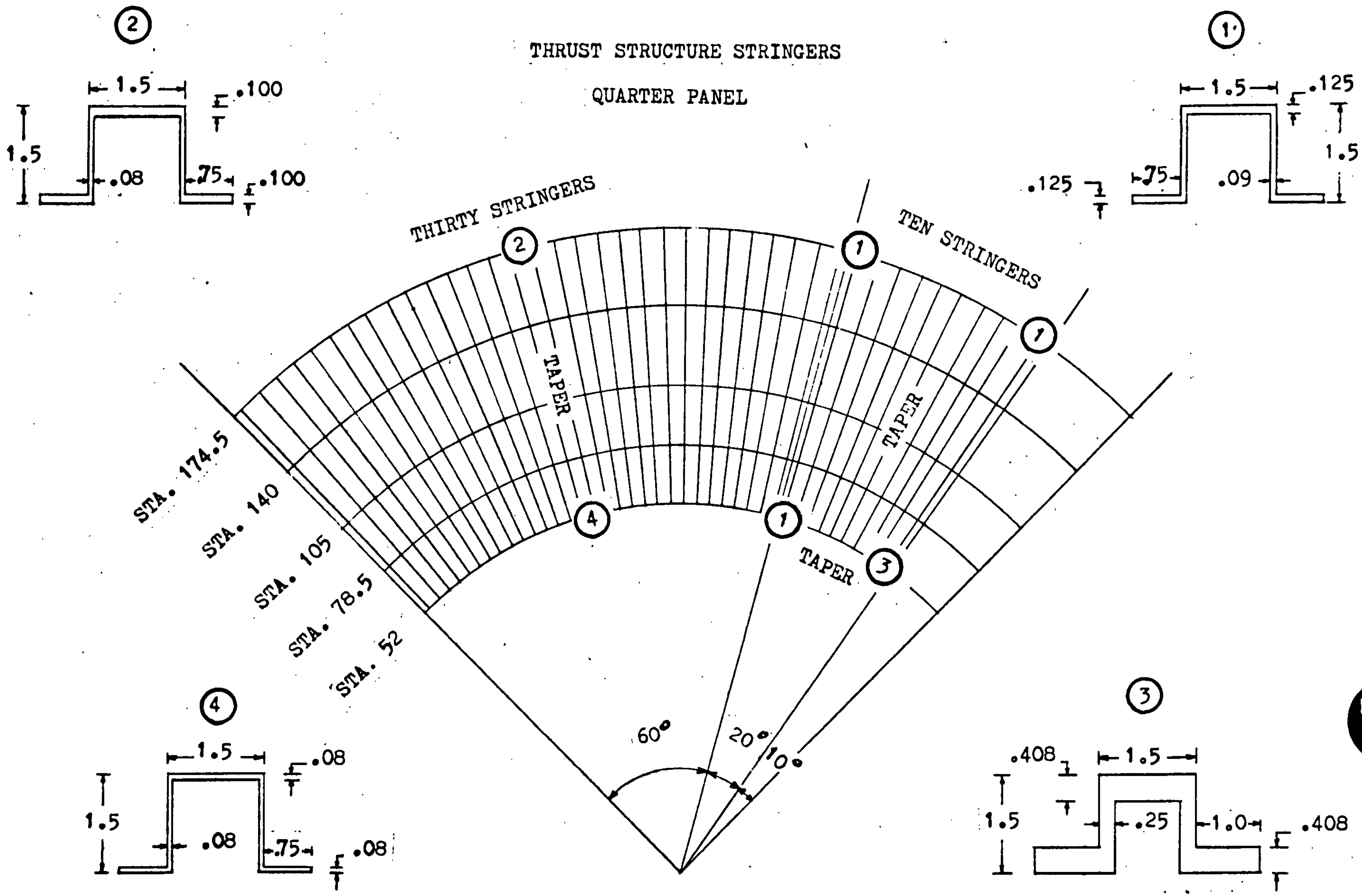

THRUST CONE FRAME 52 (15" DEPTH)

AT ENGINE

$M = 6.3 \times 10^6$ (COMP. OUTBOARD)
$P = 415{,}000$ (COMP. OUTER CAP ONLY)
$V = 200{,}000$

$$\text{OUTBOARD CAP LOAD} = \frac{M}{h'} + P = \frac{6.3\times10^6}{13} + 415{,}000$$

$$= 484{,}000 + 415{,}000 = 899{,}000\ \# \text{ COMP}$$

$$\text{REQ'D } (A_{CAP})_{OUTBOARD} = \frac{899{,}000}{60{,}000} = 15.0 \text{ IN}^2$$

$$\text{INBOARD CAP LOAD} = \frac{M}{h'} = 484{,}000\ \# \text{ TENSION}$$

$$\text{REQ'D } (A_{CAP})_{INBOARD} = \frac{484{,}000}{70{,}000} = 6.92 \text{ IN}^2$$

$$\text{REQ'D } t_{WEB} = \frac{V}{h'\tau} = \frac{200{,}000}{13 \times 41{,}000} = .376$$

AT 90°

$M = 6.15 \times 10^6$ (TENSION OUTBOARD)
$P = 150{,}000$ (TENSION OUTER CAP ONLY)
$V = 170{,}000$

$$\text{OUTBOARD CAP LOAD} = \frac{M}{h'} + P = \frac{6.15\times10^6}{13} + 150{,}000$$

$$= 473{,}000 + 150{,}000 = 623{,}000\ \# \text{ TEN.}$$

$$\text{REQ'D } (A_{CAP})_{OUTBOARD} = \frac{623{,}000}{70{,}000} = 8.9 \text{ IN}^2$$

$$\text{INBOARD CAP LOAD} = \frac{M}{h'} = 473{,}000\ \# \text{ COMP.}$$

$$\text{REQ'D } (A_{CAP})_{INBOARD} = \frac{473{,}000}{60{,}00} = 7.9 \text{ IN}^2$$

$$\text{REQ'D } t_{WEB} = \frac{V}{h'\tau} = \frac{170{,}000}{13 \times 41{,}000} = .318$$

THRUST CONE FRAME 78.5 (9" DEPTH)

LOADS

$M = 246{,}100$
$P = 11{,}090$
$V = 6260$

$$\text{CAP LOAD} = \frac{M}{h'} + \frac{P}{2} = \frac{246{,}100}{7} + \frac{11{,}090}{2}$$

$$= 35{,}200 + 5500 = 40{,}700^{\#}$$

$$\text{REQ'D } A_{CAP} = \frac{40{,}700}{50{,}000} = .814 \text{ IN}^2$$

$$\text{REQ'D } t_{WEB} = \frac{V}{h' \tau} = \frac{6260}{5 \times 41{,}000} = .031 \text{ IN}$$

USE .050 (MIN.)

THRUST CONE FRAME 105.0 (10" DEPTH)

LOADS AT 0° & 90° (AT ENGINE)

$M = 1 \times 10^6$ (COMP. INBOARD)
$P = 32,000$ (COMP. OUTBOARD CAP ONLY)
$V = 24,000$

$$\text{INBOARD CAP LOAD} = \frac{M}{h} = \frac{1 \times 10^6}{10} = 100,000 \text{ \# (COMP.)}$$

$$\text{REQ'D } (A_{CAP})_{INBOARD} = \frac{100,000}{50,000} = 2.0 \text{ IN}^2$$

$$\text{OUTBOARD CAP LOAD} = \frac{M}{h} - 32,000 = 100,000 - 32,000$$
$$= 68,000 \text{ (TENSION)}$$

$$\text{REQ'D } (A_{CAP})_{OUTBOARD} = \frac{68,000}{50,000} = 1.36 \text{ IN}^2$$

$$\text{REQ'D } t_{WEB} = \frac{V}{h\tau} = \frac{24,000}{10(30,000)} = .08''$$

LOADS 45° → 135° (CONSTANT)

$M = 600,000$ (COMP. OUTBOARD)
$P = 15,000$ (COMP. OUTB'D CAP)
$V = 6500$

$$\text{INBOARD CAP LOAD} = \frac{M}{h} = \frac{600,000}{10} = 60,000 \text{ \# (TENSION)}$$

$$\text{REQ'D } (A_{CAP})_{INBOARD} = \frac{60,000}{50,000} = 1.25 \text{ IN}^2$$

$$\text{OUTBOARD CAP LOAD} = \frac{M}{h} + P = 60,000 + 15,000 = 75,000 \text{ \# (COMP.)}$$

$$\text{REQ'D } (A_{CAP})_{OUTBOARD} = \frac{75,000}{50,000} = 1.5 \text{ IN}^2$$

$$\text{REQ'D } t_{WEB} = \frac{V}{h\tau} = \frac{6500}{10(20,000)} = .033''$$

USE .050

THRUST CONE FRAME 140 (9" DEPTH)

LOADS

$M = 393,800$
$P = 40,000$
$V = 4200$

$$CAP\ LOAD = \frac{M}{h} + \frac{P}{2} = \frac{393,800}{7} + \frac{40,000}{2}$$

$$= 56,200 + 20,000 = 76,200^{\#}$$

$$REQ'D\ \ A_{CAP} = \frac{76,200}{50,000} = 1.52$$

$$REQ'D\ \ t_{WEB} = \frac{V}{h\tau} = \frac{4200}{7(20,000)} = .030$$

USE .050

STATION 52 FRAME

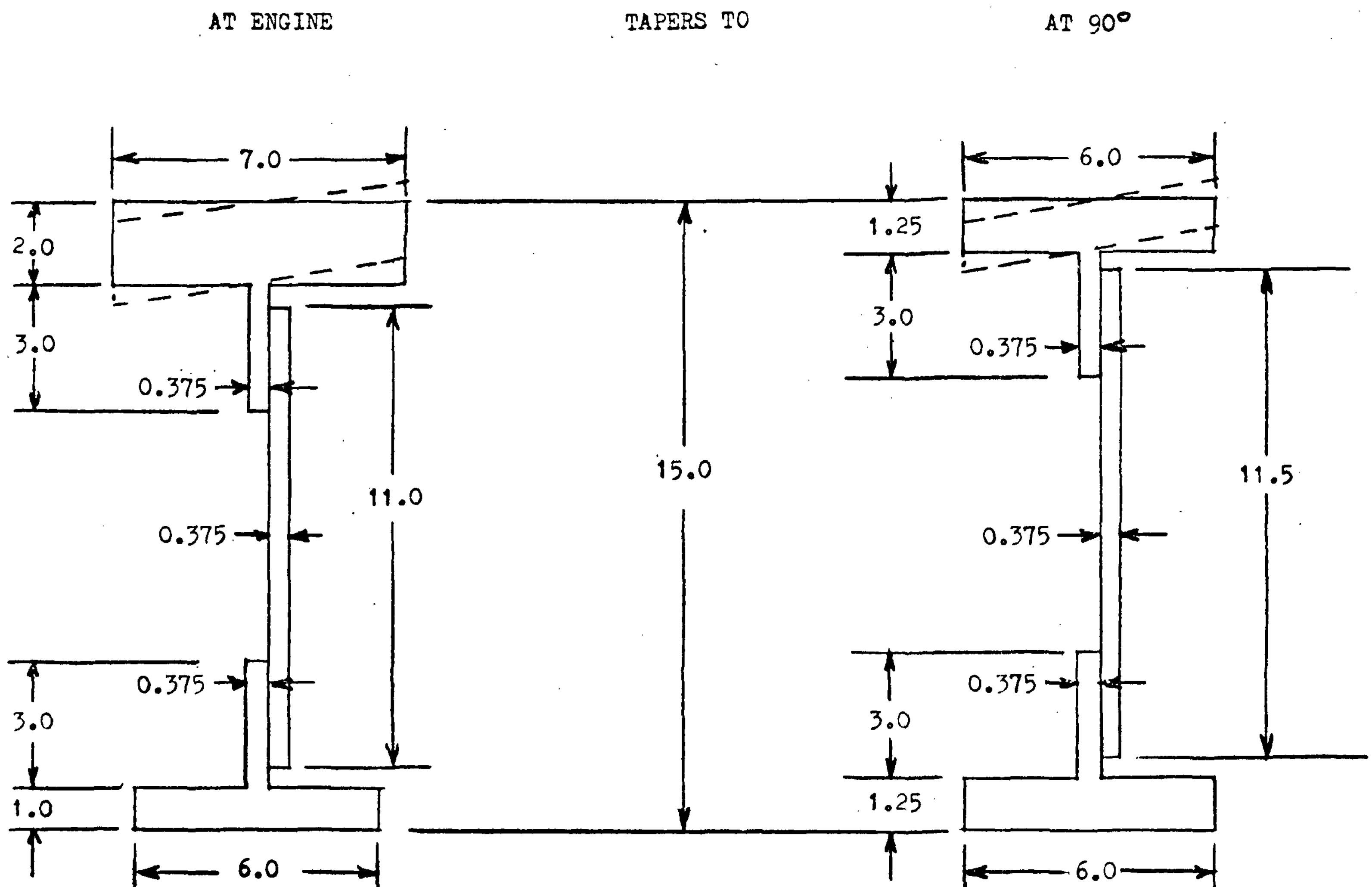

STATION 105 FRAME

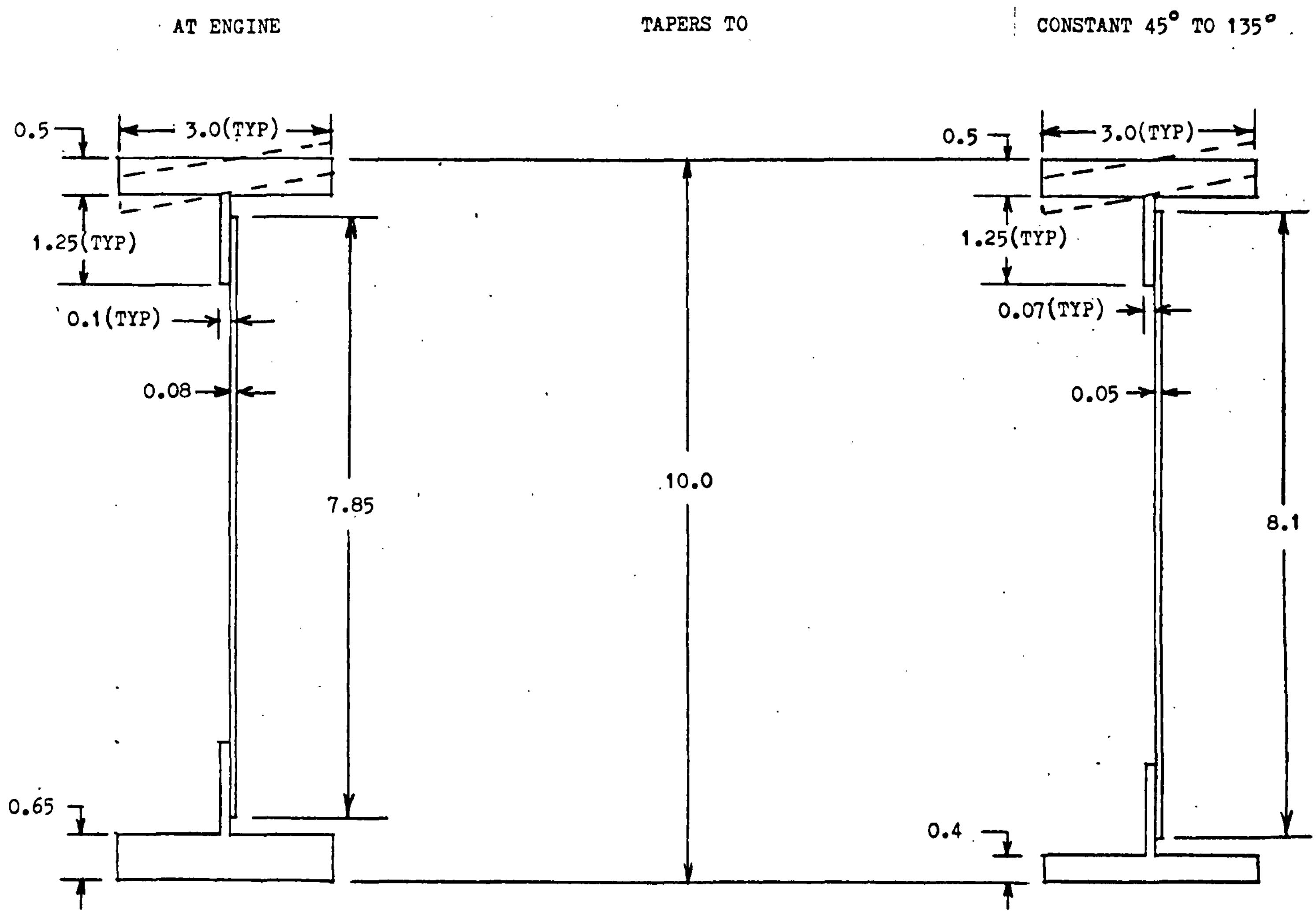

STATION 140 FRAME

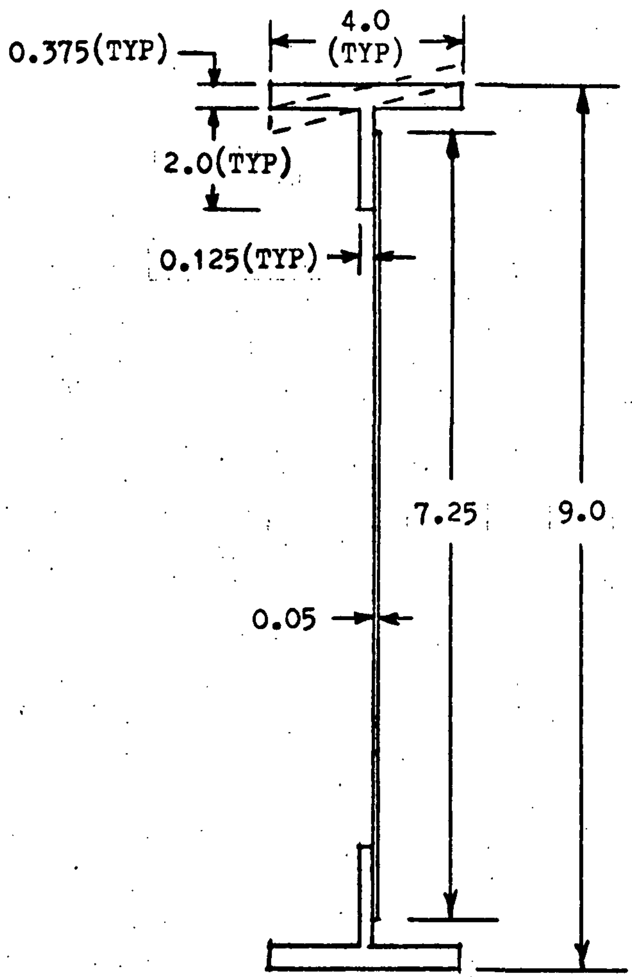

STATION 78.5 FRAME

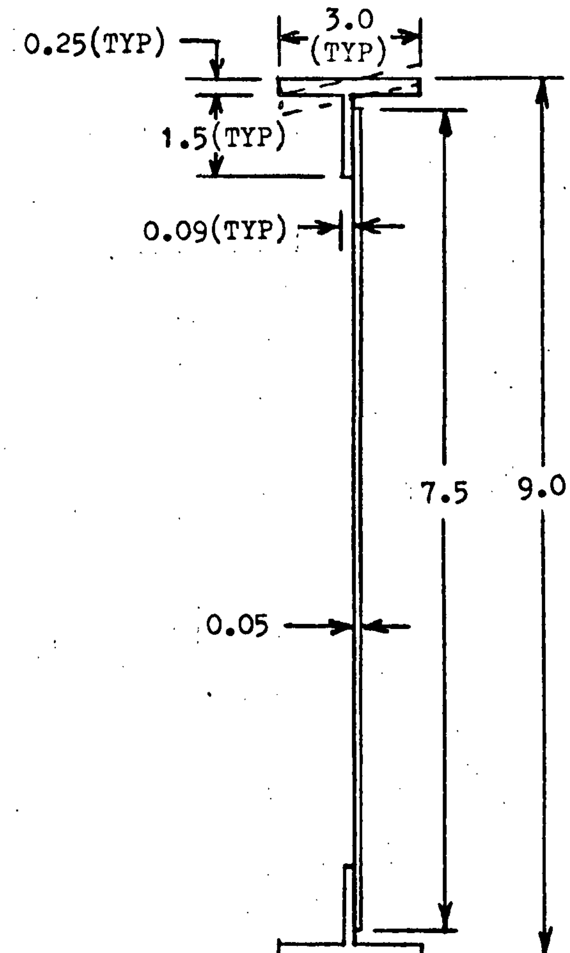

CROSS-TIE BEAM AND SUPPORT

CROSS-TIE BEAM

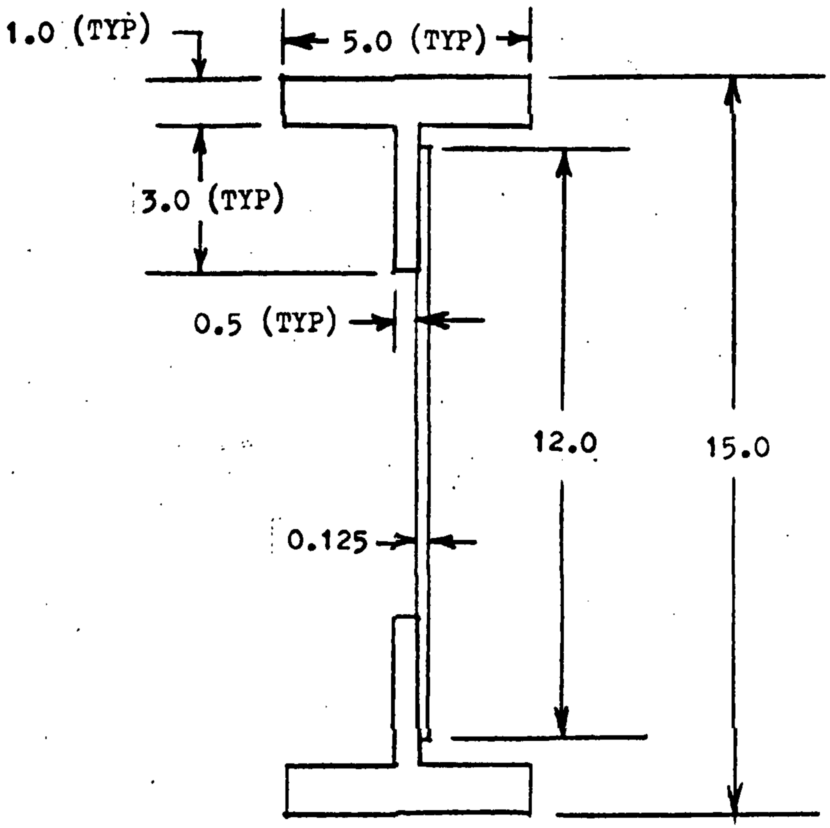

CROSS-TIE SUPPORT

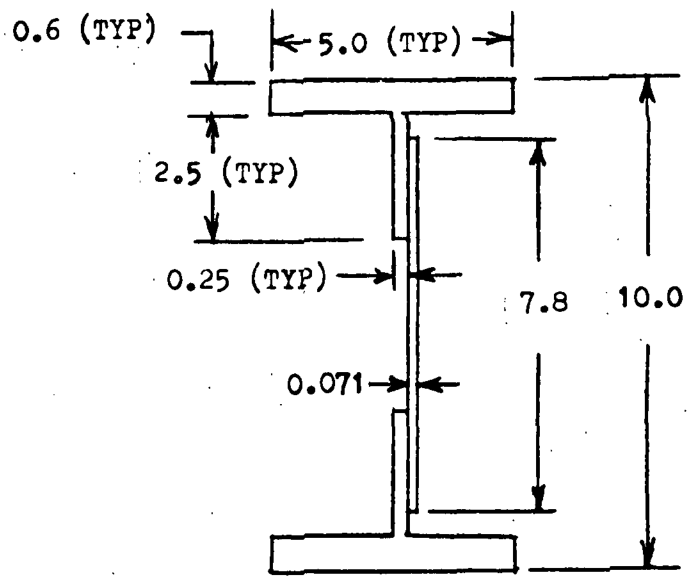

ENGINE SUPPORT BEAM
ONE ENGINE CONFIGURATION

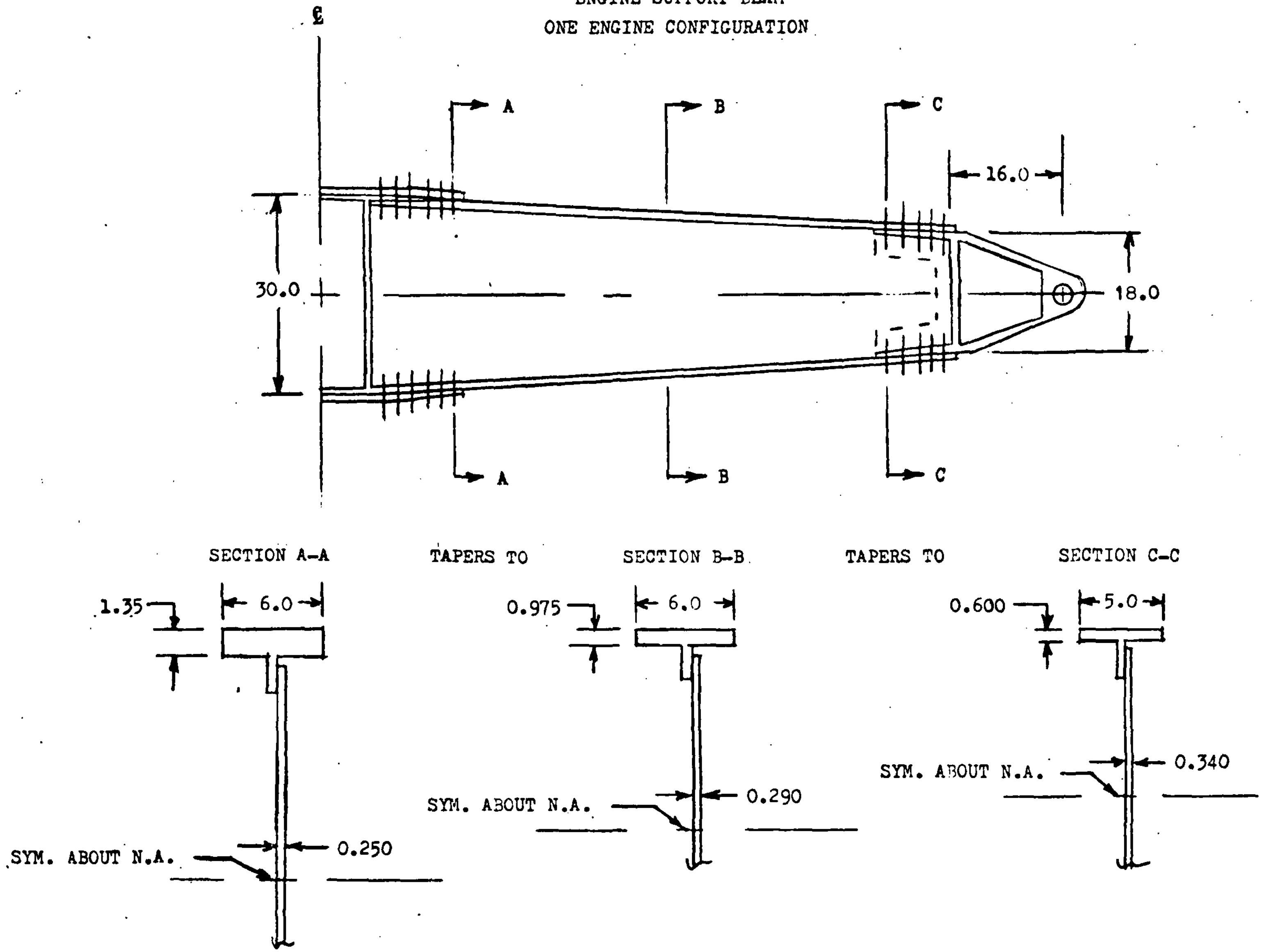

THRUST LONGERONS

STATION 52 TAPER STATION 105 STATION 105 TO STATION 174

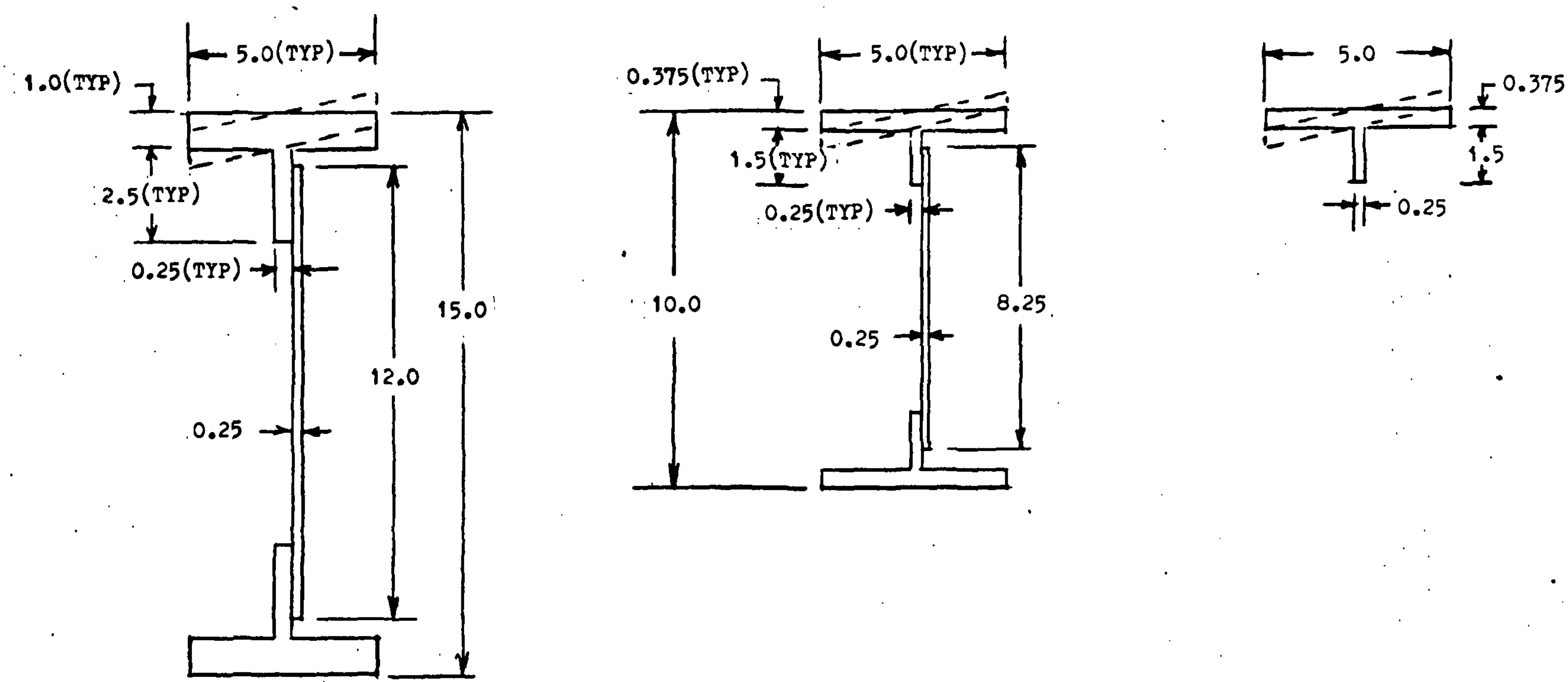

FORWARD SKIRT STRINGERS

STRINGER SPACING = 8.64 INCHES
(144 STRINGERS)

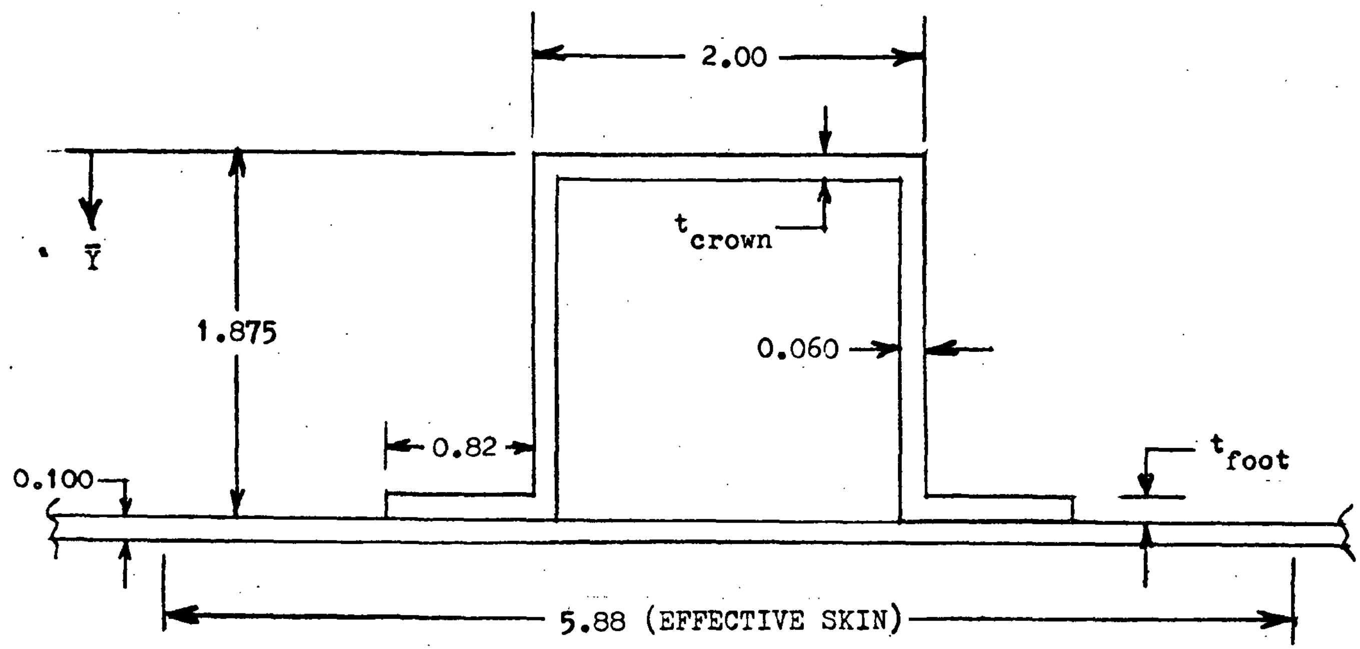

STA. - STA.	t_{crown}	t_{foot}	A	I	$\bar{Y}$
724 - 741	.070	.110	1.125	0.545	1.499
741 - 781	.075	.090	1.012	0.561	1.469
781 - 816	.085	.090	1.120	0.596	1.446
816 - 856	.085	.110	1.153	0.600	1.455

FORWARD SKIRT FRAME 767

STABILITY FRAME ONLY

$$I_{REQ'D} = \frac{\pi R^4 N_x}{4000\, E\, a} = \frac{\pi (170)^4 (2718)}{4000 (10.5 \times 10^6)(795-767)}$$

$$\therefore \quad I_{REQ'D} = 11.16$$

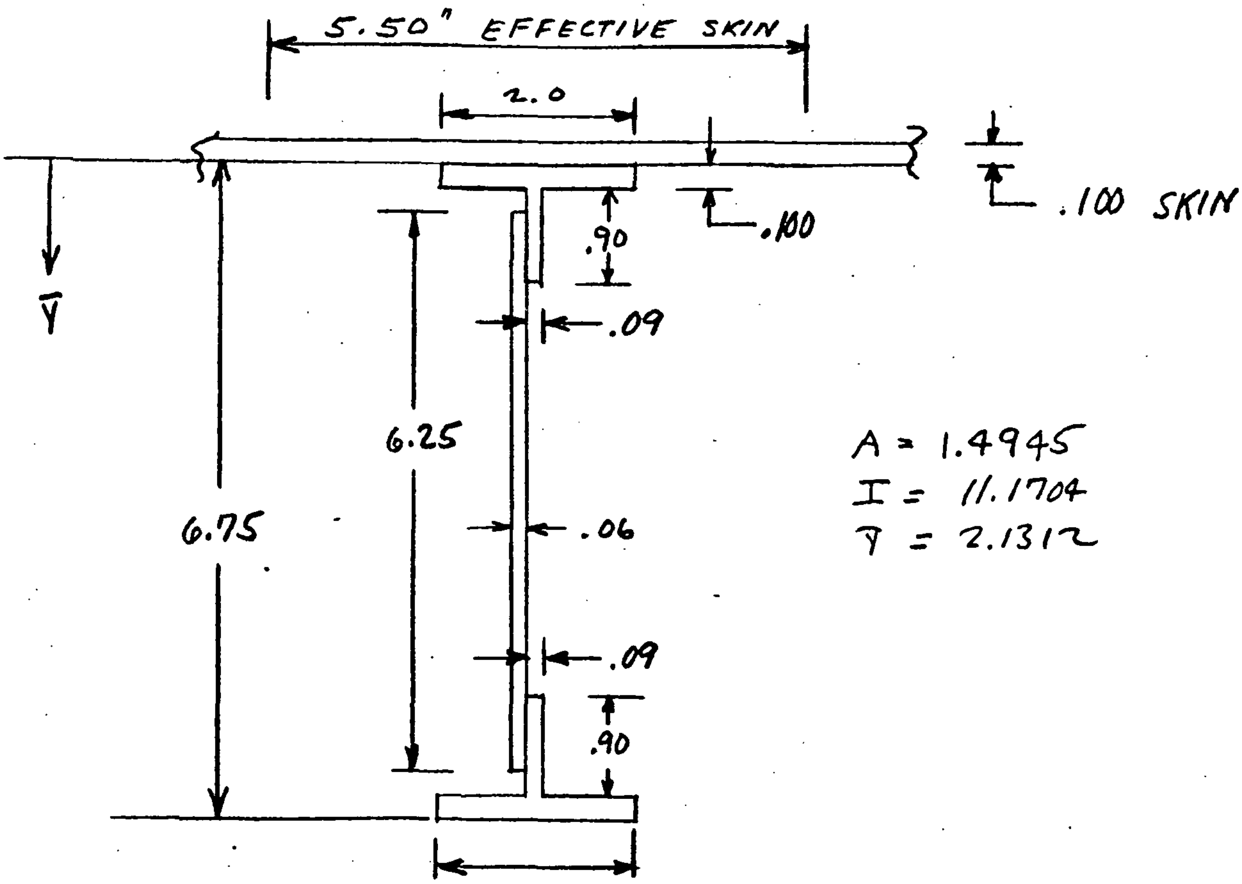

A = 1.4945
I = 11.1704
$\bar{Y}$ = 2.1312

FORWARD SKIRT STABILITY FRAME

STATION 767.0

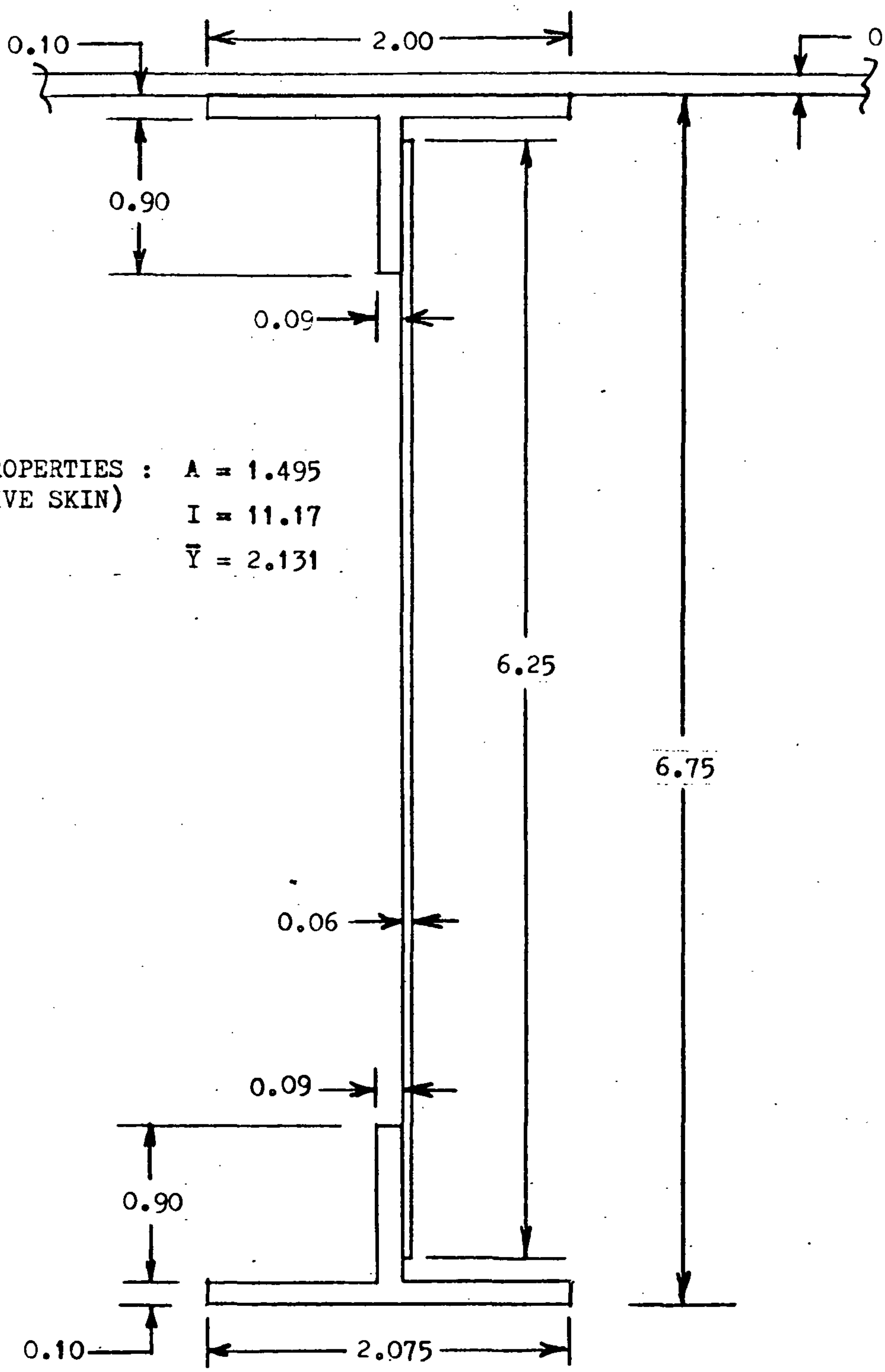

SECTION PROPERTIES : A = 1.495
(5.50" EFFECTIVE SKIN) I = 11.17
$\bar{Y}$ = 2.131

FORWARD SKIRT FRAME 795 (22" DEPTH)

P

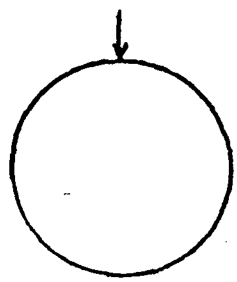

P = KICK LOAD FROM DRAG AT SEPARATION

$$P = (400{,}000 \times 1.4) \times \frac{9'' \text{ ECCENTRICITY}}{(831 - 795)}$$

$P = 140{,}000$ # ULT.

PEENEMUNDE:

$$M_{MAX} = .24(140{,}000)(198) = 6.653 \times 10^6$$
$$P = .25(140{,}000) = 35{,}000$$
$$V = .50(140{,}000) = 70{,}000$$

ASSUMPTION: FOR SIZING, USE $\frac{1}{3}$ OF PEENEMUNDE LOADS

$$\text{CAP LOAD} = \frac{M}{h'} + \frac{P}{2} = \frac{(6.653 \times 10^6/3)}{21} + \frac{(35{,}000/3)}{2}$$

$$= 105{,}600 + 5800 = 111{,}400 \text{ \#}$$

$$\text{REQ'D } A_{CAP} = \frac{111{,}400}{70{,}000} = 1.6 \text{ IN}^2$$

$$\text{REQ'D } t_{WEB} = \frac{V}{h'' T} = \frac{(70{,}000/3)}{20\,(20{,}000)} = .058$$

USE .063

FORWARD SKIRT FRAME

STATION 795.0

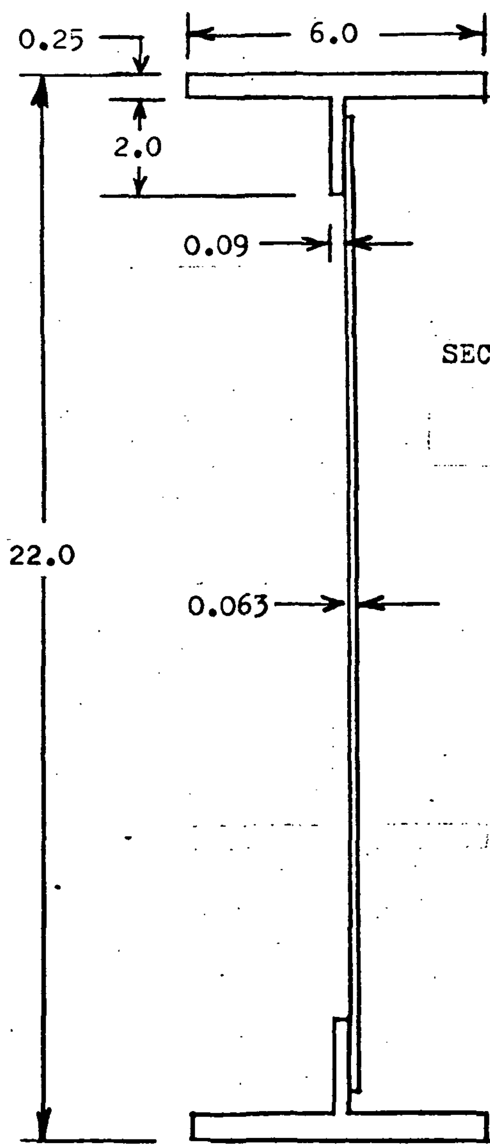

SECTION PROPERTIES : A = 4.652

I = 434.4

$\bar{Y}$ = 11.0

FORWARD SKIRT FRAME 831 (40" DEPTH)

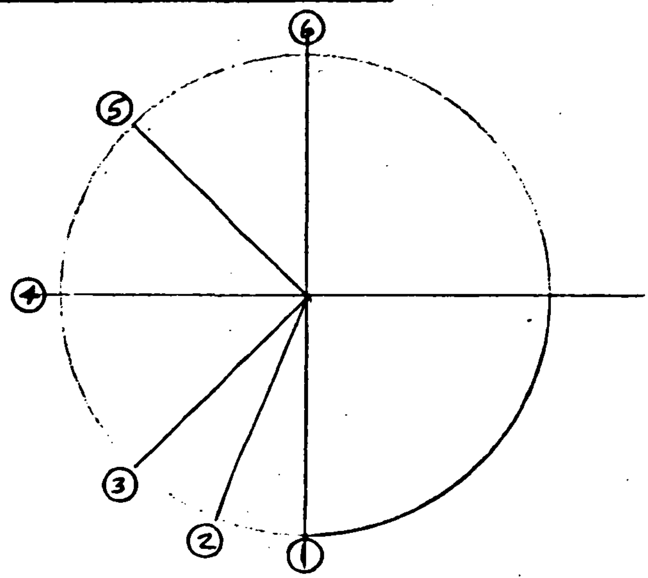

	①	②	③	④	⑤	⑥
M	4.71×10^6	9.64×10^6	-2.33×10^6	-4.46×10^6	670,000	3.2×10^6
P	365,000	389,000	213,000	31,000	29,000	56,000
V	0	172,500	41,000	37,500	36,000	0

GENERAL

$$\text{CAP LOAD} = \frac{M}{38} + \frac{P}{2}$$

WEB USE $V = 40{,}000$

$$t = \frac{V}{h\tau} = \frac{40{,}000}{40(20{,}000)} = .05$$

FORWARD SKIRT FRAME 831 (40" DEPTH)

① (6¼%)

$$\text{CAP LOAD} = \frac{4.71 \times 10^6}{38} + \frac{365,000}{2} = 123,950 + 182,500 = 306,450^{\#}$$

$$\therefore A_{CAP} = \frac{306,450}{70,000} = 4.38 \text{ IN}^2$$

② (12½%)

$$\text{CAP LOAD} = \frac{9.64 \times 10^6}{38} + \frac{389,000}{2} = 253,700 + 194,500 = 448,200^{\#}$$

$$\therefore A_{CAP} = \frac{448,200}{70,000} = 6.40 \text{ IN}^2$$

③ (18¾%)

$$\text{CAP LOAD} = \frac{2.33 \times 10^6}{38} + \frac{213,000}{2} = 61,320 + 106,500 = 167,820^{\#}$$

$$\therefore A_{CAP} = \frac{167,820}{70,000} = 2.40 \text{ IN}^2$$

④ (25%)

$$\text{CAP LOAD} = \frac{4.46 \times 10^6}{38} + \frac{31,000}{2} = 117,400 + 15,500 = 132,900^{\#}$$

$$\therefore A_{CAP} = \frac{132,900}{70,000} = 1.90 \text{ IN}^2$$

⑤ (25%)

$$\text{CAP LOAD} = \frac{670,000}{38} + \frac{29,000}{2} = 17,630 + 14,500 = 32,130$$

$$\therefore A_{CAP} = \frac{32,130}{70,000} = 0.46 \text{ IN}^2$$

⑥ (12½%)

$$\text{CAP LOAD} = \frac{3.2 \times 10^6}{38} + \frac{56,000}{2} = 84,200 + 28,000 = 112,200$$

$$\therefore A_{CAP} = \frac{112,200}{70,000} = 1.60 \text{ IN}^2$$

FORWARD SKIRT FRAME

STATION 831.0

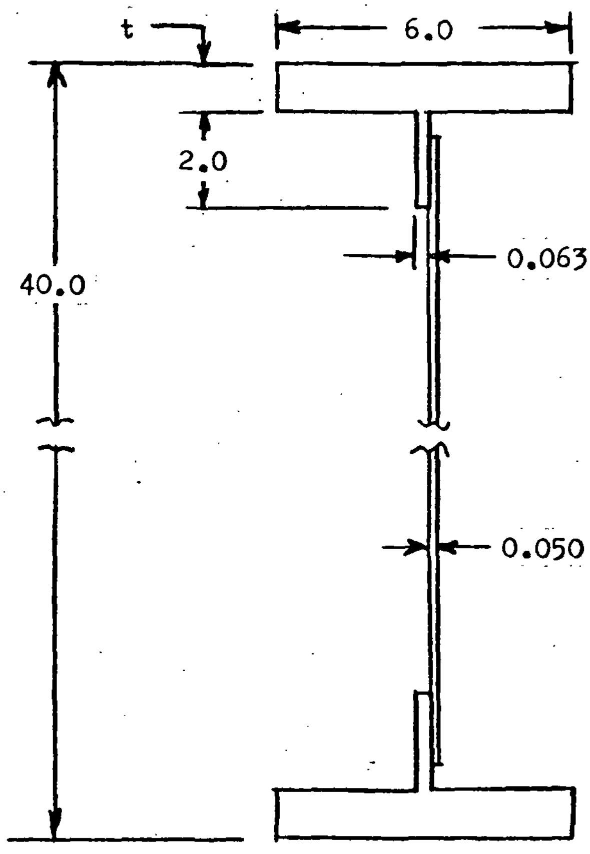

θ	t	A	I
0.00 - 11.25	0.71	10.65	3594
11.25 - 33.75	1.05	14.70	5071
33.75 - 67.50	0.38	6.72	2110
67.50 - 112.50	0.30	5.77	1743
112.50 - 157.50	0.07	3.04	670
157.50 - 180.00	0.25	5.18	1512

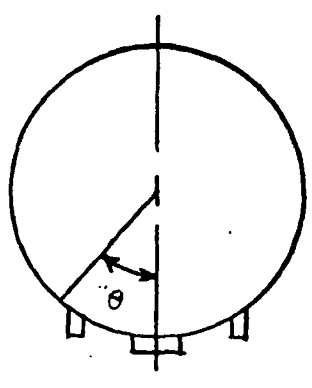

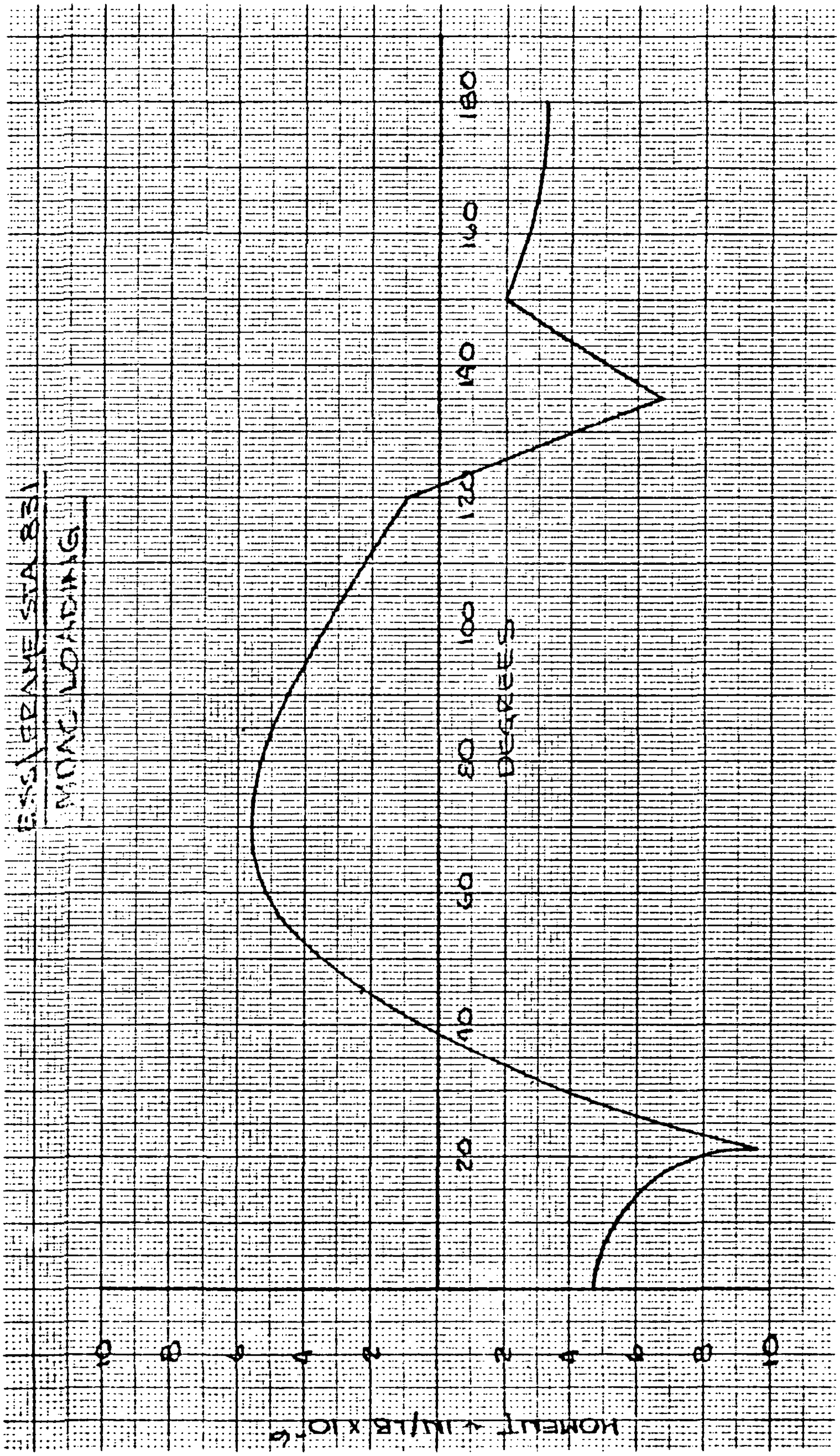
20
40
60
80
100
120
140
160
180
DEGREES

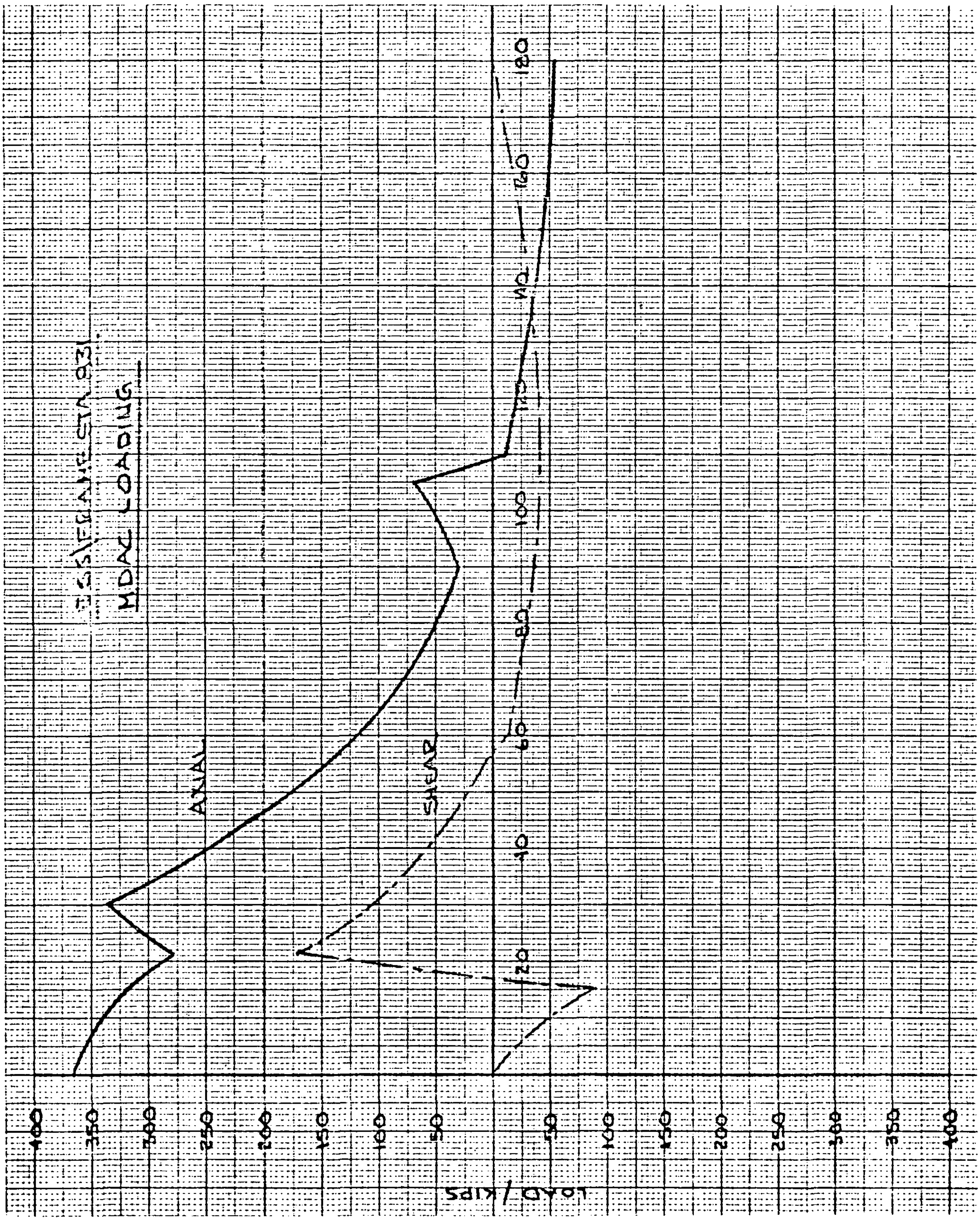
MDAC LOADING
AXIAL
SHEAR
LOAD / KIPS

AFT SKIRT STRINGERS

STRINGER SPACING = 5.76 INCHES
(216 STRINGERS)

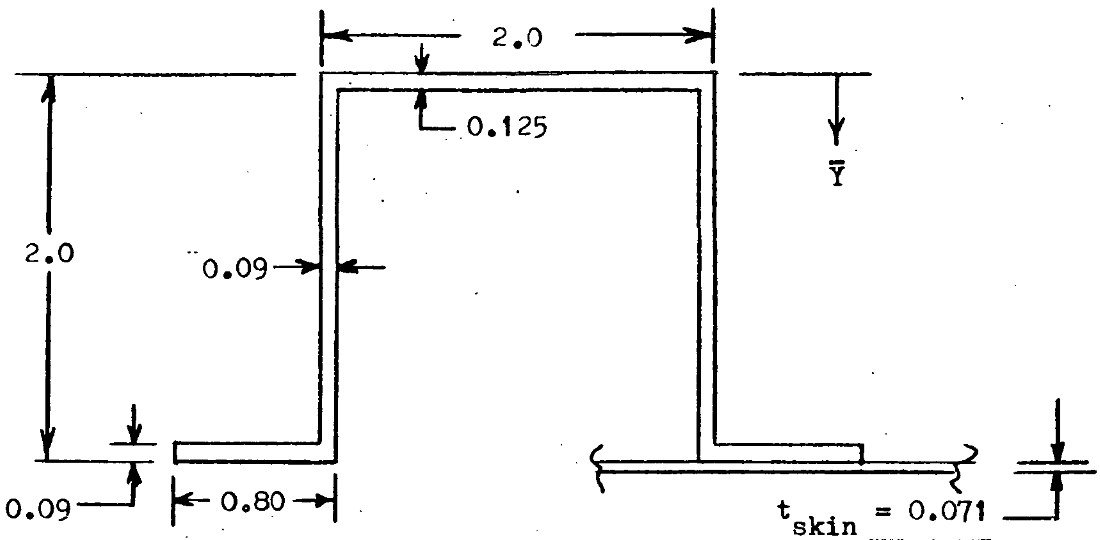

SECTION PROPERTIES : A = 1.1243
(ALL SKIN EFFECTIVE) I = 0.7774
Ȳ = 1.2955

AFT SKIRT SKIN-STRINGERS

UPPER BAY (238-283)

$$P = (3900 \times 1.4)\,5.76 = 5460 \times 5.76 = 31{,}450^{\#} \text{ ULT.}$$

(DISCONTINUITY) $M_{283} = 760 \times 5.76 = 4378$ IN-# ULT

(COMPRESSION IN CROWN)

$$J = \left(\frac{EI}{P}\right)^{1/2} = \left[\frac{(10.5 \times 10^6)(0.7774)}{31{,}450}\right]^{1/2} \doteq (259.5453)^{1/2} = 16.11$$

$$\frac{L}{J} = \frac{46}{16.11} = 2.8554 \qquad \sin\frac{L}{J} = \sin(3.1416 - 2.8554) = .282$$

(.2862 written above)

$$M' = \frac{M}{\sin\frac{L}{J}} = \frac{4378}{.282} = 15{,}525 \text{ IN-\#}$$

$$\sigma_{CROWN} = \frac{P}{A} + \frac{Mc}{I} = \frac{31{,}450}{1.1243} + \frac{15{,}525\,(1.2955)}{0.7774}$$

$$= 27{,}970 + 25{,}870$$

$$= 53{,}840 \text{ PSI}$$

CROWN

$$\frac{b}{t} = \frac{2.0}{.125} = 16.0$$

$$\sigma_{cc} = 63{,}300$$

$$M.S = \frac{63{,}300}{53{,}840} - 1 = \underline{\underline{0.18}}$$

AFT SKIRT SKIN-STRINGERS (UNDISTURBED SECTIONS)

SECTION

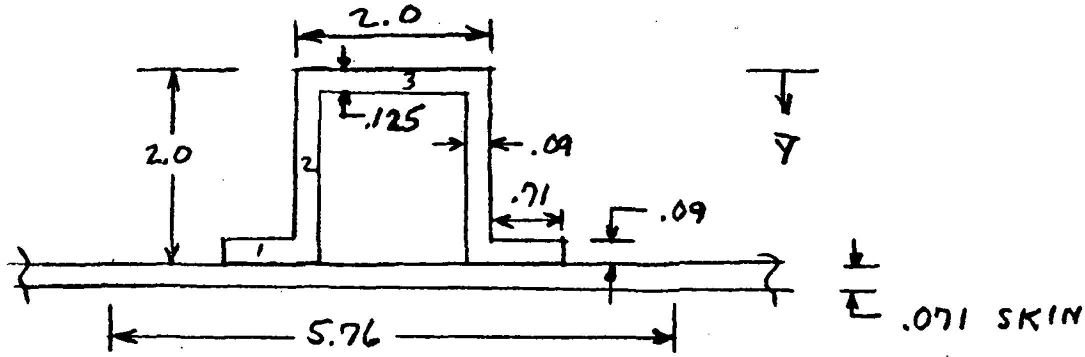

$A = 1.1243$
$I = 0.7774$
$\bar{y} = 1.2955$

$\rho = .8315$
$L' = 47.5/(1.25)^{1/2} = 42.49$
$\frac{L'}{\rho} = \frac{42.49}{.8315} = 51.10$

CRIPPLING

		A	b/t	σ_{cc}	$A \times \sigma_{cc}$
1	2×.09×.755 =	.1359	.80/.09 = 8.9	52,000	7067
2	2×.09×1.8925 =	.3407	2.0/.09 = 22.2	49,500	16,865
3	.125×1.91 =	.2387	2.0/.125 = 16.0	63,300	15,110
	Σ	.7153			39,042

$$\sigma_{cc} = \frac{39,042}{.7153} = 54,580 \text{ PSI}$$

$$\sigma_{COL\ ALLOW.} = \sigma_{cc} - \frac{\sigma_{cc}^2 (L'/\rho)^2}{4\pi^2 E}$$

$$= 54,580 - \frac{(54,580)^2 (51.10)^2}{4\pi^2 (10.5 \times 10^6)} = 35,810$$

LOAD (LOWER BAY)

$$N_x = 4883 (1.4) = 8638 \text{ \#/IN}$$

$$\sigma = \frac{P}{A} = \frac{5.76(8638)}{1.1243} = 35,020 \text{ PSI}$$

$$M.S. = \frac{35,810}{35,020} - 1 = \underline{\underline{.02}}$$

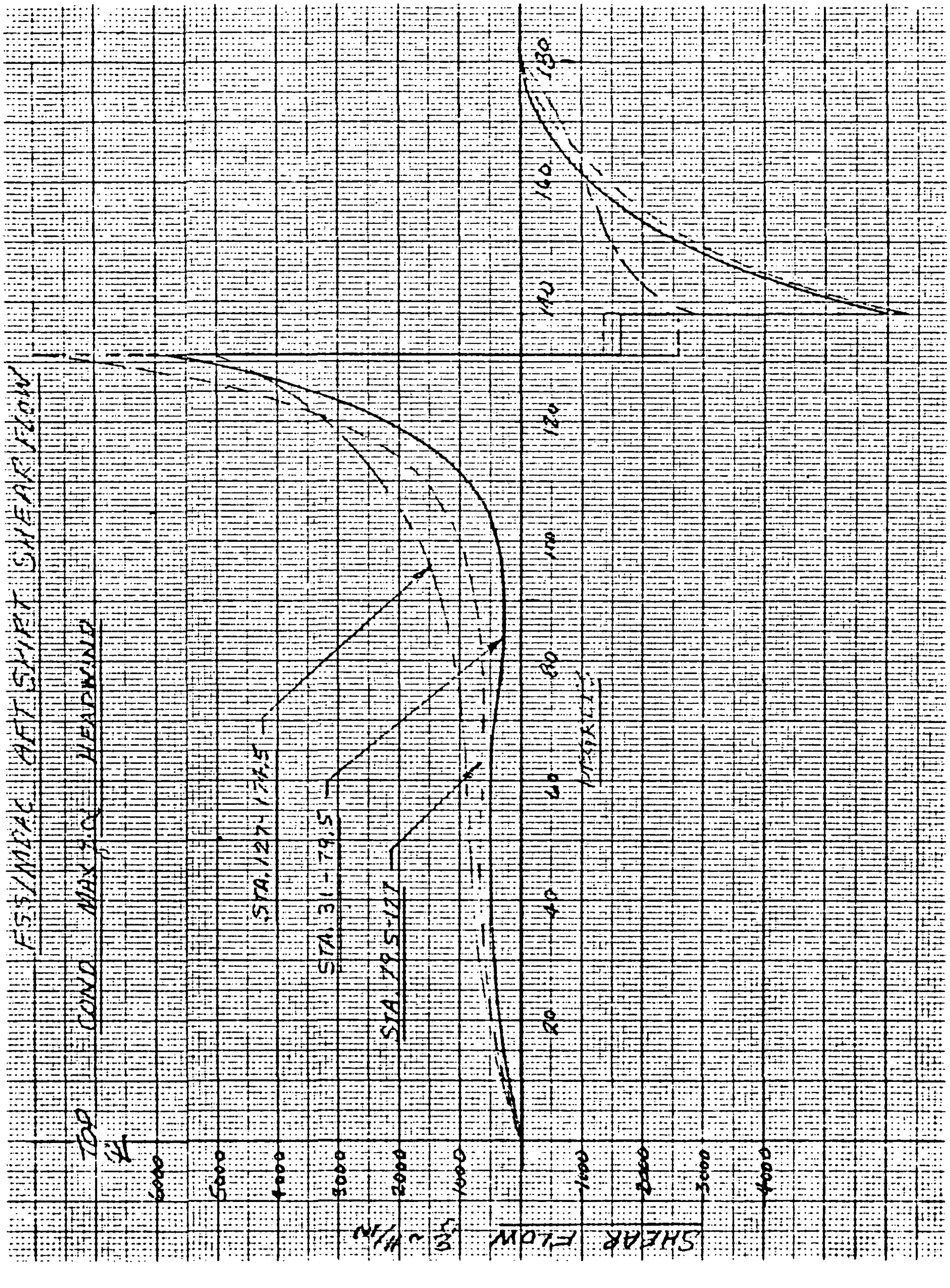
AFT SKIRT SHEAR FLOW
COND MAX q α HEADWIND
STA. 127-177.5
STA. 31-79.5
STA. 79.5-127
SHEAR FLOW ~ #/IN
6000
5000
4000
3000
2000
1000
1000
2000
3000
4000
20
40
60
80
100
120
140
160
180

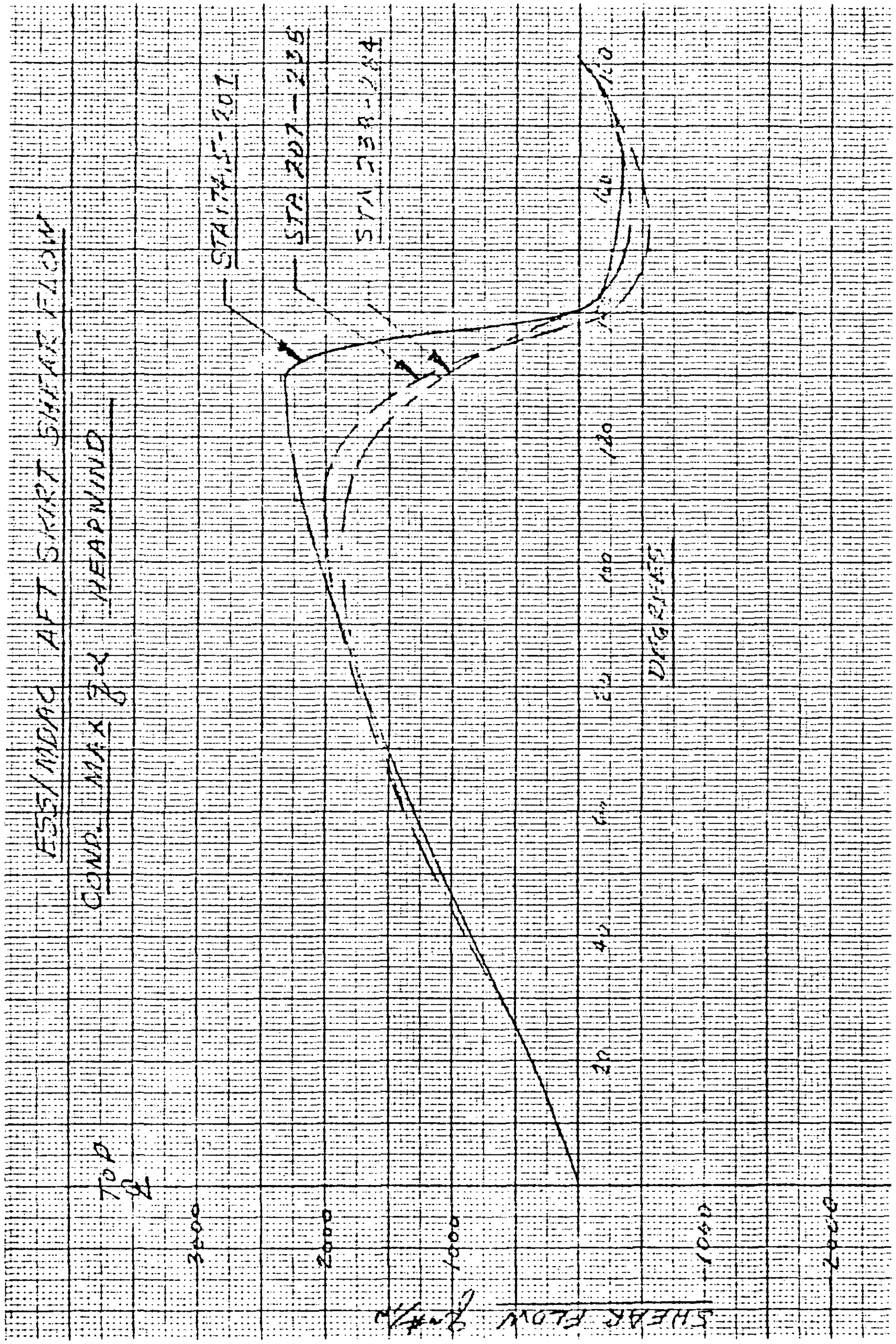
ESSI MDAC AFT SKIRT SHEAR FLOW
COND. MAX HEADWIND
STA 207-235
DEGREES
SHEAR FLOW
TOP

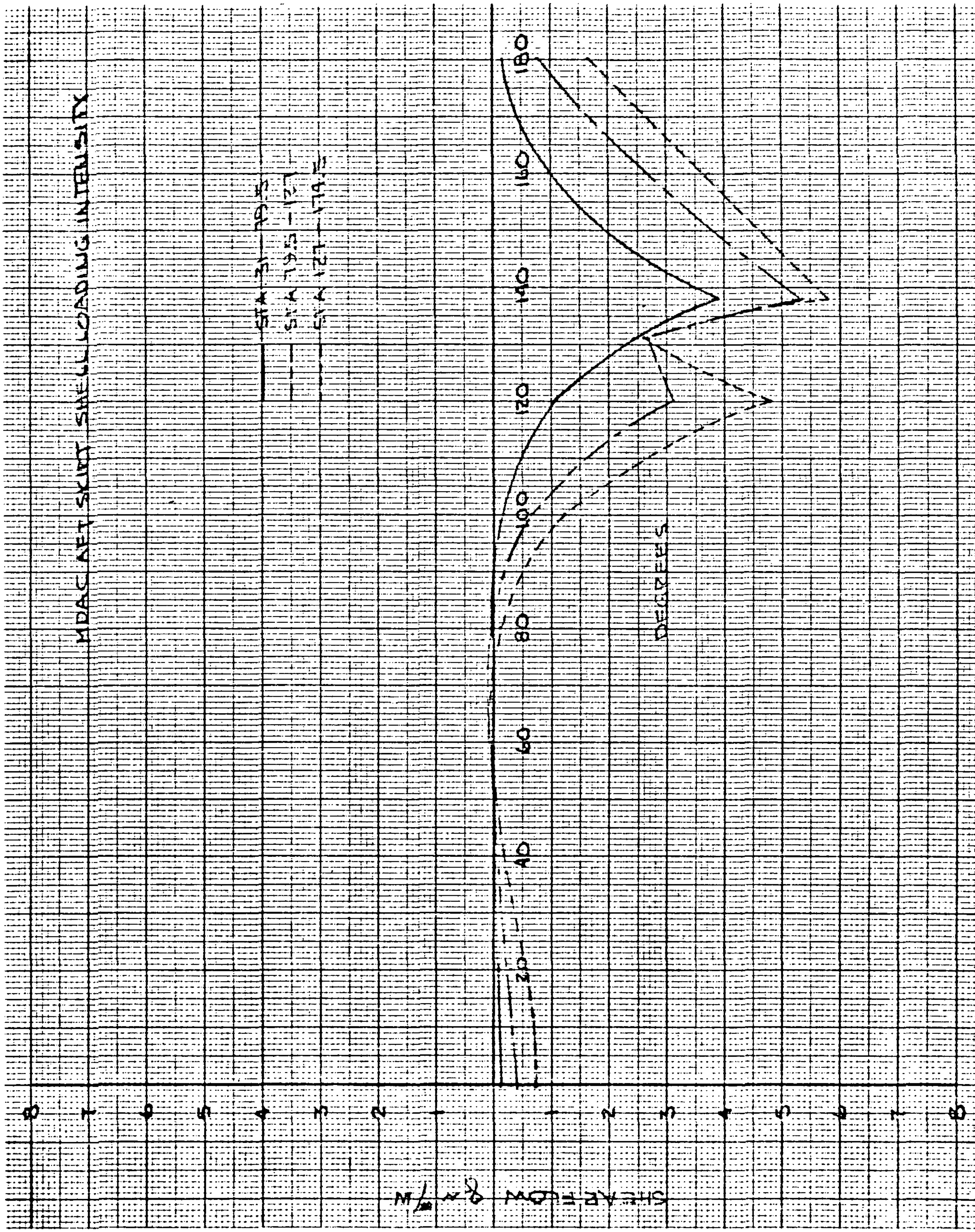
MDAC AFT SKIRT SHELL LOADING INTENSITY
STA 31 — 79.5
STA 79.5 — 127
STA 127 — 174.5
180
160
140
120
100
80
60
40
20
DEGREES
8
7
6
5
4
3
2
1
1
2
3
4
5
6
7
8

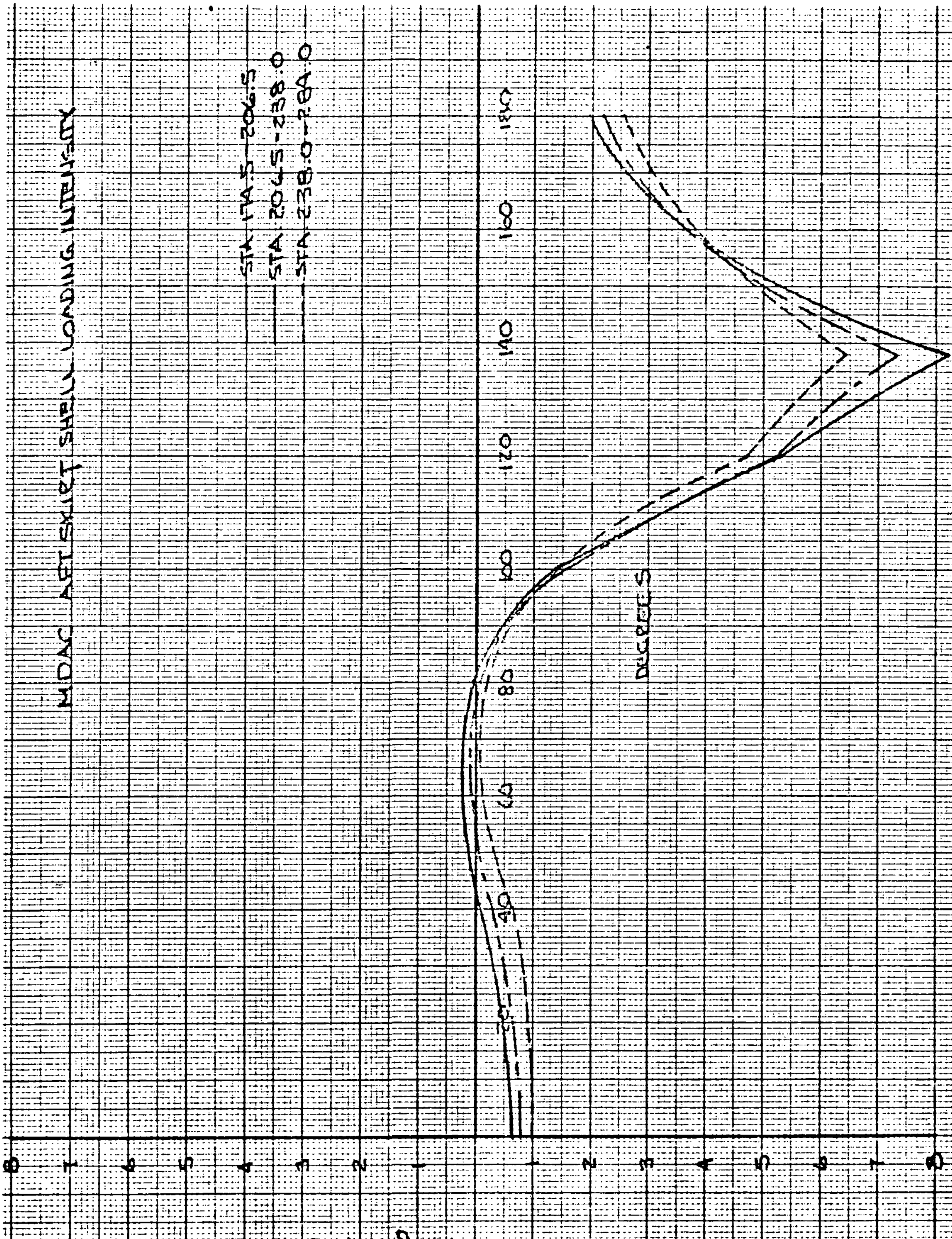

MDAC AFT SKIRT SHELL LOADING INTENSITY
STA 174.5-206.5
STA 206.5-238.0
STA 238.0-284.0
DEGREES
20
40
60
80
100
120
140
160
180

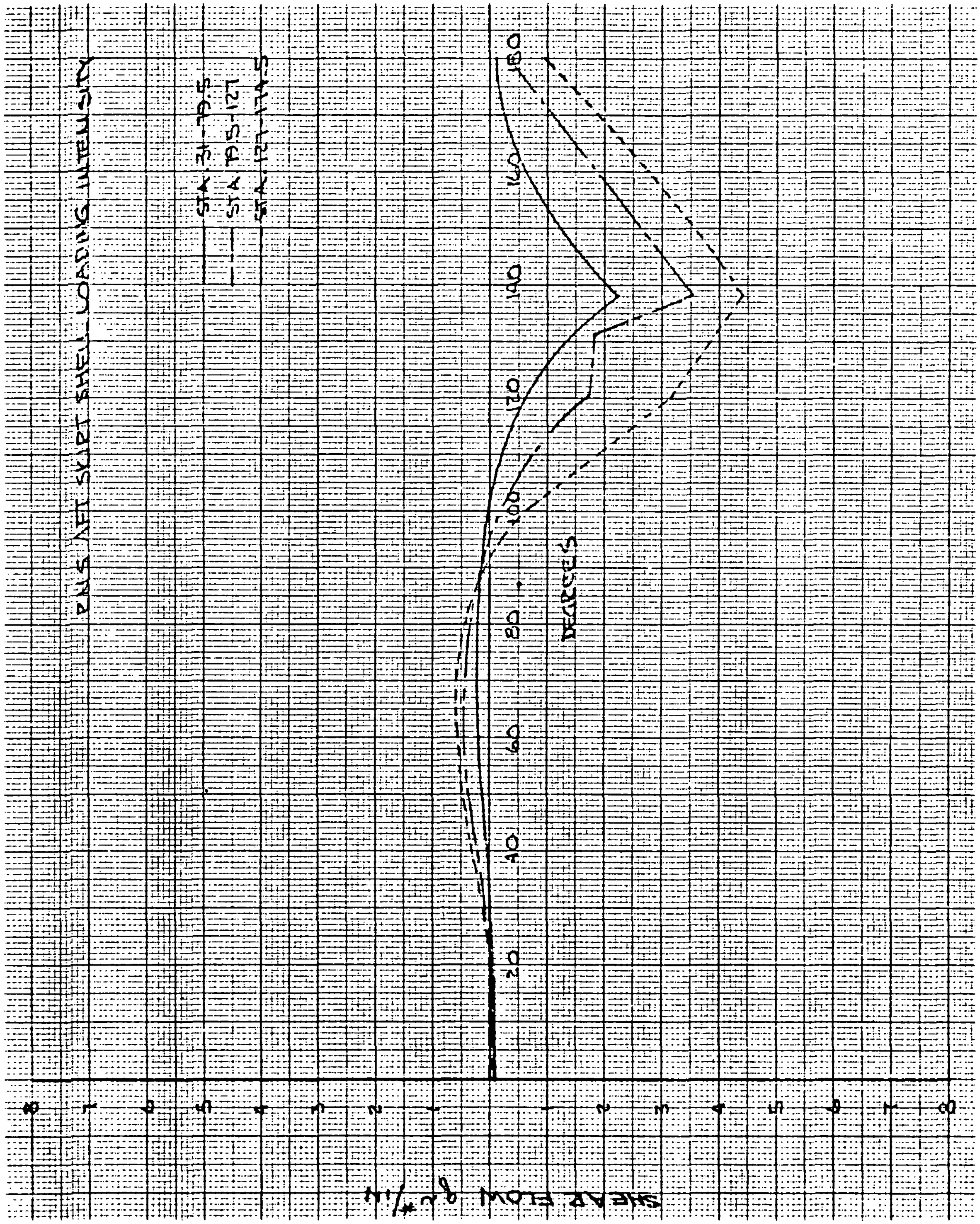

PALS AFT SKIRT SHELL LOADING INTENSITY
STA. 31-79.5
STA. 79.5-127
STA. 127-174.5
DEGREES
20
40
60
80
100
120
140
160
180
SHEAR FLOW

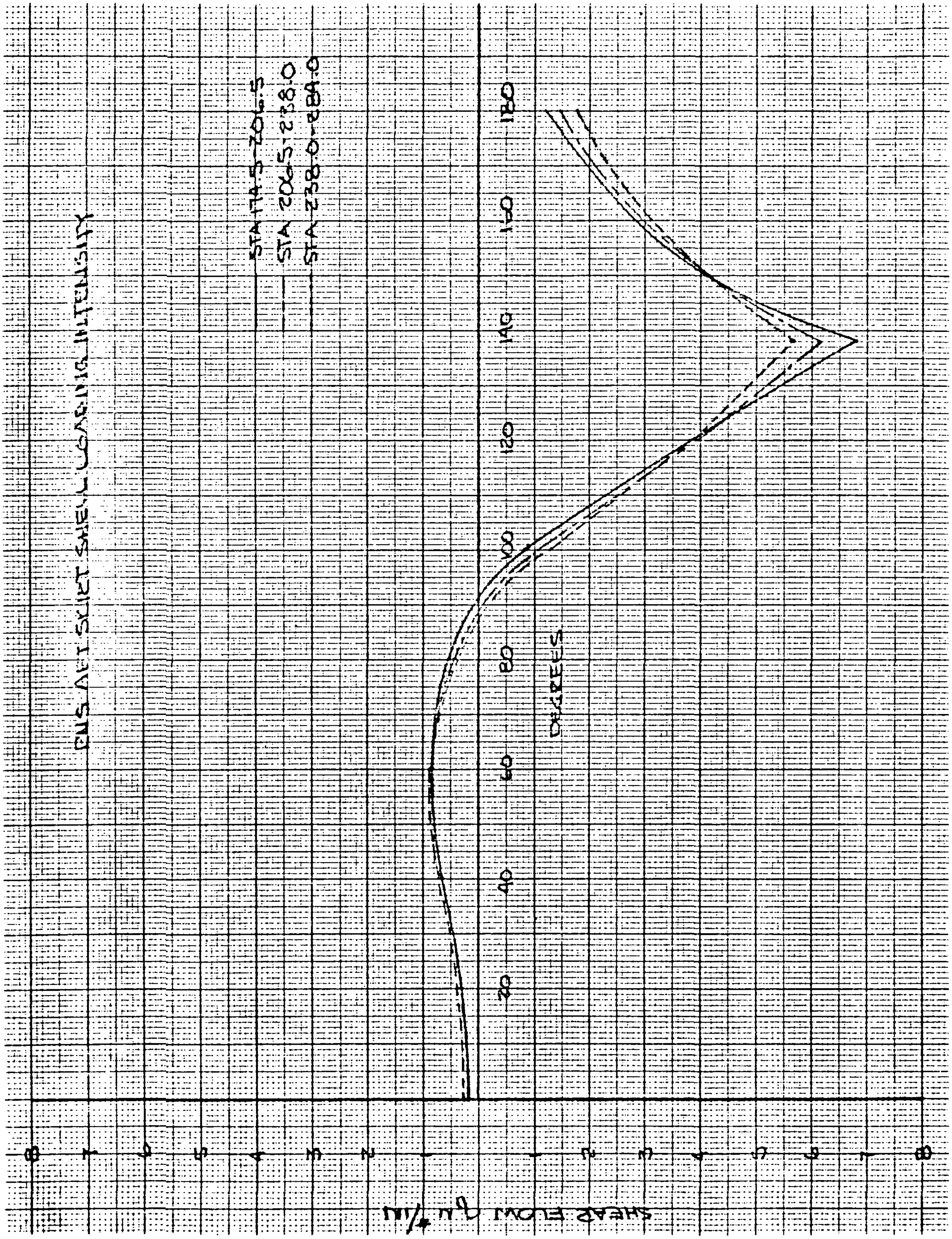
AFT SKIRT SHELL LOADING INTENSITY
STA 174.5-206.5
STA 206.5-238.0
STA 238.0-284.0
DEGREES
SHEAR FLOW q, #/IN

AFT SKIRT FRAME LOADS (FROM COMPUTER PROGRAM)

VEHICLE	θ (0° = TOP ℄)	STA. 31 P	STA. 31 V	STA. 31 $M_{\times 10^{-6}}$	STA. 82.5 P	STA. 82.5 V	STA. 82.5 $M_{\times 10^{-6}}$	STA. 128 P	STA. 128 V	STA. 128 $M_{\times 10^{-6}}$	STA. 174.5 P	STA. 174.5 V	STA. 174.5 $M_{\times 10^{-6}}$
MDAC SPACE STATION (MAX qα, HEADWIND)	10	53,566	-10,585	-2.765	23,280	-4459	-1.282	20,443	-3739	-1.193	14,670	-2501	-1.054
	30	26,491	-26,331	-2.038	13,850	-11,558	-0.976	15,254	-10,449	-0.936	15,293	-8792	-0.883
	50	-14,824	-28,599	-0.228	-2151	-13,913	-0.181	1582	-14,046	-0.218	4051	-15,056	-0.[illegible]79
	70	-53,858	-15,608	1.739	-21,692	-10,230	0.775	-21,366	-11,514	0.748	-22,520	-12,725	0.[illegible]78
	90	-81,302	8943	2.813	-46,140	391	1.479	-52,722	-1604	1.539	-51,481	3655	1.634
	110	-113,970	39,255	2.198	-77,513	21,070	1.452	-90,703	24,115	1.550	-61,107	29,358	1.382
	126 / 131	-200,380	76,478	-0.542	-108,060	46,944	0.006	-95,729	58,141	-0.108	-45,132	40,574	0.638
	134 / 138	-115,720	51,855	-3.662	-61,874	-6881	-7.859	19,381	-541	-2.431	54,896	-10,780	-2.[illegible]69
	150	-48,093	41,466	1.752	-34,201	-22,525	-7.702	-14,485	-36,252	-2.418	-21,334	-30,677	-2.[illegible]30
	170	72,405	15,786	-1.353	-33,580	-4893	-0.015	-62,936	-10,651	0.299	-54,113	-13,964	0.[illegible]69
				-2.429			0.322			1.028			1.2[illegible]9
RNS (MAX qα, TAIL WIND)	10	-19,057	3185	1.339	-8042	1493	0.502	-5875	1225	0.323	-2953	821	0.1[illegible]5
	30	-18,721	9885	1.121	-5611	4158	0.400	-1794	2867	0.239	1055	1330	0.098
	50	-11,127	16,279	0.444	274	5461	0.114	3943	2416	0.042	4673	-4734	0.0[illegible]5
	70	14,509	18,115	-0.676	8465	3848	-0.262	5066	-64	-0.125	1146	-2679	0.0[illegible]8
	90	62,821	6741	-1.918	11,416	-890	0.528	-7694	-1607	-0.121	-18,750	1178	0.2[illegible]3
	110	112,280	-26,490	-2.386	-1523	-4218	-0.466	-38,985	5383	-0.011	-35,828	13,822	0.143
	126 / 131	105,510	-66,260	-0.572	-29,824	673	-0.176	-63,569	24,669	-0.380	-32,366	24,263	-0.8[illegible]8
	134 / 138	-25,722	-153,040	2.079	-42,229	-8148	-0.201	-7764	-7301	-1.361	15,166	-16,877	-1.780
	150	63,074	95,048	6.665	-9107	-6377	-0.007	-12,450	-27,420	-1.194	-12,595	-30,940	-1.399
	170	169,840	32,180	-0.473	-1941	644	0.482	-45,660	-7422	0.861	-51,118	-12,780	0.919
				-2.675			0.433			1.368			1.798

AFT SKIRT FRAMES 206.5 & 238.0 (STABILITY)

$$N_x = 1.4\ (4883) = 6836\ \#/\text{IN}\quad (\text{ULT})$$

$$I_{REQ'D} = \frac{\pi R^4 N_x}{4000\, E\, a} = \frac{\pi (198)^4 N_x}{4000\,(10.5\times 10^6)\, a} = .115\left(\frac{N_x}{a}\right)$$

(FOR 206.5 & 238.0, $a = 31.5$)

$$\therefore\quad I_{REQ'D} = .115\left(\frac{6836}{31.5}\right) = 25.0$$

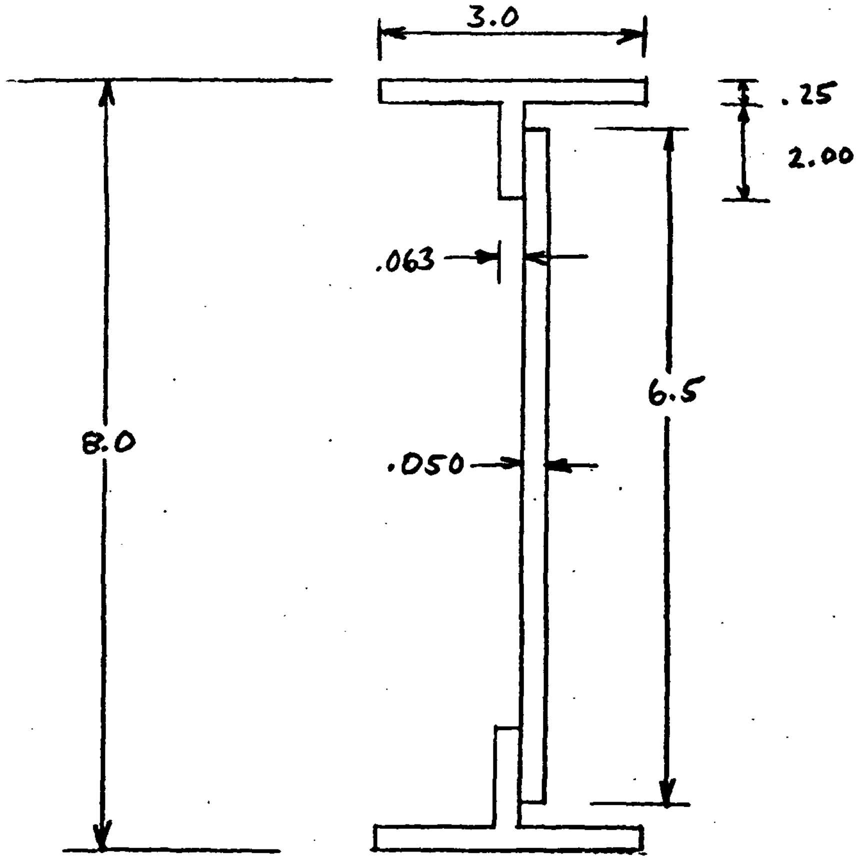

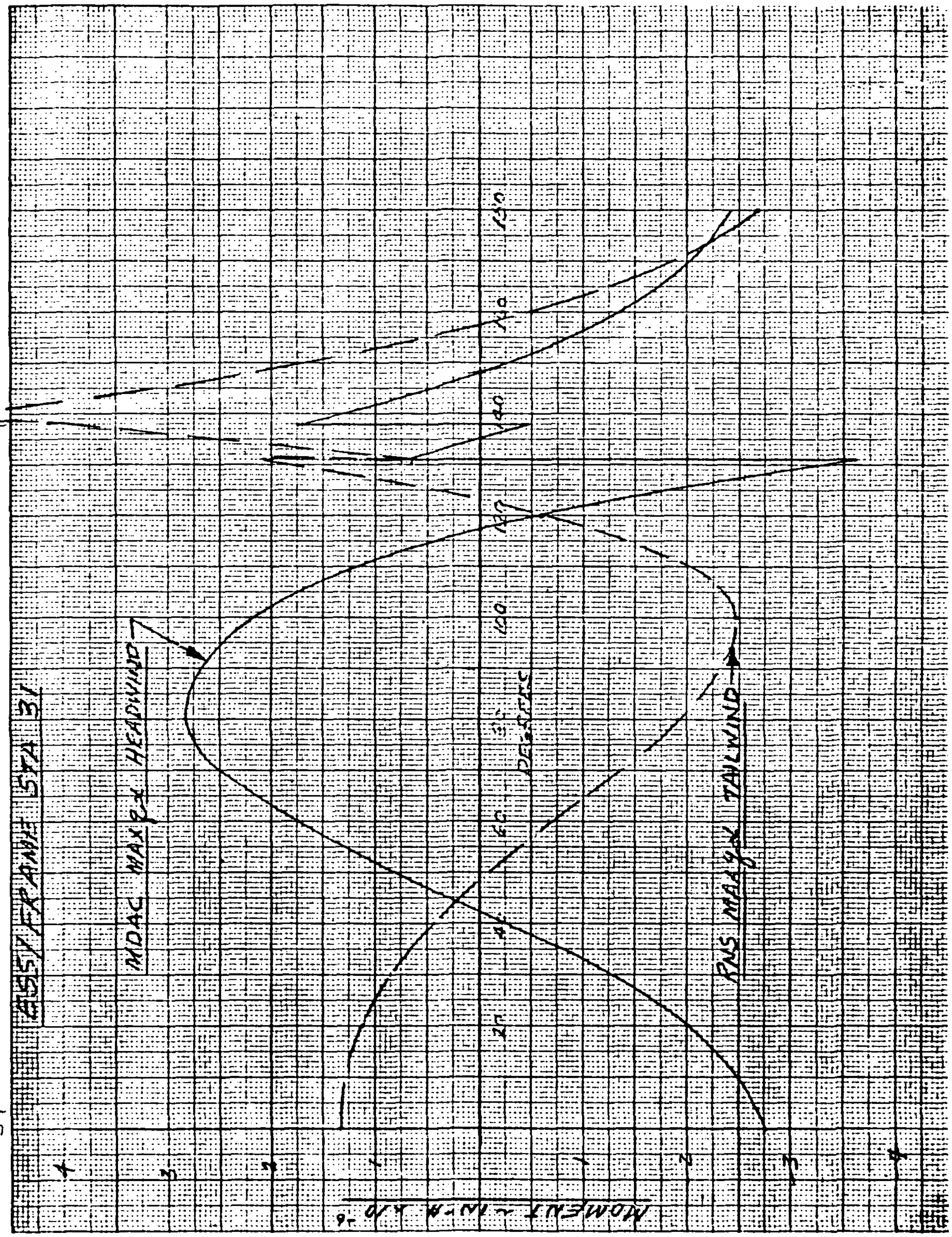
ASSY FRAME STA 31
MDAC MAX
HEADWIND
RNS MAX
TAILWIND
DEGREES
MOMENT ~ IN-#
31

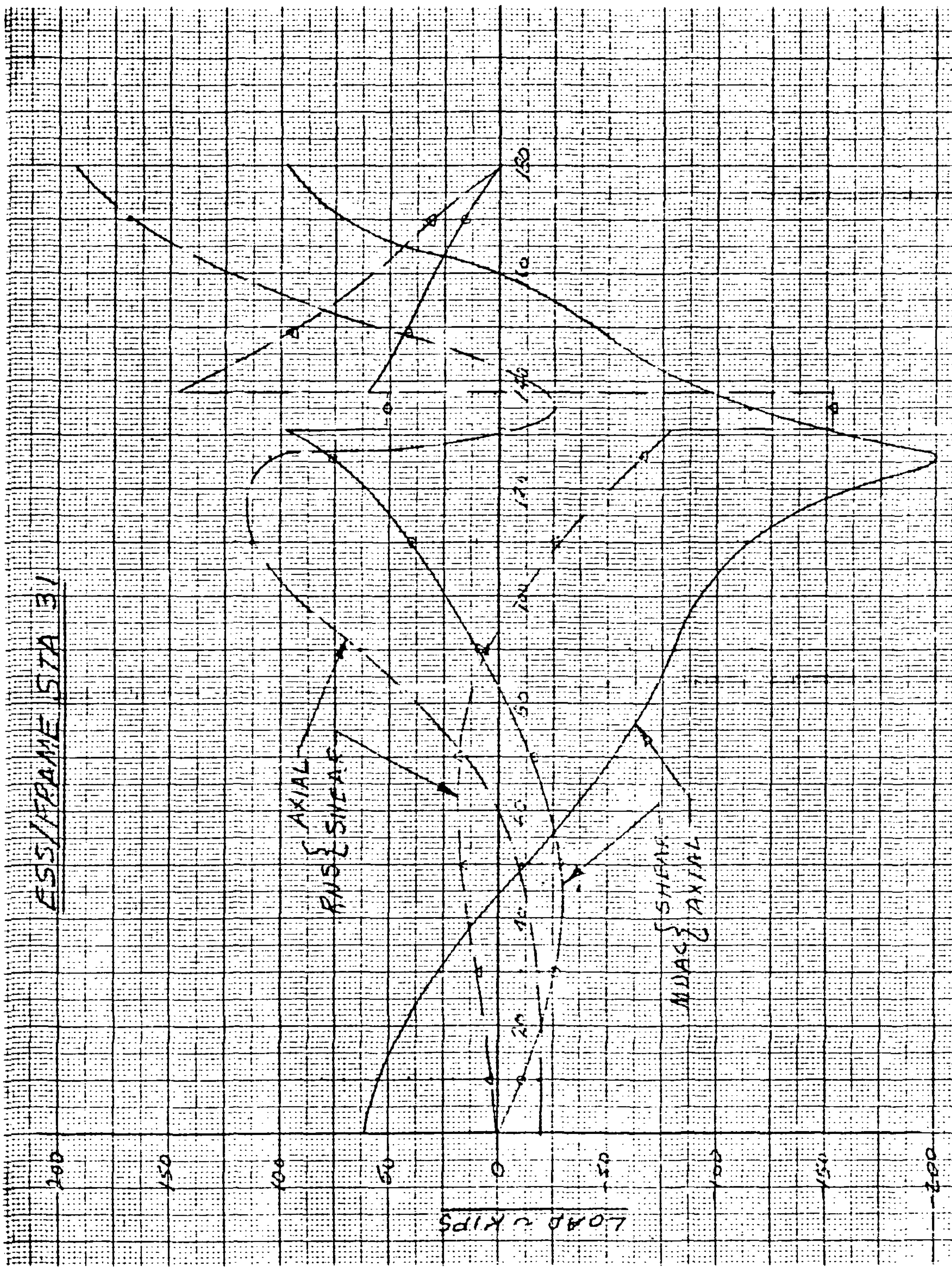
ESS/FRAME STA 31
RHS { AXIAL
SHEAR
MDAC { SHEAR
AXIAL
LOAD ~ KIPS

AFT SKIRT FRAME

STATION 31

BASIC

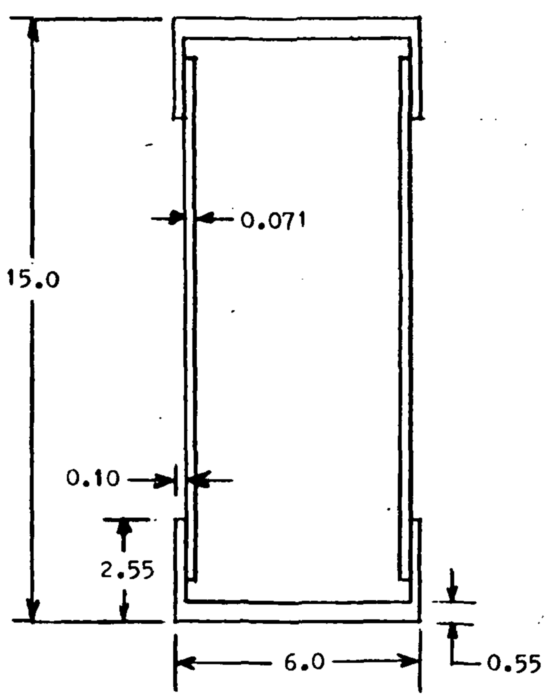

SECTION PROPERTIES : A = 9.232

I = 398.7

$\bar{Y}$ = 7.5

LOCALLY AT

POSITIONS I & III

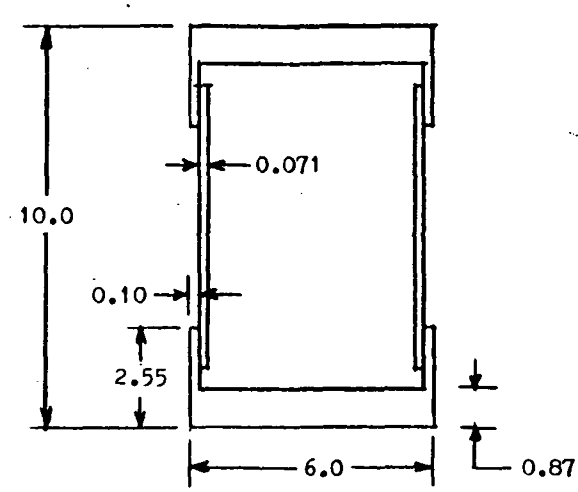

SECTION PROPERTIES : A = 12.271

I = 230.9

$\bar{Y}$ = 5.0

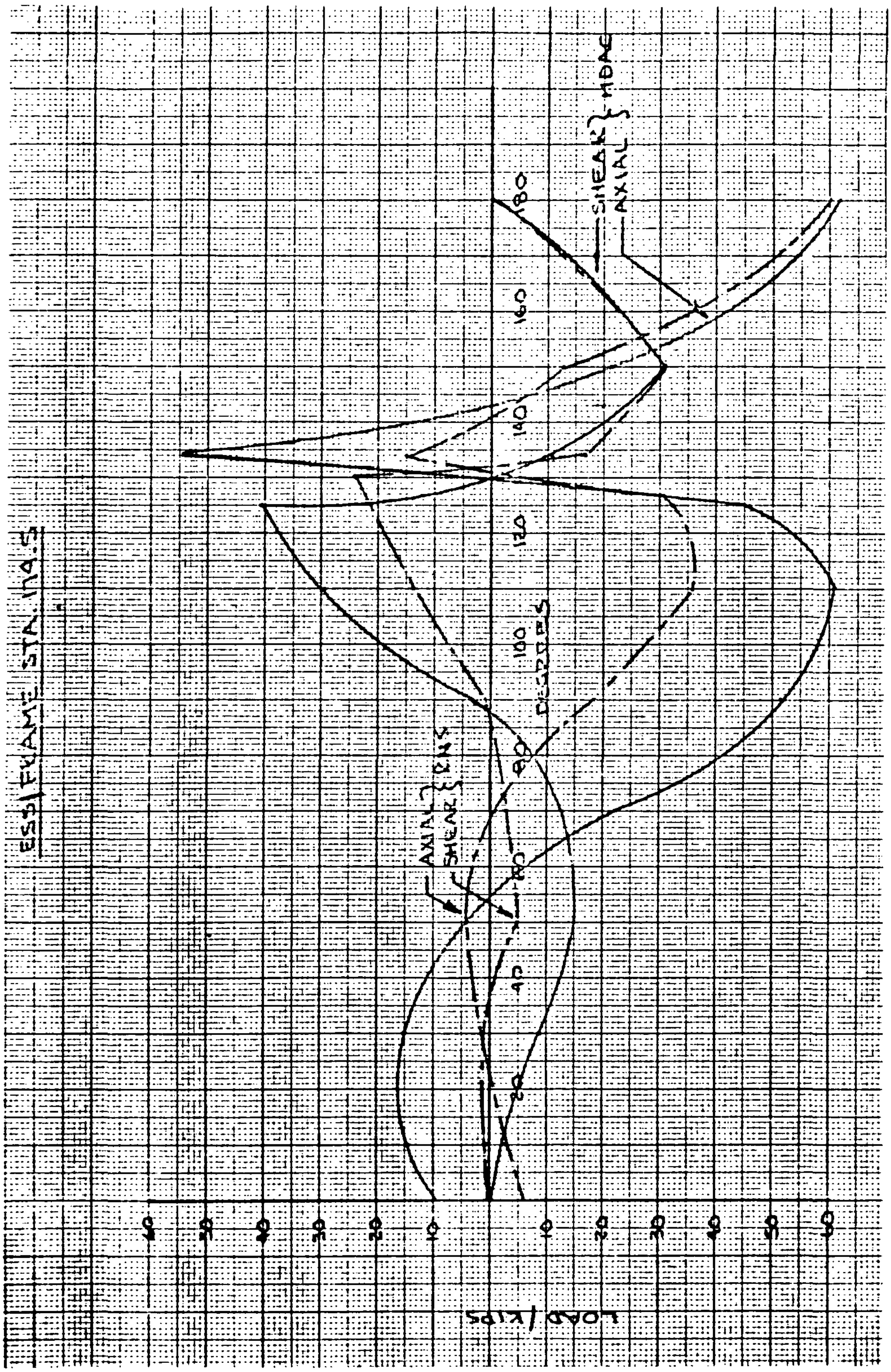

E

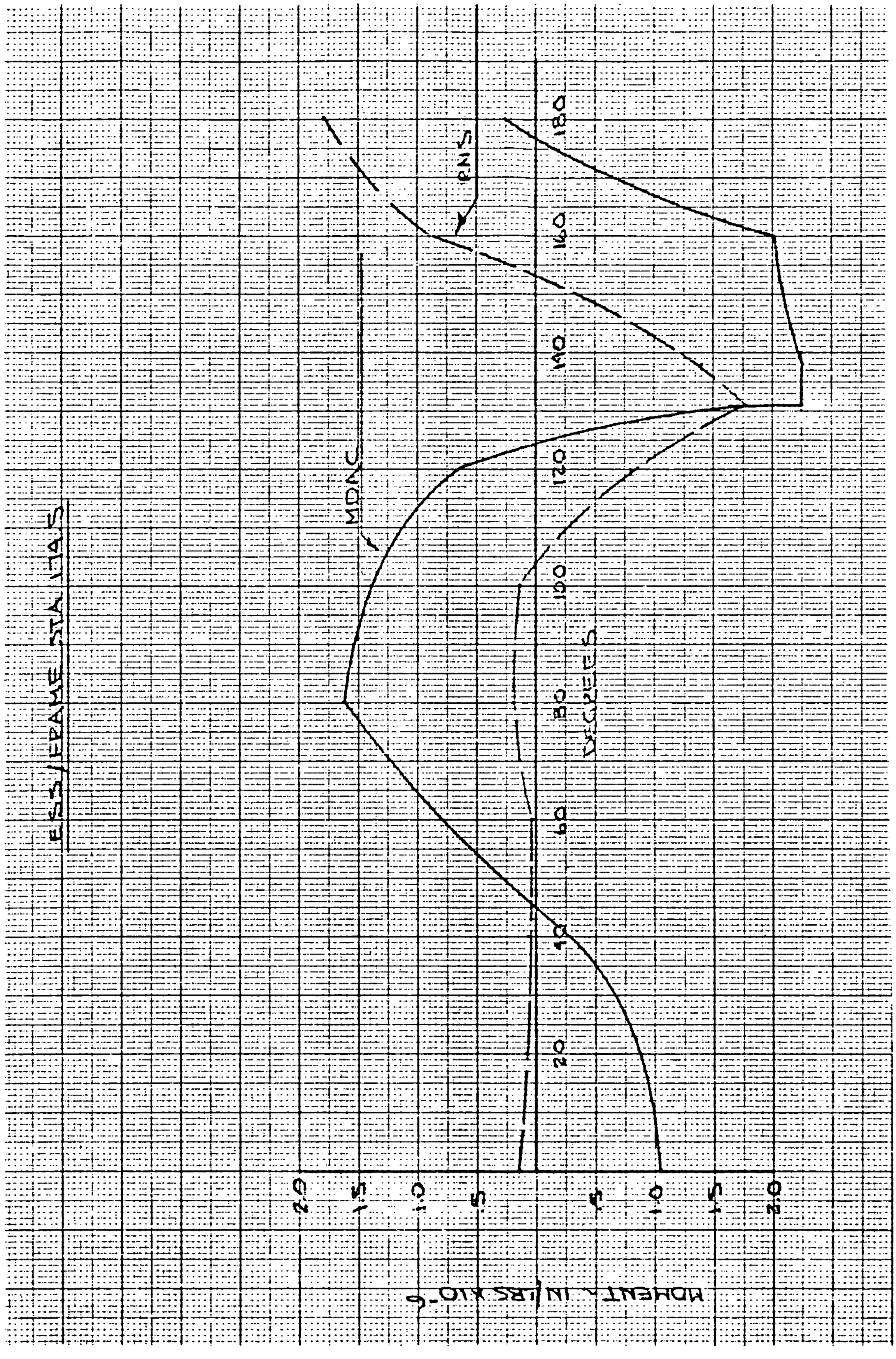
ESS/FRAME STA 1745
MDAC
RNS
DEGREES
20
40
60
80
100
120
140
160
180
2.0
1.5
1.0
.5
.5
1.0
1.5
2.0
MOMENT ~ IN/LBS X10-6

AFT SKIRT FRAMES

STA. 82.5, 128.0, & 174.5

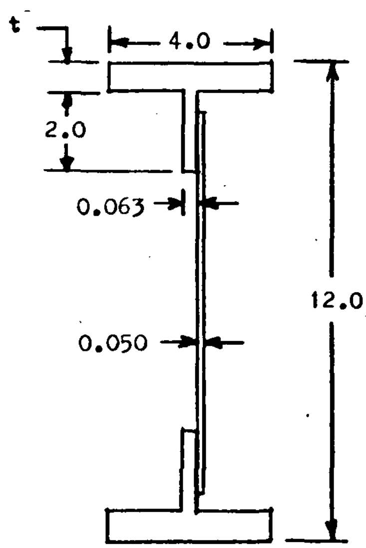

t = 0.64 (STA. 82.5)
= 0.68 (STA. 128.0)
= 0.70 (STA. 174.5)

SECTION PROPERTIES : A = 5.858 (STA. 82.5)
= 6.174 (STA. 128.0)
= 6.332 (STA. 174.5)

I = 174.0 (STA. 82.5)
= 183.0 (STA. 128.0)
= 187.4 (STA. 174.5)

$\bar{Y}$ = 6.0

STA. 206.5 & 238.0

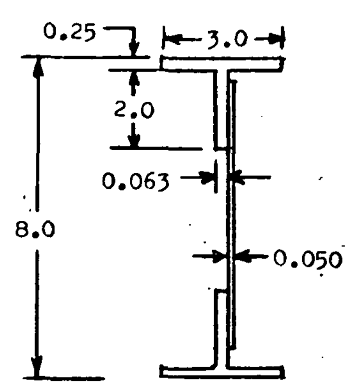

SECTION PROPERTIES : A = 2.077
I = 25.67
$\bar{Y}$ = 4.0

OIS THRUST STRUCTURE

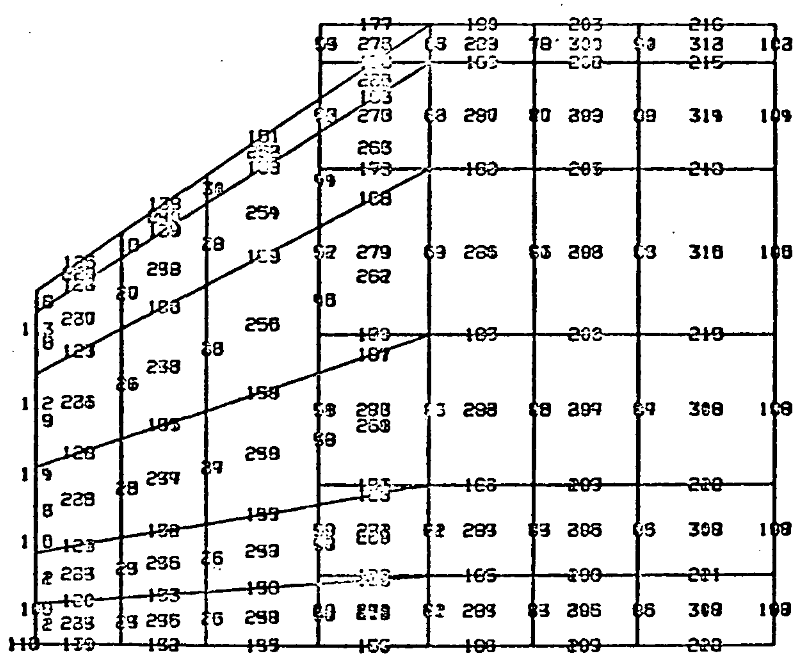

ELEMENT NUMBER X Y PROJECTION

OIS THRUST STRUCTURE

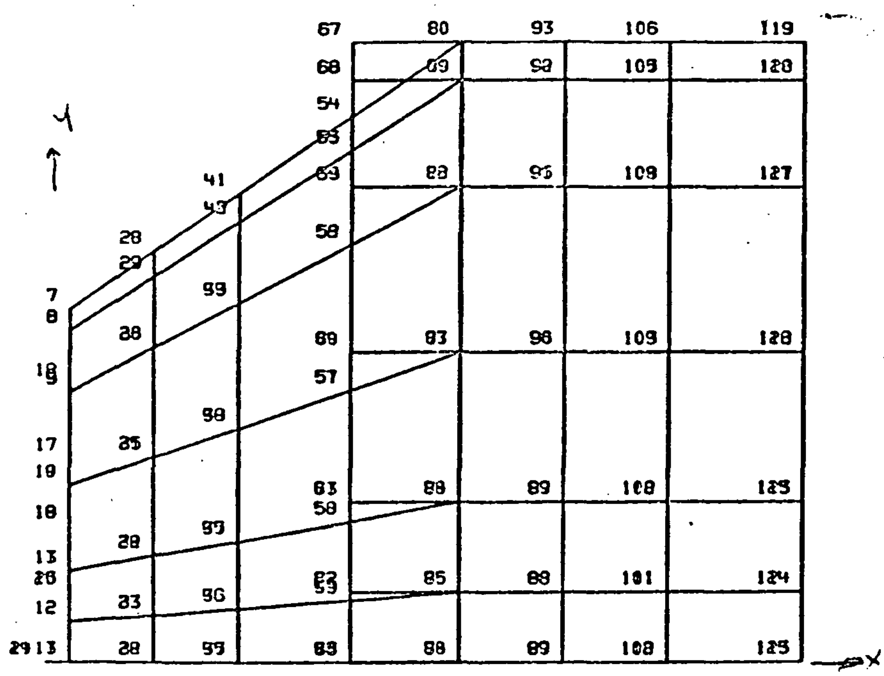

NODE NUMBER X Y PROJECTION

OIS THRUST STRUCTURE

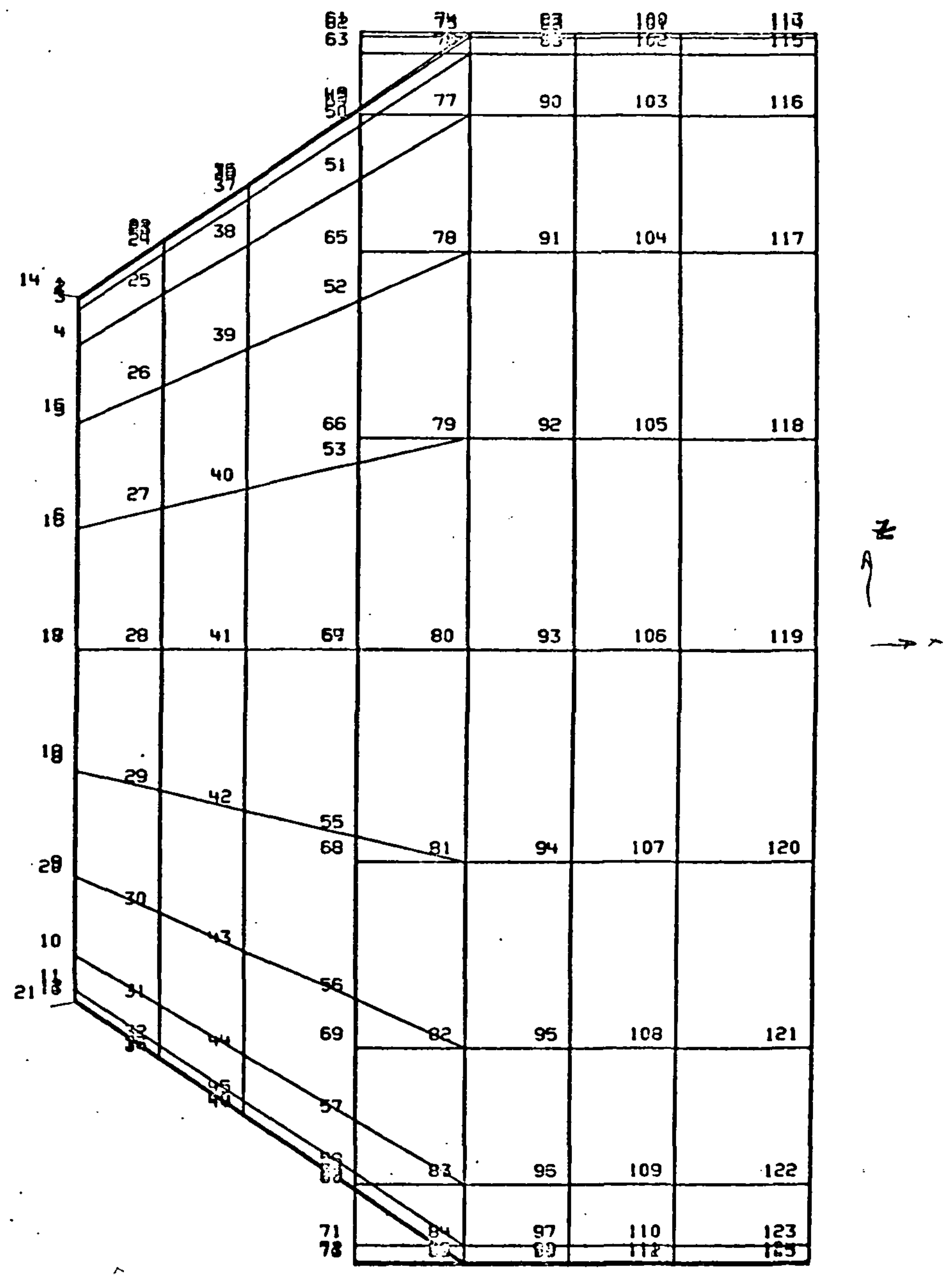

NODE NUMBER X Z PROJECTION

OIS THRUST STRUCTURE

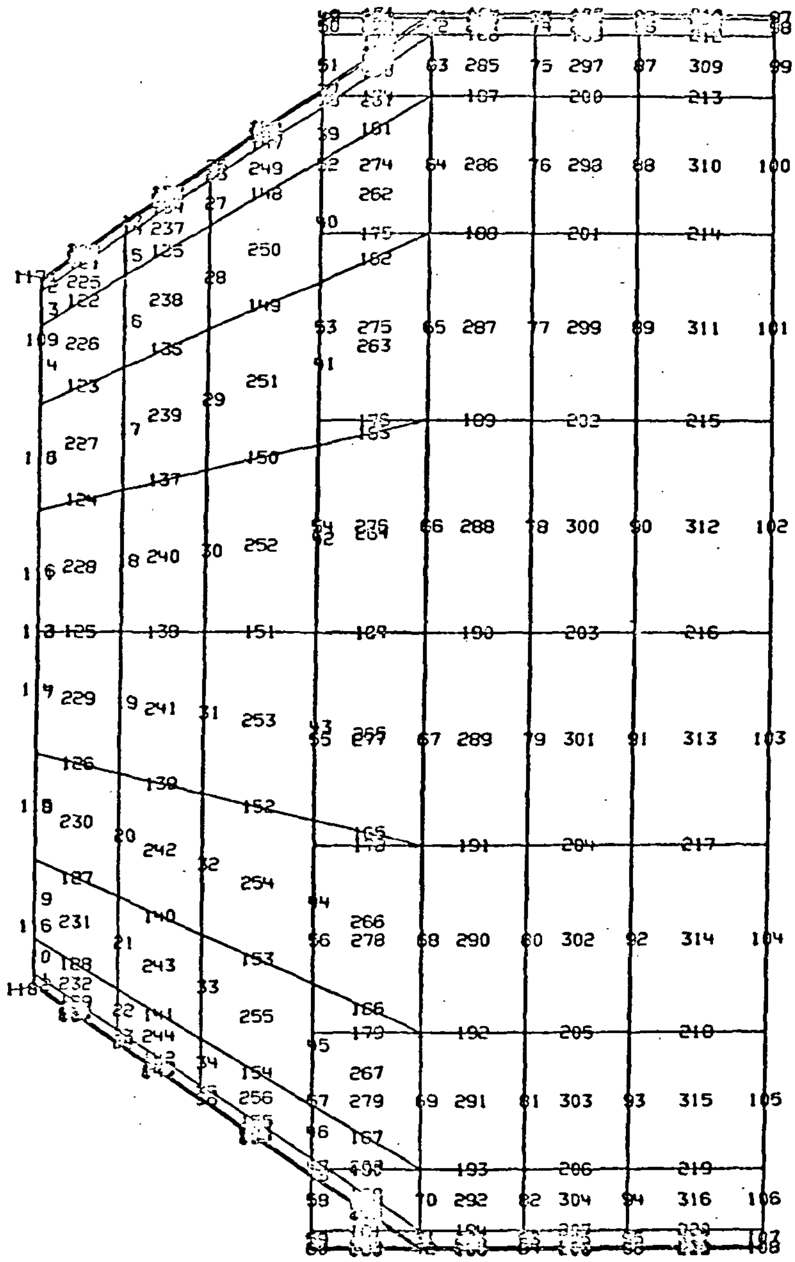

ELEMENT NUMBER X Z PROJECTION

OIS THRUST STRUCTURE

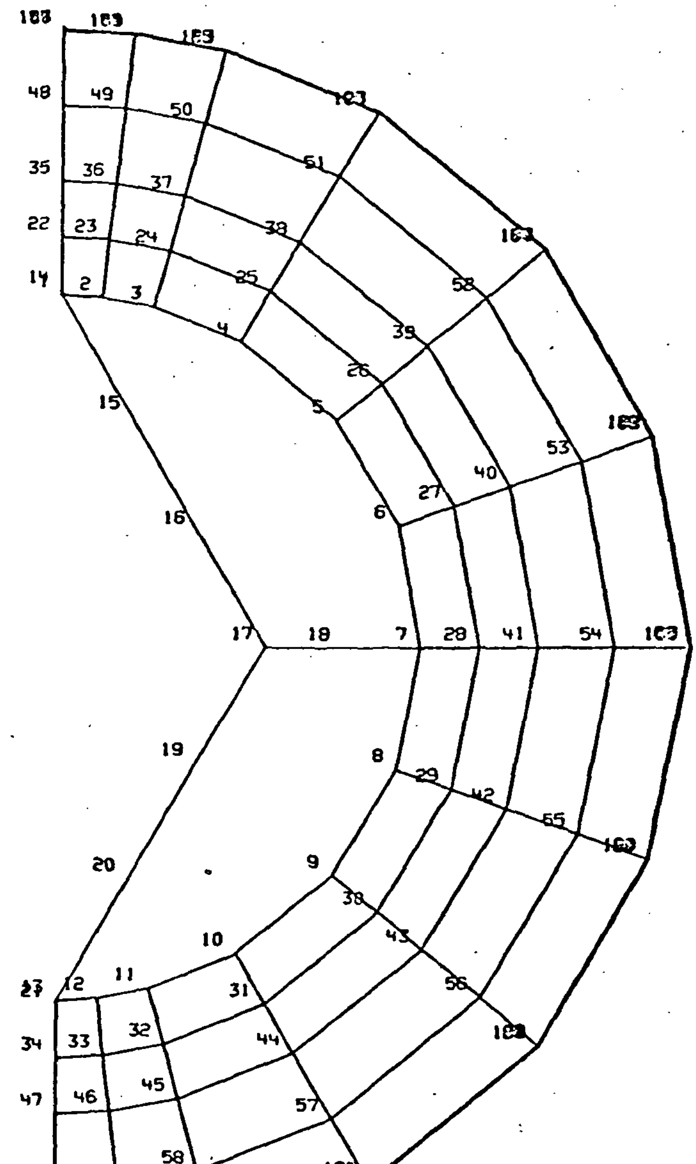

NODE NUMBER Y Z PROJECTION

OIS THRUST STRUCTURE

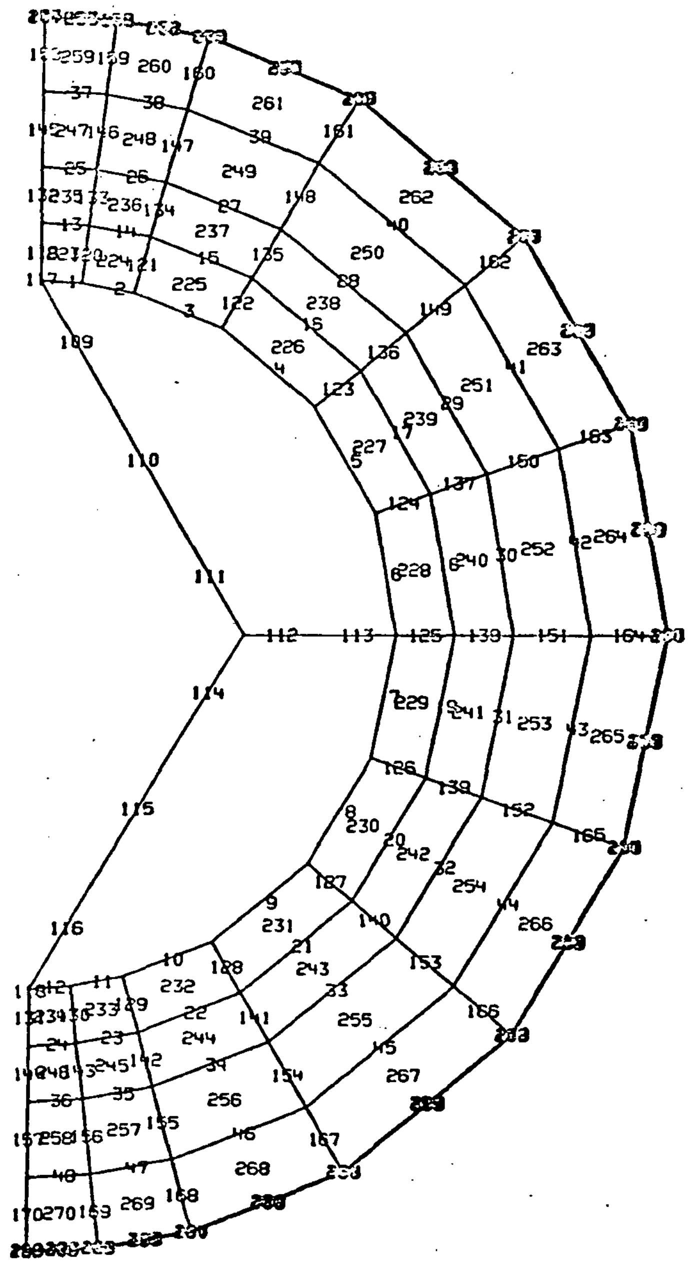

ELEMENT NUMBER Y Z PROJECTION

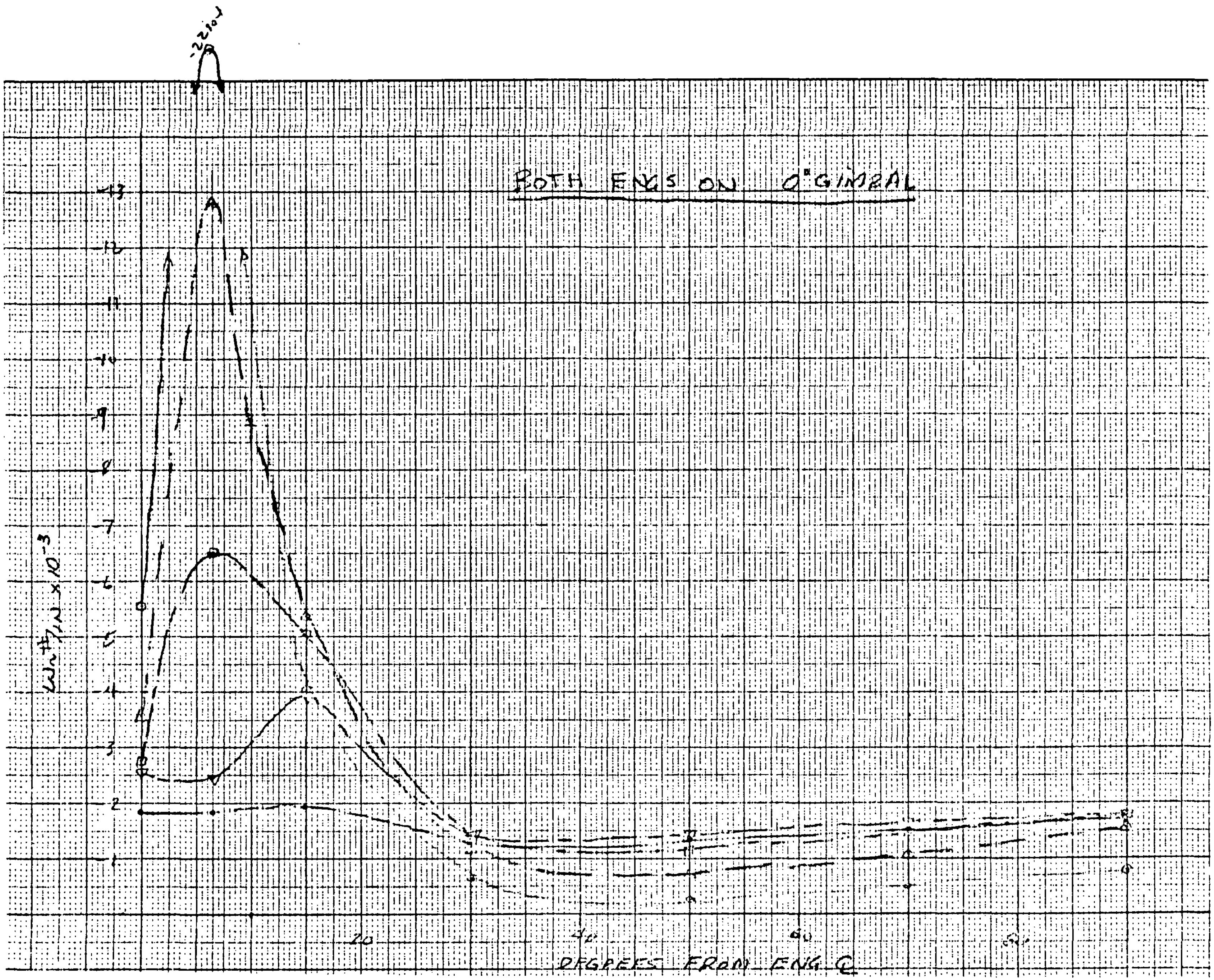

BOTH ENGS ON 0° GIMBAL
13
12
11
10
9
8
7
6
5
4
3
2
1
20
40
60
80
DEGREES FROM ENG ℄

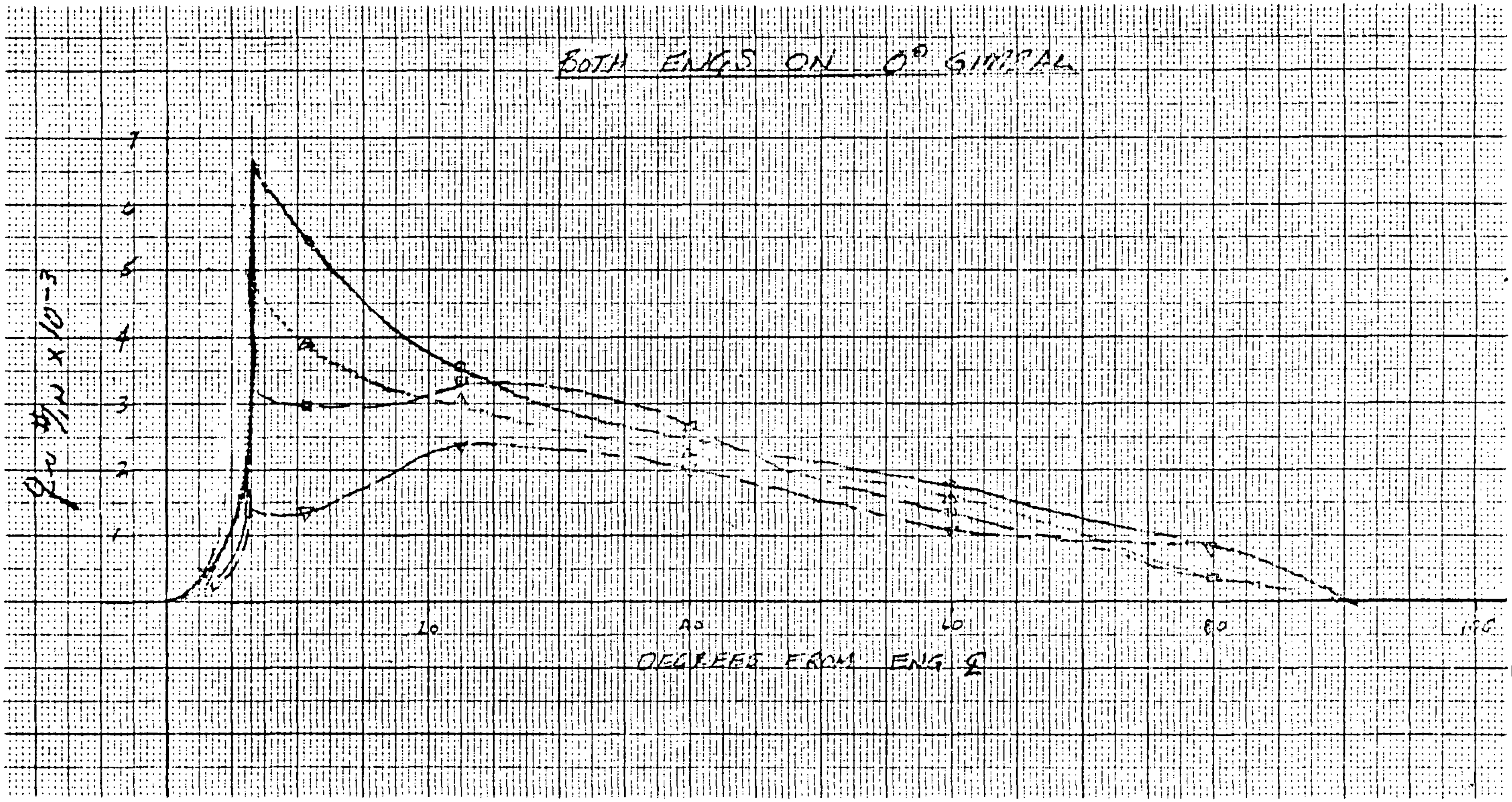
BOTH ENGS ON 0° GIMBAL
1
2
3
4
5
6
7
20
40
60
80
100
DEGREES FROM ENG ℄

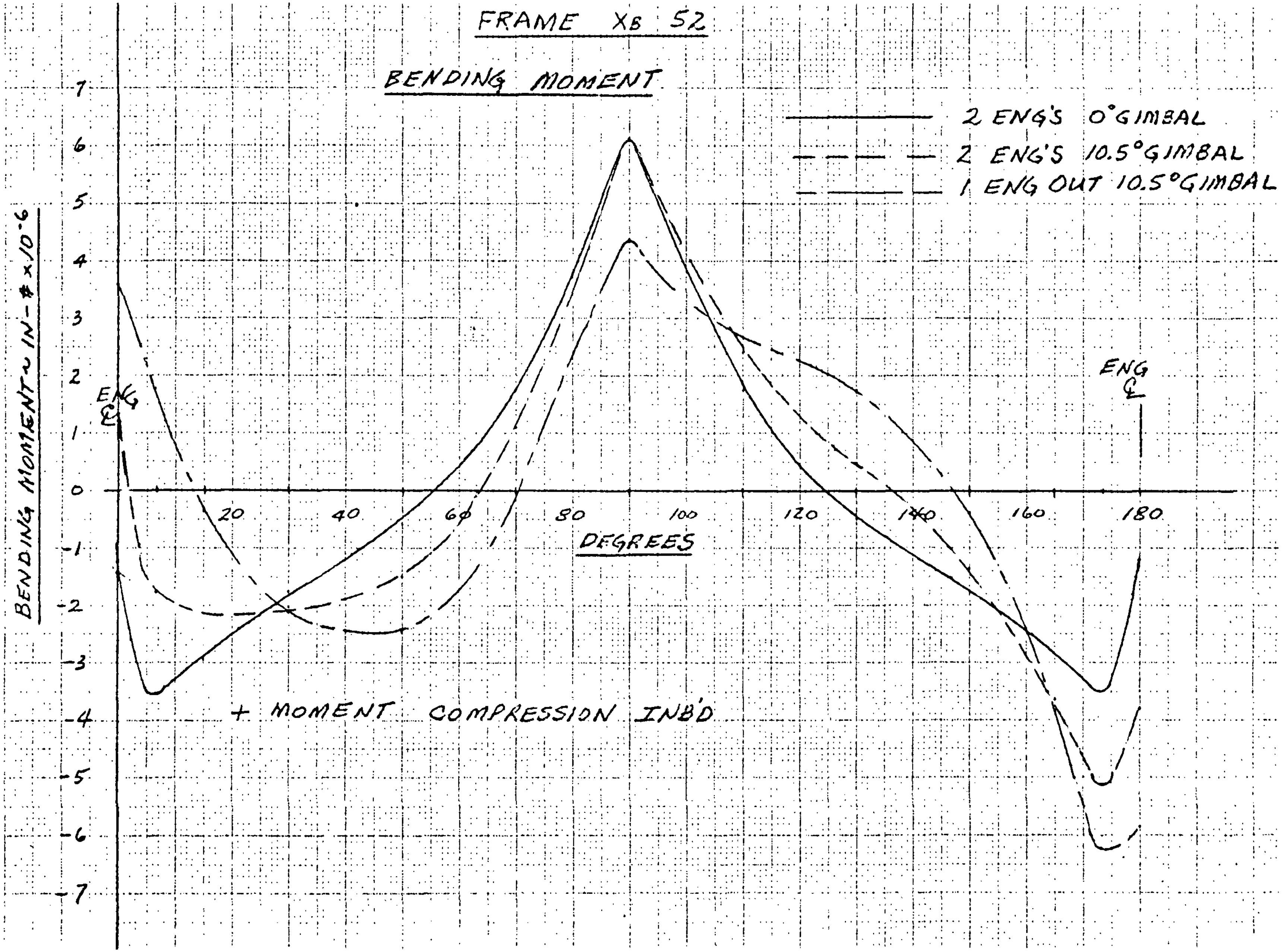

FRAME XB 52
BENDING MOMENT
2 ENG'S 0° GIMBAL
2 ENG'S 10.5° GIMBAL
1 ENG OUT 10.5° GIMBAL
BENDING MOMENT ~ IN-# x 10^-6
7
6
5
4
3
2
1
0
-1
-2
-3
-4
-5
-6
-7
ENG ℄
ENG ℄
20
40
60
80
100
120
140
160
180
DEGREES
+ MOMENT COMPRESSION INB'D

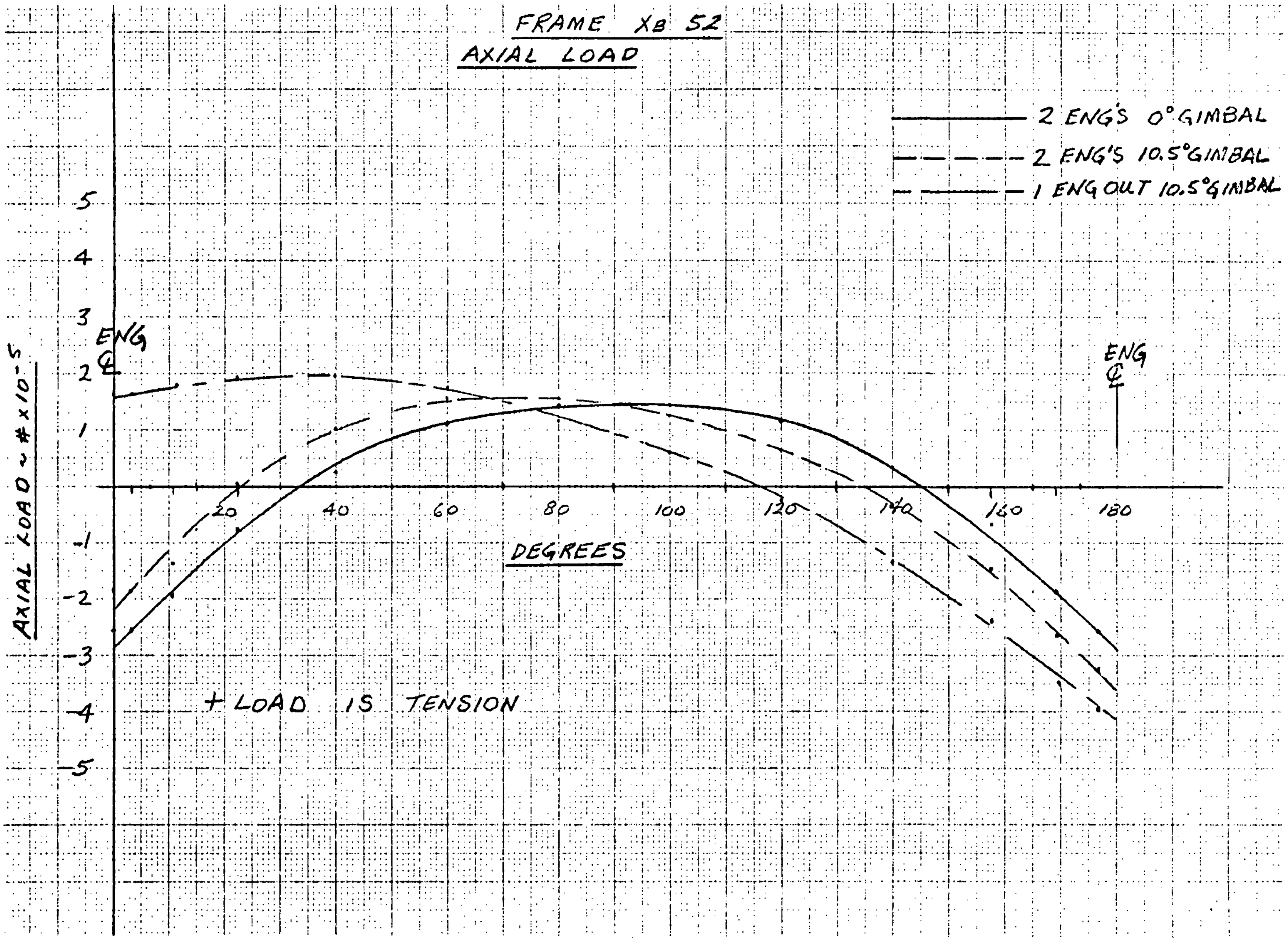

FRAME X_B 52
AXIAL LOAD
2 ENG'S 0° GIMBAL
2 ENG'S 10.5° GIMBAL
1 ENG OUT 10.5° GIMBAL
AXIAL LOAD ~ # x 10^-5
DEGREES
ENG ℄
ENG ℄
5
4
3
2
1
-1
-2
-3
-4
-5
20
40
60
80
100
120
140
160
180
+ LOAD IS TENSION

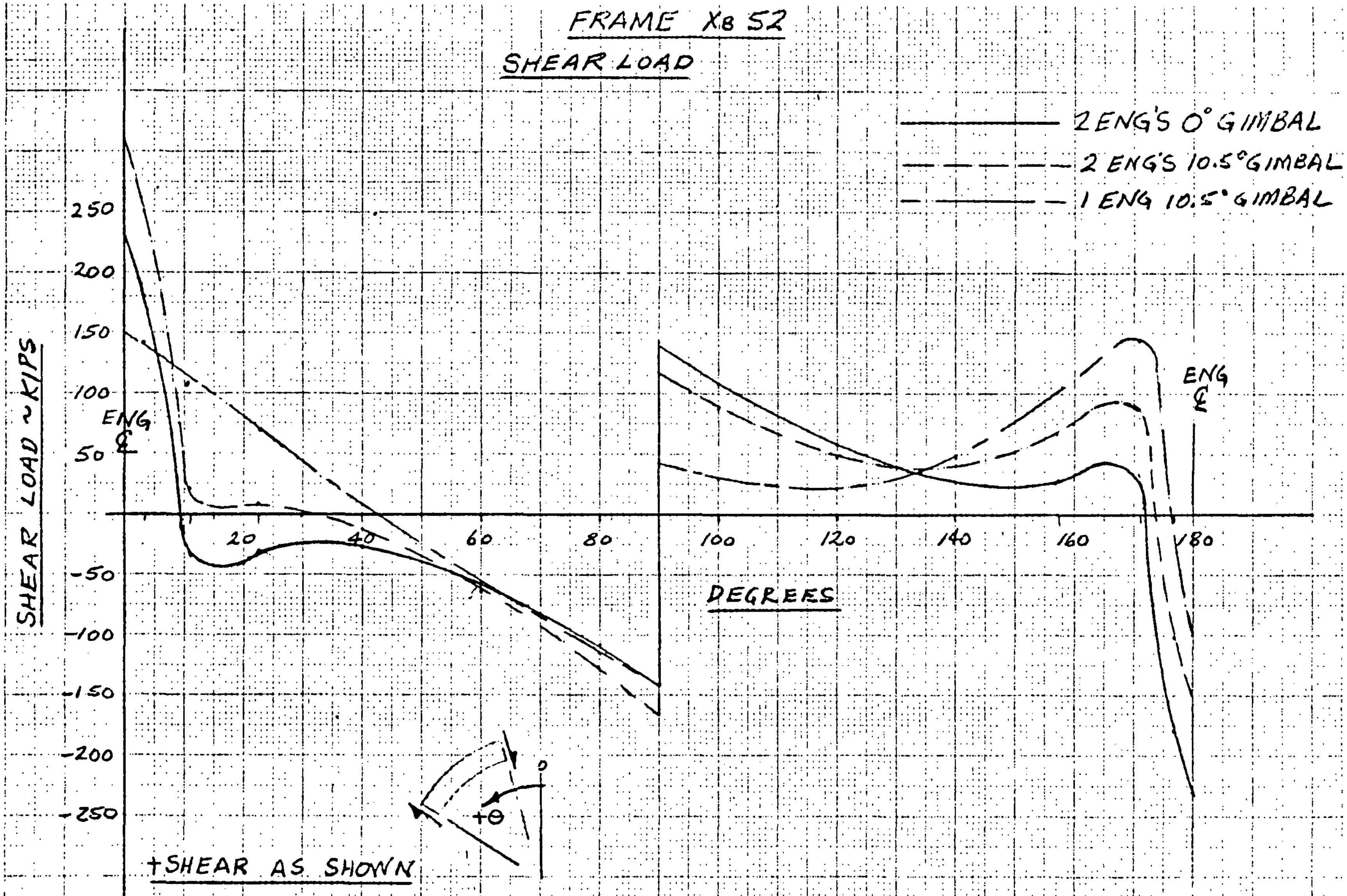
FRAME XB 52
SHEAR LOAD
2 ENG'S 0° GIMBAL
2 ENG'S 10.5° GIMBAL
1 ENG 10.5° GIMBAL
SHEAR LOAD ~ KIPS
250
200
150
100
50
-50
-100
-150
-200
-250
ENG ℄
ENG ℄
20
40
60
80
100
120
140
160
180
DEGREES
+θ
+SHEAR AS SHOWN

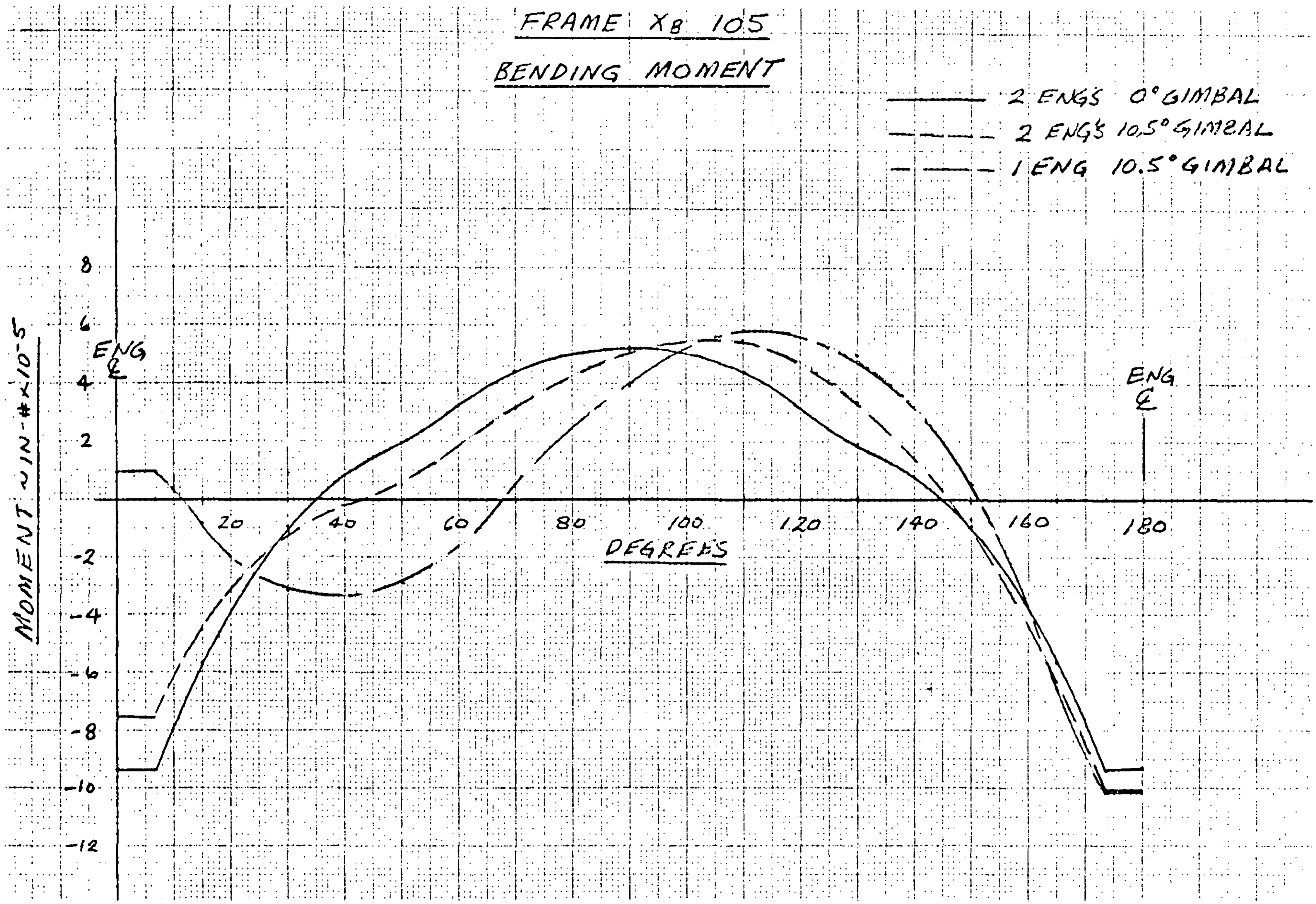

FRAME X_B 105
BENDING MOMENT
2 ENGS 0° GIMBAL
2 ENG'S 10.5° GIMBAL
1 ENG 10.5° GIMBAL
MOMENT ~IN-#×10⁻⁵
8
6
4
2
-2
-4
-6
-8
-10
-12
ENG ℄
ENG ℄
20
40
60
80
100
120
140
160
180
DEGREES

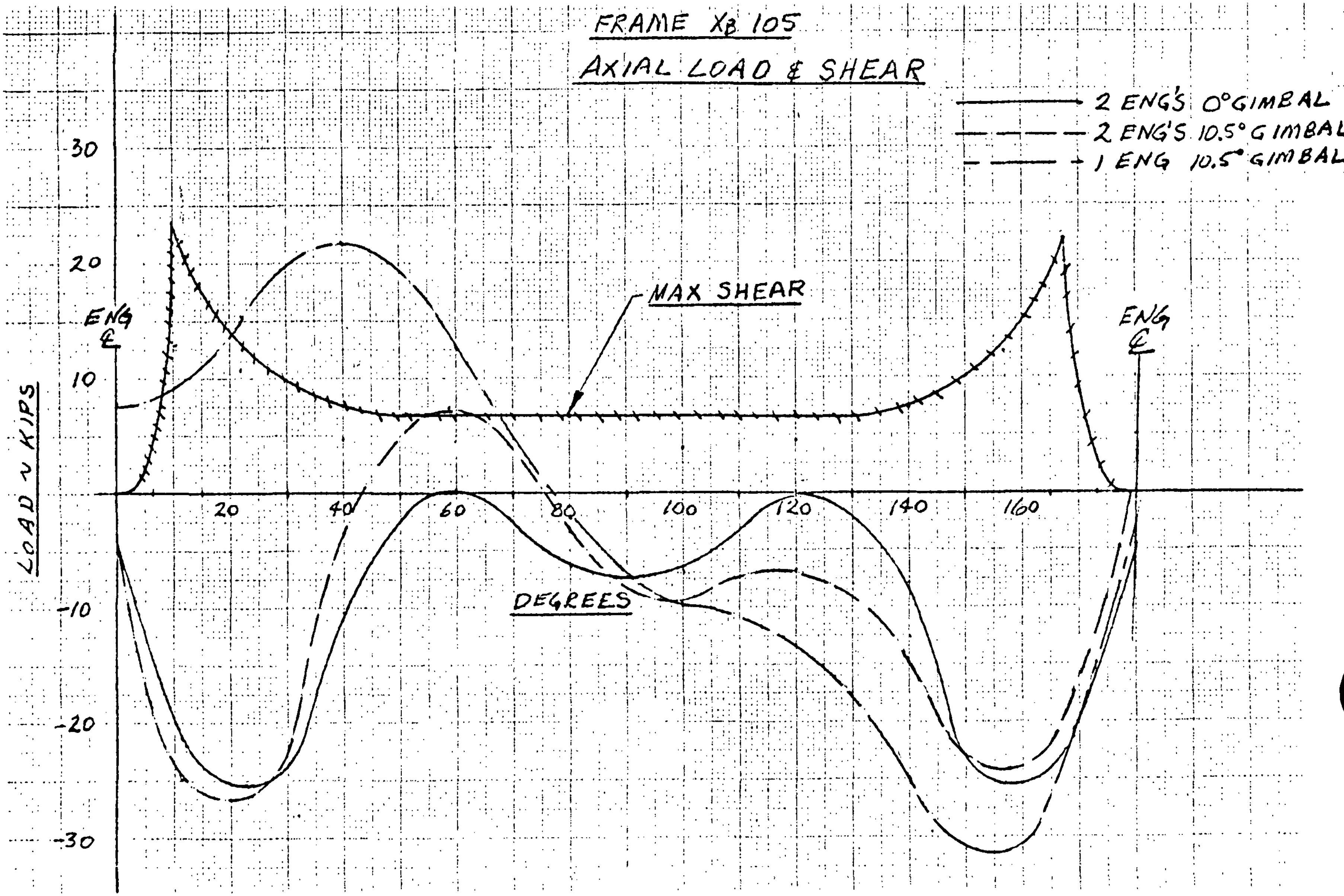

FRAME X_B 105
AXIAL LOAD & SHEAR
2 ENG'S 0° GIMBAL
2 ENG'S 10.5° GIMBAL
1 ENG 10.5° GIMBAL
MAX SHEAR
ENG ℄
ENG ℄
LOAD ~ KIPS
30
20
10
-10
-20
-30
20
40
60
80
100
120
140
160
DEGREES

THRUST CONE LONGERON

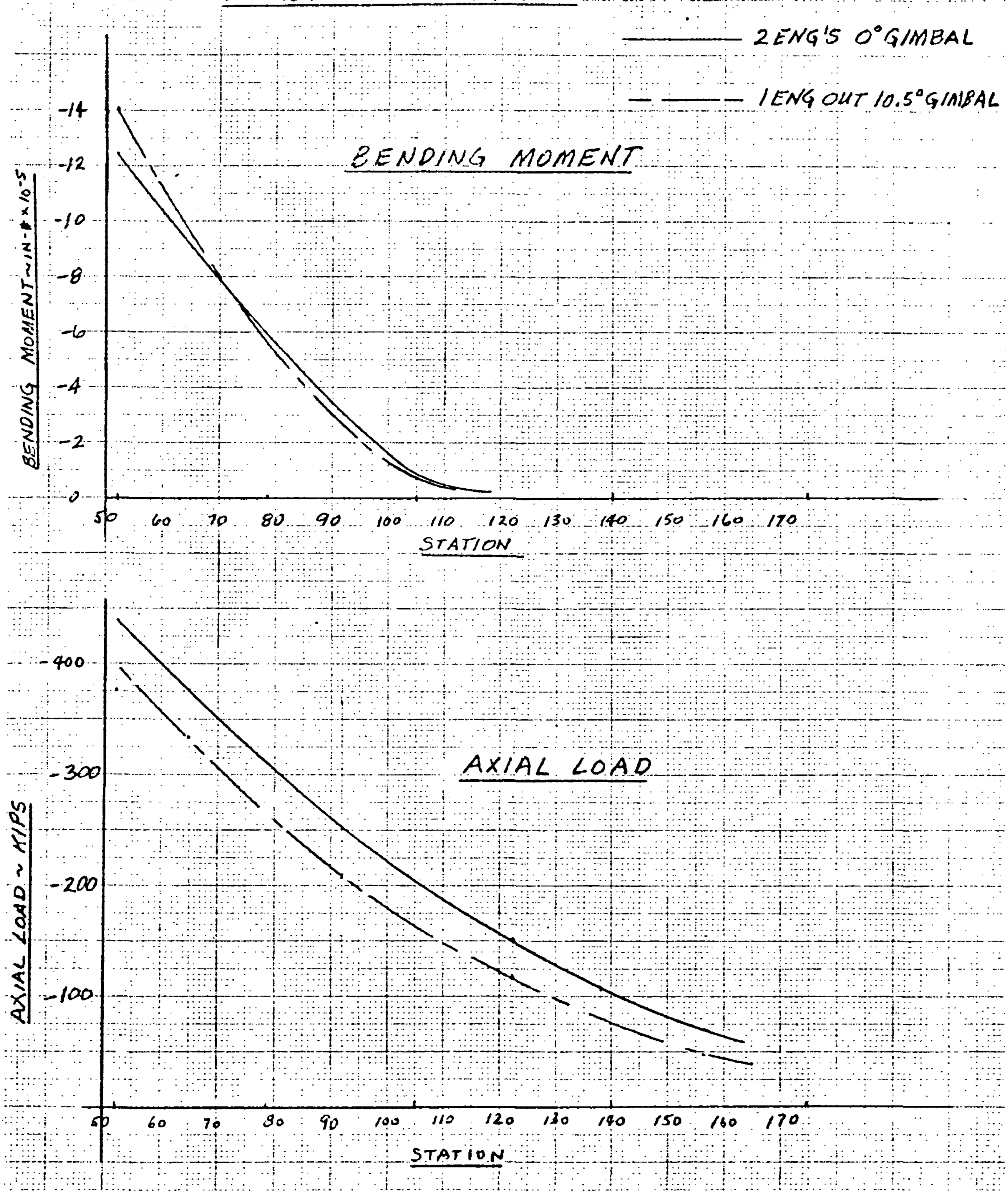

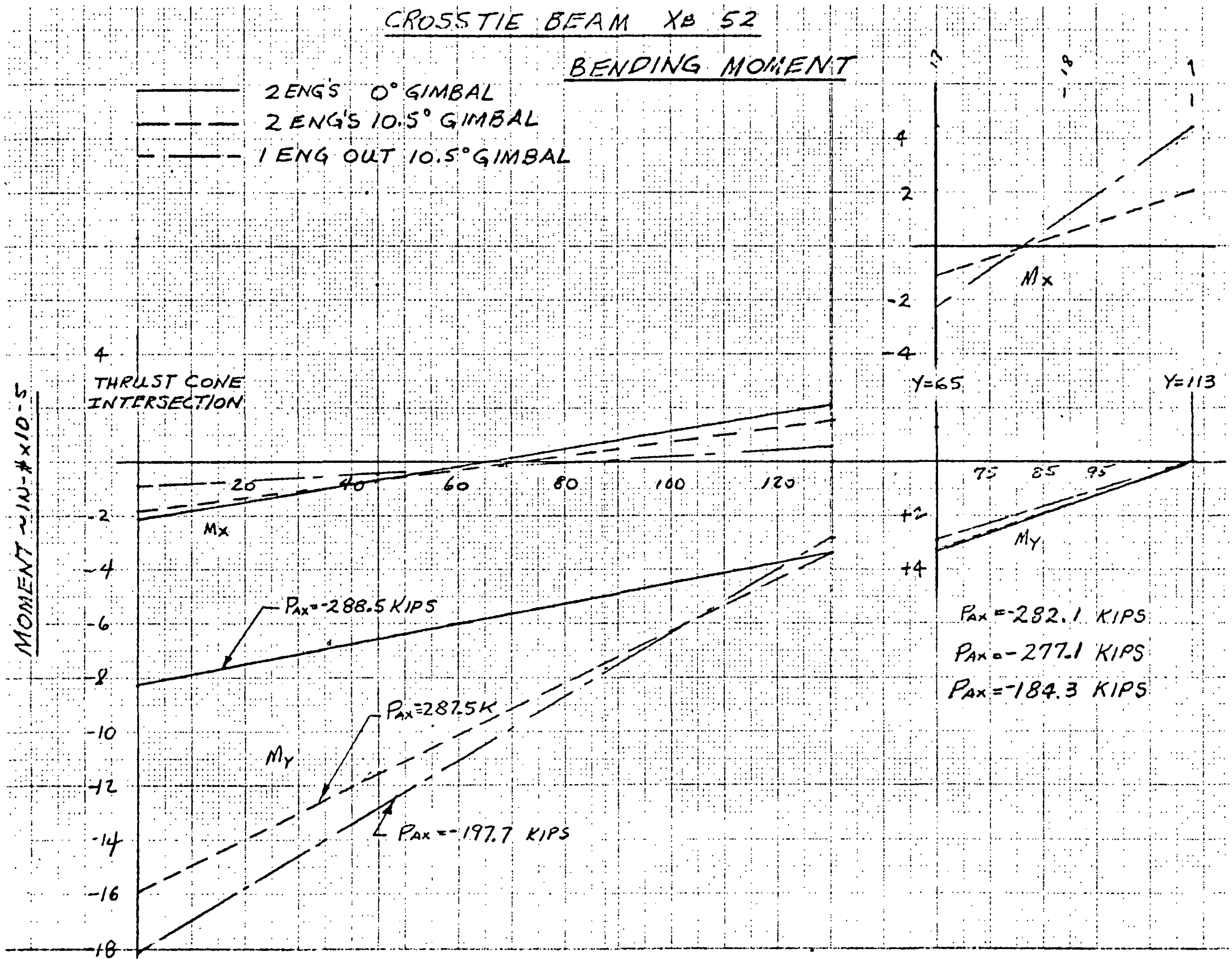
CROSSTIE BEAM XB 52
BENDING MOMENT
2 ENG'S 0° GIMBAL
2 ENG'S 10.5° GIMBAL
1 ENG OUT 10.5° GIMBAL
THRUST CONE INTERSECTION
MOMENT ~ IN-# x 10-5
Mx
My
PAX = -288.5 KIPS
PAX = 287.5K
PAX = -197.7 KIPS
Y=65
Y=113
PAX = -282.1 KIPS
PAX = -277.1 KIPS
PAX = -184.3 KIPS
20
40
60
80
100
120
75
85
95
4
2
-2
-4
-6
-8
-10
-12
-14
-16
-18
+2
+4

3.6. BOOSTER LOADS AND STRUCTURAL SIZING

The ESS launch vehicle, consisting of the shuttle booster with a modified S-II stage mounted in place of the reusable orbiter vehicle, was analyzed with the following payloads:

Space Station (MDAC configuration)

Space Tug

Nuclear Stage (RNS)

Loads and structural sizing study were determined to verify the feasibility of this launch vehicle concept and to identify structural design requirements that differ from those of the shuttle launch vehicle. The following sections describe the methodology used to conduct the loads and structural analyses.

3.6.1 GROUND RULES AND OBJECTIVES

The overall objective was to minimize the impact of the ESS, with its various payloads, on the shuttle booster. To minimize internal body loads and the amount of strengthening required in the structure at the interstage attach points, aerodynamic loading limits were established that were less than those applicable to the shuttle launch vehicle. During the maximum dynamic pressure region of flight, in particular, these limits were selected to constrain αq to within +1500 and -2900 deg-psf, and βq within ±1600 deg-psf. For αq, the -2900 deg-psf value represents, in general, the structural capacity of the aft lower portion of the hydrogen tank, and the total range of 4400 deg-psf represents the minimum control limit. The βq value of ±1600 is also a minimum control limit. The αq and βq constraints must be satisfied for the shuttle synthetic design wind conditions and without exceeding the booster thrust vector control system capability defined for shuttle. In addition, all attitude stabilization and control system modifications required by the ESS launch vehicle to achieve the essential load relief were confined to the areas of system software. Both trajectory shaping and load-relief techniques were employed to satisfy the αq and βq constraints.

3.6.2 APPROACH

The approach to booster structural sizing is shown in Figure 3-8. The booster was analyzed only in the mated configuration with each of the three payloads shown. From stage separation to booster touchdown, the shuttle

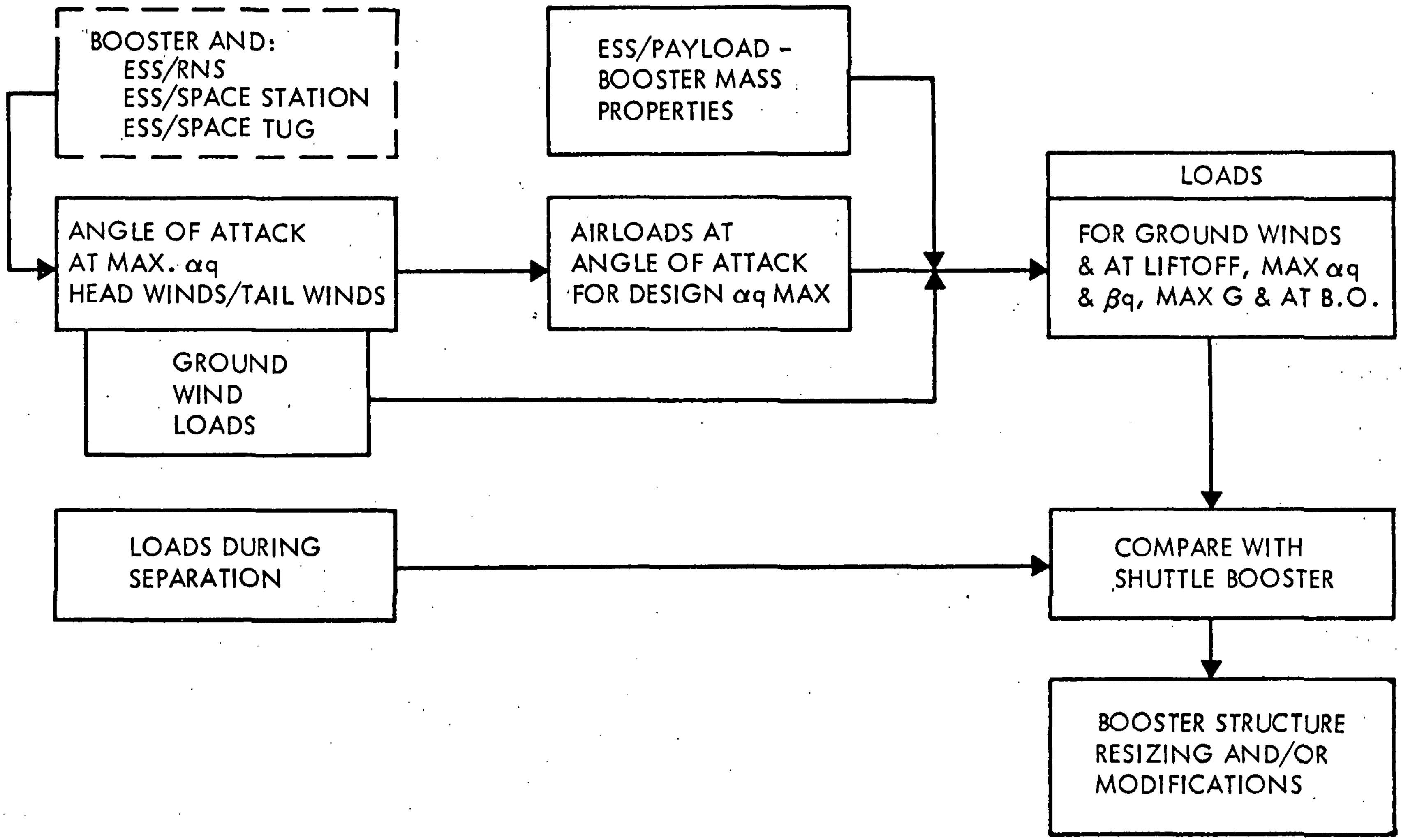

Figure 3-8. Approach to Structural Sizing

booster structural capability is adequate. The analyses conducted for each of the three mated configurations consisted of the following:

1. Booster loads were determined from a consideration of 1-hour ground winds, liftoff plus 1-hour ground winds, maximum αq, maximum βq, the point in the trajectory where the maximum thru thrust level is reached, and burnout. The loads were determined using Net Load II, a program for the determination of net loads (described below). Certain analyses were conducted separately to provide input to the loads program. These consisted of:

   a. Ground Loads. The magnitude and the point of application of these loads were determined as described below.

   b. A six-degree-of-freedom control simulation program was used to ensure that the αq and βq constraints defined above could be satisfied and to determine the angle of attack at maximum αq under headwind and tailwind conditions.

   c. Aerodynamic load distribution data were developed for the booster body plus point loads for the wing, canard, vertical tail, and ESS. The flight conditions consisted of maximum αq headwinds, maximum αq tailwinds, and maximum βq (pitch and yaw planes).

   d. Integrated system mass properties were developed for the ground and flight conditions to be investigated.

2. Separation system linkage loads and the resultant loads on the booster bulkheads during separation were determined using the six-degree-of-freedom multiple-body separation simulation digital program.

3. The body load intensities and the bulkhead loads determined in Steps 1 and 2 were compared with the shuttle booster design loads. Identified were all regions where the shuttle design loads were exceeded and the corresponding ground or flight conditions.

4. The required changes to the shuttle booster structure and the resultant weight increases were then identified. These changes basically added material to the booster bulkheads and the body skin and stringers to provide increased shear capability for local areas. Because of the nature of the structural changes, it was considered impractical to make field modifications that would provide the required "beef-up" for the ESS mission and then be

removed upon completion of the mission. It was therefore assumed that the required changes to the primary structure of the booster would be incorporated in the original design and development of the shuttle booster

3.6.3 GROUND WIND LOADS

Ground wind loads were determined for the mated configuration on the launch pad. Conditions investigated were the 2-week and 1-hour wind profile profiles defined by NASA[1]. The base of the booster is assumed to be 100 feet above mean grade. Loads are claculated by dividing the vehicle into a series of sections, computing the loads on each section for the wind velocity at that height, and integrating over the vehicle to obtain shear and bending moment distributions.

The running load at a point on the vehicle is given by

$$F = 0.00119 \, C \, C_D V^2 D$$

where F is the running load (lb/ft), C is the dynamic amplification factor (1.6 in this case), C_D is the drag coefficient (1.0 in this case), V is the wind velocity (ft/sec), and D is vehicle width (ft). The C and C_D coefficients are consistent with those used for all General Dynamics space shuttle ground wind analyses. These coefficients, considered conservative, should be verified by wind tunnel testing.

3.6.4 BOOST-PHASE STABILITY AND CONTROL

A six-degree-of-freedom digital simulation was used to analyze the time-varying stability and control aspects of the boost phase. The principal simulation activity was the determination of thrust vector control gimbal angle requirements and trajectory parameters for design wind profiles. The rigid-body stability characteristics and the blending of aerodynamic control surfaces with the TVC system were also investigated (see Volume II, Book 1).

3.6.5 BOOSTER/ESS AIR LOADS

Launch trajectory data, similar to that presented in Book 1, and component aerodynamic data versus Mach number were used to determine the design flight conditions that produced the maximum component loads. To

---

[1] Structural Design Criteria Applicable to a Space Shuttle, NASA SP-8057 (Jan. 1971).

ensure maximum loads on all components, flight conditions were explored to provide maximum positive and negative normal loads and maximum side loads. The total launch trajectory was investigated, and the design flight conditions occurred at maximum αq and βq between Mach 1.0 and 1.2.

For the design flight conditions, the total booster and component loads were determined from wind tunnel data. Interference factors were applied to these data, and total integrated booster/ESS aerodynamic data derived. Each flight configuration was balanced to the total integrated data.

3.6.6 COMPUTER PROGRAM NETLD2

This program determines net loads due to a specified loading system at any number of stations along the longitudinal reference axis of each of two interconnected vehicles. The loading system consists of the intertia loading system and the external load system. The inertia load system includes loads due to vehicle acceleration in the three coordinate directions as well as pitch, roll, and yaw accelerations. The external load system consists of air loads, point loads, engine thrust loads, and trim loads due to engine gimballing. Air loads for each vehicle, in the form of running load distributions along the longitudinal reference axis of the vehicle, are required input to the program. The air loads are given as a load distribution each for lift loads, lateral loads, and drag loads. Point loads for each vehicle are input in the form of load components and bending moment components at specified coordinate locations in the directions of the positive vehicle local axis system. Right-hand rule reference system is used. The total engine thrust for each vehicle is required input data. The user has the option of putting in either individual trim loads for each vehicle or rotational accelerations of the interconnected vehicle system.

If the trim loads are specified, the rotational accelerations of the interconnected vehicle system about the combined center of gravity are calculated as the quotient of the unbalanced moments and the combined mass moments of inertia. If the rotational accelerations are specified, the inertia moments are calculated as the product of the rotational accelerations and their respective mass moments of inertia. These moments are combined with the moments produced by the specified external load system moments. Trim loads necessary to put the system in moment balance are then determined.

Vehicle load factors are determined by summing loads in the directions of the coordinate axes and are calculated as the quotient of the resultant loads and the vehicle weight.

Interconnect loads are determined by separating the vehicles and calculating the loads required to put each vehicle in balance with the individual external and inertia loading systems of the vehicle. The interconnect loads are then included in the external loading system of the individual vehicle. Finally, net loads are determined by cutting the vehicle at the desired stations and summing the external and inertia loading systems at each station.

The net station loads are resolved into distributed load intensities at eight points around the vehicle circumference in a "load envelope" computer program. A subroutine of this program computes the thickness ($\bar{t}$) of structural material required to carry the maximum load intensity at any point, including the influences of propellant tank pressures, using stability tables derived from a separate plate-stringer optimization program (Nova). The weight of a component such as the LH_2 tank is computed by integrating the product of $\bar{t}$ and material density over the tank surface. For ESS, weight differences with the B-9U are determined by comparing the B-9U and B-9U/ESS LH_2 tank weights computed by the above method.

The weight of the thrust structure is determined by using net station and point loads in a finite-element computer model. A baseline weight is defined for the B-9U thrust structure, and, for B-9U/ESS configurations yielding higher loads, weight increments were estimated by increasing B-9U component weights by the ratio of the change in load. Attachment loads between the ESS and B-9U stages are computed with the load envelope program. They are resolved into bulkhead loading conditions at Stations 1866, 2096, 2666, and 2866 for comparison with orbiter/B-9U loads. At Stations 1866 and 2866, where ESS loads exceed baseline, weights are computed by making mathematical models of the bulkheads for use in structural sizing in General Dynamics, finite-element CLASS program.

3.6.7 LINKAGE LOADS DURING SEPARATION

General Dynamics' Digital Program P5255 was utilized to determine separation system characteristics, which included linkage loads developed during the separation maneuver. Inputs to the program consisted of mass properties data and initial condition inputs such as q, α, β, γ, altitude, velocity, and Mach number. In addition, inputs included geometric data peculiar to the ESS (plus payload)/booster linkage arrangement and ESS engine positions.

Separations were simulated which corresponded to cases where one and both engines were operative at normal staging points. Output of the simulations included link loads. Structural sizing of the mating/separation system linkage elements was based on the use of those link loads developed before separation and the complementary loads developed during the separation maneuver.

3.7. SEPARATION SYSTEM SIMULATION

3.7.1 INVESTIGATION GROUND RULES

The following ground rules were applicable:

1. Rigid-body separations were to be investigated for the following booster payloads:

   a. ESS with nuclear stage

   b. ESS with MDAC space station

   c. ESS with space tug

2. Simulations were to be made of separations occurring at normal staging points of specified trajectories, where aerodynamic effects are minimal.

3. The booster thrusted linkage separation system linkage concept - as used for the baseline booster/orbiter separation system - was to be used.

4. Staging simulations were to take into account the following conditions:

   a. Two ESS engines operative, and 10 to 12 booster engines operative

   b. One ESS engine operative, and 12 booster engines operative

3.7.2 INPUTS

General Dynamics' Digital Computer Program P5255 was used to solve the equations of motion for the booster and ESS/payload. Inputs included mass properties, shown in Tables 3-1, 3-2, and 3-3, and end boost trajectory variables shown elsewhere in this data book.

Comparison of the inputs indicated that separation simulation of the ESS/space tug configuration was not warranted since the ESS/nuclear stage and ESS/MDAC space station bounded the separation simulation kinetics

Table 3-1. Flight Sequence Mass Properties Summary (RNS)

MISSION EVENT	WEIGHT (LB)	CENTER OF GRAVITY (INCH) BOOSTER REF. AXES LOCATION			MOMENT OF INERTIA (SLUG-FT^2/10^6)			PRODUCT OF INERTIA (SLUG-FT^2/10^6)		
	W	X_{CG}	Y_{CG}	Z_{CG}	I_{XX}	I_{YY}	I_{ZZ}	I_{XY}	I_{XZ}	I_{YZ}
ESS (S-II + RNS) AT LIFTOFF *	669,420	2251.6	0	850.0	1.332	45.166	45.166	0	0	0
MODIFIED B-9U BOOSTER **										
AT LIFTOFF ***	3,298,223	2310.1	0	374.4	13.39	456.9	456.5	0	-15.8	0
AT MAX. Q	2,211,878	2543.8	0	361.9	12.27	332.0	331.8	0	-11.6	0
AT 2.5G	1,487,648	2796.3	0	343.3	11.35	225.2	225.3	0	-6.96	0
AT BURNOUT	815,916	3146.6	0	332.5	9.814	106.5	107.8	0	-2.20	0
COMBINED B-9U + ESS										
AT LIFTOFF ***	3,967,643	2300.3	0	454.7	41.89	529.6	502.0	0	-19.2	0
AT MAX. Q	2,881,298	2475.9	0	475.3	40.02	413.1	386.5	0	-27.4	0
AT 2.5G	2,157,068	2627.3	0	500.5	38.26	325.5	300.0	0	-34.5	0
AT BURNOUT	1,485,336	2743.2	0	565.7	32.40	236.5	216.5	0	-39.0	0

* Based on NAR Trajectory Program run for off-loaded booster (-900,000 lbs propellant), low q (Received 4/8/71).
** Modified B-9U Booster includes an estimate of 10,000 lbs for ESS platform and fairing.
*** Booster off-loaded by 900,000 lbs of propellant at liftoff.

Table 3-2. Flight Sequence Mass Properties Summary (MDAC)

MISSION EVENT	WEIGHT	CENTER OF GRAVITY (INCH) BOOSTER REF. AXES LOCATION			MOMENT OF INERTIA (SLUG-FT^2/10^6)			PRODUCT OF INERTIA (SLUG-FT^2/10^6)		
	W	X_{CG}	Y_{CG}	Z_{CG}	I_{XX}	I_{YY}	I_{ZZ}	I_{XY}	I_{XZ}	I_{YZ}
ESS (S-II + STA.) AT LIFTOFF *	991,687	2222.0 *	0	850.0	1.619	46.24	46.24	0	0	0
MODIFIED B-9U BOOSTER **										
AT LIFTOFF	4,198,223	2162.9	0	379.9	14.38	552.4	551.8	0	-18.5	0
AT MAX. Q	2,860,726	2393.4	0	370.5	12.96	409.6	409.2	0	-14.3	0
AT 2.06G	2,156,501	2559.2	0	360.9	12.20	324.4	324.2	0	-11.3	0
AT BURNOUT	815,916	3146.6	0	332.5	9.814	106.5	107.8	0	-2.20	0
COMBINED B-9U + ESS										
AT LIFTOFF	5,189,910	2174.2	0	469.7	54.26	637.5	598.7	0	-13.7	0
AT MAX. Q	3,852,413	2349.3	0	493.9	51.12	497.0	460.1	0	-27.4	0
AT 2.06G	3,148,188	2453.0	0	515.0	48.90	422.4	387.1	0	-35.5	0
AT BURNOUT	1,807,603	2639.3	0	616.4	37.31	261.2	236.6	0	-48.4	0

* Based on NAR Trajectory Program run for MDAC SS dated 4-12-71.

** Modification consists of the addition of 10,000 lbs for ESS platform and fairing.

* S-II STA 475 (SEE TRAJECTORY)

Table 3-3. Flight Sequence Mass Properties Summary (Space Tug)

MISSION EVENT	WEIGHT (LBS)	CENTER OF GRAVITY (INCH) BOOSTER REF. AXES LOCATION			MOMENT OF INERTIA ($SLUG-FT^2/10^6$)			PRODUCT OF INERTIA ($SLUG-FT^2/10^6$)		
	W	X_{CG}	Y_{CG}	Z_{CG}	I_{XX}	I_{YY}	I_{ZZ}	I_{XY}	I_{XZ}	I_{YZ}
ESS (S-II + SPACE TUG) AT LIFTOFF*	691,523	2254.0	0	850.0	0.753	30.45	30.45	0	0	0
MODIFIED B-9U BOOSTER **										
AT LIFTOFF	3,848,223	2217.6	0	378.1	13.92	514.3	514.3	0	-17.5	0
AT MAX. Q (407 PSF)	2,693,517	2428.4	0	368.7	12.79	390.6	390.3	0	-13.7	0
AT MAX. G (2.47)	1,651945	2725.5	0	348.9	11.57	252.4	252.4	0	-8.25	0
AT BURNOUT	815,916	3146.6	0	332.5	9.814	106.5	107.8	0	-2.20	0
COMBINED B-9U + ESS										
AT LIFTOFF	4,539,746	2223.2	0	450.0	42.85	573.6	544.9	0	-15.3	0
AT MAX. Q (407 PSF)	3,385,040	2392.7	0	467.0	41.06	452.2	424.3	0	-23.6	0
AT MAX. G (2.47)	2,343,468	2586.4	0	496.8	38.73	332.6	306.3	0	-33.1	0
AT BURNOUT	1,507,439	2737.1	0	569.9	32.2	223.0	202.6	0	-39.5	0

* Based on NAR Trajectory Program run for Space Tug dated 4-15-71.

**Booster off-loaded 350,000 lbs at liftoff. 10,000 lbs added for ESS platform and fairing.

* S-II STA 443 (SEE TRAJECTORY)

problems. Also, for those cases in which 10 or 11 booster engines are operative, a 50-percent thrust level may be maintained by increasing the thrust of the remaining booster engines. Consequently, investigation of these cases was deemed unwarranted.

3.7.3 RESULTS

The results of the computer simulations are shown in Figures 3-9 through 3-20. Tables 3-4, 3-5, and 3-6 facilitate comparison and interpretation of the graphs. A review of the results indicates that for the three integrated vehicle systems considered, satisfactory separations can be effected in those cases where one and two ESS engines are operative.

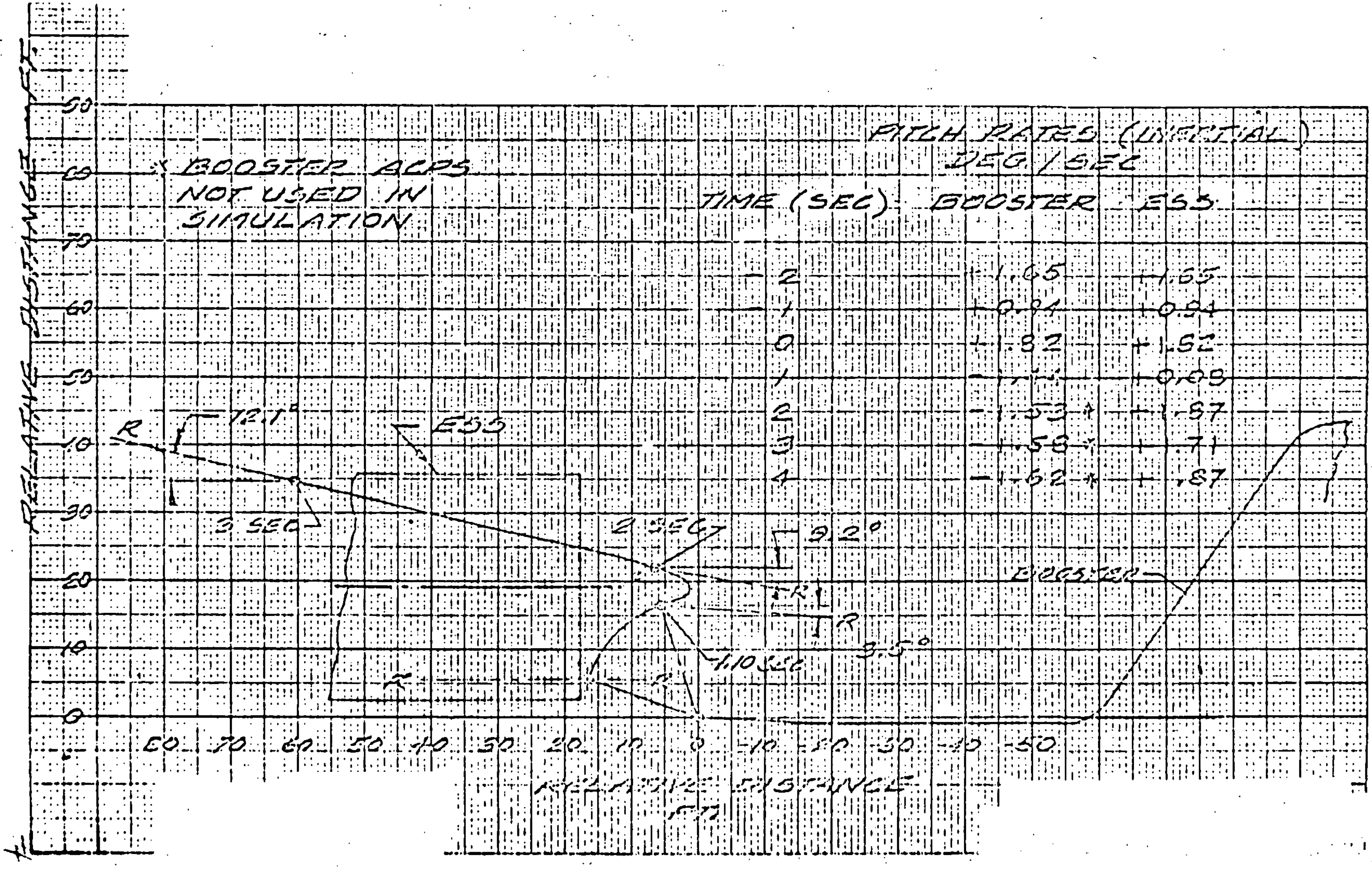

Figure 3-9. Separation Trajectory - Normal Staging of ESS With RNS Payload
(2 ESS Eng operative)

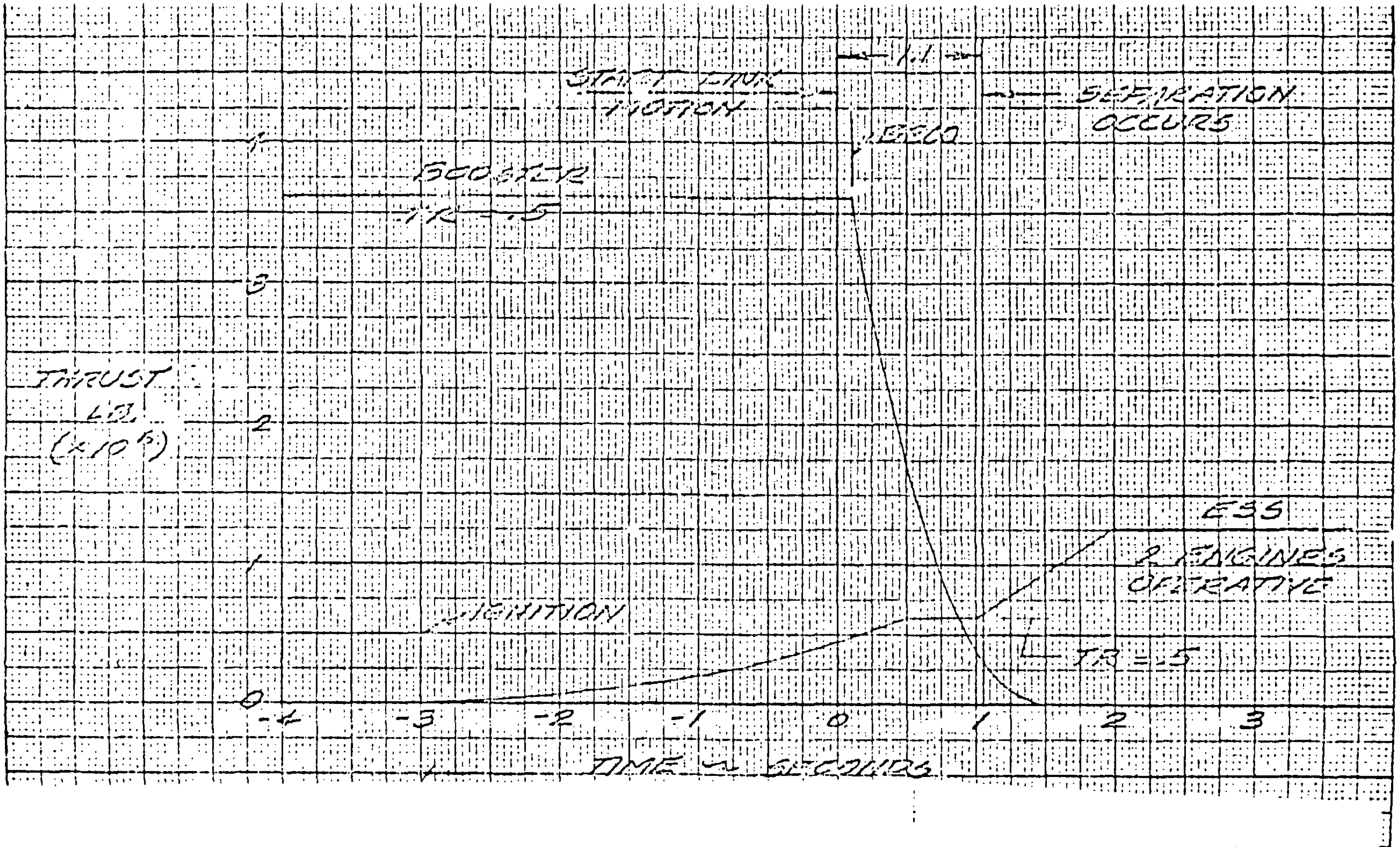

Figure 3-10. Thrust Scheduling - Normal Staging of ESS With RNS Payload

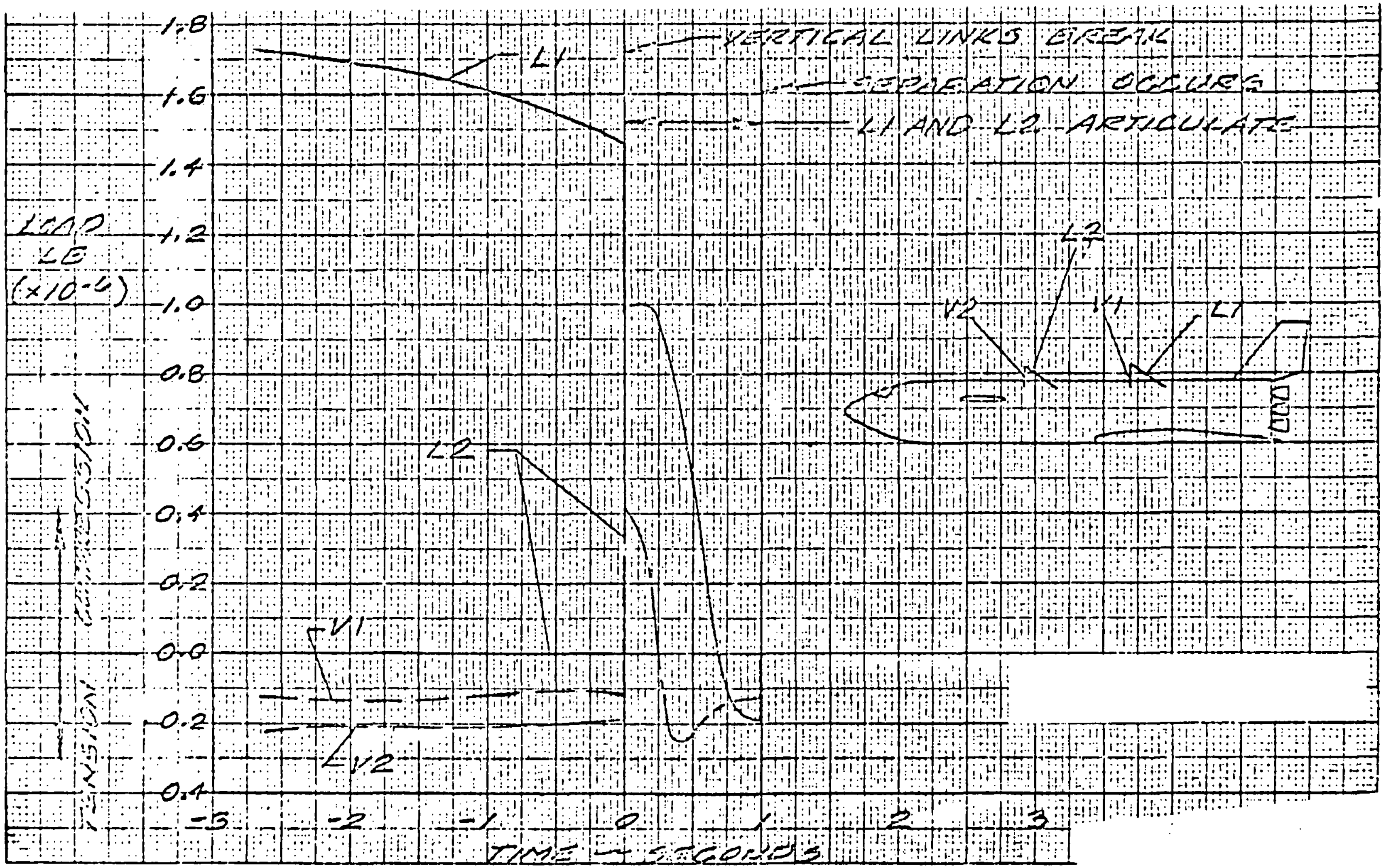

Figure 3-11. Separation System Link Loads - Normal Staging of ESS With RNS Payload

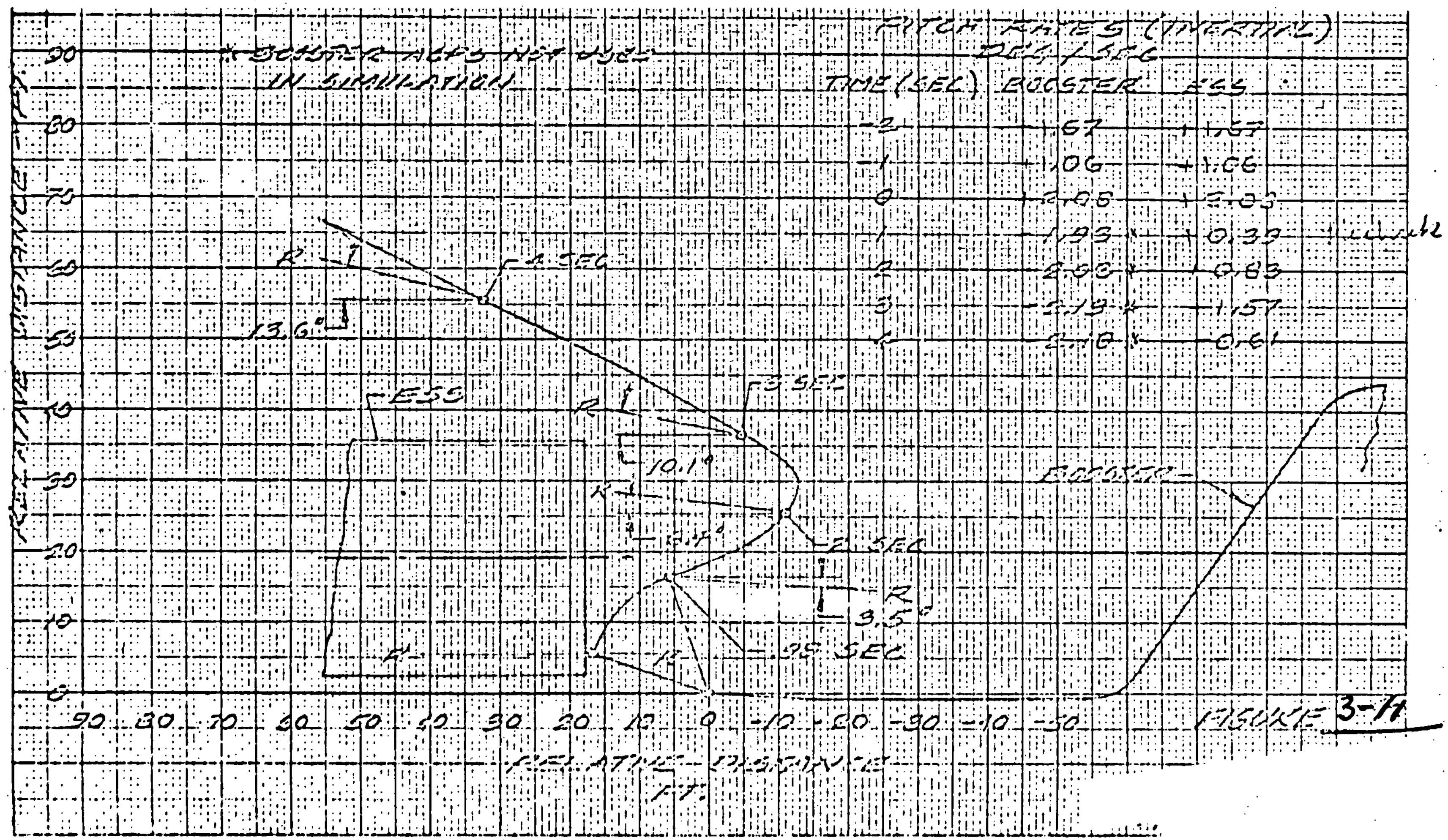

Figure 3-12. Separation Trajectory - Staging of ESS With RNS Payload
(one ESS ENG operative)

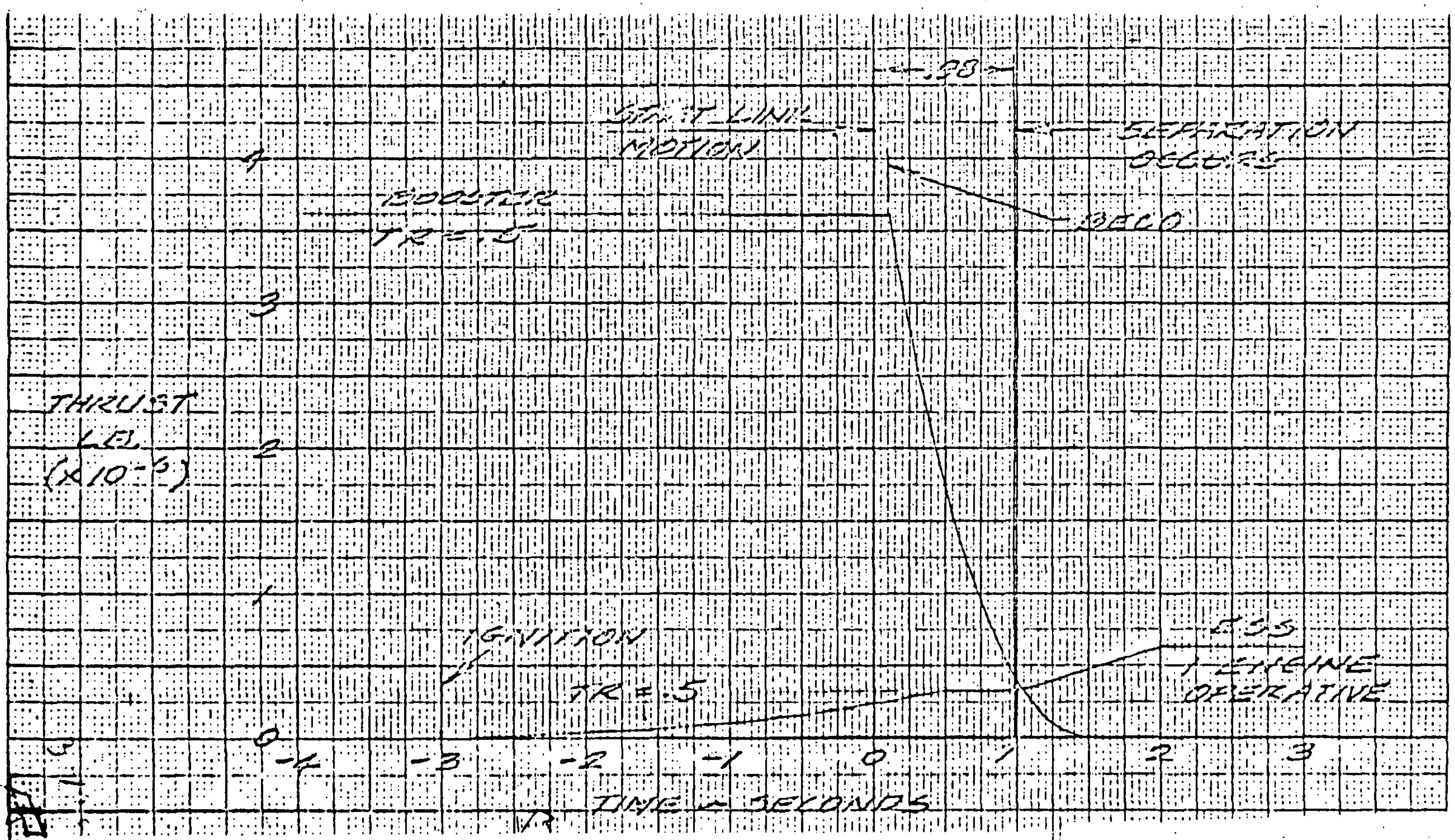

Figure 3-13. Thrust Scheduling - Staging of ESS With RNS Payload

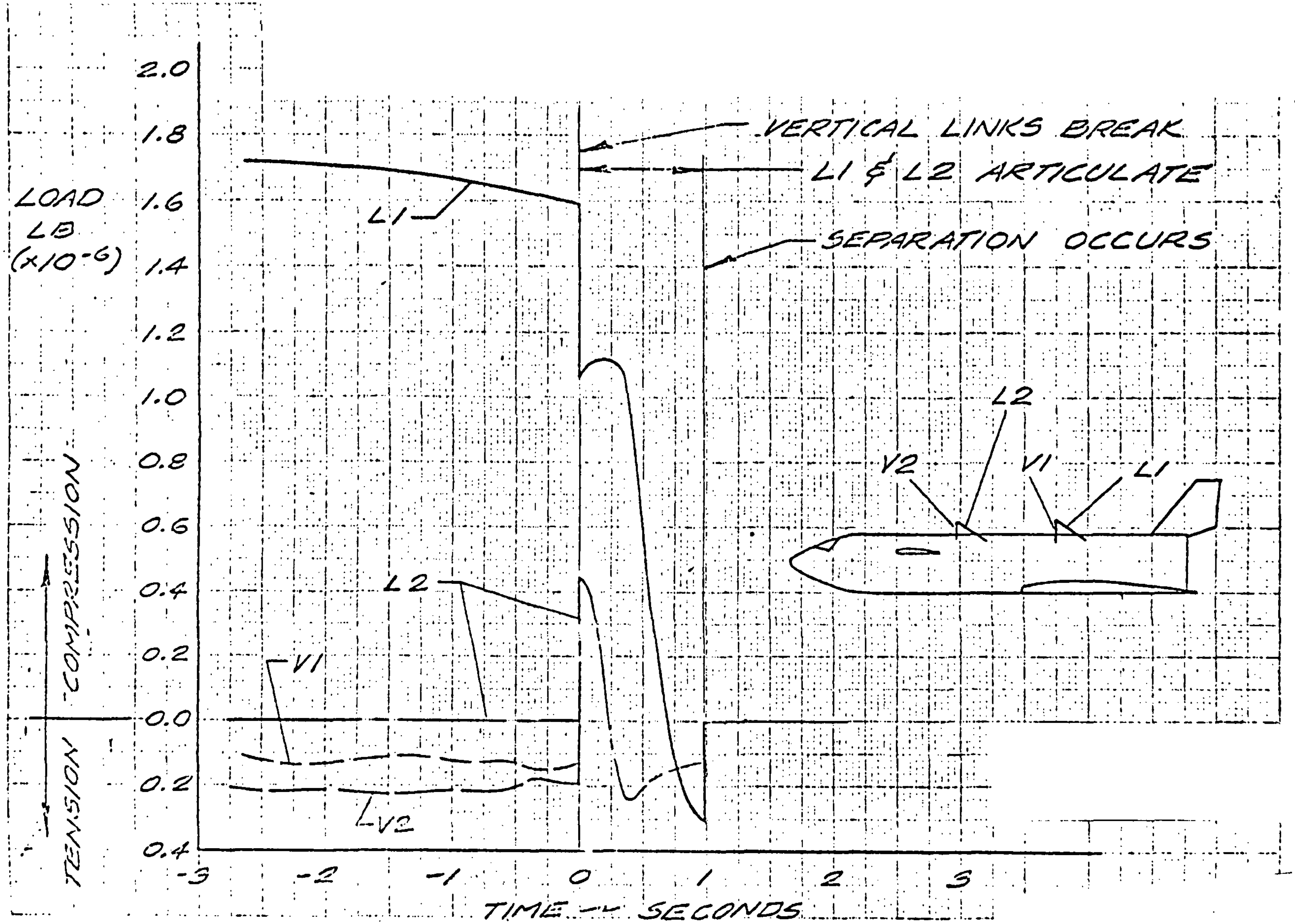

Figure 3-14. Separation System Link Loads - Staging of ESS With RNS Payload (one ESS ENG operative)

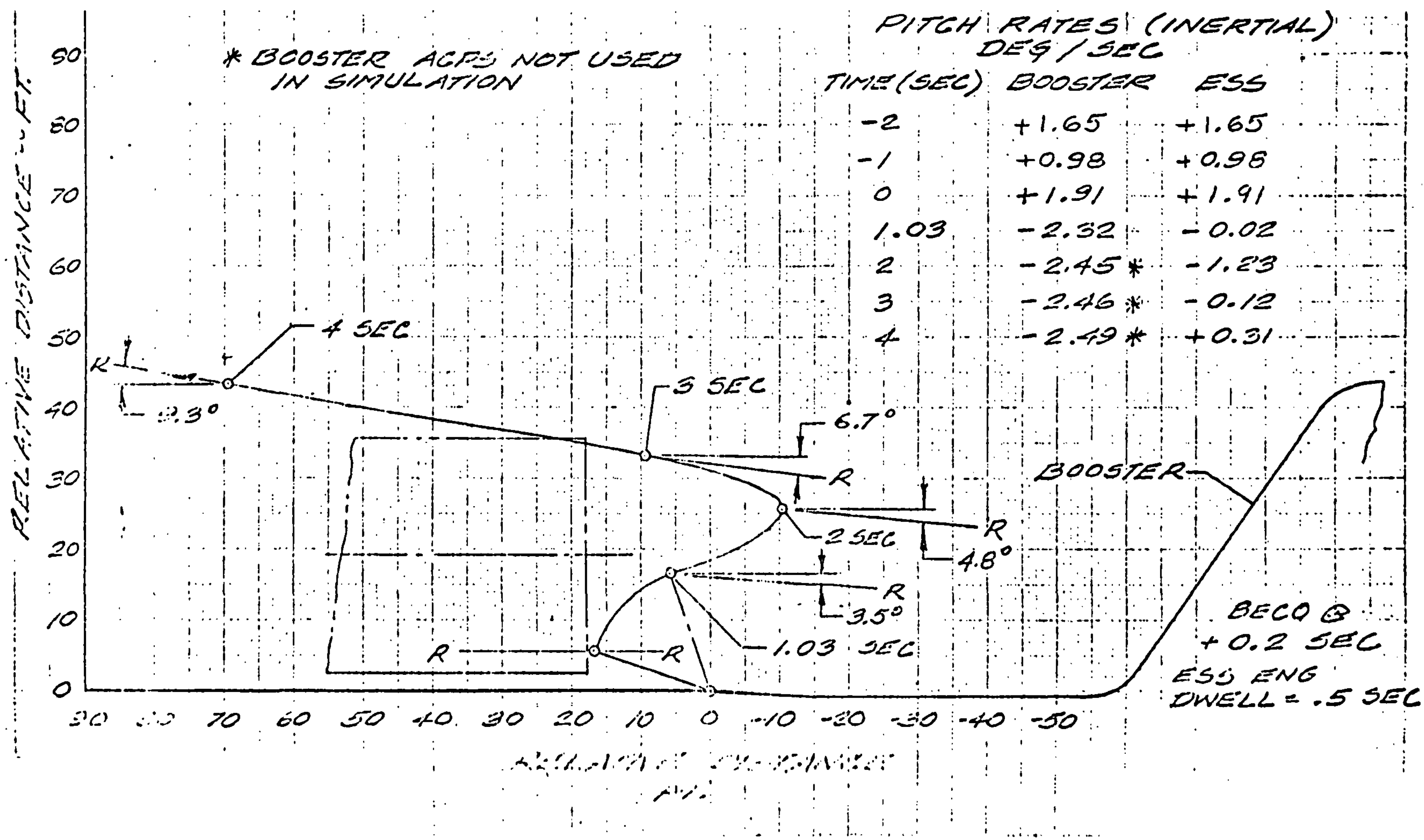

Figure 3-15. Separation Trajectory - Staging of ESS With MDAC Space Station Payload (two ESS ENG operative)

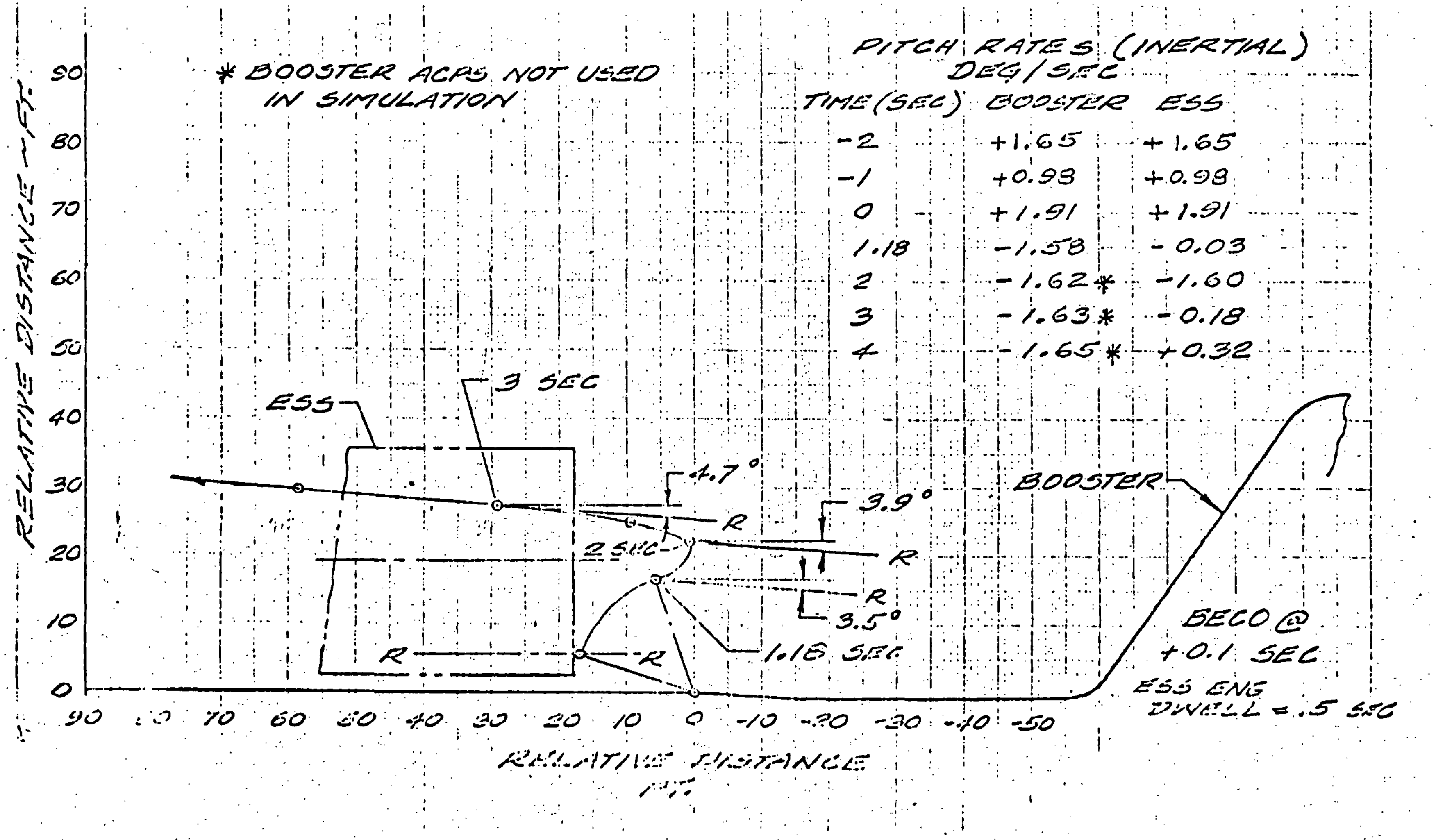

Figure 3-16. Separation Trajectory - Staging of ESS With MDAC Space Station Payload (two ESS ENG operative)

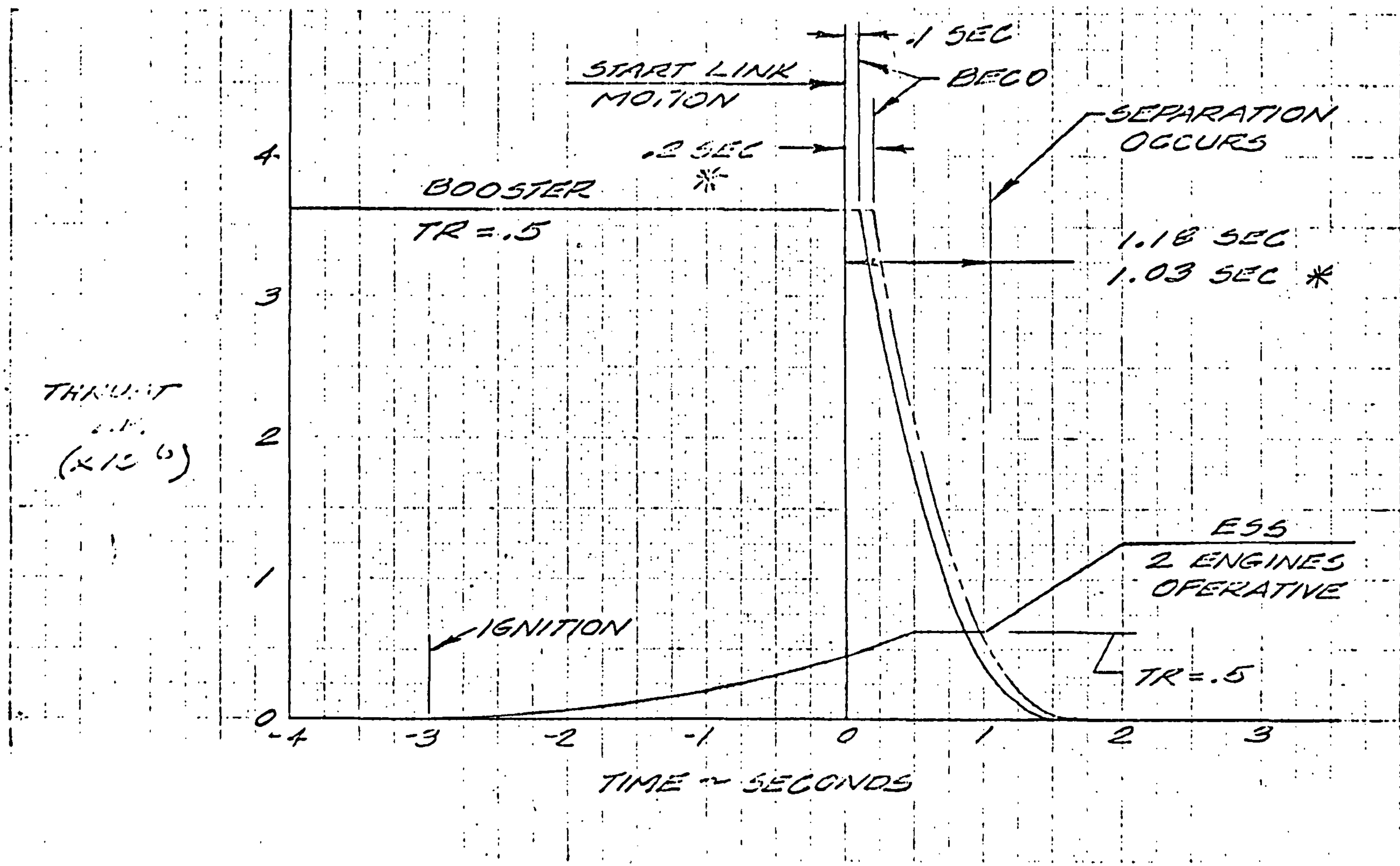

Figure 3-17. Thrust Scheduling - Normal Staging of ESS With MDAC Space Station Payload

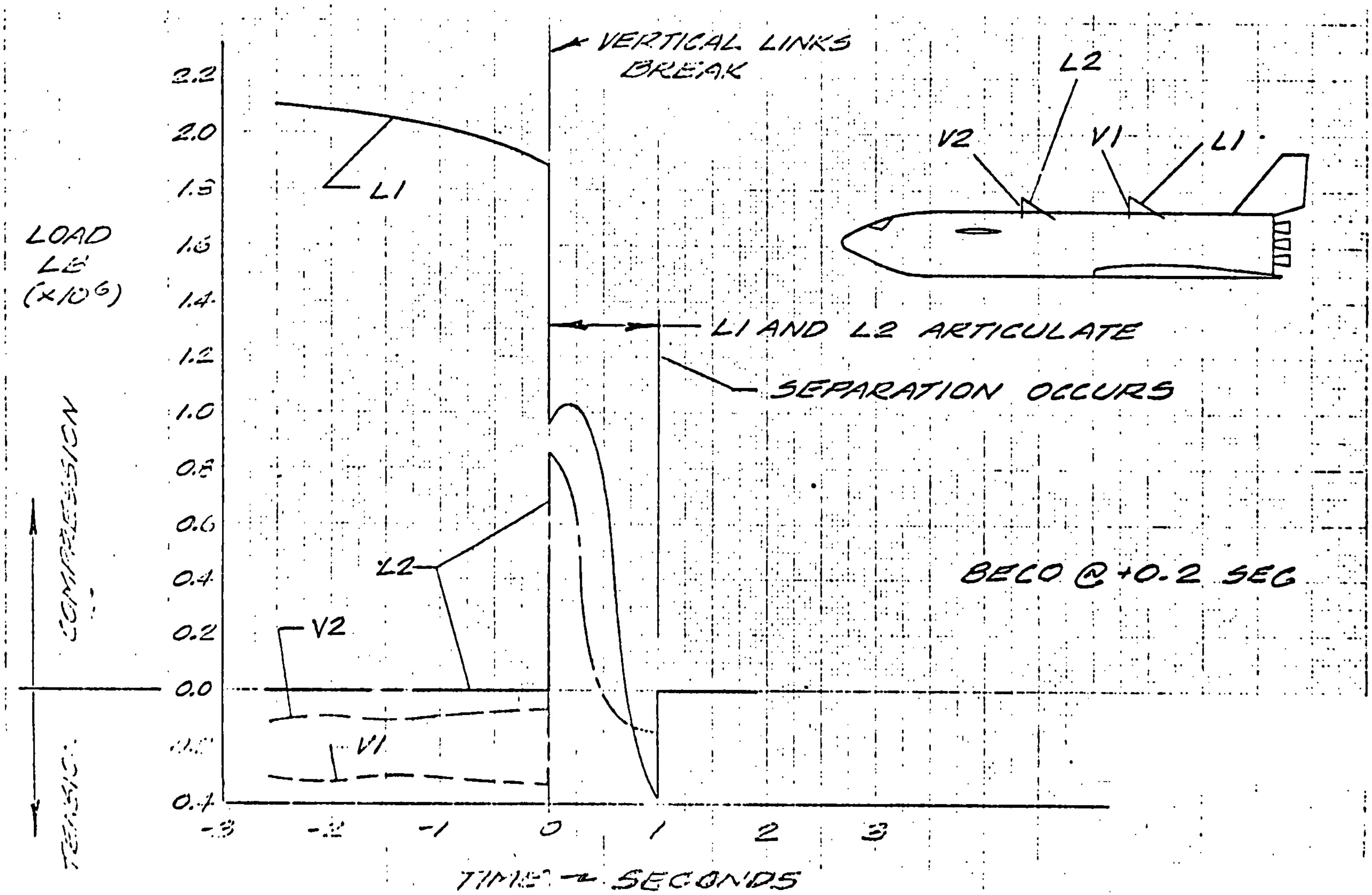

Figure 3-18. **Separation System Link Loads - Normal Staging of ESS With**
MDAC Space Station Payload

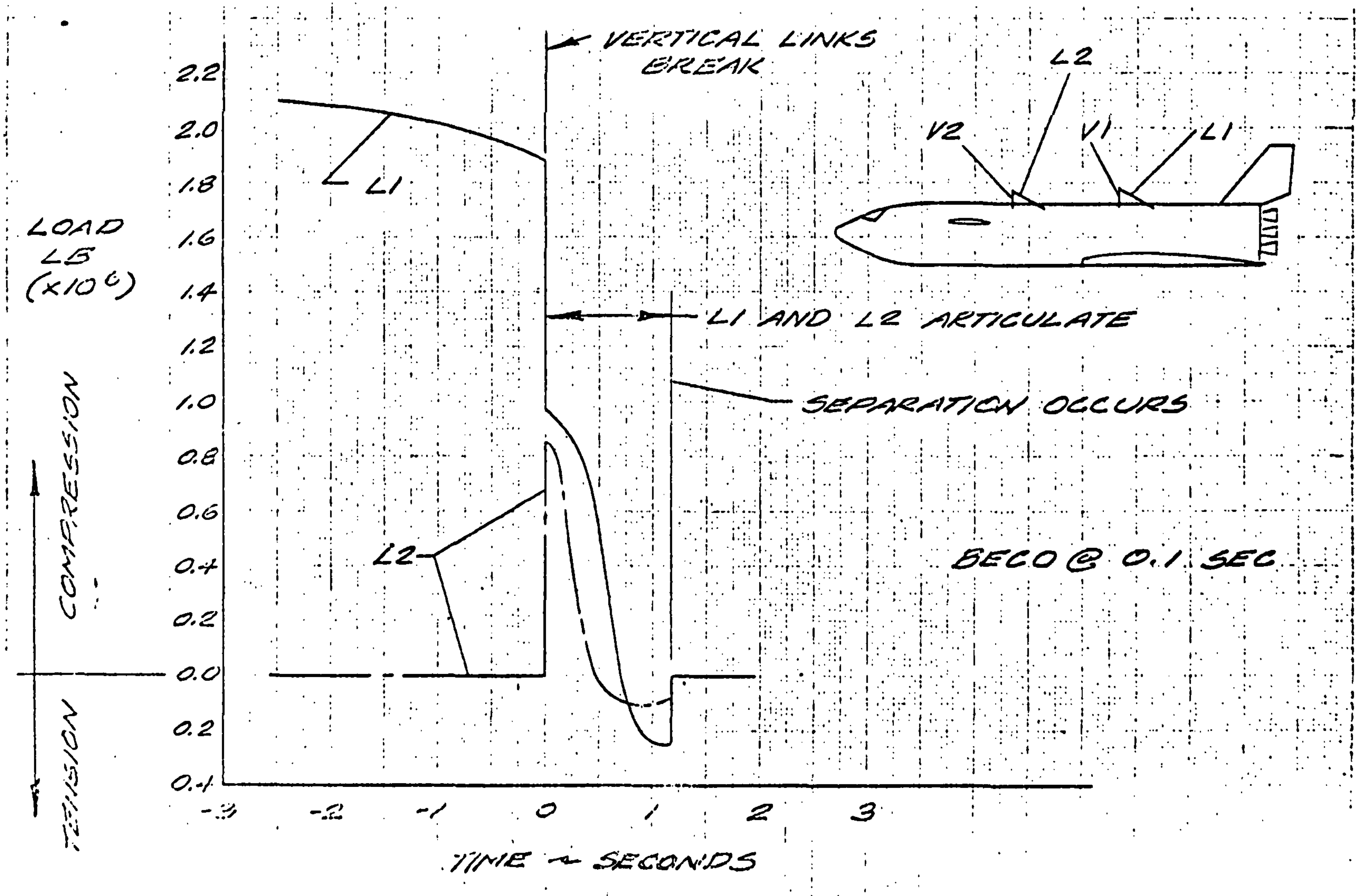

Figure 3-19. Separation System Link Loads - Normal Staging of ESS With MDAC Space Station Payload

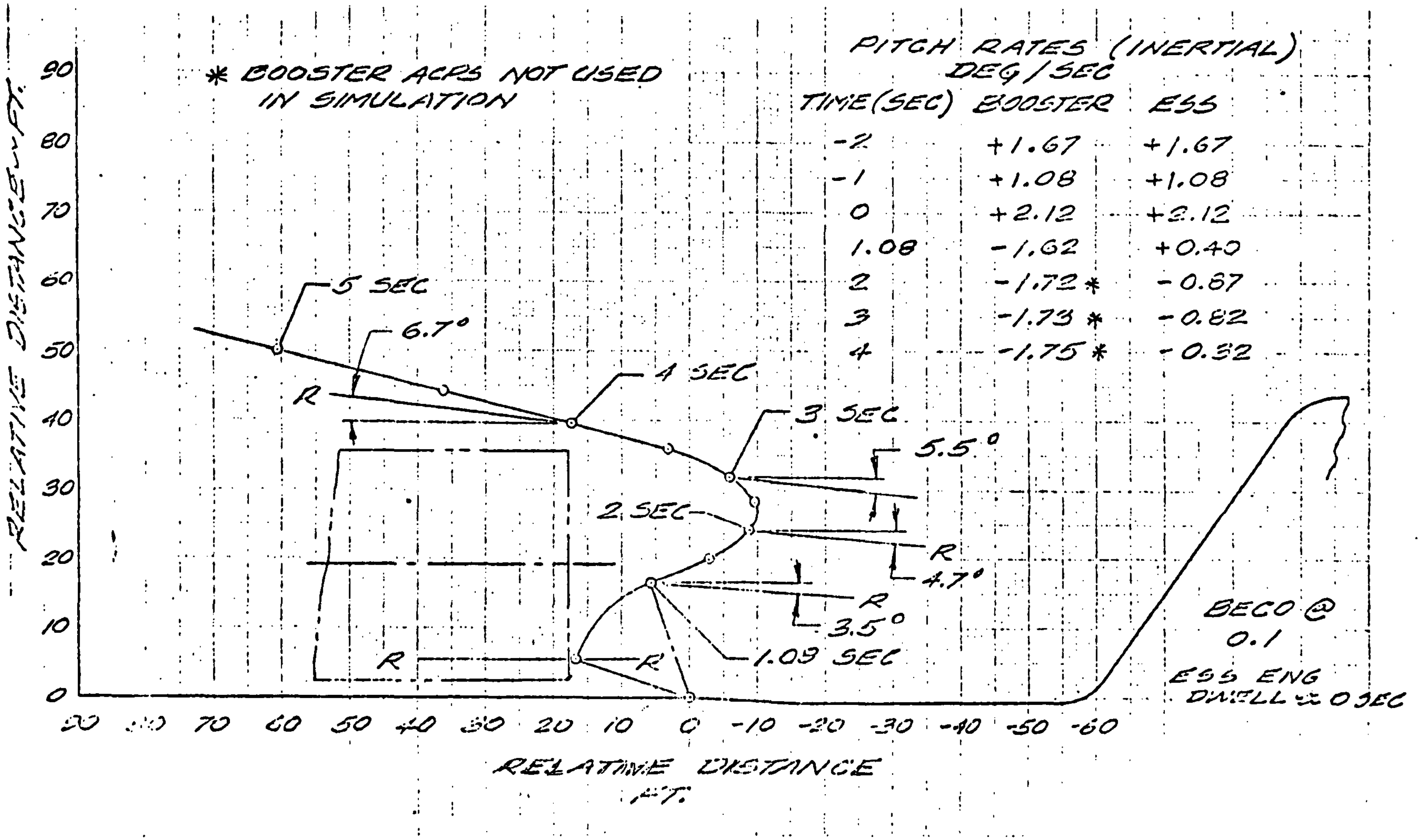

Figure 3-20. Separation Trajectory - Staging of ESS With MDAC Space Station Payload (one ESS ENG operative)

Table 3-4.

Fig.	Payload	Graph	Conditions	Comments/Conclusion
1	ESS [S-II + RNS (Nuclear Stage)]	Trajectory	2 ESS Eng. Oper., θ Release governs, BECO @ .1	Trajectory, clearances, vehicle pitch rates, attitudes satisfactory.
2		Thrust Scheduling	"	BECO @ t = 0.1 sec; BECO @ t $\leqq$ .05 sec. will not permit separation to occur.
3		Link Loads	"	Satisfactory except that graph indicates that release may be effected at t $\approx$ .75 sec.
4		Trajectory	1 ESS Eng. Oper., .5 sec. ESS Eng. Dwell, θ Release governs, BECO @ .1	Trajectory, clearances, vehicle pitch rates satisfactory. Elimination of ESS engine dwell (not used normally) would improve trajectory.
5		Thrust Scheduling	"	ESS engine dwell normally nonexistent under one engine operative conditions.
6		Link Loads	"	Satisfactory except that graph indicates that release may be effected at t $\leqq$ 1.0 sec.

Table 3-5.

Fig.	Payload	Graph	Conditions	Comments/Conclusion
7	ESS [S-II + MDAC Payload]	Trajectory	2 ESS Eng. Oper., θ Release governs, BECO @ .2 sec.	Trajectory, clearances, vehicle pitch rate and attitudes satisfactory. Longitudinal clearance less than for BECO = 0.1 sec. (Ref. Fig. 8)
9		Thrust Scheduling	2 ESS Eng. Oper., θ Release governs, BECO @ 0.1 sec. & BECO @ 0.2 sec.	Delayed BECO yields earlier release for constant θ release.
10		Link Loads	"	As could be expected, MDAC configurated ESS yields highest loads. Load histories indicate that release may be made prior to t = 1.0 sec.
8		Trajectory	2 ESS Eng. Oper., θ Release governs, BECO @ .1 sec.	Trajectory, clearances, vehicle pitch rates and attitudes satisfactory. Compare with Figure 7.
11		Link Loads	"	Note effect of BECO change by comparing with Figure 10.

C4

Table 3-6.

Fig.	Payload	Graph	Conditions	Comments/Conclusions
12		Trajectory	One ESS Eng. Oper., θ Release Governs, BECO @ .1 sec	Trajectory, attitude and inertial pitch rates satisfactory; improvement can be obtained by letting release time govern.
13		Thrust Scheduling	"	ESS eng. dwell = 0 which normal for case when one ESS engine is operative.

3.8 BOOSTER B-9U—COMPARISON OF LOADS IMPOSED BY ESS/NUCLEAR STAGE, ESS/MDAC SPACE STATION, AND ESS/SPACE TUG VERSUS NR 161C ORBITER

The loads imposed by the ESS/nuclear stage, ESS/MDAC space station, and ESS/space tug on the B-9U Booster structure were compared to those imposed by the NR 161C orbiter, which represents the present structural capability. Table 3-7 lists the loading conditions used to develop the current design load envelope. Table 3-8 and Table 3-9 give the peak tension and compression ultimate loads versus booster station for the current baseline. Figure 3-21 gives the interconnecting structural configuration used in the following loads analysis for the ESS/nuclear stage, ESS/MDAC space station, and ESS/space tug stage.

The delta weight increases, as determined by this analysis, are based on the assumption that ground support equipment will be available to render 1-day and 2-week ground wind conditions noncritical to the booster design.

3.8.1 ESS/NUCLEAR STAGE

Table 3-10 lists the loading conditions investigated for the ESS/nuclear stage. Tables 3-11 and 3-12 give the peak tension and compression ultimate loads versus booster station for this configuration.

Figures 3-22 through 3-26 are plots of the loads shown in Tables 3-8, 3-9, 3-11, and 3-12. The shaded portions indicate the areas where the ESS/nuclear stage-imposed loads exceed the current load-carrying capacity of the booster body structure. The tension side of the plots are not shaded because the booster has excess tension capability.

Figure 3-27 gives design limit attachment loads that are applied to the booster by the ESS/nuclear stage.

3.8.2 ESS/MDAC SPACE STATION

Table 3-13 lists the loading conditions investigated for the ESS/MDAC space station. Tables 3-14 and 3-15 give the peak tension and compression ultimate loads versus booster station for this configuration.

Figures 3-28 through 3-32 are plots of the loads shown in Tables 3-8, 3-9, 3-14, and 3-15. The shaded portions indicate the areas where the

ESS/MDAC space station-imposed loads exceed the current load-carrying capacity of the booster body structure. The tension side of the plots are not shaded because the booster has excess tension capability.

Figure 3-33 gives design limit attachment loads that are applied to the booster by the ESS/MDAC space station.

3.8.3 ESS/SPACE TUG

Table 3-15 lists the loading conditions investigated for the ESS/space tug. Tables 3-16 and 3-17 give the peak tension and compression ultimate loads versus booster station for this configuration.

Figures 3-34 through 3-38 are plots of the loads shown in Tables 3-8, 3-9, 3-17, and 3-18. The shaded portions indicate the areas where the ESS/space tug imposed loads exceed the current load-carrying capacity of the booster body structure. The tension side of the plots are not shaded because the booster has excess tension capability.

Figure 3-39 gives design limit attachment loads that are applied to the booster by the ESS/space tug.

3.8.4 CONCLUSIONS

The effects of the ESS/nuclear stage, ESS/MDAC space station, and ESS/space tug on the structural weight of the booster have been evaluated, and the results are presented in Figures 3-40, 3-41, and 3-42.

Table 3-7. Booster B-9U/Orbiter NR 161-C Ultimate Internal Loads (Baseline)

COND 1	BOOSTER B-9U / ORBITER NR 161-C	1 HR GROUND HEADWINDS TANKED UNPRESS
COND 2	BOOSTER B-9U / ORBITER NR 161-C	1 HR GROUND TAILWINDS TANKED UNPRESS
COND 3	BOOSTER B-9U / ORBITER NR 161-C	1 HR GROUND SIDEWINDS TANKED UNPRESS
COND 4	BOOSTER B-9U / ORBITER NR 161-C	LIFT OFF + 1 HR GROUND HEADWINDS
COND 5	BOOSTER B-9U / ORBITER NR 161-C	LIFT OFF + 1 HR GROUND TAILWINDS
COND 6	BOOSTER B-9U / ORBITER NR 161-C	LIFT OFF + 1 HR GROUND SIDEWINDS
COND 7	BOOSTER B-9U / ORBITER NR 161-C	MAX ALPHA-Q HEADWINDS AQ = 2800.
COND 8	BOOSTER B-9U / ORBITER NR 161-C	MAX ALPHA-Q TAILWINDS AQ = -2800.
COND 9	BOOSTER B-9U / ORBITER NR 161-C	MAX BETA-Q (2400)
COND 10	BOOSTER B-9U / ORBITER NR 161-C	3G MAX THRUST
COND 11	BOOSTER B-9U	BOOSTER BURNOUT
COND 12	BOOSTER B-9U	BOOSTER RECOVERY
COND 13	BOOSTER B-9U	BOOSTER SUBSONIC GUST
COND 14	BOOSTER B-9U	BOOSTER 2 POINT LANDING
COND 15	BOOSTER B-9U	BOOSTER 3 POINT LANDING
COND 16	BOOSTER B-9U	BOOSTER 2 G TAXI

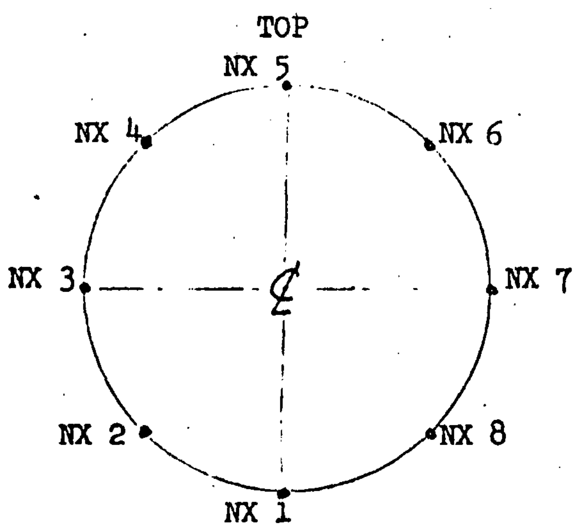

VIEW LOOKING AFT

Table 3-8. Booster B-9U/Orbiter NR 161-C Ultimate Internal Loads (Baseline)

PEAK ULTIMATE AXIAL TENSION LOAD INTENSITIES

STATION (IN)	NX1 (LB/IN)	NX2 (LB/IN)	NX3 (LB/IN)	NX4 (LB/IN)	NX5 (LB/IN)	NX6 (LB/IN)	NX7 (LB/IN)	NX8 (LB/IN)
1000	0(16)	0(16)	0(16)	0(16)	0(16)	0(16)	0(16)	0(16)
1036	5(12)	4(12)	0(15)	0(16)	1(11)	0(16)	0(15)	4(12)
1072	45(12)	32(12)	1(15)	3(11)	8(11)	3(11)	1(15)	32(12)
1131	73(12)	51(12)	3(15)	7(16)	13(8)	7(16)	3(15)	51(12)
1278	141(12)	98(12)	7(15)	28(16)	58(8)	28(16)	7(15)	98(12)
1337	173(12)	121(12)	9(15)	42(8)	89(8)	42(8)	9(15)	121(12)
1341	177(12)	124(12)	8(14)	121(15)	192(15)	121(15)	8(14)	124(12)
1477	288(12)	200(12)	14(14)	99(8)	191(8)	99(8)	14(14)	200(12)
1481	1411(12)	1322(12)	1229(10)	1280(8)	1374(8)	1280(8)	1229(10)	1322(12)
1600	1569(12)	1430(12)	1194(10)	1377(8)	1531(8)	1377(8)	1194(10)	1430(12)
1750	1820(12)	1601(12)	1149(10)	1539(8)	1791(8)	1539(8)	1153(9)	1601(12)
1864	2042(12)	1753(12)	1102(10)	1510(8)	1780(8)	1510(8)	1102(10)	1753(12)
1868	931(12)	640(12)	35(14)	86(13)	140(13)	85(13)	35(14)	640(12)
2006	1932(11)	853(11)	47(14)	155(13)	242(13)	153(13)	47(14)	853(11)
2022	2207(11)	996(11)	48(14)	166(13)	258(13)	164(13)	48(14)	996(11)
2026	2274(11)	1031(11)	45(14)	160(13)	251(13)	158(13)	45(14)	1031(11)
2042	2544(11)	1169(11)	47(14)	152(13)	242(13)	150(13)	47(14)	1169(11)
2094	3431(11)	1631(11)	52(14)	141(14)	219(13)	141(14)	52(14)	1631(11)
2098	3476(11)	1650(11)	52(14)	142(14)	217(13)	142(14)	52(14)	1650(11)
2180	3878(11)	1678(11)	60(14)	168(14)	213(14)	168(14)	60(14)	1678(11)
2184	5798(11)	3588(11)	1454(13)	1653(13)	1734(13)	1650(13)	1450(13)	3588(11)
2300	5803(11)	3577(11)	1444(13)	1656(13)	1743(13)	1653(13)	1439(13)	3577(11)
2400	5813(11)	3574(11)	1437(13)	1675(13)	1772(13)	1671(13)	1431(13)	3574(11)
2500	5820(11)	3568(11)	1433(13)	1709(13)	1821(13)	1704(13)	1426(13)	3568(11)
2600	5822(11)	3559(11)	1432(13)	1756(13)	1888(13)	1751(13)	1424(13)	3559(11)
2664	5822(11)	3552(11)	1431(13)	1793(13)	1940(13)	1787(13)	1422(13)	3552(11)

Table 3-8. Booster B-9U/Orbiter NR 161-C Ultimate Internal Loads (Baseline) (Cont)

PEAK ULTIMATE AXIAL TENSION LOAD INTENSITIES

STATION (IN)	NX1 (LB/IN)	NX2 (LB/IN)	NX3 (LB/IN)	NX4 (LB/IN)	NX5 (LB/IN)	NX6 (LB/IN)	NX7 (LB/IN)	NX8 (LB/IN)
2668	5813(11)	3545(11)	1431(13)	1795(13)	1944(13)	1789(13)	1422(13)	3545(11)
2800	5193(11)	3092(11)	1429(13)	1886(13)	2072(13)	1879(13)	1419(13)	3092(11)
2864	4889(11)	2871(11)	1429(13)	1937(13)	2144(13)	1930(13)	1418(13)	2871(11)
2868	4870(11)	2856(11)	1429(13)	1940(13)	2149(13)	1933(13)	1418(13)	2856(11)
2950	4450(11)	2977(12)	1428(13)	2015(13)	2254(13)	2007(13)	1417(13)	2977(12)
3050	3796(12)	3103(12)	1428(12)	2172(13)	2477(13)	2164(13)	1428(12)	3102(12)
3161	3683(12)	3033(12)	1464(12)	2487(13)	2921(13)	2477(13)	1464(12)	3033(12)
3165	3615(12)	2980(12)	1448(12)	2497(13)	2938(13)	2487(13)	1448(12)	2980(12)
3293	2979(12)	2538(12)	1473(12)	2631(16)	3721(16)	2631(16)	1473(12)	2538(12)
3295	2968(12)	2530(12)	1473(12)	2643(16)	3737(16)	2643(16)	1473(12)	2530(12)
3373	2475(12)	2185(12)	1486(12)	2737(13)	3272(13)	2726(13)	1486(12)	2185(12)
3377	2394(12)	2123(12)	1469(12)	2742(13)	3281(13)	2730(13)	1469(12)	2123(12)
3538	1465(12)	1471(12)	1486(12)	2654(13)	3156(13)	2642(13)	1486(12)	1471(12)
3542	1391(12)	1414(12)	1469(12)	2651(13)	3155(13)	2639(13)	1469(12)	1414(12)
3679	943(12)	1105(12)	1559(13)	2228(13)	2506(13)	2229(13)	1561(13)	1105(12)
3683	-609(12)	-442(12)	25(13)	770(16)	1088(16)	770(16)	26(13)	-442(12)
3820	-447(16)	-316(16)	16(13)	516(12)	743(12)	516(12)	16(13)	-316(16)
3921	-119(16)	-84(16)	15(13)	132(12)	196(12)	132(12)	15(13)	-84(16)
3925	538(11)	478(11)	333(10)	290(10)	272(10)	290(10)	333(10)	478(11)
4065	0(7)	1(6)	2(6)	1(6)	0(7)	0(7)	0(7)	0(7)
4069	0(16)	1(6)	2(6)	1(6)	0(6)	0(16)	0(16)	0(16)
4300	0(16)	0(16)	0(16)	0(16)	0(16)	0(16)	0(16)	0(16)

Table 3-9. Booster B-9U/Orbiter NR 161-C Ultimate Internal Loads (Baseline)

PEAK ULTIMATE AXIAL COMPRESSION LOAD INTENSITES

STATION (IN)	NX1 (LB/IN)	NX2 (LB/IN)	NX3 (LB/IN)	NX4 (LB/IN)	NX5 (LB/IN)	NX6 (LB/IN)	NX7 (LB/IN)	NX8 (LB/IN)
1000	0(16)	0(16)	0(16)	0(16)	0(16)	0(16)	0(16)	0(16)
1036	-5(11)	-4(11)	-4(9)	-4(12)	-5(12)	-4(12)	-3(9)	-4(11)
1072	-23(11)	-21(9)	-25(9)	-34(12)	-47(12)	-34(12)	-8(9)	-18(11)
1131	-57(11)	-50(9)	-59(9)	-55(9)	-75(12)	-53(12)	-24(10)	-48(11)
1278	-171(8)	-138(8)	-122(9)	-105(12)	-147(12)	-105(12)	-65(10)	-138(8)
1337	-231(8)	-184(8)	-142(9)	-132(12)	-185(12)	-132(12)	-77(10)	-184(8)
1341	-295(15)	-224(15)	-144(9)	-136(12)	-189(12)	-136(12)	-79(10)	-224(15)
1477	-435(8)	-343(8)	-205(9)	-225(12)	-313(12)	-225(12)	-131(7)	-343(8)
1481	-135(15)	-107(15)	-39(15)	-58(16)	-82(16)	-58(16)	-62(3)	-107(15)
1600	-232(6)	-167(6)	-50(2)	-111(16)	-158(16)	-111(16)	-90(3)	-176(6)
1750	-446(4)	-337(6)	-65(6)	-154(16)	-218(16)	-154(16)	-135(3)	-329(4)
1864	-665(4)	-503(6)	-117(6)	-166(16)	-234(16)	-166(16)	-178(3)	-490(4)
1868	-5396(4)	-5238(6)	-4868(6)	-4514(5)	-4388(5)	-4514(5)	-4819(4)	-5227(4)
2006	-4429(4)	-4742(4)	-5564(6)	-6397(5)	-7050(10)	-6397(5)	-5498(4)	-4742(4)
2022	-4315(4)	-4685(4)	-5648(6)	-6621(5)	-7670(10)	-6621(5)	-5579(4)	-4685(4)
2026	-4286(4)	-4671(4)	-5669(6)	-6678(5)	-7825(10)	-6678(5)	-5599(4)	-4671(4)
2042	-4171(4)	-4613(4)	-5753(6)	-7144(10)	-8447(10)	-7144(10)	-5681(4)	-4613(4)
2094	-3791(4)	-4421(4)	-6023(6)	-8733(10)	-10458(10)	-8733(10)	-5942(4)	-4421(4)
2098	-3773(4)	-4414(4)	-6043(6)	-8837(10)	-10587(10)	-8837(10)	-5962(4)	-4414(4)
2180	-3651(7)	-4437(4)	-6458(6)	-10594(10)	-12710(10)	-10594(10)	-6364(4)	-4437(4)
2184	-3166(4)	-3968(4)	-5999(6)	-8728(10)	-10852(10)	-8728(10)	-5905(4)	-3968(4)
2300	-3238(4)	-4026(4)	-6036(6)	-8773(10)	-10895(10)	-8773(10)	-5928(4)	-4026(4)
2400	-3343(7)	-4072(4)	-6062(6)	-8803(10)	-10923(10)	-8803(10)	-5944(4)	-4072(4)
2500	-4011(7)	-4118(4)	-6086(6)	-8830(10)	-10945(10)	-8830(10)	-5961(4)	-4118(4)
2600	-4675(7)	-4452(7)	-6107(6)	-8853(10)	-10963(10)	-8853(10)	-5978(4)	-4452(7)
2664	-5091(7)	-4751(7)	-6119(6)	-8866(10)	-10972(10)	-8866(10)	-5989(4)	-4751(7)

Table 3-9. Booster B-9U/Orbiter NR 161-C Ultimate Internal Loads (Baseline) (Cont)

PEAK ULTIMATE AXIAL COMPRESSION LOAD INTENSITES

STATION (IN)	NX1 (LB/IN)	NX2 (LB/IN)	NX3 (LB/IN)	NX4 (LB/IN)	NX5 (LB/IN)	NX6 (LB/IN)	NX7 (LB/IN)	NX8 (LB/IN)
2668	-5111(7)	-4766(7)	-6120(6)	-8861(10)	-10964(10)	-8861(10)	-5990(4)	-4766(7)
2800	-5563(7)	-5096(7)	-6138(6)	-8485(10)	-10412(10)	-8485(10)	-6012(4)	-5096(7)
2864	-5773(7)	-5250(7)	-6146(6)	-8301(10)	-10141(10)	-8301(10)	-6023(4)	-5250(7)
2868	-5787(7)	-5260(7)	-6146(6)	-8289(10)	-10125(10)	-8289(10)	-6023(4)	-5260(7)
2950	-6060(7)	-5463(7)	-6162(6)	-8065(10)	-9788(10)	-8065(10)	-6045(4)	-5463(7)
3050	-6519(7)	-5828(7)	-6276(6)	-7956(10)	-9525(10)	-7956(10)	-6167(4)	-5828(7)
3161	-7061(7)	-6256(7)	-6401(6)	-7817(10)	-9206(10)	-7817(10)	-6301(4)	-6256(7)
3165	-7174(7)	-6346(7)	-6405(6)	-7812(10)	-9194(10)	-7812(10)	-6306(4)	-6346(7)
3293	-7480(7)	-6597(7)	-6491(6)	-7566(5)	-8701(10)	-7566(5)	-6404(4)	-6597(7)
3295	-7485(7)	-6601(7)	-6492(6)	-7564(5)	-8693(10)	-7564(5)	-6406(4)	-6601(7)
3373	-7671(7)	-6751(7)	-6536(6)	-7484(5)	-8368(10)	-7484(5)	-6458(4)	-6751(7)
3377	-7770(7)	-6831(7)	-6536(6)	-7479(5)	-8349(10)	-7479(5)	-6459(4)	-6831(7)
3538	-7646(7)	-6771(7)	-6593(6)	-7277(5)	-7584(5)	-7277(5)	-6536(4)	-6771(7)
3542	-7732(7)	-6841(7)	-6594(6)	-7271(5)	-7576(5)	-7271(5)	-6538(4)	-6841(7)
3679	-7196(7)	-6499(7)	-6681(6)	-7125(5)	-7325(5)	-7125(5)	-6743(3)	-6499(7)
3683	-9708(7)	-9017(7)	-8198(6)	-9195(10)	-9682(10)	-9195(10)	-8162(4)	-9017(7)
3820	-8869(7)	-8464(7)	-8263(6)	-8763(10)	-8991(10)	-8763(10)	-8251(4)	-8464(7)
3921	-8474(10)	-8497(10)	-8551(10)	-8605(10)	-8627(10)	-8605(10)	-8551(10)	-8497(10)
3925	-243(12)	-184(12)	-113(9)	-124(9)	-116(9)	-94(9)	-71(9)	-184(12)
4065	-0(15)	-0(15)	-0(15)	-0(15)	-0(15)	-1(6)	-2(6)	-1(6)
4069	0(16)	0(16)	0(16)	0(16)	0(16)	-1(6)	-2(6)	-1(6)
4300	0(16)	0(16)	0(16)	0(16)	0(16)	0(16)	0(16)	0(16)

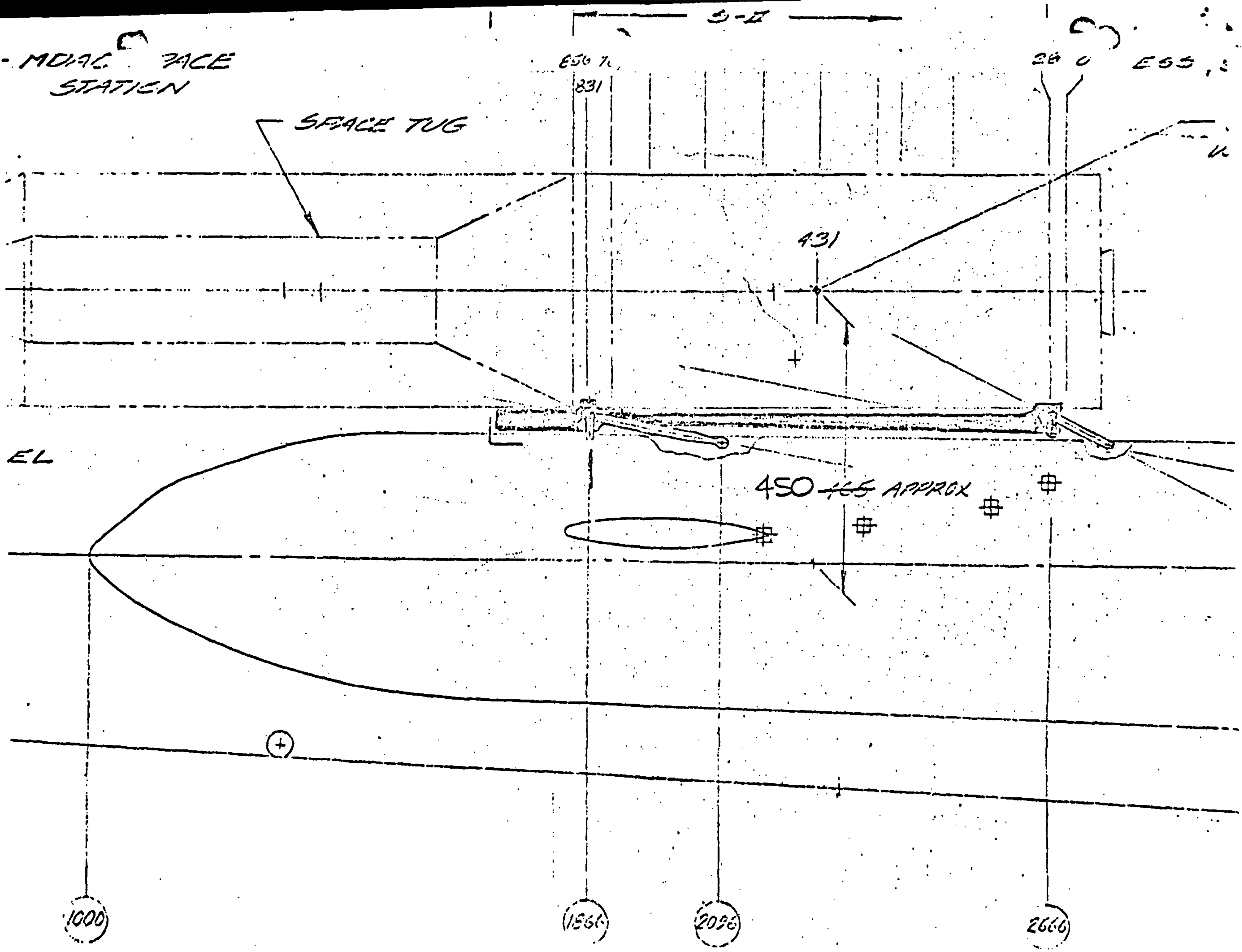

Figure 3-21. Interconnecting Configuration – Ref-Sketch-ESS/B-9U Booster Interface Concept

Table 3-10. Booster B-9U/Nuclear Stage Ultimate Internal Loads

COND 1	BOOSTER B-9U /ESS-NUCLEAR STAGE 1 HR GROUND HEADWINDS TANKED UNPRESS
COND 2	BOOSTER B-9U /ESS-NUCLEAR STAGE 1 HR GROUND TAILWINDS TANKED UNPRESS
COND 3	BOOSTER B-9U /ESS-NUCLEAR STAGE 1 HR GROUND SIDEWINDS TANKED UNPRESS
COND 4	BOOSTER B-9U / ESS-NUCLEAR STAGE LIFT OFF + 1 HR GROUND HEADWINDS
COND 5	BOOSTER B-9U / ESS-NUCLEAR STAGE LIFT OFF + 1 HR GROUND TAILWINDS
COND 6	BOOSTER B-9U / ESS-NUCLEAR STAGE LIFT OFF + 1 HR GROUND SIDEWINDS
COND 7	BOOSTER B-9U / ESS-NUCLEAR STAGE MAX ALPHA-Q HEADWINDS
COND 8	BOOSTER B-9U / ESS-NUCLEAR STAGE MAX ALPHA-Q TAILWINDS
COND 9	BOOSTER B-9U / ESS-NUCLEAR STAGE MAX BETA≠0
COND 10	BOOSTER B-9U /ESS NUCLEAR STAGE 2.5 G MAX THRUST
COND 11	BOOSTER B-9U /ESS NUCLEAR STAGE 2.5 G BOOSTER BURNOUT
COND 12	BOOSTER B-9U BOOSTER RECOVERY
COND 13	BOOSTER B-9U BOOSTER SUBSONIC GUST
COND 14	BOOSTER B-9U BOOSTER 2 POINT LANDING
COND 15	BOOSTER B-9U BOOSTER 3 POINT LANDING
COND 16	BOOSTER B-9U BOOSTER 2 G TAXI

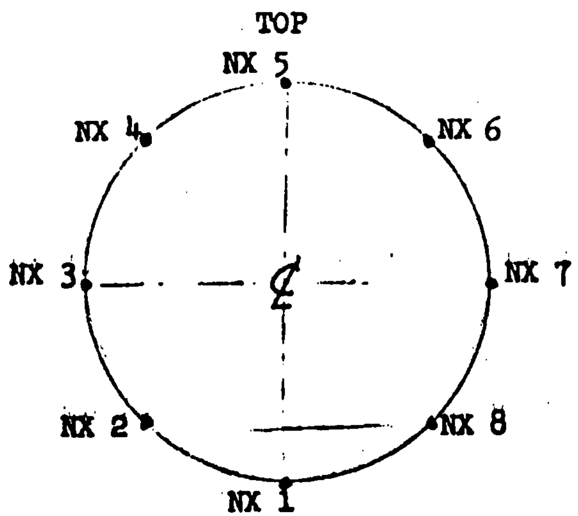

VIEW LOOKING AFT

Table 3-11. Booster B-9U/Nuclear Stage Ultimate Internal Loads

PEAK ULTIMATE AXIAL TENSION LOAD INTENSITIES

STATION (IN)	NX1 (LB/IN)	NX2 (LB/IN)	NX3 (LB/IN)	NX4 (LB/IN)	NX5 (LB/IN)	NX6 (LB/IN)	NX7 (LB/IN)	NX8 (LB/IN)
1000	0(16)	0(16)	0(16)	0(16)	0(11)	0(16)	0(16)	0(16)
1036	5(12)	4(12)	0(15)	0(16)	1(11)	0(16)	0(15)	4(12)
1072	45(12)	32(12)	1(15)	6(8)	11(8)	6(8)	1(15)	32(12)
1131	73(12)	51(12)	3(15)	13(8)	26(8)	13(8)	3(15)	51(12)
1278	141(12)	98(12)	7(15)	43(8)	80(8)	43(8)	7(15)	98(12)
1337	177(12)	121(12)	9(15)	61(8)	111(8)	61(8)	9(15)	121(12)
1341	177(12)	124(12)	8(14)	121(15)	192(15)	121(15)	8(14)	124(12)
1477	288(12)	200(12)	14(14)	124(8)	218(8)	124(8)	14(14)	200(12)
1481	1411(12)	1322(12)	1263(10)	1310(10)	1401(8)	1310(10)	1263(10)	1322(12)
1600	1569(12)	1430(12)	1230(10)	1403(8)	1558(8)	1403(8)	1230(10)	1430(12)
1750	1820(12)	1601(12)	1187(10)	1561(8)	1311(8)	1561(8)	1187(10)	1601(12)
1864	2042(12)	1753(12)	1141(10)	1873(8)	2278(8)	1873(8)	1141(10)	1753(12)
1868	931(12)	640(12)	35(14)	86(13)	140(13)	85(13)	35(14)	640(12)
2006	1453(11)	829(12)	47(14)	155(13)	242(13)	153(13)	47(14)	829(12)
2022	1649(11)	850(12)	48(14)	166(13)	258(13)	164(13)	48(14)	850(12)
2026	1698(11)	891(12)	45(14)	160(13)	251(13)	158(13)	45(14)	891(12)
2042	1903(11)	911(11)	47(14)	152(13)	242(13)	150(13)	47(14)	911(11)
2094	2508(11)	1302(11)	52(14)	141(14)	219(13)	141(14)	52(14)	1302(11)
2098	2647(11)	1322(11)	52(14)	142(14)	217(13)	142(14)	52(14)	1322(11)
2180	3118(11)	1488(11)	60(14)	168(14)	213(14)	168(14)	60(14)	1488(11)
2184	5046(11)	3407(11)	1454(13)	1653(13)	1734(13)	1650(13)	1450(13)	3407(11)
2300	5356(11)	3614(11)	1444(13)	1656(13)	1743(13)	1653(13)	1439(13)	3614(11)
2400	5622(11)	3793(11)	1437(13)	1675(13)	1772(13)	1671(13)	1431(13)	3793(11)
2500	5882(11)	3967(11)	1433(13)	1709(13)	1821(13)	1704(13)	1426(13)	3967(11)
2600	6139(11)	4139(11)	1432(13)	1756(13)	1888(13)	1751(13)	1424(13)	4139(11)
2664	6300(11)	4247(11)	1431(13)	1793(13)	1940(13)	1787(13)	1422(13)	4247(11)

Table 3-11. Booster B-9U/Nuclear Stage Ultimate Internal Loads (Cont)

PEAK ULTIMATE AXIAL TENSION LOAD INTENSITIES

STATION (IN)	NX1 (LB/IN)	NX2 (LB/IN)	NX3 (LB/IN)	NX4 (LB/IN)	NX5 (LB/IN)	NX6 (LB/IN)	NX7 (LB/IN)	NX8 (LB/IN)
2668	6296(11)	4244(11)	1431(13)	1795(13)	1944(13)	1789(13)	1422(13)	4244(11)
2800	5714(11)	3816(11)	1429(13)	1886(13)	2072(13)	1879(13)	1419(13)	3816(11)
2864	5435(11)	3612(11)	1429(13)	1937(13)	2144(13)	1930(13)	1418(13)	3612(11)
2868	5417(11)	3598(11)	1429(13)	1940(13)	2149(13)	1933(13)	1418(13)	3598(11)
2950	5042(11)	3322(11)	1428(13)	2015(13)	2254(13)	2007(13)	1417(13)	3322(11)
3050	4305(11)	3102(12)	1428(12)	2172(13)	2477(13)	2164(13)	1428(12)	3102(12)
3161	3683(12)	3033(12)	1464(12)	2487(13)	2921(13)	2477(13)	1464(12)	3033(12)
3165	3615(12)	2980(12)	1448(12)	2497(13)	2938(13)	2487(13)	1448(12)	2980(12)
3293	2979(12)	2538(12)	1473(12)	2631(16)	3721(16)	2631(16)	1473(12)	2538(12)
3295	2968(12)	2530(12)	1473(12)	2643(16)	3737(16)	2643(16)	1473(12)	2530(12)
3373	2475(12)	2185(12)	1486(12)	2737(13)	3272(13)	2726(13)	1486(12)	2185(12)
3377	2394(12)	2123(12)	1469(12)	2742(13)	3281(13)	2730(13)	1469(12)	2123(12)
3538	1465(12)	1471(12)	1486(12)	2654(13)	3156(13)	2642(13)	1485(12)	1471(12)
3542	1391(12)	1414(12)	1469(12)	2651(13)	3155(13)	2639(13)	1469(12)	1414(12)
3679	943(12)	1105(12)	1559(13)	2228(13)	2506(13)	2229(13)	1561(13)	1105(12)
3683	-609(12)	-442(12)	25(13)	770(16)	1088(16)	770(16)	26(13)	-442(12)
3820	-447(16)	-316(16)	16(13)	516(12)	743(12)	516(12)	16(13)	-316(16)
3921	-119(16)	-84(16)	15(13)	132(12)	196(12)	132(12)	15(13)	-84(16)
3925	451(11)	400(11)	280(10)	246(8)	268(8)	246(8)	280(10)	400(11)
4065	0(7)	1(6)	1(6)	1(6)	0(7)	0(7)	0(7)	0(7)
4069	0(16)	1(6)	1(6)	1(6)	0(6)	0(16)	0(16)	0(16)
4300	0(16)	0(16)	0(16)	0(16)	0(16)	0(16)	0(16)	0(16)

Table 3-12. Booster B-9U/Nuclear Stage Ultimate Internal Loads

PEAK ULTIMATE AXIAL COMPRESSION LOAD INTENSITES

STATION (IN)	NX1 (LB/IN)	NX2 (LB/IN)	NX3 (LB/IN)	NX4 (LB/IN)	NX5 (LB/IN)	NX6 (LB/IN)	NX7 (LB/IN)	NX8 (LB/IN)
1000	-1(11)	-1(11)	-0(10)	-0(6)	-0(5)	-0(5)	-0(10)	-1(11)
1036	-5(11)	-4(11)	-2(10)	-4(12)	-5(12)	-4(12)	-2(10)	-4(11)
1072	-25(8)	-19(8)	-12(9)	-34(12)	-47(12)	-34(12)	-7(7)	-19(8)
1131	-61(8)	-49(8)	-32(9)	-53(12)	-75(12)	-53(12)	-19(10)	-49(8)
1278	-174(8)	-137(8)	-86(9)	-105(12)	-147(12)	-105(12)	-47(7)	-137(8)
1337	-229(8)	-180(8)	-109(9)	-132(12)	-185(12)	-132(12)	-60(7)	-180(8)
1341	-295(15)	-224(15)	-111(9)	-136(12)	-189(12)	-136(12)	-61(7)	-224(15)
1477	-422(8)	-328(8)	-181(9)	-225(12)	-313(12)	-225(12)	-103(7)	-328(8)
1481	-135(15)	-107(15)	-39(15)	-58(16)	-82(16)	-58(16)	-57(3)	-107(15)
1600	-113(2)	-94(2)	-47(2)	-111(16)	-158(16)	-111(16)	-87(3)	-122(3)
1750	-499(6)	-359(6)	-62(2)	-154(16)	-218(16)	-154(16)	-133(3)	-369(6)
1864	-880(4)	-655(6)	-118(6)	-166(16)	-234(16)	-166(16)	-179(3)	-641(4)
1868	-4094(4)	-3867(6)	-3737(6)	-2822(5)	-2629(5)	-2822(5)	-3287(5)	-3857(4)
2006	-3264(6)	-3410(4)	-3801(4)	-4197(5)	-4578(10)	-4197(5)	-3820(6)	-3437(6)
2022	-3162(6)	-3358(5)	-3868(5)	-4383(4)	-5029(10)	-4383(4)	-3895(6)	-3390(6)
2026	-3136(6)	-3346(5)	-3884(5)	-4431(10)	-5142(10)	-4431(10)	-3913(6)	-3378(6)
2042	-3029(6)	-3296(5)	-3948(5)	-4784(10)	-5590(10)	-4784(10)	-3985(6)	-3327(6)
2094	-2697(5)	-3117(5)	-4141(5)	-5914(10)	-7034(10)	-5914(10)	-4205(6)	-3146(6)
2098	-2675(5)	-3109(5)	-4155(5)	-5989(10)	-7129(10)	-5989(10)	-4221(6)	-3138(6)
2180	-2489(5)	-3065(5)	-4454(5)	-7293(10)	-8735(10)	-7293(10)	-4563(6)	-3091(6)
2184	-2191(2)	-2597(5)	-3992(5)	-5508(4)	-6870(10)	-5518(6)	-4103(6)	-2619(6)
2300	-2278(2)	-2548(5)	-4013(5)	-5692(10)	-7239(10)	-5699(6)	-4189(6)	-2703(3)
2400	-2354(2)	-2596(2)	-4030(5)	-5922(10)	-7552(10)	-5922(10)	-4393(3)	-2786(3)
2500	-2430(2)	-2654(2)	-4047(5)	-6150(10)	-7860(10)	-6150(10)	-4626(3)	-2873(3)
2600	-2508(2)	-2712(2)	-4065(5)	-6375(10)	-8164(10)	-6375(10)	-4862(3)	-2963(3)
2664	-2560(2)	-2752(2)	-4076(5)	-6517(10)	-8356(10)	-6517(10)	-5015(3)	-3024(3)

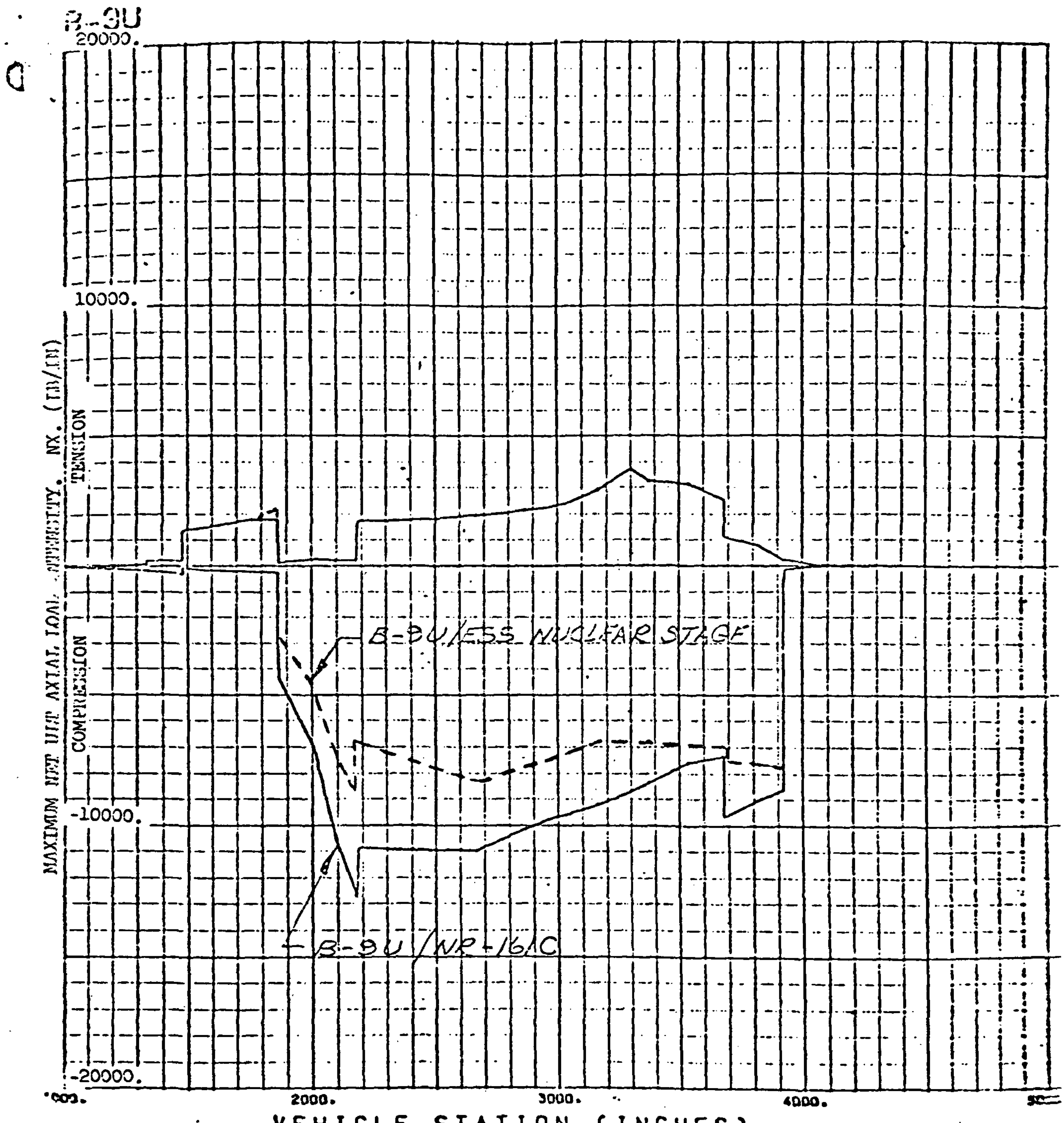

Figure 3-22. Internal Loads at the Top Centerline

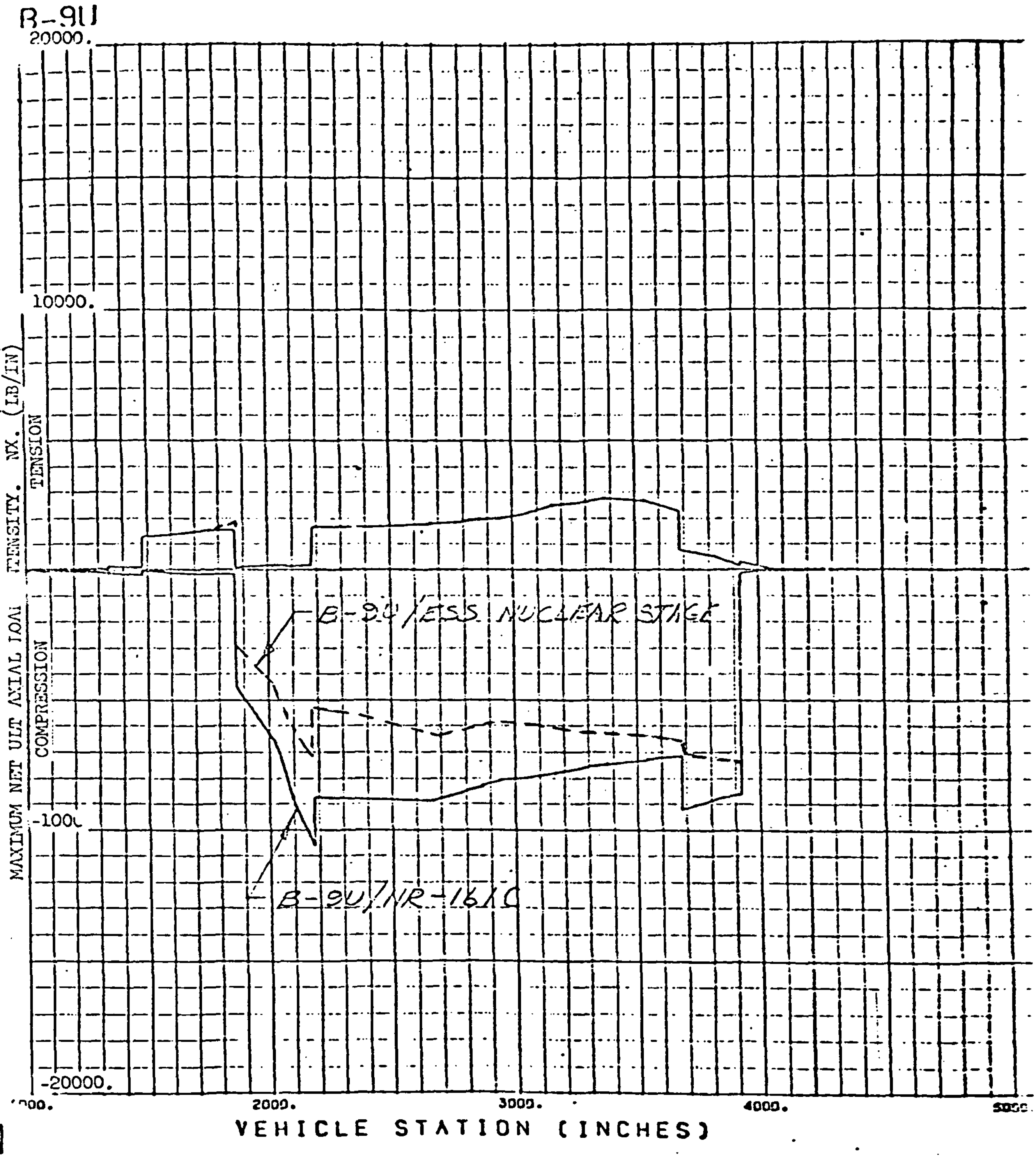

Figure 3-23. Internal Loads 45 Degrees from the Top

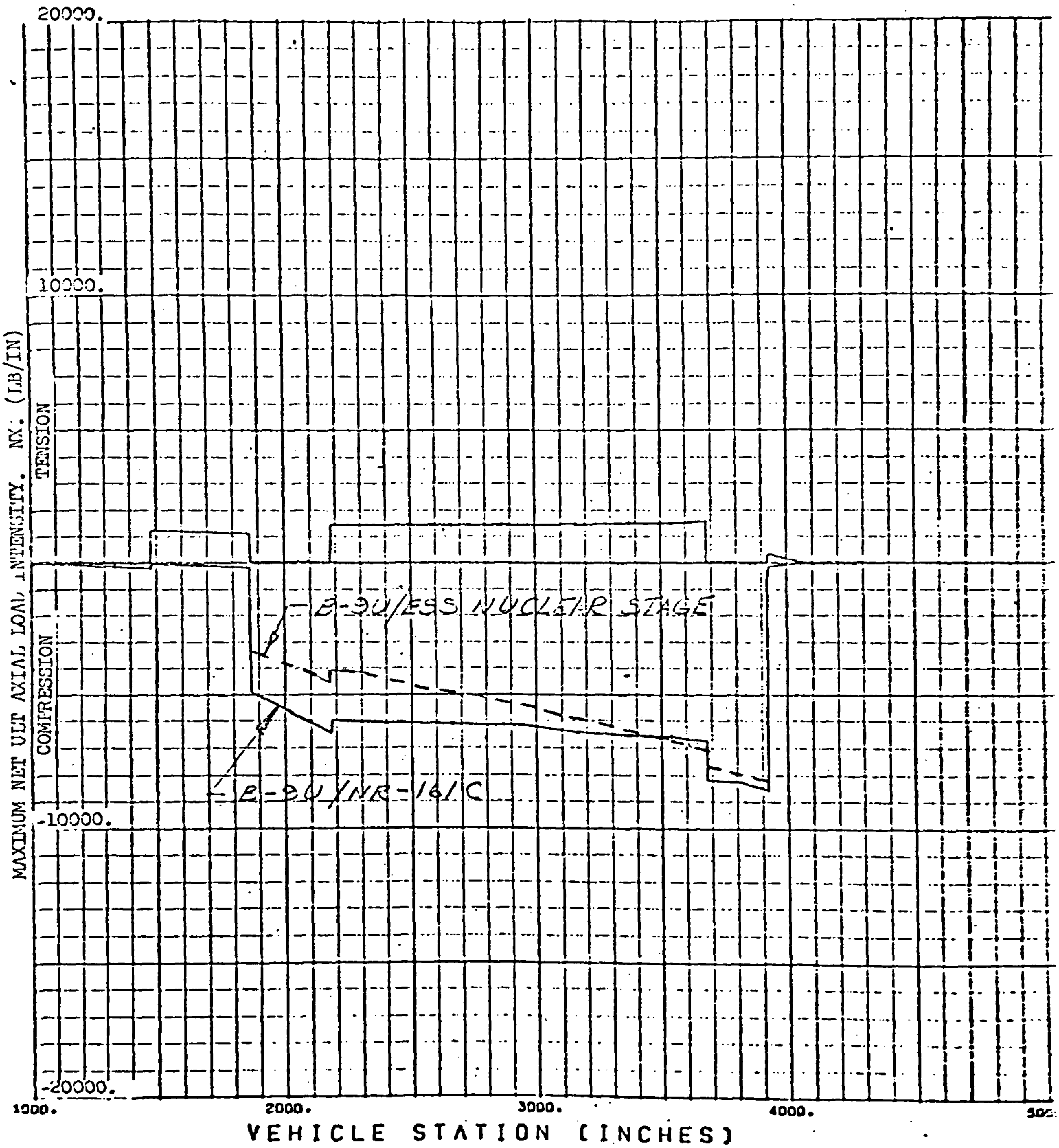

Figure 3-24. Internal Loads at the Side

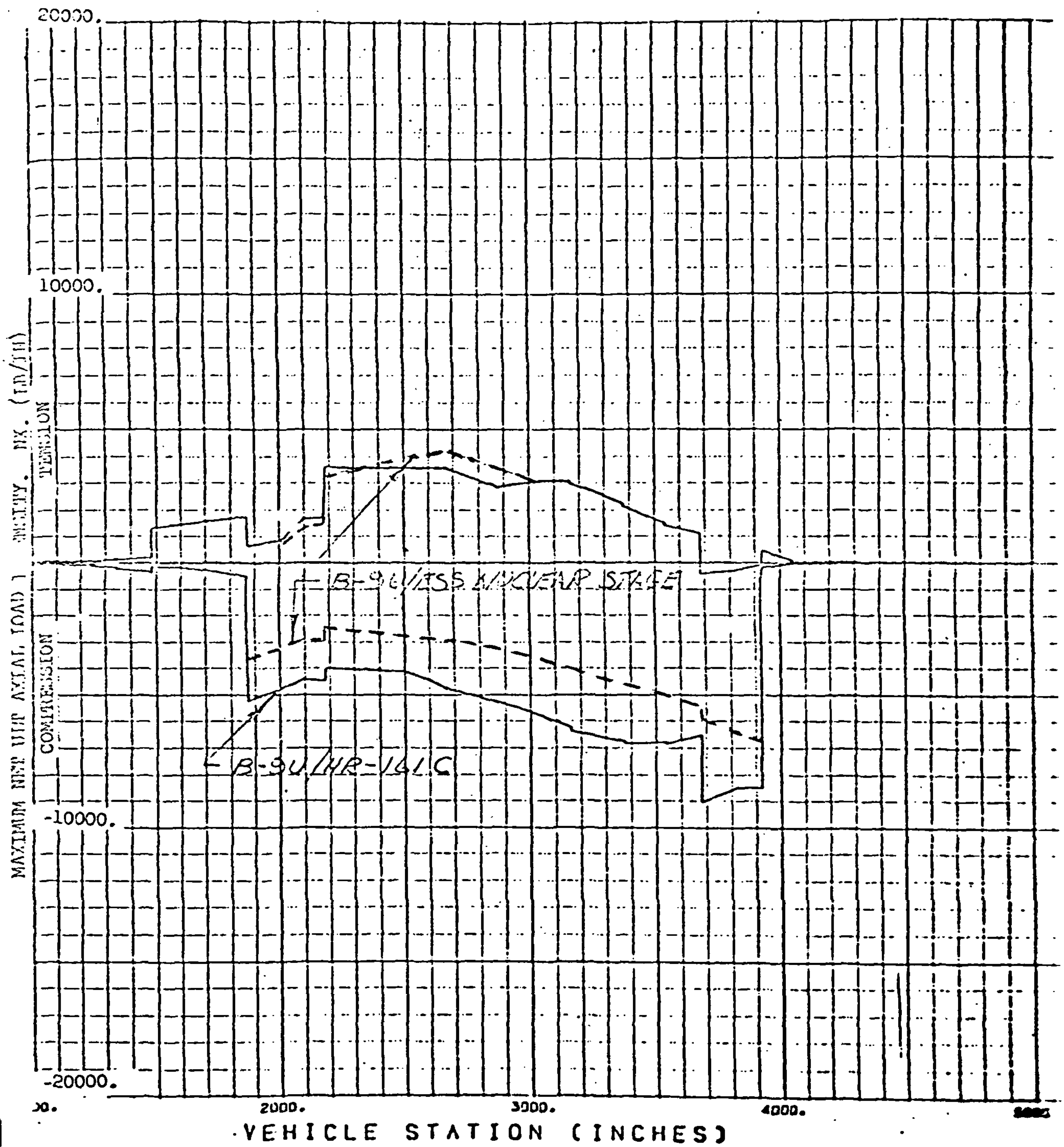

Figure 3-25. Internal Loads 45 Degrees from the Bottom

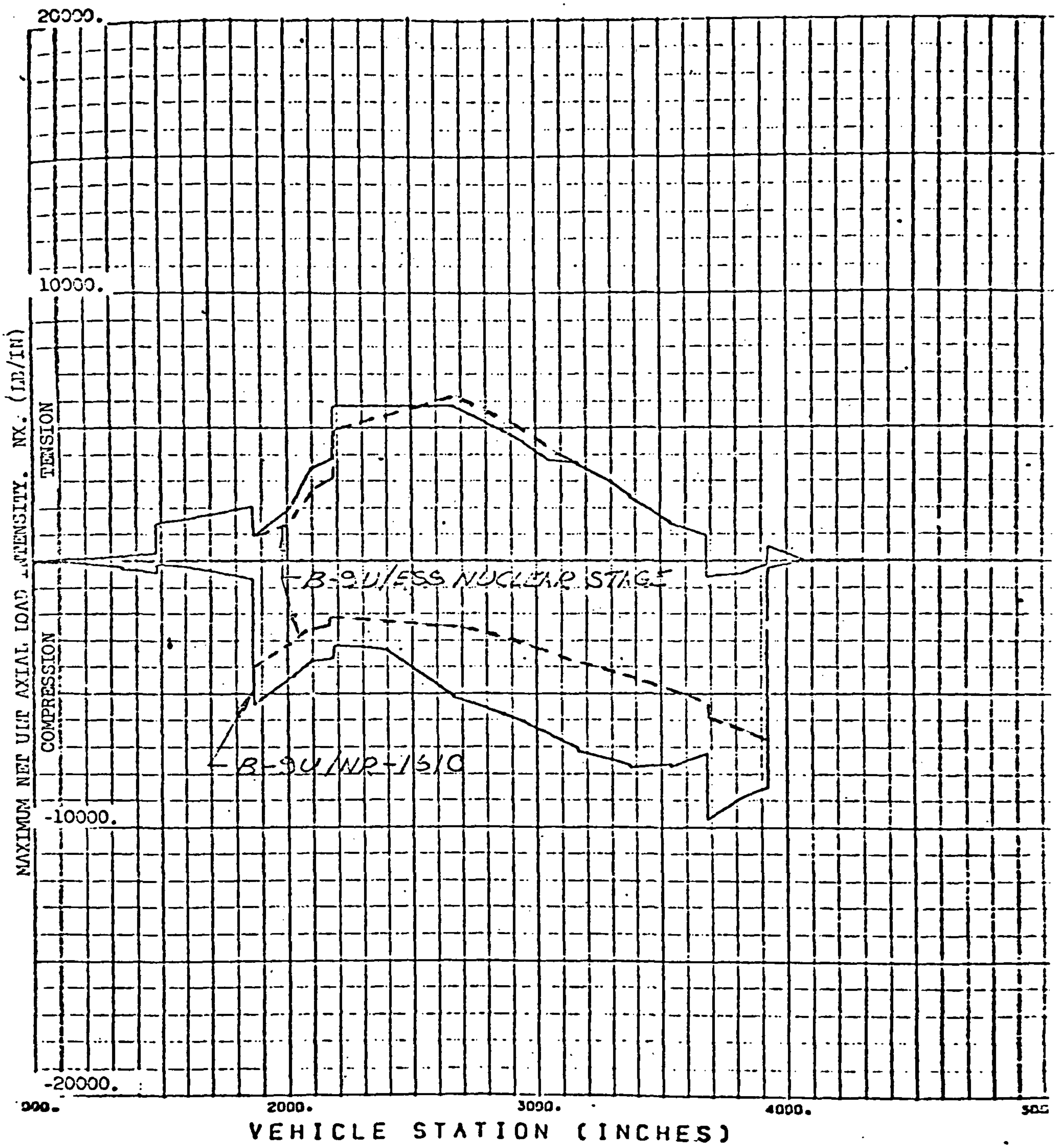

Figure 3-26. Internal Loads at Bottom Centerline

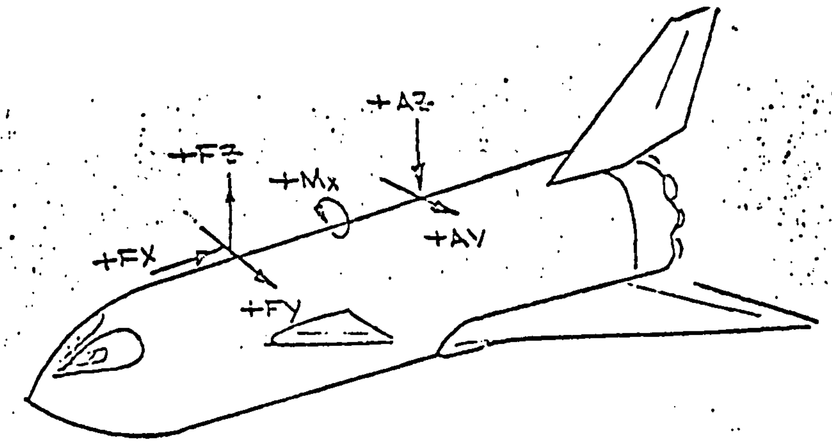

B-9U/ESS - NUCLEAR STAGE (LIMIT LOADS)

CONDITION	WIND	Fx (x 10^3 lb)	Fy (x 10^3 lb)	Fz (x 10^3 lb)	Ay (x 10^3 lb)	Az (x 10^3 lb)	Mx (10^6 in/lb)
Two Week	Head	195		426		289	
Ground Winds	Tail	195		-495		-175	
Unfueled	Side	195	±554	48.7	∓230	54.0	±70.8
1 Hour Ground	Head	669		270		249	
Winds Fueled	Tail	669		16.7		121	
Unpressurized	Side	669	±149	166	∓63.1	185	∓18.9
Dynamic Lift Off	Head	946		322		341	
+ 1 Hour Ground	Tail	946		97.1		187	
Winds	Side	945	±130	232	∓80.8	263	∓11.4
Max. α-q	Head	1243		409		567	
	Tail	1237		-130		-124	
Max. β-q	Side	1234	±247	161	∓182	237	∓13.3
2.5g Max. Thrust	-	1818		405		544	
Booster Burnout	-	1797		343		592	

Figure 3-27. Design Attachment Loads

Table 3-13. Booster B-9U/MDAC Ultimate Internal Loads

COND 1	BOOSTER B-9U/ESS-MDAC	STAGE 1HR GROUND HEADWIND TANKED UNPRESS
COND 2	BOOSTER B-9U/ESS-MDAC	STAGE 1HR GROUND TAILWIND TANKED UNPRESS
COND 3	BOOSTER B-9U/ESS-MDAC	STAGE 1HR GROUND SIDEWIND TANKED UNPRESS
COND 4	BOOSTER B-9U/ESS-MDAC	STAGE LIFT OFF +1HR GROUND HEADWINDS
COND 5	BOOSTER B-9U/ESS-MDAC	STAGE LIFT OFF +1HR GROUND TAILWINDS
COND 6	BOOSTER B-9U/ESS-MDAC	STAGE LIFT OFF +1HR GROUND SIDEWINDS
COND 7	BOOSTER B-9U /MDAC	STAGE MAX ALPHA-Q HEADWINDS
COND 8	BOOSTER B-9U /MDAC	STAGE MAX ALPHA-Q TAILWINDS
COND 9	BOOSTER B-9U /MDAC	STAGE MAX BETA-Q
COND 10	BOOSTER B-9U/ESS-MDAC	STAGE 2.06G MAX THRUST
COND 11	BOOSTER B-9U/ESS-MDAC	STAGE 2.06G BOOSTER BURNOUT
COND 12	BOOSTER B-9U	BOOSTER RECOVERY
COND 13	BOOSTER B-9U	BOOSTER SUBSONIC GUST
COND 14	BOOSTER B-9U	BOOSTER 2 POINT LANDING
COND 15	BOOSTER B-9U	BOOSTER 3 POINT LANDING
COND 16	BOOSTER B-9U	BOOSTER 2 G TAXI

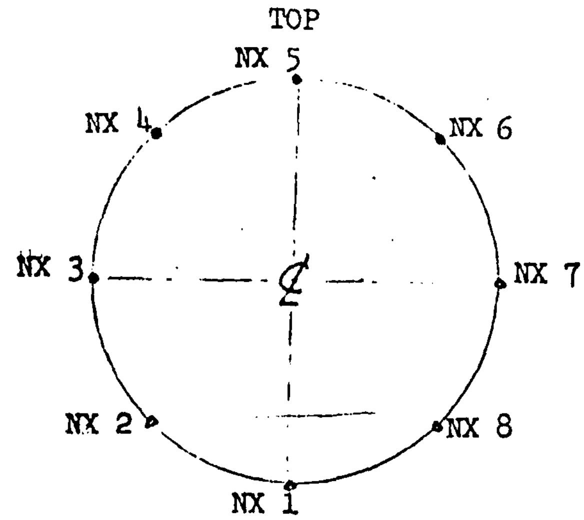

VIEW LOOKING AFT

Table 3-14. Booster B-9U/MDAC Ultimate Internal Loads

PEAK ULTIMATE AXIAL TENSION LOAD INTENSITIES

STATION (IN)	NX1 (LB/IN)	NX2 (LB/IN)	NX3 (LB/IN)	NX4 (LB/IN)	NX5 (LB/IN)	NX6 (LB/IN)	NX7 (LB/IN)	NX8 (LB/IN)
1000	0(16)	0(16)	0(16)	0(16)	0(11)	0(16)	0(16)	0(16)
1036	5(12)	4(12)	0(15)	0(16)	1(11)	0(16)	0(15)	4(12)
1072	45(12)	32(12)	1(15)	10(8)	17(8)	10(8)	1(15)	32(12)
1131	73(12)	51(12)	3(15)	25(8)	42(8)	25(8)	3(15)	51(12)
1278	141(12)	98(12)	7(15)	65(8)	110(8)	65(8)	7(15)	98(12)
1337	173(12)	121(12)	9(15)	86(8)	144(8)	86(8)	9(15)	121(12)
1341	177(12)	124(12)	8(14)	121(15)	192(15)	121(15)	8(14)	124(12)
1477	288(12)	200(12)	14(14)	154(8)	256(8)	154(8)	14(14)	200(12)
1481	1411(12)	1322(12)	1358(11)	1412(11)	1435(11)	1412(11)	1358(11)	1322(12)
1600	1569(12)	1430(12)	1332(11)	1431(8)	1596(8)	1431(8)	1332(11)	1430(12)
1750	1820(12)	1601(12)	1296(11)	1755(8)	2080(8)	1755(8)	1296(11)	1601(12)
1864	2042(12)	1753(12)	1258(11)	1416(11)	1481(11)	1416(11)	1258(11)	1753(12)
1868	931(12)	640(12)	35(14)	86(13)	140(13)	85(13)	35(14)	640(12)
2006	1963(11)	988(11)	47(14)	155(13)	242(13)	153(13)	47(14)	988(11)
2022	2213(11)	1123(11)	48(14)	166(13)	258(13)	164(13)	48(14)	1123(11)
2026	2277(11)	1157(11)	45(14)	160(13)	251(13)	159(13)	45(14)	1157(11)
2042	2534(11)	1298(11)	47(14)	152(13)	242(13)	150(13)	47(14)	1298(11)
2094	3406(11)	1786(11)	52(14)	141(14)	219(13)	141(14)	52(14)	1786(11)
2098	3454(11)	1810(11)	52(14)	142(14)	217(13)	142(14)	52(14)	1810(11)
2180	4032(11)	2018(11)	60(14)	168(14)	213(14)	168(14)	60(14)	2018(11)
2184	6012(11)	3988(11)	1454(13)	1653(13)	1734(13)	1650(13)	1450(13)	3988(11)
2300	6378(11)	4237(11)	1444(13)	1656(13)	1743(13)	1653(13)	1439(13)	4237(11)
2400	6692(11)	4450(11)	1437(13)	1675(13)	1772(13)	1671(13)	1431(13)	4450(11)
2500	7000(11)	4660(11)	1433(13)	1709(13)	1821(13)	1704(13)	1426(13)	4660(11)
2600	7304(11)	4867(11)	1432(13)	1756(13)	1888(13)	1751(13)	1424(13)	4867(11)
2664	7495(11)	4998(11)	1431(13)	1793(13)	1940(13)	1787(13)	1422(13)	4998(11)

Table 3-14. Booster B-9U/MDAC Ultimate Internal Loads (Cont)

PEAK ULTIMATE AXIAL TENSION LOAD INTENSITIES

STATION (IN)	NX1 (LB/IN)	NX2 (LB/IN)	NX3 (LB/IN)	NX4 (LB/IN)	NX5 (LB/IN)	NX6 (LB/IN)	NX7 (LB/IN)	NX8 (LB/IN)
2668	7490(11)	4994(11)	1431(13)	1795(13)	1944(13)	1789(13)	1422(13)	4993(11)
2800	6742(11)	4451(11)	1429(13)	1886(13)	2072(13)	1879(13)	1419(13)	4451(11)
2864	6382(11)	4191(11)	1429(13)	1937(13)	2144(13)	1930(13)	1418(13)	4191(11)
2868	6359(11)	4174(11)	1429(13)	1940(13)	2149(13)	1933(13)	1418(13)	4174(11)
2950	5881(11)	3827(11)	1428(13)	2015(13)	2254(13)	2007(13)	1417(13)	3827(11)
3050	5063(11)	3199(11)	1428(12)	2172(13)	2477(13)	2164(13)	1428(12)	3199(11)
3161	4063(11)	3033(12)	1464(12)	2487(13)	2921(13)	2477(13)	1464(12)	3033(12)
3165	4026(11)	2980(12)	1448(12)	2497(13)	2938(13)	2487(13)	1448(12)	2980(12)
3203	3036(11)	2538(12)	1473(12)	2631(16)	3721(16)	2631(16)	1473(12)	2538(12)
3295	3020(11)	2530(12)	1473(12)	2643(16)	3737(16)	2643(16)	1473(12)	2530(12)
3373	2492(11)	2185(12)	1486(12)	2737(13)	3272(13)	2726(13)	1486(12)	2185(12)
3377	2465(11)	2123(12)	1469(12)	2742(13)	3281(13)	2730(13)	1469(12)	2123(12)
3538	1465(12)	1471(12)	1486(12)	2654(13)	3156(13)	2642(13)	1486(12)	1471(12)
3542	1391(12)	1414(12)	1469(12)	2651(13)	3155(13)	2639(13)	1469(12)	1414(12)
3679	943(12)	1105(12)	1559(13)	2228(13)	2506(13)	2229(13)	1561(13)	1105(12)
3683	-609(12)	-442(12)	25(13)	770(16)	1088(16)	770(16)	26(13)	-442(12)
3820	-447(16)	-316(16)	16(13)	516(12)	743(12)	516(12)	16(13)	-316(16)
3921	-119(16)	-84(16)	15(13)	132(12)	196(12)	132(12)	15(13)	-84(16)
3925	373(11)	331(11)	233(10)	260(7)	274(7)	260(7)	233(10)	331(11)
4065	0(7)	1(6)	1(6)	1(6)	0(7)	0(7)	0(7)	0(7)
4069	0(16)	1(6)	1(6)	1(6)	0(6)	0(16)	0(16)	0(16)
4300	0(16)	0(16)	0(16)	0(16)	0(16)	0(16)	0(16)	0(16)

Table 3-15. Booster B-9U/MDAC Ultimate Internal Loads

PEAK ULTIMATE AXIAL COMPRESSION LOAD INTENSITES

STATION (IN)	NX1 (LB/IN)	NX2 (LB/IN)	NX3 (LB/IN)	NX4 (LB/IN)	NX5 (LB/IN)	NX6 (LB/IN)	NX7 (LB/IN)	NX8 (LB/IN)
1000	-1(11)	-1(11)	-0(10)	-0(10)	-0(10)	-0(10)	-0(10)	-1(11)
1036	-4(11)	-4(11)	-2(10)	-4(12)	-5(12)	-4(12)	-2(10)	-4(11)
1072	-30(8)	-23(8)	-7(7)	-34(12)	-47(12)	-34(12)	-7(7)	-23(8)
1131	-75(8)	-58(8)	-18(7)	-53(12)	-75(12)	-53(12)	-18(7)	-58(8)
1278	-197(8)	-152(8)	-48(7)	-105(12)	-147(12)	-105(12)	-48(7)	-152(8)
1337	-257(8)	-195(8)	-61(7)	-132(12)	-185(12)	-132(12)	-61(7)	-195(8)
1341	-295(15)	-224(15)	-62(7)	-136(12)	-189(12)	-136(12)	-62(7)	-224(15)
1477	-445(8)	-342(8)	-106(7)	-225(12)	-313(12)	-225(12)	-106(7)	-342(8)
1481	-244(6)	-181(5)	-49(4)	-58(16)	-82(16)	-58(16)	-58(6)	-194(6)
1600	-488(6)	-370(6)	-73(6)	-111(16)	-158(16)	-111(16)	-87(3)	-359(6)
1750	-856(4)	-666(6)	-142(6)	-154(16)	-218(16)	-154(16)	-133(3)	-638(4)
1864	-5601(4)	-5319(6)	-4596(6)	-3847(5)	-3580(5)	-3847(5)	-4492(4)	-5276(4)
1868	-5599(4)	-5314(6)	-4608(6)	-3875(5)	-3616(5)	-3875(5)	-4503(4)	-5271(4)
2006	-4313(4)	-4607(6)	-5306(6)	-5985(5)	-6566(10)	-5985(5)	-5239(4)	-4584(4)
2022	-4161(4)	-4524(6)	-5395(6)	-6247(5)	-7110(10)	-6247(5)	-5372(4)	-4504(4)
2026	-4122(4)	-4503(6)	-5417(6)	-6334(10)	-7246(10)	-6334(10)	-5354(4)	-4483(4)
2042	-3961(4)	-4413(6)	-5503(6)	-6759(10)	-7787(10)	-6759(10)	-5444(4)	-4395(4)
2094	-3422(4)	-4108(6)	-5769(6)	-8119(10)	-9527(10)	-8119(10)	-5720(4)	-4095(4)
2099	-3393(4)	-4093(6)	-5789(6)	-8210(10)	-9641(10)	-8210(10)	-5741(4)	-4081(4)
2180	-3051(4)	-3969(6)	-6202(6)	-9768(10)	-11559(10)	-9768(10)	-6172(4)	-3965(4)
2184	-2520(4)	-3445(6)	-5693(6)	-7938(5)	-9656(10)	-7938(5)	-5664(4)	-3441(4)
2300	-2322(4)	-3307(4)	-5688(6)	-8126(10)	-10026(10)	-8126(10)	-5685(4)	-3307(4)
2400	-2171(2)	-3193(5)	-5702(4)	-8355(10)	-10339(10)	-8355(10)	-5717(6)	-3203(6)
2500	-2127(2)	-3105(5)	-5720(4)	-8582(10)	-10648(10)	-8582(10)	-5762(6)	-3118(6)
2600	-2084(2)	-3019(5)	-5737(4)	-8806(10)	-10953(10)	-8806(10)	-5809(6)	-3044(3)
2664	-2057(2)	-2964(5)	-5748(4)	-8948(10)	-11147(10)	-8948(10)	-5840(6)	-3051(3)

Table 3-15. Booster B-9U/MDAC Ultimate Internal Loads (Cont)

PEAK ULTIMATE AXIAL COMPRESSION LOAD INTENSITES

STATION (IN)	NX1 (LB/IN)	NX2 (LB/IN)	NX3 (LB/IN)	NX4 (LB/IN)	NX5 (LB/IN)	NX6 (LP/IN)	NX7 (LB/IN)	NX8 (LB/IN)
2668	-2061(2)	-2967(5)	-5749(4)	-8946(10)	-11144(10)	-8946(10)	-5841(6)	-3056(3)
2800	-2385(2)	-3242(5)	-5778(4)	-8533(10)	-10540(10)	-8533(10)	-5989(3)	-3342(3)
2864	-2543(2)	-3375(5)	-5790(4)	-8328(10)	-10241(10)	-8328(10)	-6091(3)	-3482(3)
2868	-2553(2)	-3383(5)	-5791(4)	-8315(10)	-10223(10)	-8315(10)	-6097(3)	-3491(3)
2950	-2763(2)	-3561(5)	-5811(4)	-8070(4)	-9843(10)	-8110(6)	-6233(3)	-3675(3)
3050	-3093(2)	-3886(4)	-5917(4)	-7954(5)	-9463(10)	-7992(6)	-6461(3)	-3971(3)
3161	-3557(4)	-4287(4)	-6056(4)	-7852(5)	-9042(10)	-7932(3)	-6732(3)	-4322(3)
3165	-3572(4)	-4301(4)	-6061(4)	-7848(5)	-9026(10)	-7935(3)	-6742(3)	-4334(3)
3293	-4073(4)	-4680(4)	-6144(4)	-7656(5)	-8608(1)	-7993(3)	-7006(3)	-4683(3)
3295	-4081(4)	-4686(4)	-6145(4)	-7653(5)	-8607(1)	-7994(3)	-7010(3)	-4689(3)
3373	-4349(4)	-4881(4)	-6164(4)	-7504(5)	-8587(1)	-8011(3)	-7151(3)	-4881(4)
3377	-4363(4)	-4891(4)	-6165(4)	-7496(5)	-8586(1)	-8012(3)	-7158(3)	-4891(4)
3538	-4916(4)	-5294(4)	-6207(4)	-7447(1)	-8555(1)	-8050(3)	-7457(3)	-5294(4)
3542	-4930(4)	-5304(4)	-6208(4)	-7446(1)	-8554(1)	-8051(3)	-7464(3)	-5305(4)
3679	-5522(4)	-5763(4)	-6347(4)	-7505(1)	-8596(1)	-8149(3)	-7798(3)	-5763(4)
3683	-7265(7)	-7277(4)	-7851(4)	-8589(10)	-9294(1)	-8848(3)	-8504(3)	-7277(4)
3820	-7559(4)	-7668(4)	-7930(4)	-8233(1)	-9314(1)	-8911(3)	-8803(3)	-7668(4)
3921	-8044(5)	-8053(5)	-8076(4)	-8320(1)	-9393(1)	-9018(3)	-9091(3)	-8053(5)
3925	-243(12)	-184(12)	-42(12)	70(15)	75(1)	70(15)	-42(12)	-184(12)
4065	-0(15)	-0(15)	-0(15)	-0(15)	-0(15)	-1(6)	-1(6)	-1(6)
4069	0(16)	0(16)	0(16)	0(16)	0(16)	-1(6)	-1(6)	-1(6)
4300	0(16)	0(16)	0(16)	0(16)	0(16)	0(16)	0(16)	0(16)

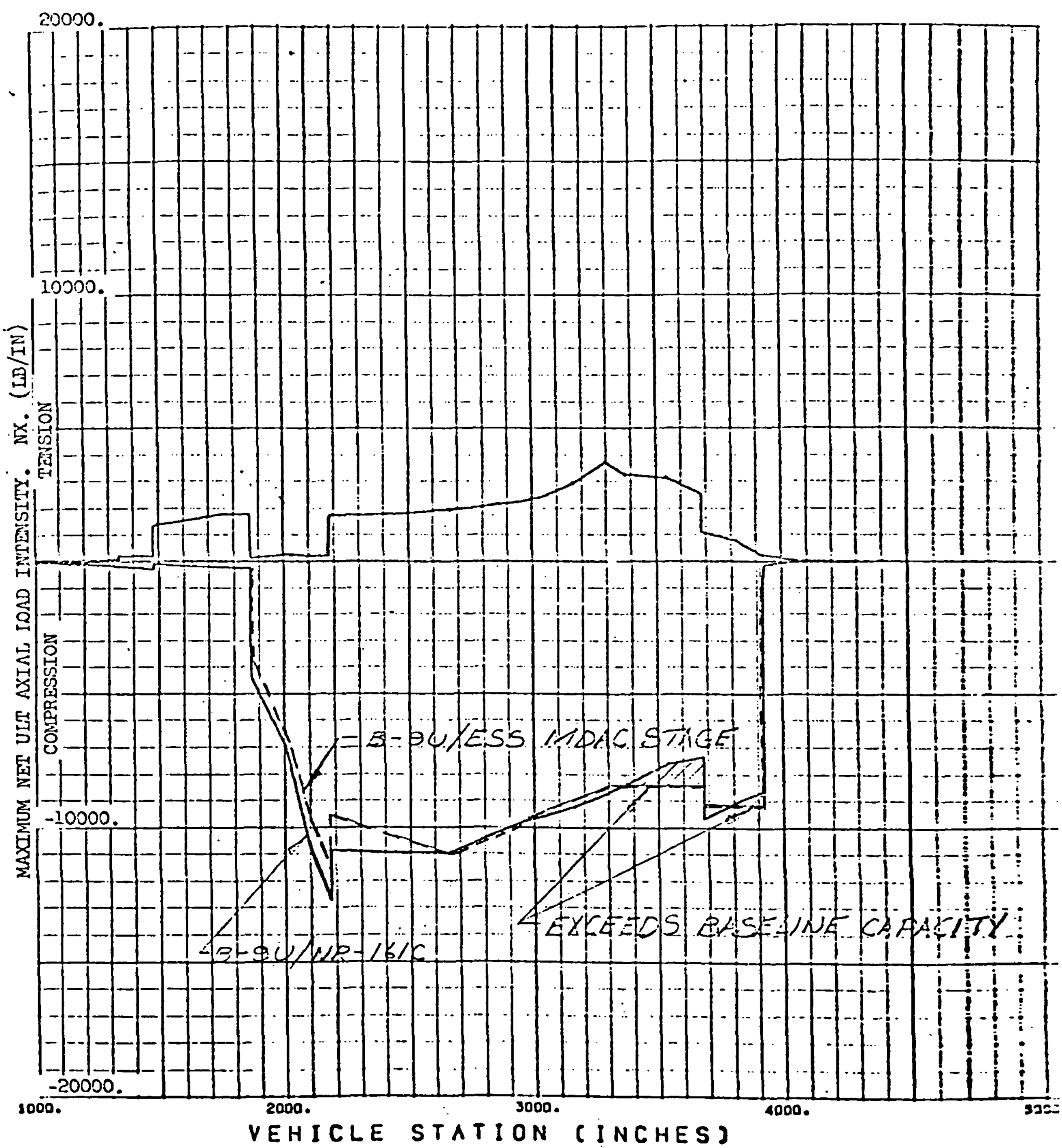

Figure 3-28. Internal Loads at the Top Centerline

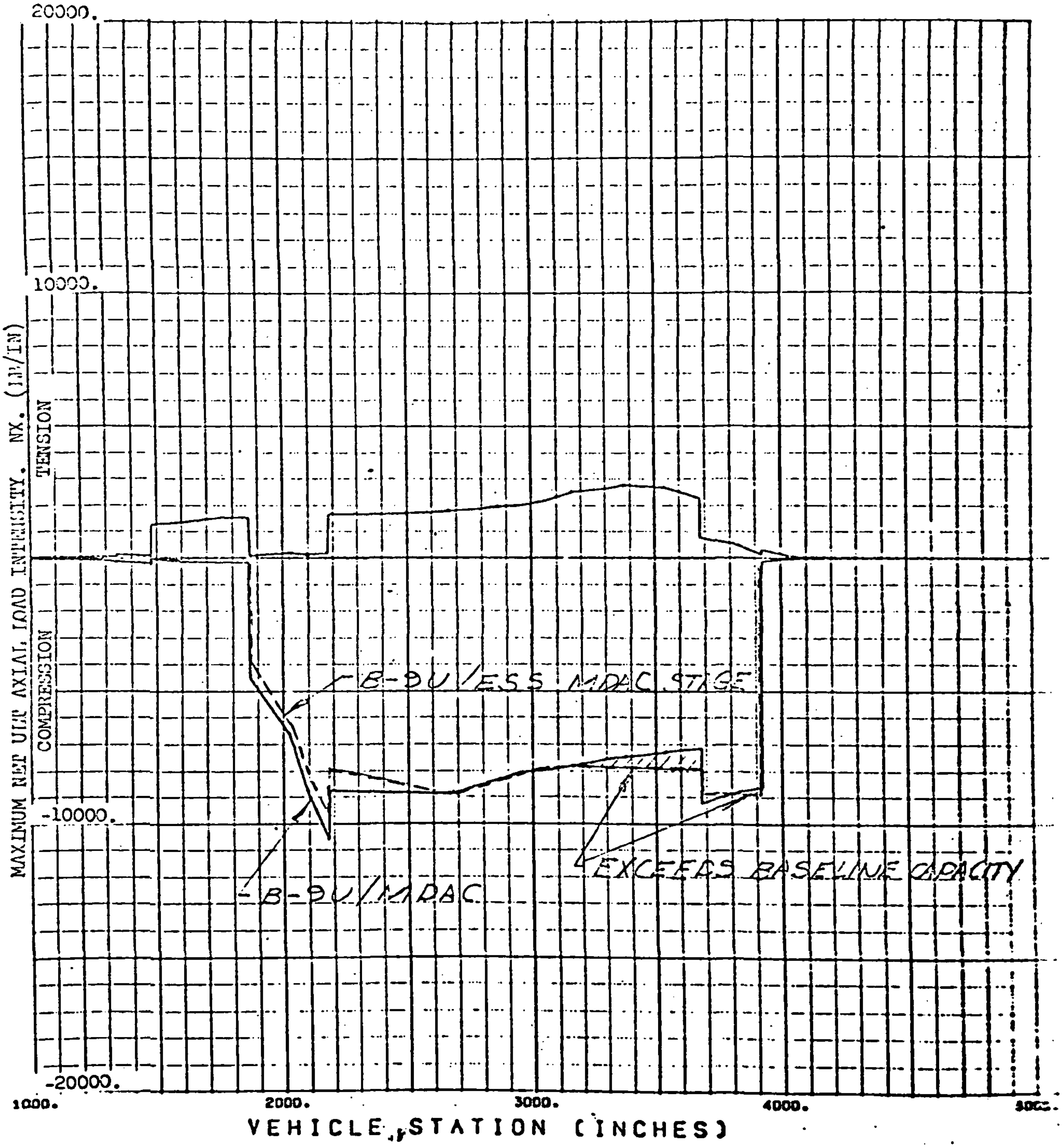

Figure 3-29. Internal Loads 45 Degrees from the Top

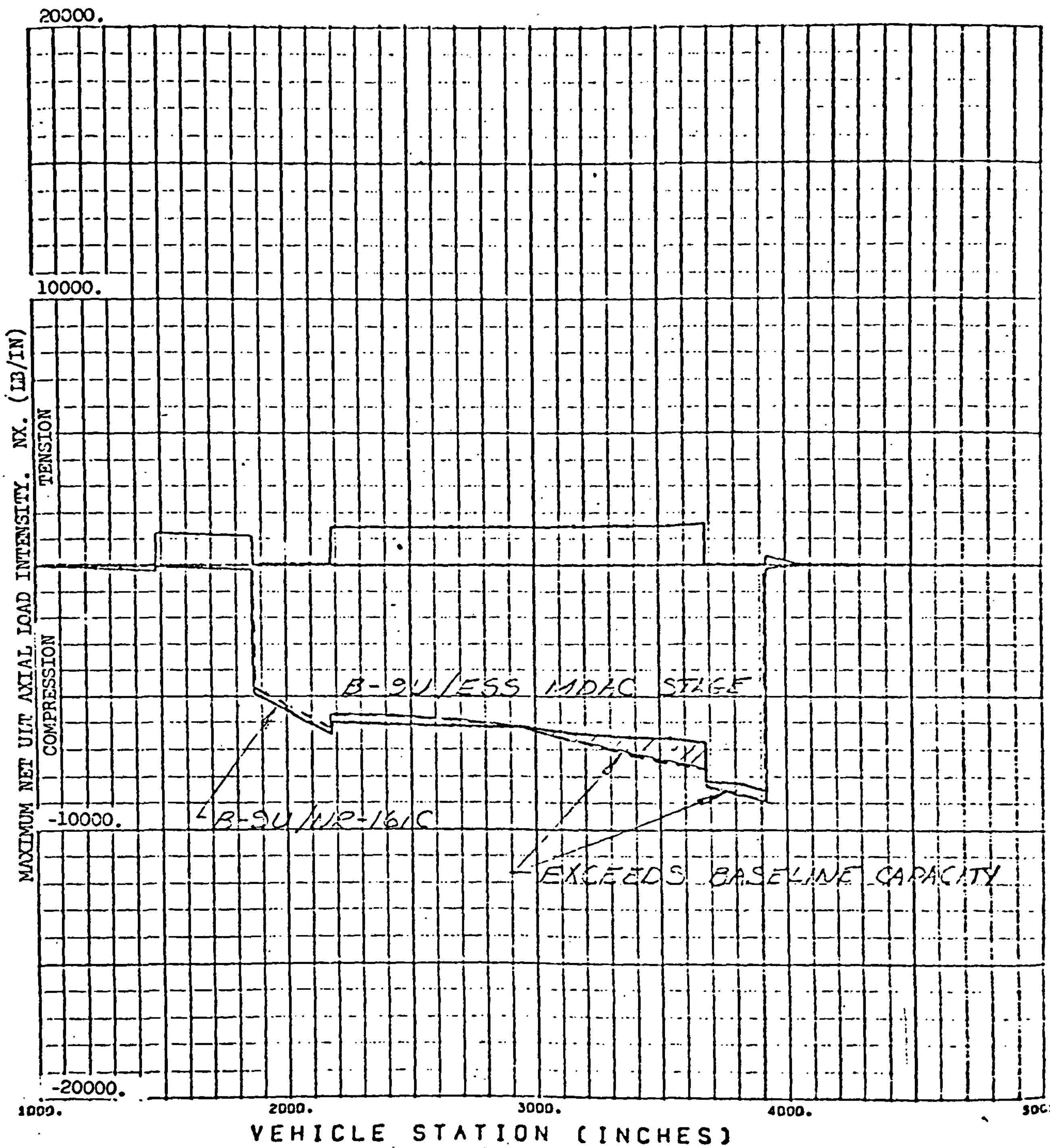

Figure 3-30. Internal Loads at the Side

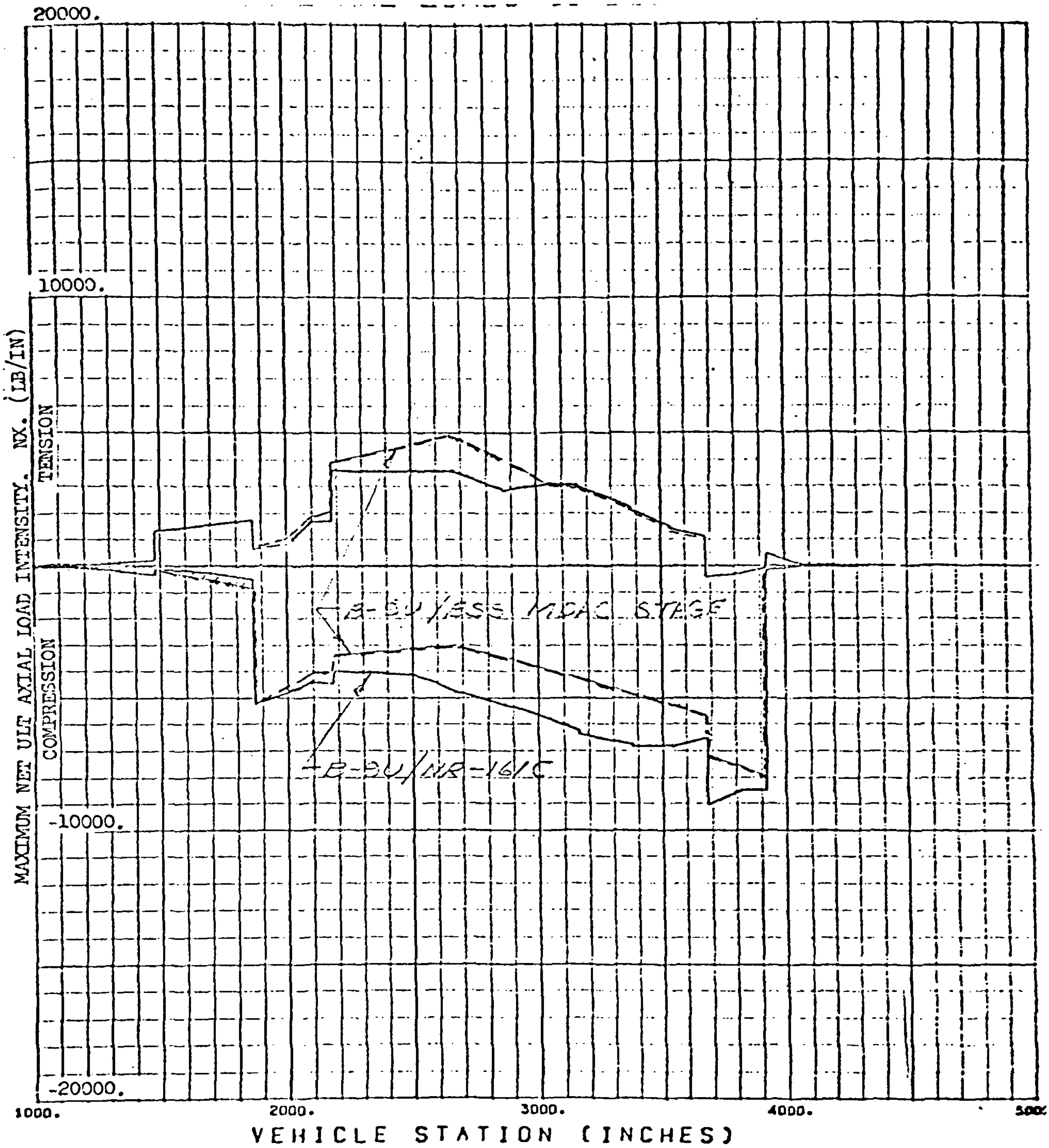

Figure 3-31. Internal Loads 45 Degrees from the Bottom

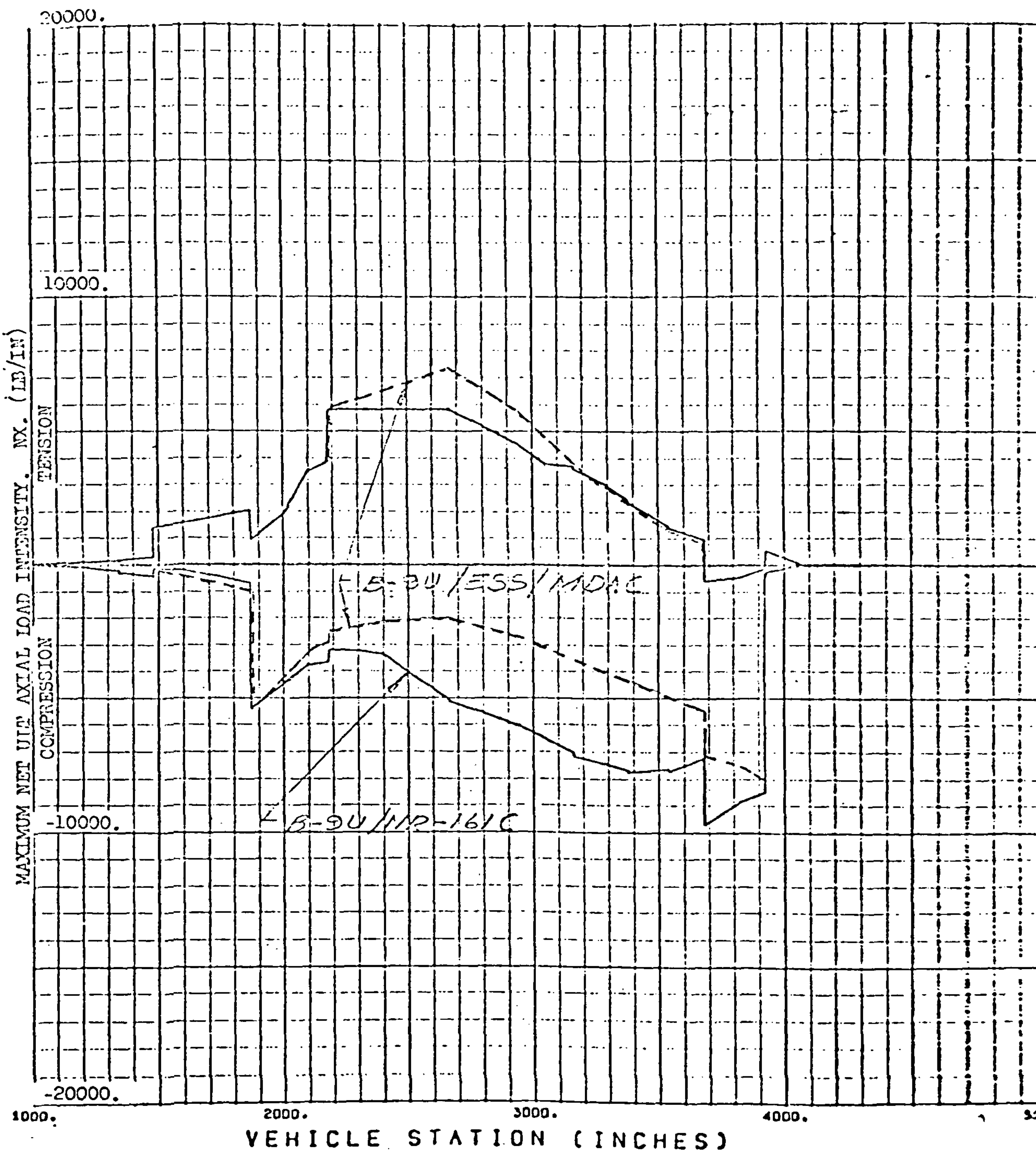

Figure 3-32. Internal Loads at Bottom Centerline

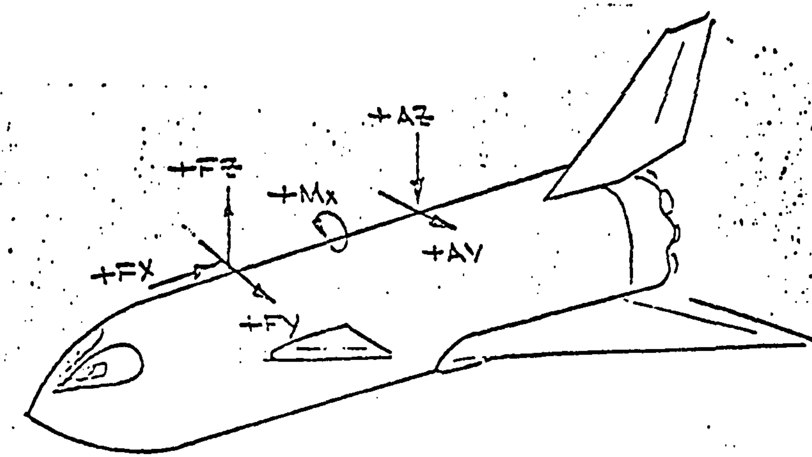

B-9U /ESS-MDAC STAGE (LIMIT LOADS)

CONDITION	WIND	Fx (x 10^3 lb)	Fy (x 10^3 lb)	Fz (x 10^3 lb)	Ay (x 10^3 lb)	Az (x 10^3 lb)	Mx (10^6 in/lb)
Two Week	Head	276		244		165	
Ground Winds	Tail	276		-286		-15.6	
Unfueled	Side	276	±354	68.8	∓92.0	76.4	∓59.0
1 Hour Ground	Head	991		293		297	
Winds Fueled	Tail	991		148		247	
Unpressurized	Side	991	± 97.4	245	∓ 25.3	272	∓15.44
Dynamic Lift Off	Head	1397		372		426	
+ 1 Hour Ground	Tail	1397		251		356	
Winds	Side	1397	± 79.5	336	∓ 39.6	391	∓8.86
Max. α-q	Head	2055		508		744	
	Tail	1964		203		255	
Max. β-q	Side	1806	±223	320	∓158	399	∓15.5
2.0g Max. Thrust	-	2239		486		669	
Booster Burnout	-	2217		377		746	

Figure 3-33. Design Attachment Loads

Table 3-16. Booster B-9U/Space Tug Ultimate Internal Loads

COND 1	BOOSTER B-9U/SPACE TUG STAGE	1HR GROUND HEADWIND TANKED UNPRESS
COND 2	BOOSTER B-9U/SPACE TUG STAGE	1HR GROUND TAILWIND TANKED UNPRESS
COND 3	BOOSTER B-9U/SPACE TUG STAGE	1HR GROUND SIDEWIND TANKED UNPRESS
COND 4	BOOSTER B-9U/SPACE TUG STAGE	LIFT OFF +1HR GROUND HEADWINDS
COND 5	BOOSTER B-9U/SPACE TUG STAGE	LIFT OFF +1HR GROUND TAILWINDS
COND 6	BOOSTER B-9U/SPACE TUG STAGE	LIFT OFF +1HR GROUND SIDEWINDS
COND 7	BOOSTER B-9U/SPACE TUG STAGE	ALPHA-Q HEADWINDS
COND 8	BOOSTER B-9U/SPACE TUG STAGE	ALPHA-Q TAILWINDS
COND 9	BOOSTER B-9U/SPACE TUG STAGE	BETA -Q
COND 10	BOOSTER B-9U/SPACE TUG STAGE	2.47G MAX THRUST
COND 11	BOOSTER B-9U/SPACE TUG STAGE	2.47G BOOSTER BURNOUT
COND 12	BOOSTER B-9U	BOOSTER RECOVERY
COND 13	BOOSTER B-9U	BOOSTER SUBSONIC GUST
COND 14	BOOSTER B-9U	BOOSTER 2 POINT LANDING
COND 15	BOOSTER B-9U	BOOSTER 3 POINT LANDING
COND 16	BOOSTER B-9U	BOOSTER 2 G TAXI

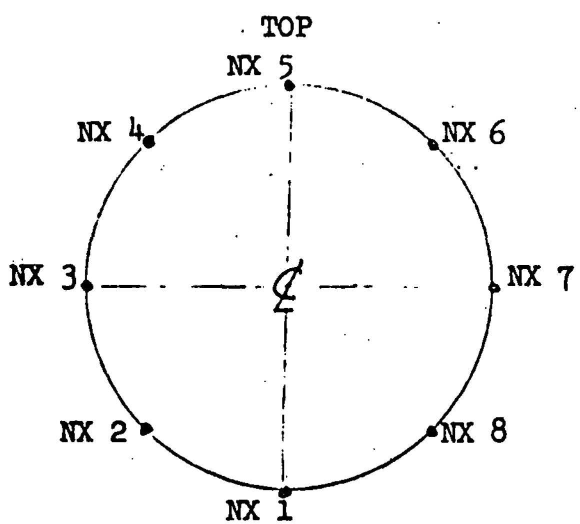

VIEW LOOKING AFT

Table 3-17. Booster B-9U/Space Tug Ultimate Internal Loads

PEAK ULTIMATE AXIAL TENSION LOAD INTENSITIES

STATION (IN)	NX1 (LB/IN)	NX2 (LB/IN)	NX3 (LB/IN)	NX4 (LB/IN)	NX5 (LB/IN)	NX6 (LB/IN)	NX7 (LB/IN)	NX8 (LB/IN)
1000	0(16)	0(16)	0(16)	0(16)	0(11)	0(16)	0(16)	0(16)
1036	5(12)	4(12)	0(15)	0(16)	1(11)	0(16)	0(15)	4(12)
1072	45(12)	32(12)	1(15)	7(8)	12(8)	7(8)	1(15)	32(12)
1131	73(12)	51(12)	3(15)	13(8)	25(8)	13(8)	3(15)	51(12)
1278	141(12)	98(12)	7(15)	37(8)	71(8)	37(8)	7(15)	98(12)
1337	173(12)	121(12)	9(15)	54(8)	99(8)	54(8)	9(15)	121(12)
1341	177(12)	124(12)	8(14)	121(15)	192(15)	121(15)	8(14)	124(12)
1477	288(12)	200(12)	14(14)	110(8)	194(8)	110(8)	14(14)	200(12)
1481	1411(12)	1322(12)	1343(11)	1405(11)	1430(11)	1405(11)	1343(11)	1322(12)
1600	1569(12)	1430(12)	1310(11)	1401(11)	1521(8)	1401(11)	1310(11)	1430(12)
1750	1820(12)	1601(12)	1268(11)	1654(8)	1935(8)	1654(8)	1268(11)	1601(12)
1864	2042(12)	1753(12)	1222(11)	1853(8)	2241(8)	1853(8)	1222(11)	1753(12)
1868	931(12)	640(12)	35(14)	86(13)	140(13)	85(13)	35(14)	640(12)
2006	1520(11)	829(12)	47(14)	155(13)	242(13)	153(13)	47(14)	829(12)
202[illegible]	724(11)	850(12)	48(14)	166(13)	258(13)	164(13)	48(14)	850(12)
202[illegible]	1776(11)	891(12)	45(14)	160(13)	251(13)	158(13)	45(14)	891(12)
2042	1988(11)	959(11)	47(14)	152(13)	[illegible]42(13)	150(13)	47(14)	959(11)
2094	2719(11)	1365(11)	52(14)	141(14)	219(13)	141(14)	52(14)	1365(11)
2098	2760(11)	1386(11)	52(14)	142(14)	217(13)	142(14)	52(14)	1386(11)
2180	3248(11)	1559(11)	60(14)	168(14)	213(14)	168(14)	60(14)	1559(11)
2184	5226(11)	3528(11)	1454(13)	1653(13)	1734(13)	1650(13)	1450(13)	3528(11)
2300	5548(11)	3743(11)	1444(13)	1656(13)	1743(13)	1653(13)	1439(13)	3743(11)
2400	5823(11)	3929(11)	1437(13)	1675(13)	1772(13)	1671(13)	1431(13)	3929(11)
2500	6094(11)	4110(11)	1433(13)	1709(13)	1821(13)	1704(13)	1426(13)	4110(11)
2600	6360(11)	4289(11)	1432(13)	1756(13)	1888(13)	1751(13)	1424(13)	4289(11)
2664	6527(11)	4401(11)	1431(13)	1793(13)	1940(13)	1787(13)	1422(13)	4401(11)

Table 3-17. Booster B-9U/Space Tug Ultimate Internal Loads (Cont)

PEAK ULTIMATE AXIAL TENSION LOAD INTENSITIES

STATION (IN)	NX1 (LB/IN)	NX2 (LB/IN)	NX3 (LB/IN)	NX4 (LB/IN)	NX5 (LB/IN)	NX6 (LB/IN)	NX7 (LB/IN)	NX8 (LB/IN)
2668	6523(11)	4398(11)	1431(13)	1795(13)	1944(13)	1789(13)	1422(13)	4397(11)
2800	5918(11)	3953(11)	1429(13)	1886(13)	2072(13)	1879(13)	1419(13)	3953(11)
2864	5627(11)	3741(11)	1429(13)	1937(13)	2144(13)	1930(13)	1418(13)	3741(11)
2868	5608(11)	3727(11)	1429(13)	1940(13)	2149(13)	1933(13)	1418(13)	3727(11)
2950	5218(11)	3440(11)	1428(13)	2015(13)	2254(13)	2007(13)	1417(13)	3440(11)
3050	4462(11)	3103(12)	1428(12)	2172(13)	2477(13)	2164(13)	1428(12)	3102(12)
3161	3683(12)	3033(12)	1464(12)	2487(13)	2921(13)	2477(13)	1464(12)	3033(12)
3165	3615(12)	2980(12)	1448(12)	2497(13)	2938(13)	2487(13)	1448(12)	2980(12)
3293	2979(12)	2538(12)	1473(12)	2631(16)	3721(16)	2631(16)	1473(12)	2538(12)
3295	2968(12)	2530(12)	1473(12)	2643(16)	3737(16)	2643(16)	1473(12)	2530(12)
3373	2475(12)	2185(12)	1486(12)	2737(13)	3272(13)	2726(13)	1486(12)	2185(12)
3377	2394(12)	2123(12)	1469(12)	2742(13)	3281(13)	2730(13)	1469(12)	2123(12)
3538	1465(12)	1471(12)	1486(12)	2654(13)	3156(13)	2642(13)	1486(12)	1471(12)
3542	1391(12)	1414(12)	1469(12)	2651(13)	3155(13)	2639(13)	1469(12)	1414(12)
3679	943(12)	1105(12)	1559(13)	2228(13)	2506(13)	2229(13)	1561(13)	1105(12)
3683	-609(12)	-442(12)	25(13)	770(16)	1088(16)	770(16)	26(13)	-442(12)
3820	-447(16)	-316(16)	16(13)	516(12)	743(12)	516(12)	16(13)	-316(16)
3921	-119(16)	-84(16)	15(13)	132(12)	196(12)	132(12)	15(13)	-84(16)
3925	452(11)	401(11)	280(10)	261(7)	277(7)	261(7)	280(10)	401(11)
4065	0(7)	1(6)	1(6)	1(6)	0(7)	0(7)	0(7)	0(7)
4069	0(16)	1(6)	1(6)	1(6)	0(6)	0(16)	0(16)	0(16)
4300	0(16)	0(16)	0(16)	0(16)	0(16)	0(16)	0(16)	0(16)

Table 3-18. Booster B-9U/Space Tug Ultimate Internal Loads

PEAK ULTIMATE AXIAL COMPRESSION LOAD INTENSITES

STATION (IN)	NX1 (LB/IN)	NX2 (LB/IN)	NX3 (LB/IN)	NX4 (LB/IN)	NX5 (LB/IN)	NX6 (LB/IN)	NX7 (LB/IN)	NX8 (LB/IN)
1000	-1(11)	-1(11)	-0(10)	-0(6)	-0(5)	-0(5)	-0(10)	-1(11)
1036	-5(11)	-4(11)	-2(10)	-4(12)	-5(12)	-4(12)	-2(10)	-4(11)
1072	-25(8)	-19(8)	-12(9)	-34(12)	-47(12)	-34(12)	-7(7)	-19(8)
1131	-58(8)	-46(8)	-31(9)	-53(12)	-75(12)	-53(12)	-19(10)	-46(8)
1278	-159(8)	-125(8)	-86(9)	-105(12)	-147(12)	-105(12)	-49(7)	-125(8)
1337	-209(8)	-164(8)	-109(9)	-132(12)	-185(12)	-132(12)	-62(7)	-164(8)
1341	-295(15)	-224(15)	-112(9)	-136(12)	-189(12)	-136(12)	-63(7)	-224(15)
1477	-384(8)	-299(8)	-181(9)	-225(12)	-313(12)	-225(12)	-107(7)	-299(8)
1481	-135(15)	-107(15)	-49(4)	-58(16)	-82(16)	-58(16)	-70(6)	-107(15)
1600	-355(5)	-270(5)	-66(4)	-111(16)	-158(16)	-111(16)	-88(6)	-283(6)
1750	-724(6)	-538(6)	-89(6)	-154(16)	-218(16)	-154(16)	-133(3)	-537(6)
1864	-1073(4)	-863(10)	-549(10)	-235(10)	-234(16)	-235(10)	-549(10)	-863(10)
1868	-4977(4)	-4714(6)	-4063(6)	-3399(5)	-3140(5)	-3399(5)	-4026(4)	-4698(4)
2006	-4130(4)	-4259(6)	-4602(6)	-4919(5)	-5071(5)	-4919(5)	-4554(4)	-4254(4)
2022	-4026(4)	-4204(6)	-4671(6)	-5111(5)	-5432(10)	-5111(5)	-4622(4)	-4201(4)
2026	-3999(4)	-4190(6)	-4688(6)	-5159(5)	-5548(10)	-5159(5)	-4639(4)	-4187(4)
2042	-3892(4)	-4133(6)	-4755(6)	-5348(5)	-6009(10)	-5348(5)	-4704(4)	-4130(4)
2094	-3525(4)	-3928(6)	-4957(6)	-6379(10)	-7495(10)	-6379(10)	-4903(4)	-3928(4)
2098	-3505(4)	-3919(4)	-4972(6)	-6456(10)	-7592(10)	-6456(10)	-4918(4)	-3919(4)
2180	-3272(4)	-3844(4)	-5284(6)	-7795(10)	-9243(10)	-7796(10)	-5225(4)	-3844(4)
2184	-2745(4)	-3322(4)	-4773(6)	-6192(6)	-7331(10)	-6188(5)	-4714(4)	-3322(4)
2300	-2607(4)	-3230(4)	-4797(6)	-6333(6)	-7704(10)	-6328(5)	-4735(4)	-3230(4)
2400	-2486(4)	-3150(4)	-4813(6)	-6450(6)	-8019(10)	-6445(5)	-4752(4)	-3150(4)
2500	-2425(2)	-3075(4)	-4827(6)	-6614(10)	-8331(10)	-6614(10)	-4770(4)	-3075(4)
2600	-2410(2)	-3000(4)	-4838(6)	-6841(10)	-8639(10)	-6841(10)	-4787(4)	-3000(4)
2664	-2401(2)	-2953(4)	-4845(6)	-6985(10)	-8833(10)	-6985(10)	-4798(4)	-2984(3)

Table 3-18. Booster B-9U/Space Tug Ultimate Internal Loads (Cont)

PEAK ULTIMATE AXIAL COMPRESSION LOAD INTENSITES

STATION (IN)	NX1 (LB/IN)	NX2 (LB/IN)	NX3 (LB/IN)	NX4 (LB/IN)	NX5 (LB/IN)	NX6 (LB/IN)	NX7 (LB/IN)	NX8 (LB/IN)
2668	-2405(2)	-2954(4)	-4846(6)	-6985(10)	-8833(10)	-6985(10)	-4799(4)	-2988(3)
2800	-2682(2)	-3163(4)	-4877(6)	-6695(10)	-8399(10)	-6695(10)	-4828(4)	-3226(3)
2864	-2818(2)	-3262(4)	-4889(6)	-6549(10)	-8184(10)	-6549(10)	-4868(3)	-3343(3)
2868	-2826(2)	-3269(4)	-4890(6)	-6541(10)	-8171(10)	-6541(10)	-4873(3)	-3350(3)
2950	-3007(2)	-3401(4)	-4908(6)	-6443(5)	-7896(10)	-6443(5)	-4983(3)	-3505(3)
3050	-3303(2)	-3659(4)	-5012(6)	-6405(5)	-7627(10)	-6405(5)	-5178(3)	-3765(3)
3161	-3658(2)	-3973(4)	-5149(6)	-6375(5)	-7328(10)	-6375(5)	-5414(3)	-4077(3)
3165	-3671(2)	-3984(4)	-5153(6)	-6374(5)	-7316(10)	-6374(5)	-5423(3)	-4089(3)
3293	-4025(2)	-4260(4)	-5233(6)	-6267(5)	-6874(10)	-6267(5)	-5645(3)	-4392(3)
3295	-4031(2)	-4264(4)	-5234(6)	-6265(5)	-6866(10)	-6265(5)	-5648(3)	-4397(3)
3373	-4225(2)	-4396(4)	-5250(6)	-6170(5)	-6566(5)	-6170(5)	-5764(3)	-4559(3)
3377	-4235(2)	-4402(4)	-5251(6)	-6165(5)	-6559(5)	-6165(5)	-5770(3)	-4567(3)
353[illegible]	-4653(2)	-4673(4)	-5284(6)	-5960(5)	-6252(5)	-5998(3)	-6017(3)	-4911(3)
3542	-4664(2)	-4680(4)	-5285(6)	-5955(5)	-6244(5)	-5999(3)	-6023(3)	-4920(3)
3679	-5127(2)	-5024(4)	-5413(6)	-5855(5)	-6140(1)	-6082(3)	-6313(3)	-5303(3)
3683	-6751(7)	-6567(7)	-6838(6)	-7522(10)	-7990(8)	-7522(10)	-6962(3)	-6567(7)
3820	-6767(7)	-6726(4)	-6906(6)	-7126(10)	-7357(10)	-7126(10)	-7217(3)	-6726(4)
3921	-7015(5)	-7024(5)	-7047(4)	-7078(4)	-7090(4)	-7078(4)	-7472(3)	-7024(5)
3925	-243(12)	-184(12)	-42(12)	70(15)	74(1)	70(15)	-42(12)	-184(12)
4065	-0(15)	-0(15)	-0(15)	-0(15)	-0(15)	-1(6)	-1(6)	-1(6)
4069	0(16)	0(16)	0(16)	0(16)	0(16)	-1(6)	-1(6)	-1(6)
4300	0(16)	0(16)	0(16)	0(16)	0(16)	0(16)	0(16)	0(16)

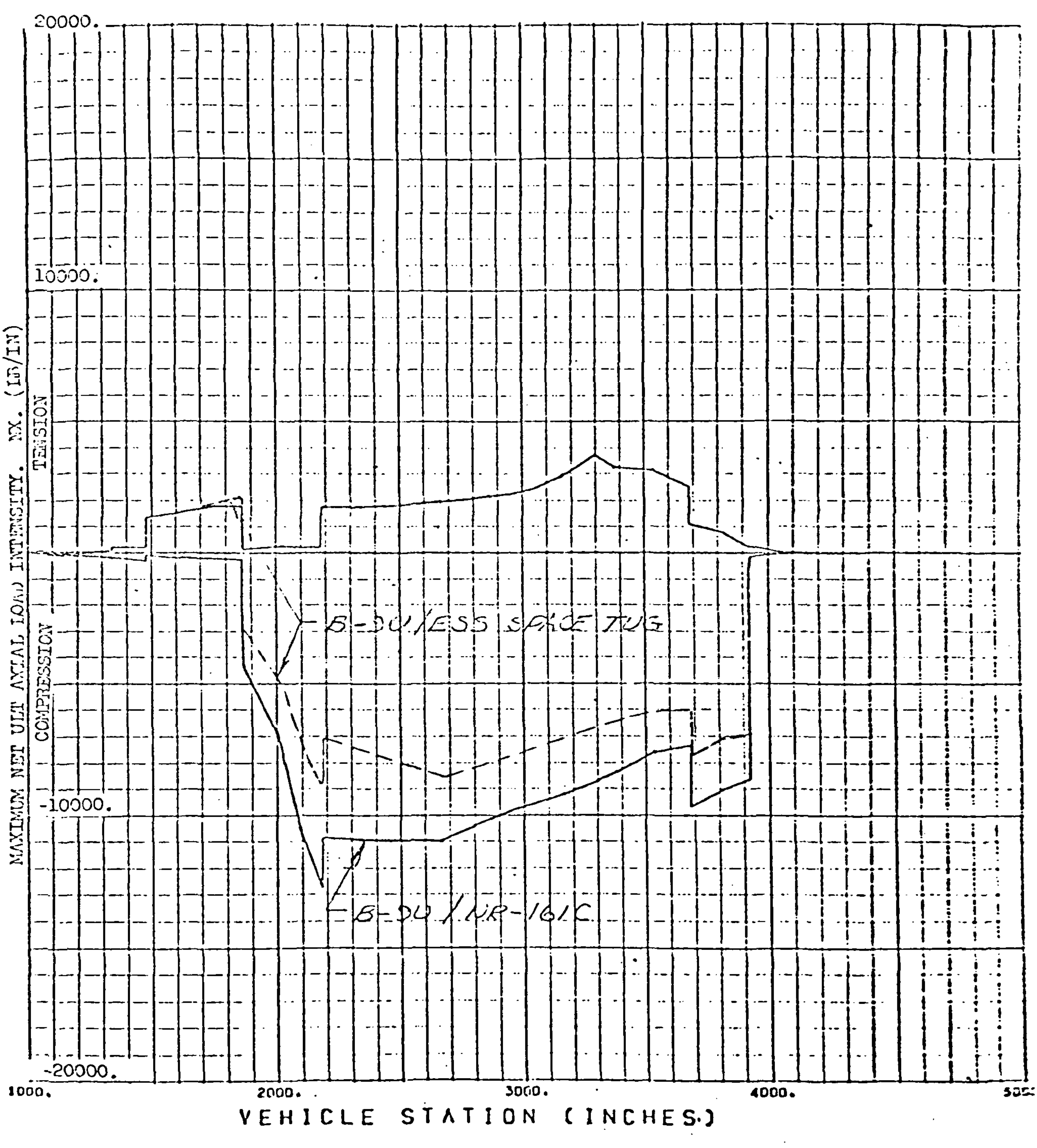

Figure 3-34. Internal Loads at the Top Centerline

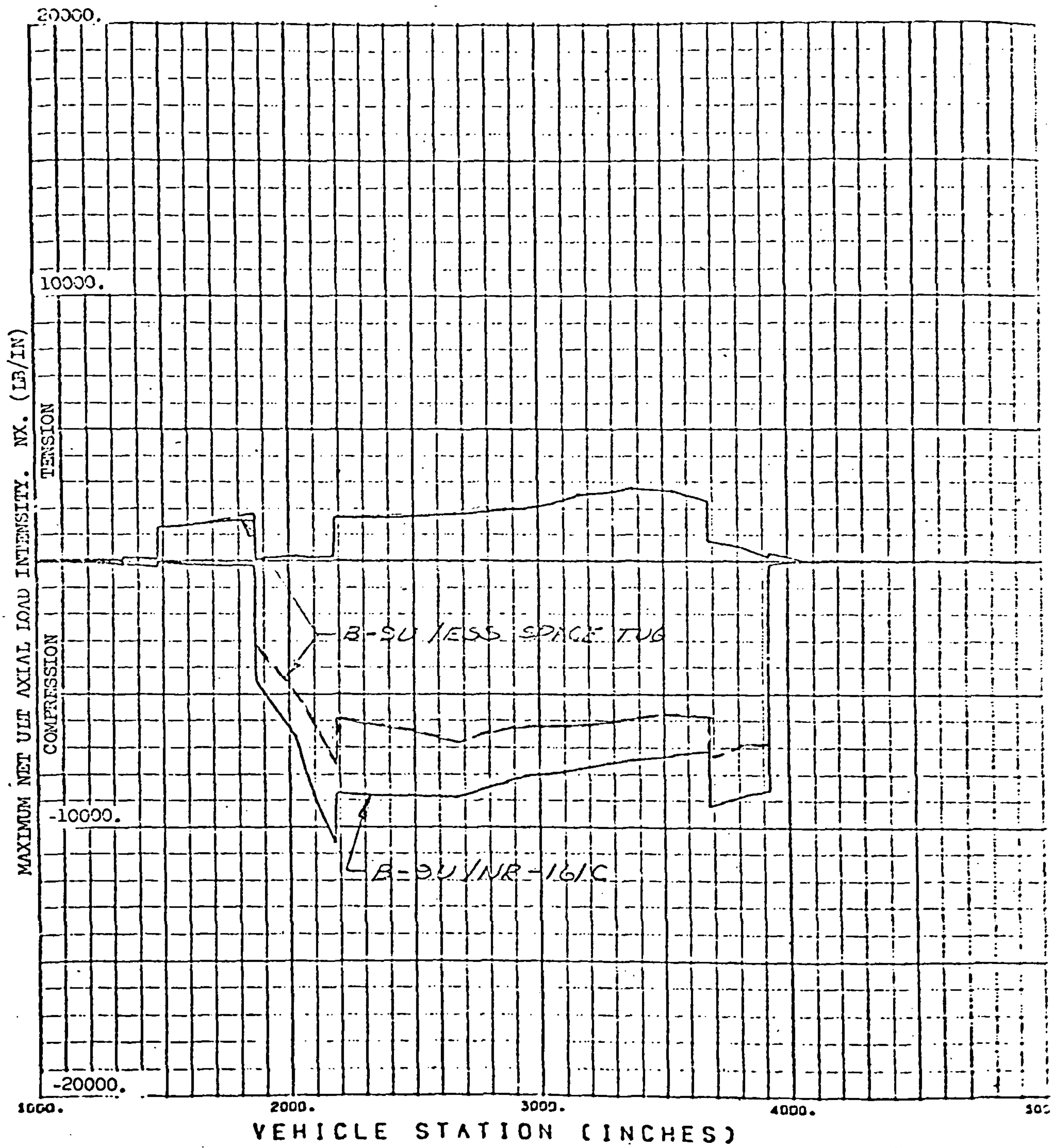

Figure 3-35. Internal Loads 45 Degrees from the Top

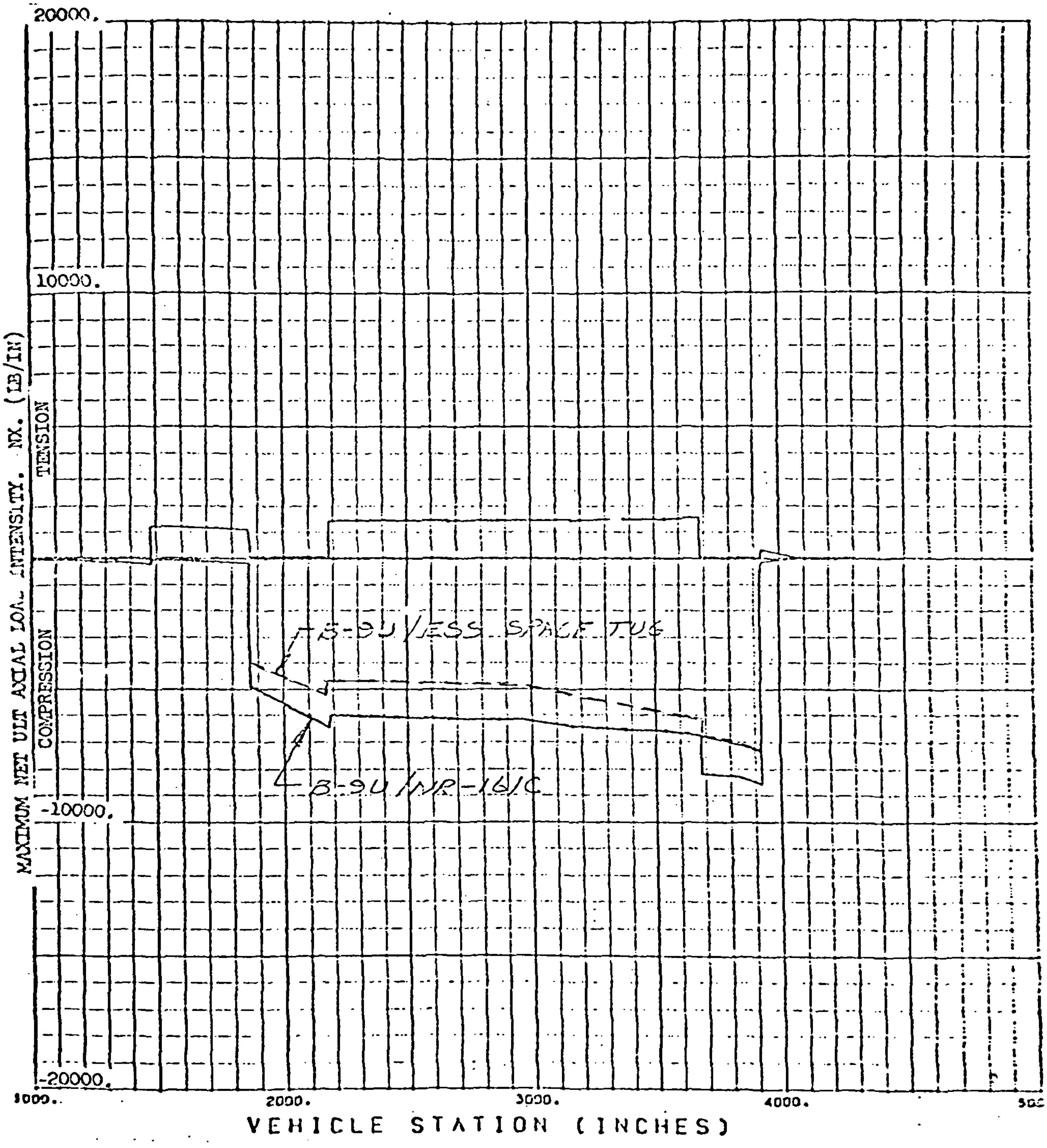

Figure 3-36. Internal Loads at the Side

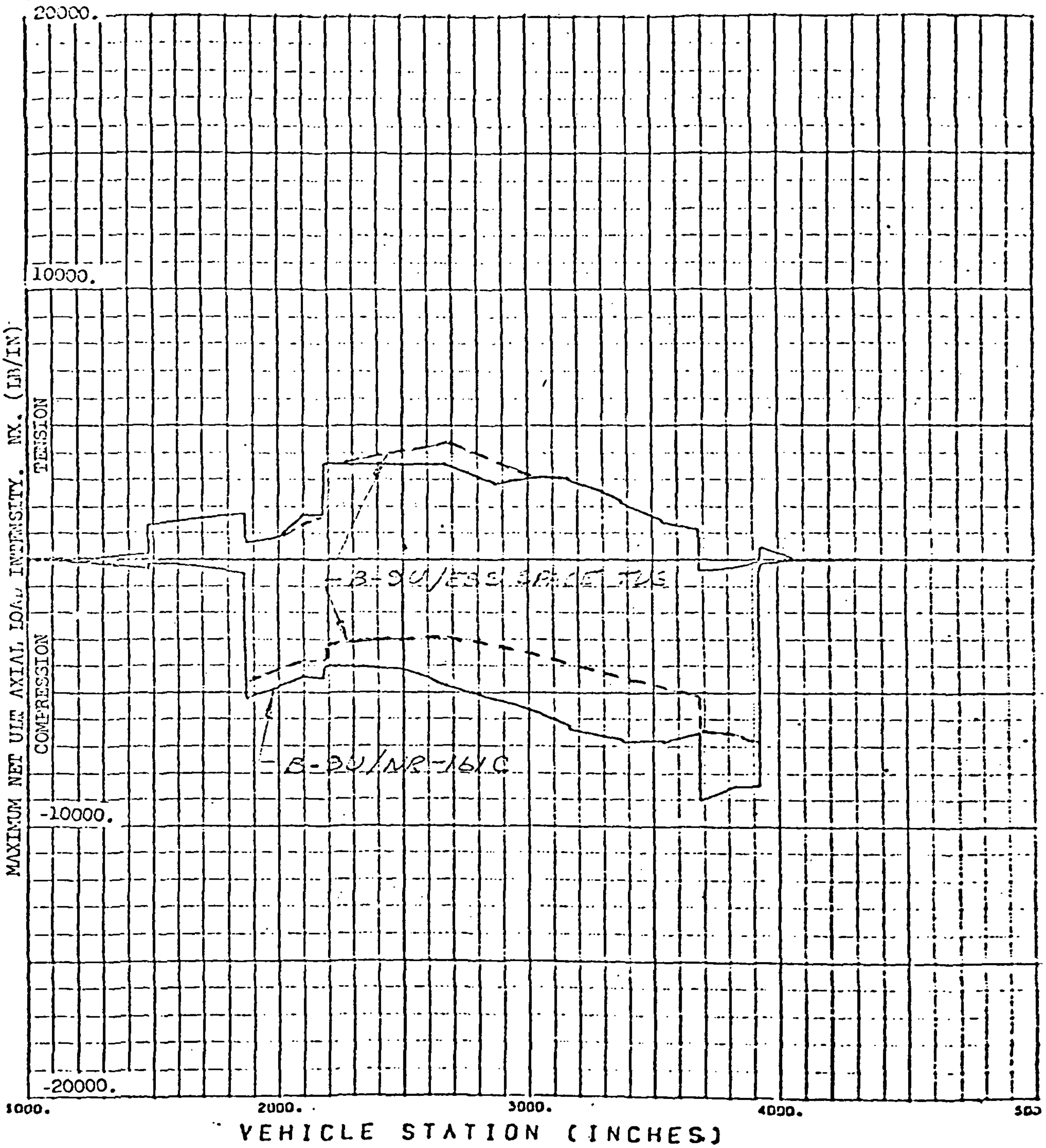

Figure 3-37. Internal Loads 45 Degrees from the Bottom

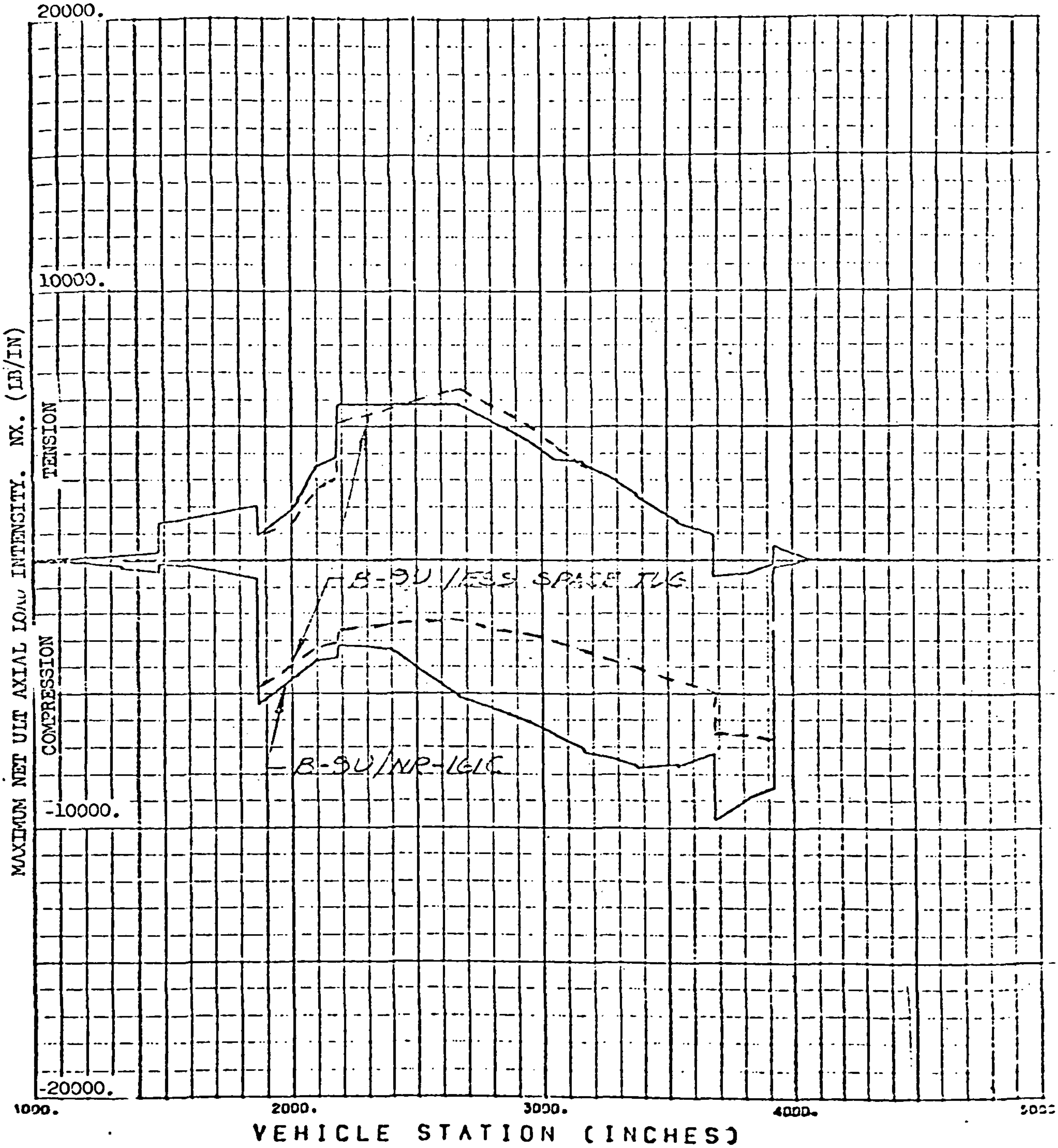

Figure 3-38. Internal Loads at Bottom Centerline

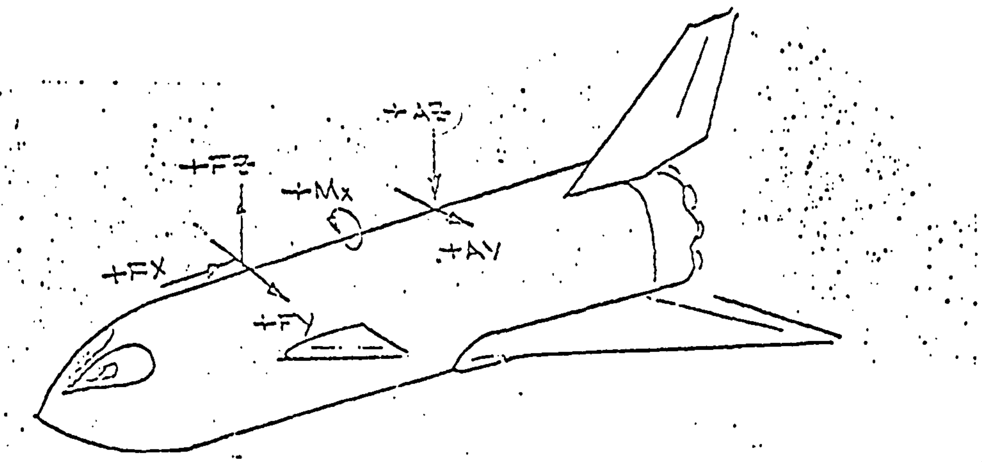

B-9U/ESS - SPACE TUG (LIMIT LOADS)

CONDITION	WIND	Fx (x 10^3 lb)	Fy (x 10^3 lb)	Fz (x 10^3 lb)	Ay (x 10^3 lb)	Az (x 10^3 lb)	Mx (10^6 in/lb)
Two Week Ground Winds Unfueled	Head	216		96.7		82.9	
	Tail	216		-108.		56.9	
	Side	216	±161	52.6	∓1.61	58.5	∓33.3
1 Hour Ground Winds Fueled Unpressurized	Head	691		184		197	
	Tail	691		128		190	
	Side	691	±44.2	172	∓ .443	191	∓9.17
Dynamic Lift Off + 1 Hour Ground Winds	Head	975		247		283	
	Tail	974		204		262	
	Side	974	±34.2	241	∓9.81	269	∓5.23
Max. α-q	Head	1506		366		511	
	Tail	1422		249		308	
Max. β-q	Side	1389	±125	302	∓38.8	393	∓18.65
2.47 Max. Thrust	-	1874		423		556	
Booster Burnout	-	1860		353		616	

Figure 3-39. Design Attachment Loads

	DELTA WEIGHT INCREASE		CRITICAL CONDITION
	THEORETICAL	INSTALLED	
LOX TANK			
DOMES	0 lbs	0 lbs	
FRAMES	0 lbs	0 lbs	
SKIN-STRINGER	0 lbs	0 lbs	
BULKHEADS	283 lbs	354 lbs	Max α q
LH_2 TANK			
DOMES	0 lbs	0 lbs	
FRAMES	0 lbs	0 lbs	
SKIN-STRINGER	30 lbs	39 lbs	1 Hour Ground Winds
BULKHEADS	597 lbs	685 lbs	2.5 g Max. Thrust
LOCAL SKIN BEEF-UP	149 lbs	186 lbs	2.5 g Max. Thrust
INTERTANK ADAPTER	0 lbs	0 lbs	
THRUST STRUCTURE	0 lbs	0 lbs	
TOTAL BOOSTER STRUCTURE		1264 lbs	

Figure 3-40. ESS/Nuclear Stage Delta Weight Estimates

	DELTA WEIGHT INCREASE		CRITICAL CONDITION
	THEORETICAL	INSTALLED	
LOX TANK			
DOMES	0 lbs	0 lbs	
FRAMES	0 lbs	0 lbs	
SKIN-STRINGER	0 lbs	0 lbs	
BULKHEADS	260 lbs	325 lbs	Max. βq
LH_2 TANK			
DOMES	0 lbs	0 lbs	
FRAMES	46 lbs	51 lbs	1 Hour Ground Winds / 2.06 g Max. Thrust
SKIN-STRINGER	371 lbs	476 lbs	1 Hour Ground Winds / 2.06 g Max. Thrust
BULKHEADS	640 lbs	735 lbs	2.06 g Max. Thrust
LOCAL SKIN BEEF-UP	160 lbs	200 lbs	2.06 g Max. Thrust
INTERTANK ADAPTER	0 lbs	0 lbs	
THRUST STRUCTURE	910 lbs	1365 lbs	1 Hour Ground Wind
TOTAL BOOSTER STRUCTURE		3152 lbs	

Figure 3-41. ESS/MDAC STage Delta Weight Estimates

4.0 PROGRAM CONCEPTS

4.1 ESS (S-II) LAUNCH PAD SERVICING STUDY

The GSE launch pad servicing of the ESS was investigated, with the following results:

OPTION I

Retain baseline ("Belly to the Tower") and redesign S-II to accept aft service connections with launcher rise-off disconnect pylon.

RATIONA-LE

1. Routing of the ESS forward connections to the aft area will add considerable weight to the ESS. New systems tunnels will be required. The LH_2 vent lines, vent valve actuation lines, tank pressure lines, thermal control line, hazardous-gas detection line, and electrical cables will have to be routed to the aft area.

2. The LH_2 fill line, LO_2 fill line, 24 pneumatic lines, and electrical cables on the S-II aft swing arm have to be rerouted for rise-off separation, which adds weight to the ESS.

3. No qualified hardware for rise-off disconnects is available.

4. The complete umbilical system will have to be redesigned and requalified.

5. Without the forward swing arm, there can be no entry into the ESS forward section for inspection or repair of the LH_2 tank and the tank vent system or entry into the payload area after T-12 hours.

6. To permit entry into the above areas before T-12 hours, the MSS will have to be modified to reach the forward access door.

OPTION II

Retain baseline and modify pad to include service tower adjacent to the launcher, with swing arms compatible with S-II service connections.

RATIONALE

1. Umbilical carrier plates, disconnects, and swing arms can be used as previously qualified for Saturn launch operations.

2. Separation at liftoff provides maximum safety for the launch vehicle.

3. No changes required for stage structures, fluid systems plumbing, or electrical cable routing.

4. Launch abort before liftoff has the umbilical connected for detanking and switchover to ground power for stage operations and safing procedures.

5. Since the new tower will be approximately 200 feet high, the flight path will have to be accurately determined.

OPTION III

Modify baseline to booster "Belly away from Tower".

RATIONALE

1. Dependent on the actual location of the ESS relative to the launch tower, the length of the swing arms and the location of the umbilical withdrawal mechanism will have to be modified.

2. The umbilical carrier plates and disconnects can be used as qualified for Saturn launch operations.

3. The service of the shuttle booster is not defined for this configuration.

4.2 CONVAIR LAUNCH PAD

Modify the ESS as required to obtain single-point aft umbilical.

- Consider ESS with nonejectable aft skirt extension.
- Consider ESS with an ejectable aft skirt extension.

Routing the LH_2 tank vent aft on either of the two configurations will violate MSFC Saturn V ground rules, which are based on engineering judgments to maintain as great a separation as possible between GH_2 and GO_2 vent systems. The GO_2 vent should face away from the tower and/or approximately 180 degrees from the LH_2 vent. GO_2 is vented to the atmosphere, GH_2 to a burn stack through a service arm. Forward and aft separation should also be as great as possible.

In order to obtain good separation between the GH_2 and GO_2 vents, additional valving in the GH_2 vent should be considered, which would provide forward venting after liftoff and prevent the aft (service arm) vent from expelling GH_2 into the ESS and/or booster engine plumes.

Routing the forward service connections aft will require an additional external tunnel large enough to contain the forward connections.

On the S-II of the Saturn V, the forward and aft swing arms are in line, in a plan view. On the ESS, therefore, as the additional tunnel containing the forward connections approaches the vicinity of the aft service connection area, the tunnel should "fan" out to a very wide tunnel, permitting the aft connections to be encompassed. This assumes that the single aft servicing point would be near the end of the aft skirt extension.

An alternative to the above approach is to use two tunnels. The second tunnel would be used for the aft service connections, and it would be "clocked" (rotated) to clear aerodynamically the forward tunnel. (The forward tunnel should remain in its current location to maintain the approximately 180-degree separation from the LO_2 tank vent.) This approach would probably require two swing arms.

An alternative to the two-tunnel approach is to locate the swing arms (probably two) at the elevation station in the aft service area. This would require only the additional tunnel for the forward connections and obviate complexities associated with running the second tunnel aft on the ESS configuration with an ejectable aft skirt. (An ejectable aft skirt would require disconnects at the separation plane.)

Refer to Volume II for a discussion of the selected system.

APPENDIX A. HEATING RATES FOR ESS WITH MDAC SPACE STATION PAYLOAD WITH PROTUBERANCES – MATED INTERFERENCE HEATING INCLUDED

Heating rates presented herein are for the ESS mated to the B-9U booster. The 2/15/71 trajectory and the 1963 Patrick atmosphere were used. The heating rates, which do not account for any separated flow region exhaust gas heating, are to be used as preliminary design values pending final definition of the configuration or wind tunnel tests, or direction from NASA.

Heat transfer coefficients, h_c, for ESS Stations 0, 451, and 962 are presented in Figures A-1a, A-1b, and A-1c, respectively. The effect of interference heating decay on the side of the ESS is also shown as a function of the local angle. The heat transfer coefficients have been determined for calorically and thermally perfect air ($\gamma = 1.4$) and a wall temperature of 540 R. The associated recovery temperature, T_r, is presented in Figure A-2.

The heat transfer rate to the 540 R wall (in the absence of ESS or payload protuberances) is obtained using $\dot{q} = h_c (T_r - T_w)$. For other wall temperatures, following NASA MSFC practice, h_c is not changed.

The protuberances on the ESS and the associated protuberance-influenced regions are shown in Figure A-3. The heating rates on these protuberances or in the protuberance-influenced regions (in the absence of payload protuberances) are found using $\dot{q} = (PF)(h_c)(T_r - T_w)$. The protuberance factors, PF, are determined using Figures A-4 through A-16. Where protuberance regions overlap, the product of the individual protuberance factors is used.

A multiplying factor, MF, is used to account for the influence of the payload protuberances on the ESS heating rates. Thus, $\dot{q} = (MF)(PF)(h_c)(T_r - T_w)$. Figure A-17 shows the variation of MF with ESS station, local angle, and flight time. The (MF) (PF) (h_c) product, which includes the effect of mated interference heating in each factor, provides an upper limit for the heating rate. A more refined study is in progress to improve the present analysis.

The protuberance factors for the protuberances in Figures A-4 through A-10 require no further explanation. However, further explanation is required for the attachment fittings and drag strut cylinders calculated using Figures A-11 through A-16. Figure A-11 shows the protuberance factors for the vicinity of the drag strut due to the radial and longitudinal struts. However, the presence of a pyramidal attachment fitting complicates the situation.

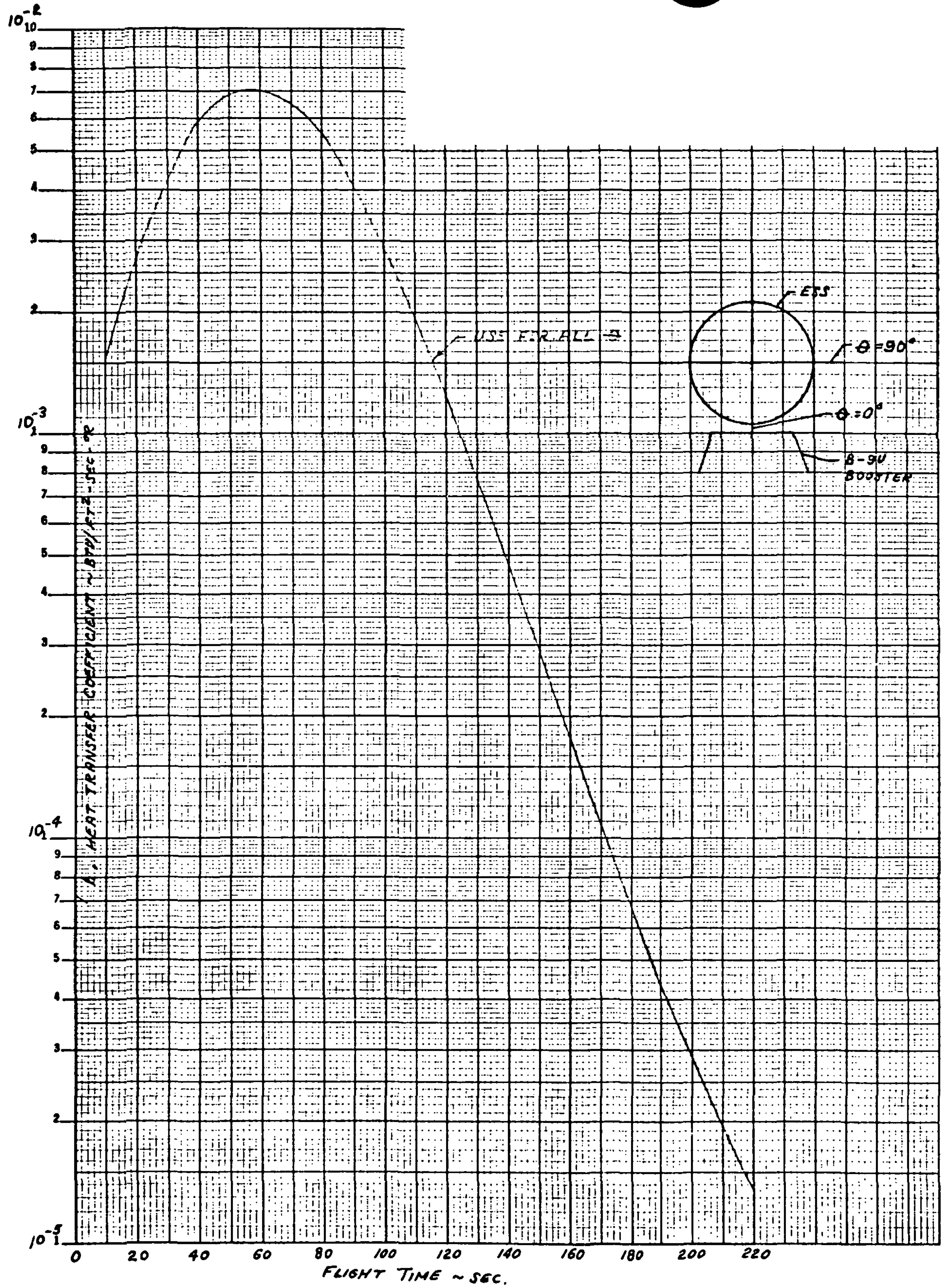

Figure A-1. ESS and MDAC Payload Basic Heat Transfer Coefficient, Including Mated Interference Heating

(a) Station 0

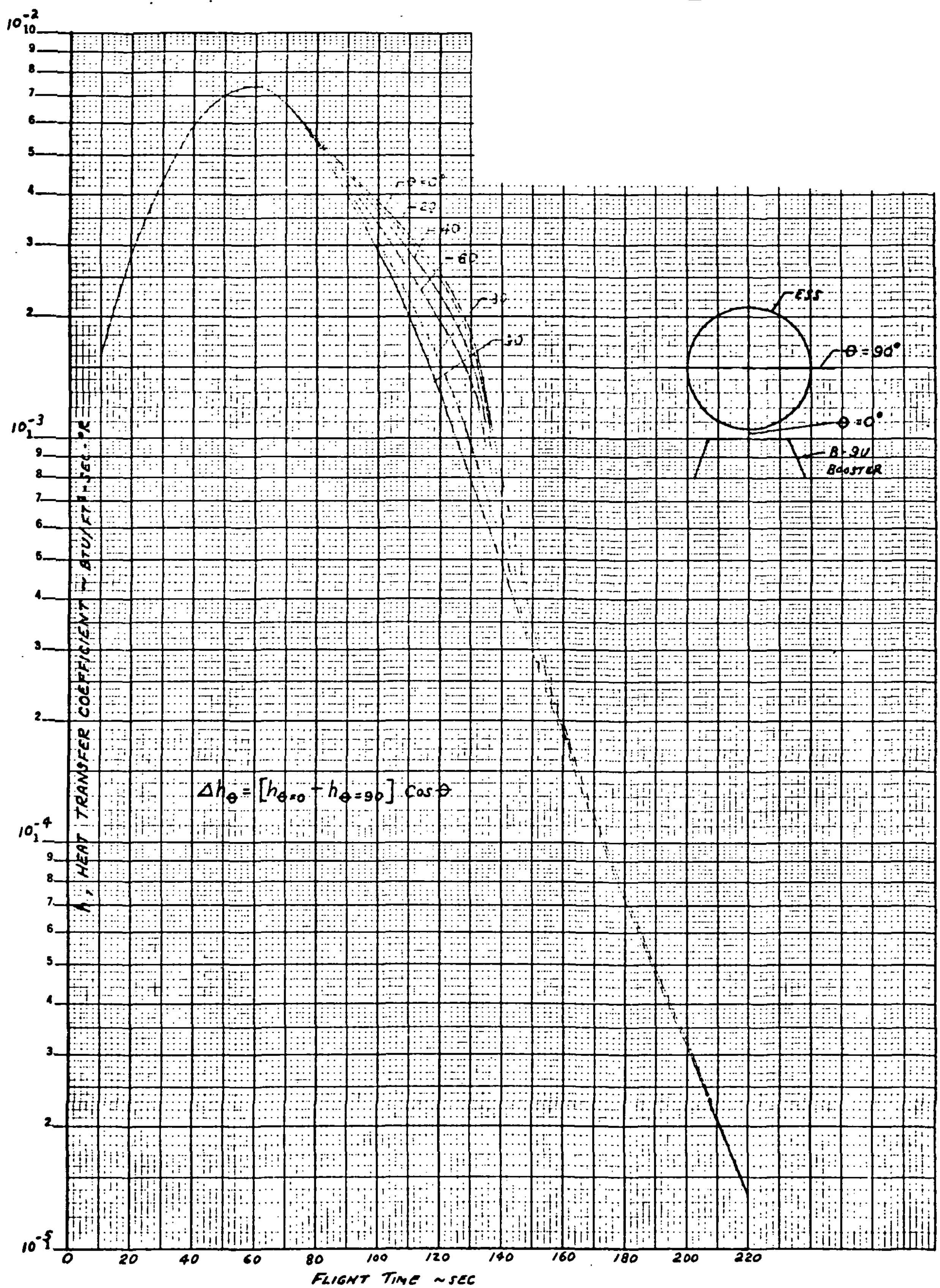

Figure A-1. ESS and MDAC Payload Basic Heat Transfer Coefficient, Including Mated Interference Heating
(b) Station 451

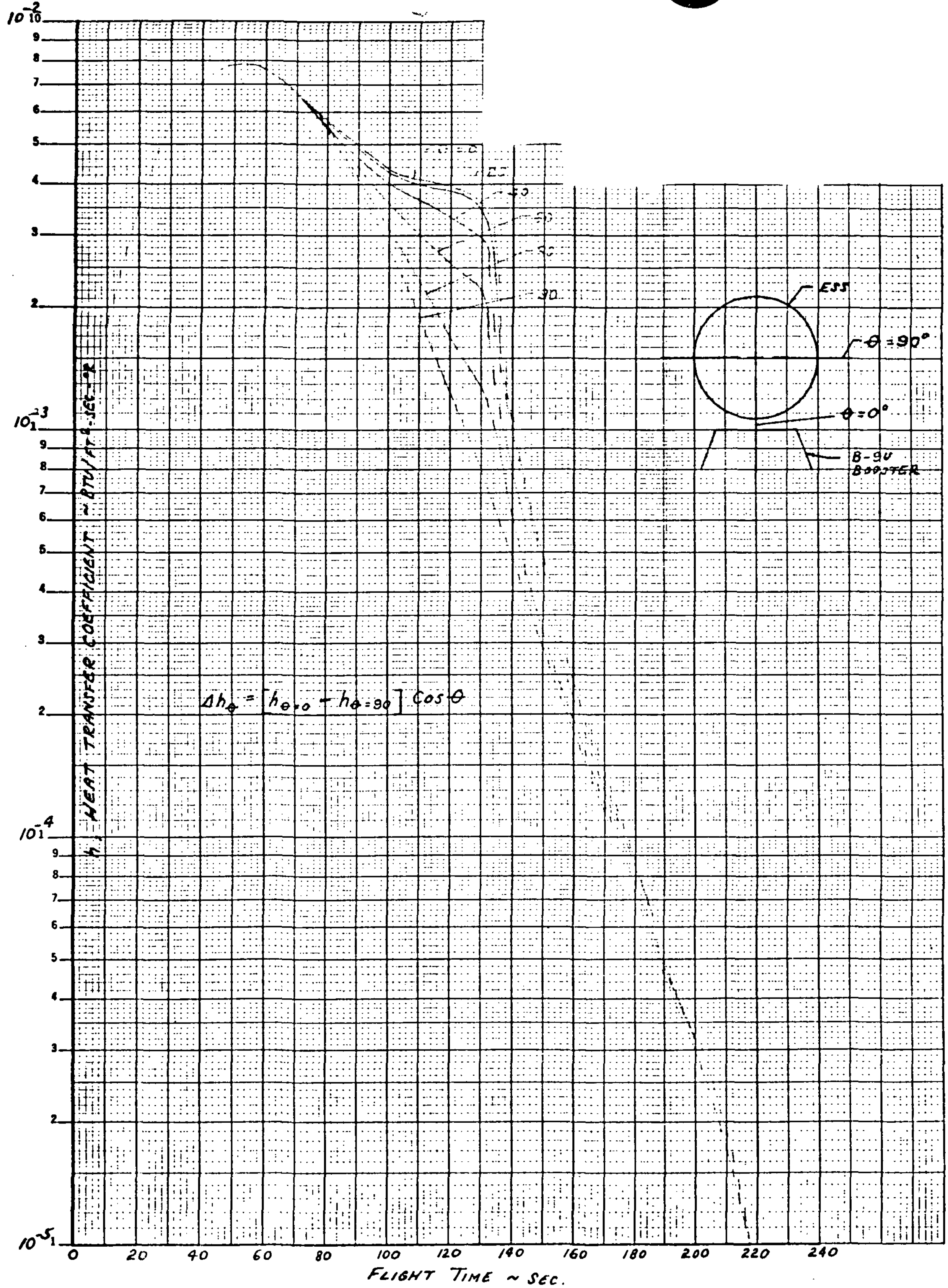

Figure A-1. ESS and MDAC Payload Basic Heat Transfer Coefficient, Including Mated Interference Heating
(c) Station 962

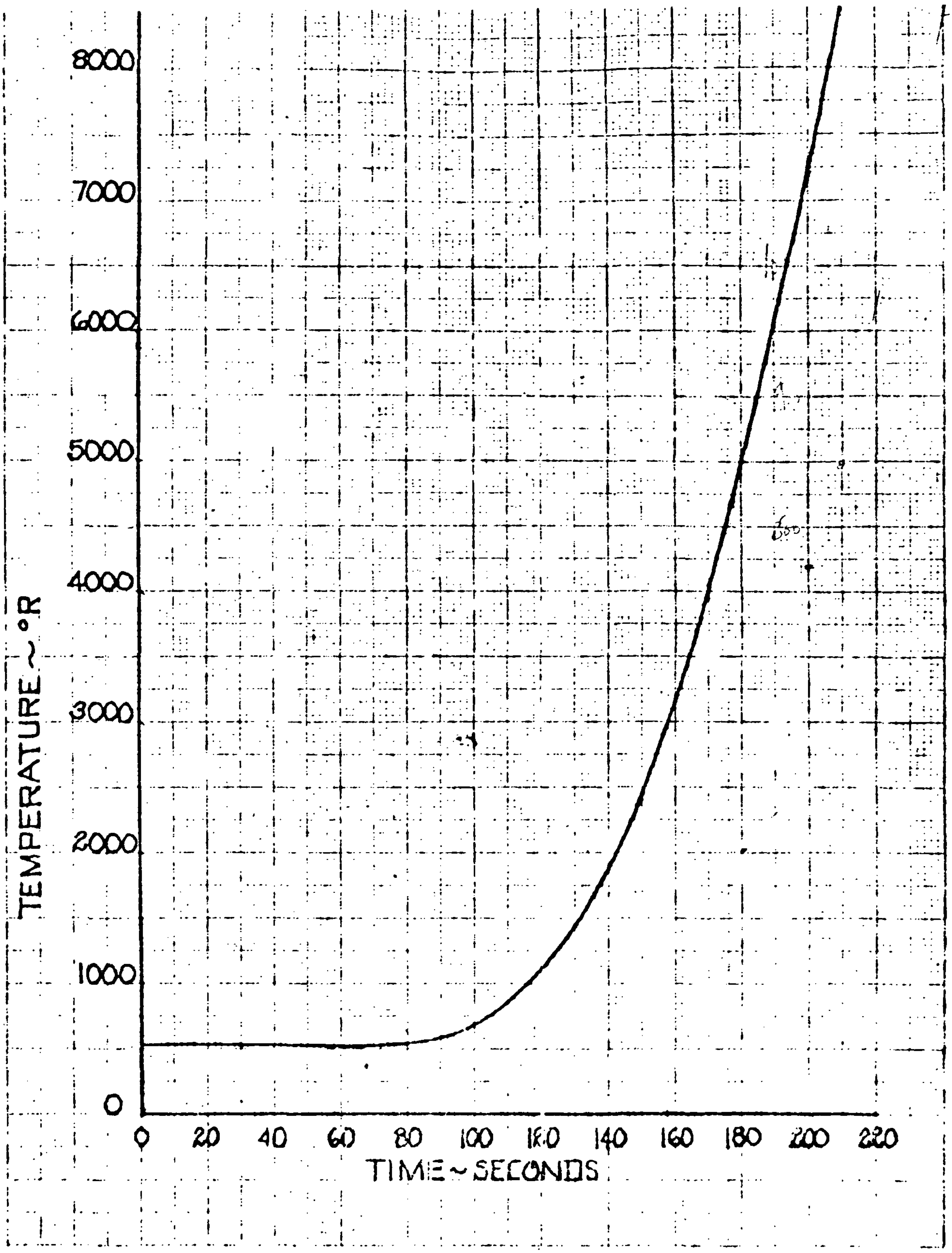

Figure A-2. Recovery Temperature for ESS Basic Sidewall

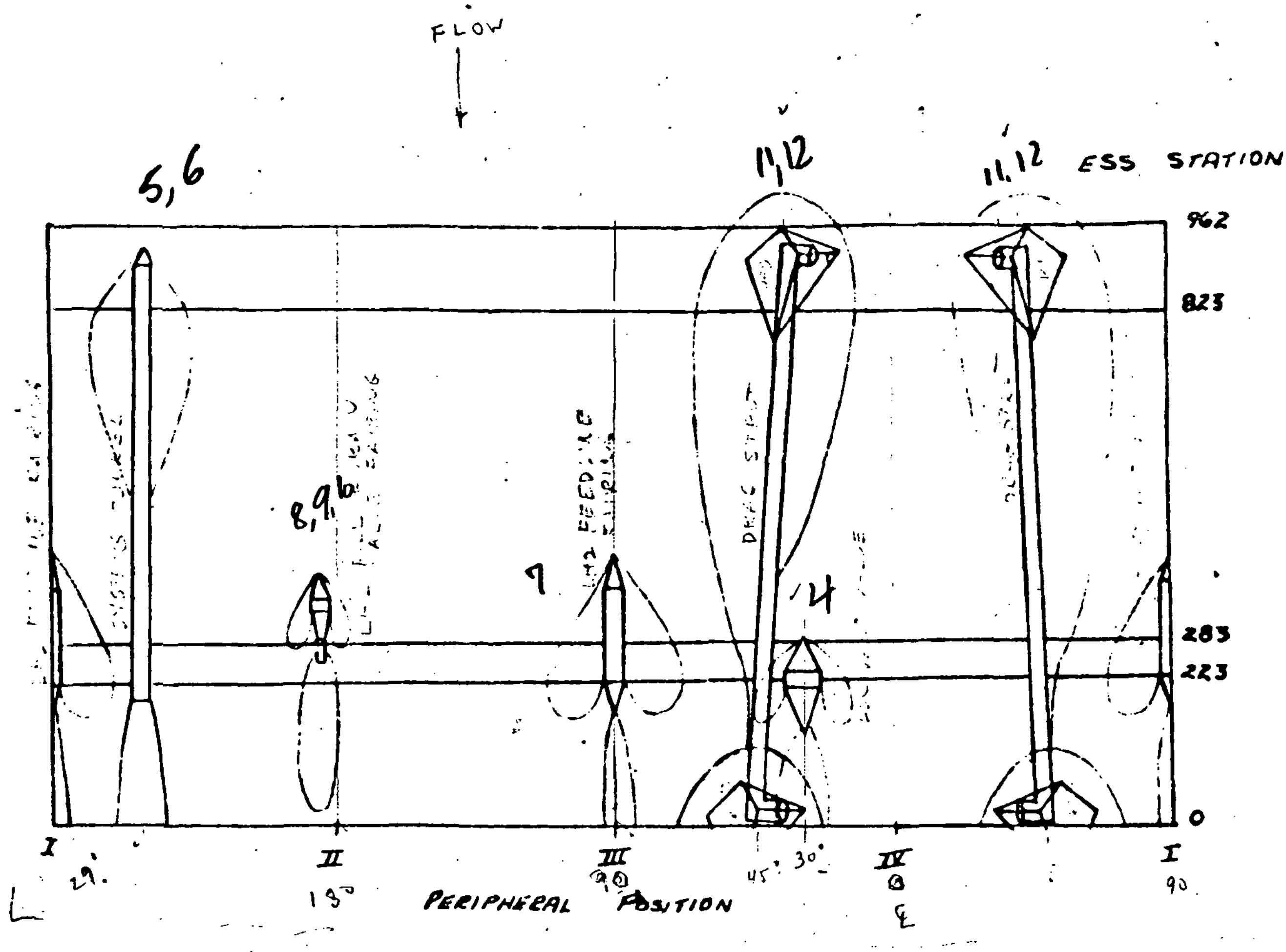

Figure A-3. ESS Protuberance and Protuberance Influenced Regions

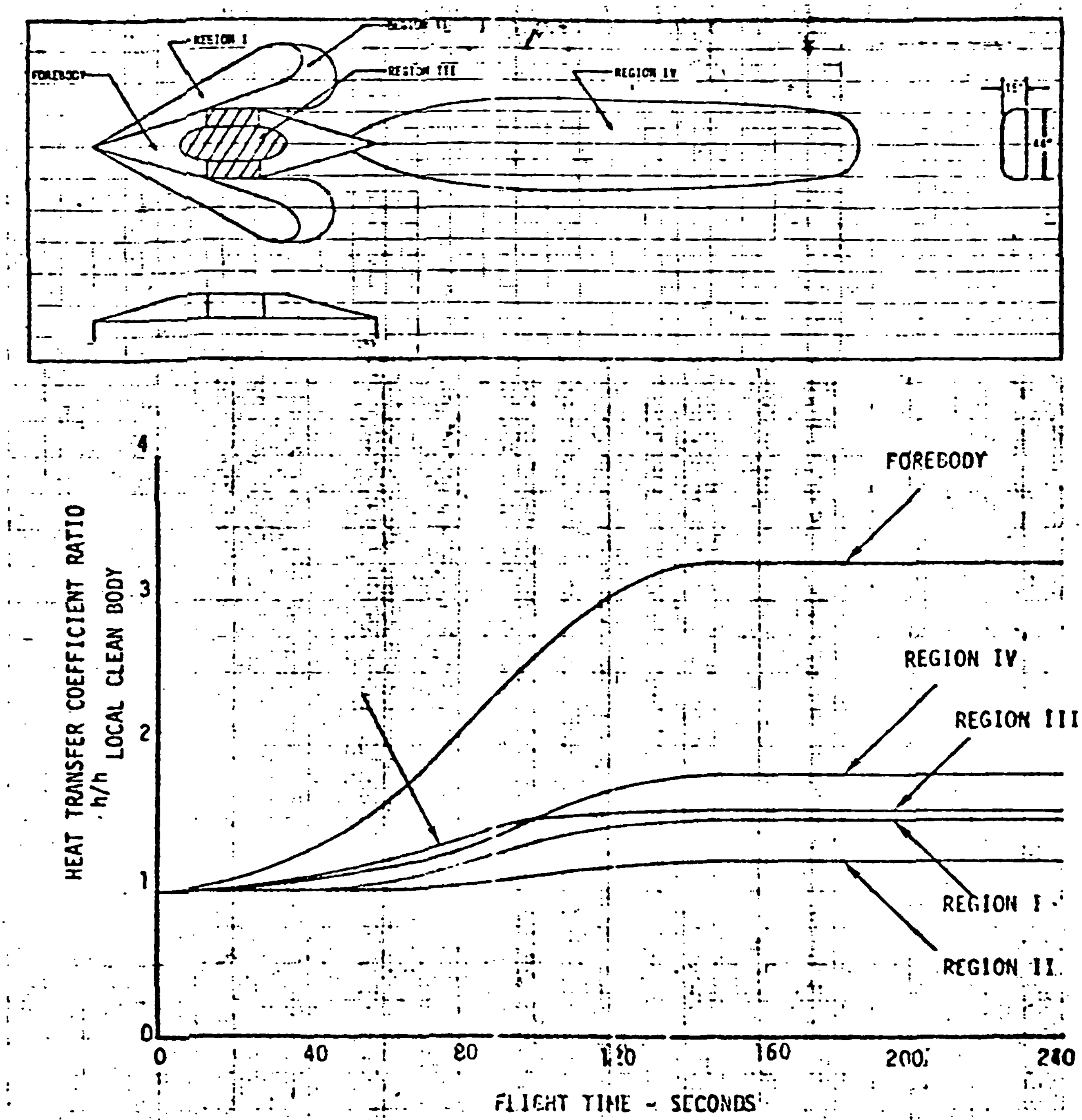

Figure A-4. Aerodynamic Heating for the LOX Vent Valve

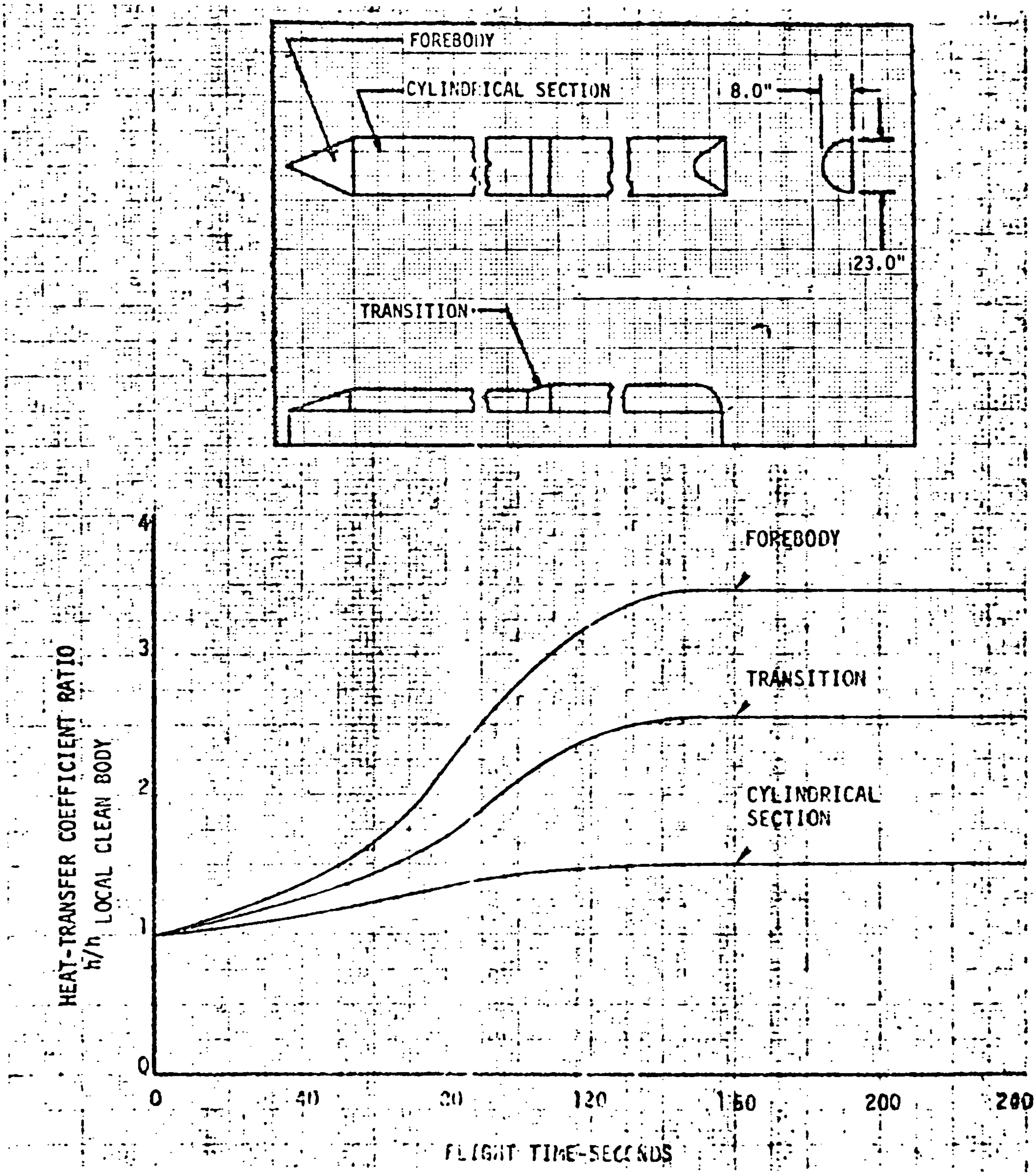

Figure A-5. Aerodynamic Heating for the Systems Tunnel Fairing

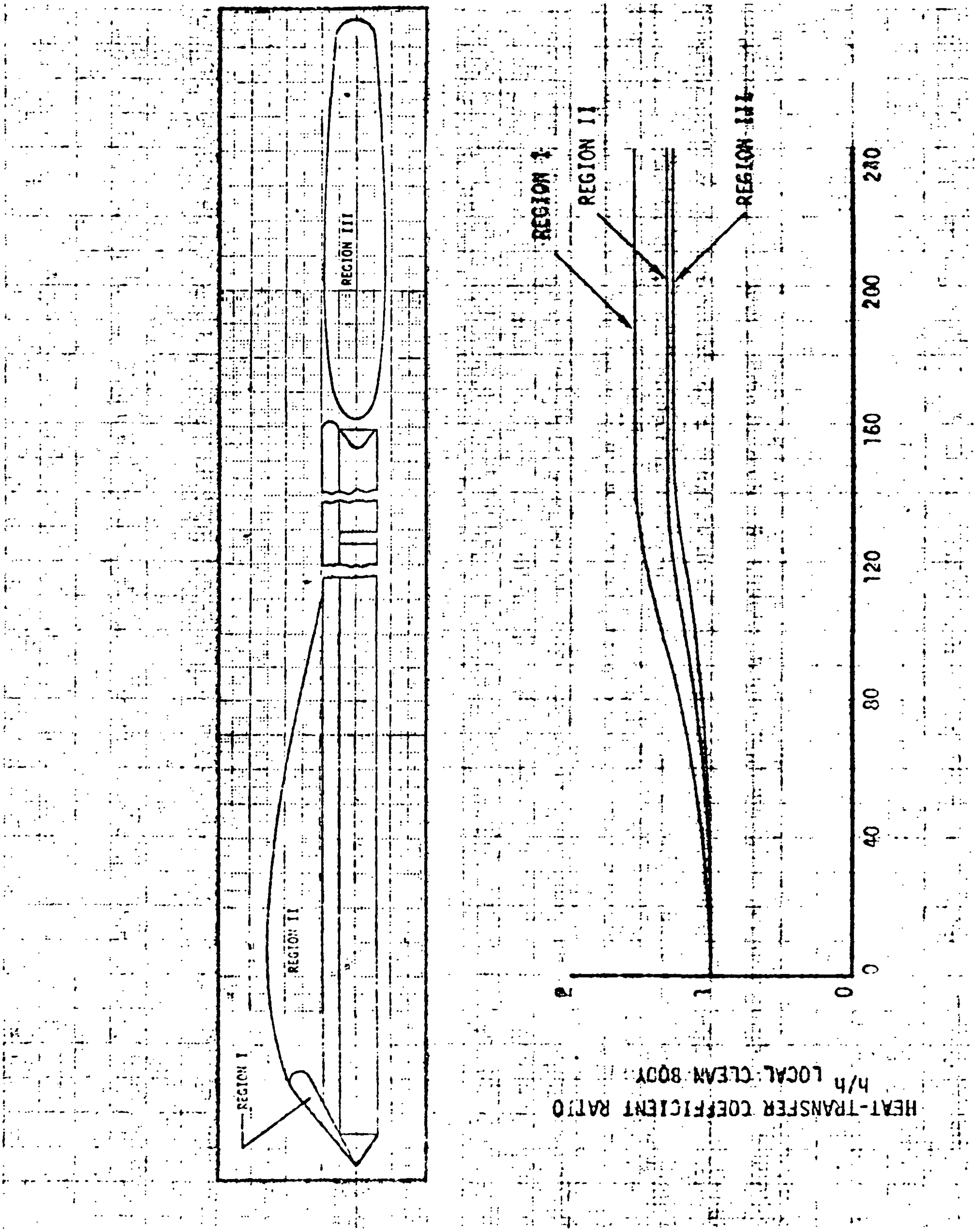

Figure A-6. Aerodynamic Heating for the Body Around the Systems Tunnel Fairing

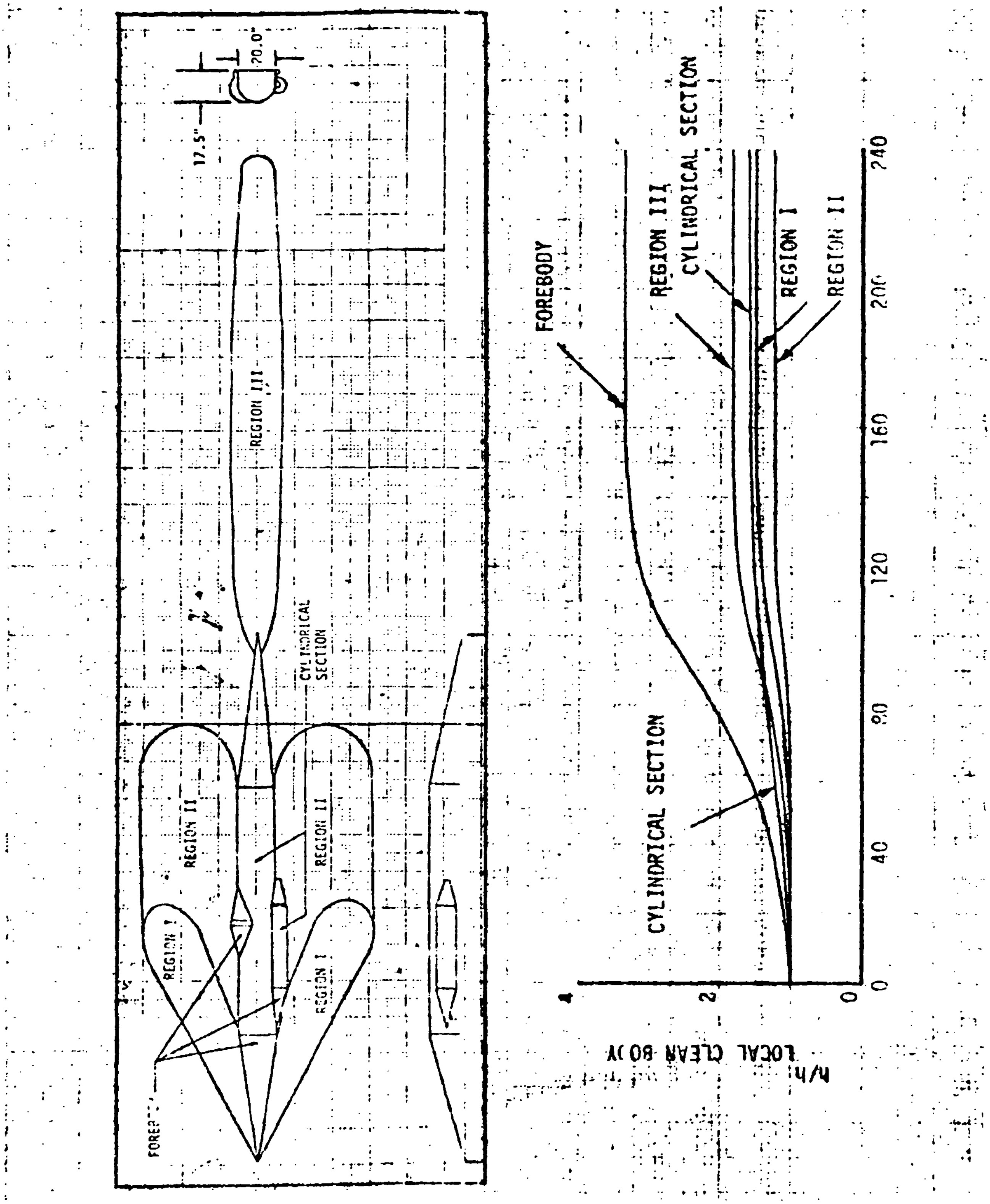

Figure A-7. Aerodynamic Heating for the LH_2 Feed Line Fairing

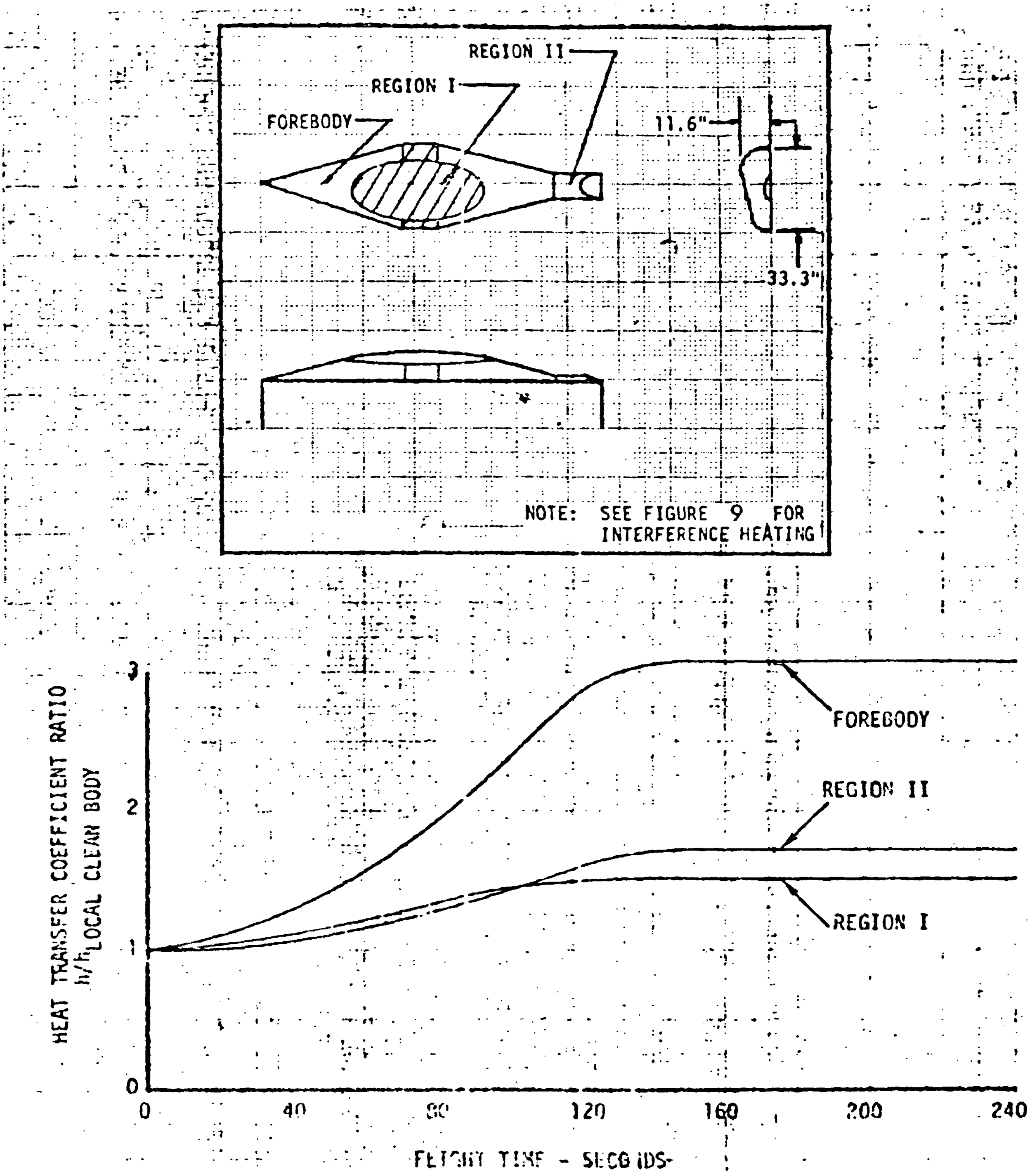

Figure A-8. Aerodynamic Heating for the LH_2 Fill and Drain Fairing

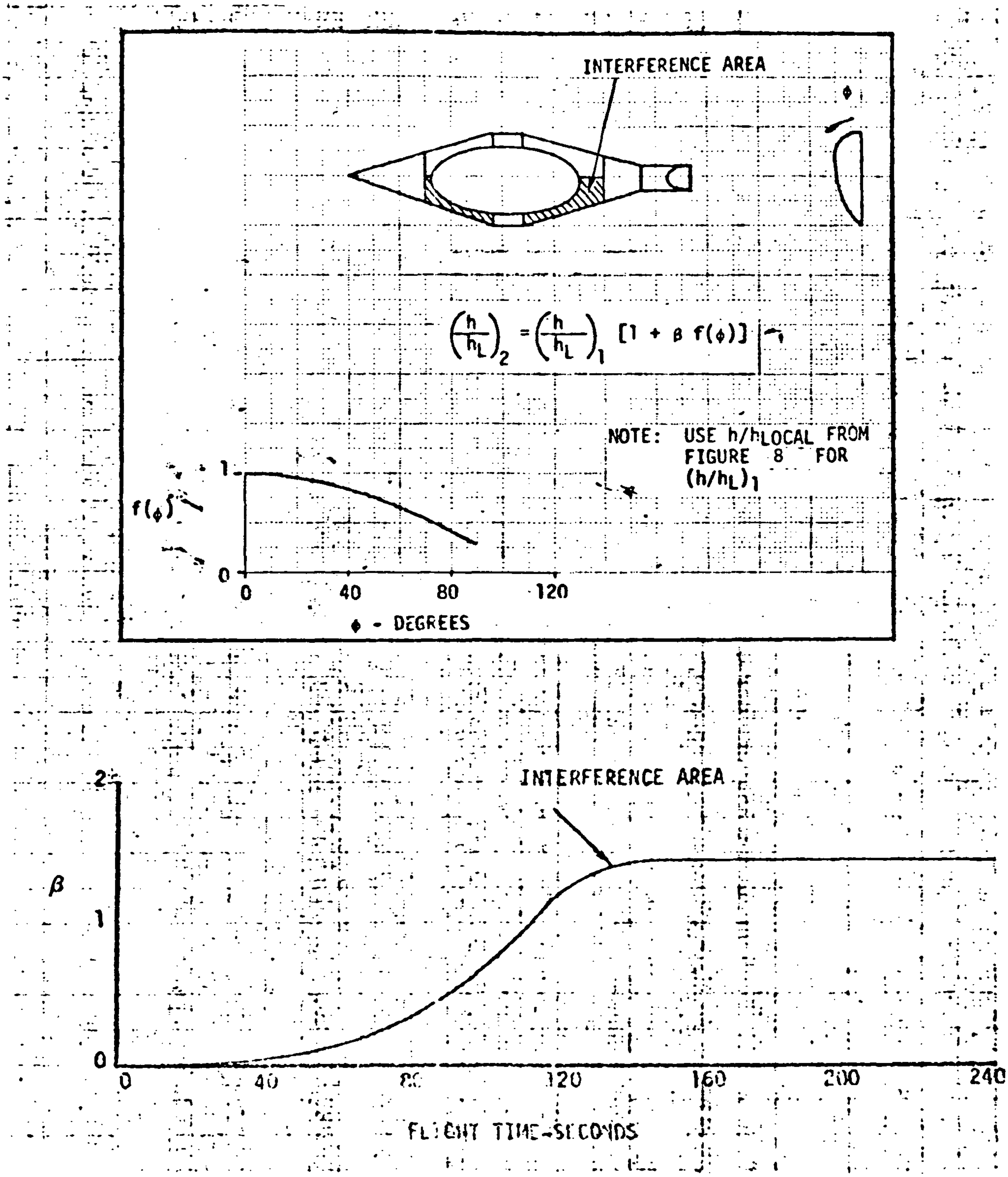

Figure A-9. Interference Heating Factor for the LH_2 Fill and Drain Fairing

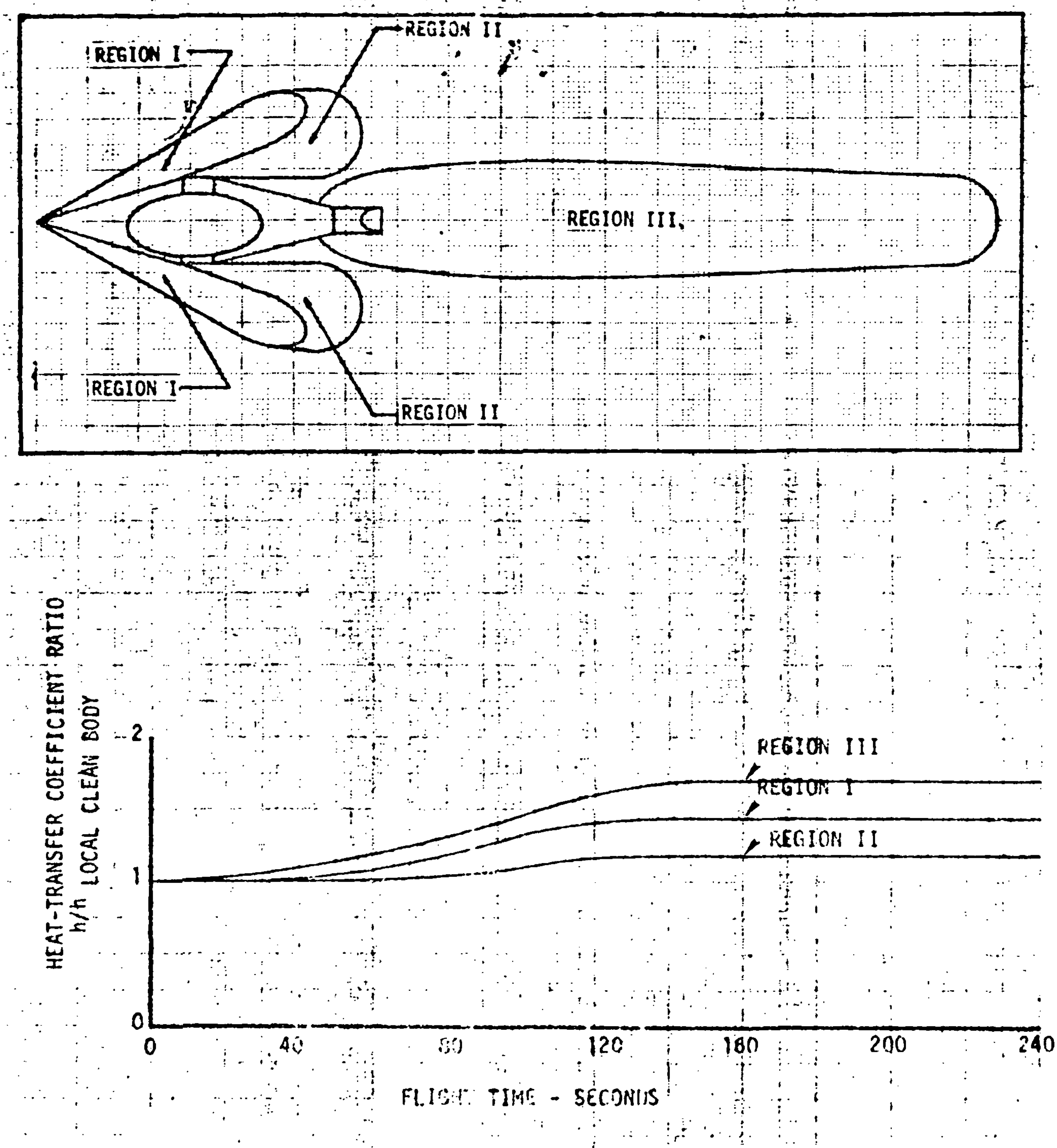

Figure A-10. Aerodynamic Heating of the Body Around the LH_2 Fill and Drain Fairing

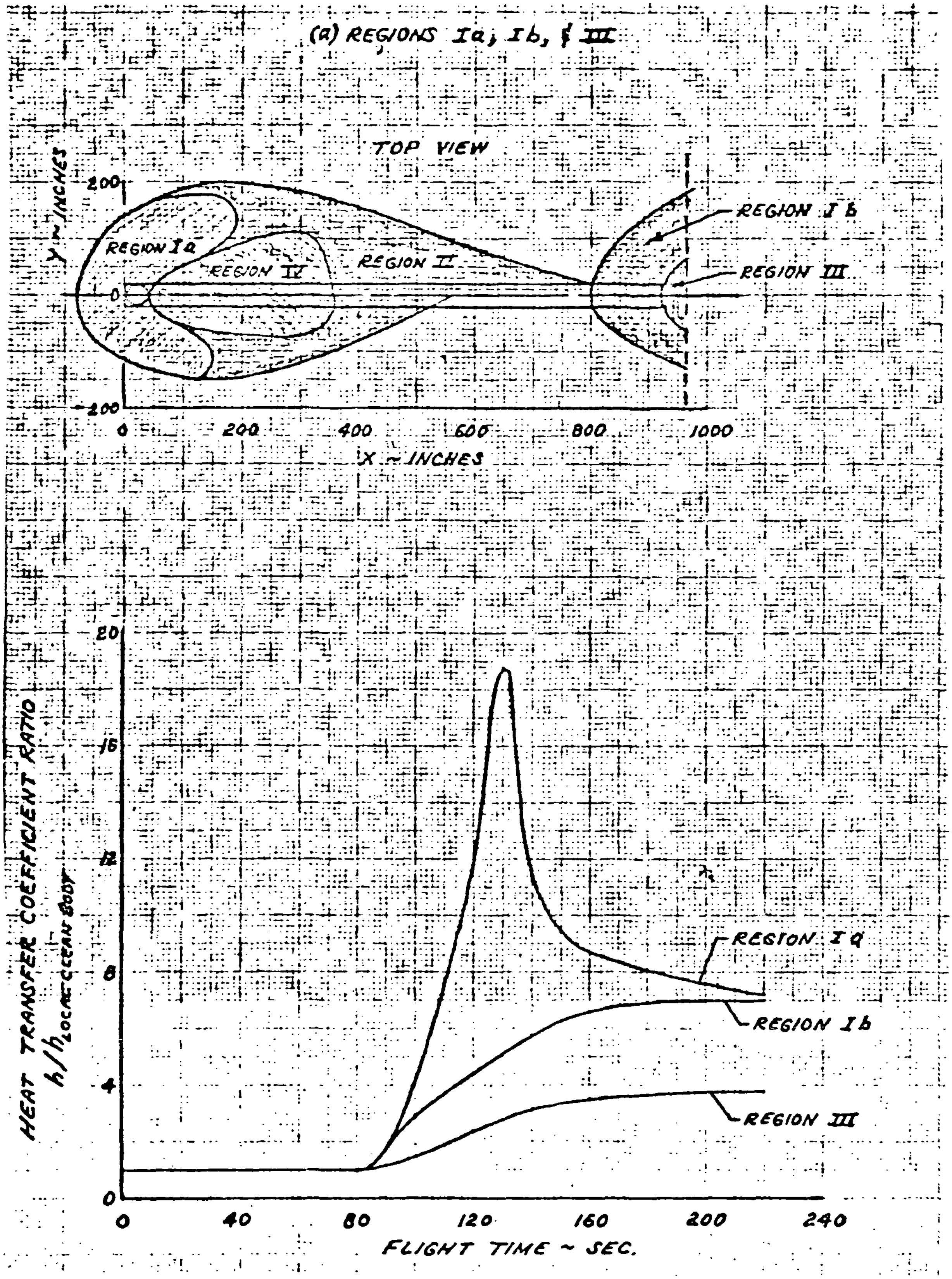

Figure A-11. Aerodynamic Heating to Body Around Drag Strut Due to Radial and Longitudinal Cylinders Including Mated Interference Heating

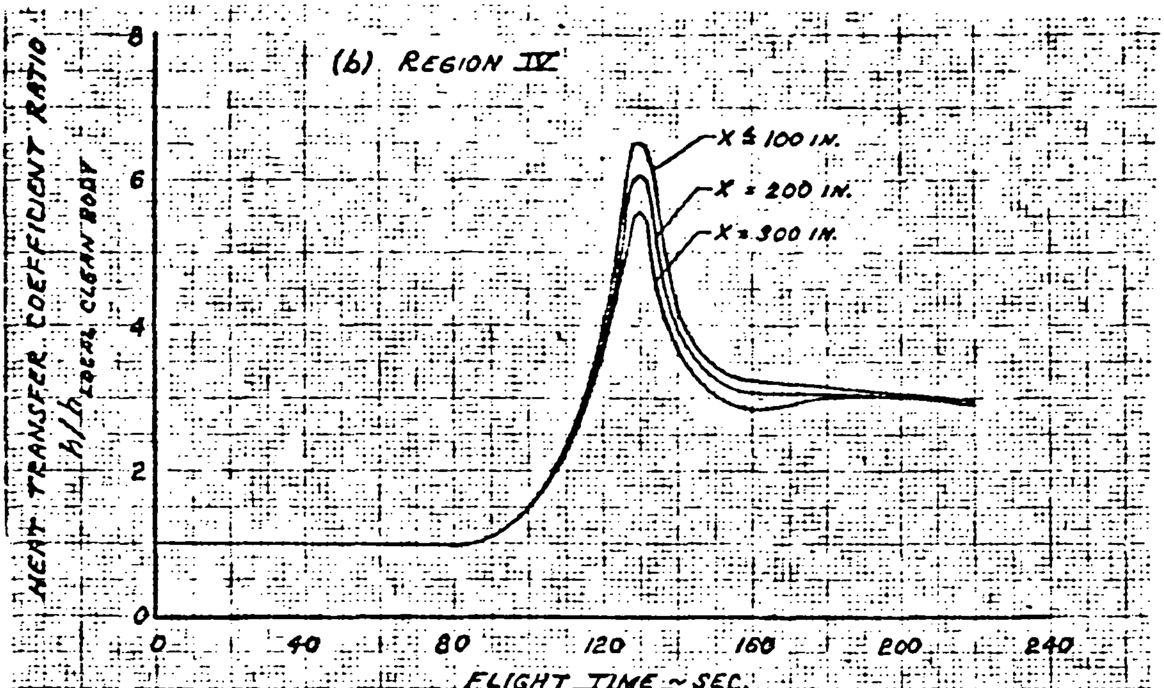

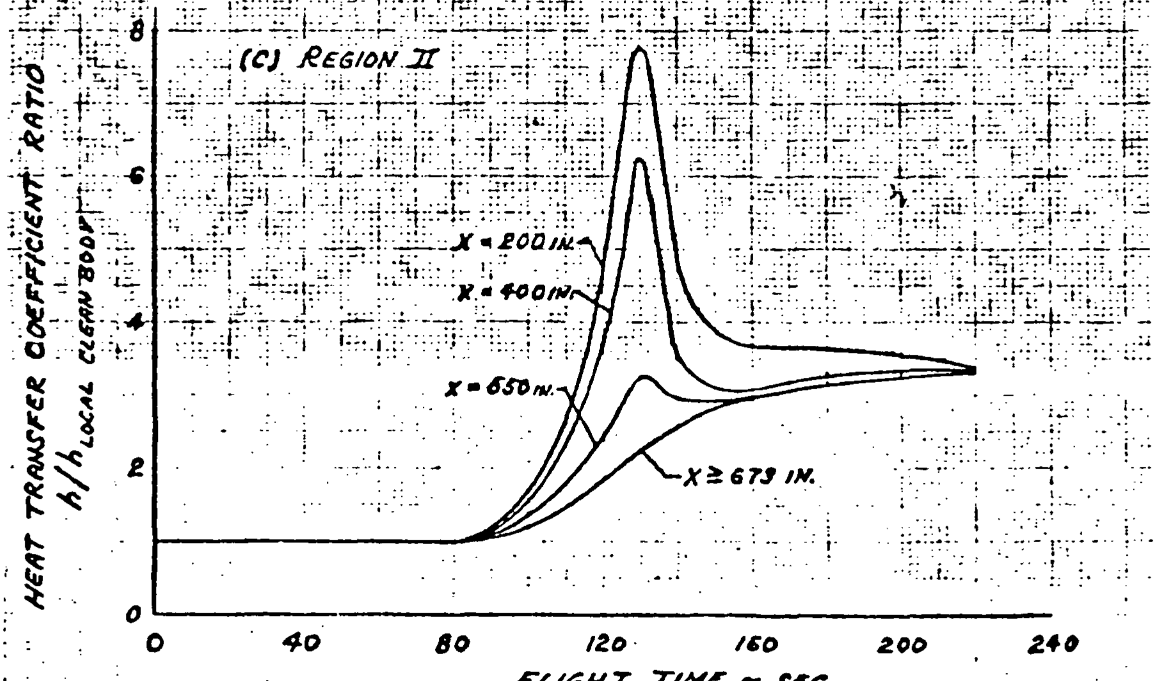

Figure A-11. Aerodynamic Heating to Body Around Drag Strut Due to Radial and Longitudinal Cylinders Including Mated Interference Heating

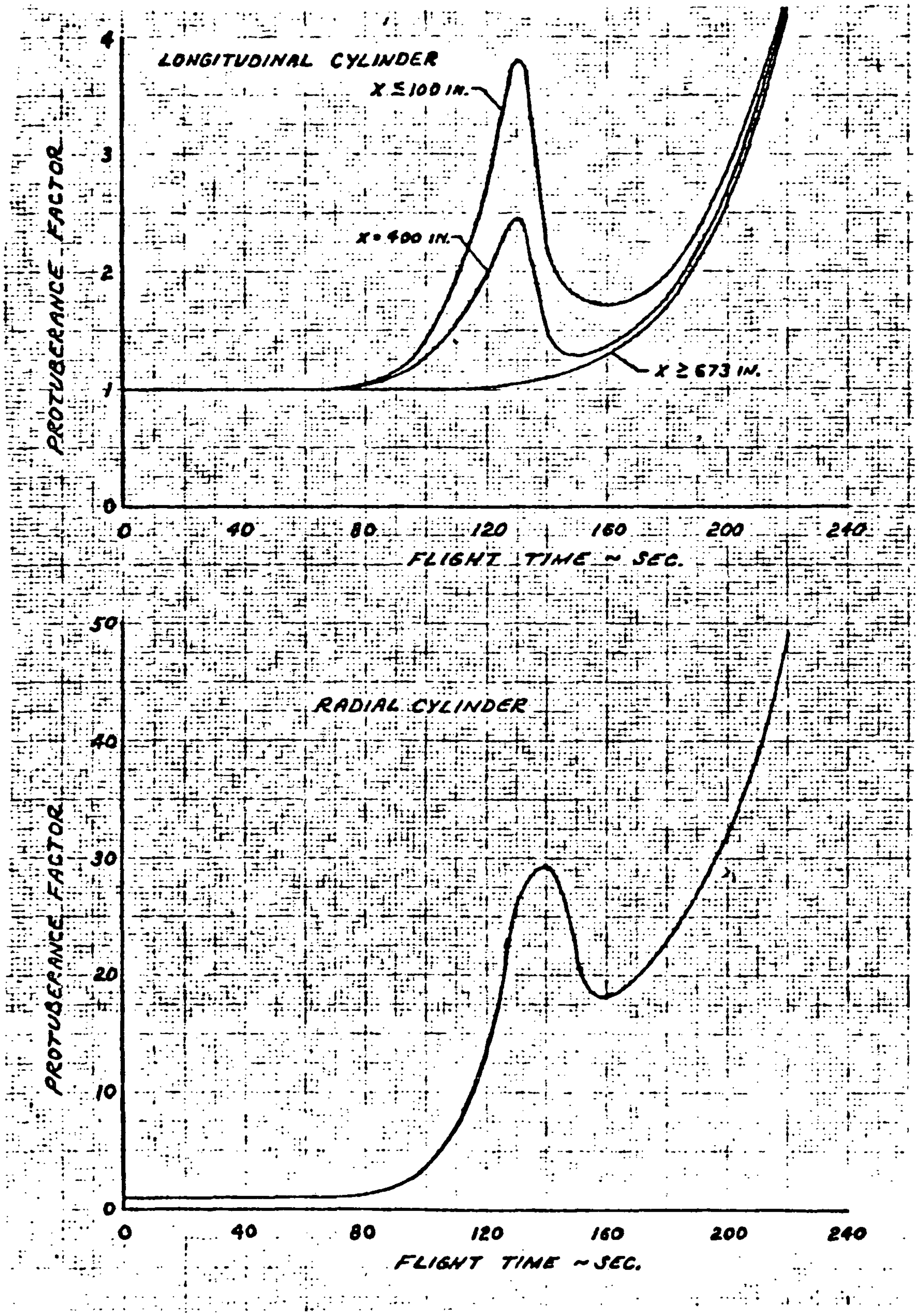

Figure A-12. Drag Strut Stagnation Line Heating Rate Protuberance Factor, Including Mated Interference Heating

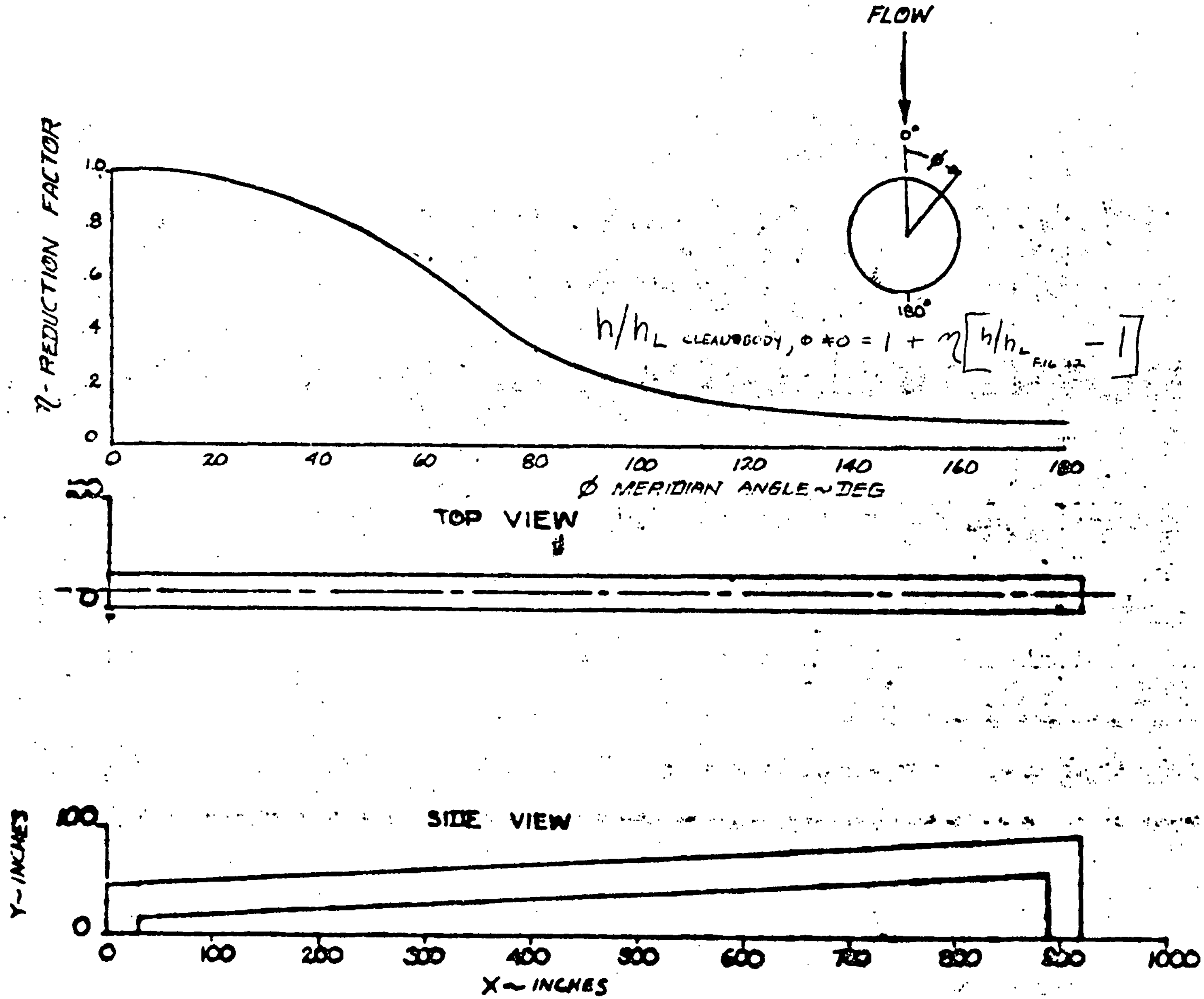

Figure A-13. Peripheral Factor for Drag Strut (Radial Cylinder)

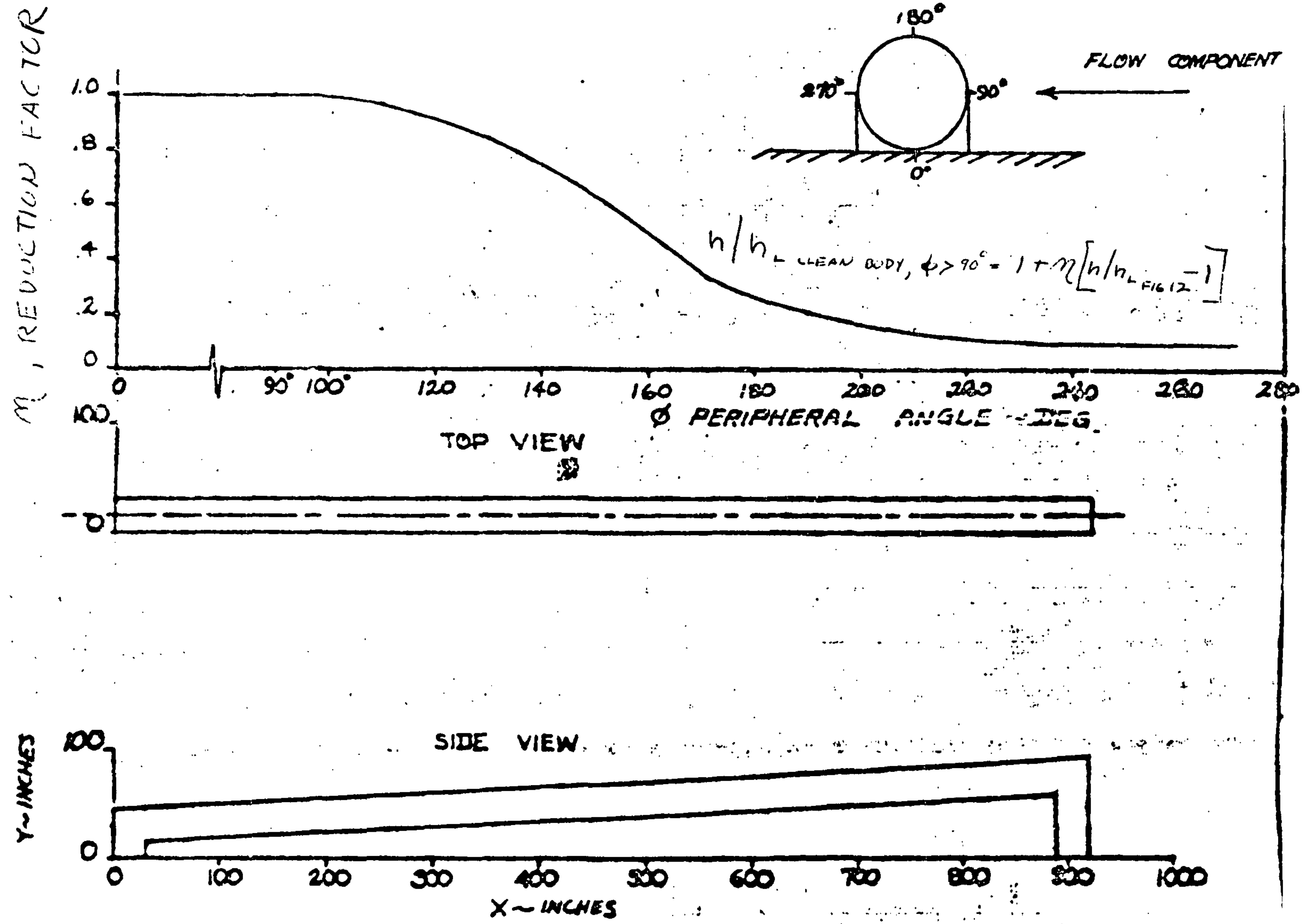

Figure A-14. Peripheral Factor for Drag Strut (Longitudinal Cylinder)

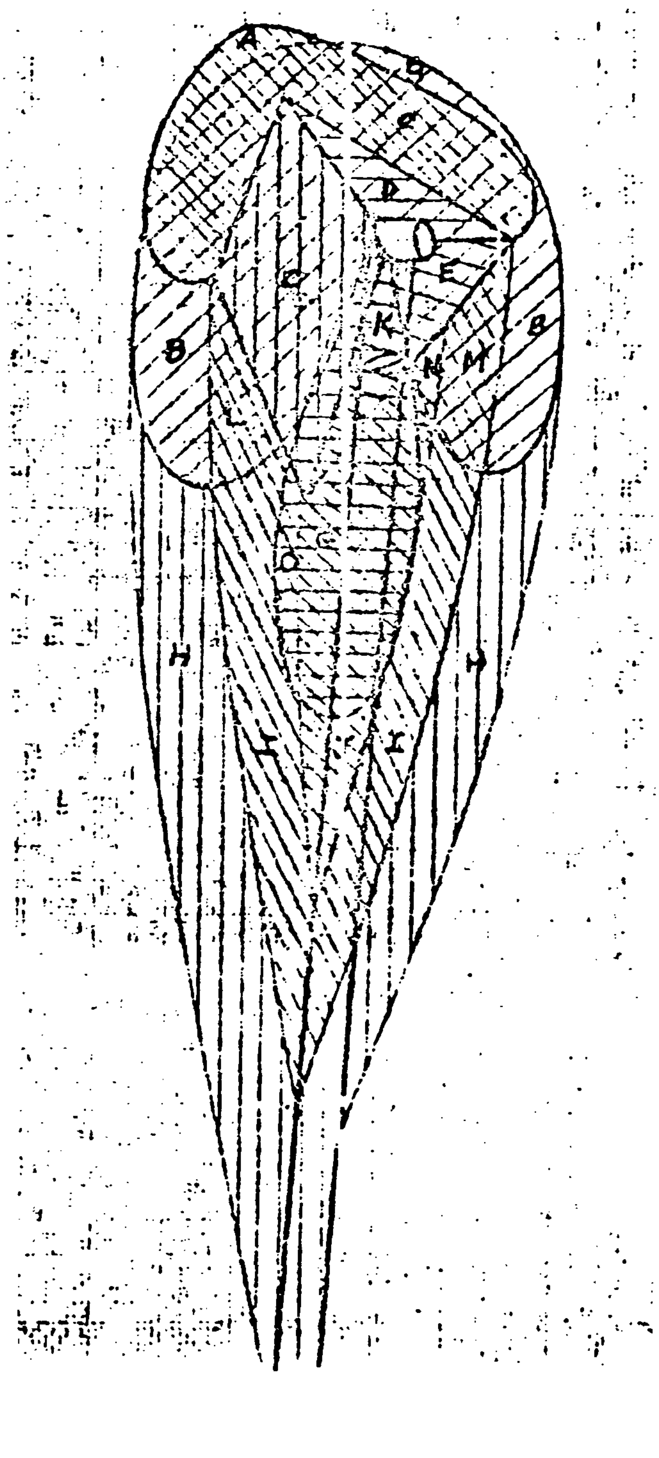

Figure A-15. Protuberance Influenced Regions in Vicinity of Attachment Fitting

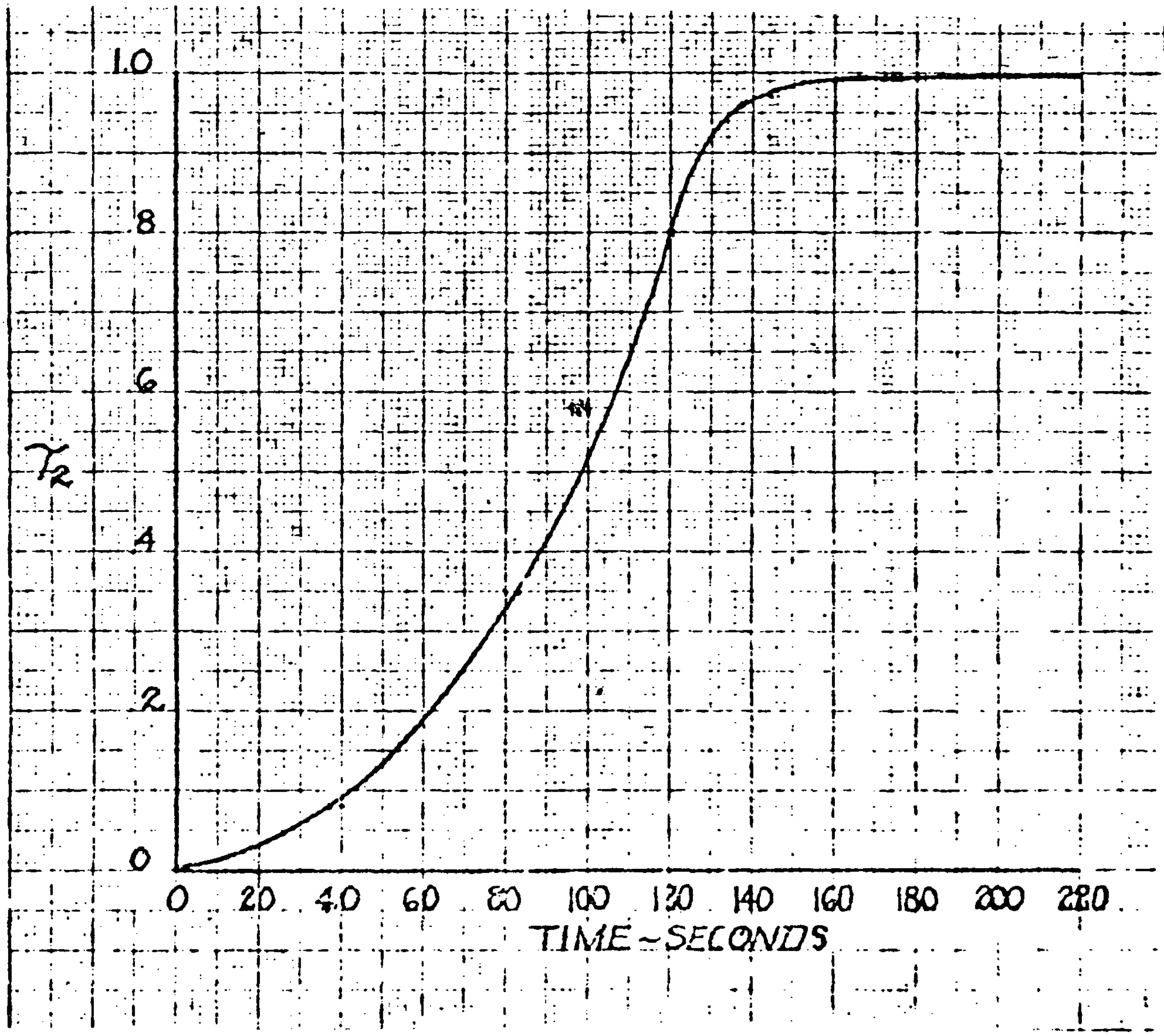

Figure A-16. Time Variation

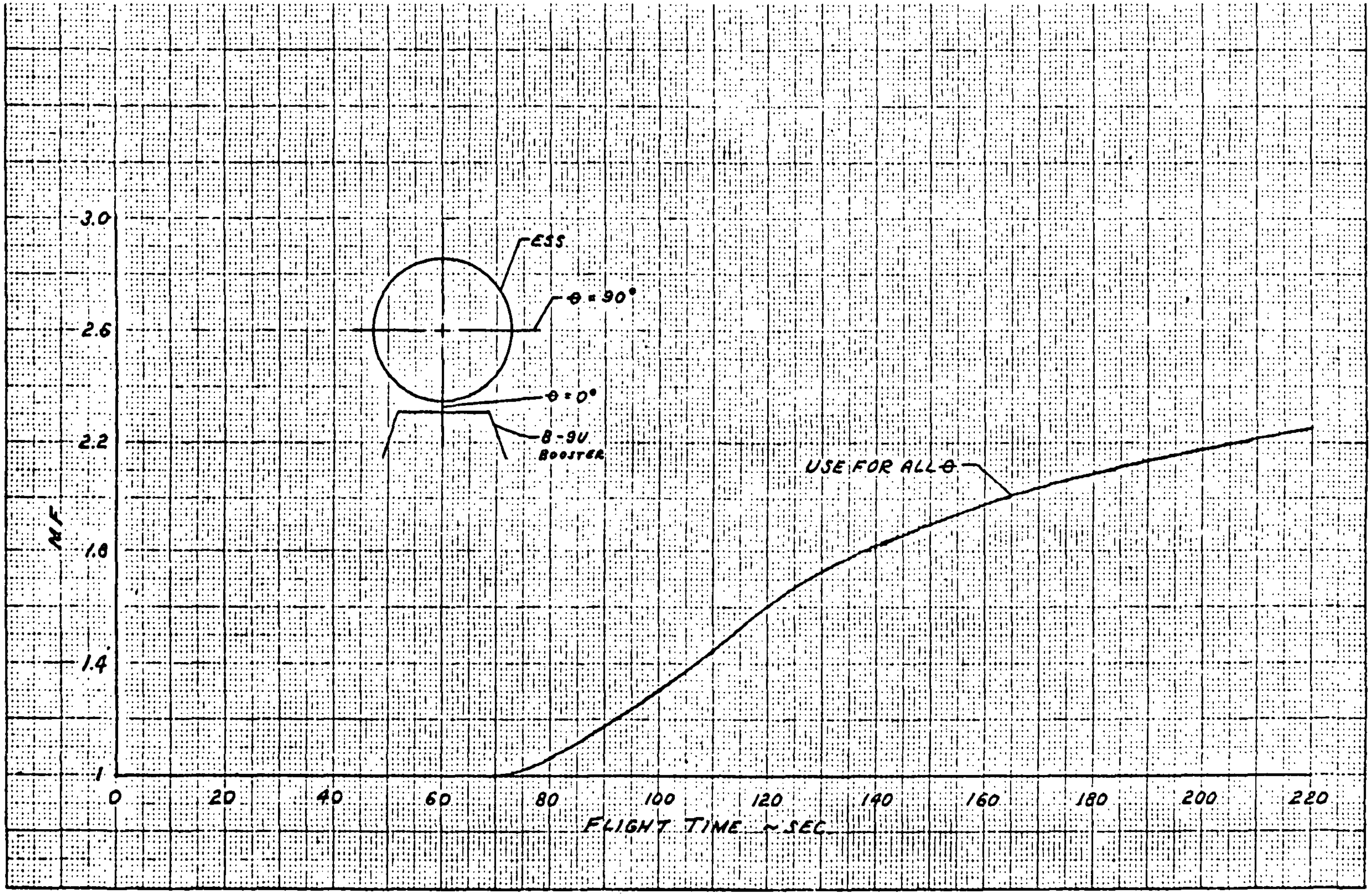

Figure A-17. ESS Payload Protuberance Multiplying Factor (MF) Including Mated Interference Heating
(a) ESS Station 0

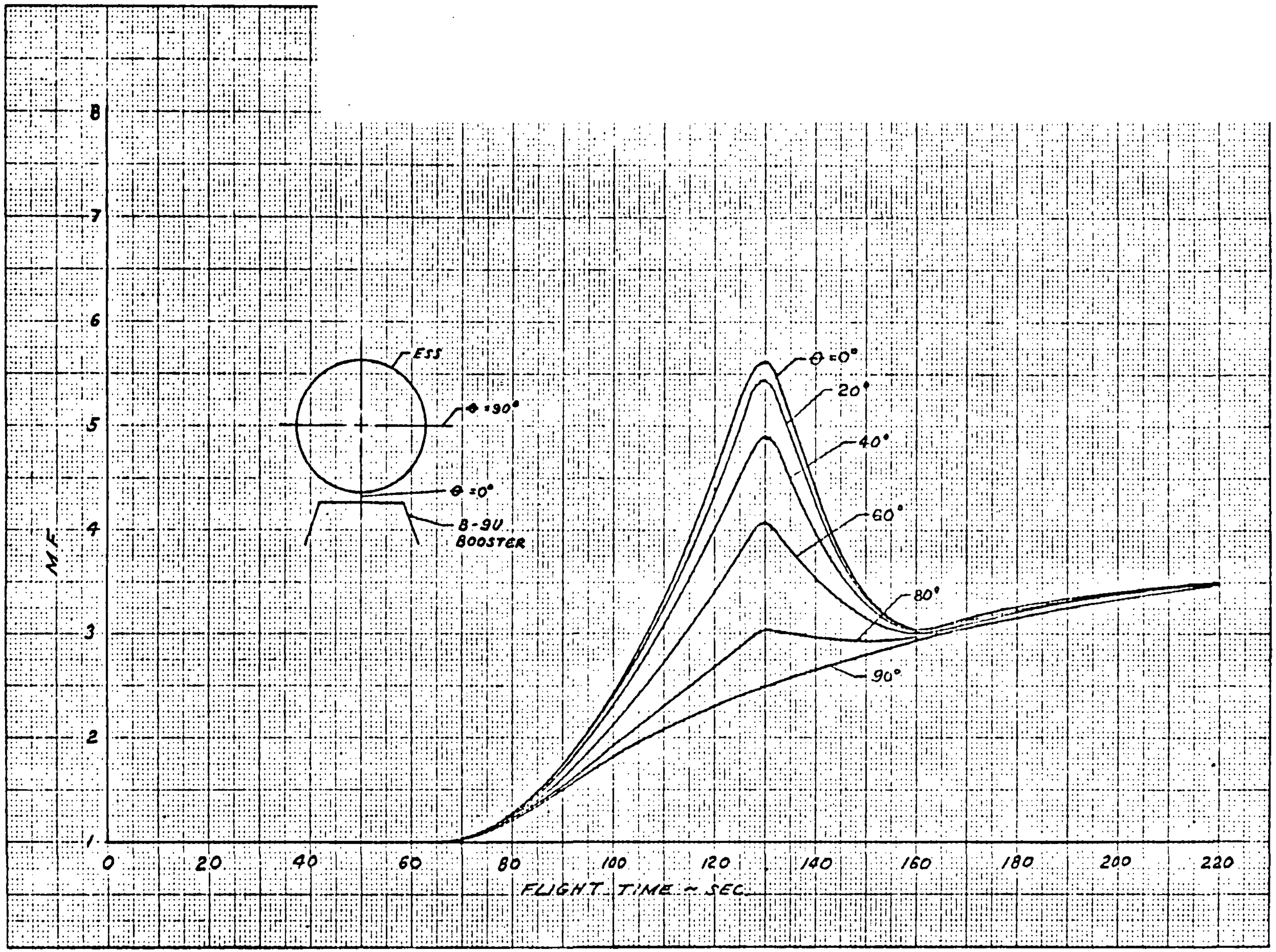

Figure A-17. ESS Payload Protuberance Multiplying Factor (MF) Including Mated Interference Heating
(b) ESS Station 451

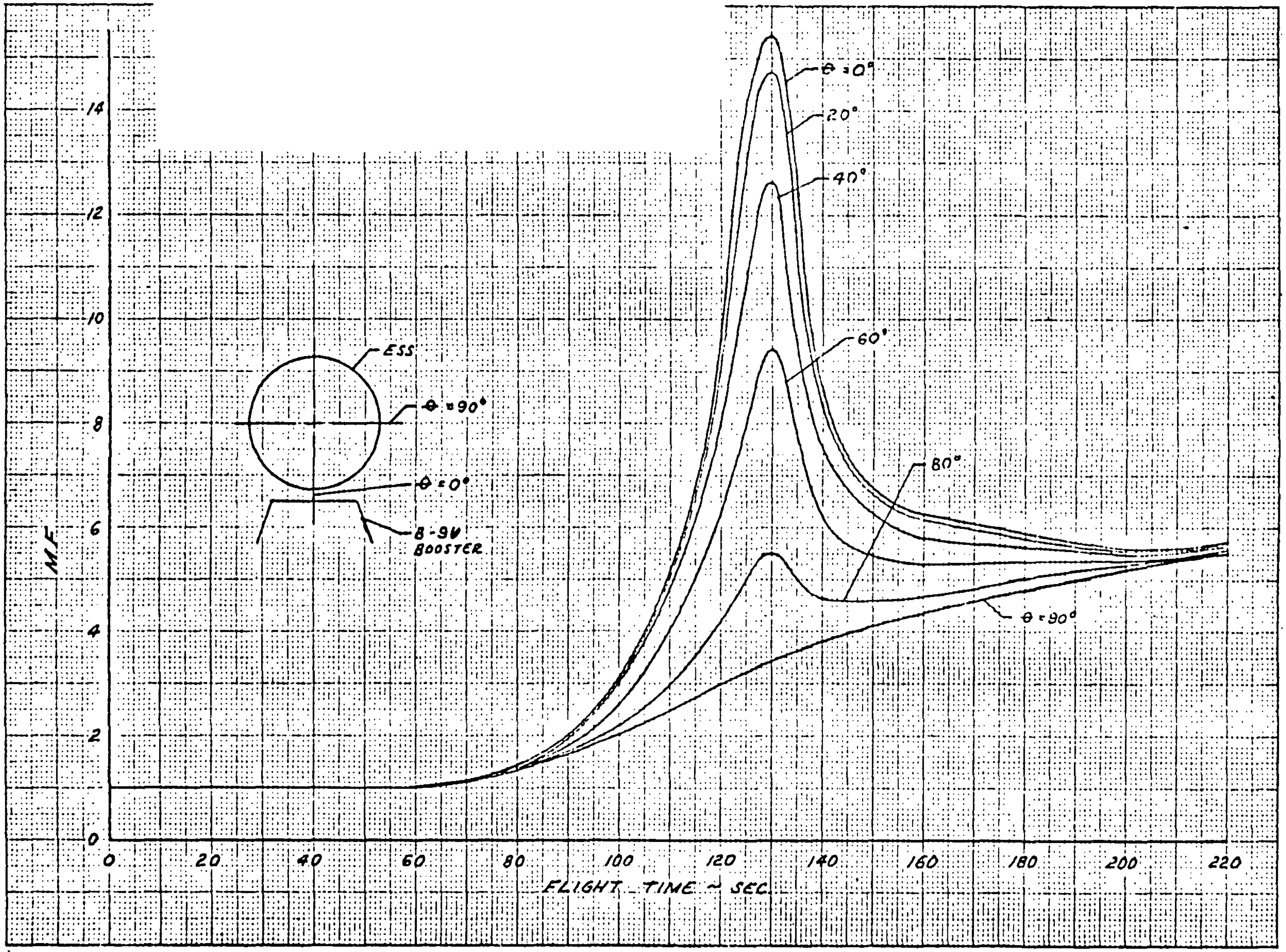

Figure A-17. ESS Payload Protuberance Multiplying Factor (MF) Including Mated Interference Heating (c) ESS Station 962

Details of the regions for the vicinity of the attachment fitting are shown in Figure A-15. The methodology for the calculation of heating rates for the attachment fitting and the adjacent structure (except drag strut) is presented in Table A-1. The heating rates for the drag strut radial cylinder are obtained using Figures A-12 and A-13. The heating rates for the longitudinal cylinder are found by multiplying the protuberance factors from Figures A-12 and A-14, by the protuberance factor for the appropriate region of the cylinder, as shown in Figure A-15.

Table A-1. Methodology for Calculating Heating Rates (Attachment Fitting and Adjacent Structure)

Region	Method
A	$PF = (1 + \tau_2^{*} K_2)$, $K_2 = 1.9$
B	PF from Figure A-11 Region I
C	Multiply Region A value by Region B value at same range time.
D	$PF = (1 + \tau_2 K_2)$ x Region B value, $K_2 = 6.7$
E	$PF = (1 + \tau_2 K_2)$ x Region B value, $K_2 = 0.9$
F	$PF = (1 + \tau_2 K_2)$ x Region B value, $K_2 = 0.3$
G	PF = (Region IV, Figure A-11, value) x $(1 = \tau_2 K_2)$, $K_2 = 3.5$
H	PF from Figure A-11, Region II
I	(PF Region H) x $(1 + \tau_2 K_2)$, $K_2 = 0.9$
J	$PF = 1 + \tau_2 K_2$, $K_2 = 3.5$
K	(PF from Region IV, Figure A-11) x $(1 + \tau_2 K_2)$, $K_2 = 0.3$
L	(PF from Region B) x $(1 + \tau_2 K_2)$, $K_2 = 0.9$
M	PF same as region L
N	(PF from Region B) x $(1 + \tau_2 K_2)$, $K_2 = 3.5$
O	(PF from Region IV, Figure A-11) x (PF Region I)

$^{*}\tau_2$ is on Figure A-16

APPENDIX B. INTERFERENCE HEATING INFLUENCE OF A FAIRING SHROUD BETWEEN ESS AND BOOSTER

Proposed is a fairing for enclosing the LO_2 vent valve and the struts between the ESS and the booster, as shown in Drawing No. V7-923147. The heating rates for the ESS hemicylinder closest to the booster is obtained using, in part, the factors shown in Figure B-1. The heating rates for the outer hemicylinder are obtained as previously stated.

RNS AND SPACE TUG

The heating rates for the hemicylinder closest to the booster are given by

$$\dot{q} = (h_c)(T_r - T_w)(h/h_{1cb}) \quad (1)$$

where

h/h_{1cb} is obtained from Figure B-1.

These ratios include both the booster interference factor and, for the forebody, shroud, and Regions I and II, the factors due to the presence of the shroud. The effect of the projections through or beyond the shroud, indicated in Drawing No. V7-923147, are not included.

MDAC SPACE STATION

The heating rates for the hemicylinder closest to the booster are obtained as follows:

$$\dot{q} = h_c (T_r - T_w)(h/h_{1cb})(MF) \quad (2)$$

These ratios include both the booster interference factor and, for the forebody, shroud, and Regions I and II, the factors due to the presence of the shroud. The effect of the projections through or beyond the shroud, indicated in Drawing No. V7-923147, are not included.

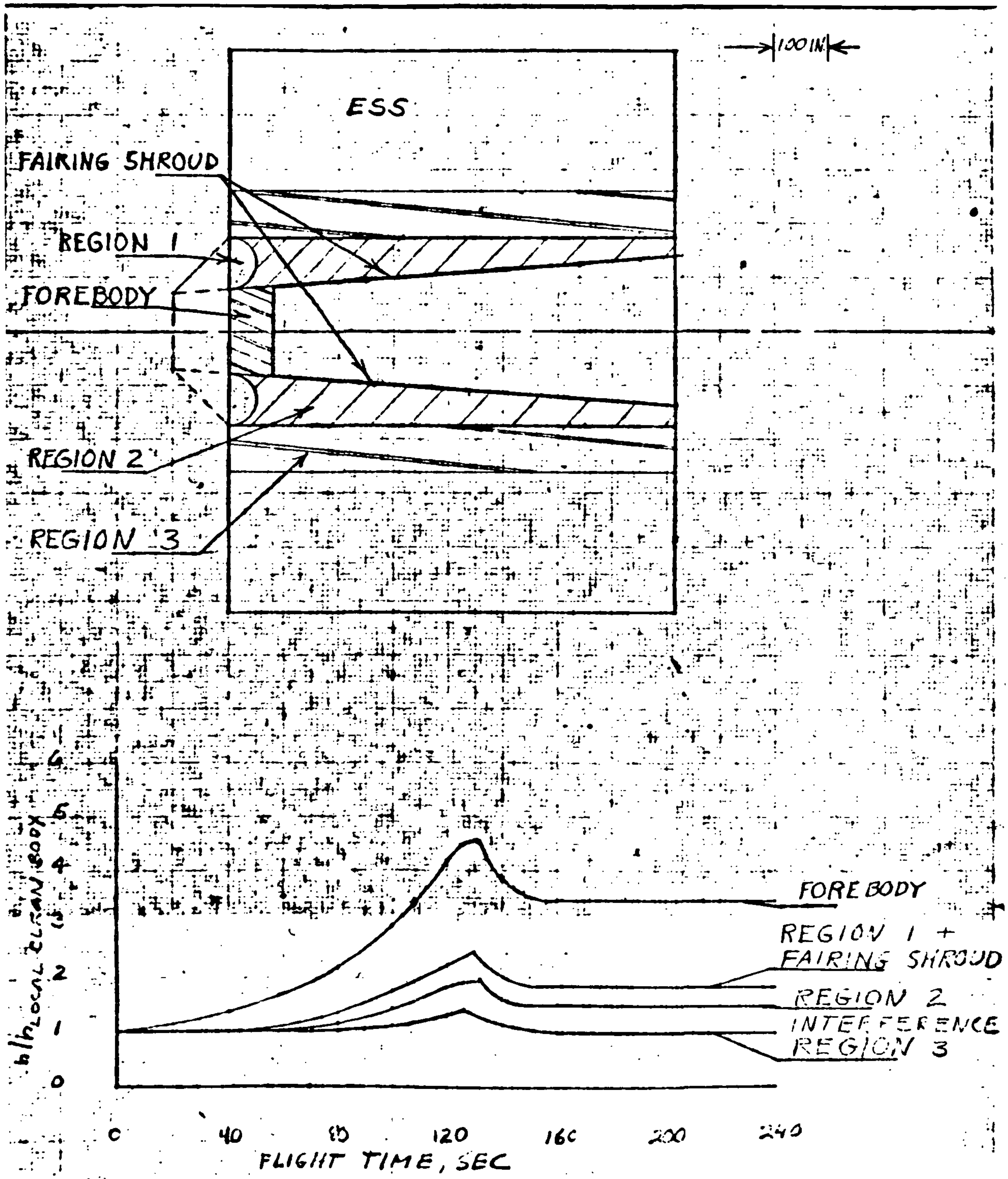

Figure B-1. Shroud- and Booster-Influenced Heating Factors

APPENDIX C. INTERFERENCE HEATING INFLUENCE OF TRAJECTORY ON ESS AND BOOSTER

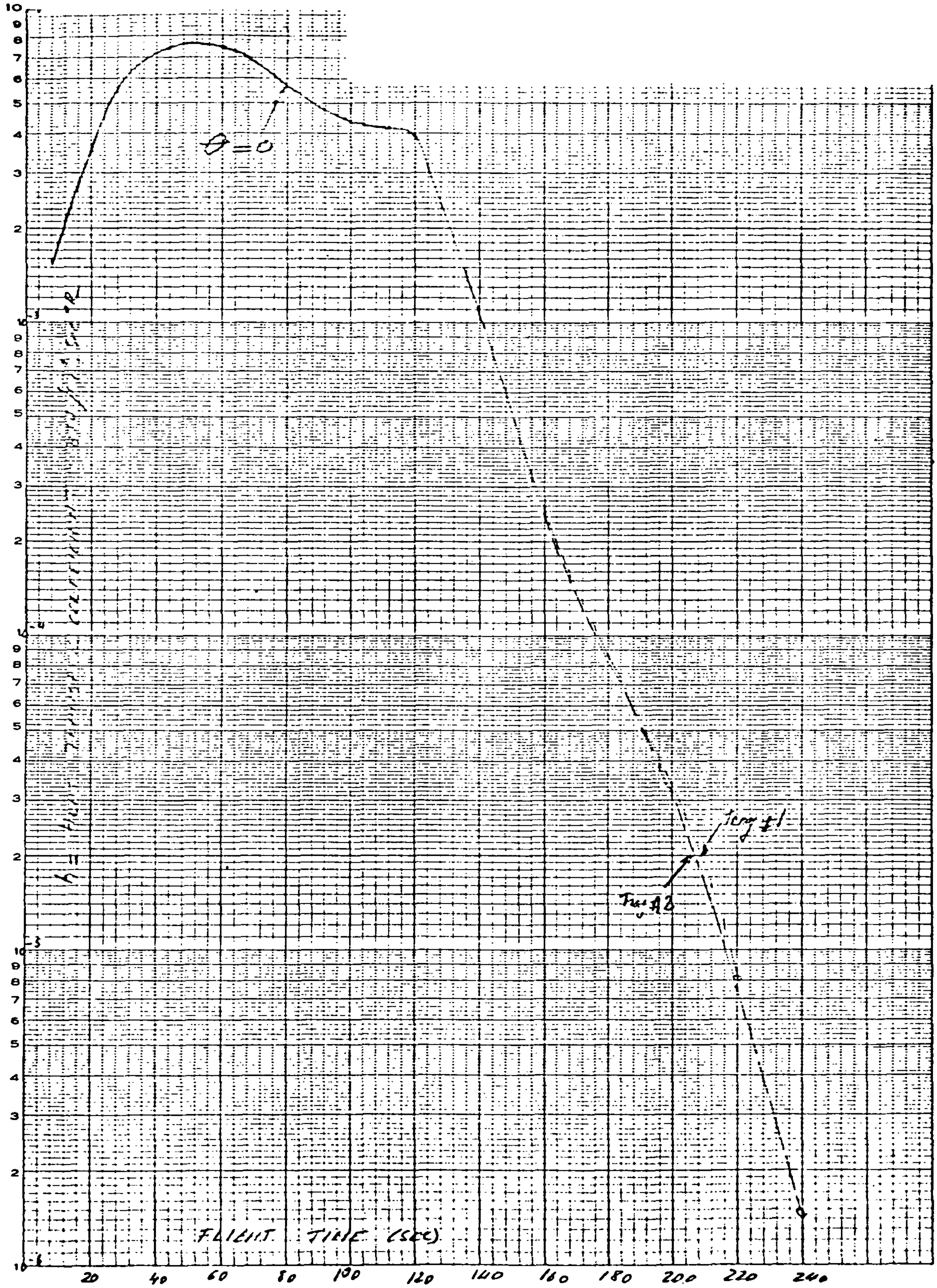

Figure C-1. ESS - MDAC Payload, Basic Heat Transfer Coefficient, Including Mated Interference Heating (C) Station 962

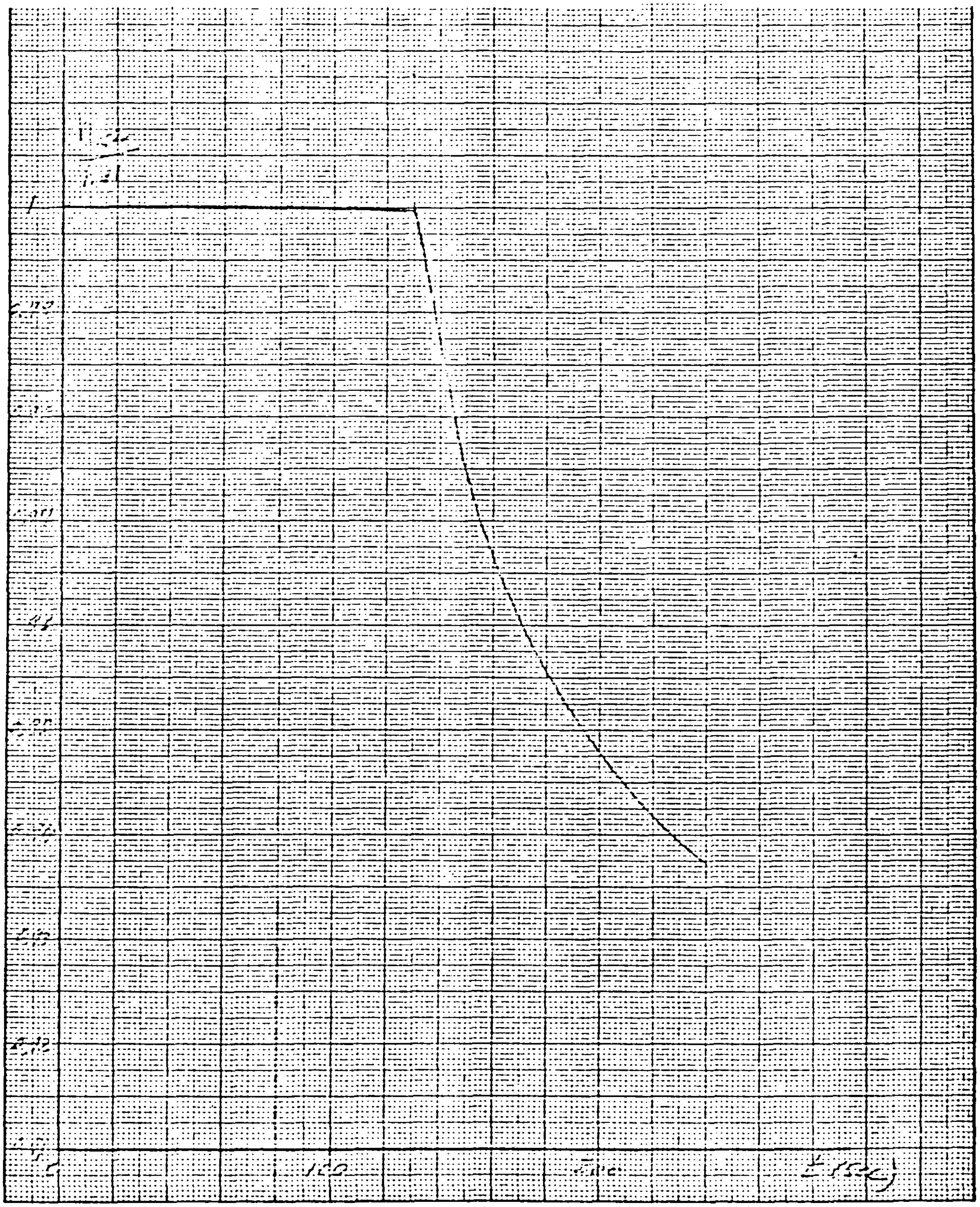

Figure C-2. ESS MDAC Payload, Ration of Basic Heat Transfer Coefficients Mated Interference Heating (C) Station 962

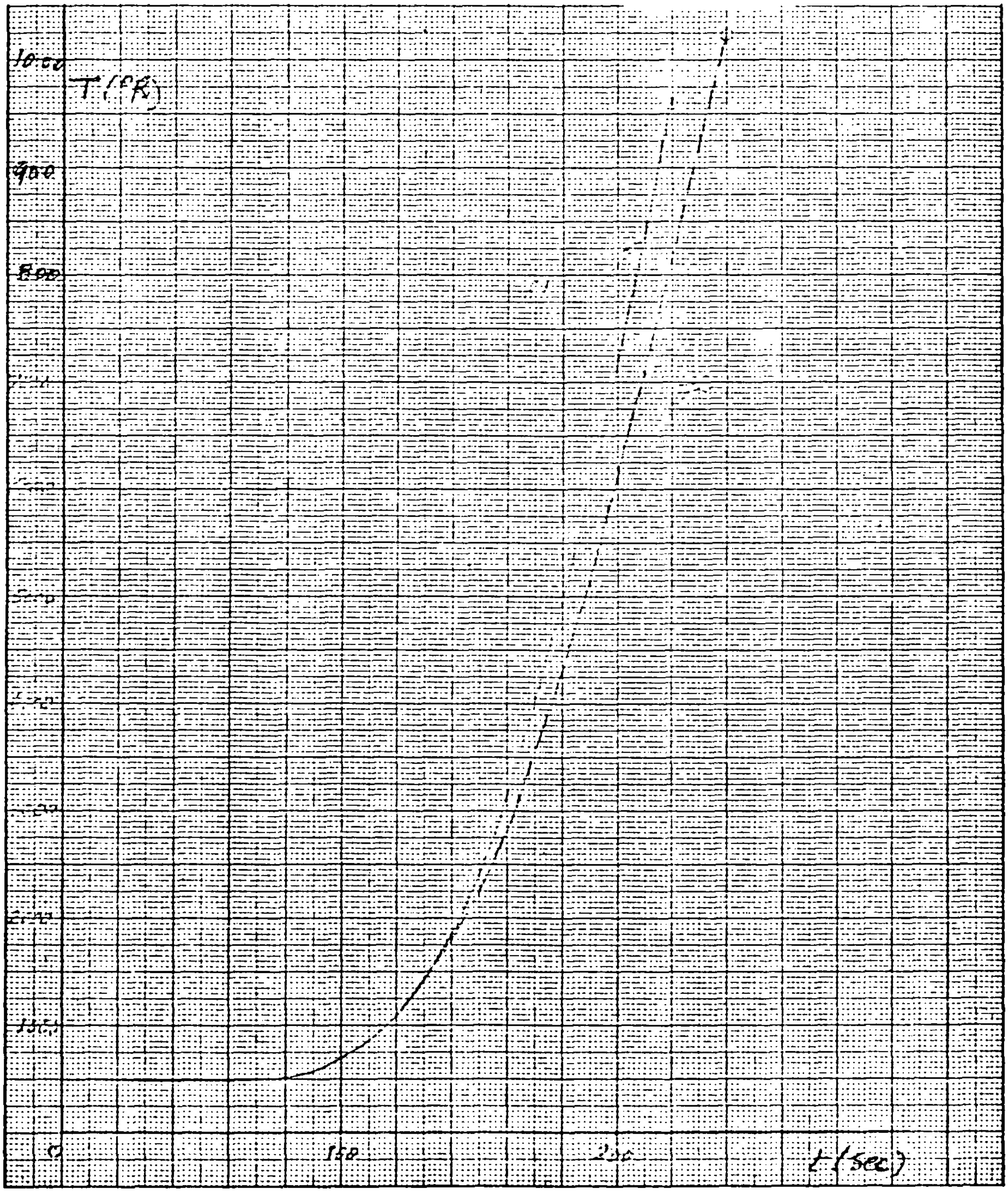

Figure C-3. Recovery Temperature for ESS Basic Sidewall

APPENDIX D. TRAJECTORY AND ANGLE-OF-ATTACK EFFECTS ON ESS HEATING RATES

The results of a study on the sensitivity of ESS heating rates to trajectory changes and to angle-of-attack are presented herein. The maximum dynamic pressure (high $\bar{q}$) trajectory (with zero angle of attack) and the low dynamic pressure (low $\bar{q}$) trajectory (with nonzero angles of attack, assuming tail winds) were used together with the 1963 Patrick reference atmosphere.

The low-$\bar{q}$ trajectories for the MDAC space station, RNS, and space tug are compared with the high-$\bar{q}$ trajectory in Figures D-1, D-2, and D-3. A comparison of trajectory and angle-of-attack effects on the heat transfer coefficient and recovery temperature for the MDAC space station payload is shown in Figures D-4 and D-5, while the effects for the RNS and space tug payloads are shown in Figures D-6, D-7, D-8, and D-9.

It should be noted that the heat transfer coefficients presented are for an area of the ESS sidewall not influenced by payload protuberances, ESS protuberances, or the presence of the booster or interstage structure (booster to ESS). Further, these values are preliminary pending final definition of the configuration, augmented by wind tunnel tests.

For this study, only the values of the heat transfer coefficient, h_c, on the windward meridian at ESS Station 885 are presented (the values of h_c at ESS Station 0 are within 10 percent of the values at ESS Station 855). The heat transfer coefficients were computed using the method of Spalding and Chi for a turbulent boundary layer. Local values of Mach number and pressure at the location were used together with an assumed constant wall temperature of 540 R. The influence of angle of attack on the heat transfer coefficient was based on the experimental results of Feller. The heat transfer rate $\dot{q}$ — determined by using $\dot{q} = h_c (T_r - T_w)$ — is the appropriate value when the supplied values of h_c and T_r are used.

The heat transfer coefficients for the high-$\bar{q}$ trajectory are higher than for the low-$\bar{q}$ trajectories, assuming zero angles of attack. However, when the angle of attack is considered the heat transfer coefficients in the high heating range of the trajectory are higher for the low-$\bar{q}$ trajectories than for the zero angle-of-attack, high-$\bar{q}$ trajectory. The heating rates (based on cold-wall assumptions) for the high-$\bar{q}$ trajectory are approximately three times as high for the low-$\bar{q}$, zero angle-of-attack condition but only 40 percent higher than the nonzero angle-of-attack, low-$\bar{q}$ heating rates. The difference in trend of the heat transfer coefficient and heating rates is due to the recovery temperatures for the trajectories.

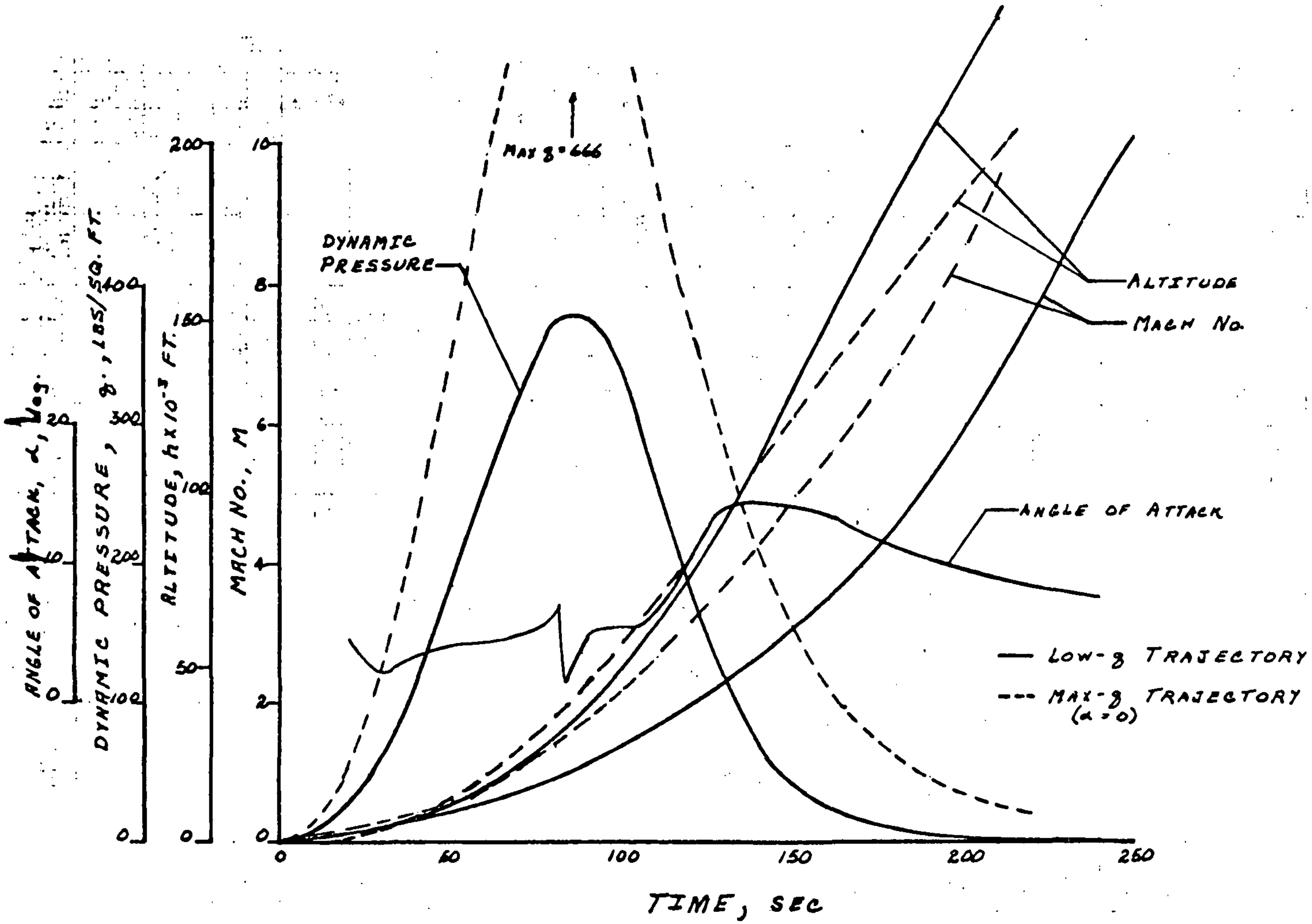

Figure D-1. ESS Ascent Trajectory, MDAC Space Station Payload

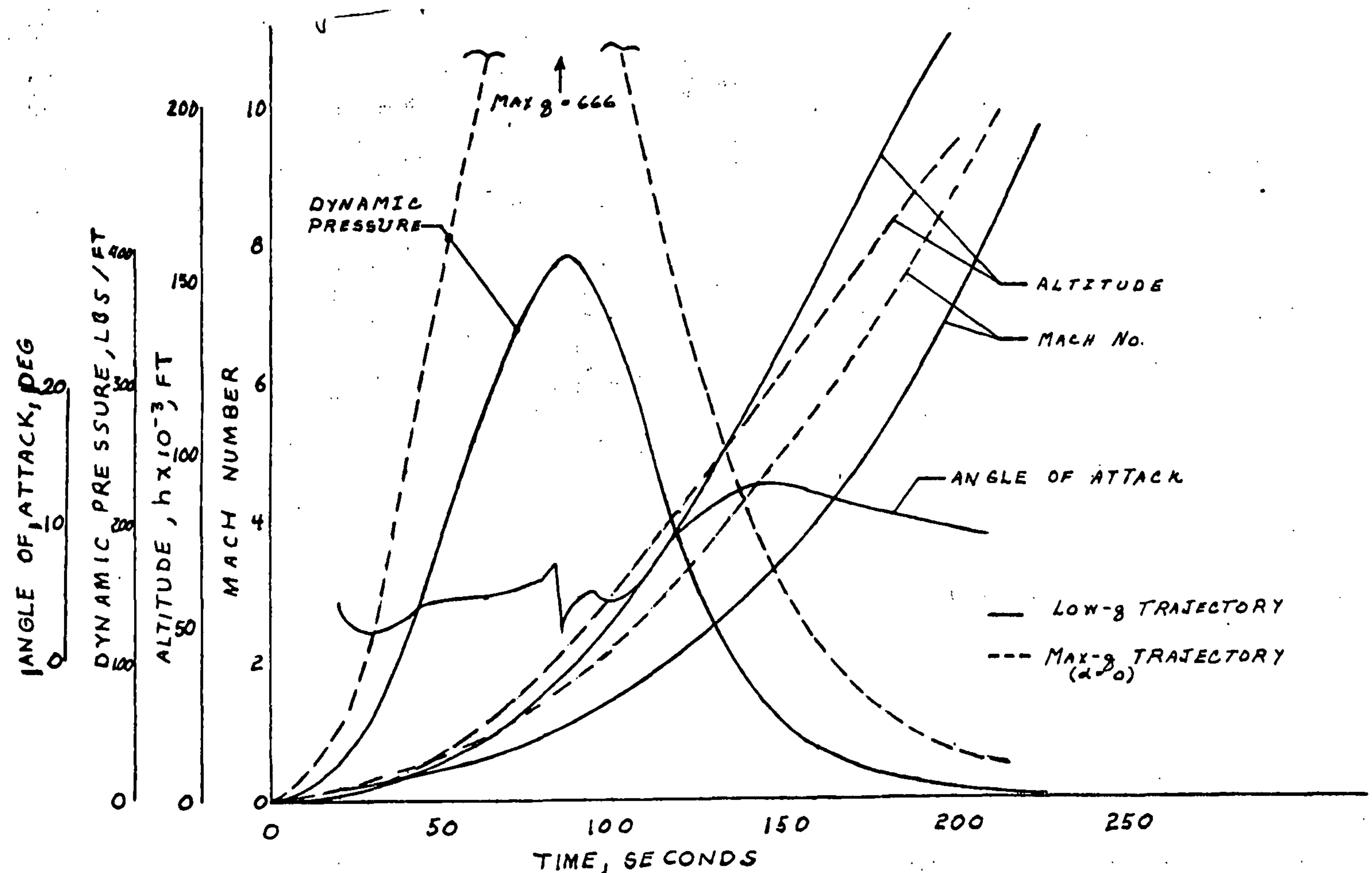

Figure D-2. ESS Ascent Trajectory, NR/RNS Payload

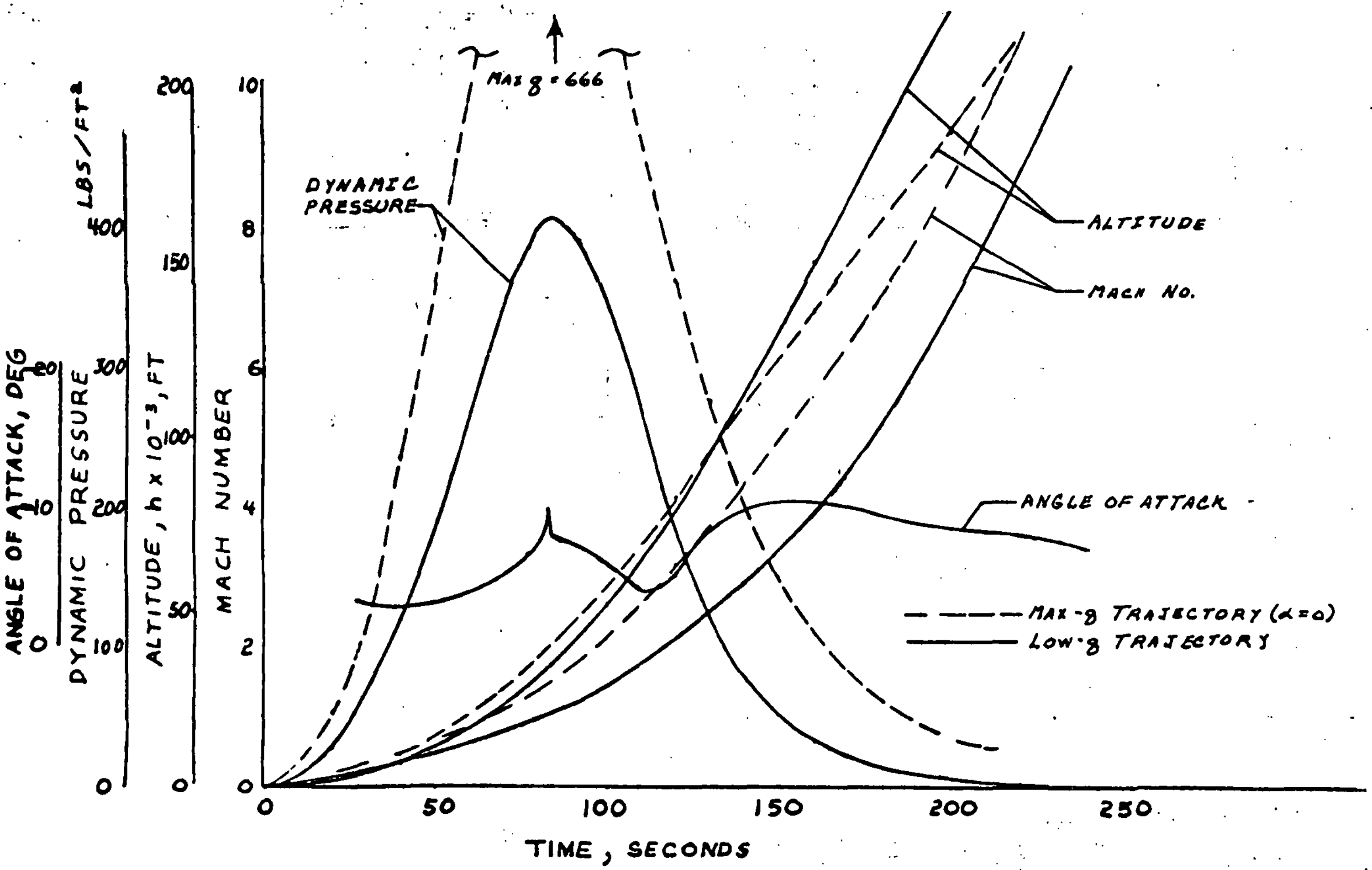

Figure D-3. ESS Ascent Trajectory, Space Tug Payload

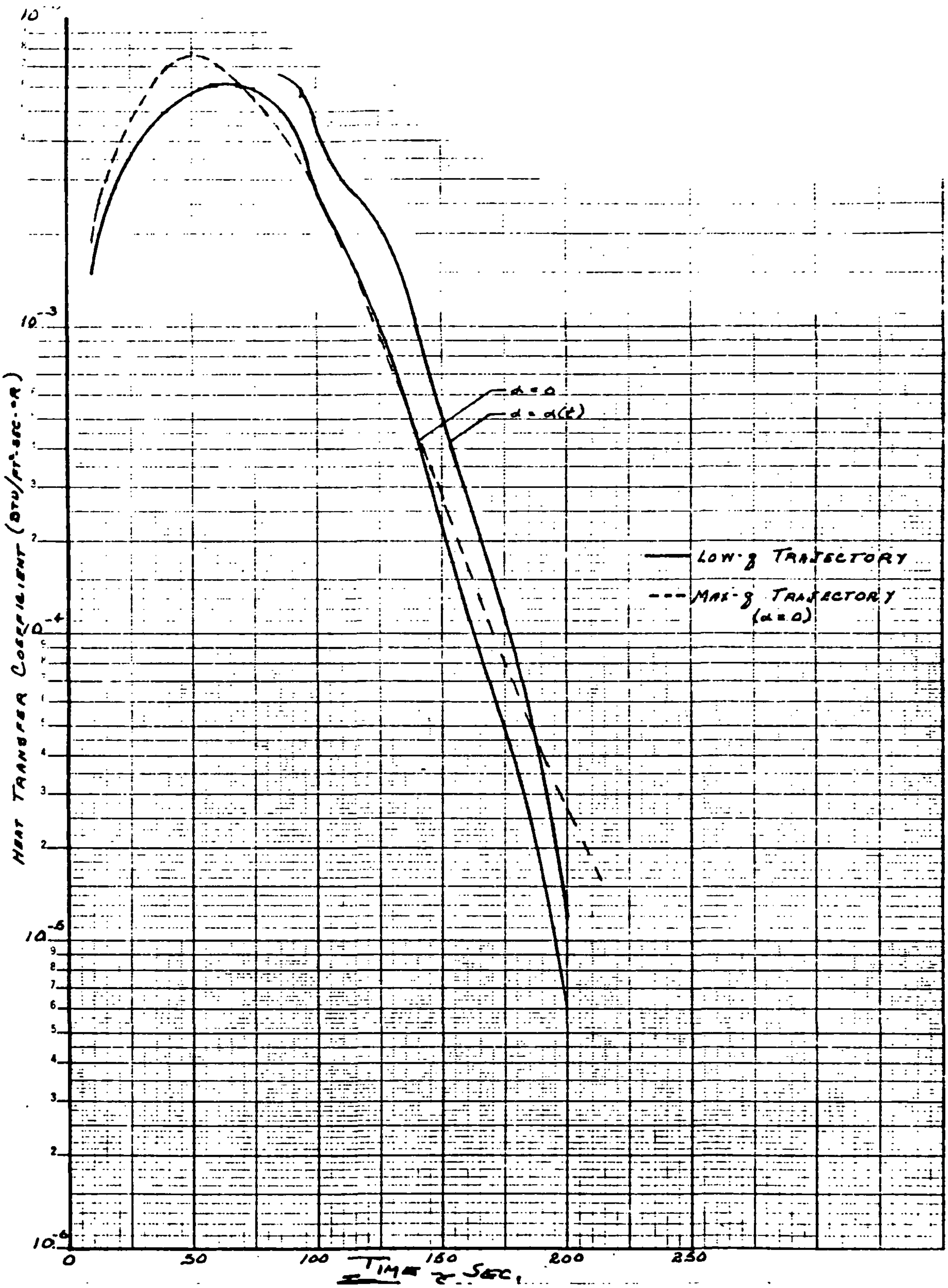

Figure D-4. ESS Sidewall Heat Transfer Coefficient, MDAC Space Station Payload ESS Station 855

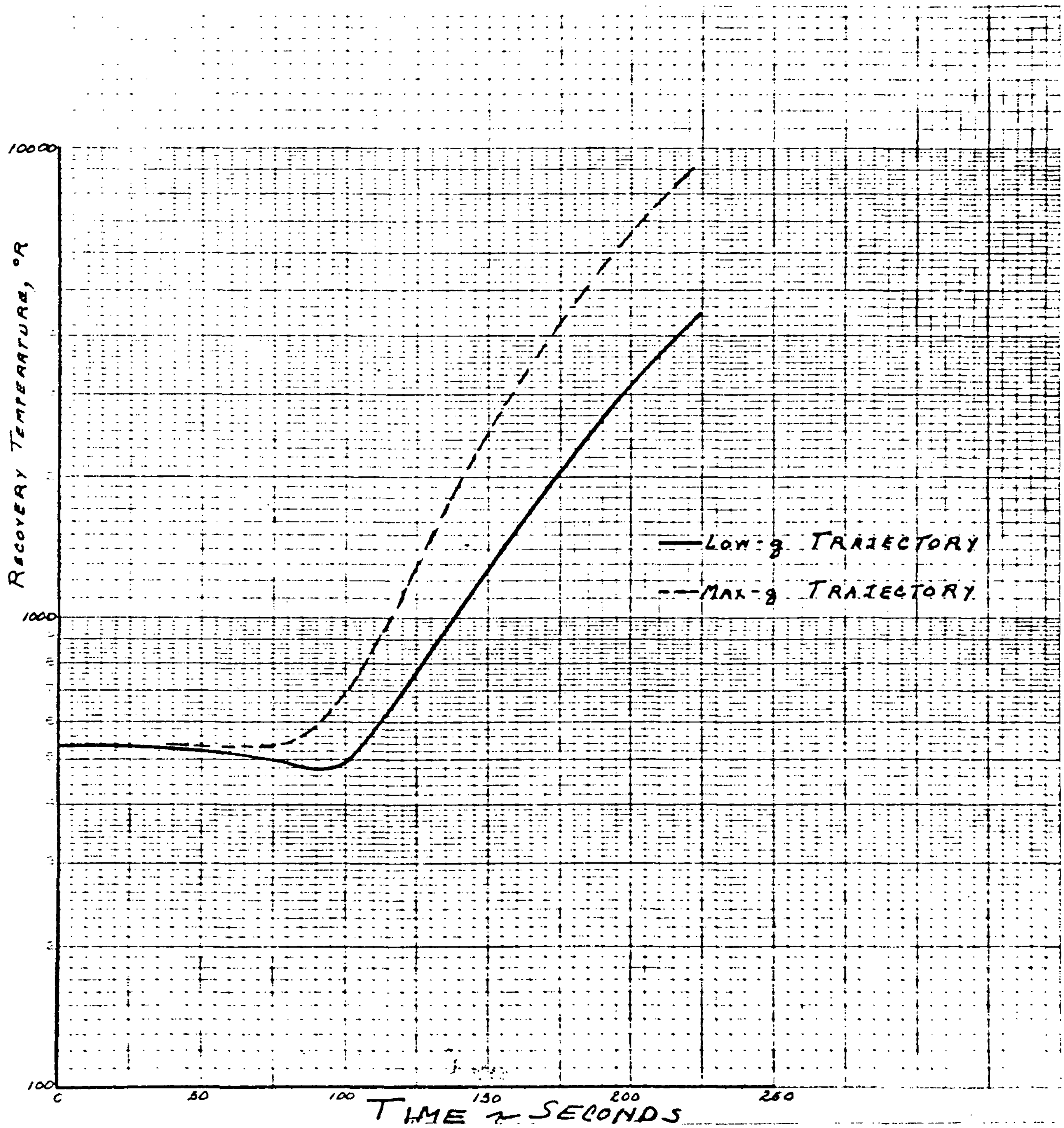

Figure D-5. ESS Sidewall Recovery Temperature, MDAC Space Station Payload ESS Station 855

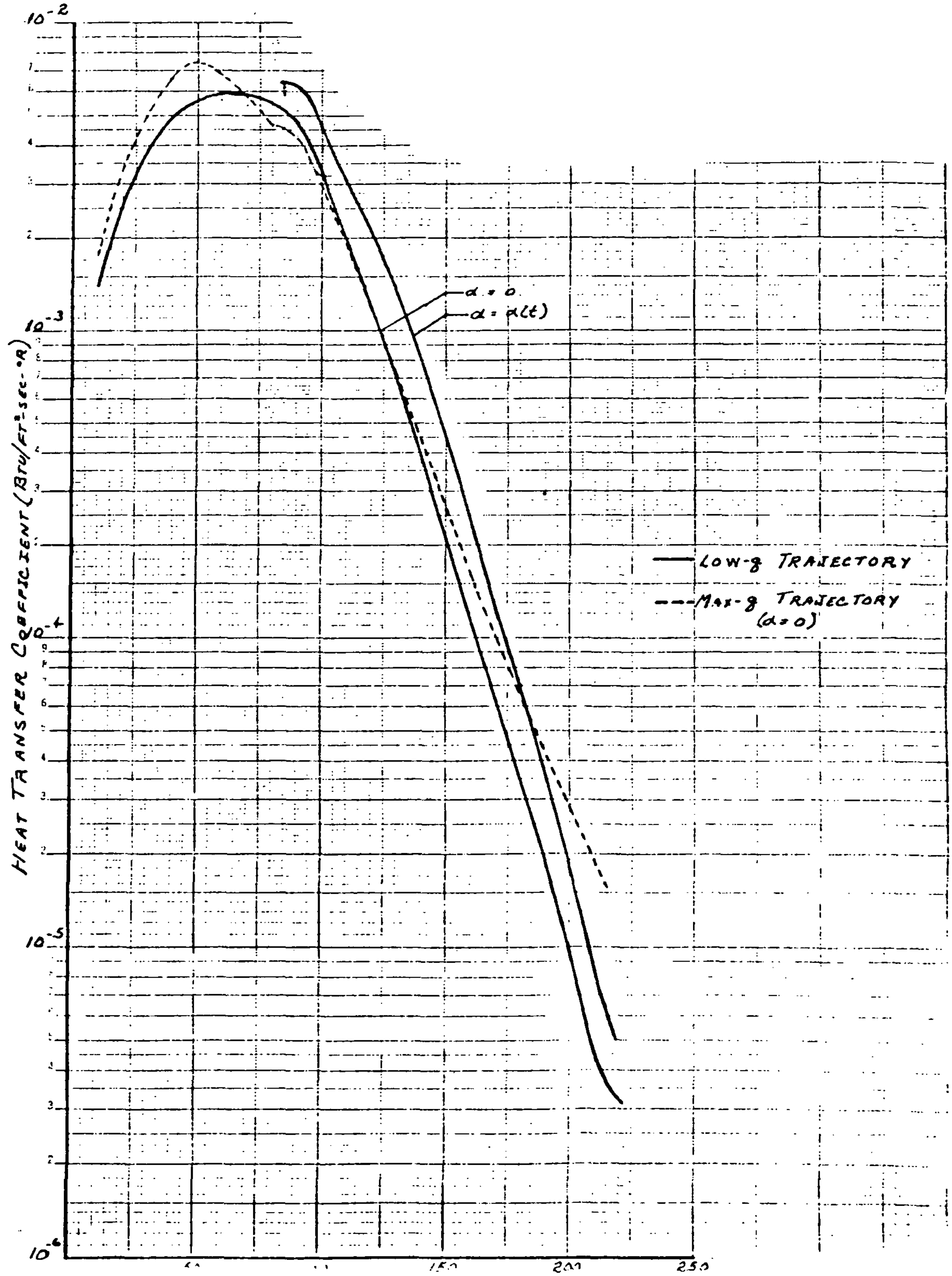

Figure D-6. ESS Sidewall Heat Transfer Coefficient, NR/RNS Payload ESS Station 855

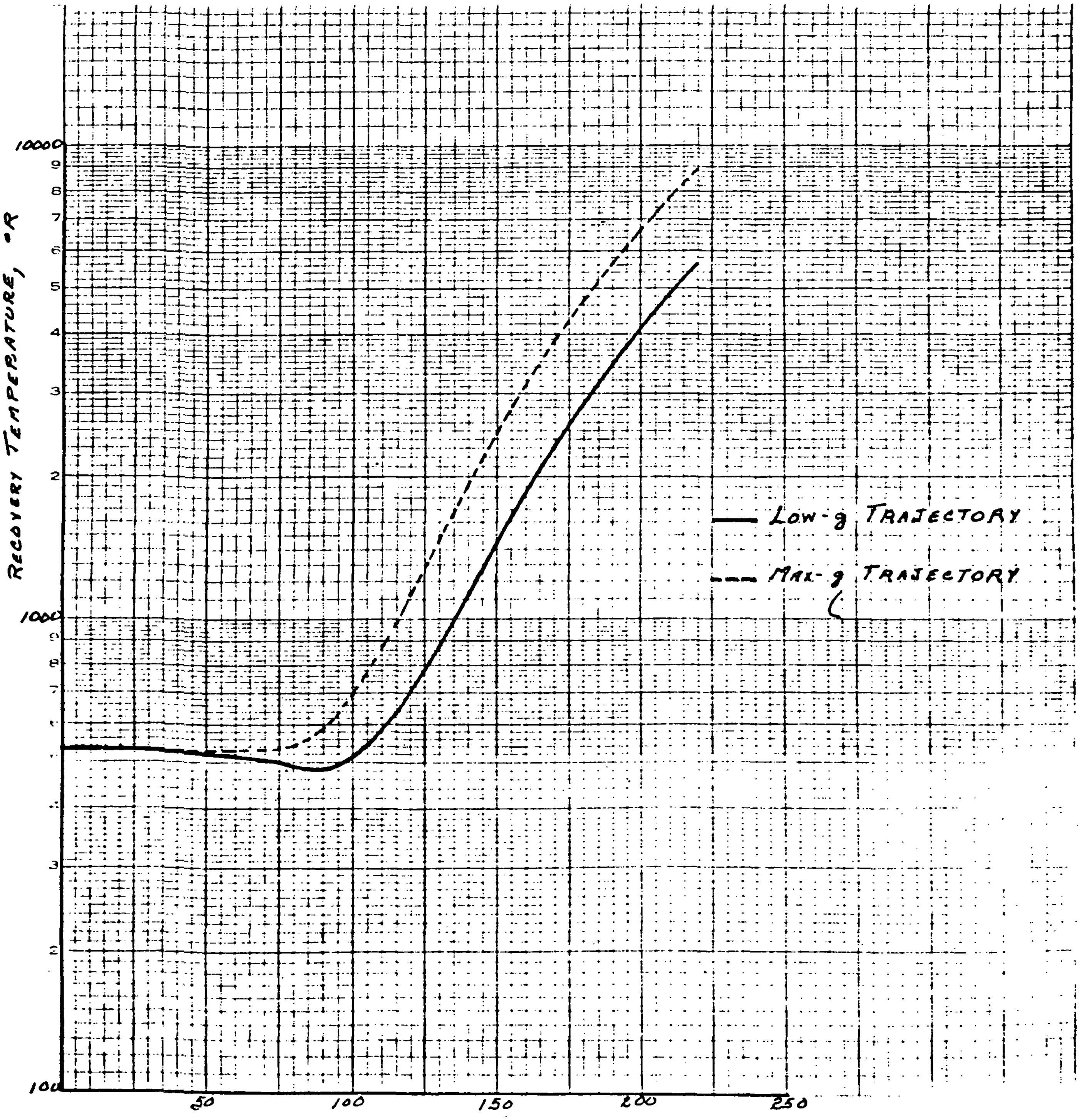

Figure D-7. ESS Sidewall Recovery Temperature, NR/RNS Payload ESS Station 855

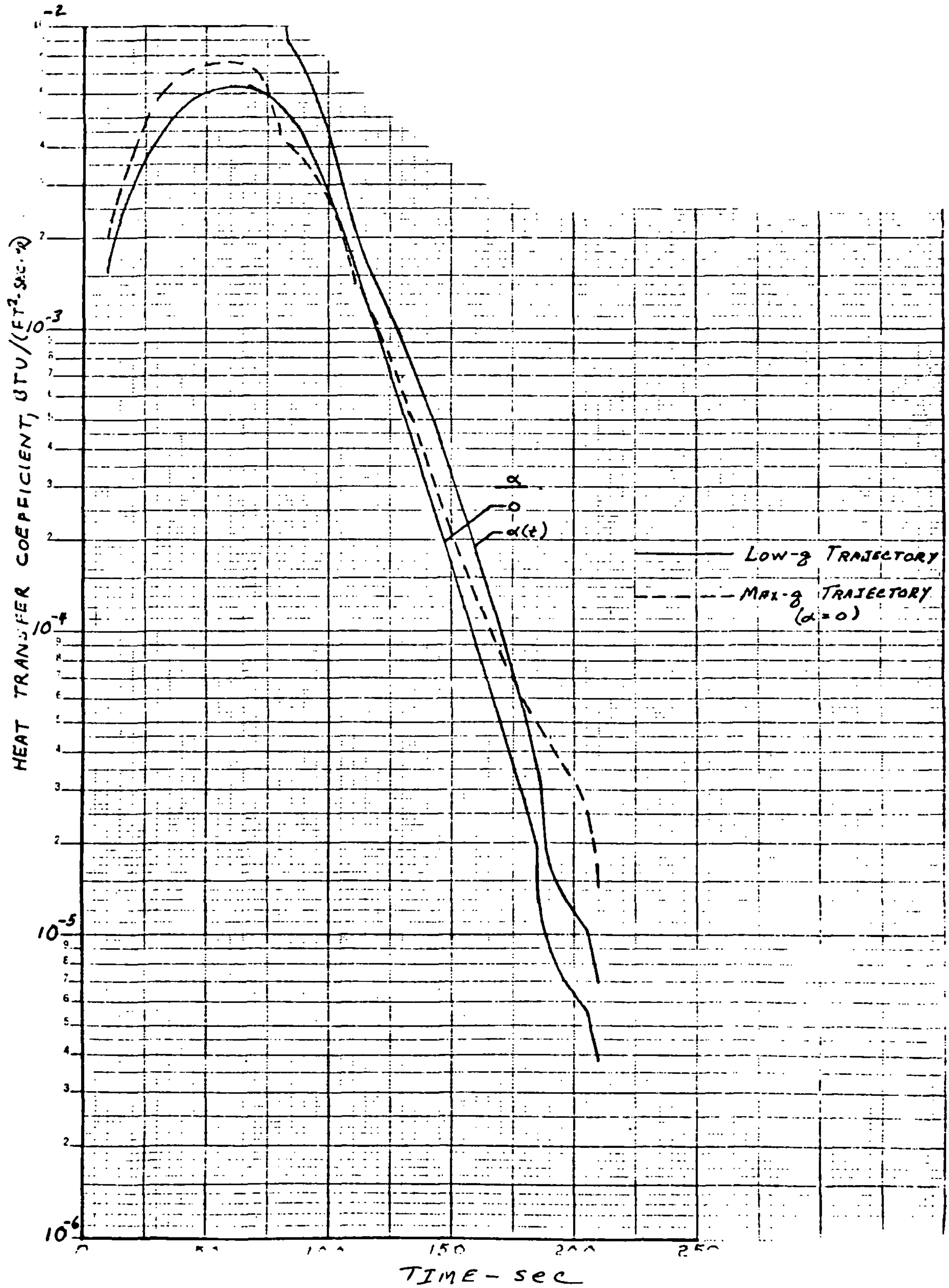

Figure D-8. ESS Sidewall Heat Transfer Coefficient, Space Tug Payload ESS Station 855

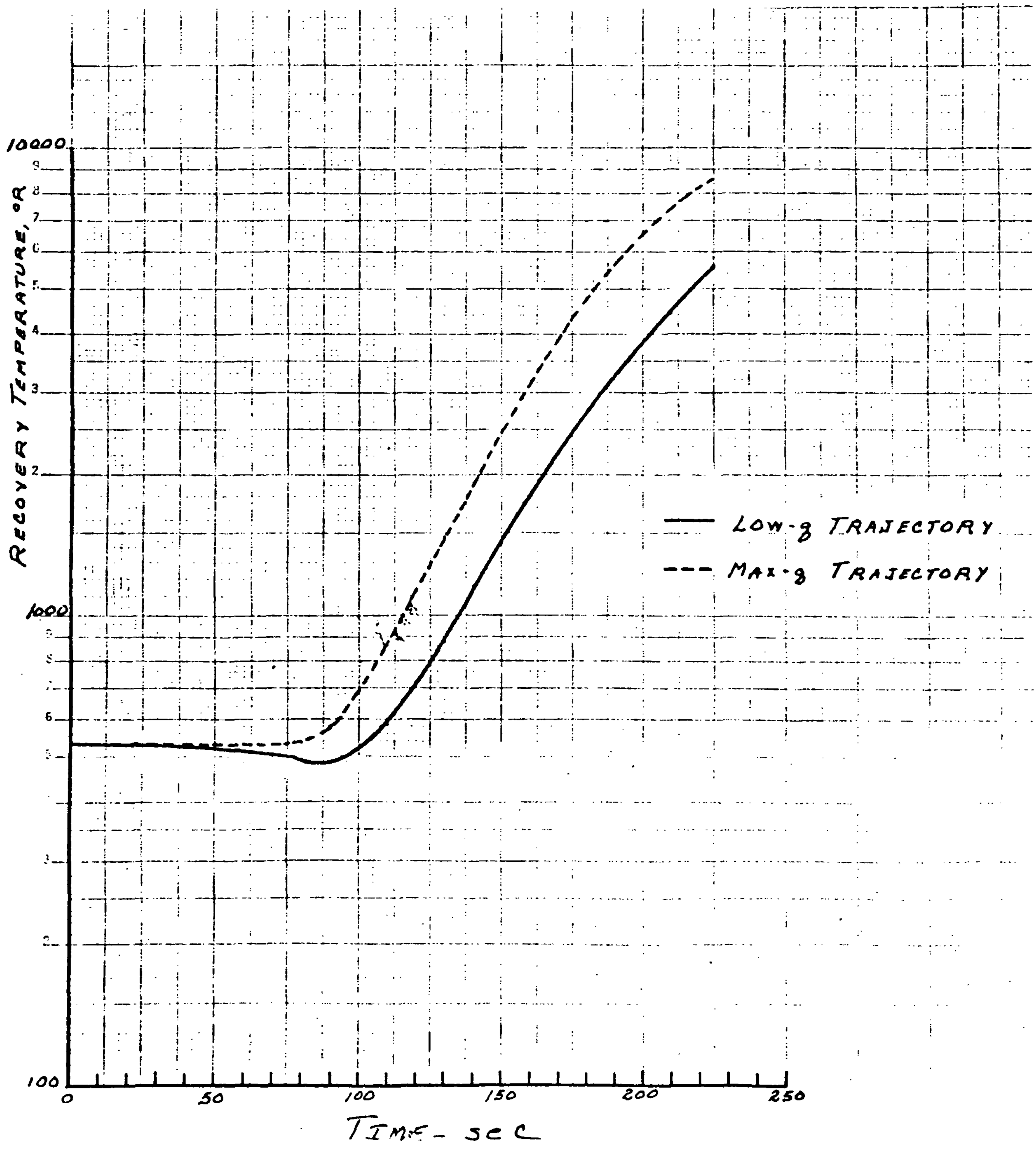

Figure D-9. ESS Sidewall Recovery Temperature, Space Tug Paylaod ESS Station 855

The aerodynamic heating indicator (AHI) has been used to indicate relative heating severity. For zero angle of attack and small trajectory changes, this is reasonable, as indicated in the Table D-1. However, for large trajectory changes and for large angle of attack, the AHI should not be used without a careful examination of all parameters that may affect the convective heat transfer rate, which is used to predict structural temperatures.

Table D-1. Comparison of Representative Heating Rates and Aero Heating Indicators

	High-q Trajectory Values/ Low-q Trajectory Values		
	MDAC	Space Tub	RNS
t = 140 sec			
q (α = 0) Btu/ft^2-sec	0.647/0.195	0.491/0.175	0.614/0.213
q ($\alpha \neq 0$) Btu/ft^2-sec	0.647/0.464	0.491/0.332	0.614/0.444
AHI x 10^{-6} (ft-lb/ft^2)	170.8/58.4	170.8/63.1	170.8/61.5
q (α = 0) ratio	3.32	2.80	2.88
q ($\alpha \neq 0$) ratio	1.39	1.47	1.38
AHI ratio	2.92	2.71	2.78
t = 160 sec			
q (α = 0) Btu/ft^2-sec	0.452/0.120	0.391/0.112	0.428/0.149
q ($\alpha \neq 0$) Btu/ft^2-sec	0.452/0.282	0.391/0.230	0.428/0.317
AHI x 10^{-6} (ft-lb/ft^2)	202.6/64.2	202.6/64.2	202.6/69.0
q (α = 0) ratio	3.77	3.47	2.87
q ($\alpha \neq 0$) ratio	1.60	1.70	1.35
HHI ratio	3.16	2.88	2.93

APPENDIX E. B-9U BOOSTER UPPER SURFACE TEMPERATURES DURING ASCENT WITH ESS AND ORBITER

The following illustrations and tables present the results of a short study to evaluate the booster upper surface skin maximum temperatures during ascent with various expendable second stages, compared with the baseline shuttle.

Three points on the booster surface were investigated for the aerodynamic heating effect of the different expendable second stages. These three points are illustrated in Figure E-1. Temperatures at these points were calculated with the booster-orbiter flying the baseline B-9U-1 trajectory, and with the booster-space tug, booster-RNS, and booster-space station configurations flying the ESS trajectory. Points A and B represent two areas on the booster forward section undergoing shock impingement due to the second stage, and their locations vary according to the second stage configuration. Point C is located in the most severe interference heating region caused by the mated attachment struts. Points A and B were modeled as 0.025-inch René-41 skin and point C as 0.025-inch René-41 skin over the LO_2 tank.

Table E-1 identifies for each point and mated configuration the view factor to space (used for radiation cooling) and the aerodynamic heating factor. The aerodynamic heating factor for the area around the mated attachment strut is shown in Figure E-2.

The maximum temperatures on the booster upper surface during ascent are summarized in Table E-2.

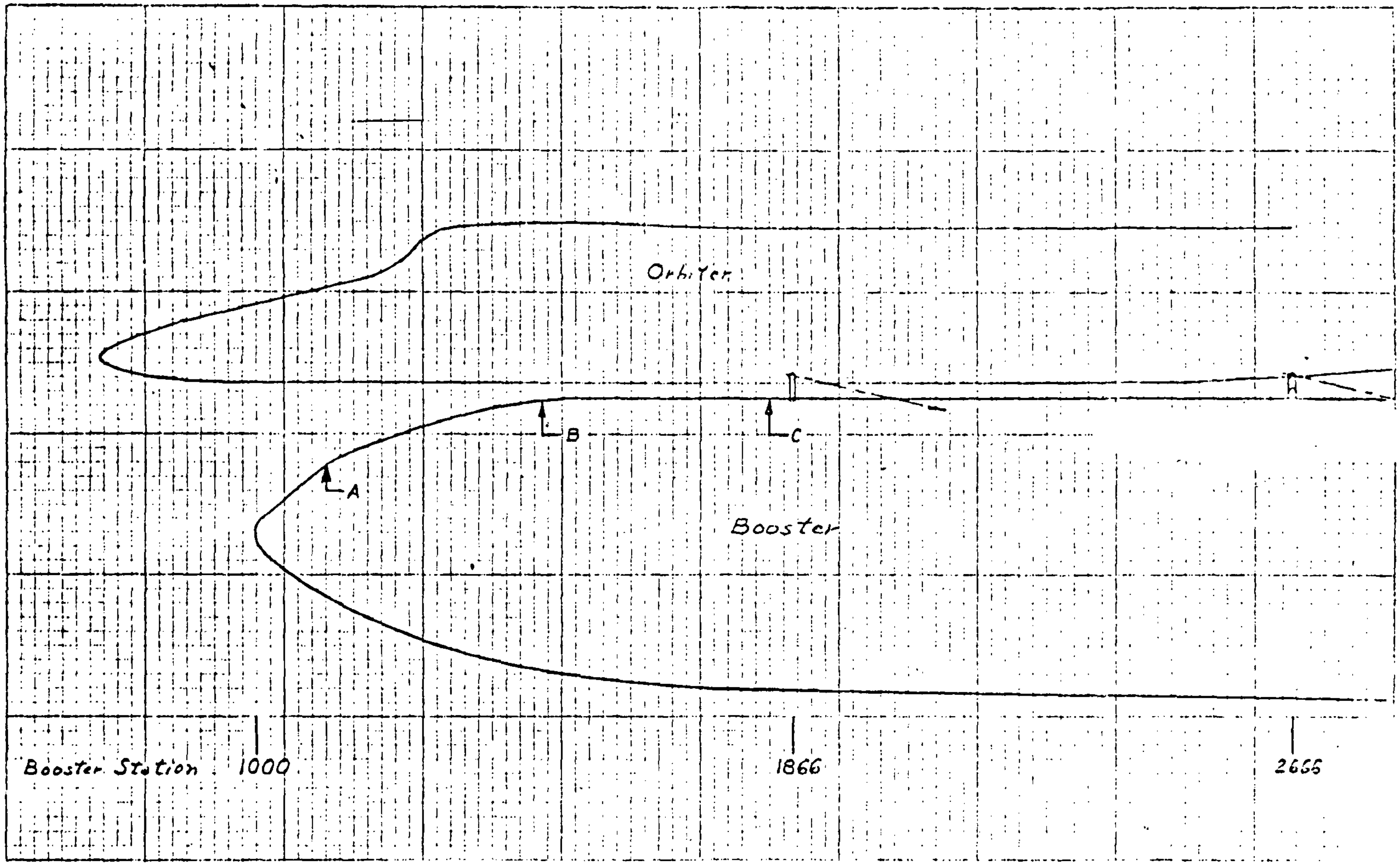

Figure E-1. Booster Top Centerline Locations Investigated

Table E-1. Heat Transfer Factors

Second Stage	Trajectory	Point A		Point B		Point C	
		View Factor to Space	Heating Factor	View Factor to Space	Heating Factor	View Factor to Space	Heating Factor
Orbiter	B 9U-1	0.55	1.0	0.10	0.5	0.083	0.16× Fig. E-2
Nuclear Stage	ESS (3-1-71)	0.54	0.5	0.10	0.5	0.10	0.16× Fig. E-2
Space Station	ESS (3-1-71)	0.60	1.0	0.10	0.5	0.10	0.16× Fig. E-2
Space Tug	ESS (3-1-71)	0.87	1.0	0.55	1.0	0.35	0.16× Fig E-2

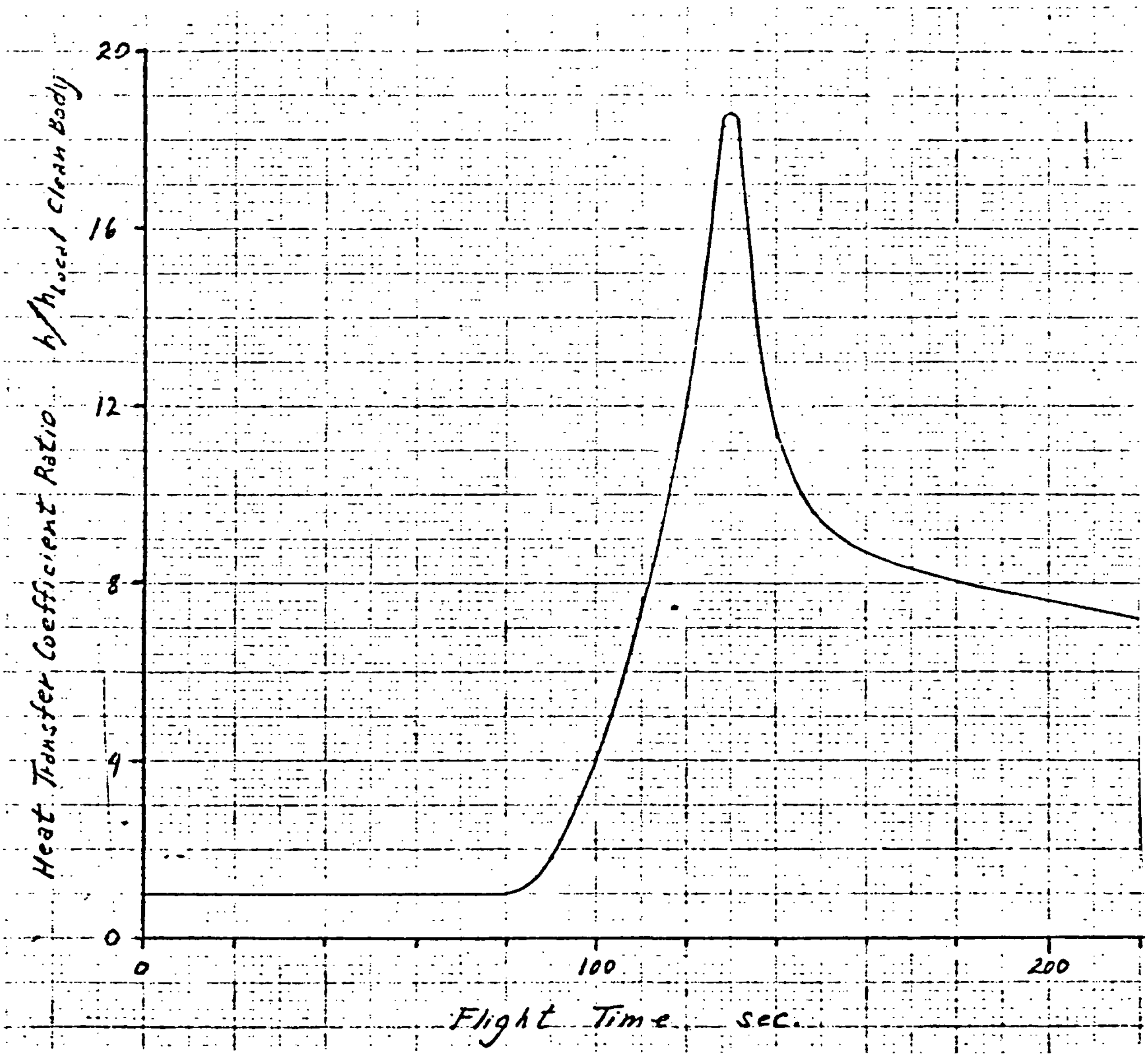

Figure E-2. Aerodynamic Heating Factor for Area Around Mated Attachment Strut

Table E-2. Peak Temperatures During Ascent on Booster Top Surface

Second Stage	Trajectory	Temperature (Deg. F)		
		Point A	Point B	Point C
Orbiter	T-B9U-1	1770	1780	2250
Nuclear Stage	ESS (3-1-71)	1500	2140	2290
Space Station	ESS (3-1-71)	1830	2140	2290
Space Tug	ESS(3-1-71)	1650	1870	1940

APPENDIX F. ORBITAL HEATING RATES FOR ESS ELECTRICAL CONTAINERS

The orbital thermal environments used in this study were generated using the Space Division's Space Vehicle Thermal Environment Program, described in SD 69-507 for the IBM 360 computer. This program was developed for computing the thermal environment encountered by multisurfaced vehicles in orbit about any of the nine planets, the moon, or the sun. The physical model of orbital motion employed in the program is an isolated dynamic system consisting of the planet, a satellite, and the sun. It is assumed the planet has a uniform spherical shape, no atmosphere, and is a diffused reflector of the solar spectrum. Orbital input data required include orbital altitude, angle between orbit plane and sun (β), position at which the satellite crosses the equator traveling from south to north, and, for elliptical orbits, the semimajor and semiminor axes. The program uses these orbital parameters to describe the position of the space vehicle relative to the planet and sun for a complete orbit, including planetary shadow effects. As output, the program provides a complete orbital history of the radiant energy incident upon each satellite surface due to direct solar radiation, planetary reflected solar radiation, and earth-emitted radiation. If desired, the program also determines the transient temperature history of the satellite surfaces for the complete orbit.

To determine the incident orbital heat loads around the ESS, the vehicle was represented by an eight-sided prism for use with the orbital heating program. Figure F-1 shows the arrangement of sides for the Y-axis perpendicular to the orbital plane (Y-POP) nose forward solar orientation. The orbital heating for each of the vehicle sides is presented as a printed output and also displayed on cathode ray tube (CRT) plots. The program also delivers the incident heating for each side as a punched-deck, which consists of direct solar and planetary reflected solar radiation combined and earth-emitted radiation. This deck is used directly as the incident radiation curve input for equipment container thermal models.

Shown in Table F-1 for a complete orbit is the integrated incident radiation on each of the eight vehicle sides as well as on the nose and base. The sum of direct solar and planetary reflected solar radiation is shown along with earth-emitted radiation for solar orientations of Y-POP nose forward at β angles of 0, 40, and 80 degrees. From this table, the maximum and minimum orbital heat loads and temperatures for each of the vehicle sides can be determined by interpolation for the range of orbital parameters under consideration.

Figures F-2 and F-3 show the temperature on the sides of the ESS relative to stage positions and axis orientation. A review of these figures indicates that containers housing high-heat-producing equipment should be installed in areas adjacent to sides 4, 5, and 6. Containers housing low-heat-producing equipment should be installed adjacent to sides 8, 9, and 10, to take advantage of solar heating.

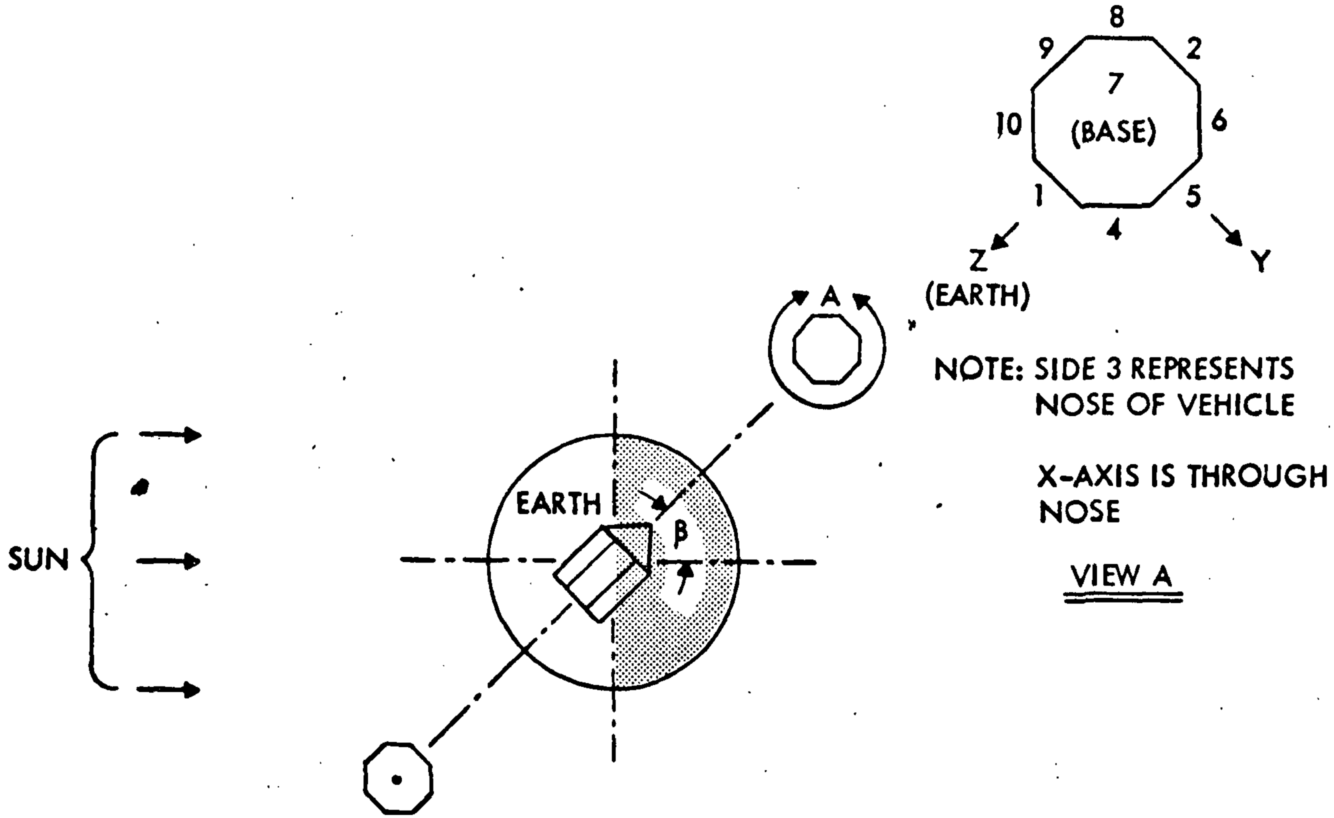

Figure F-1. Y-POP Nose Forward Solar Orientation

Table F-1. Integrated Incident Radiation for Eight-Sided Prism (with two ends) in Orbit

Side	Sun vs. Orbit Inclination Angle-β	Y-POP NOSE FORWARD SOLAR	EARTH EMITTED	MAX. TEMP °F	MIN. TEMP °F
1	0°	79.8622	98.915	+2°	
	40°	65.2903	98.915		
	80°	48.8458	98.915		-4°
2	0°	214.6548	0	+25°	
	40°	164.3048	0		
	80°	37.0768	0		-208°
3	0°	177.3812	33.4336	+12°	
	40°	142.5761	33.4336		
	80°	42.4089	33.4336		-75°
4	0°	59.4537	74.4346	-46°	
	40°	38.9037	74.4346		
	80°	8.7836	74.4346		-80°
5	0°	22.7913	33.4336	-120°	
	40°	17.4466	33.4336		
	80°	3.9411	33.4336		-135°
6	0°	154.5878	4.4912	+32°	
	40°	9.3620	4.4912		
	80°	0.5253	4.4912		-248°
7	0°	153.9719	33.4336	+10°	
	40°	121.4950	33.4336		
	80°	40.0195	33.4336		-75°
8	0°	155.0423	4.4912	+85°	
	40°	302.1195	4.4912		
	80°	471.8127	4.4912		+20°
9	0°	23.1815	33.4336	+98°	
	40°	290.6761	33.4336		
	80°	670.5327	33.4336		-75°
10	0°	59.5514	74.4346	+82°	
	40°	132.5509	74.4346		
	80°	480.1972	74.4346		-46°

These are sample or reference minimum and maximum temperatures for a piece of 0.20-inch aluminum, with $\alpha = 0.25$ and $\epsilon = 0.85$.

C5

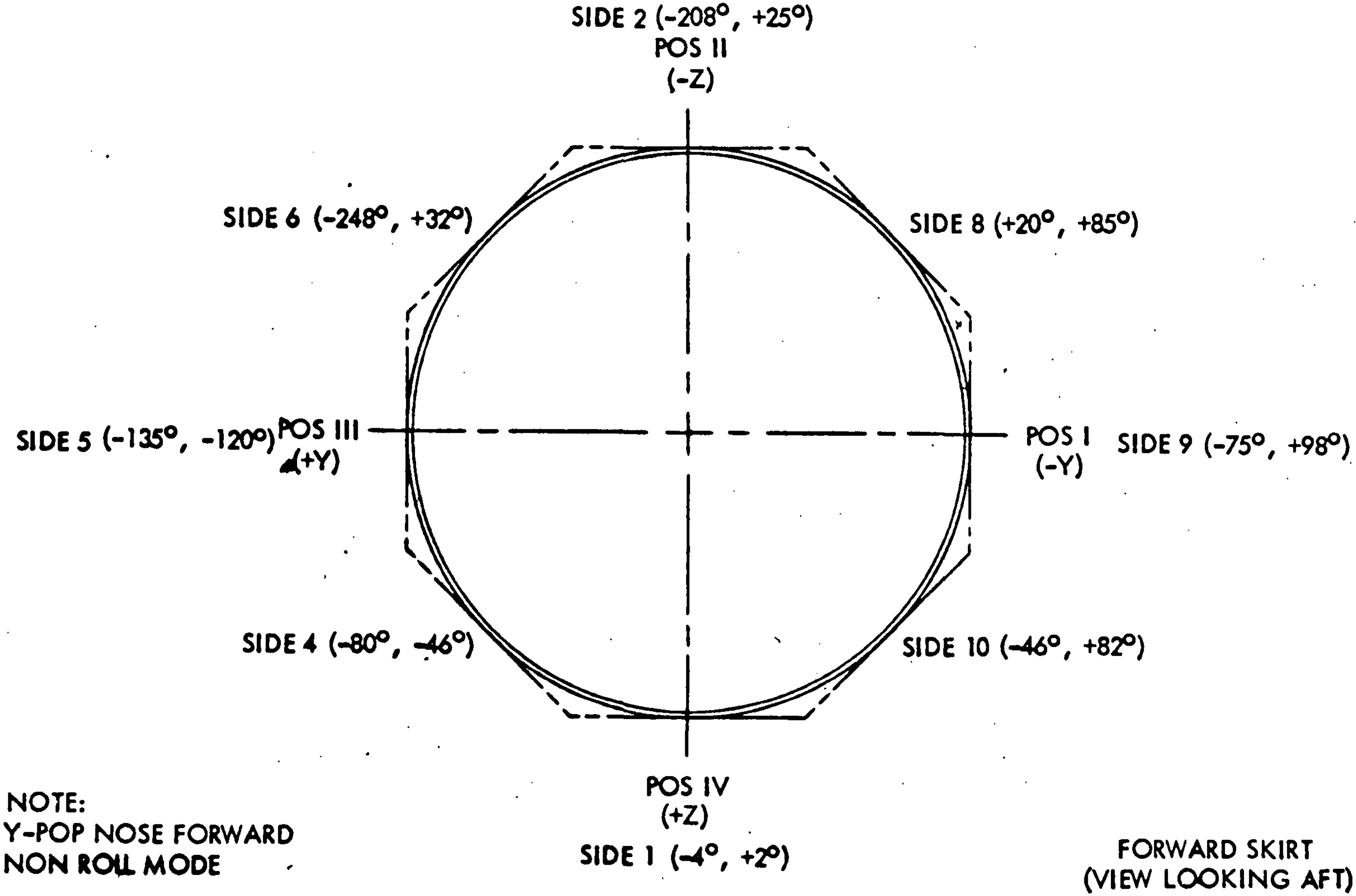

Figure F-2. Forward Skirt On-Orbit Temperatures

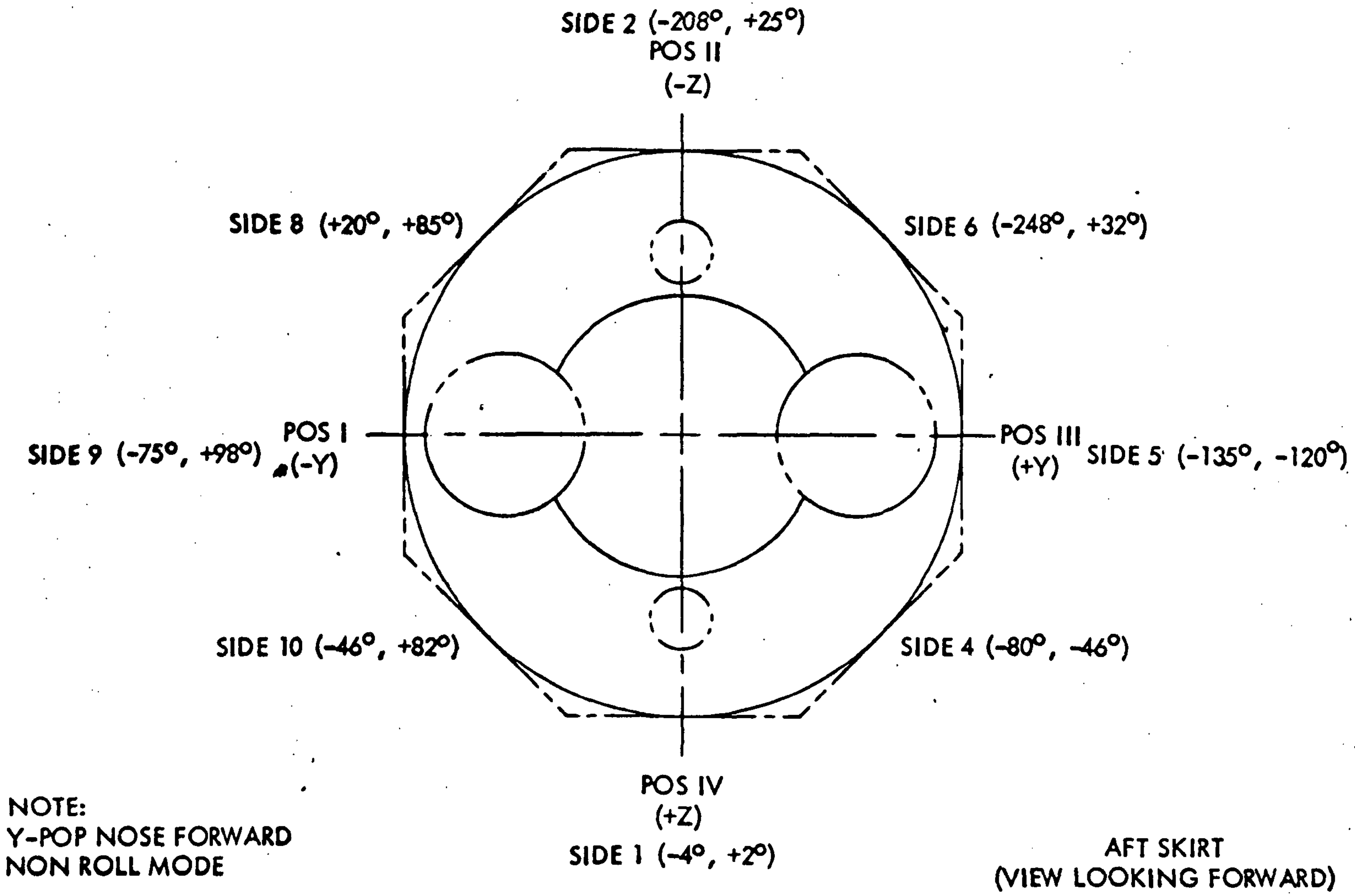

Figure F-3. Aft Skirt On-Orbit Temperatures

APPENDIX G. ESS BODY LOADS

The following figures define the body loads on the ESS vehicle structure that were not critical in the basic design. Included are all pre-launch loads and space tug loads.

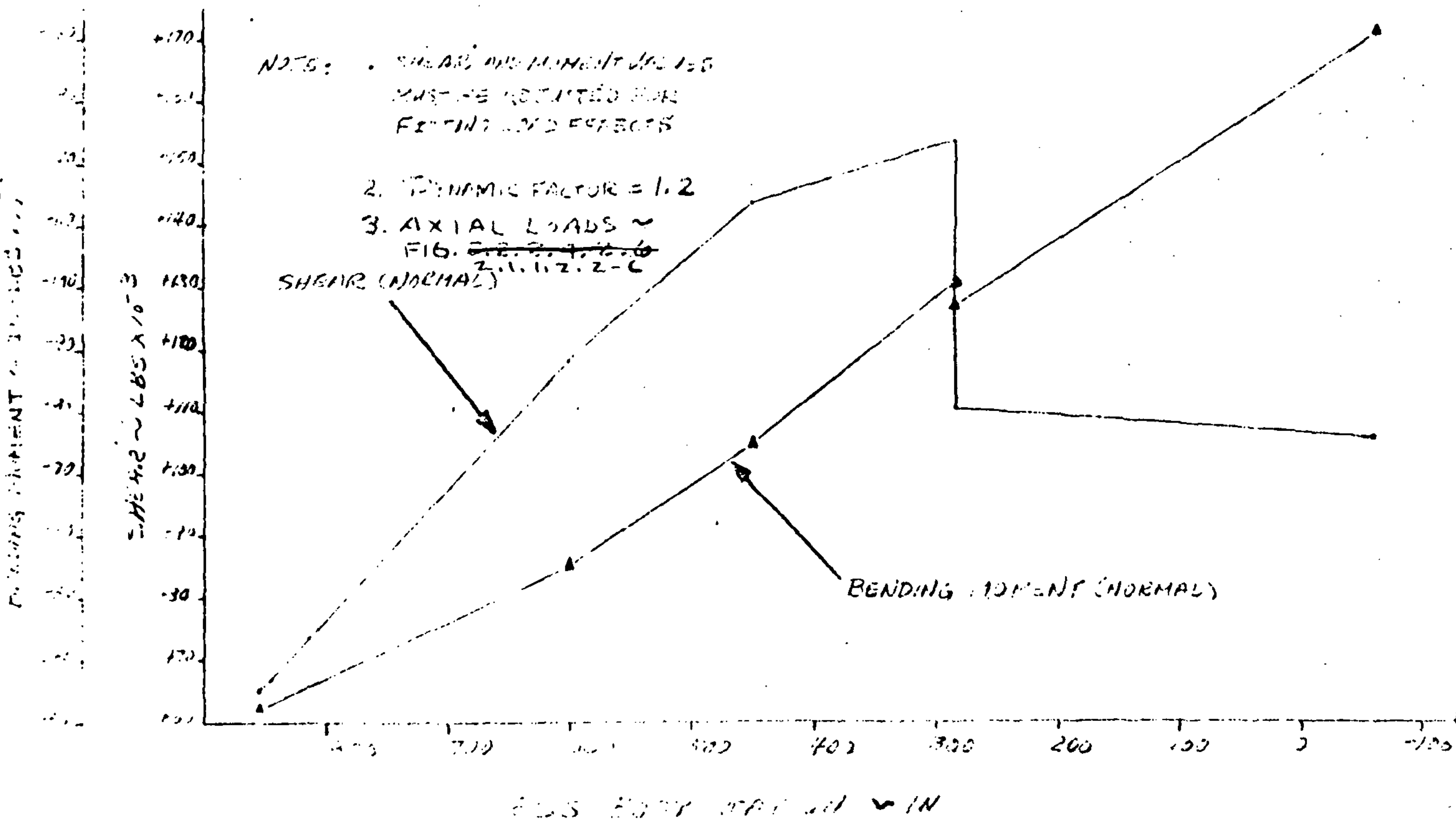

Figure G-1. ESS/Space Tug Max qα Normal Body Loads, q = 336.5 PSF α = -8.62°
(Tailwind Case)

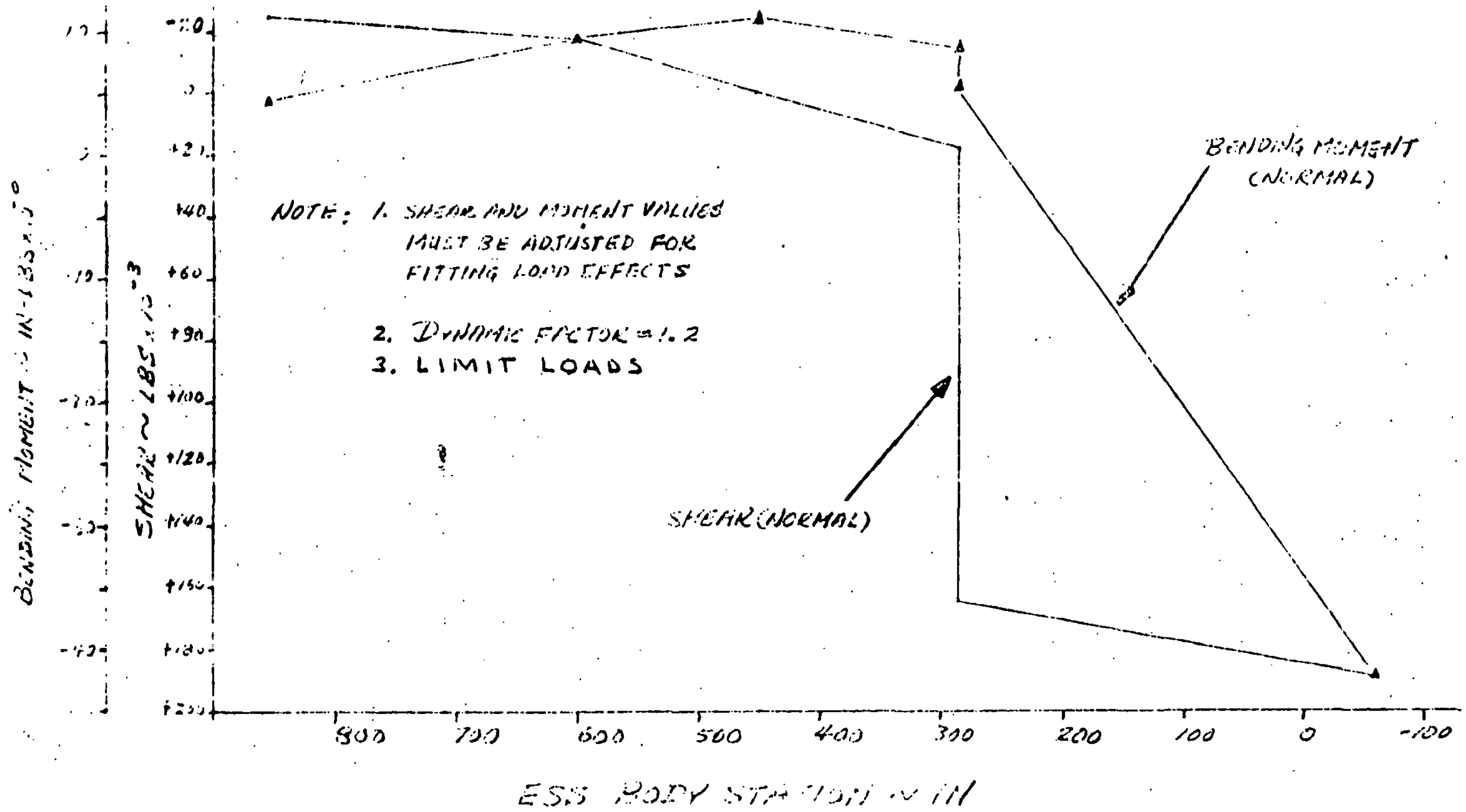

Figure G-2. ESS/Space Tug Max qα Normal Body Loads, q = 525.0 PSF α = 2.97°

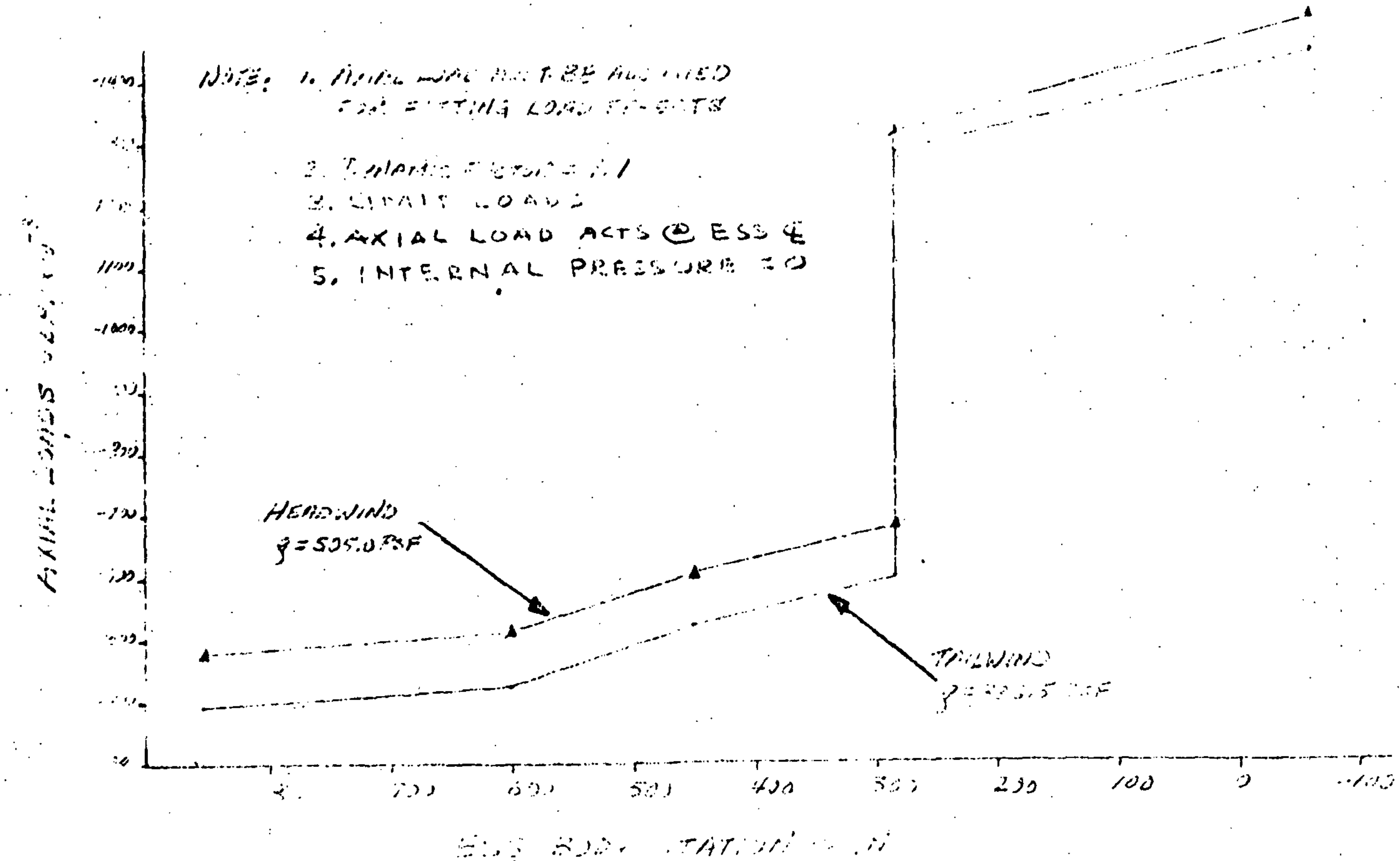

Figure G-3. ESS/Space Tug Max qα Axial Body Loads

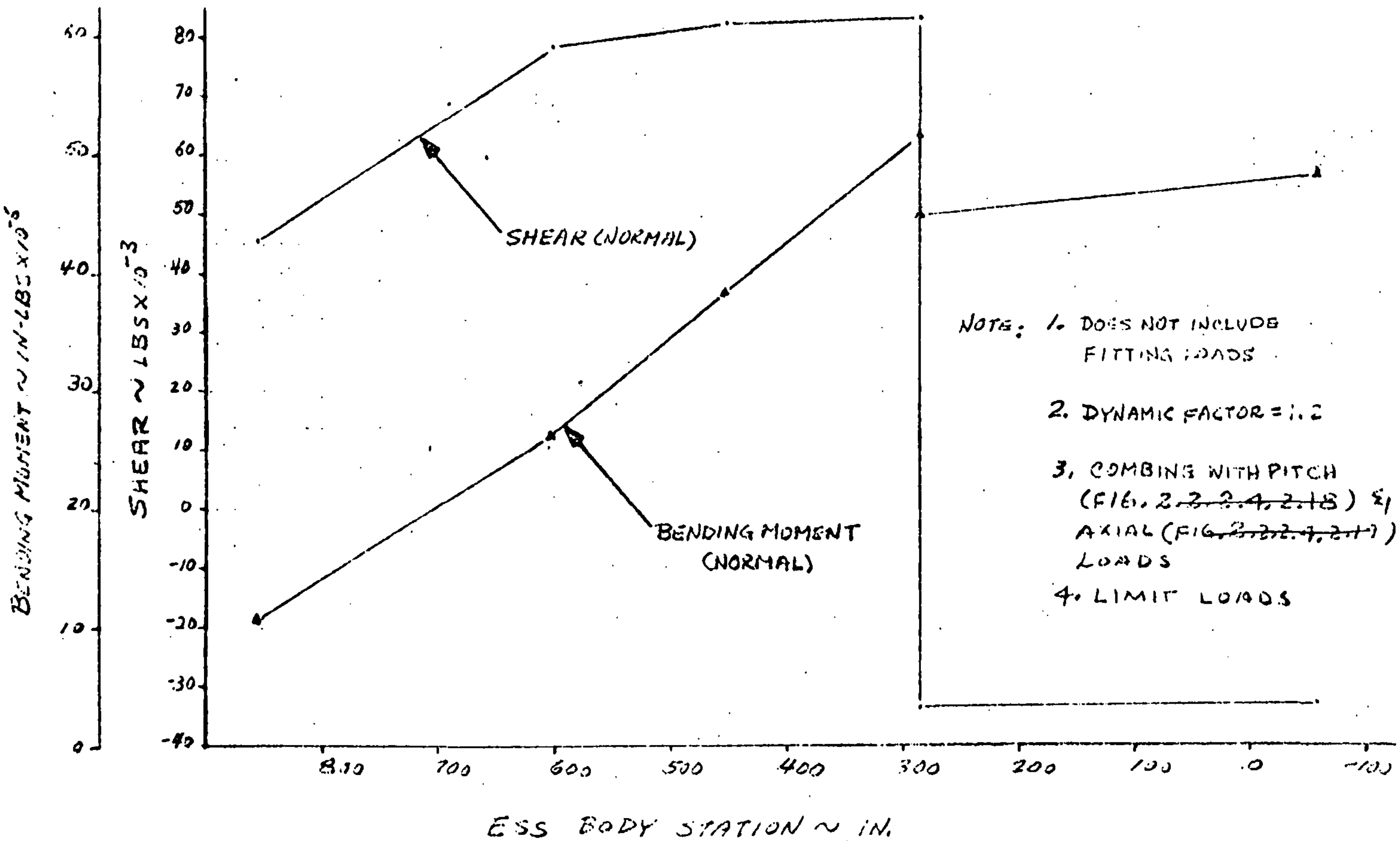

Figure G-4. ESS/Space Tug Max qα Trim Yaw Body Loads
q = 401.8 PSF α = -2.72°

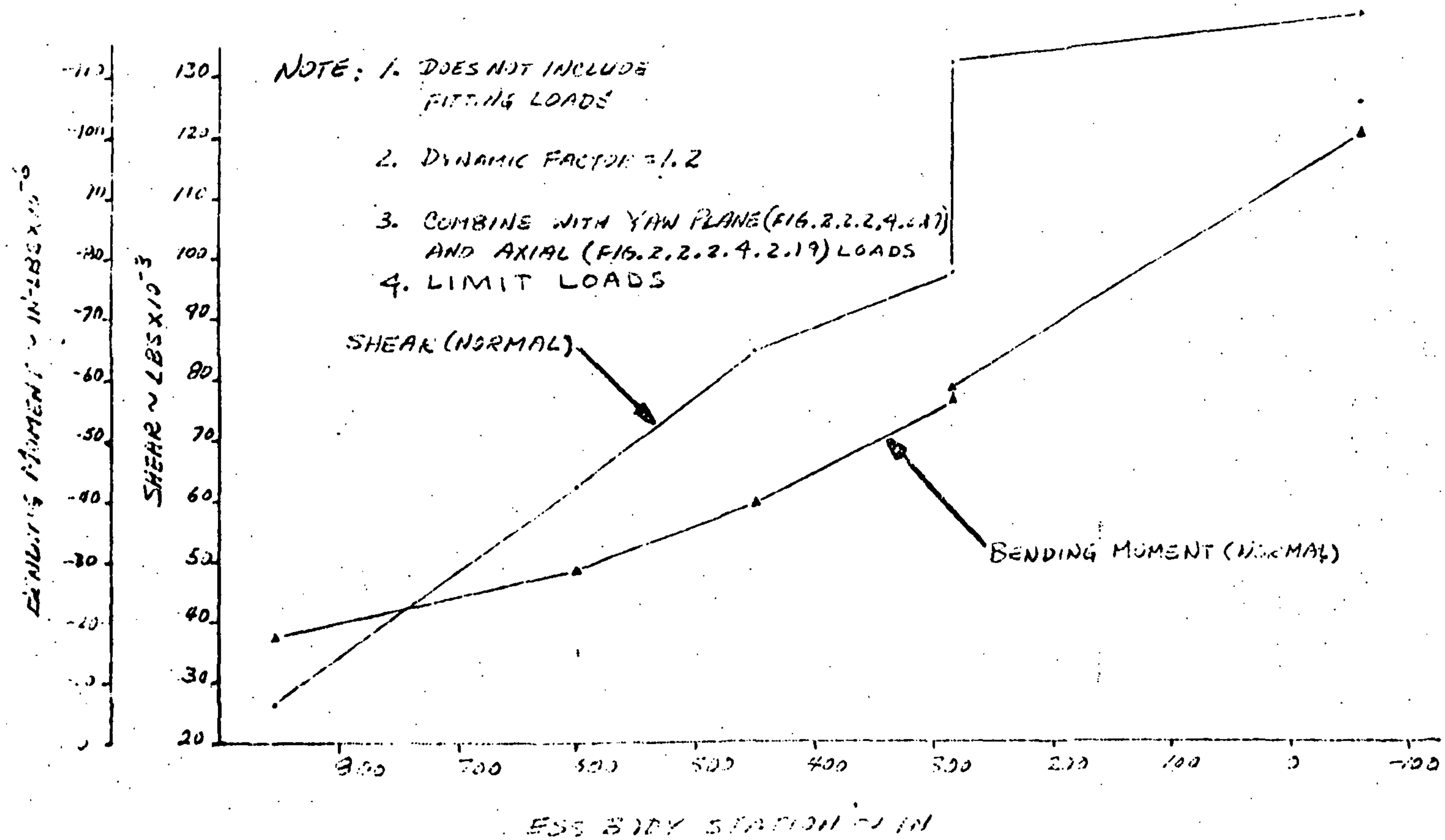

Figure G-5. ESS/Space Tug Max qα Trim Pitch Body Loads
q = 401.8 PSF α = 2.72° β = 4.0°

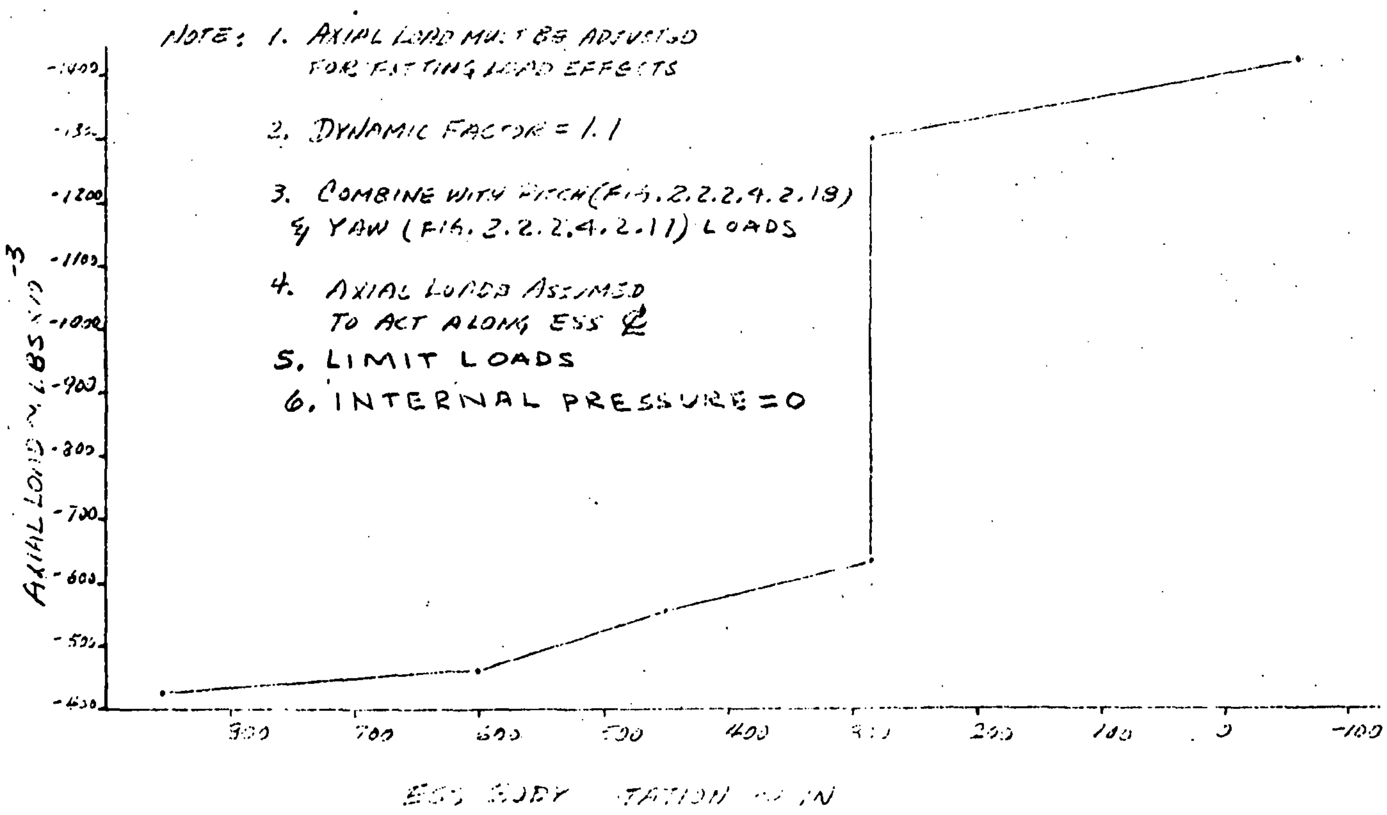

Figure G-6. ESS/Space Tug Max qα Trim Axial Body Loads
q = 401.8 PSF α = -2.72°

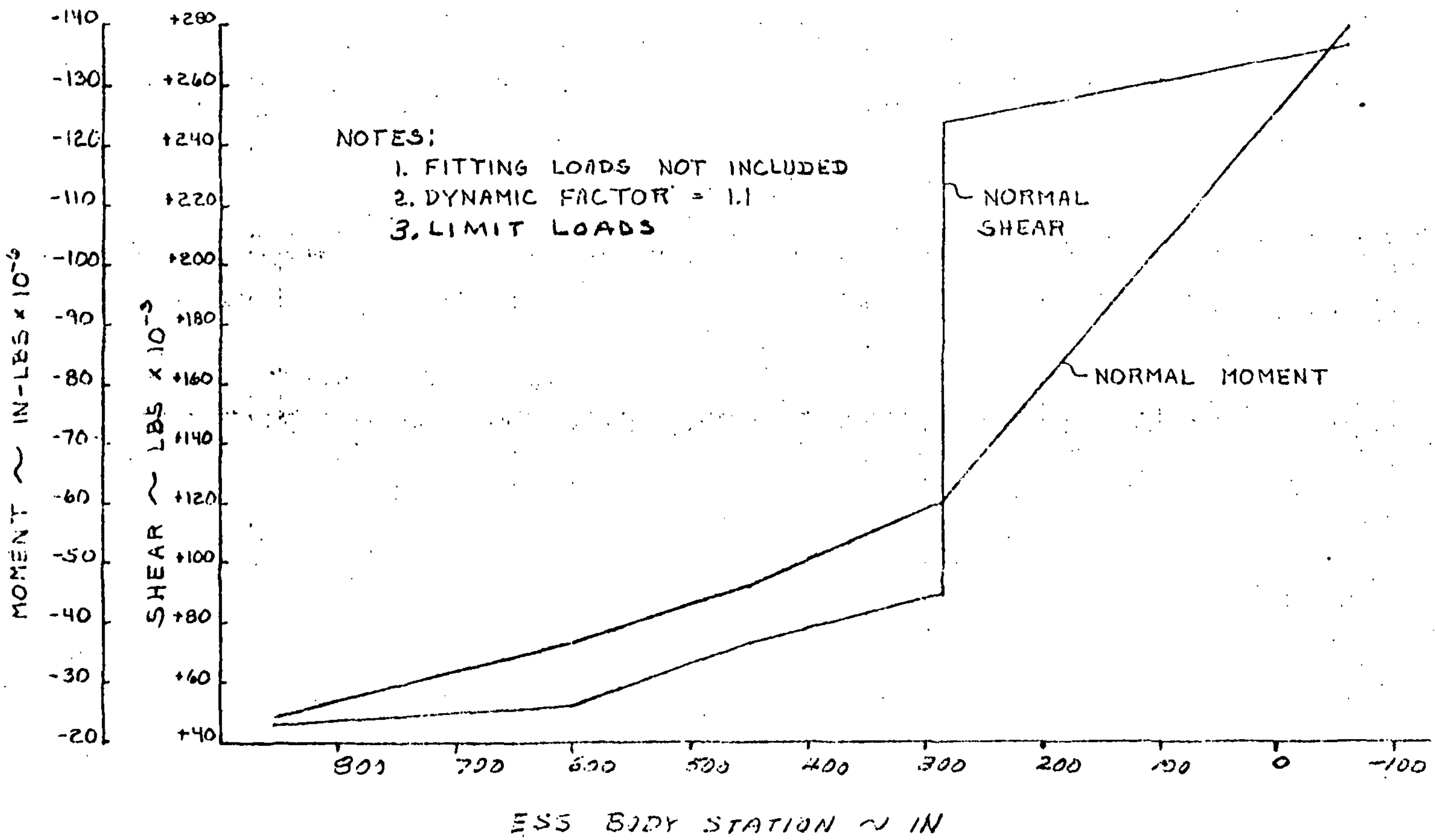

Figure G-7. ESS/Space Tug End Boost Normal Body Loads

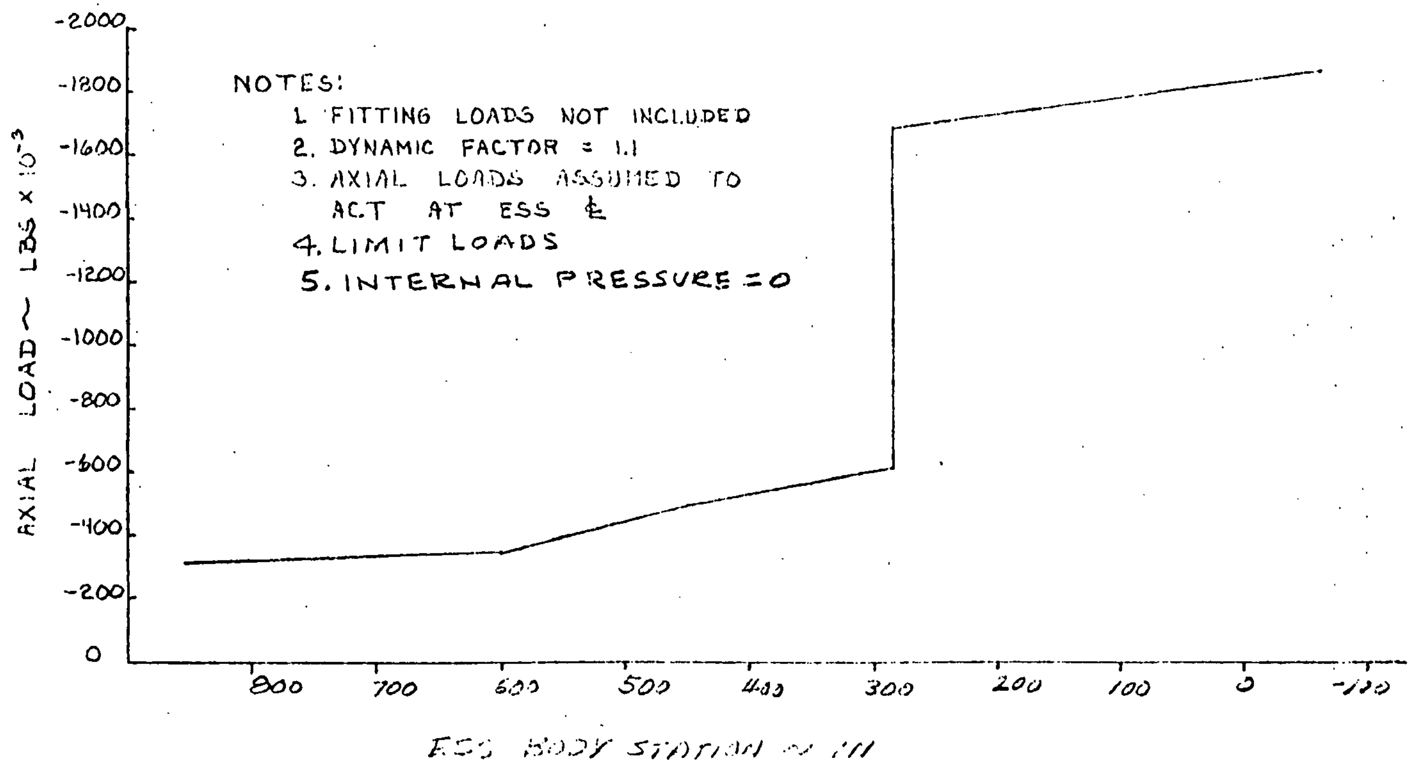

Figure G-8. ESS/Space Tug End Boost Axial Body Loads

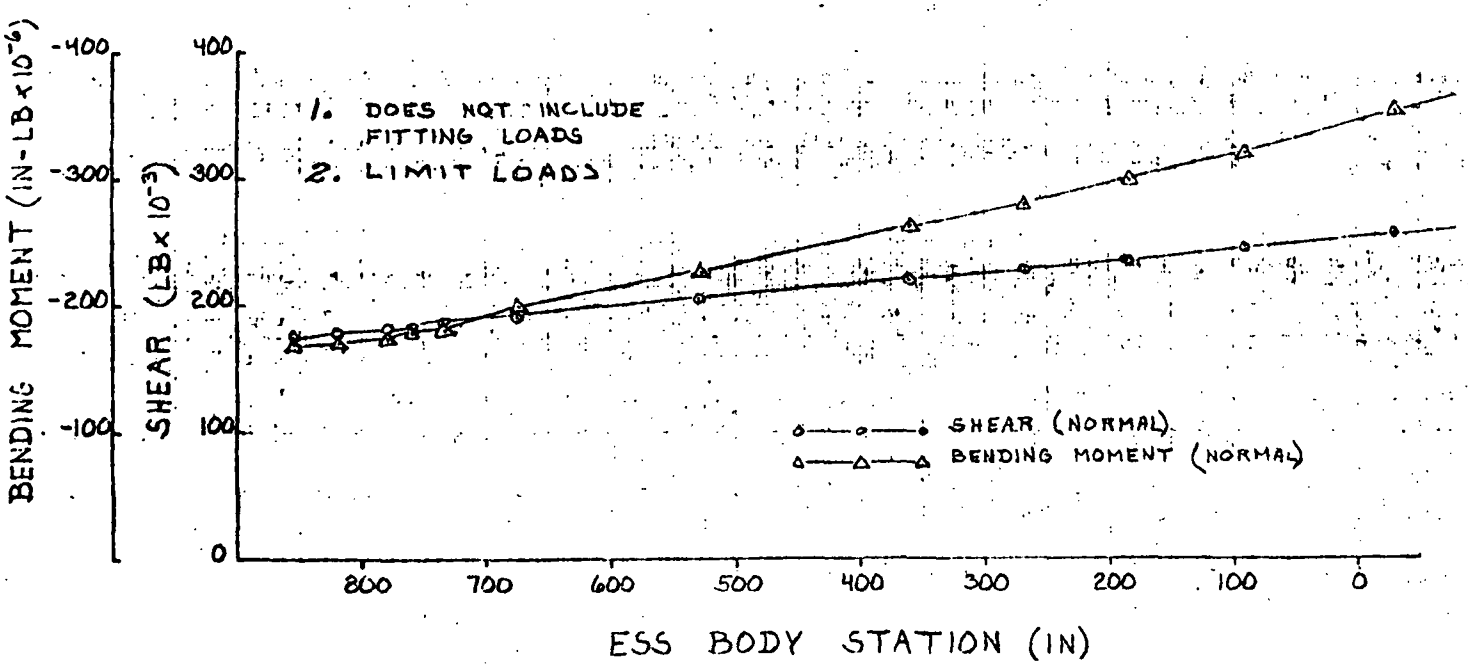

Figure G-9. Prelaunch Loads on Unfueled ESS/RNS Due to 14 Day Wind and Von Karman Effects (Winds in Direction of ESS to Booster) Headwind

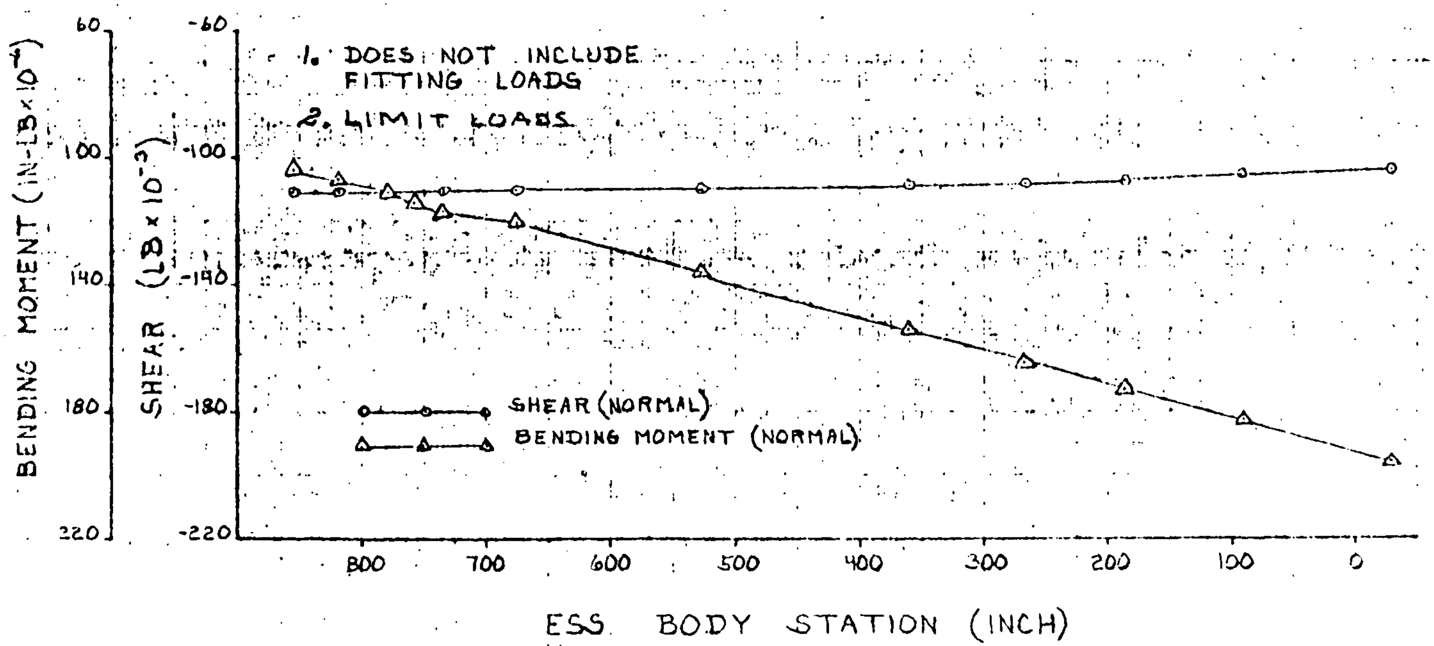

Figure G-10. Prelaunch Loads on Unfueled ESS/RNS Due to 14 Day Wind and Von Karman Effects
(Wind in Direction of Booster to ESS)
Tailwind Partial Shielding

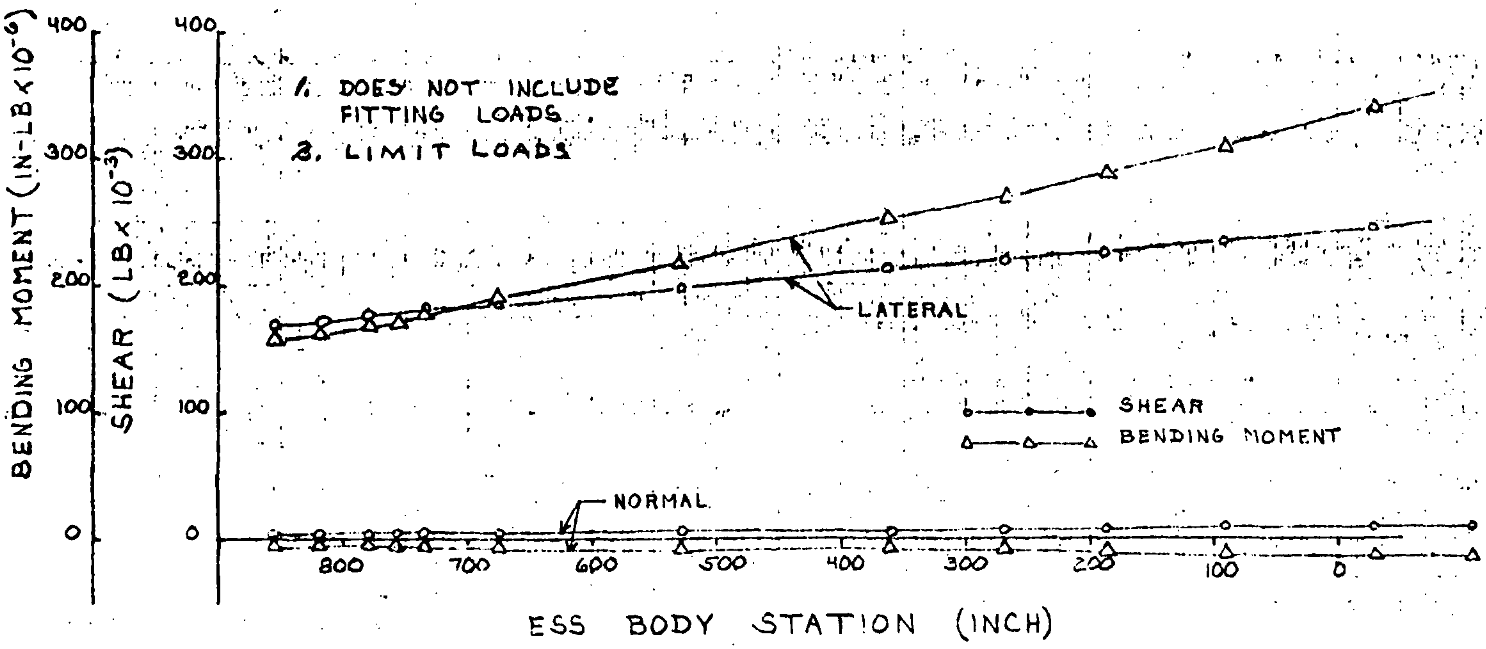

Figure G-11. Prelaunch Loads on Unfueled ESS/RNS Due to 14 Day Wind and Von Karman Effects (Winds in Lateral Direction to ESS) Crosswind

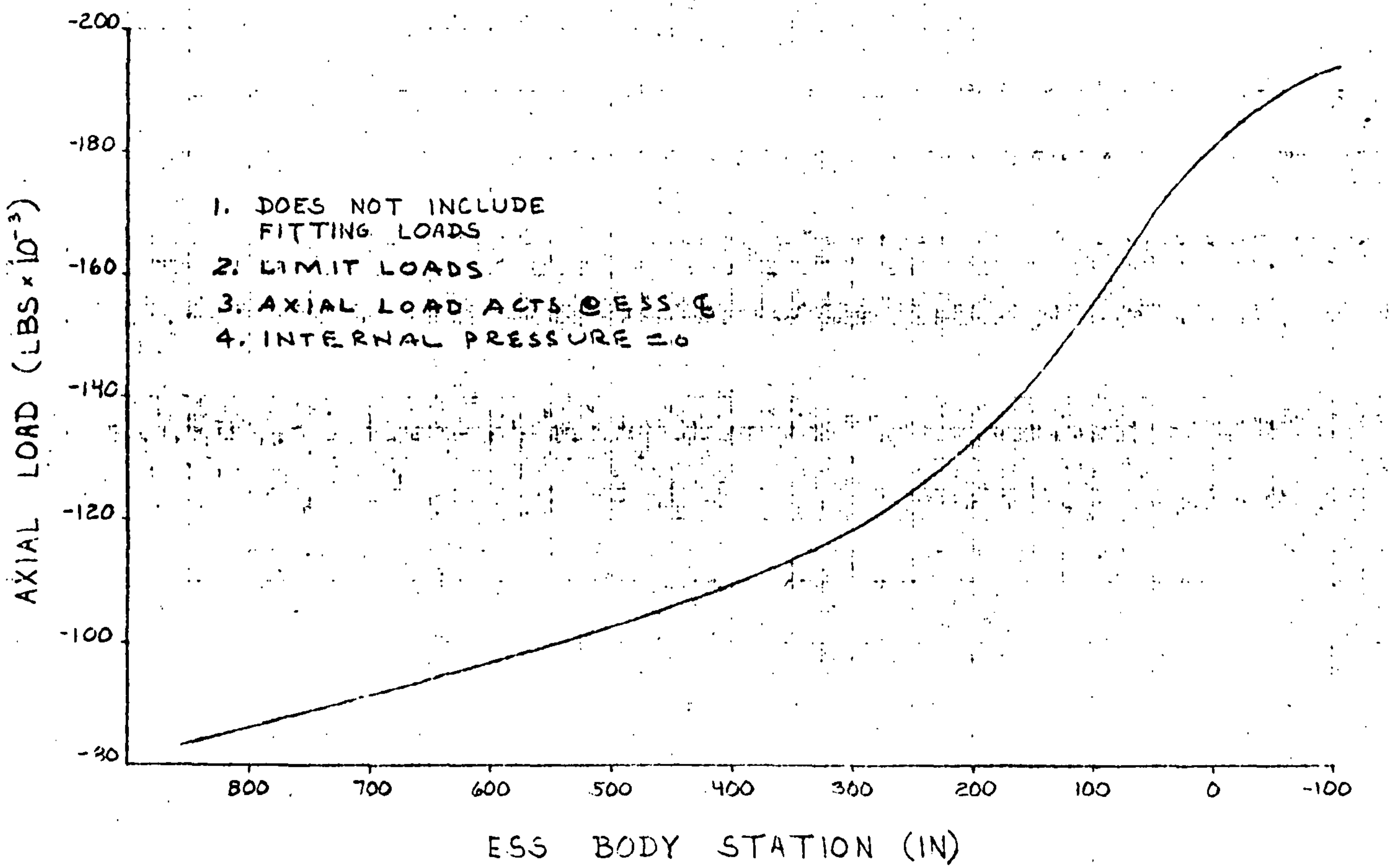

Figure G-12. Prelaunch Loads on Unfueled ESS/RNS Axial Loads for Use With 14-Day Wind Conditions

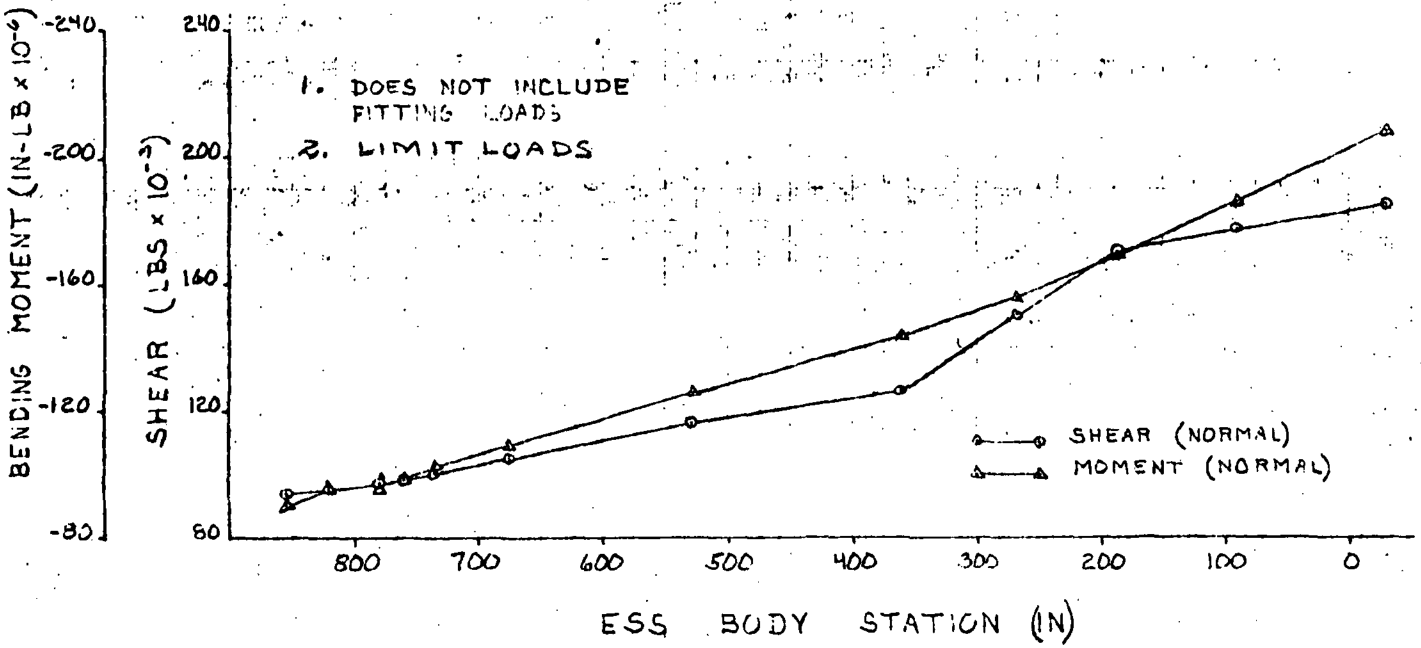

Figure G-13. Prelaunch Loads on Fueled ESS/RNS Due to 1-Day Wind and Von Karman Effect (Wind in Direction of ESS to Booster) Headwind

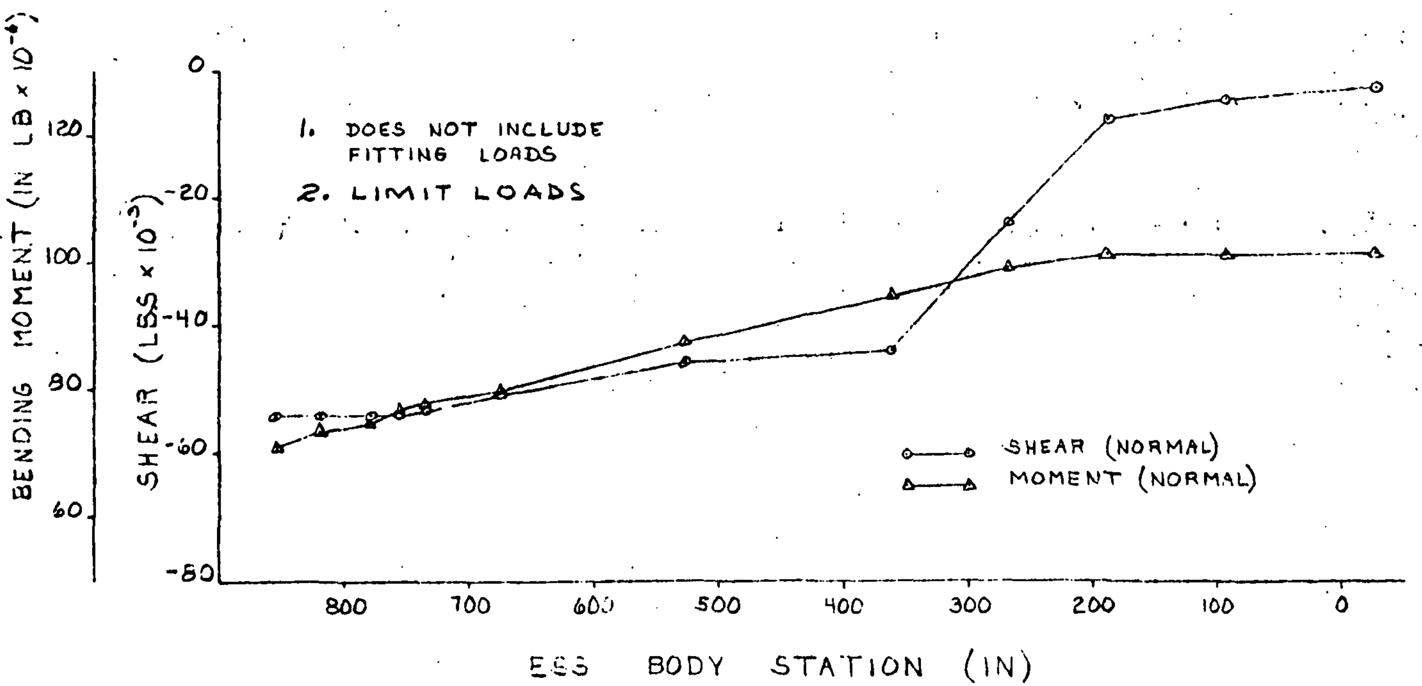

Figure G-14. Prelaunch Loads on Fueled ESS/RNS Due to 1-Day Wind and Von Karman Effect (Wind in Direction of Booster to ESS) Tailwind

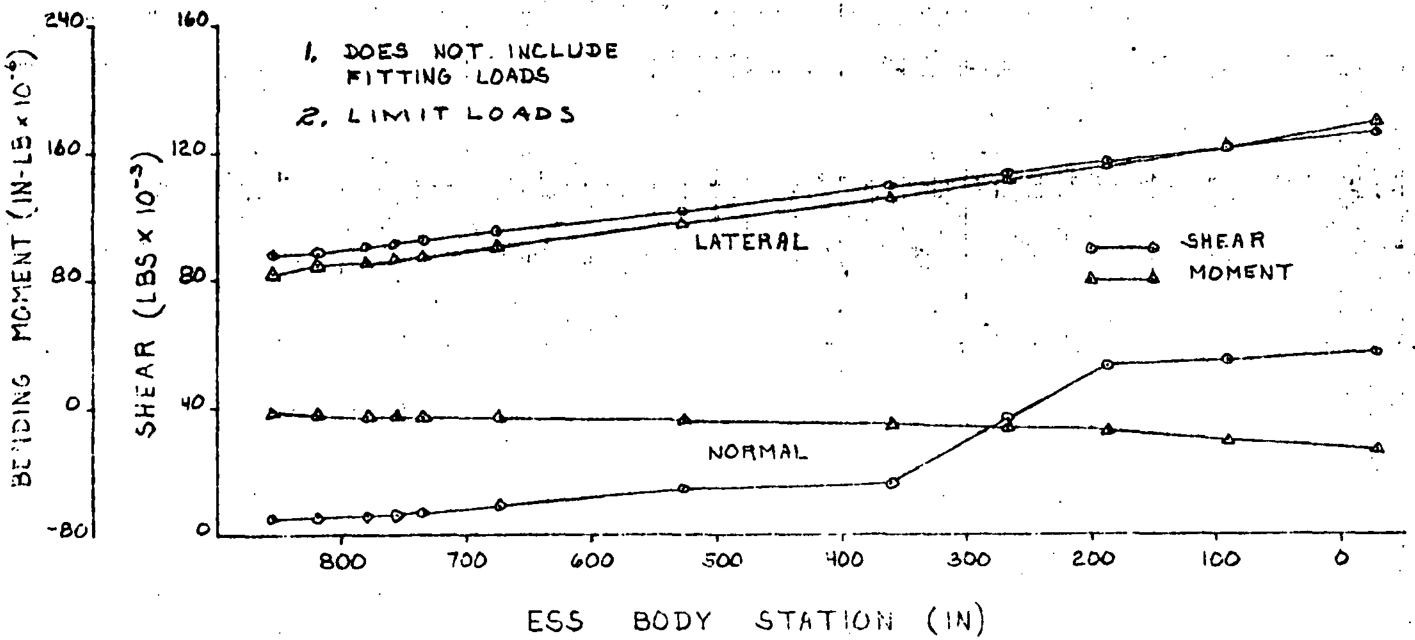

Figure G-15. Prelaunch Loads on Fueled ESS/RNS Due to 1-Day Wind and Von Karman Effect (Wind in Laterial Direction to ESS) Crosswind

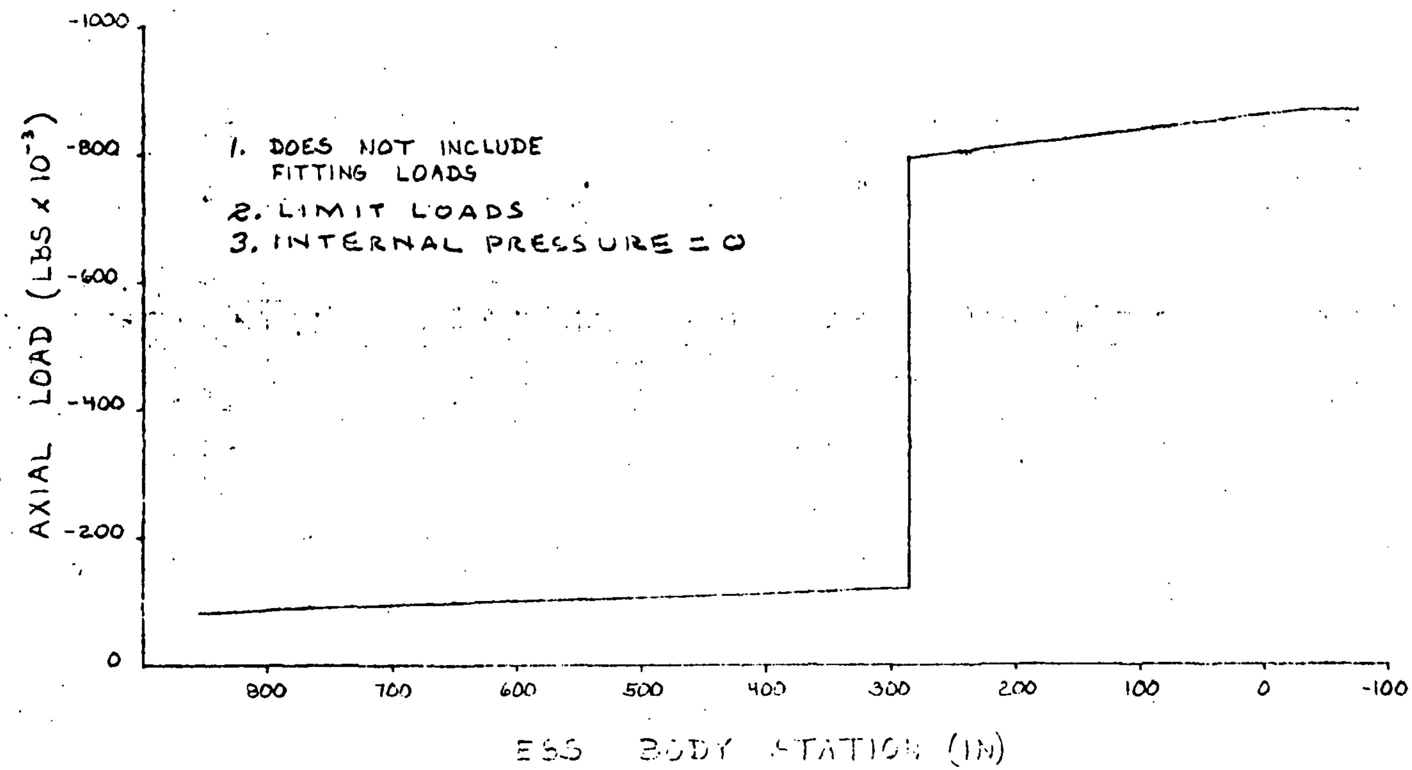

Figure G-16. Prelaunch Loads on Fueled ESS/RNS Axial Loads for Use With 1-Day Wind

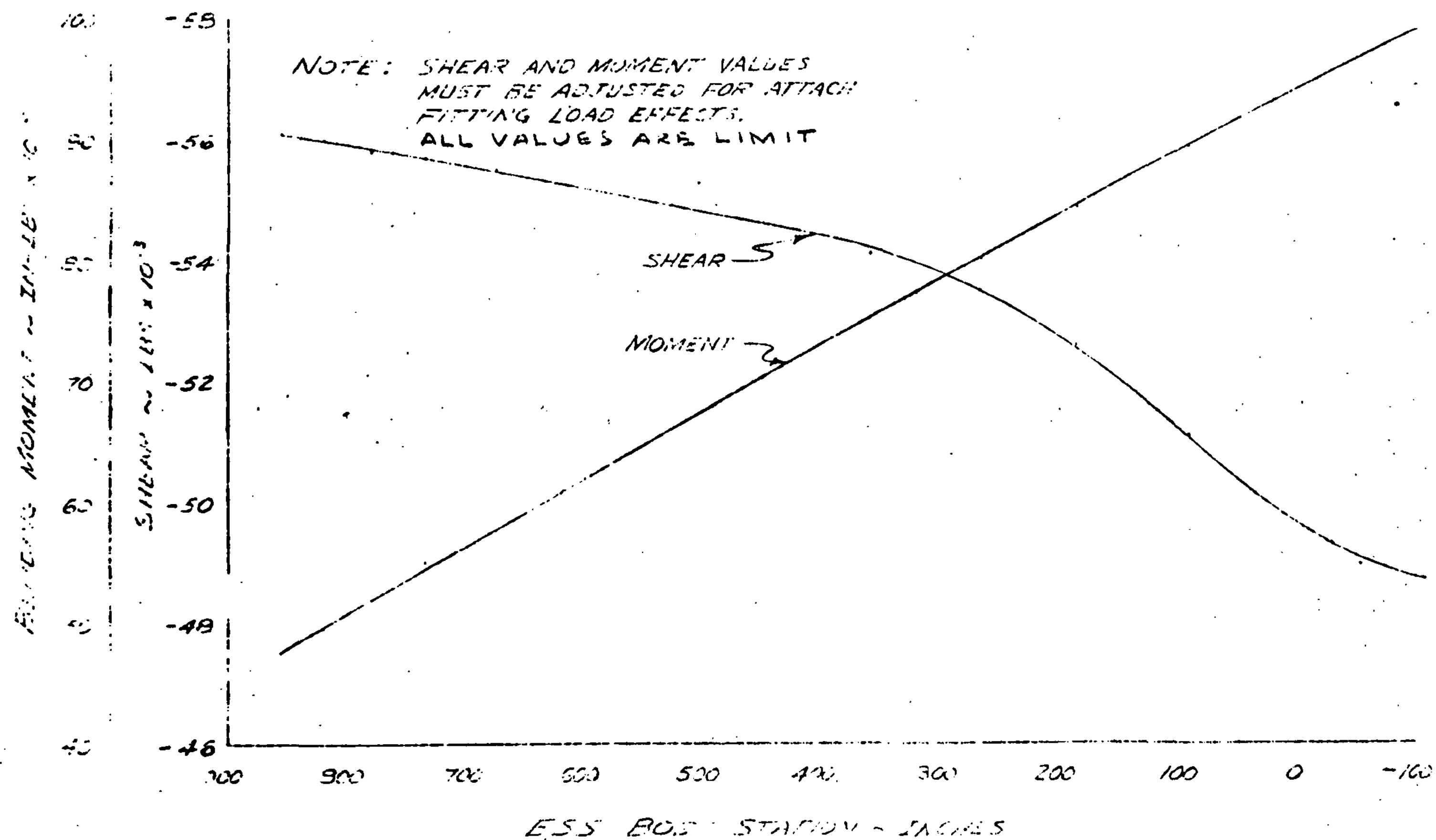

Figure G-17. Prelaunch 14-Day Headwind Loads on Unfueled ESS/MDAC (Without Fittings)

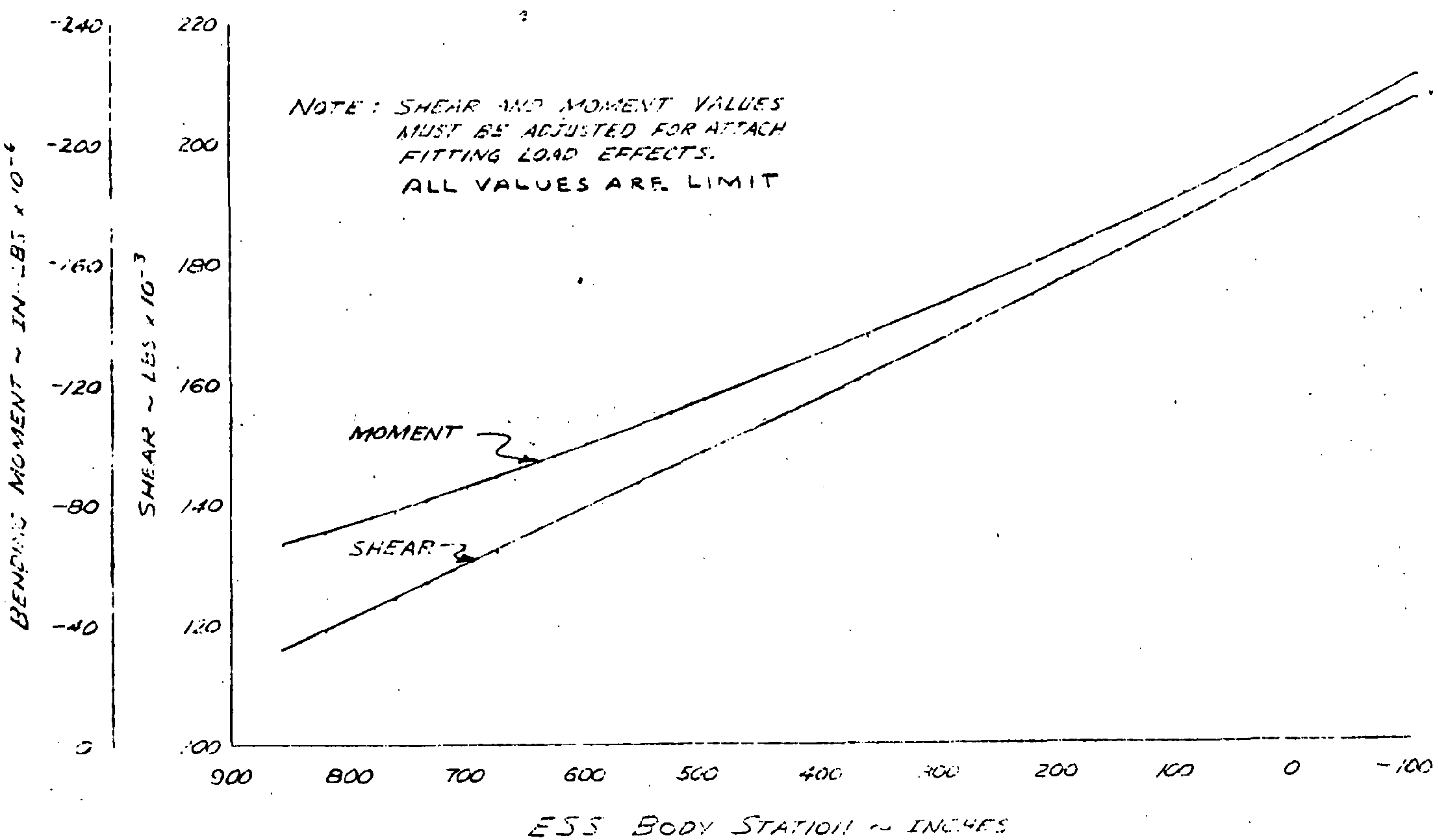

Figure G-18. Prelaunch 14-Day Tailwind Loads on Unfueled ESS/MDAC (Without Fittings)

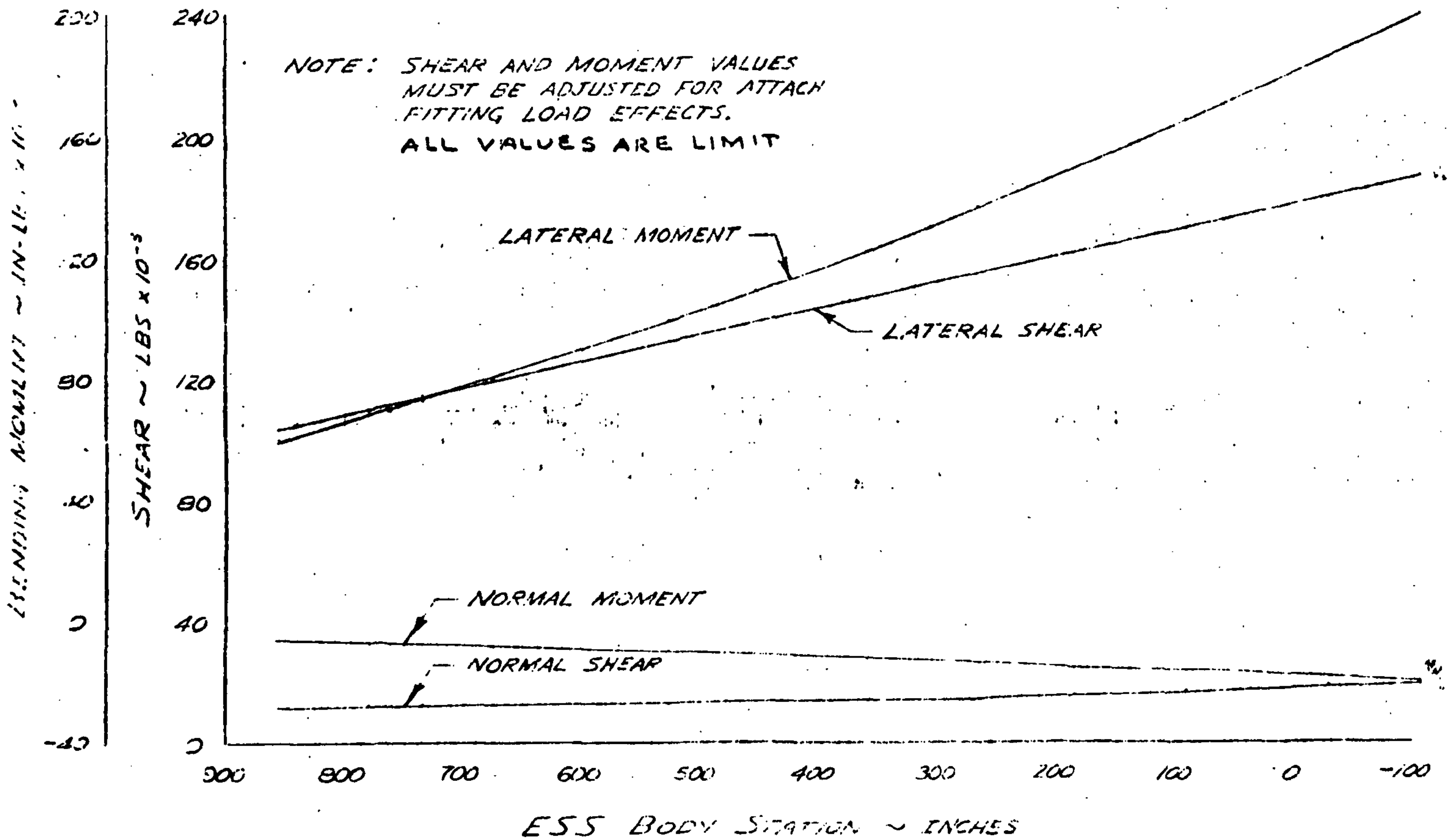

Figure G-19. Prelaunch 14-Day Sidewind Loads on Unfueled ESS/MDAC (Without Fittings)

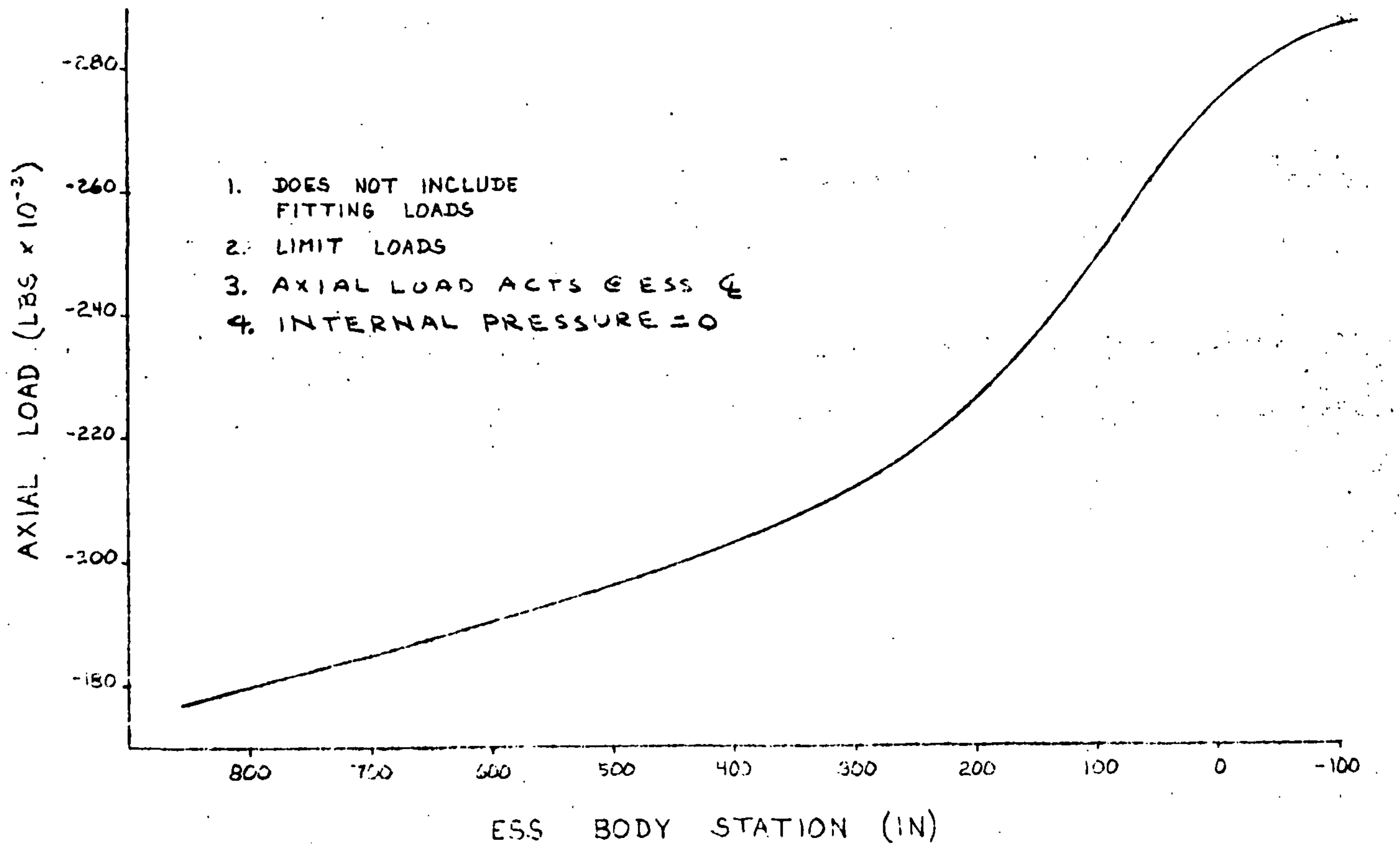

Figure G-20. Prelaunch Loads on Unfueled ESS/MDAC Axial Loads for Use With 14-Day Wind Conditions

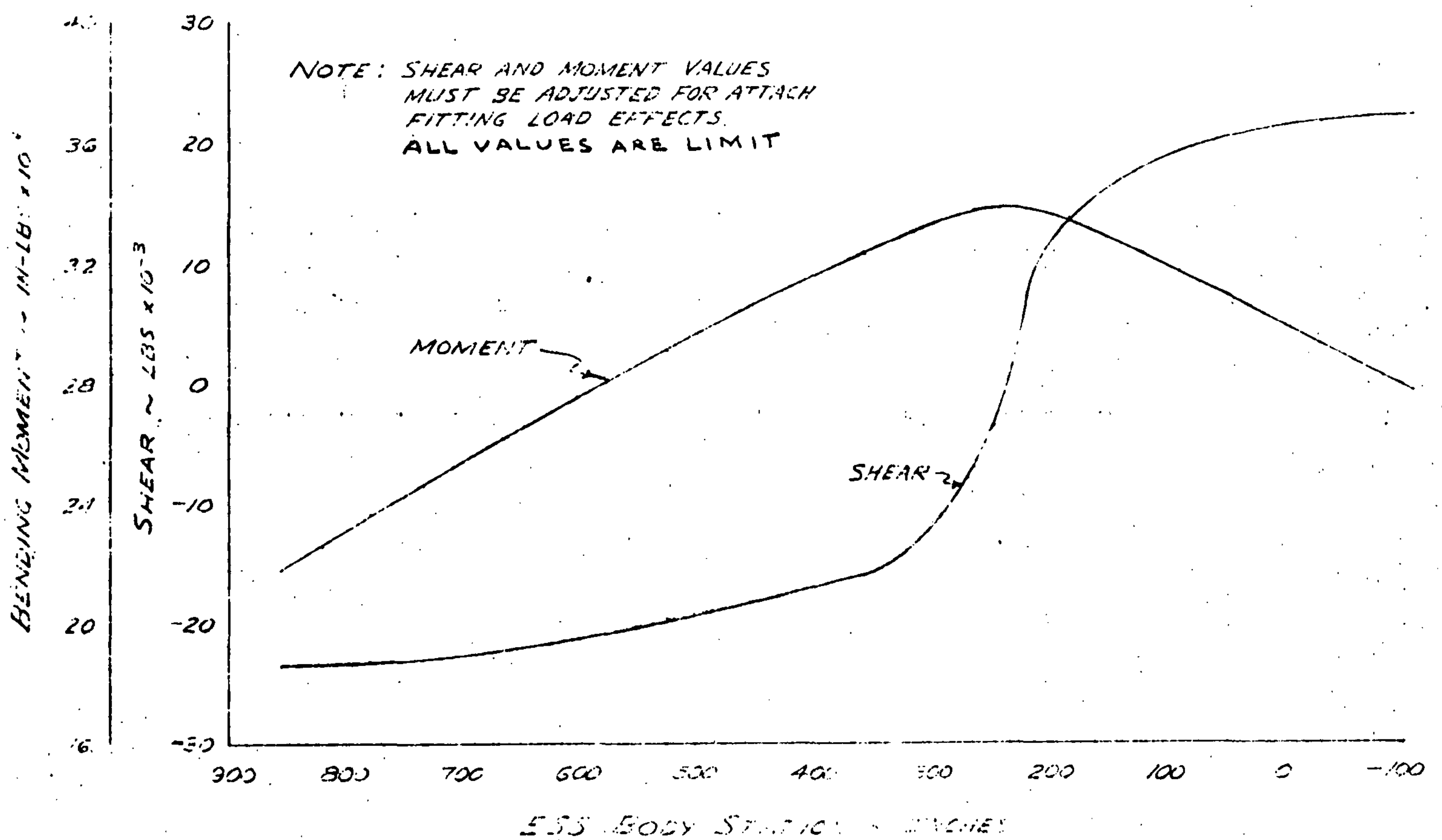

Figure G-21. Prelaunch One Day Headwind Loads on Fueled ESS/MDAC (Without Fittings)

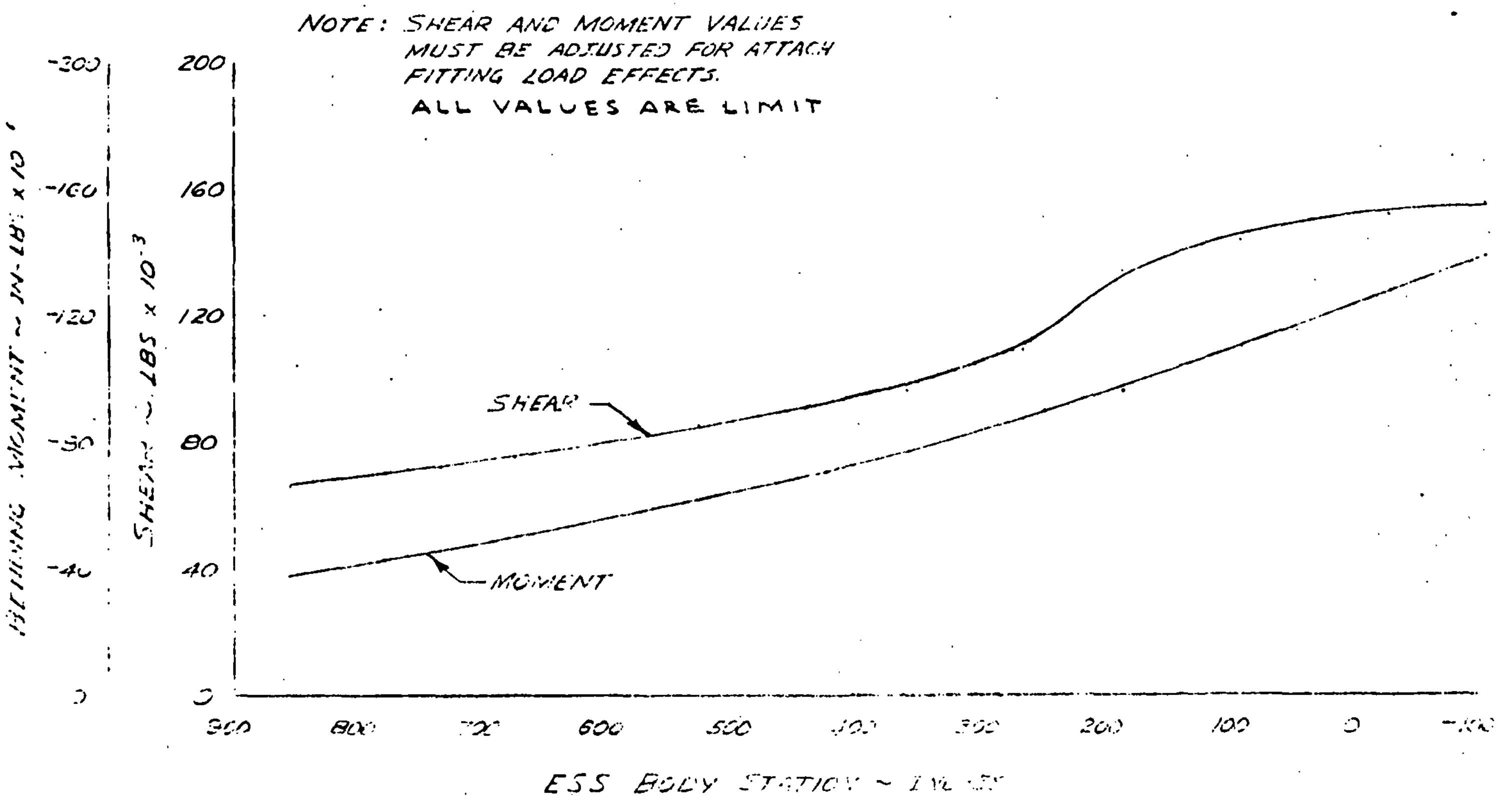

Figure G-22. Prelaunch One Day Tailwind Loads on Fueled ESS/MDAC (Without Fittings)

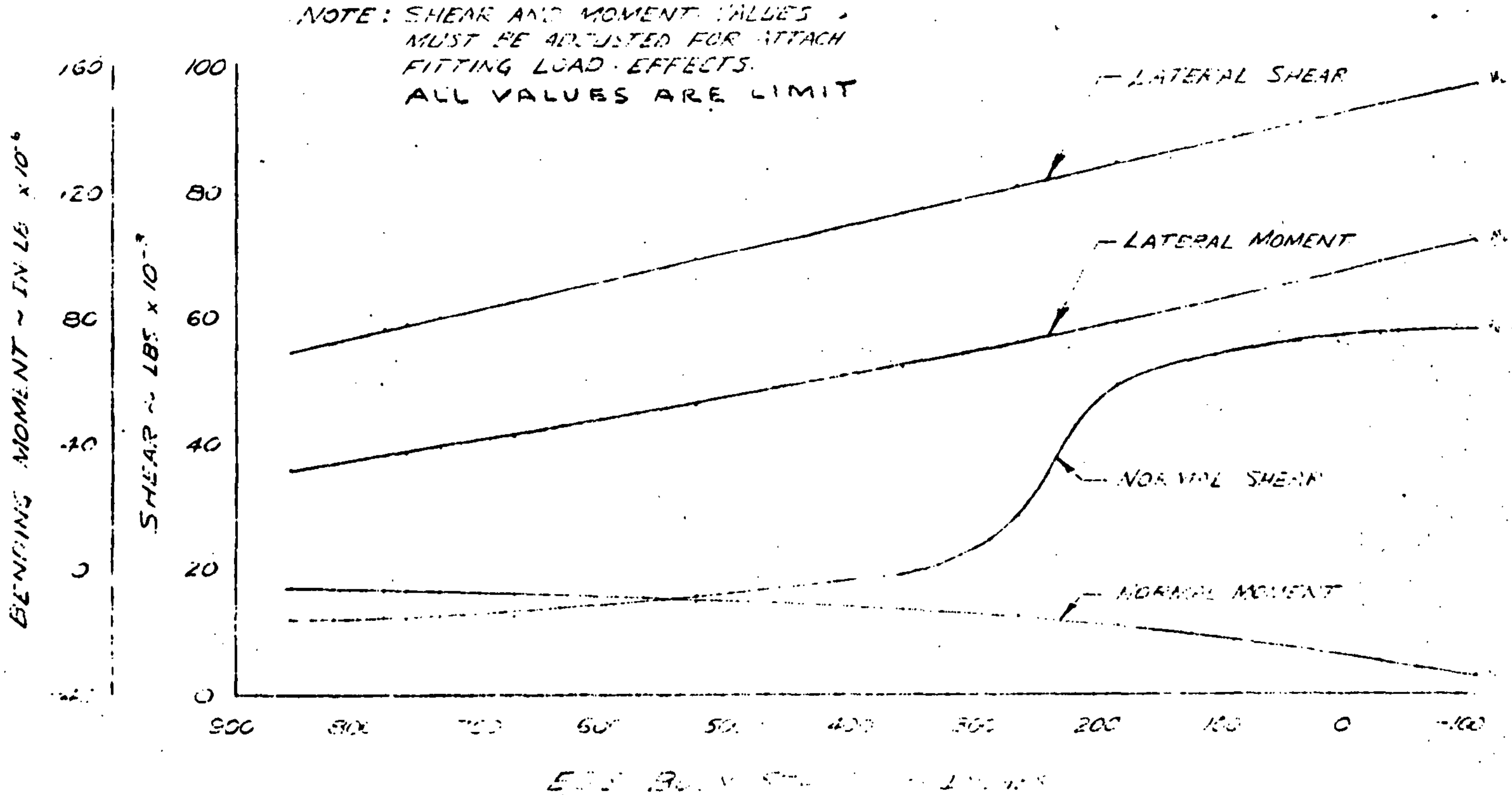

Figure G-23. Prelaunch One Day Sidewind Loads on Fueled ESS/MDAC (Without Fittings)

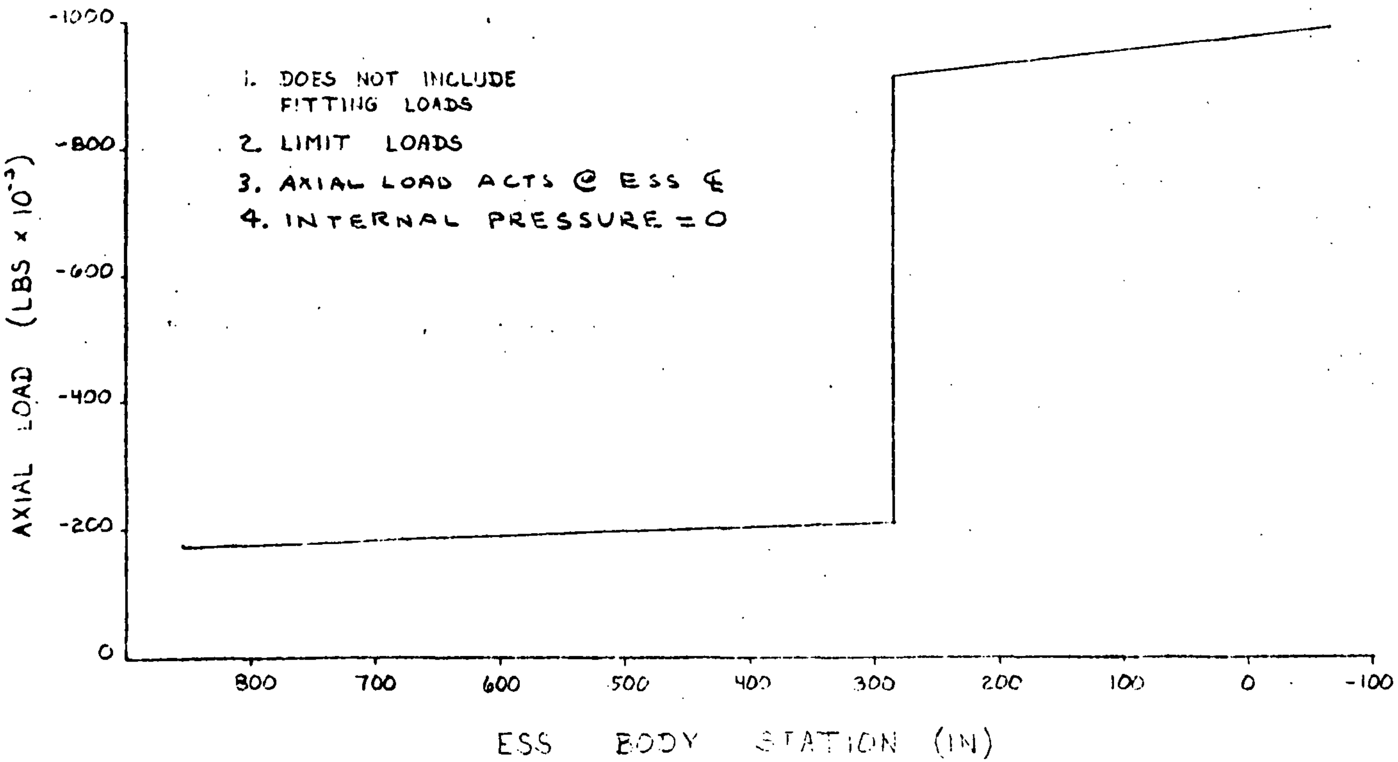

Figure G-24. Prelaunch Loads on Fueled ESS/MDAC Axial Loads for Use With 1-Day Wind Conditions

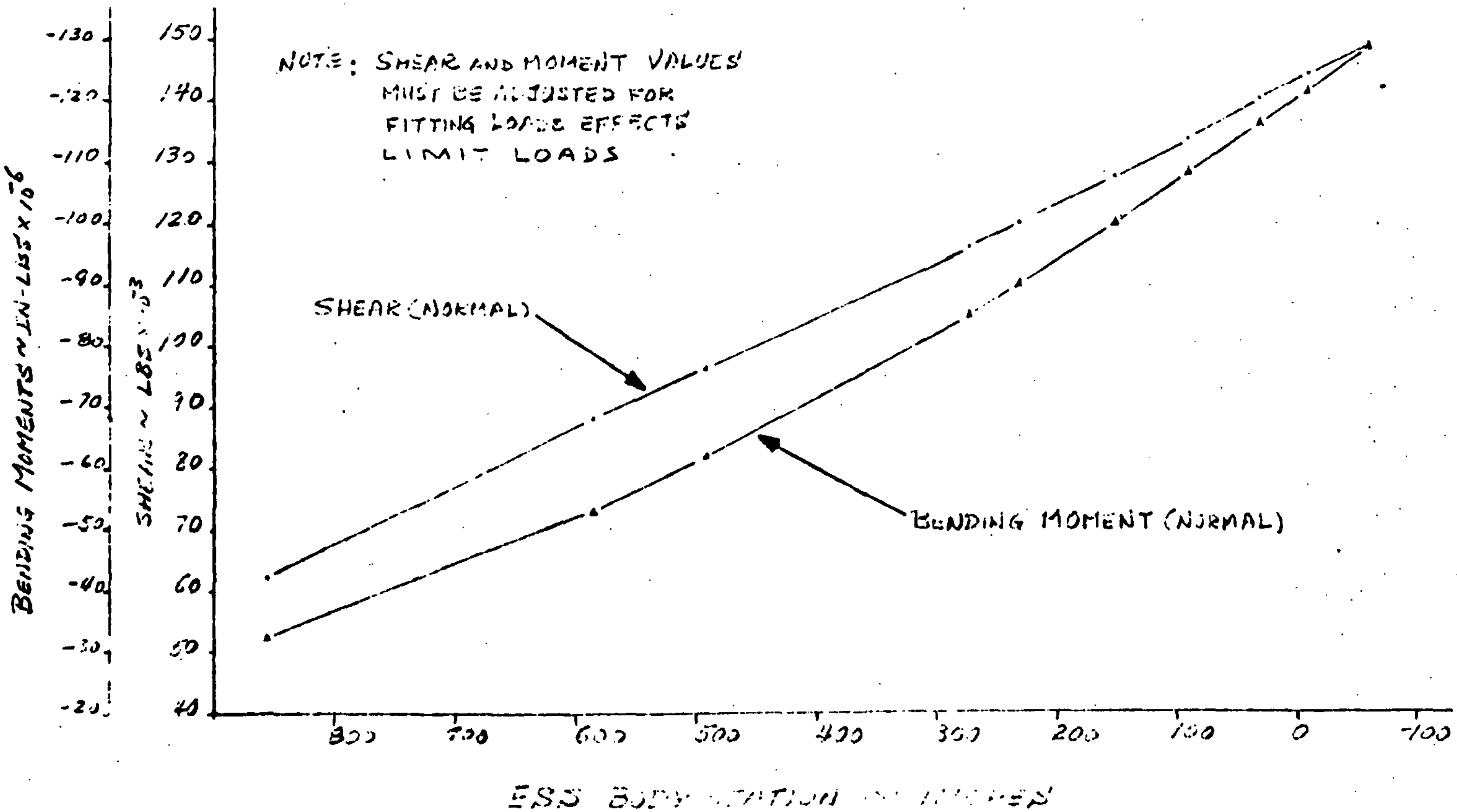

Figure G-25. Unfueled ESS/Space Tug Prelaunch Loads Due to 14-Day Wind and Von Karman Effect Winds in Direction of ESS to Booster (Headwind)

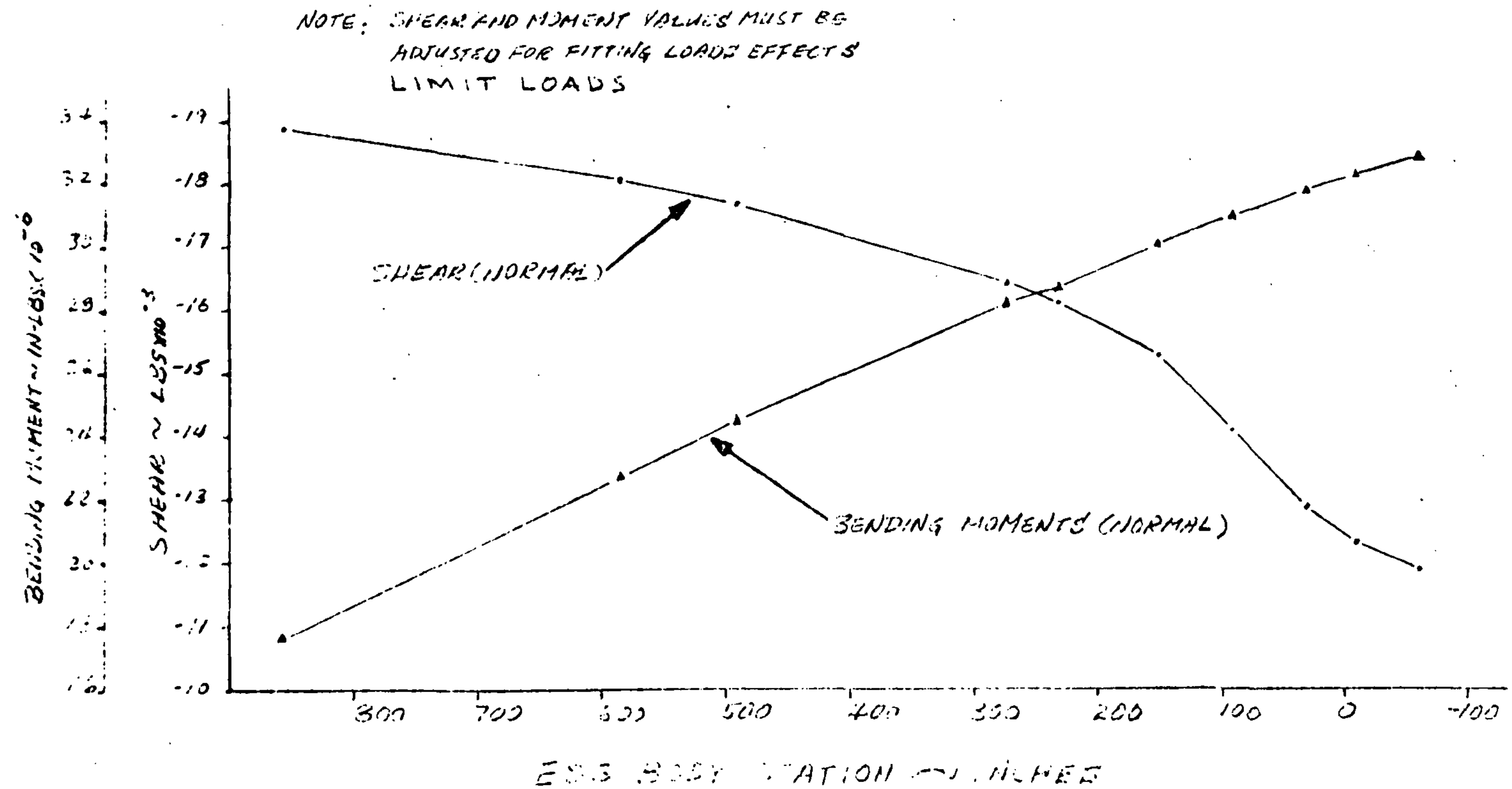

Figure G-26. Unfueled ESS/Space Tug Prelaunch Loads Due to 14-Day Wind and Von Karman Effect Winds in Direction of Booster to ESS (Tailwind) (Partial Shielding)

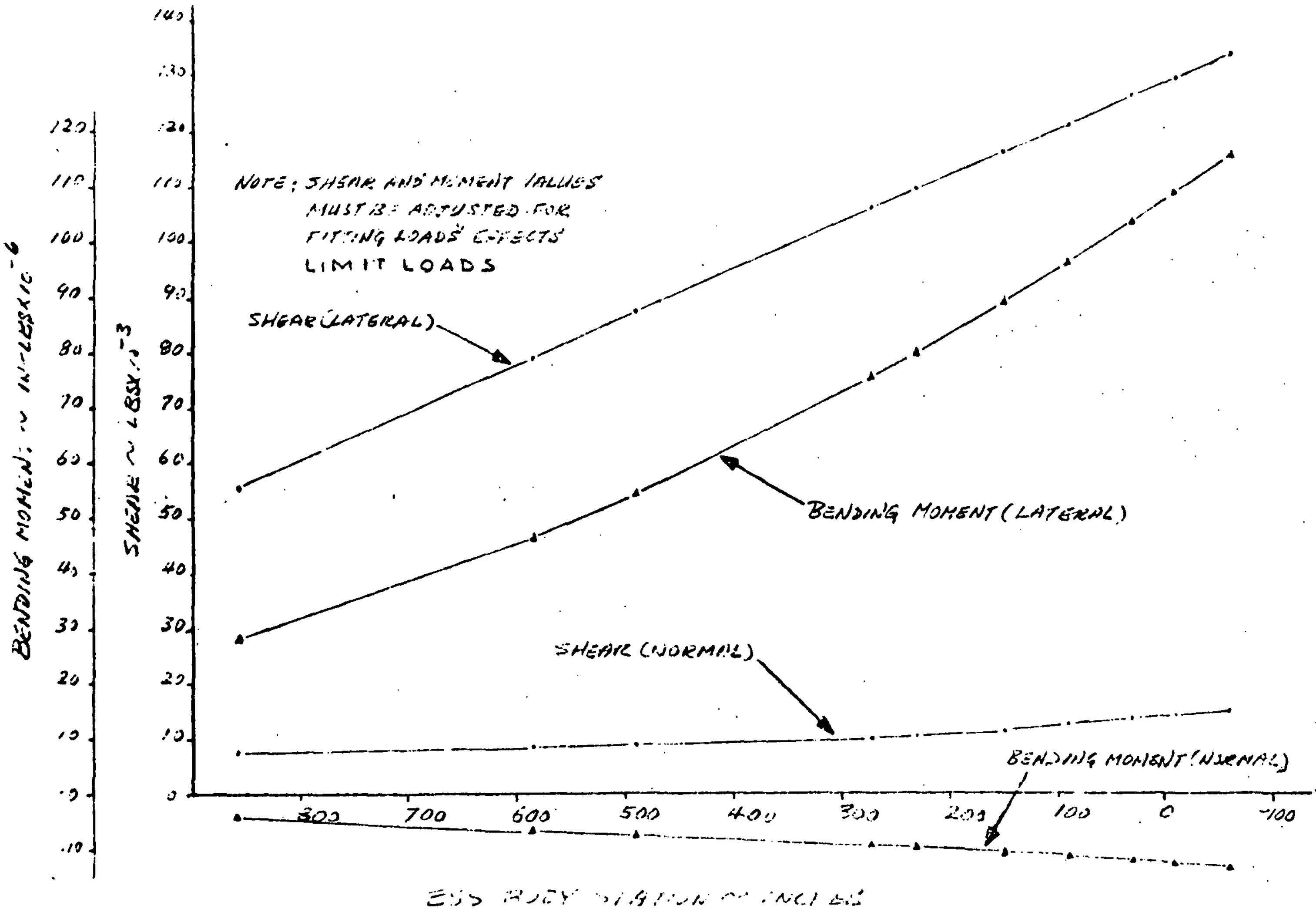

Figure G-27. Unfueled ESS/Space Tug Prelaunch Loads Due to 14-Day Wind and Von Karman Effect Winds in Laterial Direction to ESS (Crosswind)

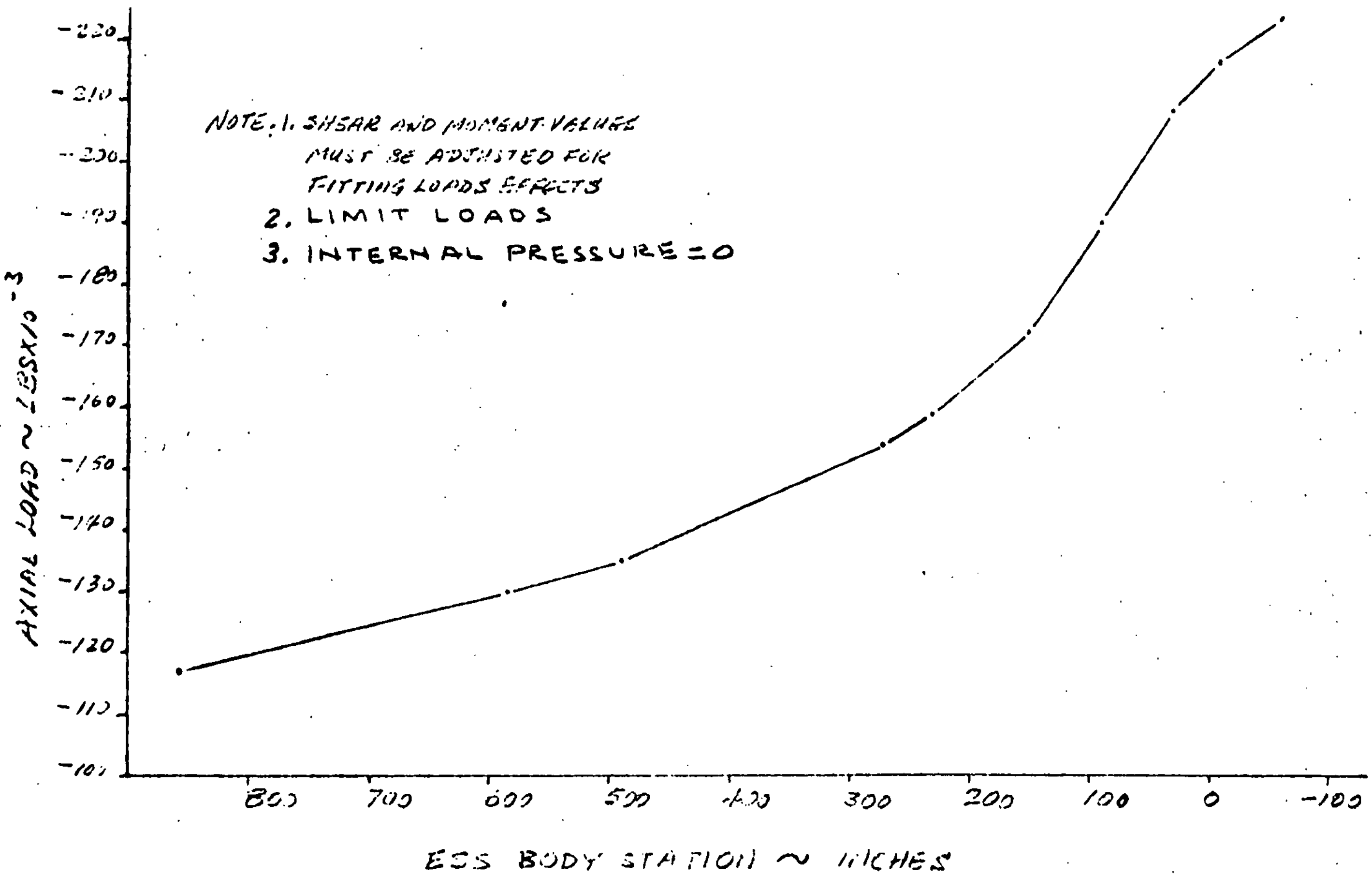

Figure G-28. Unfueled ESS/Space Tug Prelaunch Loads Axial Loads for Use With 14-Day Wind Conditions

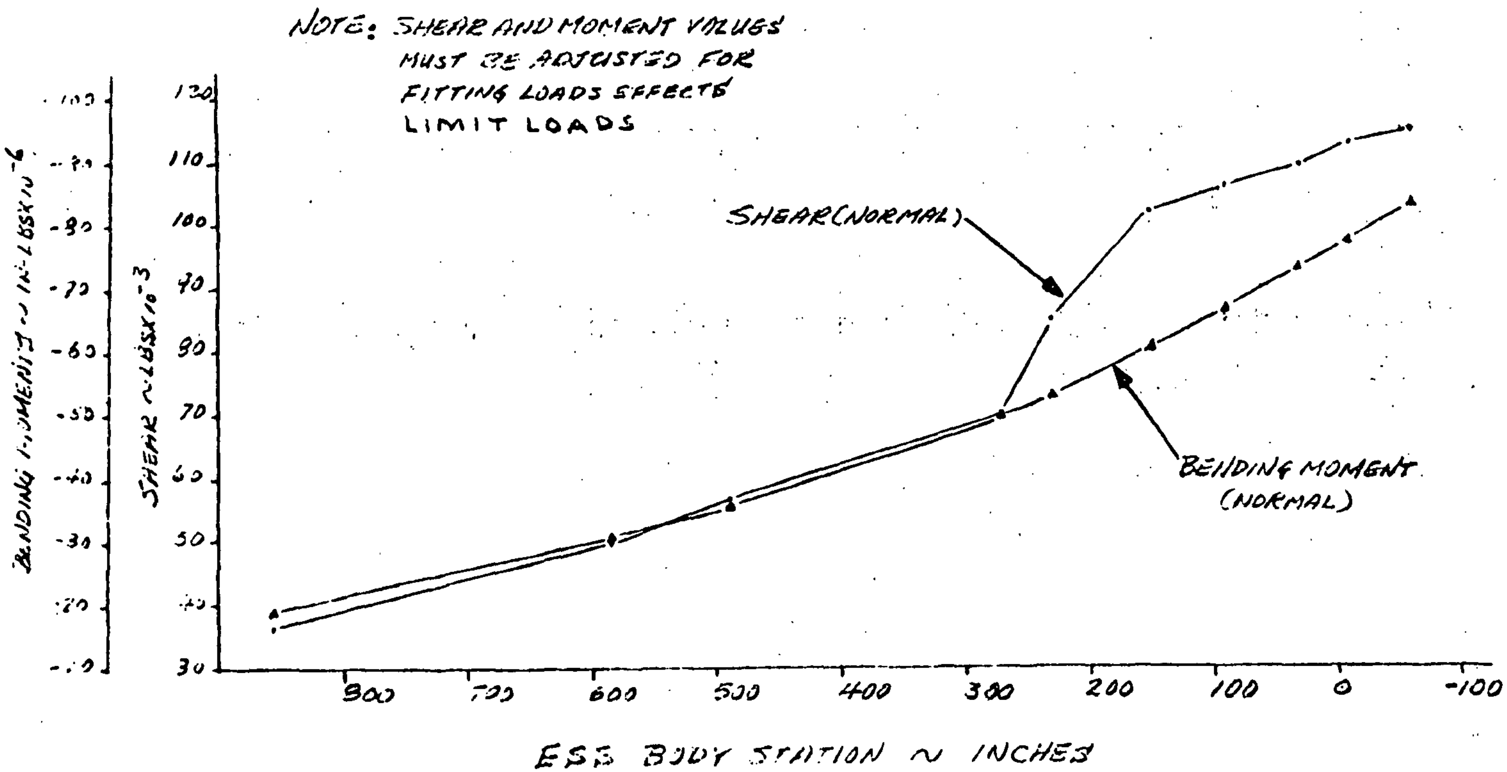

Figure G-29. Fueled ESS/Space Tug Prelaunch Loads Due to 1-Day Wind and Von Karman Effect Wind in Direction of ESS to Booster (Headwind)

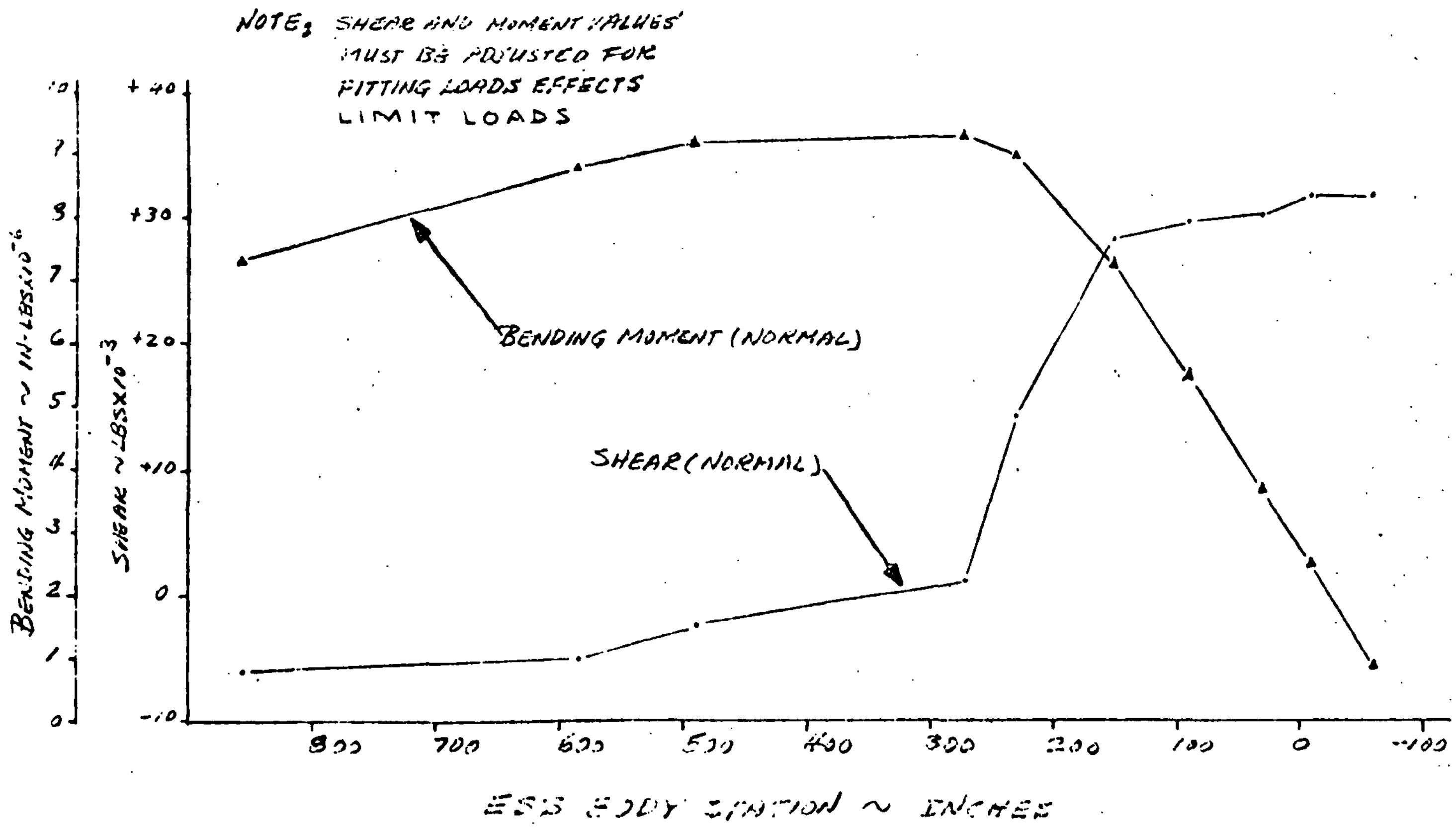

Figure G-30. Fueled ESS/Space Tug Prelaunch Loads Due to 1-Day Wind with Von Karman Effect Wind in Direction of Booster to ESS (Tailwind) (Partial Shielding)

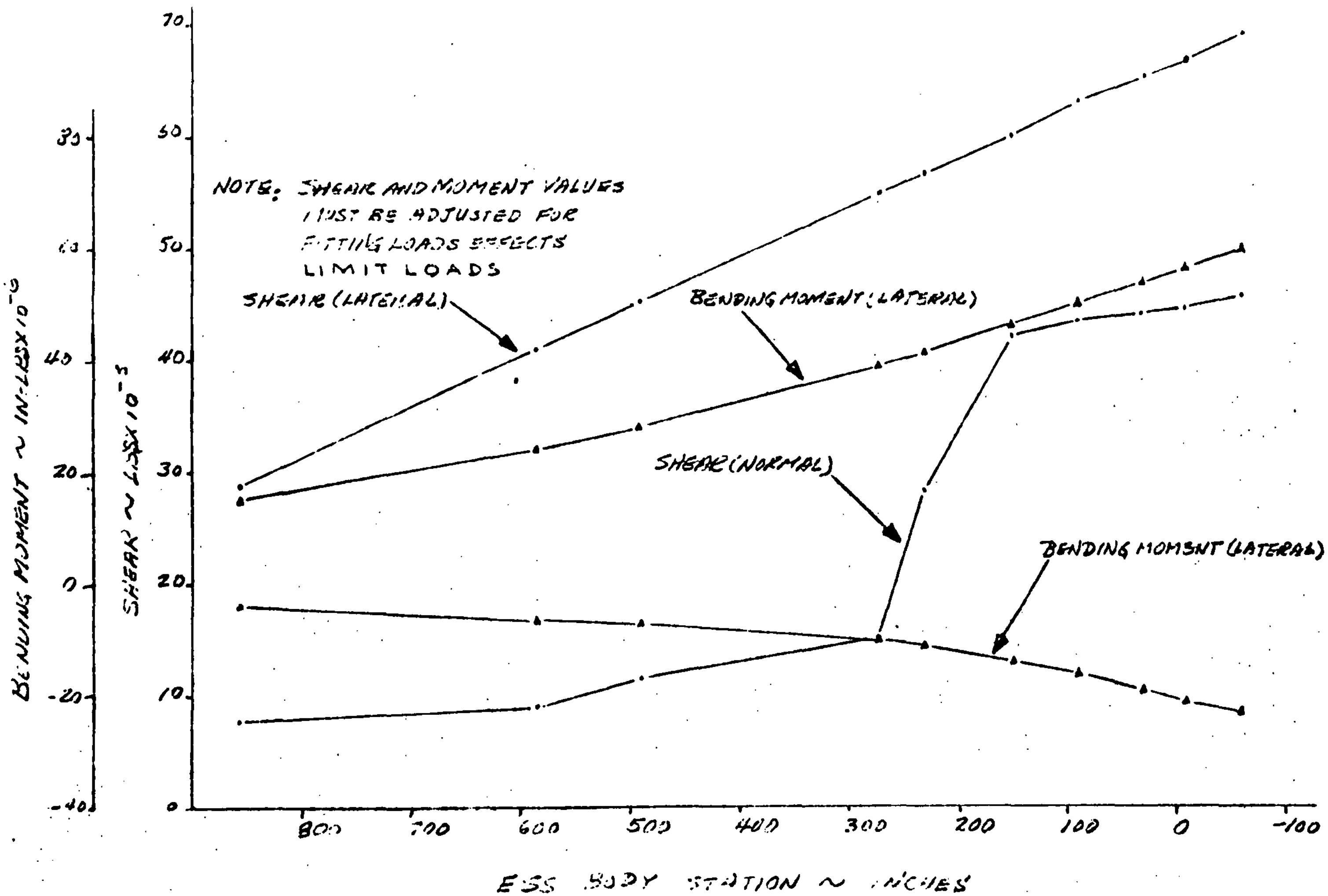

Figure G-31. Fueled ESS/Space Tug Prelaunch Loads Due to 1-Day Wind and Von Karman Effect Wind in Lateral Direction to ESS (Crosswind)

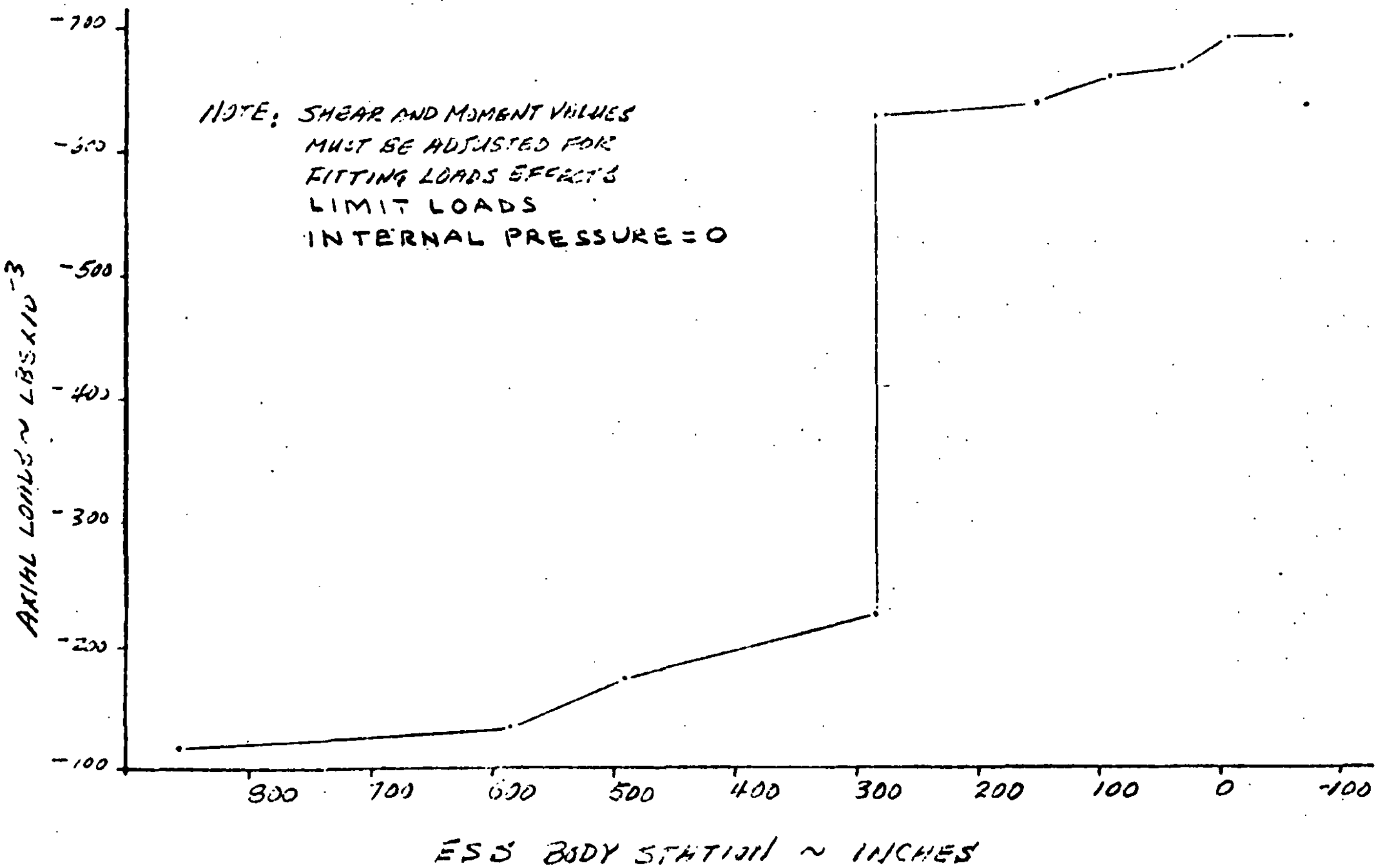

Figure G-32. Fueled ESS/Space Tug Prelaunch Loads Axial Loads for Use with 1-Day Wind Conditions